

January 15, 1968

N90-70428

Unclas  
00/15 0257071

FF No. 602(D)

(ACCESSION NUMBER) 522 (PAGES)

(NASA CR OR TMX OR AD NUMBER) ~~602(D)~~ TMX-60911

(THRU) 20 (CODE) 5 (CATEGORY)

PREPARED BY  
SATURN V FLIGHT EVALUATION WORKING GROUP



NATIONAL AERONAUTICS AND SPACE ADMINISTRATION



GEORGE C. MARSHALL SPACE FLIGHT CENTER

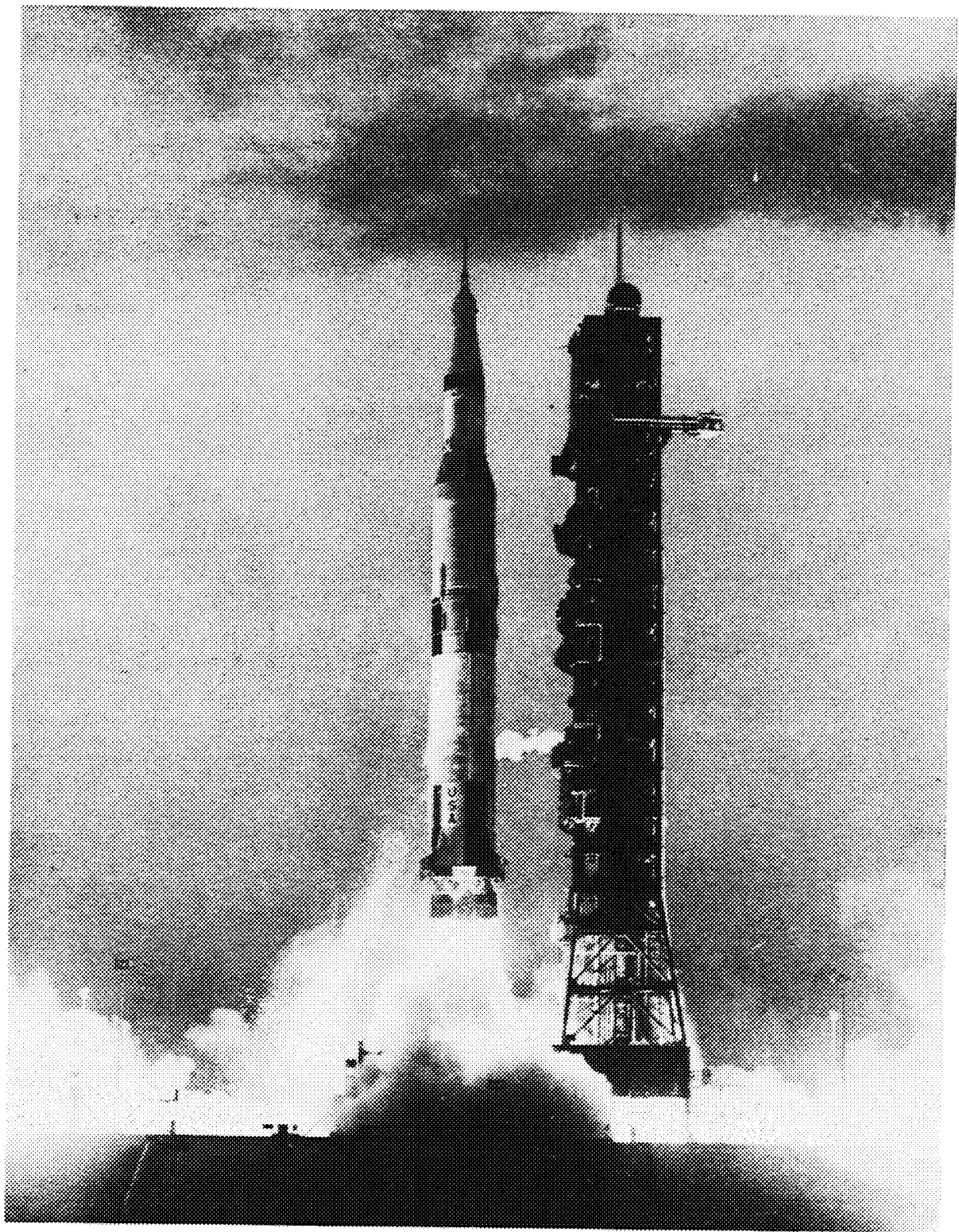
MPR-SAT-FE-68-1

**SATURN V LAUNCH VEHICLE  
FLIGHT EVALUATION REPORT - AS-501  
APOLLO 4 MISSION**

PREPARED BY  
SATURN V FLIGHT EVALUATION WORKING GROUP







Frontispiece



MPR-SAT-FE-68-1

SATURN V LAUNCH VEHICLE FLIGHT EVALUATION REPORT - AS-501  
APOLLO 4 MISSION

By

Saturn Flight Evaluation Working Group

George C. Marshall Space Flight Center

ABSTRACT

Saturn V AS-501 (Apollo 4 Mission) was launched at 0700:01 Eastern Standard Time on November 9, 1967 from KSC LC39, Pad A. The vehicle lifted off on schedule, on a launch azimuth of 90 degrees east of north and rolled to a flight azimuth of 72 degrees east of north. The actual trajectory was near nominal.

All major systems performed within design limits and close to predicted values throughout flight. Although no malfunctions or deviations occurred that adversely affected flight or mission, certain refinements for future flights are indicated in camera coverage, S-IVB CVS instrumentation, S-IC propulsion, S-II propulsion, and S-IVB propulsion.

Any questions or comments pertaining to the information contained in this report are invited and should be directed to:

Director, George C. Marshall Space Flight Center  
Huntsville, Alabama 35812

Attention: Chairman, Saturn Flight Evaluation Working Group  
R-AERO-F (Phone 876-4575)



# TABLE OF CONTENTS

Section		Page
	TABLE OF CONTENTS	iii
	LIST OF ILLUSTRATIONS	xiii
	LIST OF TABLES	viii
	ACKNOWLEDGEMENT	xxvii
	ABBREVIATIONS AND SYMBOLS	xxviii
	FLIGHT TEST SUMMARY	xxxviii
1	INTRODUCTION	
	1.1 Purpose	1-1
	1.2 Scope	1-1
2	EVENT TIMES	
	2.1 Summary of Events	2-1
	2.2 Sequence of Events	2-1
3	LAUNCH OPERATIONS	
	3.1 Summary	3-1
	3.2 Prelaunch Milestones	3-1
	3.3 Countdown Events	3-4
	3.4 Propellant and Cold Helium Loading	3-5
	3.4.1 RP-1 Loading	3-5
	3.4.2 LOX Loading	3-6
	3.4.3 LH <sub>2</sub> Loading	3-6
	3.4.4 Cold Helium Loading	3-8
	3.4.5 Auxiliary Propulsion System Propellant Loading	3-8
	3.4.6 S-IC Stage Propellant Load	3-9
	3.4.7 S-II Stage Propellant Load	3-9
	3.4.8 S-IVB Stage Propellant Load	3-12
	3.5 S-II Insulation Purge and Leak Detection	3-12
	3.6 Ground Support Equipment	3-15

## TABLE OF CONTENTS (CONTINUED)

Section		Page
4	TRAJECTORY ANALYSIS	
	4.1 Summary	4-1
	4.2 Ascent Trajectory	4-1
	4.2.1 Tracking Data Utilization	4-1
	4.2.2 Trajectory Evaluation	4-5
	4.3 Parking Orbit Trajectory	4-14
	4.3.1 Tracking Data Utilization	4-14
	4.3.2 Trajectory Evaluation	4-15
	4.4 Injection Phase Trajectory	4-17
	4.4.1 Tracking Data Utilization	4-17
	4.4.2 Trajectory Evaluation	4-17
	4.5 Waiting Orbit Trajectory	4-17
	4.5.1 Tracking Data Utilization	4-17
	4.5.2 Trajectory Evaluation	4-21
5	S-IC PROPULSION	
	5.1 S-IC Propulsion Summary	5-1
	5.2 S-IC Ignition Transient Performance	5-2
	5.3 S-IC Main Stage Performance	5-2
	5.4 S-IC Engine Shutdown Transient Performance	5-7
	5.5 S-IC Stage Propellant Management	5-8
	5.6 S-IC Pressurization System	5-9
	5.6.1 S-IC Fuel Pressurization System	5-9
	5.6.2 S-IC LOX Pressurization System	5-12
	5.7 S-IC Pneumatic Control Pressure and Purge System	5-14
6	S-II PROPULSION	
	6.1 Summary	6-
	6.2 S-II Chillo down and Buildup Transient Performance	6-

## TABLE OF CONTENTS (CONTINUED)

Section		Page
6.3	S-II Main Stage Performance	6-11
6.4	S-II Shutdown Transient Performance	6-11
6.5	S-II Propellant Management	6-16
6.6	S-II Pressurization System	6-19
6.6.1	S-II Fuel Pressurization System	6-19
6.6.2	S-II LOX Pressurization System	6-21
6.7	S-II Pneumatic Control Pressure System	6-26
6.8	Camera Ejection System	6-28
6.9	Helium Injection System	6-28
7	S-IVB PROPULSION	
7.1	Summary	7-1
7.2	S-IVB Chilldown and Buildup Transient Performance for First Burn	7-2
7.3	S-IVB Mainstage Performance for First Burn	7-6
7.4	S-IVB Shutdown Transient Performance for First Burn	7-8
7.5	S-IVB Coast Phase Conditioning	7-10
7.6	S-IVB Chilldown and Buildup Transient Performance for Second Burn	7-16
7.7	S-IVB Mainstage Performance for Second Burn	7-19
7.8	S-IVB Shutdown Transient Performance for Second Burn	7-24
7.9	S-IVB Stage Propellant Utilization	7-24
7.10	S-IVB Pressurization System	7-31
7.10.1	S-IVB LH <sub>2</sub> Tank Pressurization	7-31
7.10.2	S-IVB LOX Pressurization System	7-37
7.11	S-IVB Pneumatic Control and Purge System	7-45
7.12	S-IVB Auxiliary Propulsion System	7-52

## TABLE OF CONTENTS (CONTINUED)

Section		Page
8	HYDRAULIC SYSTEM	
	8.1 Summary	8-1
	8.2 S-IC Hydraulic System	8-1
	8.3 S-II Hydraulic System	8-1
	8.4 S-IVB Hydraulic System (First Burn)	8-4
	8.5 S-IVB Hydraulic System (Coast Phase)	8-6
	8.6 S-IVB Hydraulic System (Second Burn)	8-7
9	STRUCTURES	
	9.1 Summary	9-1
	9.2 Total Vehicle Structures Evaluation	9-1
	9.2.1 Longitudinal Loads	9-1
	9.2.2 Bending Moments	9-2
	9.2.3 Vehicle Dynamic Characteristics	9-7
	9.2.4 S-IC Fin Dynamics	9-11
	9.3 Vibration Evaluation	9-11
	9.3.1 S-IC Stage and Engine Evaluation	9-11
	9.3.2 S-II Stage and Engine Evaluation	9-18
	9.3.3 S-IVB Stage and Engine Evaluation	9-18
	9.3.4 Instrument Unit Evaluation	9-26
10	GUIDANCE AND NAVIGATION	
	10.1 Summary	10-1
	10.2 Guidance System Description	10-1
	10.3 Guidance Intelligence Errors	10-2
	10.4 Navigation and Guidance Scheme Evaluation	10-5
	10.4.1 Guidance Comparisons	10-5
	10.4.2 Evaluation of Programed Flight Maneuvers	10-9
	10.4.3 Orbital Routines	10-12
	10.5 Guidance System Component Evaluation	10-13



## TABLE OF CONTENTS (CONTINUED)

Section		Page
	10.5.1 ST-124M-3 Inertial Platform Subsystem	10-13
	10.5.2 Launch Vehicle Digital Computer and Launch Vehicle Data Adapter	10-13
11	CONTROL	
	11.1 Summary	11-1
	11.2 Control System Description	11-1
	11.3 S-IC Control System Evaluation	11-2
	11.3.1 Liftoff Clearances	11-3
	11.3.2 S-IC Flight Dynamics	11-6
	11.4 S-II Control System Evaluation	11-25
	11.4.1 Attitude Control Dynamics and Stability	11-26
	11.4.2 Liquid Propellant Dynamics and Their Effects on Flight Control	11-28
	11.5 S-IVB Control System Evaluation	11-29
	11.5.1 Control System Evaluation During First Burn	11-36
	11.5.2 Control System Evaluation During Parking Orbit	11-36
	11.5.3 Control System Evaluation During Second Burn	11-45
	11.5.4 Control System Evaluation During Waiting Orbit	11-52
	11.6 Instrument Unit Control Components Evaluation	11-52
	11.6.1 Control - EDS Rate Gyros/Control Signal Processor Analysis	11-52
	11.6.2 Flight Control Computer Performance	11-52
	11.6.3 Gimbal Actuators Analysis	11-57
12	SEPARATION	
	12.1 Summary	12-1
	12.2 S-IC/S-II Separation Evaluation	12-1

## TABLE OF CONTENTS (CONTINUED)

Section		Page
	12.2.1 S-IC Retro Motor Performance	12-1
	12.2.2 S-II Ullage Motor Performance	12.4
	12.2.3 S-IC/S-II Separation Dynamics	12.4
	12.3 S-II Second Plane Separation Dynamics	12.6
	12.4 S-II/S-IVB Separation Evaluation	12-13
	12.4.1 S-II Retro Motor Performance	12-13
	12.4.2 S-IVB Ullage Motor Performance	12-13
	12.4.3 S-II/S-IVB Separation Dynamics	12-17
	12.5 S-IVB-IU/CSM Separation Evaluation	12-24
13	ELECTRICAL NETWORKS	
	13.1 Summary	13-1
	13.2 S-IC Stage Electrical System	13-1
	13.3 S-II Stage Electrical System	13-1
	13.4 S-IVB Stage Electrical System	13-6
	13.5 Instrument Unit Electrical System	13-11
14	RANGE SAFETY AND COMMAND SYSTEMS	
	14.1 Summary	14-1
	14.2 Range Safety Command Systems	14-1
	14.3 Command and Communications System	14-2
15	EMERGENCY DETECTION SYSTEM	
	15.1 Summary	15-1
	15.2 System Description	15-1
	15.3 System Evaluation	15-1
	15.3.1 General Performance	15-1
	15.3.2 Propulsion System Sensors	15-1
	15.3.3 Flight Dynamics and Control Sensors	15-3
	15.3.4 Network Sequential Events	15-3

## TABLE OF CONTENTS (CONTINUED)

Section		Page
16	VEHICLE PRESSURE AND ACOUSTIC ENVIRONMENT	
	16.1 Summary	16-1
	16.2 Surface Pressure and Compartment Venting	16-1
	16.2.1 S-IC Stage	16-1
	16.2.2 S-II Stage	16-1
	16.2.3 S-IVB Stage	16-7
	16.3 Base Pressures	16-7
	16.3.1 S-IC Base Pressures	16-7
	16.3.2 S-II Base Pressures	16-10
	16.4 Acoustic Environment	16-11
	16.4.1 External Acoustics	16-11
	16.4.2 Internal Acoustics	16-15
17	VEHICLE THERMAL ENVIRONMENT	
	17.1 Summary	17-1
	17.2 S-IC Base Heating and Separation Environment	17-1
	17.3 S-II Base Heating and Separation Environment	17-9
	17.4 S-II/S-IVB Separation Environment	17-14
	17.5 Vehicle Aeroheating Thermal Environment	17-14
	17.5.1 S-IC Stage Aeroheating Environment	17-14
	17.5.2 S-II Stage Aeroheating Environment	17-18
	17.5.3 S-IVB Stage Aeroheating Environment	17-23
	17.5.4 Instrument Unit Aeroheating Environment	17-26
	17.6 Vehicle Orbital Heating Environment	17-26
18	ENVIRONMENTAL CONTROL SYSTEM	
	18.1 Summary	18-1
	18.2 S-IC Environmental Control	18-1
	18.3 S-II Environmental Control	18-2
	18.4 S-IVB Environmental Control	18-2
	18.4.1 Ascent Powered Flight Phase	18-2
	18.5 IU Environmental Control	18-3

## TABLE OF CONTENTS (CONTINUED)

Section		Page
	18.5.1 Thermal Conditioning System	18-3
	18.5.2 ST-124M Gas Bearing System	18-5
19	DATA SYSTEMS	
	19.1 Summary	19-1
	19.2 Vehicle Measurements Evaluation	19-1
	19.2.1 S-IC Stage Measurement Analysis	19-2
	19.2.2 S-II Stage Measurement Analysis	19-2
	19.2.3 S-IVB Stage Measurement Analysis	19-11
	19.2.4 Instrument Unit Measurement Analysis	19-13
	19.3 Airborne Telemetry Systems	19-13
	19.3.1 S-IC Stage Telemetry System	19-13
	19.3.2 S-II Stage Telemetry System	19-16
	19.3.3 S-IVB Stage Telemetry System	19-16
	19.3.4 Instrument Unit Telemetry System	19-17
	19-4 Airborne Tape Recorders	19-17
	19.4.1 S-IC Stage Recorder	19-18
	19.4.2 S-II Stage Recorder	19-19
	19.4.3 S-IVB Stage Recorder	19-20
	19.4.4 Instrument Unit Recorder	19-20
	19.5 RF Systems Evaluation	19-20
	19.5.1 Telemetry Systems RF Propagation Evaluation	19-20
	19.5.2 Tracking Systems RF Propagation Evaluation	19-22
	19.5.3 Command Systems RF Evaluation	19-28
	19.6 Optical Instrumentation	19-28
	19.6.1 Onboard Cameras	19-28
	19.6.2 Ground Engineering Cameras	19-34
20	VEHICLE AERODYNAMIC CHARACTERISTICS	
	20.1 Summary	20-1
	20.2 Vehicle Axial Force Characteristics	20-1
	20.3 Vehicle Static Stability	20-3
	20.4 Fin Pressure Loading	20-4

## TABLE OF CONTENTS (CONTINUED)

Section	Page
21	MASS CHARACTERISTICS
21.1	Summary 21-1
21.2	Mass Evaluation 21-1
22	MALFUNCTIONS AND DEVIATIONS
22.1	Summary 22-1
22.2	System Malfunctions and Deviations 22-1
23	SPACECRAFT SUMMARY
23.1	Summary 23-1
23.2	Spacecraft Performance Evaluation 23-1
Appendix	
A	ATMOSPHERIC SUMMARY
A.1	Summary A-1
A.2	General Atmospheric Conditions at Launch Time A-1
A.3	Surface Observations at Launch Time A-1
A.4	Upper Air Measurements A-1
A.4.1	Wind Speed A-1
A.4.2	Wind Direction A-5
A.4.3	Pitch Wind Component A-5
A.4.4	Yaw Wind Component A-5
A.4.5	Component Wind Shears A-9
A.5	Thermodynamic Data A-9
A.5.1	Temperature A-9
A.5.2	Density A-9
A.5.3	Pressure A-9
A.5.4	Optical Index of Refraction A-9

## TABLE OF CONTENTS (CONTINUED)

Appendix		Page
B	AS-501 LAUNCH VEHICLE DESCRIPTION	
	B.1 Vehicle	B-1
	B.1.1 Vehicle Structure	B-1
	B.1.2 Vehicle Propulsion	B-1
	B.1.3 Vehicle Systems	B-3
	B.2 S-IC Stage	B-8
	B.2.1 S-IC Stage Structure	B-8
	B.2.2 S-IC Stage Propulsion System	B-8
	B.3 S-II Stage	B-10
	B.3.1 S-II Stage Structure	B-11
	B.3.2 S-II Stage Propulsion System	B-11
	B.4 S-IVB Stage	B-14
	B.4.1 S-IVB Stage Structure	B-14
	B.4.2 S-IVB Stage Propulsion System	B-15
	B.5 Instrument Unit	B-17
	B.5.1 Instrument Unit Structure	B-17
	B.5.2 Instrument Unit Electrical System	B-18
	B.5.3 Instrument Unit Environment Control System	B-18
	B.6 Spacecraft	B-19
	B.6.1 Spacecraft Structure	B-19
	B.6.2 Spacecraft Subsystems	B-19
C	MISSION OBJECTIVES	
	C.1 SA-501 Launch Vehicle Flight Objectives	C-1
D	PREFLIGHT VERSUS POSTFLIGHT COMPARISONS OF INSERTION AND INJECTION CONDITIONS	D-1

## LIST OF ILLUSTRATIONS

Figure		Page
4-1	Ascent Trajectory Position Comparison	4-6
4-2	Ascent Trajectory Earth-Fixed Velocity Comparison	4-7
4-3	Injection Phase Space-Fixed Velocity Comparison	4-8
4-4	Ascent Trajectory Acceleration Comparison	4-10
4-5	Dynamic Pressure and Mach Number Vs Range Time	4-11
4-6	Acceleration Due to Venting in Parking Orbit	4-16
4-7	AS-501 Ground Track	4-18
4-8	Injection Phase Space-Fixed Velocity Comparison	4-19
4-9	Injection Phase Acceleration Comparison	4-20
5-1	S-IC Start Box Requirements	5-3
5-2	S-IC Engine Buildup Transient	5-4
5-3	S-IC Steady State Operation	5-5
5-4	S-IC Engine Shutdown Transient Performance	5-11
5-5	S-IC Fuel Ullage Pressure During Countdown	5-12
5-6	S-IC Helium Pressurization System (Inlet to 60B49029 Duct)	5-13
5-7	S-IC Fuel Ullage Pressure During Boost	5-15
5-8	S-IC Helium Bottle Pressure for Fuel Pressurization	5-15
5-9	S-IC LOX Ullage Pressure	5-16
5-10	S-IC Pneumatic Control Regulator Outlet Pressure	5-16
6-1	S-II Thrust Chamber Temperatures	6-4
6-2	S-II Engine Start Tank Performance	6-5
6-3	S-II Start Box Requirements	6-7
6-4	S-II LH <sub>2</sub> Recirculation System Performance	6-8
6-5	S-II Engine Thrust Buildup	6-9
6-6	S-II Chamber Pressure Buildup on Engine Number 4	6-10
6-7	S-II Steady State Operation	6-12

# LIST OF ILLUSTRATIONS (CONTINUED)

Figure		Page
6-8	S-II Engine Shutdown Transient	6-15
6-9	S-II PU Valve Position	6-17
6-10	S-II LOX and LH <sub>2</sub> Probe/Tank Mismatch	6-18
6-11	Stage Mass at S-II Ignition and Cutoff	6-20
6-12	S-II LH <sub>2</sub> Tank Ullage Pressure During Prepress and S-IC Boost	6-22
6-13	S-II LH <sub>2</sub> Ullage Pressure During S-II Burn	6-22
6-14	S-II Fuel Pump Inlet Conditions	6-23
6-15	S-II LOX Ullage Pressure During Prepress and S-IC Boost	6-24
6-16	S-II LOX Ullage Pressure During Burn	6-24
6-17	S-II Heat Exchanger Performance	6-25
6-18	S-II LOX Pump Inlet Conditions	6-27
6-19	S-II Pneumatic Control Regulator Outlet Pressure	6-29
6-20	S-II Camera Ejection System Pressures	6-29
7-1	S-IVB Start Box and Run Requirements - First Burn	7-3
7-2	S-IVB Thrust Chamber Temperature - First Burn	7-4
7-3	S-IVB Start Tank Performance	7-5
7-4	S-IVB Buildup Transient - First Burn	7-5
7-5	S-IVB Steady-State Operation - First Burn	7-7
7-6	S-IVB Shutdown Transient Performance - First Burn	7-9
7-7	S-IVB Continuous Vent System Schematic	7-11
7-8	S-IVB CVS Performance - Coast Phase	7-12
7-9	S-IVB LH <sub>2</sub> Ullage Conditions - Coast Phase	7-14
7-10	S-IVB Start Box and Run Requirements - Second Burn	7-17
7-11	S-IVB Thrust Chamber Temperature - Second Burn	7-18
7-12	S-IVB LOX Pump Chillover Performance - Second Burn	7-18
7-13	S-IVB Buildup Transient - Second Burn	7-20
7-14	S-IVB Steady State Operation - Second Burn	7-21



# LIST OF ILLUSTRATIONS (CONTINUED)

Figure		Page
7-15	S-IVB Shutdown Transient - Second Burn	7-25
7-16	S-IVB Ignition and Cutoff Best Estimate Masses	7-26
7-17	S-IVB PU Valve Positions	7-28
7-18	S-IVB PU System Nonlinearities	7-29
7-19	S-IVB PU Indicated Mass - Second Burn	7-30
7-20	S-IVB LH <sub>2</sub> Ullage Pressure	7-32
7-21	S-IVB CVS Performance - Orbital Coast	7-34
7-22	S-IVB LH <sub>2</sub> Ullage Pressure - Second Burn	7-36
7-23	S-IVB Fuel Pump Inlet Conditions - First Burn	7-38
7-24	S-IVB Fuel Pump Inlet Conditions - Second Burn	7-39
7-25	S-IVB LOX Ullage Pressure - First Burn	7-40
7-26	S-IVB LOX Tank Ullage - Second Burn	7-42
7-27	S-IVB Cold Helium Sphere Condition - Coast Phase	7-44
7-28	S-IVB LOX Pump Inlet Conditions - First Burn	7-46
7-29	S-IVB LOX Pump Inlet Conditions - Second Burn	7-47
7-30	S-IVB Pneumatic Control Helium Bottle Pressure	7-48
7-31	S-IVB Pneumatic Control Performance	7-49
7-32	S-IVB Pneumatic Control Performance - Second Burn	7-50
7-33	S-IVB Pneumatic Control System Schematic	7-51
7-34	S-IVB APS Pressurization System Performance	7-53
7-35	S-IVB APS Propellant Consumption	7-56
7-36	S-IVB APS Propellant Conditions	7-57
8-1	S-IC Hydraulic System Performance	8-2
8-2	S-II Hydraulic System Performance	8-3
8-3	S-IVB Hydraulic System Performance - First Burn	8-5
8-4	S-IVB Hydraulic System Performance - Coast Phase	8-6
8-5	S-IVB Hydraulic System Performance - Second Burn	8-8

# LIST OF ILLUSTRATIONS (CONTINUED)

Figure		Page
9-1	Longitudinal Structural Dynamic Response Due to Thrust Buildup and Release	9-3
9-2	Longitudinal Loads at Maximum Bending Moment and Inboard Engine Cutoff	9-4
9-3	Longitudinal Structural Dynamic Response at the Instrument Unit and Command Module During S-IC/S-II Separation	9-5
9-4	Lateral (Pitch) Structural Dynamic Response During Thrust Buildup and release	9-6
9-5	Maximum Bending Moment at MAX Q ( $t = 78.7$ sec.)	9-7
9-6	First Longitudinal Modal Frequencies and Amplitudes During S-IC Powered Flight	9-8
9-7	First Longitudinal Mode Shapes During S-IC Powered Flight	9-9
9-8	Lateral Modal Frequencies and Amplitudes During S-IC Powered Flight	9-10
9-9	Pitch Mode Shapes During Powered Flight	9-12
9-10	S-IC Fin Vibration Response and Bending and Torsional Modal Frequencies	9-13
9-11	S-IC Stage Structure Vibrations Envelopes	9-14
9-12	S-IC Stage Engine Vibration Envelopes (Turbopump)	9-16
9-13	S-IC Stage Components Vibration Envelopes	9-17
9-14	S-II Stage Structure Vibration Envelopes	9-19
9-15	S-II Stage Engine Vibration Envelopes	9-21
9-16	S-II Stage Component Vibration Envelopes	9-22
9-17	S-IVB Stage Vibration Envelopes	9-24
9-18	Comparison of Similar Forward and Aft Skirt Vibration Measurements (AS-501 and IB Flights)	9-25
9-19	Instrument Unit Vibration Envelopes	9-27
9-20	Power Spectral Densities of Inertial Platform Input Vibration	9-28
10-1	Navigation, Guidance, and Control System Block Diagram	10-3

# LIST OF ILLUSTRATIONS (CONTINUED)

Figure		Page
10-2	Velocity from Glotrac Minus Velocity from Guidance	10-4
10-3	Accelerometer Pickup Outputs Vs Time (Liftoff)	10-14
10-4	Platform Sensed Vibration for S-IU-202 and S-IU-501	10-15
11-1	Control Components Block Diagram	11-2
11-2	Liftoff Vertical Motion	11-5
11-3	Motion At The Base of The S-IC Stage (Position 1)	11-7
11-4	Protective Hood - Holddown Post Clearance (Position 1)	11-8
11-5	Engine Bell Clearance	11-9
11-6	Liftoff Trajectories of Fin Tip "A"	11-10
11-7	S-IC Plume Angles and Center Engine Trajectories	11-12
11-8	Vehicle Attitude During S-IC Burn	11-13
11-9	Pitch Plane Dynamics During S-IC Burn	11-14
11-10	Yaw Plane Dynamics During S-IC Burn	11-15
11-11	Roll Plane Dynamics During S-IC Burn	11-16
11-12	Wind Velocity During S-IC Powered Flight	11-17
11-13	Free Stream Angle-of-Attack During S-IC Burn	11-18
11-14	Normal Acceleration During S-IC Powered Flight	11-19
11-15	Predominant Slosh Frequencies During S-IC Burn	11-20
11-16	S-IC Propellant Slosh Amplitudes During S-IC Burn	11-21
11-17	S-II Propellant Slosh Amplitudes During S-IC Burn	11-22
11-18	S-IC Engine Deflection Response to Propellant Slosh	11-23
11-19	Telemetered and Command Attitude Angles	11-27
11-20	Attitude Errors During S-II Powered Flight	11-30
11-21	S-II Stage Attitude Rates	11-31
11-22	Average S-II Engine Deflections	11-32
11-23	LH <sub>2</sub> and LOX Slosh Amplitudes During S-II Flight	11-33
11-24	Slosh Frequencies	11-34
11-25	J-2 Engine Pitch and Yaw Response to S-II Stage Sloshing	11-35

# LIST OF ILLUSTRATIONS (CONTINUED)

Figure		Page
11-26	Attitude Error and Auxiliary Propulsion System Engine Firings During S-IVB First Burn	11-37
11-27	Angular Velocities During First Burn	11-38
11-28	S-IVB Pitch and Yaw Actuator Positions During First Burn	11-39
11-29	Vehicle Attitude During S-IVB First Burn	11-40
11-30	Vehicle Attitude During S-IVB First Burn	11-41
11-31	Vehicle Attitude Following S-IVB First Burn Cutoff	11-43
11-32	Vehicle Attitude During Restart Orientation Maneuver	11-44
11-33	Attitude Error and Auxiliary Propulsion System Engine Firing During S-IVB Second Burn	11-46
11-34	Angular Velocities During Second Burn	11-47
11-35	S-IVB Pitch and Yaw Actuator Positions During Second Burn	11-48
11-36	Vehicle Attitude During S-IVB Second Burn	11-49
11-37	S-IVB Slosh Heights During Second Burn	11-50
11-38	Vehicle Attitude Prior to Spacecraft Separation	11-51
11-39	Vehicle Attitude Following Spacecraft Separation	11-52
12-1	S-IC Retro Motors Thrust	12-5
12-2	S-II Ullage Motor Thrust	12-7
12-3	S-IC/S-II Relative Velocity and Longitudinal Acceleration	12-8
12-4	S-IC/S-II Separation Distance	12-9
12-5	S-II Stage Attitude Errors During S-IC/S-II Separation	12-10
12-6	S-IC Pitch and Yaw Dynamic Following S-IC/S-II First Plane Separation	12-11
12-7	S-IC/S-II Second Plane Separation	12-12
12-8	Relative Velocity, Interstage Clearance Distance and Axial Separation Distance During Second Plane Separation	12-13
12-9	S-II Retro Motor Thrusts	12-14
12-10	S-IVB Ullage Motor Thrust	12-15
12-11	S-II/S-IVB Separation Distance	12-16
12-12	S-II/S-IVB Longitudinal Acceleration	12-17
12-13	Vehicle Angular Velocities During S-II/S-IVB Separation	12-18

# LIST OF ILLUSTRATIONS (CONTINUED)

Figure		Page
12-14	Lateral Acceleration	12-22
12-15	S-II/S-IVB Relative Velocity	12-23
12-16	S-IVB-IU Attitude Errors During Spacecraft Separation	12-25
12-17	S-IVB Angular Rate During Separation from Spacecraft	12-26
13-1	S-IC Stage Voltage and Current, Bus, 1D10	13-2
13-2	S-IC Stage Voltage and Current, Bus, 1D20	13-2
13-3	S-II Stage Main DC Bus Voltage and Current	13-4
13-4	S-II Stage Instrumentation Bus Voltage and Current	13-4
13-5	S-II Stage Recirculation DC Bus Voltage and Current	13-5
13-6	S-II Stage Ignition DC Voltage	13-5
13-7	S-IVB Stage FWD Battery No. 1 Voltage, Current, and Temperature	13-7
13-8	S-IVB Stage FWD Battery No. 2 Voltage, Current, and Temperature	13-8
13-9	S-IVB Stage AFT Battery No. 1 Voltage, Current, and Temperature	13-9
13-10	S-IVB Stage AFT Battery No. 2 Voltage, Current, and Temperature	13-10
13-11	IU Battery 6D10 Voltage, Current, and Temperature	13-12
13-12	IU Battery 6D20 Voltage, Current, and Temperature	13-12
13-13	IU Battery 6D30 Voltage, Current, and Temperature	13-13/13-14
13-14	IU Battery 6D40 Voltage, Current, and Temperature	13-13/13-14
15-1	EDS Functional Diagram	15-2
15-2	Q-Ball $\Delta P$ Versus Flight Times	15-5
16-1	S-IC Engine Fairing Compartment Pressure Differential and Aerodynamic Loads	16-2
16-2	S-IC Compartment Pressure Differentials	16-3
16-3	S-IC Compartment Pressure Loads	16-4
16-4	Forward Skirt Differential Pressures	16-5
16-5	Sidewall Insulation Differential Pressures	16-6
16-6	S-II/S-IVB Interstage Pressure Differential	16-8
16-7	S-II/S-IVB Interstage Pressure Loading	16-8
16-8	S-IC Base Heat Shield Pressure Environment	16-9

# LIST OF ILLUSTRATIONS (CONTINUED)

Figure		Page
16-9	S-II Base Pressures	16-10
16-10	Vehicle External Overall Sound Pressure Level at Liftoff	16-11
16-11	Vehicle Overall Fluctuating Pressure Level	16-12/16-13
16-12	Vehicle External Fluctuating Pressure Spectral Densities	16-14
16-13	S-IC Acoustic Environment, Acoustic Measurement Summary - Intertank, Internal	16-16
16-14	S-IVB Internal Sound Pressure Levels	16-17
17-1	S-IC Base Heat Shield Thermal Environment	17-3
17-2	F-1 Engine Thermal Environment	17-4
17-3	S-IC Fin Aft Face Thermal Environment	17-5
17-4	S-IC Interstage Thermal Environment During Separation	17-6
17-5	S-IC Base Heat Shield Structural Temperatures	17-7
17-6	S-II Heat Shield Heating Rates	17-10
17-7	S-II Base Region Thermal Environment	17-12
17-8	Thrust Cone Area Temperatures	17-13
17-9	S-IC Body Aerodynamic Heating	17-15
17-10	S-IC Fin and Fairing Temperature Histories	17-16
17-11	Fairing Heat Rate	17-20
17-12	Forward Skirt Skin and Insulation Temperatures	17-21
17-13	S-II Structural Temperatures	17-22
17-14	S-IVB Aeroheating Environment	17-24
17-15	S-IVB Protuberance Aeroheating Environment	17-25
17-16	Instrument Unit Skin Temperature	17-28
17-17	APS Fairing Orbital Temperature	17-28
17-18	LH <sub>2</sub> Heating During Orbit and Tank Skin Temperatures	17-29
17-19	Instrument Unit Inner Skin Orbital Temperature	17-30
18-1	Methanol/Water Bulk Temperature $\frac{C11 + 15}{2}$	18-3
18-2	Sublimator Inlet and Exit Temperatures	18-4

# LIST OF ILLUSTRATIONS (CONTINUED)

Figure		Page
18-3	Sublimator Cooling Rate	18-5
18-4	Modulating Flow Control Valve Performance	18-5
18-5	Selected Component Temperatures	18-6
18-6	GN <sub>2</sub> Supply Pressure and Temperatures	18-7
18-7	Platform Internal Pressure	18-8
18-8	Heat Exchanger GN <sub>2</sub> and Methanol/Water Temperatures	18-8
19-1	VHF Telemetry Coverage, Launch Phase 100 to 200 Seconds	19-23
19-2	VHF Telemetry Coverage Summary	19-24
19-3	ODOP Coverage Summary	19-26
19-4	Azusa/Glotrac Coverage Summary	19-27
19-5	C-Band Radar Coverage Summary	19-29
19-6	Merritt Island CCS Down Link Carrier Signal Strength, AS-501	19-30
19-7	Bermuda CCS Down Link Carrier Signal Strength, AS-501	19-30
19-8	Ascension CCS Down Link Carrier Signal Strength, AS-501	19-31
19-9	Carnarvon CCS Down Link Carrier Signal Strength, AS-501	19-31
19-10	Command and Communications (CCS) Coverage Summary	19-32
20-1	Vehicle Axial Force Characteristics	20-2
20-2	Base Pressure Increment During S-II Boost	20-3
20-3	S-IC Fin Pressure Differential	20-5
21-1	Vehicle Mass, Center of Gravity, and Mass Moment of Inertia During S-IC Stage Powered Flight	21-3
21-2	Total Vehicle Mass, Center of Gravity, and Mass Moment of Inertia During S-II Stage Powered Flight	21-4
21-3	Vehicle Mass, Center of Gravity, and Mass Moment of Inertia During S-IVB Stage Powered Flight	21-5

# LIST OF ILLUSTRATIONS (CONTINUED)

Figure		Page
A-1	AS-501 Scalar Launch Wind	A-3
A-2	AS-501 Launch Time Wind Direction	A-4
A-3	AS-501 Launch Time Pitch Wind Component ( $W_x$ )	A-7
A-4	AS-501 Launch Time Yaw Wind Component ( $W_z$ )	A-8
A-5	AS-501 Launch Time Pitch ( $S_x$ ) and Yaw ( $S_z$ ) Component Wind Shears	A-11
A-6	Relative Deviation of AS-501 Temperature and Density from PAFB (63) Reference Atmosphere	A-12
A-7	Relative Deviation of Pressure and Absolute Deviation of the Index of Refraction from the PAFB (63) Reference Atmosphere AS-501	A-13
B-1	Saturn V Apollo Flight Configuration	B-2



## LIST OF TABLES

Table		Page
2-1	Time Base Summary	2-2
2-2	Events Time Summary	2-3
2-3	Sequence of Events	2-6
2-4	Ground Commanded Switch Selector Events Beginning at 15:07:22 UT	2-15
3-1	AS-501 Milestones	3-2
3-2	Countdown Events	3-5
3-3	S-IC Stage Propellant Mass at Ignition Command	3-10
3-4	S-II Stage Propellant Mass at S-IC Ignition Command	3-11
3-5	S-IVB Stage Propellant Mass at S-IC Ignition Command	3-13
3-6	Effluent Gas Concentrations	3-14
4-1	Summary of AS-501 Orbital C-Band Tracking Stations	4-2
4-2	Comparisons of Cutoff Events	4-3
4-3	Comparisons of Separation Events	4-4
4-4	Velocity Gains Sensed by Guidance System after ECO Signal	4-9
4-5	Comparison of Significant Trajectory Events	4-12
4-6	Stage Impact Location	4-13
4-7	Parking Orbit Radar Stations	4-14
4-8	Parking Orbit Insertion Conditions	4-15
4-9	Waiting Orbit Injection Conditions	4-21
5-1	S-IC Engine Performance Deviations	5-6
5-2	Comparison of S-IC Stage Flight Reconstruction Data with Trajectory Simulation Results	5-7
5-3	Velocity and Time Deviation Analysis at OECO (Simulation versus Predicted)	5-8
5-4	S-IC Propellant Consumption	5-9
5-5	S-IC Residuals at Outboard Engine Cutoff Signal	5-10
6-1	S-II Engine Performance Deviations	6-13
6-2	S-II Flight Reconstruction Comparison with Simulation Trajectory Match Results	6-14

# LIST OF TABLES (CONTINUED)

Table		Page
6-3	S-II Propellant Consumption	6-19
6-4	S-II Helium Mass	6-26
6-5	S-II Camera Ejection System Helium Mass Usage	6-28
7-1	S-IVB Steady State Performance - First Burn	7-6
7-2	Comparison of S-IVB Stage Flight Reconstruction Data - First Burn	7-8
7-3	S-IVB Cutoff Impulse - First Burn	7-9
7-4	S-IVB Steady State Performance - Second Burn	7-20
7-5	Comparison of S-IVB Stage Reconstruction Data - Second Burn	7-23
7-6	S-IVB Cutoff Impulse - Second Burn	7-25
7-7	S-IVB Stage Propellant Mass History	7-27
7-8	S-IVB Helium Bottle Mass	7-52
7-9	S-IVB APS Propellant Consumption	7-55
8-1	S-IVB Hydraulic System Pressures	8-4
9-1	S-IC Stage Vibration Summary	9-15
9-2	S-II Stage Vibration Summary	9-20
9-3	S-IVB Vibration Summary	9-23
10-1	Guidance Inertial Velocity Comparisons	10-6
10-2	Guidance Comparisons (Navigation System)	10-7
10-3	Parameter Comparisons	10-8
10-4	Comparison of Velocity Changes Time Base 6 to Orbital Injection	10-10
10-5	Injection Comparisons (Second S-IVB Cutoff plus 10 Seconds)	10-11
11-1	SA-501 Liftoff Misalignment	11-4
11-2	Summary of Liftoff Clearances	11-11
11-3	Maximum Control Parameters During S-IC Flight	11-26

# LIST OF TABLES (CONTINUED)

Table		Page
11-4	S-IC Dynamic End Conditions	11-26
11-5	Maximum Control Parameters During S-II Stage Powered Flight	11-29
11-6	Maximum Values of Critical Flight Control Parameters - First Burn	11-42
11-7	Maximum Values of Critical Flight Control Parameters - Second Burn	11-51
11-8	APS Impulse Requirements	11-55
11-9	Vehicle Angular Rates Developed and Angles Commanded at Significant Events	11-56
12-1	Commanded Separation Event Times	12-2
12-2	S-IC Retro Motors System Performance	12-3
12-3	S-II Ullage Motor Performance	12-6
12-4	S-II Retro Motor Data	12-15
12-5	S-IVB Ullage Motor Performance	12-15
13-1	S-II Battery Consumption	13-3
13-2	S-IVB Battery Consumption	13-6
14-1	CCS Command History, AS-501	14-3
15-1	Performance Summary of Thrust OK Pressure Switches	15-4
15-2	Discrete EDS Events	15-6
15-3	Switch Selector EDS Events	15-7
19-1	Vehicle Measurements Summary	19-2
19-2	Measurements Waived Prior to Launch	19-3
19-3	Measurement Malfunctions During Flight	19-5
19-4	Measurements with Insufficient Range	19-10
19-5	AS-501 Launch Vehicle Telemetry Links	19-14
19-6	Tape Recorders Summary	19-18
19-7	AS-501 Onboard Tracking Systems	19-22

# LIST OF TABLES (CONTINUED)

Table		Page
21-1	Total Vehicle Mass - S-IC Burn Phase (Kilograms)	21-6
21-2	Total Vehicle Mass - S-IC Burn Phase (Pounds Mass)	21-7
21-3	Total Vehicle Mass - S-II Burn Phase (Kilograms)	21-8
21-4	Total Vehicle Mass - S-II Burn Phase (Pounds Mass)	21-9
21-5	Total Vehicle Mass - S-IVB First Burn Phase (Kilograms)	21-10
21-6	Total Vehicle Mass - S-IVB First Burn Phase (Pounds Mass)	21-11
21-7	Total Vehicle Mass - S-IVB Second Burn Phase (Kilograms)	21-12
21-8	Total Vehicle Mass - S-IVB Second Burn Phase (Pounds Mass)	21-13
21-9	Flight Sequence Mass Summary	21-14
21-10	Mass Characteristics Comparison	21-17
22-1	Summary of Malfunctions and Deviations	22-2
A-1	Surface Observations at AS-501 Launch Time	A-2
A-2	Solar Radiation Data (0.35 to 4.0 microns) at AS-501 Launch	A-2
A-3	Systems Used to Measure Upper Air Wind Data, AS-501	A-5
A-4	Maximum Wind Speed in High Dynamic Pressure Region	A-6
A-5	Extreme Wind Shear in High Dynamic Pressure Region	A-10
C-1	SA-501 Launch Vehicle Flight Objectives	C-1
D-1	Parking Orbit Insertion Parameters Comparison	D-2
D-2	Waiting Orbit Injection Parameters Comparison	D-3

## ACKNOWLEDGEMENTS

This report is published by the Saturn Flight Evaluation Working Group--composed of representatives of Marshall Space Flight Center, John F. Kennedy Space Center, and MSFC'S prime contractors--and in cooperation with the Manned Spacecraft Center. Significant contributions to the evaluation have been made by:

George C. Marshall Space Flight Center

Research and Development Operations

Aero-Astroynamics Laboratory

Astrionics Laboratory

Computation Laboratory

Propulsion and Vehicle Engineering Laboratory

Industrial Operations

John F. Kennedy Space Center

Manned Spacecraft Center

The Boeing Company

Douglas Aircraft Company

International Business Machines Corporation

North American Rockwell/Rocketdyne Division

North American Rockwell/Space Division

# ABBREVIATIONS AND SYMBOLS

AGC	Automatic gain control	GOX	Gaseous oxygen
APS	Auxiliary propulsion system	gpm	Gallon per minute
ATI	Automated telemetry inspection	GRR	Guidance reference release
CCS	Command and communications system	GSE	Ground Support Equipment
CDS	Command destruct system	GSFC	Goddard Space Flight Center
CIF	Central instrumentation facility	HFCV	Helium fuel control valve
DDAS	Digital data acquisition system	HOSC	Huntsville Operations Support Center
EBW	Explosive bridge wire	IBM	International Business Machines
ECO	Engine cutoff	IECO	Inboard engine cutoff
ECP	Engineering change proposal	IGM	Iterative guidance mode
EDS	Emergency detection system	IP&C	Instrumentation program and components
EMR	Engine mixture ratio	KSC	Kennedy Space Center
ESC	Engine start command	Lb <sub>f</sub>	Pounds force
ESC	Engineering sequential cameras	Lb <sub>m</sub>	Pounds mass
FEP	Flight evaluation panel	LEM	Lunar excursion module
FEWG	Flight evaluation working group	LES	Launch escape system
GFCV	GOX flow control valve	LET	Launch escape tower
GMT	Greenwich mean time	LIEF	Launch information exchange facility
		LOC	Launch operations center

LOR	Lunar orbit rendezvous	PMR	Programmed mixture ratio
LVDA	Launch vehicle digital adapter	PRESS	Pressurization
LVDC	Launch vehicle digital computer	PRN	Pseudo random noise
MECO	Main engine cutoff	PSD	Power spectral density
MFV	Main fuel valve	PSRD	Program support requirements document
MILA	Merritt Island Launch Area	PT	Point
MOV	Main oxidizer valve	PTCS	Propellant tanking computer system
MR	Mixture ratio	PU	Propellant utilization
MSC	Manned Spacecraft Center	RCS	Reaction Control System
MSF	Manned Space Flight	RECIRC	Recirculation
MSFC	Marshall Space Flight Center	RET	Reynolds number
MSFN	Manned space flight network	RMR	Reference mixture ratio
MTF	Mississippi Test Facility	RMS	Root mean square
n mi	Nautical miles	RSC	Range safety command
NPSH	Net positive suction head	RT	Range time
NPSP	Net positive suction pressure	SAFER	Saturn flight evaluation retrieval
ODOP	Offset frequency doppler	STCSV	Start tank control solenoid valve
OECD	Outboard engine cutoff	STDV	Start tank discharge valve
OMPT	Observed mass point trajectory	TVC	Thrust vector control
OSRO	Operations support requirements office	USB	Unified S-Band
PDRD	Processed data requirements document		

SYMBOL	DEFINITION	UNIT
CIP/BOP	Ratio of gradients of angular acceleration, pitch	Dimensionless
Ciy/BOY	Ratio of gradients of angular acceleration, yaw	Dimensionless
CP	Center of aerodynamic pressure	Meters
$C_p$	Pressure coefficient = $\frac{P_c - P_\infty}{q}$	Dimensionless
$C_{p_L}$	Pressure loading = $\frac{P_c - P_L}{q}$	Dimensionless
D	Diameter of S-IC stage	Meters
$D\dot{X}_0$	X- Accelerometer timing error	M/S
$DY_0$	Y-Accelerometer timing error	M/S
$D\dot{Z}_0$	Z-Accelerometer timing error	M/S
FCD	Chilldown thrust - S-IVB stage only during start transients	N
FCL	Local chamber thrust	N
FCSL	Sea level chamber thrust	N
FEL	Local engine thrust	N
FESL	Sea level engine thrust	N
FEV	Vacuum engine thrust	N
FHH	Helium heater thrust	N
FTEL	Local turbine exhaust thrust	N
FTESL	Sea level turbine exhaust thrust	N
FVL	Local longitudinal vehicle thrust	N
FVSL	Sea level vehicle thrust	N
FVV	Vacuum vehicle thrust	N
$F_s$	Standard engine thrust derived from static engine test firings	N
$I_p$	Pitch mass moment of inertia	kg-m <sup>2</sup>



SYMBOL	DEFINITION	UNIT
$I_R$	Roll mass moment of inertia	$\text{kg-m}^2$
$I_y$	Yaw mass moment of inertia	$\text{kg-m}^2$
$L_p$	Radial CG offset, pitch plane	Meters
$L_y$	Radial CG offset, yaw plane	Meters
$I_{SP}^{CL}$	Local chamber specific impulse	sec
$I_{SP}^{CSL}$	Sea level chamber specific impulse	sec
$I_{SP}^{EL}$	Local engine specific impulse	sec
$I_{SP}^{ESL}$	Sea level engine specific impulse	sec
$I_{SP}^{EV}$	Vacuum engine specific impulse	sec
$I_{SP}^{VL}$	Local longitudinal vehicle specific impulse	sec
$I_{SP}^{VSL}$	Sea level vehicle specific impulse	sec
$I_{SP}^{VV}$	Vacuum vehicle specific impulse	sec
$LH_2$	Liquid hydrogen	Dimensionless
$LOX$	Liquid oxygen	Dimensionless
$M$	Total vehicle mass	kg
$MA$	Mach number	Dimensionless
$M_{xz}$	Accelerometer misalignment (non-orthogonality) of the altitude (X) accelerometer rotated about the range (Z) axis. A positive misalignment: when the angle between the altitude (X) and cross range (Y) accelerometers is less than 90 degrees.	deg
$M_{xy}$	Accelerometer misalignment (non-orthogonality) of the altitude (X) accelerometer rotated about the cross range (Y) axis. A positive misalignment: when the angle between the altitude (X) and range (Z) accelerometers is greater than 90 degrees.	deg

SYMBOLS	DEFINITION	UNIT
$M_{zx}$	Accelerometer misalignment (non-orthogonality) of the range (Z) accelerometer rotated about the altitude (X) axis. A positive misalignment: when the angle between the range (Z) and cross range (Y) accelerometers is greater than 90 degrees.	deg
$M_{zy}$	Accelerometer misalignment (non-orthogonality) of the range (Z) accelerometer rotated about the cross range (Y) axis. A positive misalignment: when the angle between the range (Z) and altitude (X) accelerometers is less than 90 degrees.	deg
$M_{yz}$	Accelerometer misalignment (non-orthogonality) of the cross range (Y) accelerometer about the range (Z) axis. A positive misalignment: when the angle between the cross range (Y) and altitude (X) accelerometers is greater than 90 degrees.	deg
$M_{yx}$	Accelerometer misalignment (non-orthogonality) of the cross range (Y) accelerometer about the altitude (X) axis. A positive misalignment: when the angle between the cross range (Y) and range (Z) accelerometers is less than 90 degrees.	deg
P	Static pressure	$N/cm^2$
PA	Ambient pressure	$N/cm^2$
PASL	Sea level atmospheric pressure	$N/cm^2$
PC	Thrust chamber pressure	$N/cm^2$
$P_c$	Compartment pressure	$N/cm^2$
$P_L$	Local static exterior pressure	$N/cm^2$
$P_\infty$	Free stream ambient pressure	$N/cm^2$
Q,q	Dynamic pressure	$N/cm^2$
$\dot{q}$	Total heating rate	Watts/cm <sup>2</sup>
$\dot{q}_c$	Convective heating rate	Watts/cm <sup>2</sup>
$\dot{q}_R$	Radiation heating rate	Watts/cm <sup>2</sup>
R	Radius	Meters

SYMBOLS	DEFINITION	UNIT
Re	Reynolds number based on reference body diameter	Dimensionless
$R_o$	Radial distance from missile longitudinal axis to the outboard engine gimbal point	Meters
SMCX	Steering misalignment correction angle in yaw	deg
SMCZ	Steering misalignment correction angle in pitch	deg
STA	Station	Meters
STR	Stringer	Dimensionless
$S_z$	Scale factor error in range (Z) accelerometer	g/g
$S_x$	Scale factor error in altitude (X) accelerometer	g/g
$S_y$	Scale factor error in cross range (Y) accelerometer	g/g
T	Temperature	°K
Tas	Computer time from GRR	sec
TBN	Time base N (N = 1,2,3...,N)	sec
$V_s$	Magnitude of the space-fixed velocity vector	m/s
$\dot{W}$	Flowrate	kg/s
$\dot{W}_A$	Auxiliary flowrate	kg/s
$\dot{W}_{CT}$	Chamber flowrate, total	kg/s
$\dot{W}_{ET}$	Engine flowrate, total	kg/s
$\dot{W}_{FGG}$	Gas generator fuel flowrate	kg/s
$\dot{W}_{HC}$	Chamber hydrogen flowrate	kg/s
$\dot{W}_{HCD}$	S-IVB chilldown LOX flowrate	kg/s
$\dot{W}_{HEH}$	Helium heat exchanger flowrate	kg/s
$\dot{W}_{HHH}$	Helium heat exchanger hydrogen flowrate	kg/s
$\dot{W}_{LC}$	Chamber LOX flowrate	kg/s

SYMBOL	DEFINITION	UNIT
$\dot{W}_{LCD}$	S-IVB chilldown LOX flowrate	kg/s
$\dot{W}_{LGG}$	Gas generator LOX flowrate	kg/s
$\dot{W}_{LHH}$	Heat exchanger LOX flowrate	kg/s
$\dot{W}_S$	Stage flowrate (propellant only)	kg/s
$\dot{W}_{VL}$	Vehicle weight loss rate (ice, lube, oil, propellant, etc.)	kg/s
$\dot{x}_x, \dot{x}_y, \dot{x}_z$	Command rates	deg/sec
$x_x, x_y, x_z$	Computed guidance command	deg
$\dot{x}_m, \dot{y}_m, \dot{z}_m$	Scaled summation of the X, Y, Z accelerometer pulses	m/s
$x_e, y_e, z_e$	Components of vehicle displacement along earth-fixed Cartesian X, Y, and Z axes respectively	m
$\dot{x}_e, \dot{y}_e, \dot{z}_e$	Vehicle velocity components along earth-fixed Cartesian X, Y, and Z axes respectively	m/s <sup>2</sup>
$\ddot{x}_e, \ddot{y}_e, \ddot{z}_e$	Vehicle acceleration components along earth-fixed Cartesian X, Y, and Z axes respectively	m/s <sup>2</sup>
$V_e$	Vehicle total earth-fixed velocity vector (earth vel)	m/s
$x_s, y_s, z_s$	Components of vehicle displacement along space-fixed X, Y, and Z axes respectively with origin at the center of the earth and space-fixed at GRR.	m
$\dot{x}_s, \dot{y}_s, \dot{z}_s$	Vehicle velocity components along space-fixed X, Y, and Z axes respectively	m/s
$\ddot{x}_s, \ddot{y}_s, \ddot{z}_s$	Vehicle acceleration components along space-fixed X, Y, and Z axes respectively	m/s <sup>2</sup>

SYMBOL	DEFINITION	UNIT
$V_s$	Vehicle total space-fixed velocity magnitude (space vel)	m/s
$h$	Altitude of the vehicle (above the reference ellipsoid)	km
$r$	Distance of vehicle from the earth center	m
$R$	Range along surface of the earth	km
$\psi$	Geocentric latitude	deg
$\lambda$	Longitude	deg
$\epsilon$	The angle between the earth-fixed vehicle velocity vector and the local horizontal (vel elev)	deg
$\alpha$	Total angle of attack	deg
$a$	Semi-major axis	km
$e$	Eccentricity	Dimensionless
$i$	Inclination	deg
$\Omega$	Right ascension of ascending node	deg
$v$	True anomaly	deg
$\theta$	Mean sidereal time	deg
$\alpha_s$	Azimuth of space-fixed velocity	deg
$\epsilon_s$	Elevation of space-fixed velocity	deg
$\ddot{X}_{sg}, \ddot{Y}_{sg}, \ddot{Z}_{sg}$	Components of gravitational acceleration in the $X_s, Y_s, Z_s$ system.	m/s
$\dot{X}_{sg}, \dot{Y}_{sg}, \dot{Z}_{sg}$	Components of gravitational velocity in the $X_s, Y_s, Z_s$ system	m/s
$\alpha_p$	Angle-of-attack, pitch plane	deg
$\alpha_y$	Angle-of-attack, yaw plane	deg
$\alpha_{qp,y}$	Pitch, yaw, Q-ball angle of attack	deg
$\alpha_{ox}$	X-accelerometer g-sensitive error (due to acceleration along output axis)	deg/hr/g

SYMBOL	DEFINITION	UNIT
$\alpha_{oy}$	Y-accelerometer g-sensitive error (due to acceleration along output axis)	deg/hr/g
$\alpha_{oz}$	Z-accelerometer g-sensitive error (due to acceleration along output axis)	deg/hr/g
$\alpha_{sx}$	X-accelerometer g-sensitive error (due to acceleration along spin reference axis)	deg/hr/g
$\alpha_{sy}$	Y-accelerometer g-sensitive error (due to acceleration along spin reference axis)	deg/hr/g
$\alpha_{sz}$	Z-accelerometer g-sensitive error (due to acceleration along spin reference axis)	deg/hr/g
$\beta_{1,2,3,4p}$	Telemetered angle of engine deflection, pitch	deg
$\beta_{1,2,3,4y}$	Telemetered angle of engine deflection, yaw	deg
$\beta_p$	Average angle of engine deflection, pitch	deg
$\beta_y$	Average angle of engine deflection, yaw	deg
$\gamma_o$	Cant angle of outboard engine	deg
$\gamma_i$	Cant angle of inboard engine	deg
$\ddot{\gamma}_p$	Pitch control acceleration	m/s <sup>2</sup>
$\ddot{\gamma}_y$	Yaw control acceleration	m/s <sup>2</sup>
$\delta_z$	Initial platform (yaw) leveling error about the range (Z) axis. Positive when cross range (Y) accelerometer is rotated to give a negative output of the cross range (Y) accelerometer	deg
$\delta_x$	Initial azimuth alignment (roll) error. Positive when the azimuth is less than the prescribed azimuth	deg
$\delta_y$	Initial platform (pitch) leveling error about the cross range (Y) axis. Positive when the range (Z) accelerometer is rotated to give a positive output of the range (Z) accelerometer	deg

SYMBOL	DEFINITION	UNIT
$\dot{\delta}_z$	Constant platform drift rate about the range (Z) axis. Signs are consistent with leveling error, $\delta_z$ .	deg/hr
$\dot{\delta}_x$	Constant platform drift rate about the altitude (X) axis. Signs are consistent with azimuth alignment error, $\delta_x$ .	deg/hr
$\dot{\delta}_y$	Constant platform drift rate about the cross range (Y) axis. Signs are consistent with leveling error, $\delta_y$ .	deg/hr
$\dot{\delta}_{z/\ddot{z}}$	Platform g-dependent drift about the range (Z) axis proportional to the range (Z) acceleration.	deg/hr/g
$\dot{\delta}_{z/\ddot{x}}$	Platform g-dependent drift about the range (Z) axis proportional to the altitude (X) acceleration.	deg/hr/g
$\dot{\delta}_{x/\ddot{z}}$	Platform g-dependent drift about the altitude (X) axis proportional to the range (Z) acceleration.	deg/hr/g
$\dot{\delta}_{x/\ddot{x}}$	Platform g-dependent drift about the altitude (X) axis proportional to the altitude (X) acceleration.	deg/hr/g
$\dot{\delta}_{y/\ddot{z}}$	Platform g-dependent drift about the cross range (Y) axis proportional to the range (Z) acceleration.	deg/hr/g
$\dot{\delta}_{y/\ddot{x}}$	Platform g-dependent drift about the cross range (Y) axis proportional to the altitude (X) acceleration.	deg/hr/g
$\theta_{X, Y, Z}$	Platform gimbal angles	deg
$\dot{\phi}_{P, Y, R}$	Body-fixed rate gyro control signals	deg/s
$\psi_{P, Y, R}$	Pitch, yaw, roll vehicle attitude error signals (ladder output)	deg

## FLIGHT TEST SUMMARY

Saturn V Space Vehicle AS-501 (Apollo 4 Mission), first of the Saturn V series vehicles, was launched at 07:00:01 EST on November 9, 1967, and placed Apollo Spacecraft 017 in orbit. The flight was the first in a series of R&D test flights in which the primary objective is to qualify the Saturn V launch vehicles, the Apollo spacecraft, and the ground systems for the Lunar Landing Mission. Three highly significant milestones were successfully achieved on this mission; the first flight of the S-IC stage, the first flight of the S-II stage, and the re-ignition in orbit of the S-IVB stage. All mission objectives as listed in Appendix C were achieved.

AS-501 was launched from Complex 39, Pad A at Cape Kennedy, Florida, on schedule. Two unscheduled holds occurred because of: 1) minor difficulties causing launch operations to fall behind the clock, and 2) a range safety command receiver check difficulty. The 3 hours and 59 minutes lost by these unscheduled holds were absorbed by the 7.5 hours of scheduled hold time. No recycling of the count was required because of these holds.

The vehicle was launched on an azimuth of 90 degrees east of north and after 11.06 seconds of vertical flight, (which included a small yaw maneuver for tower clearance) AS-501 began to roll into a flight azimuth of 72 degrees east of north. The actual trajectory of AS-501 was close to nominal. The space-fixed velocity at S-IC OECO was 19.80 m/s (64.96 ft/s) lower than nominal. At S-II cutoff it was 38.61 m/s (126.67 ft/s) lower than nominal and 1.24 m/s (4.06 ft/s) lower than nominal at S-IVB first burn cutoff. At S-IVB first burn cutoff the altitude was 1.17 kilometers (0.63 n mi) higher than nominal and the surface range was 44.17 kilometers (23.85 n mi) greater than nominal. The cross range velocity deviated 1.52 m/s (4.99 ft/s) to the right of nominal at S-IVB first burn cutoff. At waiting orbit injection the actual values of the targeting parameters were very close to nominal. The eccentricity was 0.0028 less than nominal, the inclination was 0.011 degrees less than nominal, the node was 0.004 degrees greater than nominal and C3 was 187,669 m<sup>2</sup>/s<sup>2</sup> (2,020,050 ft<sup>2</sup>/s<sup>2</sup>) less than nominal. At waiting orbit injection the total space-fixed velocity was 11.4 m/s (37.4 ft/s) greater than nominal and the altitude was 24.25 kilometers (13.09 n mi) less than nominal.

All S-IC stage propulsion systems performed satisfactorily throughout flight. The stage thrust and propellant flowrates were 0.41 percent and 0.80 percent higher, and the specific impulse was 0.39 percent lower than predicted,



based upon flight simulation results. Stage reconstruction indicated that the thrust was 0.6 percent higher and the specific impulse and flowrate were 0.19 and 0.233 percent lower than predicted respectively. Inboard engine cutoff occurred approximately as predicted, and outboard engine cutoff occurred 1.13 seconds earlier than predicted. Outboard engine cutoff was initiated by LOX depletion.

The S-II propulsion system operation was satisfactory. On the basis of flight simulation, the overall average S-II stage thrust and mass loss rate were 1.17 percent and 1.30 percent lower than predicted respectively. The specific impulse was higher by 0.14 percent during high mixture ratio operation. At the 60 second time slice the stage reconstruction showed the thrust and mass loss rate to be 1.4 and 1.7 percent lower than predicted, and the specific impulse to be 0.23 percent higher than predicted. The propellant management system performed satisfactorily. Because of lower than predicted propellant flowrates and mixture ratios during the high EMR portion of S-II operation, PU step time was later than predicted by 15 seconds but well within the allowable of  $\pm 50$  seconds. S-II burn time was approximately five seconds longer than predicted due to low propellant flowrates and a lower than predicted reference mixture ratio (RMR) setting. All supporting subsystems performed satisfactorily. However, some out-of-band behavior did occur as discussed in Section 6.

The S-IVB Stage propulsion system performance was satisfactory throughout S-IVB powered flight. The J-2 engine was successfully restarted in space following the two revolution coast period. During first burn, based on flight simulation results, the stage thrust and mass loss rate was 0.70 percent, and 0.72 percent lower than predicted respectively, and the specific impulse was 0.02 percent higher than predicted. During second burn, the flight average thrust and mass loss rate were 2.36 percent and 2.61 percent higher than predicted respectively, while the flight average specific impulse was 0.24 percent lower than predicted. Based on stage reconstruction results the first burn thrust and specific impulse were 0.91 and 0.08 percent lower than predicted and the second burn thrust and specific impulse were 1.68 percent higher and 0.42 percent lower than predicted respectively. The first burn time was 6.2 seconds longer than predicted. This longer burn time can be attributed to lower thrust, mass flow rate, and separation velocity, combined with a higher initial mass flow rate, and separation velocity, combined with a higher initial mass and a higher separation altitude. A 15.18 seconds shorter second burn time was primarily due to high EMR operation for the first 55 seconds of mainstage. All supporting systems performed their functions satisfactorily. However, the stage pneumatic control system leaked causing the control sphere pressure to drop below regulator setting after the end of the mission. Corrective action is under study. Out-of-band behavior on other systems is discussed in Section 7.

The Auxiliary Propulsion System (APS) performed satisfactorily with less than 75 percent consumption of propellants. However, a marked deterioration in thrust for APS engine IIV and III may have been experienced after spacecraft separation.

The hydraulic systems on all stages performed within predicted limits, and the entire system operated satisfactorily throughout the flight.

The structural loads and dynamic environment experienced by the AS-501 launch vehicle were well within the vehicle structural capability. Vehicle loads, due to the combined rigid body and dynamic longitudinal load and bending moment, were well below limit design values. Tank pressures, compartment pressures, and structural temperatures also remained within limit design values. Vehicle dynamic characteristics followed the trends established by preflight analyses. As predicted prior to launch, small thrust oscillations of magnitudes less than 0.1 percent of total thrust occurred in the 4.5 to 5.5 hertz frequency range and excited the first longitudinal mode to small amplitudes. However, no longitudinal instability phenomenon occurred. Fin bending and torsional modes compared well with analytical predictions. No fin flutter occurred. S-IC, S-II, and S-IVB stage vibrations were as expected except for the inertial platform input vibrations which exceeded the random test specification at liftoff. No adverse effects were noted in platform performance due to vibration.

The navigation and guidance system of AS-501 performed satisfactorily throughout boost phase of flight. The accumulation of velocity pulses near liftoff as observed in the Z (cross range) axis during the AS-202 flight, did not occur in the X, Y, or Z axes during the AS-501 flight. Gimbal angle reasonableness test failure, as observed in the X gimbal angle on the AS-202 flight, did not occur on the AS-501 flight. Initial pitch, yaw, and roll maneuvers were performed as expected. Shortly after S-II stage ignition, a +1.3 degree ladder output was generated by the Launch Vehicle Digital Computer/Launch Vehicle Digital Adapter (LVDC/LVDA) due to a positive clockwise torque which developed a positive roll in the vehicle. The positive roll rate was nulled out by the ladder command and a +1.3 degree roll offset remained throughout S-II stage burn. At S-II stage engine cutoff, the positive clockwise roll torque was removed. Cause of the roll offset may be attributed to a combination of engine misalignment and center of gravity offset.

Steering misalignment corrections were developed by the LVDC shortly after Iterative Guidance Mode (IGM) initiation. From 11,595 seconds to 11,620 seconds, commanded (CHI) rates of a maximum 1.0 degree per second in positive pitch and negative yaw were commanded in response to fifth phase IGM calculations. During this time, a positive roll torque on the vehicle was observed. The roll reached a maximum value of 2.2 degrees at 11,617 seconds range time and decreased to zero at 11,638.4 seconds when CHI rates reached zero. All programmed maneuvers were completed satisfactorily during AS-501 orbital guidance.

The control system performed throughout flight as expected. Liftoff transients and drift were well within expected tolerances. Vehicle lift-off acceleration, however, was substantially less than predicted possibly due to higher than expected soft release rod forces. During S-IC powered flight the maximum values of attitude errors were 1.3 degrees in pitch, and 1.0 degree in yaw and roll. Angles of attack in the Max Q region were 1.48 degrees pitch and 1.29 degrees yaw. The control system performance during S-II Stage burn was as expected. The S-II control system responded to the guidance commands to counteract the +1.3 degree roll offset. The S-IVB stage engine control system performed satisfactorily during first and second burns. Auxiliary Propulsion System (APS) attitude control engine operation was nominal throughout burn and coast periods. S-IVB control system activity during the initial portion of second burn was greater than expected due to approximately 55 seconds of J-2 engine operation at the high EMR thrust levels. Vehicle attitudes and rates remained within design tolerances during S-IC/S-II, S-II/S-IVB, and S-IVB/SC separations.

All separation systems performed as required. S-IC/S-II separation and associated sequencing was accomplished as planned with the S-IC retro motors performing satisfactorily. Subsequent S-IC dynamics provided adequate positive clearances between the stages following separation. Performance of the S-II separation system was satisfactory with no anomalies noted. The S-II ullage motors functioned as predicted within the required limits. Photographic coverage provided evidence that S-II second plane separation was satisfactory. The four retro motors mounted on the S-II stage performed satisfactorily in separating the S-II and S-IVB stages. S-IVB ullage motor performance was also satisfactory. Separation of the S-IVB stage from the S-II stage was accomplished as expected within the desired time period. S-IVB attitude control was normal during S-IVB spacecraft separation.

The performance of all launch vehicle stage electrical systems was satisfactory throughout the flight period. Battery voltages and currents were satisfactory and remained within predicted tolerances. All battery temperatures were indicated as falling within acceptable limits.

Data indicated that the redundant Secure Range Safety Command Systems (SRSCS) on the S-IC, S-II, and S-IVB stages were ready to perform their functions properly on command if flight conditions had required and that the safe-disconnect system responded properly to command. The performance of the command and communications system in the Instrument Unit (IU) was excellent.

The performance of the Emergency Detection System (EDS), which was flown in the "open-loop" configuration, was satisfactory. The automatic abort circuit was deactivated in the spacecraft. No abort limits were reached and no false indications were sensed by the system. The sequential events all occurred at the proper times.

The vehicle pressure and acoustic environment was in general agreement with predictions and well within the values to which the structure was designed.

The AS-501 vehicle thermal environment was generally less severe than that for which the vehicle was designed.

The effectiveness of the insulation on the S-IC forward skirt in reducing protuberance induced heating could not be determined due to large variations in the insulation thickness. The only suspected anomaly noted in the thermal protection system appears to be the loss of a small section of the S-IC base heat shield M-31 to the level of the open face honeycomb. However, since the base region environment was substantially below the design level, temperatures in this area did not exceed design limits.

All Environmental Control Systems performed satisfactorily. The S-IC forward and aft conditioning systems maintained compartment and canister temperatures within design limits. S-II forward and aft control systems maintained container temperatures within mid-range of design limits throughout prelaunch and boost. Hydrogen and oxygen concentrations were well below the allowable 3 percent maximum. The S-IVB aft interstage control system maintained an Auxiliary Propulsion System temperature within design limits. The Instrument Unit control subsystem held pressures, temperatures and flow rates within the required ranges except for the ST-124M internal ambient pressure which did not decay to the specified lower limit. This did not cause any platform system operation problem and was not considered a failure. Also the IU internal ambient temperature dropped below the redline limit prior to liftoff but a waiver was obtained and no adverse effects were noted. A redline change is being considered.

Of the 2687 measurements active at the start of the AS-501 automatic count-down sequence, 45 failed in flight, resulting in an overall measuring system reliability of 98.3 percent. The Airborne Telemetry System operated satisfactorily including preflight calibrations, inflight calibrations, and tape recorder operation. Performance of the RF systems including telemetry, tracking, and command systems was good.

## SECTION 1 INTRODUCTION

### 1.1 PURPOSE

This report provides the National Aeronautics and Space Administration (NASA) Headquarters, and other interested agencies, with the launch vehicle evaluation results of the AS-501 flight test. The basic objective of flight evaluation is to acquire, reduce, analyze, evaluate and report on flight test data to the extent required to assure future mission success and vehicle reliability. To accomplish this objective, actual flight malfunctions and deviations must be identified, their causes accurately determined, and complete information made available so that corrective action can be accomplished within the established flight schedule.

### 1.2 SCOPE

This report presents the results of the early engineering flight evaluation of the AS-501 launch vehicle. The contents are centered on the performance evaluation of the major launch vehicle systems, with special emphasis on malfunctions and deviations. Summaries of launch operations and spacecraft performance are included for completeness.

The official MSFC position at this time is represented by this report. It will not be followed by a similar report unless continued analysis or new information should prove the conclusions presented herein to be significantly incorrect. Final stage evaluation reports will, however, be published by the stage contractors. Reports covering major subjects and special subjects will be published as required.



## SECTION 2 EVENT TIMES

### 2.1 SUMMARY OF EVENTS

The Time Base range times and the signal for initiating each Time Base are presented in Table 2-1. The sequence and times of major events for AS-501 are listed in Table 2-2. Guidance Reference Release (GRR), which is Time Base Zero ( $T_0$ ), was initiated at 11:59:43.362 UT. Liftoff, the start of Time Base 1 ( $T_1$ ), was determined from the Launch Vehicle Digital Computer (LVDC) as having occurred 17.901 seconds after GRR, at 12:00:01.263 UT, thereby establishing Range Zero as 12:00:01 UT. All times referenced in this report, unless otherwise noted, are referenced to this time. First motion of the vehicle occurred at -0.48 seconds and liftoff at +0.263 seconds. The most significant deviations from predicted shown in the table are: S-II Engine Mixture Ratio (EMR) shift and second phase Iterative Guidance Mode (IGM); S-IVB Chi Tilde ( $\chi$ ) steering; S-IVB Engine Cutoff (ECO) velocity, first burn; start of Time Base 5 ( $T_5$ ); coast period ON; IGM termination and start Chi Tilde steering; start of Time Base 7 ( $T_7$ ); coast period ON; and start Launch Vehicle (LV) and spacecraft (SC) separation. Reasons for these time deviations are discussed in detail in Sections 6, 7, and 10.

### 2.2 SEQUENCE OF EVENTS

Table 2-3 lists the sequence of switch selector events. Range time is calculated as the elapsed time, in seconds, from Range Zero time. Seven switch selector functions were not verified during the boost phase because of telemetry dropout at S-IC/S-II stage separation. However, the functions did occur. Two switch selector functions were missed at the end of  $T_6$  due to early cutoff of S-IVB stage second burn. Switch selector events scheduled to occur 0.1 second apart immediately after the start of a time base occurred as much as 0.09 second late due to hardware design limitations. The remaining switch selector events have not been verified.

Table 2-4 lists inflight switch selector events activated by ground stations, beginning at 15:07:22 UT.

Table 2-1. Time Base Summary

TIME BASE	RANGE TIME SEC (HR:MIN:SEC)	SIGNAL START
T <sub>0</sub>	-17.638 (-00:00:17.638)	Guidance Reference Release
T <sub>1</sub>	0.263 (00:00:00.263)	IU Umbilical Disconnect
T <sub>2</sub>	135.469 (00:02:15.469)	LVDC Monitors IECO, S-IC
T <sub>3</sub>	150.769 (00:02:30.769)	OECO, S-IC
T <sub>4</sub>	519.759 (00:08:39.759)	ECO, S-II
T <sub>5</sub>	665.884 (00:11:05.884)	Velocity Cutoff, S-IVB
T <sub>6</sub>	11159.576 (03:05:59.576)	Restart Equation Solution, S-IVB
T <sub>7</sub>	11786.479 (03:16:26.479)	Velocity Cutoff, S-IVB



Table 2-2. Event Times Summary

EVENT	RANGE TIME		TIME FROM BASE	
	ACTUAL SEC (HR:MIN:SEC)	ACT-PRED SEC	ACTUAL SEC	PREDICTED SEC
1. First Motion	-0.48 -00:00:00.48			
2. Range Zero 12:00:01 UT	0.00 00:00:00			
3. Liftoff and Start of Time Base 1 ( $T_1$ )	0.263 00:00:00.263		$T_1$	0.000
4. Begin Yaw Maneuver	1.263 00:00:01.263	0.263	1.000	1.000
5. End Yaw Maneuver	10.16 00:00:10.16	0.09	9.90	9.81
6. Start Roll	11.06 00:00:11.06	0.000	10.80	10.80
7. Start Pitch	11.06 00:00:11.06	0.000	10.80	10.80
8. End Roll	31.99 00:00:31.99	1.65	31.73	30.08
9. Start of Time Base 2 ( $T_2$ )	135.469 00:02:15.469	0.000	$T_2$	0.000
10. S-IC Inboard Engine Cutoff (IECO)	135.52 00:02:15.52	0.04	0	0.04
11. Tilt Arrest	145.07 00:02:25.07	0.60	9.60	9.00
12. S-IC Outboard Engine Cutoff (OECO) and Start of Time Base 3 ( $T_3$ )	150.769 00:02:30.769	-1.13	$T_3$	0.000
13. S-IC/S-II Separation	151.43 00:02:31.43	-1.16	0.66	0.70

Table 2-2. Event Times Summary (Continued)

EVENT	RANGE TIME		TIME FROM BASE	
	ACTUAL SEC (HR:MIN:SEC)	ACT-PRED SEC	ACTUAL SEC	PREDICTED SEC
14. S-II Engine Start Command (ESC)	152.12 00:02:32.12	-1.18	1.35	1.40
15. S-IC/S-II Second Plane Separation	181.44 00:03:01.44	-1.16	30.67	30.70
16. Launch Escape Tower (LET) Jettison	187.13 00:03:07.13	-1.17	36.36	36.40
17. Initiate Iterative Guidance Mode (IGM)	190.88 00:03:10.88	-0.39	40.11	40.50
18. S-II Engine Mixture Ratio (EMR) Shift and Second Phase IGM	435.69 00:07:15.69	15.92	284.92	269.00
19. S-II Engine Cutoff (ECO) and Start of Time Base 4 ( $T_4$ )	519.759 00:08:39.759	3.44	$T_4$	0.000
20. S-II/S-IVB Separation	520.53 00:08:40.53	3.41	0.77	0.81
21. S-IVB Engine Start Sequence	520.72 00:08:40.72	3.40	0.95	4.00
22. Third Phase Iterative Guidance Mode (IGM)	527.65 00:08:47.65	0.69	7.90	7.20
23. Jettison S-IVB Ullage Motor Cases	532.53 00:08:52.53	3.41	12.77	12.80
24. S-IVB Chi Tilde ( $\tilde{\chi}$ ) Steering	632.25 00:10:32.25	7.99	112.49	104.50
25. S-IVB Engine Cut-off (ECO)(Velocity)	665.64 00:11:05.64	9.65	-	-
26. Start of Time Base 5 ( $T_5$ )	665.884 00:11:05.884	9.69	$T_5$	0.000

Table 2-2. Event Times Summary (Continued)

EVENT	RANGE TIME		TIME FROM BASE	
	ACTUAL SEC (HR:MIN:SEC)	ACT-PRED SEC	ACTUAL SEC	PREDICTED SEC
27. Coast Period ON	667.15 00:11:07.15	9.66	1.26	1.30
28. Initiate S-IVB Restart Sequence and Start of Time Base 6 ( $T_6$ )	11159.576 03:05:59.576	2.07	$T_6$	0.000
29. S-IVB Engine Start ON	11486.57 03:11:26.57	2.06	326.99	327.00
30. Fourth Phase Iterative Guidance Mode (IGM)	11499.99 03:11:39.99	-0.59	340.41	341.10
31. Iterative Guidance Mode Termination and Start Chi Tilde ( $\tilde{\chi}$ ) Steering	11758.18 03:15:58.18	-11.30	598.60	609.90
32. S-IVB Engine Cutoff (ECO) (Velocity)	11786.27 03:16:26.27	-13.12	-0.22*	-0.20*
33. Start of Time Base 7 ( $T_7$ )	11786.479 03:16:26.479	-13.11	$T_7$	0.000
34. Coast Period ON	11787.66 03:16:27.66	-13.13	1.15	1.15
35. Start Launch Vehicle (LV) and Spacecraft (SC) Separation	12386.47 03:26:26.47	-13.12	599.95	600.00
36. LV/SC Separation (MSC)	12388.244 03:26:28.244	-	-	-
*Referenced to $T_7$ .				

Table 2-3. Sequence of Events

FUNCTION	ACTUAL RANGE TIME	PREDICTED (SEC)	ACT-PRED SEC
Range Zero is defined as 12:00:01 UT	-	-	-
<u>Liftoff and Start of Time Base 1</u>	0.263	-	-
IU Auto-Abort Enable Relays Reset	5.21	5.26	-0.05
S-IC Multiple Engine Cutoff Enable	14.21	14.26	-0.05
S-IC Telemeter Calibrate ON	25.21	25.26	-0.05
IU Telemetry Calibrator Inflight Calibrate ON	27.23	27.26	-0.03
S-IC Telemeter Calibrate OFF	30.04	30.06	-0.02
IU Launch Vehicle Engines EDS Cutoff Enable	30.21	30.26	-0.05
IU Telemetry Calibrator Inflight Calibrate OFF	32.22	32.26	-0.04
S-IC Fuel Pressurizing Valve No. 2 Open and Tape Recorder Record	49.72	49.76	-0.04
S-II Start Data Recorders	74.32	74.36	-0.04
IU Telemetry Calibrator Inflight Calibrate ON	90.22	90.26	-0.04
IU Telemetry Calibrator Inflight Calibrate OFF	95.22	95.26	-0.04
S-IC Fuel Pressurizing Valve No. 3 Open	95.52	95.56	-0.04
IU Flight Control Computer Switch Point No. 1	105.21	105.26	-0.05
S-IC Telemeter Calibrate ON	115.21	115.26	-0.05
S-IVB Special Calibrate Relays ON	119.24	119.26	-0.02
S-IVB Regular Calibrate Relays ON	119.41	119.46	-0.05
IU Flight Control Computer Switch Point No. 2	120.21	120.26	-0.05
S-IC Telemeter Calibrate OFF	120.43	120.46	-0.03
S-IVB Regular Calibrate Relays OFF	124.43	124.46	-0.03
S-IVB Special Calibrate Relays OFF	124.62	124.66	-0.04
S-IC Fuel Pressurizing Valve No. 4 Open	133.73	133.76	-0.03
S-IVB Fast Record ON	134.12	134.16	-0.04
IU Tape Recorder Record ON	134.21	134.26	-0.05
IU S-IC Two Engines Out Auto-Abort Inhibit Enable	134.43	134.46	-0.03
IU S-IC Two Engines Out Auto-Abort Inhibit	134.61	134.66	-0.05
IU Excess Rate (P,Y,R) Auto-Abort Inhibit Enable	134.82	134.86	-0.04
IU Excess Rate (P,Y,R) Auto-Abort Inhibit	135.04	135.06	-0.02
S-IC Two Adjacent Outboard Engines Out Cutoff Enable	135.21	135.26	-0.05
<u>S-IC Start of Time Base 2</u>	135.47	135.47	0.00
S-IC Inboard Engine Cutoff	135.52	135.47	+0.05
S-II Start First PAM/FM/FM Calibration	135.82	135.86	-0.04
S-II Stop First PAM/FM/FM Calibration	140.82	140.86	-0.04
S-II Ordnance Arm	144.32	144.36	-0.04
S-IC Separation and Retro EBW Firing Units Arm	144.53	144.56	-0.03
IU Q-Ball Power OFF	144.72	144.76	-0.04
S-II Camera Lights ON	144.93	144.96	-0.03
S-IC Telemetry Measurement Switch Over	145.12	145.16	-0.04
S-IC Outboard Engines Cutoff Enable	145.33	145.36	-0.03

Table 2-3. Sequence of Events (Continued)

FUNCTION	ACTUAL RANGE TIME	PREDICTED (SEC)	ACT-PRED SEC
<u>S-IC Outboard Engines Cutoff and Start of Time Base 3</u>	150.77	151.90	-1.13
S-II Camera Motor On	150.85	152.00	-1.15
S-II LH <sub>2</sub> Recirculation Pumps OFF	150.94	152.10	-1.16
S-II Ullage Trigger	151.24	152.40	-1.16
S-II Camera Event Mark	151.34	152.50	-1.16
S-II S-IC/S-II Separation	151.43	152.60	-1.16
IU Switch Engine Control to S-II; S-II Engine Out Indication "A" Enable; S-II Aft Interstage Separation Indication "A" Enable	151.52	152.70	-1.18
S-II Engines Cutoff Reset	151.62(1)	152.80	-1.18
S-II Engines Ready Bypass	151.72(1)	152.90	-1.18
S-II Prevalves Lockout Reset	151.82(1)	153.00	-1.18
S-II Engine Start	152.12(1)	153.30	-1.18
S-II Camera Event Mark	152.22(1)	153.40	-1.18
IU, S-II Engine Out Indication "B" Enable and S-II Aft Interstage Separation Indication "B" Enable	152.32(1)	153.50	-1.18
S-II Engines Ready Bypass Reset	152.52(1)	153.70	-1.18
S-II Hydraulic Accumulators Unlock	153.72	154.90	-1.18
S-II Chilldown Valves Close	157.12	158.30	-1.18
S-II Start Phase Limiter Cutoff Arm	157.42	158.60	-1.18
S-II Activate PU System	157.64	158.80	-1.16
S-II Start Phase Limiter Cutoff Arm Reset	158.44	159.60	-1.16
IU Tape Recorder Record OFF	161.82	163.00	-1.18
S-II Stop Data Recorders	162.04	163.20	-1.16
S-IVB Fast Record OFF	162.22	163.40	-1.18
IU Water Coolant Valve Open	178.32	179.50	-1.18
S-II Second Plane Separation	181.44	182.60	-1.16
S-II Camera Event Mark	181.54	182.70	-1.16
S-II Camera Event Mark	182.53	183.70	-1.17
IU Launch Escape Tower Jettison "A" ON	187.13	188.30	-1.17
IU Launch Escape Tower Jettison "B" ON	187.32	188.50	-1.18
S-II Camera Eject No. 1	188.72	189.90	-1.18
S-II Camera Eject No. 2	189.33	190.50	-1.17
S-II Camera Eject No. 3	189.84	191.00	-1.16
IU Flight Control Computer Switch Point No. 3	212.13	213.30	-1.17
S-II Start Second PAM/FM/FM Calibration	275.74	276.90	-1.16
S-II Stop Second PAM/FM/FM Calibration	280.72	281.90	-1.18
IU Flight Control Computer Switch Point No. 4	342.12	343.30	-1.18
IU Telemetry Calibrator Inflight Calibrate ON	348.32	349.50	-1.18
IU Telemetry Calibrator Inflight Calibrate OFF	353.33	354.50	-1.17
S-II Measurement Control Switch No. 2 Activate	363.43	364.60	-1.17

Table 2-3. Sequence of Events (Continued)

FUNCTION	ACTUAL RANGE TIME	PREDICTED (SEC)	ACT-PRED SEC
S-II Start Third PAM/FM/FM Calibration	375.72	376.90	-1.18
S-II Stop Third PAM/FM/FM Calibration	380.72	381.90	-1.18
S-II LH <sub>2</sub> Step Pressurization	470.72	471.90	-1.18
S-IVB Special Calibrate Relays ON	475.73	476.90	-1.17
S-IVB Regular Calibrate Relays ON	475.92	477.10	-1.18
IU Telemetry Calibrator Inflight Calibrate ON	476.14	477.30	-1.16
S-IVB Regular Calibrate Relays OFF	480.73	481.90	-1.17
S-IVB Special Calibrate Relays OFF	480.94	482.10	-1.16
IU Telemetry Calibrator Inflight Calibrate OFF	481.12	482.30	-1.18
S-IVB Rate Gyro OFF	481.33	482.50	-1.17
S-IVB Charge Ullage Ignition ON	481.54	482.70	-1.16
S-II/S-IVB Ordnance Arm	481.72	482.90	-1.18
IU Tape Recorder Record ON	481.94	483.10	-1.16
S-IVB Fast Record ON	482.12	483.30	-1.18
S-II Start Data Recorders	482.33	483.50	-1.18
S-II LOX Depletion Sensor Cutoff Arm	482.52	483.70	-1.18
S-II LH <sub>2</sub> Depletion Sensor Cutoff Arm	482.73	483.90	-1.18
S-II Start of Time Base 4	519.76	516.32	+3.44
S-II Redundant S-II Cutoff Switch Selector	519.85	516.32	+3.53
S-II Start Recorder Timers	519.94	516.42	+3.52
S-IVB Prevalves Close OFF	520.03	516.52	+3.51
S-IVB Engine Cutoff OFF	520.13	516.62	+3.51
S-IVB Engine Ready Bypass	520.22	516.82	+3.40
S-IVB LOX Chilldown Pump OFF	520.32	516.92	+3.40
S-IVB Fire Ullage Ignition ON	520.44	517.02	+3.42
S-IVB S-II/S-IVB Separation	520.53	517.12	+3.41
S-IVB Engine Start Interlock Bypass ON	520.63	517.22	+3.41
S-IVB Engine Start ON	520.72	517.32	+3.40
IU Flight Control Computer S-IVB Burn Mode On "A"	520.93	517.52	+3.41
IU Flight Control Computer S-IVB Burn Mode On "B"	521.03	517.62	+3.41
IU S-IVB Engine Out Indication "A" Enable	521.32	517.92	+3.40
IU S-IVB Engine Out Indication "B" Enable	521.53	518.12	+3.41
S-IVB Fuel Chilldown Pump OFF	521.92	518.52	+3.40
S-IVB LOX Tank Flight Pressure System ON	523.52	520.12	+3.40
S-IVB Fuel Injection Temperature OK Bypass	523.74	520.32	+3.42
S-IVB Engine Start OFF	523.91	520.52	+3.39
S-IVB First Burn Relay ON	525.52	522.12	+3.40
S-IVB Emergency Playback Enable ON	527.53	524.12	+3.41
S-IVB Fast Record OFF	527.72	524.32	+3.40
S-IVB PU Activate ON	528.72	525.32	+3.40

Table 2-3. Sequence of Events (Continued)

FUNCTION	ACTUAL RANGE TIME	PREDICTED TIME (SEC)	ACT-PRED SEC
S-IVB Charge Ullage Jettison ON	530.03	526.62	+3.41
S-IVB Fire Ullage Jettison ON	532.53	529.12	+3.41
S-IVB Ullage Charging Reset	535.82	532.42	+3.40
S-IVB Ullage Firing Reset	536.03	532.62	+3.41
IU Tape Recorder Record OFF	538.63	535.22	+3.41
S-IVB Emergency Playback Enable OFF	541.02	537.62	+3.40
IU Telemetry Calibrator Inflight Calibrate ON	542.12	538.72	+3.40
IU Telemetry Calibrator Inflight Calibrate OFF	547.11	543.72	+3.40
S-IVB Regular Calibrate Relays ON	551.51	548.12	+3.39
S-IVB Regular Calibrate Relays OFF	556.51	553.12	+3.39
S-IVB Chilldown Shutoff Pilot Valve Close ON	625.02	621.62	+3.40
S-IVB Engine Pump Purge Control Valve Enable ON	658.69	649.19	+9.50
S-IVB Cutoff S-IVB Engine (Velocity)	665.64	656.09	+9.65
S-IVB Start of Time Base 5	665.88	656.19	+9.69
S-IVB Cutoff S-IVB Engine (Redundant)	665.97	-	-
S-IVB Point Level Sensor Disarming	666.07	656.29	+9.78
S-IVB Ullage Engine No. 1 ON	666.16	656.49	+9.67
S-IVB Ullage Engine No. 2 ON	666.28	656.59	+9.69
IU S-IVB Ullage Thrust Present Indication ON	666.45	656.79	+9.66
S-IVB First Burn Relay OFF	666.58	656.89	+9.69
S-IVB PU Activate OFF	666.74	657.09	+9.65
S-IVB Prevalves Close ON	666.84	657.19	+9.65
S-IVB LOX Tank Flight Pressure System OFF	666.94	657.29	+9.65
S-IVB Coast Period ON	667.15	657.49	+9.66
S-IVB Engine Pump Purge Control Valve Enable ON	667.36	657.69	+9.67
S-IVB PU Fuel Boiloff Bias Cutoff ON	667.54	657.89	+9.65
IU Flight Control Computer S-IVB Burn Mode OFF "B"	669.14	659.49	+9.65
IU Flight Control Computer S-IVB Burn Mode OFF "A"	669.36	659.69	+9.67
S-IVB Aux. Hydraulic Pump Coast Mode ON	669.54	659.89	+9.65
S-IVB Aux. Hydraulic Pump Flight Mode OFF	669.75	660.09	+9.66
IU S-IVB Engine Out Indication "A" Enable Reset	675.86	666.19	+9.67
IU S-IVB Engine Out Indication "B" Enable Reset	676.04	666.39	+9.65
S-IVB SS/FM Transmitter OFF	688.04	678.39	+9.65
S-IVB SS/FM Group OFF	688.25	678.59	+9.66
S-IVB LH <sub>2</sub> Tank Continuous Vent Valve Open ON	724.84	715.19	+9.65
IU Telemetry Calibrator Inflight Calibrate ON	725.44	715.79	+9.65
S-IVB Prevalves Close OFF	726.35	716.69	+9.66
S-IVB Chilldown Shutoff Pilot Valve Close OFF	726.56	716.89	+9.67
S-IVB LH <sub>2</sub> Tank Continuous Vent Valve Open OFF	726.86	717.19	+9.67
IU Telemetry Calibration Inflight Calibrate OFF	730.44	720.79	+9.65

Table 2-3. Sequence of Events (Continued)

FUNCTION	ACTUAL RANGE TIME	PREDICTED (SEC)	ACT-PRED SEC
S-IVB Ullage Engine No. 1 OFF	753.84	744.19	+9.65
S-IVB Ullage Engine No. 2 OFF	753.94	744.29	+9.65
IU S-IVB Ullage Thrust Present Indication OFF	754.15	744.49	+9.66
S-IVB Emergency Playback Enable ON	764.15	754.49	+9.66
IU Tape Recorder Playback Reverse ON	767.33	758.69	+8.64
IU Tape Recorder Playback Reverse OFF	853.34(2)	843.69	+9.65
S-IVB Emergency Playback Enable OFF	854.14	844.49	+9.65
S-IVB Slow Record ON	954.14	944.49	+9.65
S-IVB Slow Record ON	957.14(2)	947.49	+9.65
S-IVB Engine Pump Purge Control Valve Enable OFF	1268.44	1258.79	+9.65
S-IVB Slow Record ON	2232.15(2)	2222.49	+9.66
S-IVB Slow Record OFF	2264.15	2254.49	+9.66
S-IVB Recorder Playback ON	2264.35	2254.69	+9.66
S-IVB Recorder Playback OFF	2429.35	2419.69	+9.66
S-IVB Slow Record ON	2511.14	2501.49	+9.65
S-IVB Slow Record ON	2514.14(2)	2504.49	+9.65
IU Telemetry Calibrator Inflight Calibrate ON	3116.2	3106.49	+9.71
S-IVB Special Calibrate Relays ON	3116.34	3106.69	+9.65
S-IVB Regular Calibrate Relays ON	3116.54	3106.89	+9.65
IU Telemetry Calibrator Inflight Calibrate OFF	3121.34	3111.69	+9.65
S-IVB Regular Calibrate Relays OFF	3121.54	3111.89	+9.65
S-IVB Special Calibrate Relays OFF	3121.74	3112.09	+9.65
IU Telemetry Calibrator Inflight Calibrate ON	5279.4	5269.69	+9.71
S-IVB Slow Record ON	5279.45(2)	5269.89	+9.56
S-IVB Special Calibrate Relays ON	5279.65	5270.09	+9.56
S-IVB Regular Calibrate Relays ON	5279.88	5270.29	+9.59
IU Telemetry Calibrator Inflight Calibrate OFF	5284.03(2)	5274.69	+9.34
S-IVB Regular Calibrate Relays OFF	5284.63	5275.29	+9.34
S-IVB Special Calibrate Relays OFF	5284.88	5275.49	+9.39
S-IVB Slow Record OFF	5311.78	5301.89	+9.89
S-IVB Recorder Playback ON	5311.78	5302.09	+9.69
S-IVB Recorder Playback OFF	5661.95	5652.29	+9.66
S-IVB Slow Record ON	5662.15	5652.49	+9.66
S-IVB Slow Record ON	5665.15	5655.49	+9.66
IU Telemetry Calibrator Inflight Calibrate ON	6318.97	6309.29	+9.68
S-IVB Special Calibrate Relays ON	6319.16	6309.49	+9.67
S-IVB Regular Calibrate Relays ON	6319.37	6309.69	+9.68
IU Telemetry Calibrator Inflight Calibrate OFF	6323.95	6314.29	+9.66
S-IVB Regular Calibrate Relays OFF	6324.35	6314.69	+9.66
S-IVB Special Calibrate Relays OFF	6324.55	6314.89	+9.66



Table 2-3. Sequence of Events (Continued)

FUNCTION	ACTUAL RANGE	PREDICTED TIME (SEC)	ACT-PRED SEC
S-IVB Slow Record ON	(3)	7723.49	
S-IVB Slow Record OFF	(3)	7755.49	
S-IVB Recorder Playback ON	(3)	7755.69	
S-IVB Recorder Playback OFF	8009.15	7999.49	+9.66
S-IVB Slow Record ON	8009.35	7999.69	+9.66
S-IVB Slow Record ON	8012.35(2)	8002.69	+9.66
S-IVB Special Calibrate Relays ON	8685.04	8675.49	+9.55
S-IVB Regular Calibrate Relays ON	8685.21	8675.69	+9.52
IU Telemetry Calibrator Inflight Calibrate ON	8685.6	8675.89	+9.71
S-IVB Regular Calibrate Relays OFF	8690.21	8680.69	+9.52
S-IVB Special Calibrate Relays OFF	8690.41	8680.89	+9.52
IU Telemetry Calibrator Inflight Calibrate OFF	8690.61(2)	8681.09	+9.52
S-IVB Slow Record ON	10225.17	10215.49	+9.68
S-IVB Slow Record OFF	10257.18	10247.49	+9.69
S-IVB Recorder Playback ON	10257.38	10247.69	+9.69
S-IVB Recorder Playback OFF	10541.37	10531.69	+9.68
S-IVB Slow Record ON	10541.57	10531.89	+9.68
S-IVB Slow Record ON	10544.57	10534.89	+9.68
IU Telemetry Calibrator Inflight Calibrate ON	10866.0	10856.29	+9.71
S-IVB Special Calibrate Relays ON	(4)	10856.49	-
S-IVB Regular Calibrate Relays ON	(4)	10856.69	-
IU Telemetry Calibrator Inflight Calibrate OFF	(4)	10861.29	-
S-IVB Regular Calibrate Relays OFF	(4)	10861.69	-
S-IVB Special Calibrate Relays OFF	(4)	10861.89	-
S-IVB Aux. Hydraulic Pump Flight Mode ON	10913.87	10904.19	+9.68
S-IVB Aux. Hydraulic Pump Coast Mode OFF	10914.08	10904.39	+9.69
S-IVB Fuel Chillover Pump ON	10918.88	10909.19	+9.69
S-IVB LOX Chillover Pump ON	10923.87	10914.19	+9.68
S-IVB Prevalves Close ON	10933.87	10924.19	+9.68
<u>S-IVB Begin Restart Preparations and Start of Time Base 6</u>	11159.58	11157.51	+2.07
S-IVB Ullage Engine No. 1 ON	11159.78	11157.71	+2.07
S-IVB Ullage Engine No. 2 ON	11159.87	11157.81	+2.06
IU S-IVB Ullage Thrust Present Indication ON	11160.08	11158.01	+2.07
S-IVB LH <sub>2</sub> Tank Vent Valve Boost Close ON	11160.38	11158.31	+2.07
S-IVB LOX Tank Vent Valve Boost Close ON	11160.57	11158.51	+2.06
S-IVB LH <sub>2</sub> Tank Continuous Vent Valve Close ON	11160.78	11158.71	+2.07
S-IVB LH <sub>2</sub> Tank Repressurization Control Valve Open ON	11161.78	11159.71	+2.07
S-IVB LH <sub>2</sub> Tank Vent Valve Boost Close OFF	11162.37	11160.31	+2.06
S-IVB LOX Tank Vent Valve Boost Close OFF	11162.58	11160.51	+2.07

Table 2-3. Sequence of Events (Continued)

FUNCTION	ACTUAL RANGE TIME	PREDICTED (SEC)	ACT-PRED SEC
S-IVB LH <sub>2</sub> Tank Continuous Vent Valve Close OFF	11162.79	11160.71	+2.08
S-IVB Fuel Chilldown Pump ON	11165.59	11163.52	+2.07
S-IVB LOX Chilldown Pump ON	11170.51	11168.51	+2.00
S-IVB Prevalves Close ON	11180.58	11178.51	+2.07
IU Telemetry Calibrator Inflight Calibrate ON	11375.06	11373.01	+2.05
S-IVB Special Calibrate Relays ON	11375.26	11373.21	+2.05
S-IVB Regular Calibrate Relays ON	11375.48	11373.41	+2.07
IU Telemetry Calibrator Inflight Calibrate OFF	11380.06	11378.01	+2.05
S-IVB Regular Calibrate Relays OFF	11380.47	11378.41	+2.06
S-IVB Special Calibrate Relays OFF	11380.65	11378.61	+2.04
S-IVB SS/FM Group ON	11380.86	11378.81	+2.05
S-IVB SS/FM Transmitter ON	11381.08	11379.01	+2.07
S-IVB LOX Tank Repressurization Control Valve Open ON	11416.56	11414.51	+2.05
S-IVB PU Activate ON	11466.56	11464.51	+2.05
S-IVB PU Valve Hardover Position ON	11466.78	11464.71	+2.07
S-IVB Prevalves Close OFF	11475.77	11473.71	+2.06
IU S-IVB Restart Alert	11476.55	11474.51	+2.04
S-IVB Engine Cutoff OFF	11485.15	11483.11	+2.04
S-IVB Engine Ready Bypass	11485.36	11483.31	+2.05
S-IVB LH <sub>2</sub> Tank Repressurization Control Valve Open OFF <sup>2</sup>	11485.58	11483.51	+2.07
S-IVB Fuel Chilldown Pump OFF	11485.76	11483.71	+2.05
S-IVB LOX Chilldown Pump OFF	11485.97	11483.91	+2.06
S-IVB LOX Tank Pressurization Control Valve Open OFF	11486.35	11484.31	+2.04
S-IVB Engine Start ON	11486.57	11484.51	+2.06
IU S-IVB Engine Out Indication "A" Enable	11487.35	11485.31	+2.04
IU S-IVB Engine Out Indication "B" Enable	11487.57	11485.51	+2.06
S-IVB Ullage Engine No. 1 OFF	11489.56	11487.51	+2.05
S-IVB Ullage Engine No. 2 OFF	11489.65	11487.61	+2.04
IU S-IVB Ullage Thrust Present Indication OFF	11489.86	11487.81	+2.05
IU Flight Control Computer S-IVB Burn Mode On "B"	11494.17	11492.11	+2.06
IU Flight Control Computer S-IVB Burn Mode On "A"	11494.36	11492.31	+2.05
S-IVB Fuel Injection Temperature OK Bypass	11494.60	11492.51	+2.09
S-IVB LOX Tank Flight Pressure System ON	11494.76	11492.71	+2.05
S-IVB Coast Period OFF	11494.96	11492.91	+2.05
S-IVB Engine Start OFF	11495.16	11493.11	+2.05
S-IVB Second Burn Relay ON	11497.17	11495.11	+2.06
S-IVB PU Valve Hardover Position OFF	11499.56	11497.51	+2.05
S-IVB SS/FM Transmitter OFF	11752.07	11750.01	+2.06
S-IVB SS/FM Group OFF	11752.26	11750.21	+2.05

Table 2-3. Sequence of Events (Continued)

FUNCTION	ACTUAL RANGE TIME	PREDICTED TIME (SEC)	ACT-PRED SEC
IU Flight Control Computer Switch Point No. 5	11756.56	11754.51	+2.05
IU Telemetry Calibrator Inflight Calibrate ON	11758.17	11756.11	+2.06
S-IVB Special Calibrate Relays ON	11758.36	11756.31	+2.05
S-IVB Regular Calibrate Relays ON	11758.57	11756.51	+2.06
IU Telemetry Calibrator Inflight Calibrate OFF	11763.17	11761.11	+2.06
S-IVB Regular Calibrate Relays OFF	11763.56	11761.51	+2.05
S-IVB Special Calibrate Relays OFF	11763.78	11761.71	+2.07
S-IVB Chilldown Shutoff Pilot Valve	(5)	-	-
S-IVB Point Level Sensor Arming	(5)	-	-
S-IVB Cutoff S-IVB Engine (Velocity)	11786.27	11799.39	-13.12
<u>S-IVB Start of Time Base 7</u>	11786.48	11799.59	-13.11
S-IVB Cutoff S-IVB Engine (Redundant)	11786.60	-	-
S-IVB LOX Tank Vent Valve Open	11786.69	11799.79	-13.10
S-IVB Point Level Sensors Disarming	11786.78	11799.89	-13.11
S-IVB LH <sub>2</sub> Tank Vent Valve Open	11786.88	11799.99	-13.11
S-IVB Second Burn Relay OFF	11787.26	11800.39	-13.13
S-IVB LOX Tank Flight Pressure System OFF	11787.47	11800.59	-13.12
S-IVB Prevalves Close ON	11787.57	11800.69	-13.12
S-IVB Coast Period ON	11787.66	11800.79	-13.13
S-IVB PU Activate OFF	11787.87	11800.99	-13.12
S-IVB PU Inverter and DC Power OFF	11787.97	11801.09	-13.12
S-IVB LOX Chilldown Pump Purge Control Valve Open OFF	11788.06	11801.19	-13.13
IU Flight Control Computer S-IVB Burn Mode OFF "B"	11789.76	11802.89	-13.13
IU Flight Control Computer S-IVB Burn Mode OFF "A"	11789.97	11803.09	-13.12
S-IVB Aux. Hydraulic Pump Flight Mode OFF	11790.16	11803.29	-13.13
S-IVB LOX Tank Vent Valve Close	11796.46	11809.59	-13.13
S-IVB LOX Tank Vent Valve Boost Close ON	11799.47	11812.59	-13.12
S-IVB LOX Tank Vent Valve Boost Close OFF	11801.47	11814.59	-13.12
S-IVB Prevalves Close OFF	11846.97	11860.09	-13.12
S-IVB Chilldown Shutoff Pilot Valve Close OFF	11847.17	11860.29	-13.12
S-IVB LH <sub>2</sub> Tank Vent Valve Close	11906.47	11919.59	-13.12
S-IVB LH <sub>2</sub> Tank Vent Valve Boost Close ON	11909.47	11922.59	-13.12
S-IVB LH <sub>2</sub> Tank Vent Valve Boost Close OFF	11911.47	11924.59	-13.12
IU LV/SC Separation Sequence Start	12386.47	12399.59	-13.12
IU Switch PCM to Low Gain Antenna (Fail Safe)	13519.81	13532.89	-13.08
IU Switch CCS to Low Gain Antenna	13520.01	13533.09	-13.08
IU Telemetry Calibrator Inflight Calibrate ON	14124.57	14137.69	-13.12
S-IVB Special Calibrate Relays ON	14124.77	14137.89	-13.12
S-IVB Regular Calibrate Relays ON	14124.97	14138.09	-13.12

Table 2-3. Sequence of Events (Continued)

FUNCTION	ACTUAL RANGE TIME (SEC)	PREDICTED TIME (SEC)	ACT-PRED SEC
IU Telemetry Calibrator Inflight Calibrate OFF	14129.56	14142.69	-13.13
S-IVB Regular Calibrate Relays OFF	14129.96	14143.09	-13.13
S-IVB Special Calibrate Relays OFF	14130.16	14143.29	-13.13
IU Switch PCM to High Gain Antenna	16099.77	16112.89	-13.12
IU Switch CCS to High Gain Antenna (Fail Safe)	16100.00	16113.09	-13.09
IU Switch PCM to Low Gain Antenna (Fail Safe)	19399.76	19412.89	-13.13
IU Switch CCS to Low Gain Antenna	19399.96	19413.09	-13.13
IU CCS Transmitter Inhibit	20186.52	20199.59	-13.07
IU Switch PCM to OMNI Antenna	26899.77	26912.89	-13.12
IU Switch CCS to OMNI Antenna	26899.97	26913.09	-13.12
<u>C-Band Transponder</u>			
No. 1 and No. 2 ON	5074.87	(6)	(6)
No. 2 OFF	5074.87		
No. 1 and No. 2 ON	5098.37		
No. 1 OFF	5098.37		
No. 1 and No. 2 ON	5698.47		
No. 2 OFF	5698.54		
No. 1 and No. 2 ON	11809.61		
No. 1 OFF	11809.68		
No. 1 and No. 2 ON	11881.52		
No. 2 OFF	11881.59		
No. 1 and No. 2 ON	11889.72		
No. 1 OFF	11889.79		
No. 1 and No. 2 ON	11897.93		
No. 2 OFF	11898.01		
No. 1 and No. 2 ON	11906.55		
No. 1 OFF	11906.62		
No. 1 and No. 2 ON	11929.67		
No. 2 OFF	11929.75		
No. 1 and No. 2 ON	12129.86		
No. 1 OFF	12129.93		
No. 1 and No. 2 ON	12306.26		
No. 2 OFF	12306.33		
No. 1 and No. 2 ON	12530.55		
No. 1 OFF	12530.62		
No. 1 and No. 2 ON	12657.59		
No. 2 OFF	12657.67	(6)	(6)
NOTES: (1) Data dropout-computed values. (2) Computed values. (3) Late acquisition at Tananarive. (4) Recorder playback not programmed. (5) Not issued because of early S-IVB engine cutoff. (6) These columns left blank because the events occur at variable times.			

Table 2-4. Ground Commanded Switch Selector Events  
Beginning at 15:07:22 UT

EVENT	RANGE TIME (SEC)
LH <sub>2</sub> Tank Prepressurization Control Valve Open OFF	11242.06
LH <sub>2</sub> Tank Continuous Vent Close ON	11242.93
S-IVB Stage Select Address Zero (Time Spacer)	11243.82
LH <sub>2</sub> Tank Continuous Vent Valve Close OFF	11244.69
LH <sub>2</sub> Tank Repressurization Control Valve Open OFF	11295.39
LH <sub>2</sub> Tank Continuous Vent Valve Close ON	11296.27
S-IVB Stage Select Address Zero (Time Spacer)	11297.15
LH <sub>2</sub> Tank Continuous Vent Valve Close OFF	11298.05
LH <sub>2</sub> Tank Repressurization Control Valve Open OFF	11325.41
LH <sub>2</sub> Tank Continuous Vent Valve Close ON	11326.29
S-IVB Stage Select Address Zero (Time Spacer)	11327.22
LH <sub>2</sub> Tank Continuous Vent Valve Close OFF	11328.11
Switch PCM to Low Gain Antenna (Fail Safe)	13252.32
Switch CCS to Low Gain Antenna	13255.30
Switch CCS to High Gain Antenna (Fail Safe)	13410.19
Switch CCS to OMNI Antenna	13411.19
Switch PCM to Low Gain Antenna (Fail Safe)	13412.24
Switch PCM to OMNI Antenna	13413.24
Switch CCS to High Gain Antenna (Fail Safe)	15782.42
Switch CCS to OMNI Antenna	15783.64
Switch PCM to Low Gain Antenna (Fail Safe)	15784.84
Switch PCM to OMNI Antenna	15786.08
CCS Transponder Inhibit ON	19979.35
CCS Transponder Inhibit OFF	20159.49
CCS Transponder Inhibit OFF	20186.46



## SECTION 3 LAUNCH OPERATIONS

### 3.1 SUMMARY

The Apollo 4 was the first of two missions designed to qualify the Saturn V system for manned flight. This also was the first Apollo mission utilizing a Saturn V launch vehicle (AS-501), a Lunar Module Boilerplate (LTA/10R), and a Command Service Module (CSM 017). The launch was the first to be made from Launch Complex 39A at Kennedy Space Center.

The launch countdown for AS-501 proceeded smoothly without any major holds and culminated in the successful launch of the vehicle at 0700 hours EST November 9, 1967.

Ground systems performance was exceptionally good; minor anomalies that occurred did not pose any serious constraint to the vehicle nor contribute to a significant hold. Photographic coverage experienced the most significant deviation from standard performance. A dropout of both camera power and timing signals was experienced just prior to liftoff. This resulted in the cameras not starting, short runs, jamming, and a lack of timing signals. The problem has been documented by UCR and is under investigation.

Launch damage, while extensive in isolated areas, (the LUT level platform was completely destroyed and the engine service platform was damaged extensively), was in general, less than expected.

There were no major range safety problems during the countdown. The actual trajectory of the vehicle appeared near nominal on all the range safety charts during flight. The command destruct receivers on the S-IVB stage were successfully "safed" by the Bermuda Range Safety Officer after first S-IVB cutoff.

### 3.2 PRELAUNCH MILESTONES

A chronological sequence of events and the preparation which led to the successful launch of AS-501 is presented in Table 3-1.

Table 3-1. AS-501 Milestones

DATE	EVENT
August 15, 1966	S-IVB stage arrived and moved into VAB low bay
August 25, 1966	IU arrived
September 9, 1966	SLA arrived
September 12, 1966	S-IC stage arrived at KSC via barge, and was off-loaded and moved into VAB transfer aisle on this date
October 27, 1966	S-IC stage erected on Mobile Launcher No. 1 in high bay 1
October 31, 1966	S-II stage spacer erected
November 1, 1966	S-IVB stage erected
November 2, 1966	IU stage erected
November 7, 1966	Initial power applied to S-IC stage
November 16, 1966	Initial IU bus power application
November 21, 1966	Launch vehicle electrical mate completed
December 12, 1966	Launch vehicle emergency detection system test completed
December 16, 1966	Sequential malfunction test completed
December 20, 1966	Guidance and control system checks completed
December 21, 1966	SM arrived
December 24, 1966	CM arrived
January 12, 1967	Apollo S/C erected
January 21, 1967	S-II stage arrived at KSC via barge, and was off-loaded and transported to the VAB low bay for checkout
January 23, 1967	Spacecraft systems integrated tests with launch vehicle simulator started
January 24, 1967	Launch vehicle overall test (OAT) No. 1 completed
February 13, 1967	S/C de-erected and transported to the Manned Space Operations Building for testing
February 13, 1967	IU de-erected
February 14, 1967	S-IVB de-erected
February 15, 1967	S-IVB modifications started
February 15, 1967	S-II stage spacer de-erected
February 23, 1967	S-II stage erected
February 24, 1967	IU and S-IVB stages erected
March 1, 1967	Launch vehicle electrical mate accomplished
March 17, 1967	Power transfer test completed
March 22, 1967	Launch vehicle electrical support equipment (ESE) modifications started
April 6, 1967	S/C Facility Verification Vehicle FVV erected
April 8, 1967	Launch vehicle electrical support equipment modification verification completed
April 14, 1967	Launch vehicle overall test (OAT) No. 2 completed
May 24, 1967	Swing arm compatibility test performed
May 25, 1967	S-II stage LOX tank inspection for presence of structural flaws
May 26, 1967	De-erect S/C FVV
May 27, 1967	De-erect IU



Table 3-1. AS-501 Milestones (Continued)

May 27, 1967	De-erect S-IVB stage
May 28, 1967	S-II LOX tank dye penetrant inspection start
June 3, 1967	S-II stage de-erected
June 5, 1967	S-II stage LH <sub>2</sub> tank inspection started
June 12, 1967	S/C cabin leak check test accomplished
June 16, 1967	S-II stage LH <sub>2</sub> tank inspection completed
June 18, 1967	S-II stage erected
June 19, 1967	S-IVB stage erected
June 19, 1967	IU stage erected
June 20, 1967	S/C erected
June 23, 1967	Launch vehicle electrical mate accomplished
July 14, 1967	Launch vehicle overall test (OAT) No. 2 completed
July 24, 1967	Space vehicle electrical mate and emergency detection system (EDS) test was accomplished
August 1, 1967	Space vehicle overall test (OAT) No. 1 plugs in, completed
August 6, 1967	Space vehicle overall test (OAT) No. 2 plugs out accomplished
August 7, 1967	S/C ordnance installed
August 18, 1967	Space vehicle simulated flight test completed
August 24, 1967	S-II stage LH <sub>2</sub> insulation modifications completed
August 26, 1967	Space vehicle transferred to pad A
September 7, 1967	S/C GSE mobile service structure/mobile launcher interface tests completed
September 20, 1967	LOX and LH <sub>2</sub> cold flow tests completed
September 27, 1967	RP-1 loading of the S-IC stage was completed in preparation for the start of the countdown demonstration test (CDDT)
September 27, 1967	Countdown demonstration test was started with the completion of the precount section on September 29.
September 29, 1967	CDDT terminal count section started and continued through October 14 as a result of numerous problems encountered
--	During this portion of the test it became necessary to change out the fuel cells in the Apollo S/M. This activity was not actually completed until after the test was completed.
October 14, 1967	Terminal count portion of the CDDT procedure was completed
October 19, 1967	Fuel cell changeout completed
October 22, 1967	Inspection S-II stage LOX tank anti-vortex baffle complete
October 26, 1967	Space vehicle - Flight Readiness Test (FRT) completed
November 3, 1967	Space vehicle hypergolic loading completed in preparation for the start of launch countdown
November 4, 1967	S-IC stage RP-1 loading accomplished in preparation for the start of launch countdown
November 4, 1967	Launch vehicle precount started at -104 hours on Saturday, November 4, 1967, at 1200 EST
November 6, 1967	Launch vehicle terminal count was picked up at -49 hours on Monday, November 6, 1967, at 2230 EST and progressed through all scheduled holds without dropping behind in the count
November 9, 1967	Liftoff occurred on schedule at 0700 hours EST

### 3.3 COUNTDOWN EVENTS

The launch countdown for AS-501 was divided into two segments; precount, from -104 hours to -49 hours and countdown from -49 hours to -0 hours. Two holds were preplanned, one of 6 hours duration at -6.5 hours, and a second hold of 1.5 hours duration at -4 hours.

The precount was picked up at -104 hours at 1200 EST on Saturday, November 4, 1967. It proceeded smoothly with only two noninterruptive problems on November 5, 1967:

- a. A scratched seal on the S-IC helium flow control valve No. 4 which required replacement.
- b. Several hydraulic leaks on the swing arms during pressurization.

On November 6, 1967, a series of early morning alarm reports resulted in the initiation of an emergency evacuation of the LUT. However, this evacuation was cancelled when it was confirmed the alarms had been accidentally initiated. Later in the day the S-IVB experienced some difficulty with propellant utilization calibrations and an erratic LOX pump inlet transducer had to be replaced. A LOX pressurization regulator had to be replaced in the S-II stage, and the spacecraft experienced some difficulty because of leaks in pneumatically operated disconnects.

The launch countdown was picked up at -49 hours at 2230 EST on November 6, 1967. The count continued smoothly through 2210 EST November 7, 1967, when the spacecraft reported a potential problem with heat loss in the fuel cell LH<sub>2</sub> tank. At 0532 on November 8, 1967, the decision was made to continue the count without reloading LH<sub>2</sub>. At 1231 EST November 8, 1967, an unscheduled hold was called at -11 hours. This hold consumed 1 hour 59 minutes of the scheduled 6-hour hold and was primarily to allow the launch vehicle to catch up with the clock. Minor difficulties had compounded to cause an approximate 2.5 hour lag. At -8.5 hours at 1700 EST November 8, 1967, a second 2-hour unscheduled hold was called because of difficulties encountered with range safety command receiver checks. The S-IVB Electrical Bridge Wire No. 2 did not charge because of low deviation from the range. A procedure rewrite was required. The count was picked up again at 1900 EST. Prior to entering the hold, the spacecraft experienced difficulties with LOX pressure; however, analysis indicated a high probability that the pressure would be nominal at liftoff and therefore would not constrain the count.

At 2100 EST the -6.5 scheduled hold point was attained, and the count was held for the 2 hours and 1 minute of the hold that remained. The count was picked up at 2301 EST November 8, 1967, and continued smoothly to the second hold at -4 hours. The clock was held at 0130 EST and was released at 0300 EST as planned. No major problems were encountered from the time the countdown clock was released until liftoff at 0700 hours November 9, 1967.

Table 3-2 presents a summary of unscheduled holds.

Table 3-2. Countdown Events

<u>COUNTDOWN STOPPED</u>	<u>TIME LOST</u>	<u>CAUSE</u>
-11 hrs.	1 hr. 59 mins.	Allow launch vehicle to catch up with clock
-8 hrs. 30 mins.	2 hrs.	Range Safety Command Receiver check difficulty. S-IVB EBW No. 2 did not charge. Procedure rewrite required.

### 3.4 PROPELLANT AND COLD HELIUM LOADING

#### 3.4.1 RP-1 Loading

RP-1 loading for launch countdown was accomplished on November 3, 1967. To compensate for thermal shrinkage and later filling of F-1 engine lines, a flight mass overload of 2 percent was used. The level adjust operation was completed ahead of schedule on November 9, 1967. The RP-1 mass readouts did not recover to the previous value following power transfer test at -27 minutes. However, since no valves had opened since level adjust, the correct level for launch was assured. There were approximately 769.953 meters<sup>3</sup> (203,400 gal) of RP-1 onboard at liftoff.

The RP-1 system operated satisfactorily through FRT and launch countdown with no delays and only a few minor problems.

The following anomalies and problems were encountered:

- a. Mast cutoff valve A9651 did not close during terminal count, therefore, the RP-1 lines were contaminated at liftoff. This valve is intended to close at completion of RP-1 level adjust/line inert. During FRT, the valve opened at commit because the valve control system deenergized. Design evaluation indicated the valve could remain open for AS-501, so no changes were made. Redesign is recommended to ensure mast cutoff valve closure for subsequent launches.
- b. RP-1 vent trap A4120 in room 4A leaked about 0.0076 meters<sup>3</sup> (2 gal) of RP-1 on the pad. The actual time of leakage cannot be determined as this area was cleared during RP-1 loading. Possible causes may have been momentary float binding as RP-1 entered the component, or continuous leakage throughout loading. Inspection per NCR 019916 will ensure acceptability before use on AS-503.

- c. The RP-1 mass readout decreased approximately 0.16 percent during power transfer test. Recurrence could prevent accurate mass readout monitoring and cause the mass readout indicator to drop out of flight mass tolerance after about -27 minutes. Power transfer also affects the S-IC fuel probe package 60B43006-27-G readout in the Propellant Tanking Computer System (PTCS).

CR 5-8531-136 and UCR KSC300216 cover this problem. Work is in process to develop a more reliable readout for AS-502.

#### 3.4.2 LOX Loading

The LOX consumption on S-IC stage totaled 2093.33 meters<sup>3</sup> (553,000 gal) from start of count to system securing. About 1703.43 meters<sup>3</sup> (450,000 gal) were aboard at liftoff. S-II LOX 100 percent mass, 359,037 kilograms (791,542 lbm), was attained at -4 hours during the built-in hold, after which time the count was resumed. At liftoff, the indicated S-IVB LOX load was 87,624 kilograms (193,179 lbm). The PTCS indicated 99.96 percent at liftoff. The LOX load required for launch was 87,667.2 ± 437.7 kilograms (193,273 ± 965 lbm). The total loss of LOX due to boiloff after loading was complete and prior to liftoff was 10,269 kilograms (22,640 lbm).

The LOX system supported FRT, and AS-501 launch from -6.5 hours through -0 with no serious problems or delays. Vehicle flight mass at liftoff was within specifications. There was no unexpected or excessive damage to either the storage area or LUT LOX equipment. An S-IC LOX tank overfill occurred as a result of launch vehicle power transfer test at -27 minutes. This was rectified and the vehicle launched with an acceptable LOX flight mass.

During storage tank pressurization (0017 EST), LOX vaporizer flow control valve A12 did not respond to control pressure. At -4 hours 29 minutes 57 seconds (0100:03 EST) the valve broke loose from the fully open position and thereafter functioned normally. It was checked out during securing from launch and functioned properly. Ice accumulation on the valve probably caused the failure. A more adequate purge will minimize icing.

#### 3.4.3 LH<sub>2</sub> Loading

The system performance was excellent, with no major delays because of malfunctions during the fill sequences. The system consumed or delivered to the S-IC stage 1627.73 meters<sup>3</sup> (430,000 gal) of LH<sub>2</sub>. The S-II LH<sub>2</sub> 100 percent mass, 69,694.5 kilograms (153,650 lbm), was attained at -1 hour and 45 minutes. At liftoff, the indicated S-IVB LH<sub>2</sub> load was 18,656 kilograms (41,129 lbm). The PTCS indicated 99.85 percent. The LH<sub>2</sub> load required for launch was 18,698 ± 93.4 kilograms (41,222 ± 206 lbm). The total loss of LH<sub>2</sub> due to boiloff, after loading was complete and prior to liftoff, was 1,746 kilograms (3,850 lbm).

The following anomalies were noted:

- a. During PTCS checkout, S-II Automatic Pneumatic On was lost at the S-II LH<sub>2</sub> console in the LCC. The setting of pressure switch 3 was too close to the operating pressure of the valve control assembly on level 120 and caused a dropout when the valve was cycled. The low resolution gages used to reverify the regulator pressure settings aggravated the problem. The pressures were set by installation of a Heise gage and adjusting the regulators accordingly. This anomaly could cause a hold in AS-502 testing or launch if no corrective action is taken to increase the differential pressure between the pressure switch and regulator settings.
- b. The vehicle vent system filling with water at the burn pond after a loading operation was an anomaly common to both CDDT and launch count-down. This was attributed to a siphoning action through the standpipes, which was initiated by rapid closing of the S-II and S-IVB vent valves after stage vent. The fluid dynamics of the GH<sub>2</sub> in the vent system caused a negative pressure when the vents were closed and pulled a small vacuum at the standpipes, thus starting the siphoning. This could result in an inability to vent GH<sub>2</sub> through the vehicle vent system during AS-502 CDDT and launch if no corrective action is taken. A procedural change to initiate a purge in the vent line during venting has been incorporated as a workaround.

Recommendations for corrective action are as follows:

- a. Change valve control assembly pressure settings and install high quality calibrated gages.
- b. Install an automatic helium purge system in the LH<sub>2</sub> storage area.
- c. Install a purge regulator and gage in the LH<sub>2</sub> storage area for maintaining standby helium blanket pressure.
- d. Install vent line valves to isolate the burn pond from the LUT vent lines.
- e. Relocate the S-IVB heat exchanger purge line closer to the DAC/Boeing interface for a more efficient purge.
- f. Provide a means for venting the hydrogen transport trailers after a tank fill operation.
- g. Install pneumatic console reliefs to prevent cabinet rupture during launch.
- h. Provide a stronger support bracket on the S-II drain line at the 100-foot level.

- i. Install a vacuum pumpdown valve on the  $\text{LH}_2$  storage tank boot.
- j. Install a sample vent valve on the 4-inch storage area vent line for safer  $\text{LH}_2$  sampling.

#### 3.4.4 Cold Helium Loading

Pressurization of the four cold helium spheres in the S-IC LOX tank was accomplished in two steps utilizing helium from the ground support equipment (GSE) cold gas system. Prior to LOX loading, the spheres were pressurized to approximately  $1034 \text{ N/Cm}^2$  (1500 psia) to prevent them from collapsing as they cooled during the initial part of the LOX loading. After 98 percent of the LOX had been tanked, the sphere pressure was raised to  $2082 \text{ N/Cm}^2$  (3020 psia) where it remained until liftoff.

The eight S-IVB cold helium spheres in the  $\text{LH}_2$  tank were also filled in two steps. The final liftoff mass in the spheres was 151 kilograms (332 lbm) at a pressure of  $2006 \text{ N/Cm}^2$  (2910 psia).

#### 3.4.5 Auxiliary Propulsion System Propellant Loading

The Auxiliary Propulsion System (APS) functioned as expected during propellant loading and no delays resulted.

The APS loading history prior to launch follows:

##### a. Module 1

##### (1) Oxidizer System (Nitrogen Tetroxide, $\text{N}_2\text{O}_4$ )

Volume loaded  $67,219.74 \text{ centimeters}^3$  ( $4102 \text{ in.}^3$ ) at  $300^\circ\text{K}$  ( $81^\circ\text{F}$ )

Volume off-loaded  $6095.99 \text{ centimeters}^3$  ( $372 \text{ in.}^3$ ) at  $298^\circ\text{K}$  ( $76^\circ\text{F}$ )

Volume removed with bubble bleed during burp firing  $458.84 \text{ centimeters}^3$  ( $28 \text{ in.}^3$ ) at  $304^\circ\text{K}$  ( $87^\circ\text{F}$ )

Volume removed with bubble bleed during countdown  $2458.06 \text{ centimeters}^3$  ( $150 \text{ in.}^3$ ) at  $304^\circ\text{K}$  ( $87^\circ\text{F}$ )

##### (2) Fuel System

Volume loaded  $67,219.74 \text{ centimeters}^3$  ( $4102 \text{ in.}^3$ ) at  $302^\circ\text{K}$  ( $84^\circ\text{F}$ )

Volume off-loaded  $1442.06 \text{ centimeters}^3$  ( $88 \text{ in.}^3$ ) at  $298^\circ\text{K}$  ( $77^\circ\text{F}$ )

Volume removed during countdown  $327.74 \text{ centimeters}^3$  ( $20 \text{ in.}^3$ ) at  $304^\circ\text{K}$  ( $87^\circ\text{F}$ )

b. Module 2

(1) Oxidizer System (Mono Methyl Hydrazine, MMH)

Volume loaded 67,219.74 centimeters<sup>3</sup> (4102 in.<sup>3</sup>) at 300°K (81°F)

Volume off-loaded 6095.99 centimeters<sup>3</sup> (372 in.<sup>3</sup>) at 299°K (79°F)

Volume removed with bubble bleed during burp firing 1147.09 centimeters<sup>3</sup> (70 in.<sup>3</sup>) at 304°K (87°F)

Volume removed with bubble bleed during countdown 327.74 centimeters<sup>3</sup> (20 in.<sup>3</sup>) at 304°K (87°F)

(2) Fuel System

Volume loaded 67,219.74 centimeters<sup>3</sup> (4102 in.<sup>3</sup>) at 302°K (84°F)

Volume off-loaded 1442.06 centimeters<sup>3</sup> (88 in.<sup>3</sup>) at 302°K (84°F)

Volume removed with bubble bleed during countdown 409.68 centimeters<sup>3</sup> (25 in.<sup>3</sup>) at 304°K (87°F)

3.4.6 S-IC Stage Propellant Load

Initial propellant loads obtained from the KSC weight and balance log were checked against the continuous level sensor data. The LOX load agreed very well, but the fuel load was approximately 1115 kilograms (2459 lbm) less. The reconstruction, utilizing an RPM match, was able to follow the continuous level sensor data for both LOX and fuel with an accuracy of  $\pm 1.27$  centimeters ( $\pm 0.5$  in.). It also matched the residuals calculated from level sensor and line pressure data, indicating that the propellant loads calculated from the level sensor data are accurate. The reconstructed fuel load was 0.18 percent low, which is well within the predicted 3 sigma limits of  $\pm 0.5$  percent. Total propellants onboard at ignition command are shown in Table 3-3.

3.4.7 S-II Stage Propellant Load

The S-II LOX tank was entirely filled through the 6-inch replenish line at a slow rate of 0.0574 m<sup>3</sup>/sec (900 gpm) maximum. The facility Propellant Tanking Control System (PTCS) functioned satisfactorily during S-II loading and replenishing. The LOX capacitance probe fine mass indication was slightly high (87.87 vs 87.72 percent planned). The best estimates of propellants loaded are 69,416 kilograms (153,036 lbm) LH<sub>2</sub> and 358,416 kilograms (790,171 lbm) LOX based on flowmeter integration from the 3 percent point sensor indicated mass and the 2 percent LOX point sensor indicated mass. This compares to predicted values of 69,569 kilograms (153,375 lbm) LH<sub>2</sub> and 359,037 kilograms (791,542 lbm) LOX. Table 3-4 presents the S-II stage propellant load at S-IC ignition command.

3-10

MASS REQUIREMENTS				MASS INDICATIONS			MASS DEVIATIONS	
PROPELLANT	UNITS	PREDICTED PRIOR TO LAUNCH <sup>1</sup>	LOADING TABLE AT IGNITION <sup>2</sup>	KSC MASS READOUT	RECONSTRUCTED LOAD <sup>2</sup>	KSC MINUS IGNITION	RECONS'T MINUS IGNITION	RECONS'T MINUS PREDICTED
Lox	kg lbm %	1,421,113 3,133,018	1,421,434 3,133,726	Same As Loading Table Data At Ign.	1,421,434 3,133,726	0 0	0 0 0	321 708 .02
Fuel	kg lbm %	616,309 1,358,729	615,988 1,358,021		614,873 1,355,562	0 0	-1115 -2459 -0.18	-1436 -3167 -0.23
Total	kg lbm %	2,037,422 4,491,747	2,037,422 4,491,747		2,036,307 4,489,288	0 0	-1115 -2459 -0.05	-1115 -2459 -0.05

<sup>1</sup> Based on LOX density of 1137.31 kg/m<sup>3</sup> (71.00 lbm/ft<sup>3</sup>) and fuel density of 802.52 kg/m<sup>3</sup> (50.100 lbm/ft<sup>3</sup>)

<sup>2</sup> Based on LOX density of 1136.11 kg/m<sup>3</sup> (70.93 lbm/ft<sup>3</sup>) and fuel density of 802.12 kg/m<sup>3</sup> (50.075 lbm/ft<sup>3</sup>)



Table 3-4. S-II Stage Propellant Mass At S-IC Ignition Command

PROPELLANT	UNITS	PREDICTED PRIOR TO LAUNCH	INDICATED	BEST ESTIMATE	INDICATED MINUS PREDICTED	BEST ESTIMATE MINUS PREDICTED
LOX	kg	359,037	359,013	358,416	-24	- 621
	lbm	791,542	791,489	790,171	-53	-1371
	%				- 0.007	- 0.17
Fuel	kg	69,569	69,596	69,416	27	- 153
	lbm	153,375	153,432	153,036	57	- 339
	%				0.04	- 0.22
Total	kg	428,606	428,609	427,832	3	- 774
	lbm	944,917	944,921	943,207	4	-1710
	%				0.0004	- 0.18

### 3.4.8 S-IVB Stage Propellant Load

The best estimate S-IVB propellant mass values at S-IC ignition command were 88,141 kilograms (194,318 lbm) LOX and 18,656 kilograms (41,130 lbm) LH<sub>2</sub> as compared to desired mass values of 87,667 kilograms (193,273 lbm) LOX and 18,698 kilograms (41,222 lbm) LH<sub>2</sub>. These values were well within required loading accuracies. Table 3-5 presents the S-IVB stage propellant load at S-IC ignition command.

### 3.5 S-II INSULATION PURGE AND LEAK DETECTION

Performance of the S-II insulation to control the LH<sub>2</sub> boiloff rate was well within specification requirements. Heat transmitted through the insulation to the liquid hydrogen is calculated as  $1.85 \times 10^8$  watts (180,000 Btu), which is 16 percent below the maximum allowable specification requirement of  $2.27 \times 10^8$  watts (215,000 Btu). External insulation surface temperatures were lower than predicted.

Hazardous gas concentrations were low in all circuits during the prelaunch hold. No concentration of GH<sub>2</sub> or GO<sub>2</sub> was detected in any circuit greater than 100 ppm. GN<sub>2</sub> concentrations in the common bulkhead reached 700 ppm during LH<sub>2</sub> fill. However, this is consistent with previous data from Mississippi Test Facility (MTF) operations (see Table 3-6). Gas concentrations are launch constraints only when GO<sub>2</sub> is in excess of 450 ppm in the common bulkhead prior to LH<sub>2</sub> loading, or when GH<sub>2</sub> reaches 10,000 ppm in the common bulkhead or 100,000 ppm in the feedline circuit after initiation of LH<sub>2</sub> fill.

During the countdown the following anomalies were noted in this system:

- a. During operational television (OTV) scan of S-II insulation at the start of LH<sub>2</sub> fill, using OTV cameras 34 and 35 at ground level (420 feet from the Mobile Launcher) and cameras 9 and 16 on the Mobile Launcher (160 foot level), helium vapor was detected near feedlines 1, 4, and 5. It appeared to be venting from under the fairings covering these LH<sub>2</sub> feedlines. The source of the vapor could not be determined since it was not shown that the leak came from the insulation; and since any defect in the insulation would have been protected by fairings from wind stream in flight, no action was taken.
- b. OTV scan 45 minutes prior to launch detected two blisters in the close-out seal at approximately stringer 120, Station 565. They were less than 2 inches diameter as shown by honeycomb cell outline. No vapor was observed coming from the area which indicated no external leakage or surface defect. Insulation integrity was judged acceptable due to excellent OTV inspection detail and the absence of any change in sidewall insulation pressure.

Table 3-5. S-IVB Stage Propellant Mass At S-IC Ignition Command

PROPELLANT	UNITS	PREDICTED PRIOR TO LAUNCH	INDICATED	BEST ESTIMATE	INDICATED MINUS PREDICTED	BEST ESTIMATE MINUS PREDICTED
LOX	Kg	87,667	87,624	88,141	-43	474
	LBM	193,273	193,179	194,318	-94	1,045
	%				- 0.05	-0.54
Fuel	Kg	18,698	18,656	18,656	-42	-42
	LBM	41,222	41,129	41,130	-93	-92
	%				-0.23	-0.22
TOTAL	Kg	106,365	106,280	106,797	-85	432
	LBM	234,495	234,308	235,448	-187	953
	%				-0.08	0.41

Table 3-6. Effluent Gas Concentrations

	MAXIMUM GAS CONCENTRATION MTF - LH <sub>2</sub> TANK ULLAGE PRESSURE 15 N/cm <sup>2</sup> (22 psig)									AS-501 CDDT			AS-501 COUNTDOWN				
	TEST 523				TEST 525				TEST 526								
	H <sub>2</sub>	O <sub>2</sub>	N <sub>2</sub>		H <sub>2</sub>	O <sub>2</sub>	N <sub>2</sub>		H <sub>2</sub>	O <sub>2</sub>	N <sub>2</sub>	H <sub>2</sub>	O <sub>2</sub>	N <sub>2</sub>	H <sub>2</sub>	O <sub>2</sub>	N <sub>2</sub>
Forward Bulkhead Insulation	25 PPM	100 PPM	100 PPM	35 PPM	100 PPM	100 PPM	--	100 PPM	100 PPM								100 PPM
Forward Bulkhead Uninsulated	100 PPM	100 PPM	100 PPM	40 PPM	100 PPM	100 PPM	--	100 PPM	100 PPM	Less than 100 PPM	Less than 100 PPM	Less than 100 PPM	Less than 100 PPM	Less than 100 PPM	Less than 100 PPM	Less than 100 PPM	100 PPM
Sidewall	20 PPM	100 PPM	100 PPM	700 PPM	100 PPM	100 PPM	--	100 PPM	100 PPM	Less than 100 PPM	Less than 100 PPM	Less than 100 PPM	Less than 100 PPM	Less than 100 PPM	Less than 100 PPM	Less than 100 PPM	100 PPM
Common Bulkhead	30 PPM	100 PPM	100 PPM	25 PPM	100 PPM	100 PPM	--	100 PPM	100 PPM								700 PPM
J-Ring	20 PPM	100 PPM	100 PPM	25 PPM	100 PPM	100 PPM	--	100 PPM	100 PPM								100 PPM
Feedline elbows	--	100 PPM	100 PPM	--	100 PPM	100 PPM	--	100 PPM	100 PPM								100 PPM

- c. The 30-minute pressure test of the common bulkhead forward facing sheet after LH<sub>2</sub> fill was deleted. This decision was based on the effect back pressure from the facility venting system would have on other stages at the time of S-II depressurization and the time required (in excess of 1 hour) to re-establish thermal stability. Past experience at MTF has revealed no leakage, the pressure test of the aft facing sheet after S-II LOX loading indicated no G<sub>02</sub> leakage, and a measurement of GH<sub>2</sub> leakage is obtained during the hold period just prior to launch.
- d. Feedline outlet pressure fell to 0.34N/Cm<sup>2</sup> (0.5 psig) during LH<sub>2</sub> fill and flowmeter indication was lost during cryogenic fill. These facts indicate closure of the back pressure regulator which would invalidate gas concentrations data for this circuit.

### 3.6 GROUND SUPPORT EQUIPMENT

Ground systems performance was exceptionally good. Swing arms, holddown arms, tail service masts, propellant tanking systems and all other ground equipment functioned well together to support the AS-501 launch. Minor anomalies that occurred did not present any serious problems. A dropout of ground camera power and timing signals experienced just prior to liftoff was the most significant deviation from expected performance. This resulted in cameras not starting, short runs, jamming, and a lack of timing signals.

Launch damage was, in general, less than expected. However, there were specific items that received extensive damage. Refurbishment is not expected to have any impact on future launch schedules. The following conditions of major damage were observed:

- a. Fires in the swing arm hinge areas on arms 1, 2, 3, and 4 exposed hinges, hinge bearings, retract cylinders, flex hoses and tubing, in these areas, to high temperatures.
- b. All tail service mast hoods were carried away by exhaust blast allowing the aft umbilical carriers and service lines to be damaged by engine blast and fire.
- c. Holddown arm hoods were slightly warped and electrical line and pneumatic distributors inside damaged by flame.
- d. The LUT level platform was completely destroyed and the engine service platform and transporter damaged extensively. The transporter winches were also damaged significantly.
- e. Storage racks and stored equipment on the LUT 60, 100, and 120 foot levels were badly damaged.
- f. Six OTV cameras were destroyed and four were damaged but can be repaired.



## SECTION 4 TRAJECTORY ANALYSIS

### 4.1 SUMMARY

The actual trajectory of AS-501 was close to nominal. The vehicle was launched on an azimuth of 90 degrees east of north. At 11.06 seconds, the vehicle started a maneuver to a flight azimuth of 72 degrees east of north. The space-fixed velocity at S-IC OECO was 19.80 m/s (64.96 ft/s) lower than nominal. At S-II cutoff it was 38.61 m/s (126.67 ft/s) lower than nominal and 1.24 m/s (4.07 ft/s) lower than nominal at S-IVB first burn cutoff. At S-IVB first burn cutoff the altitude was 1.17 kilometers (0.63 n mi) higher than nominal and the surface range was 44.17 kilometers (23.85 n mi) greater than nominal. The cross range velocity deviated 1.52 m/s (4.99 ft/s) to the right of nominal at S-IVB first burn cutoff.

At waiting orbit injection the actual values of the targeting parameters were very close to nominal. The eccentricity was 0.0028 less than nominal, the inclination was 0.011 degrees less than nominal, the node was 0.004 degrees greater than nominal and C3 was 187,669 m<sup>2</sup>/s<sup>2</sup> (2,020,050 ft<sup>2</sup>/s<sup>2</sup>) less than nominal. At waiting orbit injection the total space-fixed velocity was 11.4 m/s (37.4 ft/s) greater than nominal and the altitude was 24.25 kilometers (13.09 n mi) less than nominal.

The loss of telemetry signal of the S-IC stage occurred at approximately 410.0 seconds. This is close to time when the S-IC stage lost its structural integrity. At this time the actual surface range and altitude as determined from a theoretical free-flight simulation were within 1.1 kilometers (0.59 n mi) and 0.8 kilometer (0.4 n mi), respectively, of nominal. The free-flight trajectory indicates the S-II stage impacted 197.76 kilometers (106.78 n mi) short of the nominal impact point. The S-IVB free-flight trajectory indicates the impact occurred close to the nominal, but almost 11 minutes earlier than nominal.

A summary of all AS-501 orbital C-band tracking performed by various stations is presented in Table 4-1.

### 4.2 ASCENT TRAJECTORY

#### 4.2.1 Tracking Data Utilization

Tracking data was obtained during the period from 0.03 seconds through parking orbit insertion. This data, excluding radars, showed less than

0.05 kilometers (0.03 n mi) deviation in position components measured by the various systems in the period up to 266 seconds. After 266 seconds, GLOTRAC Segment I was the only precision tracking system that furnished data.

The postflight trajectory was established from a least squares curve fit of the fixed camera data tied to a best estimate trajectory. The telemetered guidance values were used as a model for obtaining the proper velocity and acceleration profiles through the transient areas. These data points were adjusted in magnitude to match the best estimate trajectory.

The best estimate trajectory, as determined by the GATE program, utilized the telemetered guidance velocities as the generating parameters to fit data from GLOTRAC Station I, and six different C-Band radar tracking stations. These data points were fit through a nine term guidance error model and constrained to the insertion vector obtained from the orbital solution. Comparison of the best estimate trajectory with data from all the tracking systems yielded reasonable agreement.

GLOTRAC Segment I provided the only precision tracking data after 266 seconds. The GLOTRAC Segment I data and the best estimate trajectory agree to within 0.04 kilometers (0.02 n mi) in X (downrange), 0.13 kilometers (0.070 n mi) in Z (cross range) and 0.72 kilometers (0.39 n mi) in Y (vertical). The vertical component experienced a discontinuity at handovers. Before handover the vertical component difference was about 0.25 kilometers (0.14 n mi); this indicates that the vertical component in the trajectory was less accurate than the other components. The GLOTRAC Segment I data were not used in the final trajectory due to late arrival and a tape format problem.

Table 4-1. Summary of AS-501 Orbital C-Band Tracking Stations

STATION	REVOLUTION 1	REVOLUTION 2	REVOLUTION 3
Bermuda (FPS-16)	X		X
Bermuda (FPQ-6)		X	X
Carnarvon	X	X	
Hawaii		X	
White Sands	X	X	
California	X	X	
Grand Bahama			X
Merritt Island			X
Antigua			X
Canary Island		X	X
Tananarive		X	
Woomera	X		
Ascension			X

X - Station performing tracking



Table 4-2. Comparisons of Cutoff Events

PARAMETER	ACTUAL	NOMINAL	ACT-NOM	ACTUAL	NOMINAL	ACT-NOM
S-IC IEEO			S-IC OEEO			
Range Time sec	135.5	135.5	0.0	150.8	151.9	-1.1
Altitude km (n mi)	49.64 (26.80)	48.46 (26.17)	1.18 (0.63)	63.70 (34.40)	63.61 (34.35)	0.09 (0.05)
Surface Range km (n mi)	54.29 (29.31)	53.75 (29.02)	0.54 (0.29)	82.63 (44.62)	85.01 (45.90)	-2.38 (-1.28)
Space-Fixed Velocity m/s (ft/s)	2207.20 (7241.47)	2179.62 (7150.98)	27.58 (90.49)	2691.81 (8831.49)	2711.61 (8896.36)	-19.80 (-64.87)
Flight Path Angle deg	23.275	22.955	0.320	20.955	20.330	0.625
Heading Angle deg	75.952	76.376	-0.424	75.293	75.624	-0.331
Cross Range km (n mi)	0.45 (0.24)	0.76 (0.41)	-0.31 (-0.17)	0.56 (0.30)	1.12 (0.60)	-0.56 (-0.30)
Cross Range Velocity m/s (ft/s)	7.82 (25.66)	21.34 (70.01)	-13.52 (-44.35)	5.45 (17.89)	21.16 (69.42)	-15.71 (-51.53)
S-II ECO			S-IVB ECO			
Range Time sec	519.8	516.3	3.5	665.6	656.0	9.6
Altitude km (n mi)	192.34 (103.86)	189.74 (102.45)	2.60 (1.41)	192.61 (104.00)	191.44 (103.37)	1.17 (0.63)
Surface Range km (n mi)	1477.64 (797.86)	1471.79 (794.70)	5.85 (3.16)	2448.25 (1321.95)	2404.08 (1298.10)	44.17 (23.85)
Space-Fixed Velocity m/s (ft/s)	6813.99 (22,355.61)	6852.60 (22,482.28)	-38.61 (-126.67)	7789.76 (25,556.96)	7791.00 (25,561.02)	-1.24 (-4.06)
Flight Path Angle deg	0.642	0.523	0.119	0.015	-0.001	0.016
Heading Angle deg	81.485	81.429	0.056	87.210	86.965	0.241
Cross Range km (n mi)	21.62 (11.67)	22.99 (12.41)	-1.37 (-0.74)	51.25 (27.67)	51.03 (27.55)	0.22 (0.12)
Cross Range Velocity m/s (ft/s)	155.84 (511.29)	152.91 (501.67)	2.93 (9.62)	256.69 (842.16)	255.17 (837.17)	1.52 (4.99)
S-IVB (2) ECO						
Range Time sec	11,786.3	11,799.4	-13.1			
Altitude km (n mi)	538.44 (290.73)	562.32 (303.63)	-23.88 (-12.90)			
Space-Fixed Velocity m/s (ft/s)	9412.73 (30,881.65)	9399.93 (30,839.67)	12.80 (41.98)			
Flight Path Angle deg	14.766	15.026	-0.260			
Heading Angle deg	102.379	102.641	-0.262			

Table 4-3. Comparisons of Separation Events

S-IC/S-II SEPARATION			
PARAMETER	ACTUAL	NOMINAL	ACT-NOM
Range Time sec	151.4	152.7	-1.3
Altitude km (n mi)	64.35 (34.75)	64.34 (34.74)	0.01 (0.01)
Surface Range km (n mi)	84.01 (45.36)	86.65 (46.79)	-2.64 (-1.43)
Space-Fixed Velocity m/s (ft/s)	2700.71 (8860.60)	2721.20 (8927.82)	-20.49 (-67.22)
Flight Path Angle deg	20.855	20.214	0.641
Heading Angle deg	75.287	75.619	-0.332
Cross Range km (n mi)	0.56 (0.30)	1.14 (0.62)	-0.58 (-0.32)
Cross Range Velocity m/s (ft/s)	5.46 (17.91)	21.24 (69.69)	-15.78 (-51.78)
S-II/S-IVB SEPARATION			
PARAMETER	ACTUAL	NOMINAL	ACT-NOM
Range Time sec	520.5	517.2	3.3
Altitude km (n mi)	192.40 (103.89)	189.89 (102.53)	2.51 (1.36)
Surface Range km (n mi)	1481.87 (800.15)	1477.27 (797.66)	4.60 (2.49)
Space-Fixed Velocity m/s (ft/s)	6816.54 (22,363.98)	6857.48 (22,498.29)	-40.94 (-134.31)

Table 4-3. Comparisons of Separation Events (Cont)

S-II/S-IVB SEPARATION (CONT)			
PARAMETER	ACTUAL	NOMINAL	ACT-NOM
Flight Path Angle deg	0.632	0.514	0.118
Heading Angle deg	81.510	81.461	0.049
Cross Range km (n mi)	21.72 (11.73)	23.13 (12.49)	-1.41 (-0.76)
Cross Range Velocity m/s (ft/s)	156.26 (512.66)	153.46 (503.48)	2.80 (9.18)
S-IVB/CSM SEPARATION			
PARAMETER	ACTUAL	NOMINAL	ACT-NOM
Range Time sec	12,388.2	12,399.6	-11.4
Altitude km (n mi)	2423.30 (1308.48)	2457.37 (1326.87)	-34.07 (-18.39)
Space-Fixed Velocity m/s (ft/s)	7995.02 (26,230.38)	7984.96 (26,197.38)	10.06 (33.00)
Flight Path Angle deg	26.542	26.715	-0.173
Heading Angle deg	116.450	116.496	-0.046

#### 4.2.2 Trajectory Evaluation

Actual and nominal altitude, surface range, and cross range for the first powered phase are presented in Figure 4-1. The actual and nominal total earth-fixed velocities and the elevation angles of the velocity vectors are shown in Figure 4-2. Actual and nominal space-fixed velocity and flight path angle during ascent are shown in Figure 4-3. Comparisons of the actual and nominal cutoff events are shown in Table 4-2. Comparisons of the actual and nominal separation events are shown in Table 4-3. The nominal trajectory is presented in "Saturn V AS-501 Launch Vehicle Operational Flight Trajectory-Final," Boeing document D5-15551(F)-1.

Through the major portion of the first powered phase the altitude was greater than nominal and the surface range was slightly less than nominal. The total

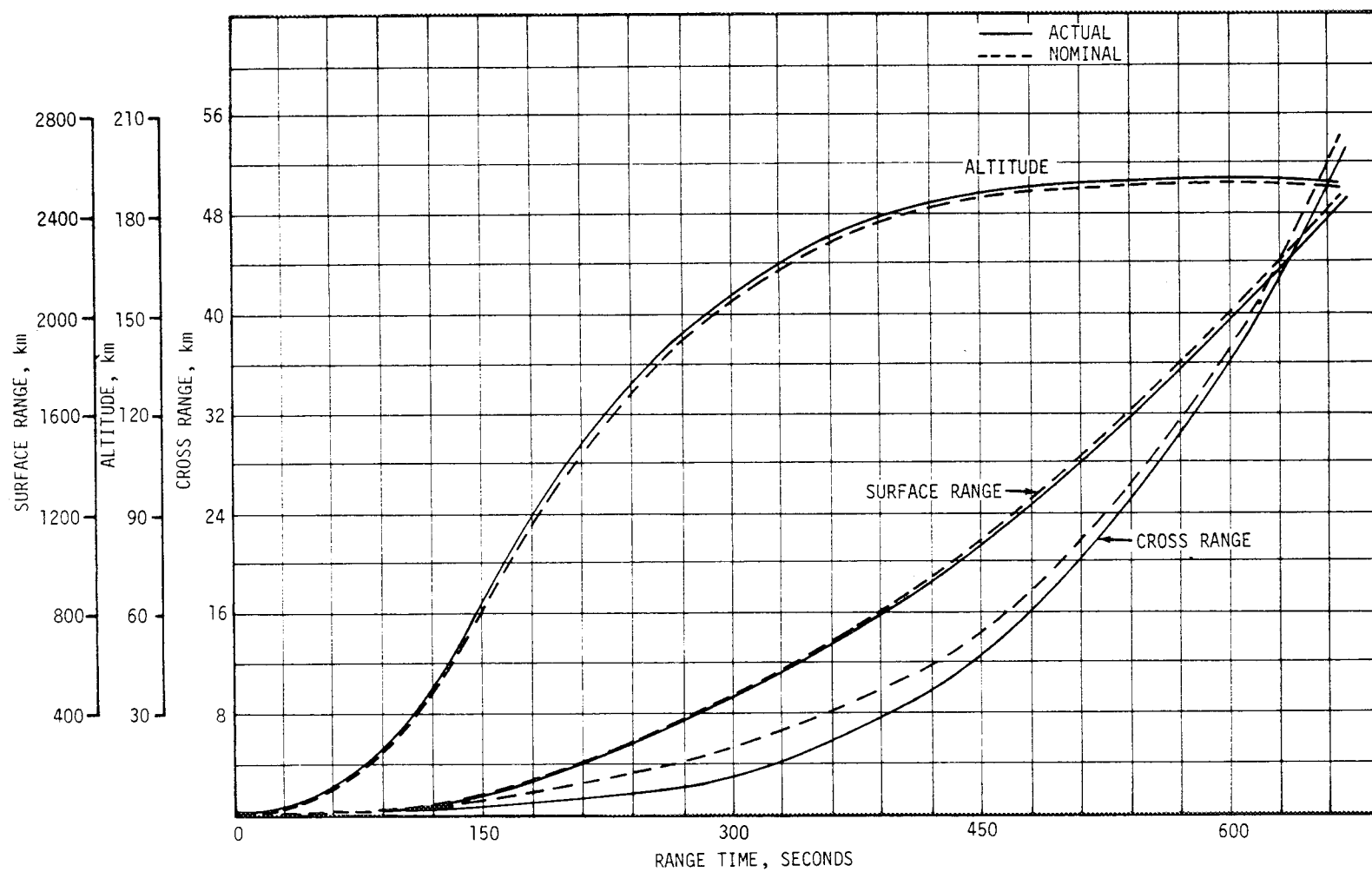


Figure 4-1. Ascent Trajectory Position Comparison

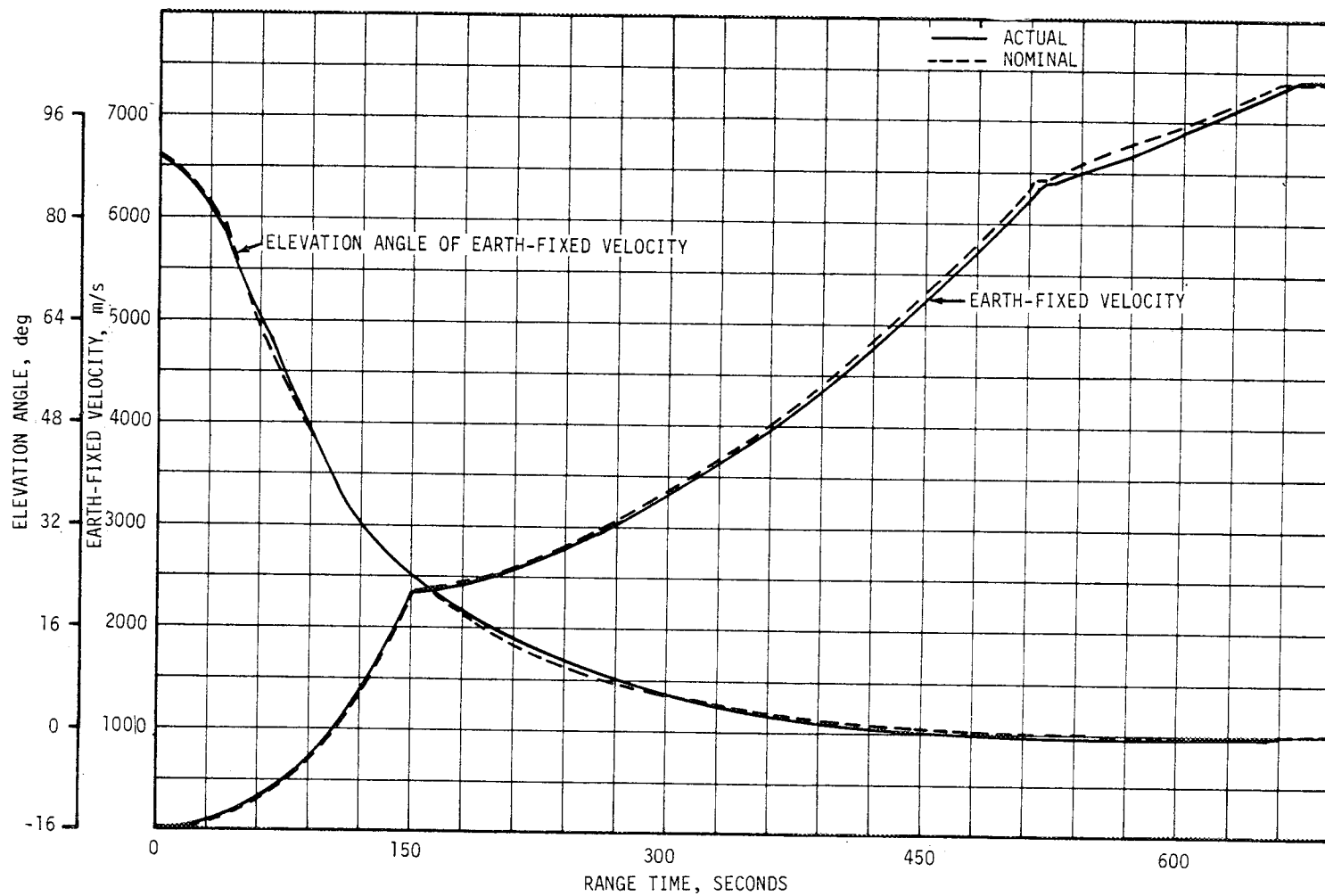


Figure 4-2. Ascent Trajectory Earth-Fixed Velocity Comparison

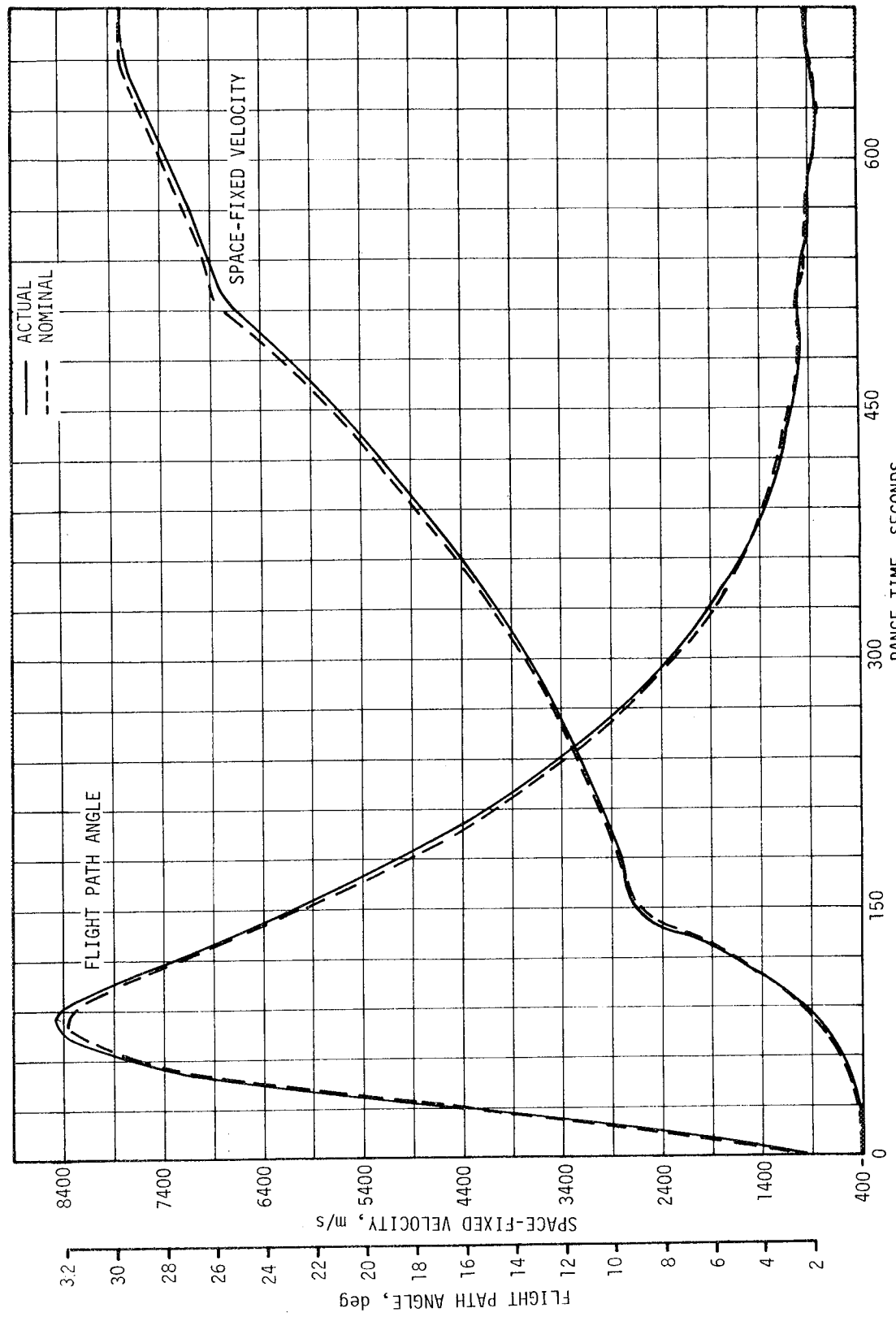


Figure 4-3. Ascent Space-Fixed Velocity Comparison

inertial acceleration shown in Figure 4-4 was greater than nominal for the S-IC phase and less than nominal for the S-II and S-IVB first burn phases.

The combined burn time of the S-IC, S-II, and S-IVB first burn was 9.6 seconds longer than nominal. The S-IC burned 1.1 seconds less than nominal, the S-II burned 4.6 seconds longer than nominal and the S-IVB first burn was 6.1 seconds longer than nominal. The total space-fixed velocity at the S-IVB first burn cutoff was 1.24 m/s (4.07 ft/s) lower than nominal. The longer burn time explains the 44.17 kilometers (23.85 n mi) greater surface range at the S-IVB first burn cutoff. The altitude at S-IVB first burn cutoff was 1.17 kilometers (0.63 n mi) greater than nominal. The accuracy of the trajectory at S-IVB first burn cutoff is estimated to be  $\pm 1.0$  m/s (3.3 ft/s) velocity and  $\pm 0.7$  kilometers (0.4 n mi) altitude.

The guidance sensed velocity increase, due to engine cutoff impulse, during the time period from guidance signal for S-IC OECO to first plane separation is shown in Table 4-4. A similar velocity increase during the period from S-II ECO signal to S-II/S-IVB separation signal is also shown. Also shown is the guidance sensed velocity increase due to complete engine cutoff impulse after S-IVB first burn ECO signal. The S-IVB first burn ECO signal was given by the guidance computer at 665.6 seconds.

Mach number and dynamic pressure are shown in Figure 4-5. These parameters were calculated using measured meteorological data to an altitude of 52.5 kilometers (28.3 n mi). Above this altitude the measured data were merged into the U.S. Standard Reference Atmosphere.

Table 4-4. Velocity Gains Sensed by Guidance System after ECO Signal

	ACTUAL m/s (ft/s)	NOMINAL m/s (ft/s)
S-IC OECO	9.1 (29.9)	11.0 (36.1)
S-II ECO	4.7 (15.4)	4.2 (13.8)
First S-IVB ECO	1.7 (5.6)	2.1 (6.9)

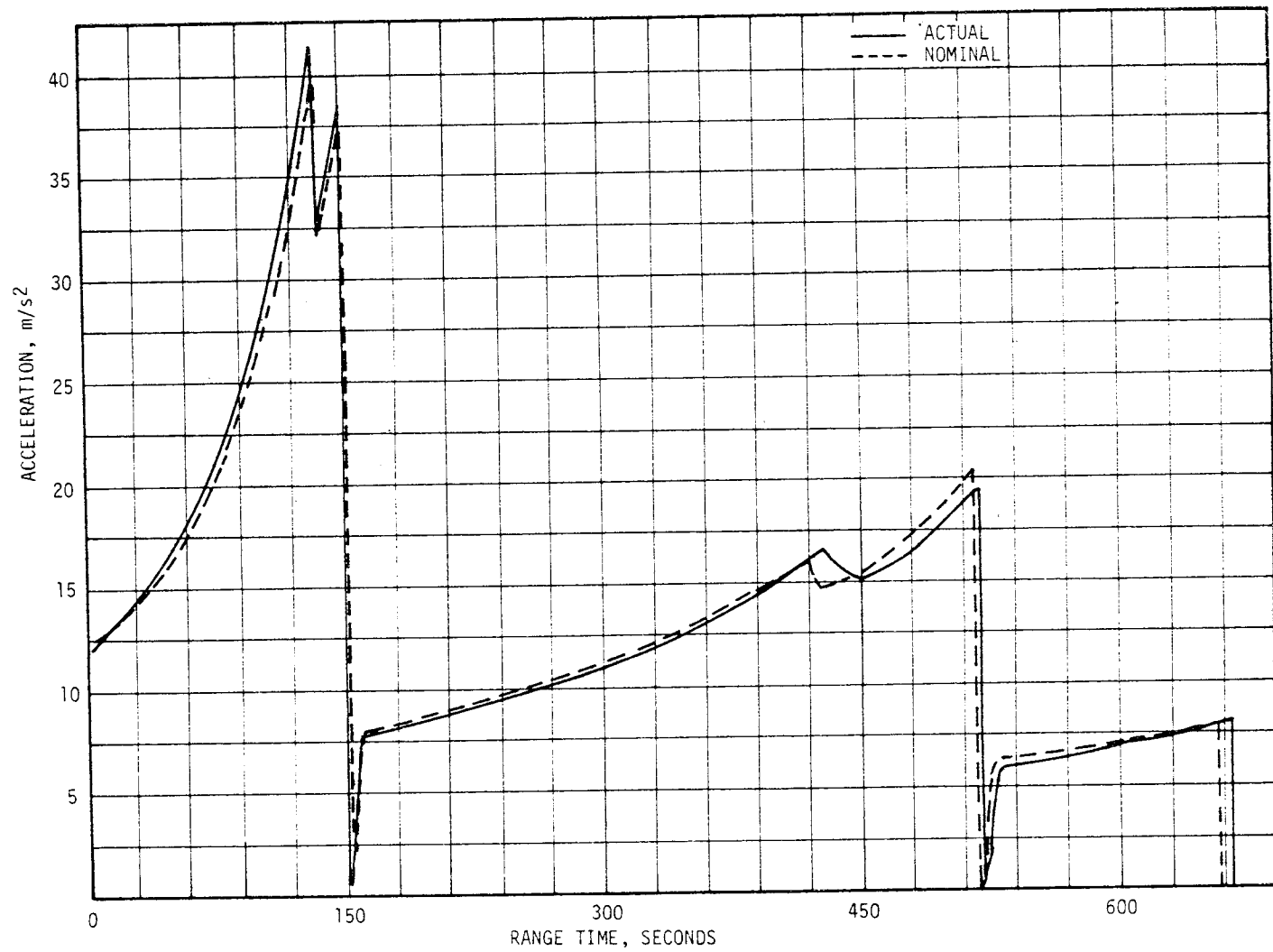


Figure 4-4. Ascent Trajectory Acceleration Comparison



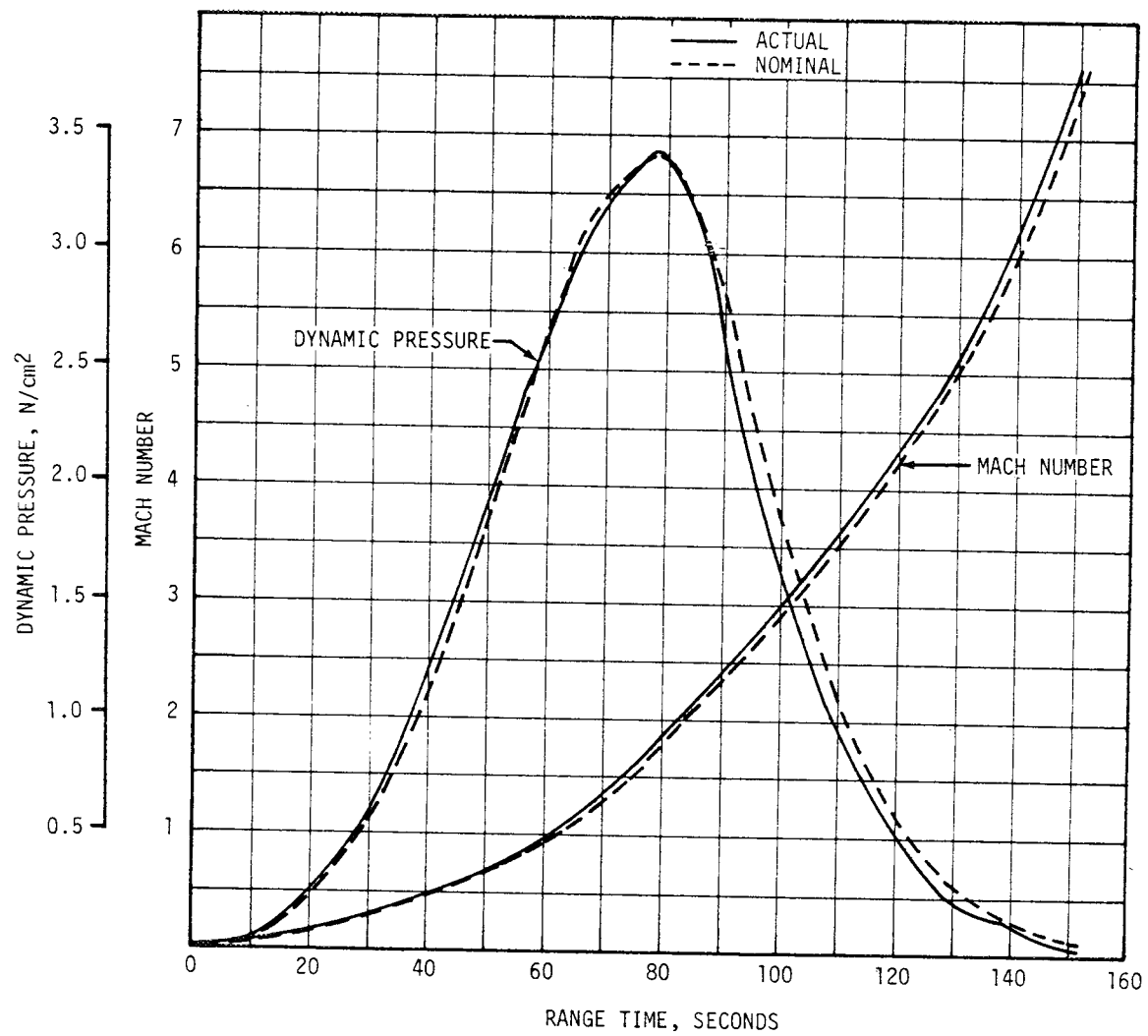


Figure 4-5. Dynamic Pressure and Mach Number vs Range Time

Table 4-5. Comparison of Significant Trajectory Events

EVENT	PARAMETER	ACTUAL	NOMINAL	ACT-NOM
First Motion	Range Time sec	-0.48	-0.48	0.00
	Total Inertial Acceleration m/s <sup>2</sup> (ft/s <sup>2</sup> )	10.02 (32.87)	12.21 (40.06)	-2.19 (-7.19)
Mach 1	Range Time sec	61.4	62.0	-0.6
	Altitude km (n mi)	7.35 (3.97)	7.53 (4.07)	-0.18 -0.10
Maximum Dyanmic Pressure	Range Time sec	78.4	78.4	0.0
	Dynamic Pressure N/cm <sup>2</sup> (psia)	3.437 (4.98)	3.424 (4.97)	0.013 (0.01)
	Altitude km (n mi)	13.26 (7.16)	13.21 (7.13)	0.05 (0.03)
Maximum Total Inertial	Range Time sec	135.6	135.1	0.5
Acceleration (S-IC Stage)	Acceleration m/s <sup>2</sup> (ft/s <sup>2</sup> )	41.27 (135.40)	40.26 (132.09)	1.01 (3.31)
Maximum Total Inertial	Range Time sec	520.0	516.4	3.6
Acceleration (S-II Stage)	Acceleration m/s <sup>2</sup> (ft/s <sup>2</sup> )	19.48 (63.91)	20.35 (66.77)	-0.87 (-2.86)
Maximum Total Inertial	Range Time sec	665.7	656.1	9.6
Acceleration (S-IVB)	Acceleration m/s <sup>2</sup> (ft/s <sup>2</sup> )	8.25 (27.07)	7.93 (26.02)	0.32 (1.05)
Apex (S-IC Stage)	Range Time sec	263.2	263.5	-0.3
	Surface Range km (n mi)	314.84 (170.00)	319.23 (172.37)	-4.39 (-2.37)
	Altitude km (n mi)	117.67 (63.54)	115.66 (62.45)	2.01 (1.09)
	Altitude km (n mi)	117.67 (63.54)	115.66 (62.45)	2.01 (1.09)
Apex (S-II Stage)	Range Time sec	556.0	547.5	8.5
	Surface Range km (n mi)	1701.90 (918.95)	1668.19 (900.75)	33.71 (18.20)
	Altitude km (n mi)	193.70 (104.59)	190.78 (103.01)	2.92 (1.58)
	Altitude km (n mi)	193.70 (104.59)	190.78 (103.01)	2.92 (1.58)
Apex (S-IVB Stage)	Range Time sec	20,202.5	20,543.0	-340.5
	Altitude km (n mi)	16,745.90 (9042.06)	17,410.00 (9400.65)	-664.10 (-358.59)
	Altitude km (n mi)	16,745.90 (9042.06)	17,410.00 (9400.65)	-664.10 (-358.59)
	Altitude km (n mi)	16,745.90 (9042.06)	17,410.00 (9400.65)	-664.10 (-358.59)
Loss of Telemetry (S-IC Stage)	Range Time sec	410.0	410.0	0.0
	Altitude km (n mi)	28.01 (15.12)	27.25 (14.71)	0.76 (0.41)
	Surface Range km (n mi)	604.78 (326.56)	605.89 (327.15)	-1.11 (-0.59)
	Elevation Angle From Pad deg	-0.018	-0.032	0.014
Maximum Earth-Fixed	Range Time sec	151.7	152.9	-1.2
Velocity (S-IC Stage)	Velocity m/s (ft/s)	2345.32 (7694.62)	2363.04 (7752.76)	-17.72 (-58.14)
Maximum Earth-Fixed	Range Time sec	520.8	517.5	3.3
Velocity (S-II Stage)	Velocity m/s (ft/s)	6419.21 (21,060.40)	6459.35 (21,192.09)	-40.14 (-131.69)
Maximum Earth-Fixed	Range Time sec	11,786.8	11,799.9	-13.1
Velocity (S-IVB Stage)	Velocity m/s (ft/s)	8997.63 (29,519.78)	8985.09 (29,478.64)	12.54 (41.14)
S-IVB Engine Restart	Range Time sec	11,486.6	11,484.5	2.1
Command	Altitude km (n mi)	203.62 (109.95)	204.73 (110.55)	-1.11 (-0.60)
	Space Fixed Velocity m/s (ft/s)	7786.65 (25,546.75)	7787.89 (25,550.82)	-1.24 (-4.07)
	Space-Fixed Flight Path Angle deg	-0.001	-0.009	0.008
	Space-Fixed Heading Angle deg	97.537	97.346	0.191
	Earth-Fixed Velocity m/s (ft/s)	7382.75 (24,221.62)	7383.87 (24,225.30)	-1.12 (-3.68)
	Geodetic Latitude deg	31.9509	31.9795	-0.0286
	Longitude deg	-82.3260	-82.7026	0.3766
	Longitude deg	-82.3260	-82.7026	0.3766
	Longitude deg	-82.3260	-82.7026	0.3766

Table 4-6. Stage Impact Location

PARAMETER	ACTUAL	NOMINAL	ACT-NOM
S-IC STAGE IMPACT			
Range Time sec	571.0	537.5	33.5
Surface Range km (n mi)	630.59 (340.49)	638.71 (344.88)	-8.12 (-4.39)
Cross Range km (n mi)	6.88 (3.71)	11.51 (6.21)	-4.63 (-2.50)
Geodetic Latitude deg	30.163	30.141	0.022
Longitude deg	-74.354	-74.261	-0.093
S-II STAGE IMPACT			
Range Time sec	1126.7	1153.2	-26.5
Surface Range km (n mi)	3915.74 (2114.33)	4113.50 (2221.11)	-197.76 (-106.78)
Cross Range km (n mi)	114.35 (61.74)	124.32 (67.13)	-9.97 (-5.39)
Geodetic Latitude deg	32.203	31.983	0.220
Longitude deg	-39.825	-37.746	-2.079
S-IVB STAGE IMPACT			
Range Time sec	28,987.2	29,645.3	-658.1
Geodetic Latitude deg	23.435	24.212	-0.777
Longitude deg	161.207	161.297	-0.090

Comparisons of actual and nominal parameters at significant trajectory event times are given in Table 4-5

The theoretical free-flight trajectory data for the discarded S-IC and S-II stages were based on initial conditions obtained from the final postflight

trajectory at separation. Some radar prints from an aircraft in the recovery area represented the only data available on the discarded S-IC stage. These radar prints can be correlated with a theoretical free-flight trajectory. They agree best with a free-flight which assumes a 90 degree angle-of-attack. Therefore, this case is used as the S-IC stage trajectory. Visual observation and the radar prints prove that the S-IC stage lost its structural integrity before impact.

There was no tracking coverage of the discarded S-II stage. A tumbling drag coefficient was assumed in the free-flight trajectory of the S-II stage. The impact times and locations of the S-IC stage pieces and the S-II stage are presented in Table 4-6.

#### 4.3 PARKING ORBIT TRAJECTORY

##### 4.3.1 Tracking Data Utilization

Table 4-7 presents a summary of the stations furnishing data for use in determining the parking orbit trajectory.

The orbital trajectory was obtained by taking the insertion conditions and integrating them forward at the desired time intervals. The insertion conditions were obtained by a differential correction procedure which adjusted the estimated insertion conditions to fit the tracking data in accordance with the weights assigned to the data.

Table 4-7. Parking Orbit Radar Stations

STATION	REVOLUTION 1	REVOLUTION 2
Bermuda (FPS-16)	X	
Carnarvon (FPQ-6)	X	
White Sands (FPS-16)	X	
Bermuda (FPQ-6)		X
Carnarvon (FPQ-6)		X
Hawaii (FPS-16)		X
White Sands (FPS-16)		X
Merritt Island (TPQ-18)		X*
Grand Bahama Island (TPQ-18)		X*
* Just prior to S-IVB second burn		

The Bermuda (FPS 16), Merritt Island and Grand Bahama Island radars provided comparatively few data points. The Bermuda data points were necessary to determine the insertion point accurately. The Merritt Island and Grand Bahama Island radars, which were tracking immediately prior to the S-IVB

second burn were used to determine initial conditions for the S-IVB second burn. Therefore, to insure reasonable agreement between the orbital and powered phases these data points were weighted more heavily than the data from the other stations

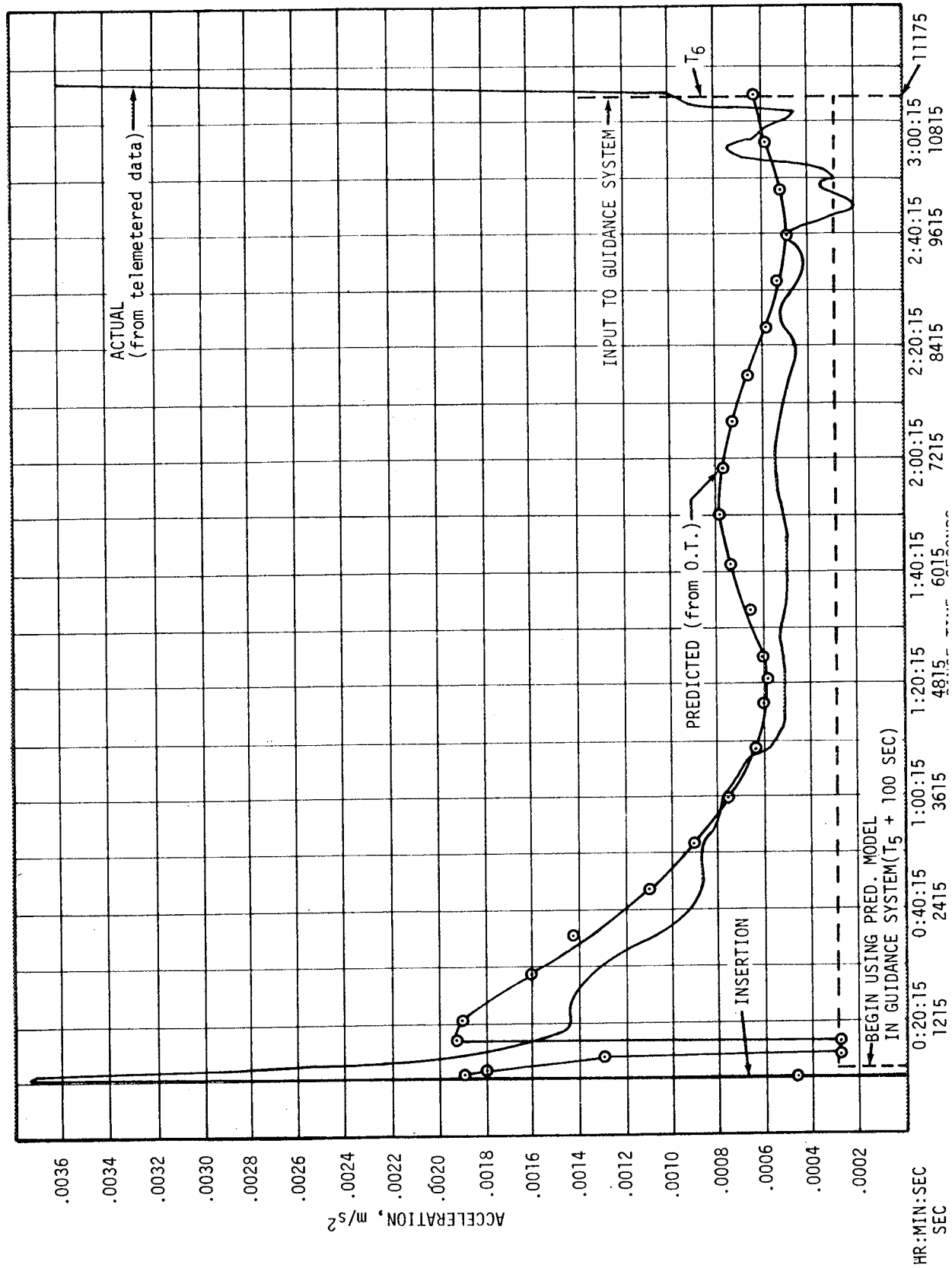
#### 4.3.2 Trajectory Evaluation

The acceleration during parking orbit due to venting is presented in Figure 4-6. Shown in this figure are the predicted venting accelerations used in the operational trajectory, the venting acceleration implemented in the guidance computer, and the actual venting acceleration obtained from the telemetered guidance data. The actual venting acceleration was obtained by differentiating the compressed guidance velocity data, removing accelerometer biases and the effect of drag.

Scatter in insertion parameter values was obtained depending upon the combination of data used and the weights applied to the data. The solutions that were considered reasonable had a spread of about  $\pm 0.5$  kilometers (0.3 n mi) in position components and  $\pm 1.0$  m/s (3.3 ft/s) in velocity components. The actual and nominal parking orbit insertion parameters are presented in Table 4-8.

Table 4-8. Parking Orbit Insertion Conditions

PARAMETER	ACTUAL	NOMINAL	ACT-NOM
Range Time sec	675.6	666.0	9.6
Space Fixed Velocity m/s (ft/s)	7791.8 (25,563.7)	7793.8 (25,570.2)	-2.0 (-6.5)
Flight Path Angle deg	0.014	0.001	0.013
Inclination deg	32.573	32.561	0.012
Eccentricity	0.0003	0.0002	0.0001
Apogee km (n mi)	187.23 (101.10)	187.85 (101.43)	-0.62 (-0.33)
Perigee km (n mi)	183.60 (99.14)	185.26 (100.03)	-1.66 (-0.89)
Altitude km (n mi)	192.53 (103.96)	191.45 (103.37)	1.08 (0.59)
Period min	88.20	88.22	-0.02



Ground track of the vehicle during flight is shown in Figure 4-7. The first and second revolution of the parking orbit are numbered.

#### 4.4 INJECTION PHASE TRAJECTORY

##### 4.4.1 Tracking Data Utilization

C-band radar data from four sites (Grand Bahama Island, Merritt Island, Antigua and Bermuda) were used to determine the injection phase trajectory. The Grand Bahama Island and Merritt Island data were available for a considerable time before S-IVB restart and were used in both the parking orbit trajectory and the injection phase trajectory to assure there would be no discontinuities. The data from these four radars were used as inputs to the GATE program. These data were consistent and showed excellent agreement with the resulting best estimate trajectory.

GLOTRAC Segment I data for the injection phase were received approximately one month after launch. This was too late for data to be used in the construction of the trajectory, but this data agreed well with the trajectory obtained from the radars. The maximum differences between the GLOTRAC Segment I data and the best estimate trajectory for the injection phase are 0.07 kilometers (0.04 n mi) in X (downrange), 0.1 kilometers (0.05 n mi) in Y (vertical) and 0.11 kilometers (0.059 n mi) in Z (cross range).

##### 4.4.2 Trajectory Evaluation

Comparisons between the actual and nominal total space-fixed velocity and flight path angle are shown in Figure 4-8. The actual and nominal total inertial acceleration comparisons are presented in Figure 4-9. The acceleration is greater than nominal for the early portion of the S-IVB second burn due to the propellant mixture ratio being higher than expected. The velocity reflects the acceleration difference and is also greater than nominal for the S-IVB second burn.

The cutoff signal was given by the guidance computer at 11,786.3 seconds. At this time the altitude was 23.88 kilometers (12.90 n mi) less than nominal and the total space-fixed velocity was 12.80 m/s (41.98 ft/s) greater than nominal. The S-IVB second burn was 15.2 seconds shorter than nominal. The larger portion of this difference is attributed to the greater acceleration during the early portion of flight. The increase in the total velocity due to thrust decay was 1.7 m/s (5.6 ft/s) which is 0.8 m/s (2.6 ft/s) less than nominal.

#### 4.5 WAITING ORBIT TRAJECTORY

##### 4.5.1 Tracking Data Utilization

The waiting orbit trajectory from injection to S-IVB/CSM separation was obtained in the same manner as the injection phase. The Antigua and Bermuda radars furnished data for this portion of flight. These data points were

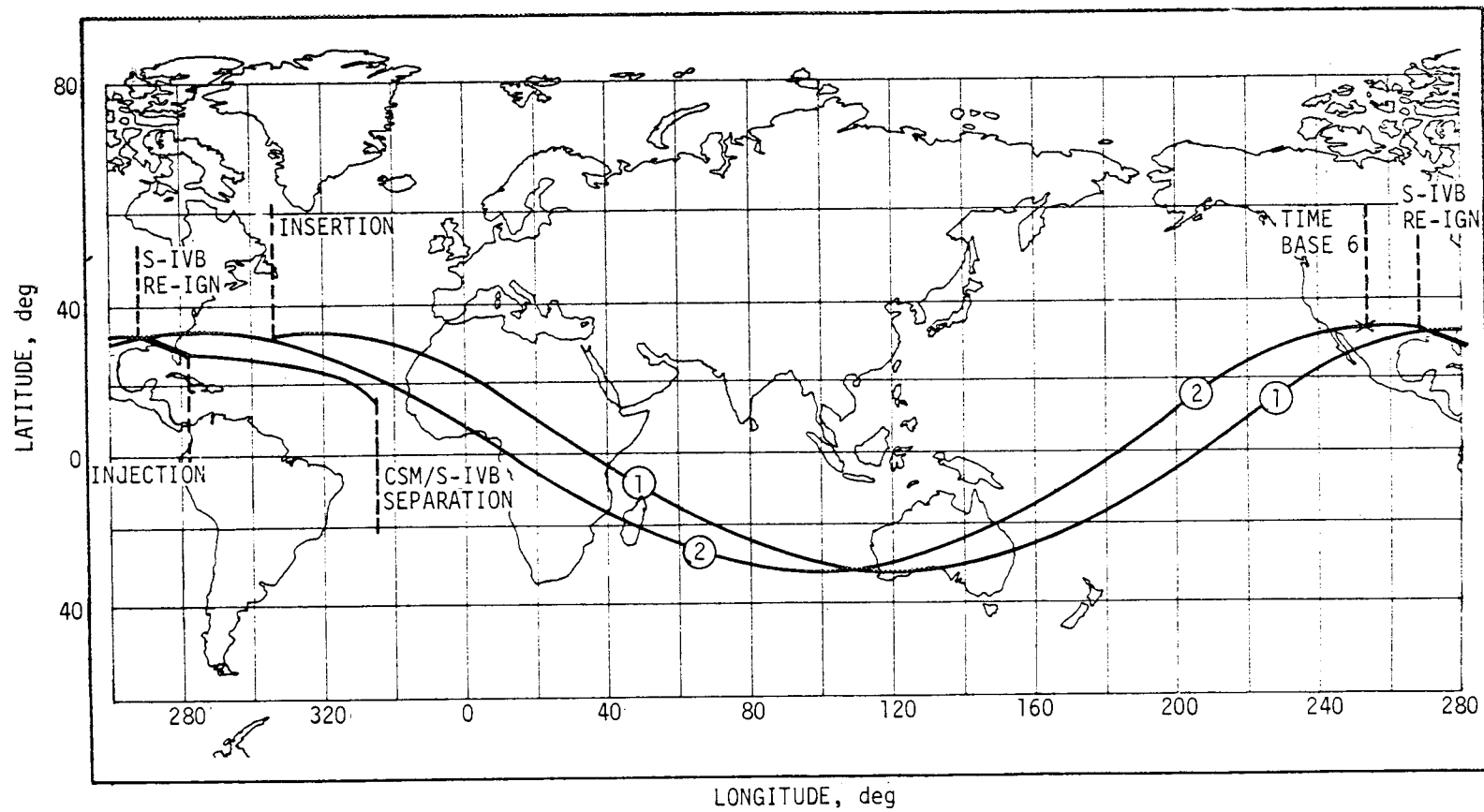


Figure 4-7. AS-501 Ground Track



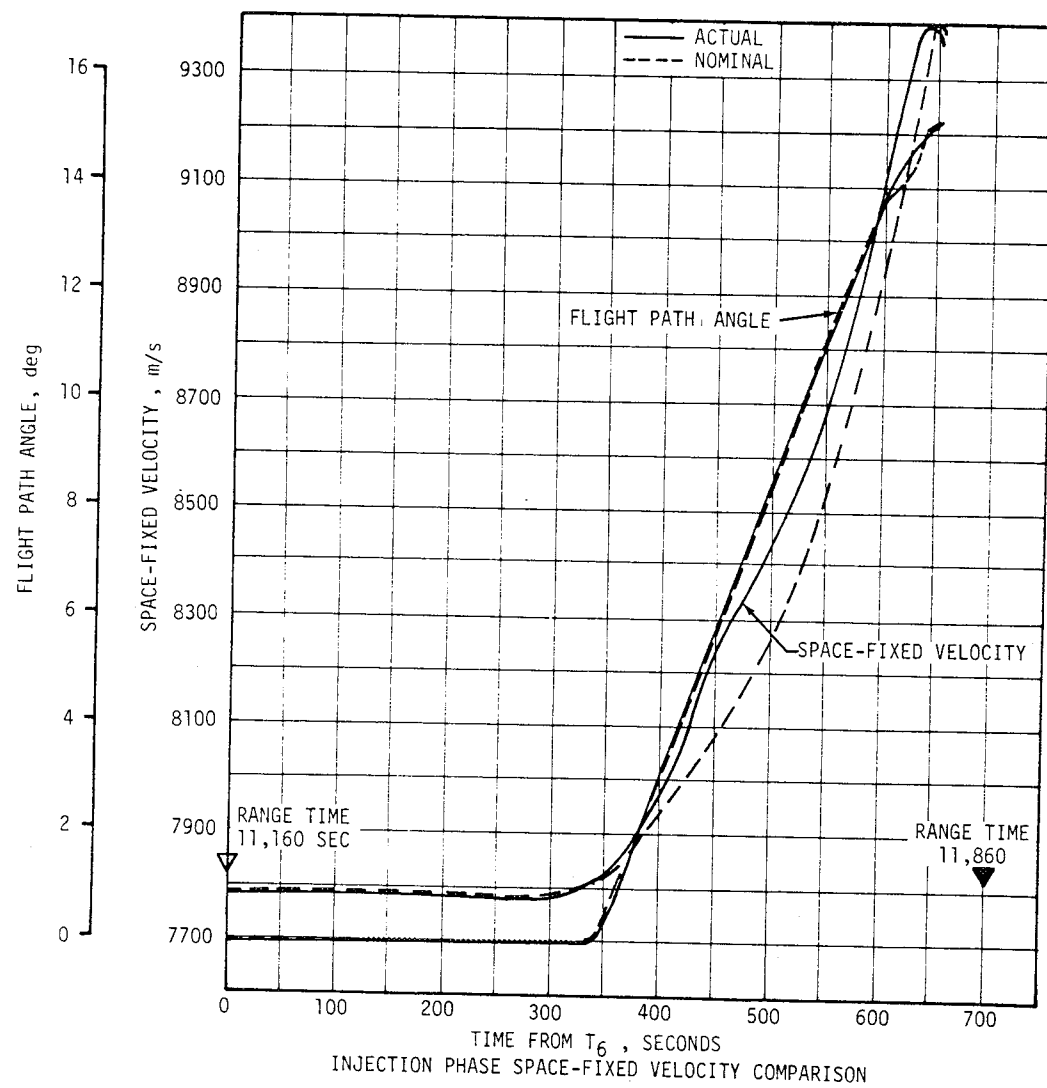


Figure 4-8. Injection Phase Space-Fixed Velocity Comparison

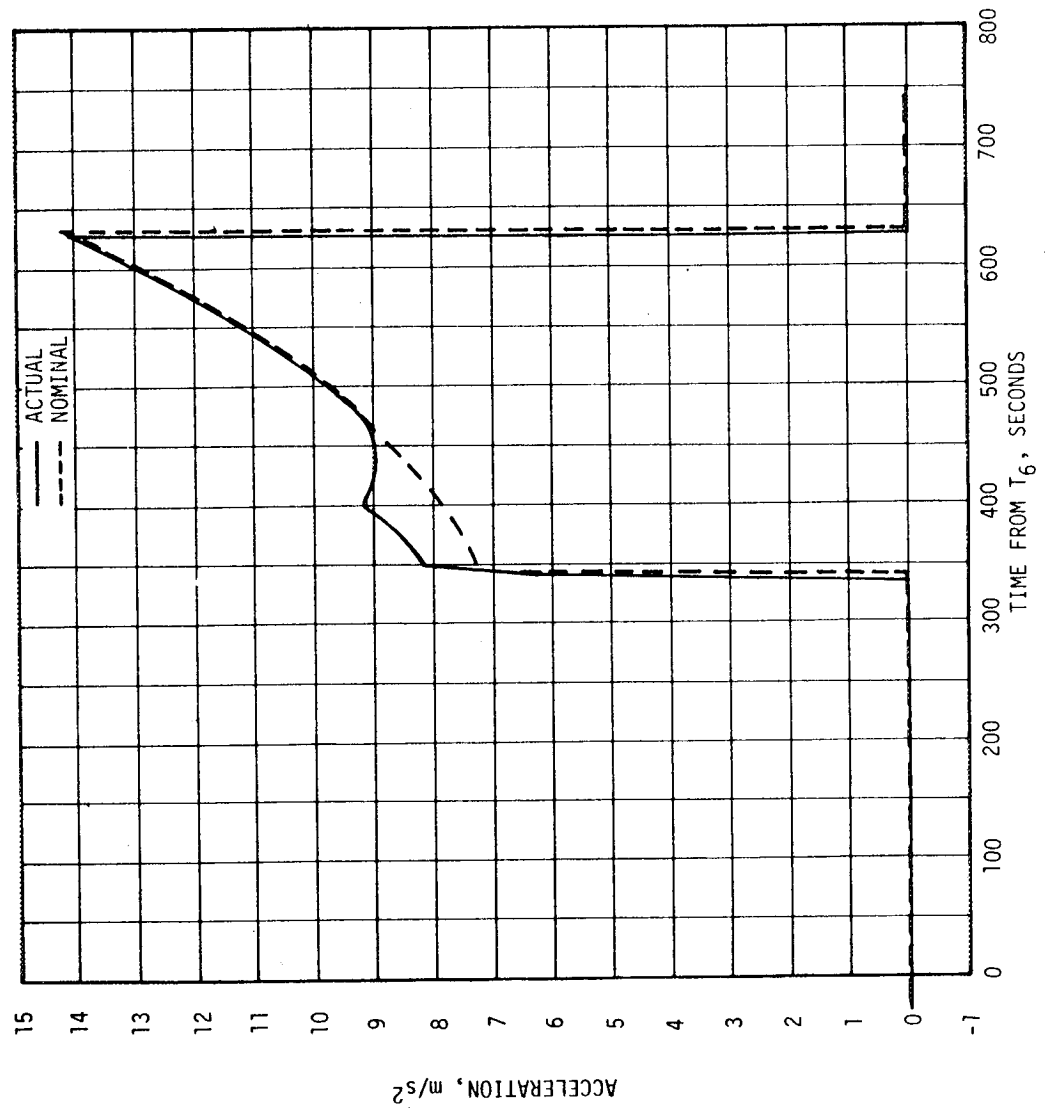


Figure 4-9. Injection Phase Acceleration Comparison

used as inputs to the GATE program. The trajectory, starting before S-IVB restart to S-IVB/CSM separation, was obtained through a single solution. GLOTRAC Segment 1 data were received for the first 200 seconds of the waiting orbit. These data points were received too late to be used in the trajectory but agree very well with the trajectory obtained from the radar data.

#### 4.5.2 Trajectory Evaluation

A comparison between the actual and nominal waiting orbit injection conditions is presented in Table 4-9. A comparison of the actual and nominal conditions at S-IVB/CSM separation is presented in Table 4-3. After S-IVB/CSM separation the Canary Island radar tracked the S-IVB stage. However, these data were not usable for determination of the S-IVB trajectory. The trajectory of the S-IVB stage was obtained by generating a theoretical free-flight trajectory using the actual S-IVB/CSM separation conditions as the starting point. Comparison of the actual and nominal impact conditions for the S-IVB stage are shown in Table 4-6.

Table 4-9. Waiting Orbit Injection Conditions

PARAMETER	ACTUAL	NOMINAL	ACT-NOM
Range Time sec	11,796.3	11,809.4	-13.1
Space-Fixed Velocity m/s (ft/s)	9394.9 (30,823.2)	9383.5 (30,785.8)	11.4 (37.4)
Flight Path Angle deg	15.030	15.288	-0.258
Inclination deg	30.302	30.313	-0.011
Node deg	135.435	135.431	0.004
C3 m <sup>2</sup> /s <sup>2</sup> (ft <sup>2</sup> /s <sup>2</sup> )	-26,672,329 (-287,098,560)	-26,484,660 (-285,078,510)	-187,669 (-2,020,050)
Eccentricity	0.5789	0.5817	-0.0028
Apogee km (n mi)	17,217.25 (9296.57)	17,426.87 (9409.76)	-209.62 (-113.19)
Perigee km (n mi)	-84.69 (-45.73)	-82.51 (-44.55)	-2.18 (-1.18)
Altitude km (n mi)	562.58 (303.77)	586.83 (316.86)	-24.25 (-13.09)
Period min	303.02	306.25	-3.23



## SECTION 5 S-IC PROPULSION

### 5.1 S-IC PROPULSION SUMMARY

All S-IC propulsion systems performed satisfactorily. Overall performance was as expected, and in general all performance flight data fell close to the nominal predictions. Stage thrust averaged 0.6 percent higher than predicted as compared with the average specific impulse which was 0.19 percent lower than predicted. Propellant consumption from Engine Start Command (ESC) to separation was 0.233 percent less than predicted.

The postflight performance simulation-trajectory match analysis confirmed S-IC propulsion system performance. This simulation analysis showed that the performance of thrust and specific impulse agreed with propulsion reconstruction within -0.18 percent.

Outboard engine cutoff occurred 1.13 seconds earlier than predicted, which was caused by the thrust, specific impulse, buildup and holddown consumption, and residual deviations. However, this cutoff time deviation was well within the predicted three sigma limit of  $\pm 2.98$  seconds.

The usable residuals resulting from the earlier than expected Outboard Engine Cutoff (OECO) were 3597 kilograms (7929 lbm) of LOX compared to the usable zero predicted and 1916 kilograms (4224 lbm) of fuel compared to 2419 kilograms (5333 lbm) predicted. The higher than expected LOX residual was due to the short timer setting with respect to first gas ingestion into the suction lines. If the flight of AS-502 indicates repeatability, then the timer settings will be re-evaluated for AS-503 and subsequent flight.

The subsystem operationally met all performance requirements. Higher than specification pressures were experienced in the fuel tank pressurization system immediately downstream of the helium flow control valves between launch commit and aft umbilical disconnect. This was expected, and was due to commanding the number 1 helium control valve open at launch commit while ground prepressurization gas continued to flow through the aft umbilical until it was disconnected. This was an overlap of approximately one second. Sequencing will be changed to command the number 1 valve open at aft umbilical disconnect on AS-502 and subsequent vehicles.

The LOX pressurization system had a  $1.17 \text{ N/cm}^2$  (1.7 psi) overshoot. This overshoot was caused by the closing response time of a ground support equip-

ment (GSE) valve, and the high pressure helium in the GSE supply system that "blows-down" into the tank after the GSE valve is closed. This operation was typical for AS-501 and was in no way detrimental to the launch vehicle.

## 5.2 S-IC IGNITION TRANSIENT PERFORMANCE

The fuel pump inlet preignition pressure and temperature was  $30.9 \text{ N/cm}^2$  (44.8 psia) and  $277^\circ\text{K}$  ( $39^\circ\text{F}$ ), respectively. These fuel pump inlet conditions were within the F-1 engine model specification limits as shown in Figure 5-1. The preignition temperature at the fuel pump inlet was considerably lower than the fuel bulk temperature of  $292.6^\circ\text{K}$  ( $67^\circ\text{F}$ ). Similarly, the LOX pump inlet preignition temperature and pressure was  $55.4 \text{ N/cm}^2$  (80.3 psia) and  $96.4^\circ\text{K}$  ( $-286^\circ\text{F}$ ), respectively. The LOX pump inlet conditions were also within the F-1 engine model specification limits as shown in Figure 5-1. The fuel and LOX ullage pressures were  $20.1 \text{ N/cm}^2$  (29.2 psia) and  $18.2 \text{ N/cm}^2$  (26.39 psia) respectively at ignition.

The engine startup sequence was nominal. A 1-2-2 start was planned and attained. Engine position starting order was 5, 3-1, 4-2. Two engines are considered to start together if their combustion chamber pressures reach  $79 \text{ N/cm}^2$  (100 psig) in a 100-millisecond time period. Figure 5-2 shows the thrust build-up of each engine indicative of the successful 1-2-2 start. A combustion chamber pressure spike of approximately  $82.7 \text{ N/cm}^2$  (120 psi) occurred at -2.93 seconds during the startup of engine position 2. This type pressure perturbation has been observed during engine production and development testing and is associated with thrust chamber fuel system priming characteristics. The pressure perturbation is not considered detrimental to engine operation. The main oxidizer valve (MOV), main fuel valve (MFV) and gas generator (GG) ball valve opening times during engine transient were nominal and compared well with the predicted values based on stage acceptance test data.

The propellants consumed during holddown were 42,012 kilograms (92,621 lbm) by the level sensor data as compared to 42,077 kilograms (92,764 lbm) by the reconstruction analysis. These consumptions are less than the predicted consumption of 44,889 kilograms (98,964 lbm). The less than predicted hold down consumption resulted in best estimate liftoff propellant loads of 1,389,147 kilograms (3,062,544 lbm) for LOX and 605,148 kilograms (1,334,121 lbm) for fuel.

## 5.3 S-IC MAIN STAGE PERFORMANCE

S-IC stage propulsion performance was completely satisfactory. Analysis of the performance was accomplished by applying the F-1 engine flight data to the reconstruction program of the S-IC propulsion system. All stage propulsion performance parameters fell within the predicted three sigma limits. Stage thrust averaged over flight time was 0.60 percent higher than predicted. Stage specific impulse was 0.19 percent lower than predicted with the difference being essentially constant throughout flight. All of the above engine performance parameters compared well with the nominal predictions as shown in Figure 5-3.

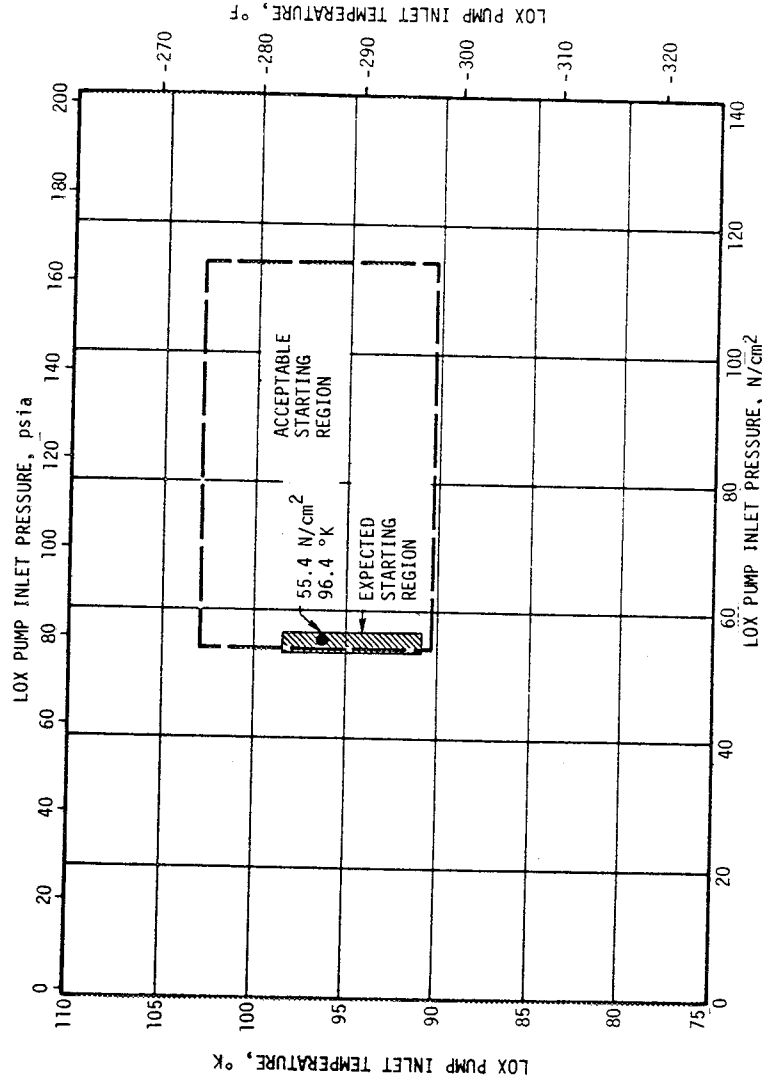
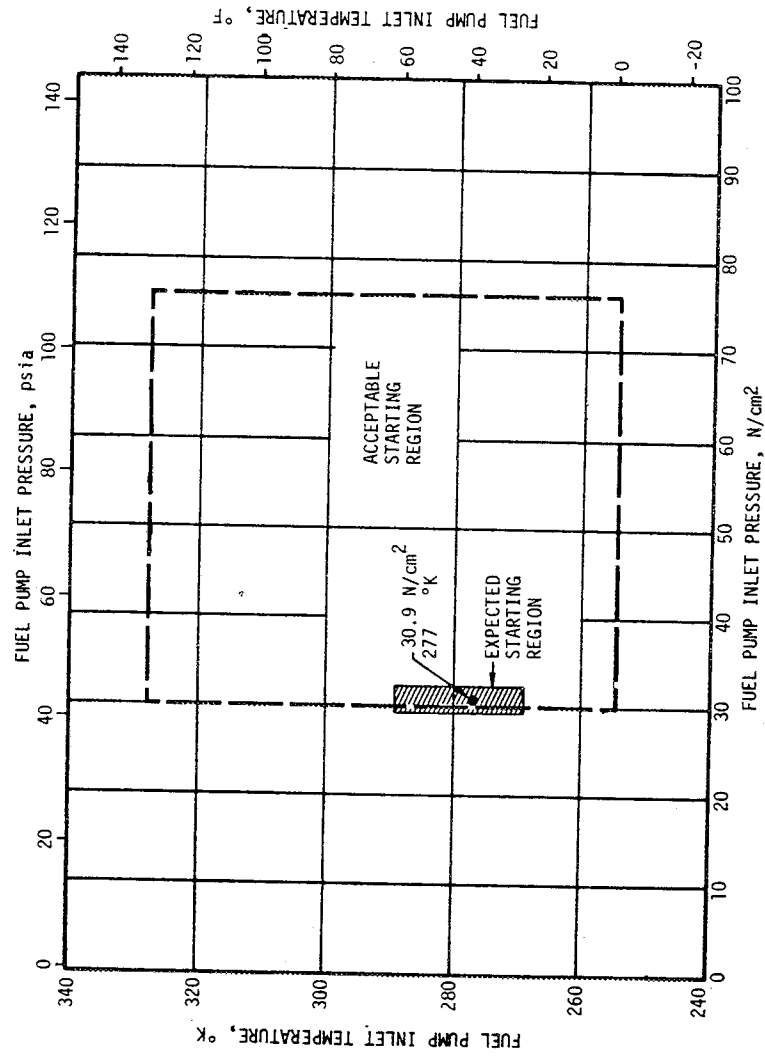


Figure 5-1. S-IC Start Box Requirements

Individual engine parameters also fell within predicted limits. The thrusts of engine positions 1, 2, and 3 were slightly lower than predicted tag values when reduced to standard conditions. Engine positions 4 and 5 were higher than predicted with engine position 5 exhibiting the greatest deviation from the predicted. Engine standard sea level performance is summarized in Table 5-1.

A trajectory simulation program was employed to adjust the propulsion reconstruction analysis results using a differential correction procedure. This simulation determined adjustments to the reconstructed thrust, mass flow, and aerodynamic axial force coefficient to yield a simulated trajectory which closely matched the observed mass point trajectory. The results obtained using the differential correction procedure are that the sea level thrust was reduced by -0.18 percent, and the propellant flowrate was unchanged. Total impulse was slightly lower than predicted. The resulting aerodynamic axial force coefficient is discussed in paragraph 20.2.

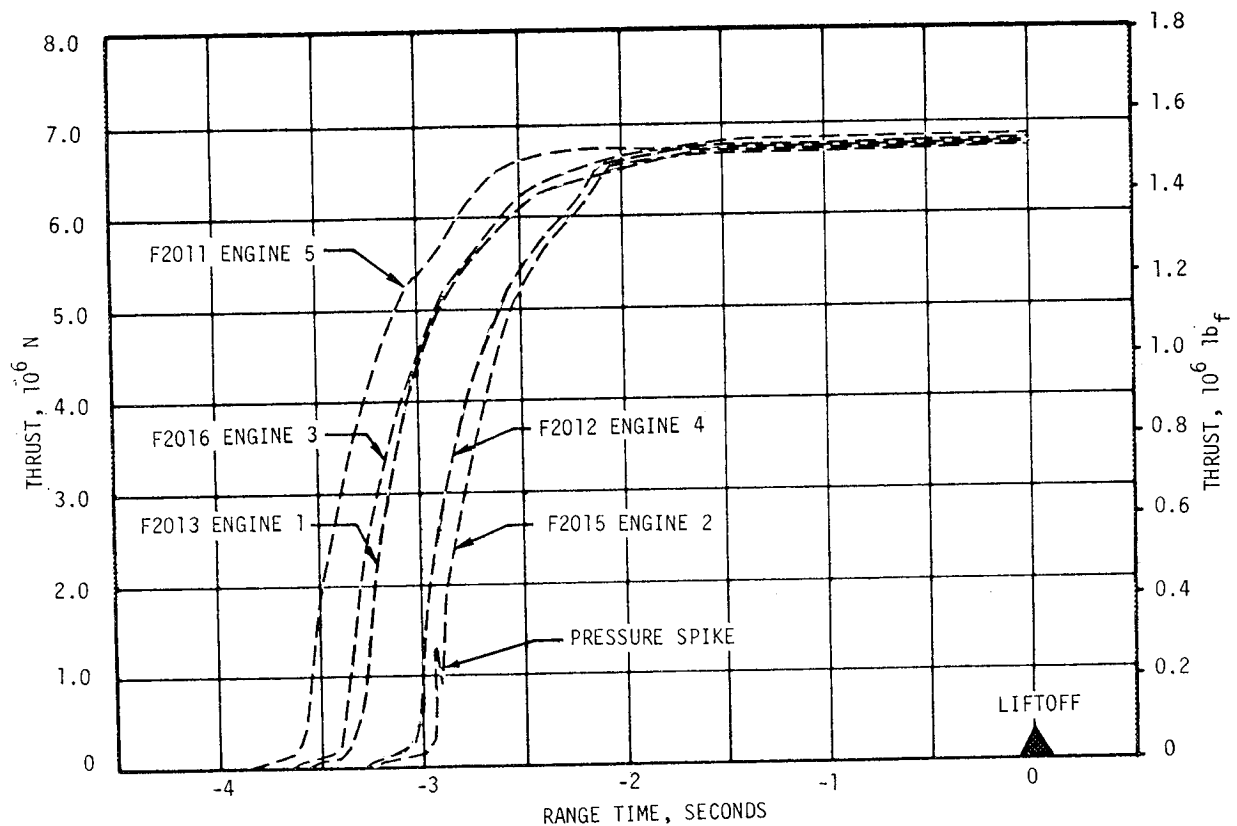


Figure 5-2. S-IC Engine Buildup Transient



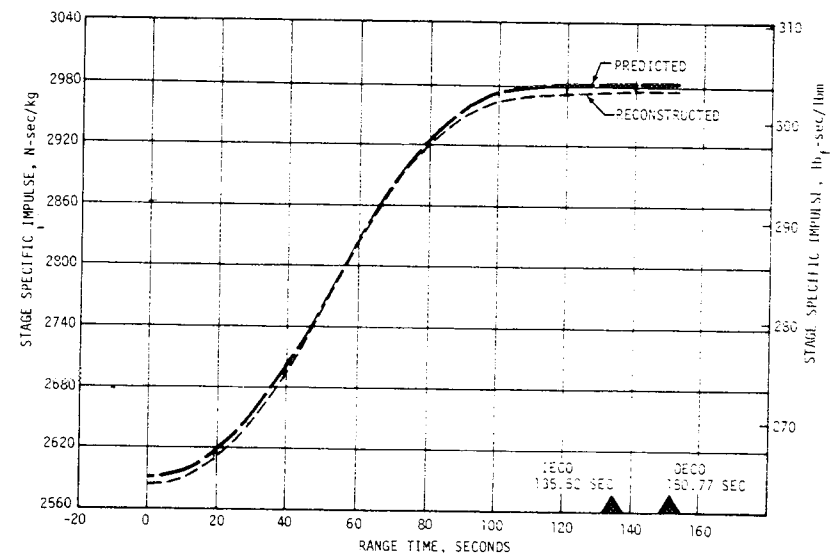
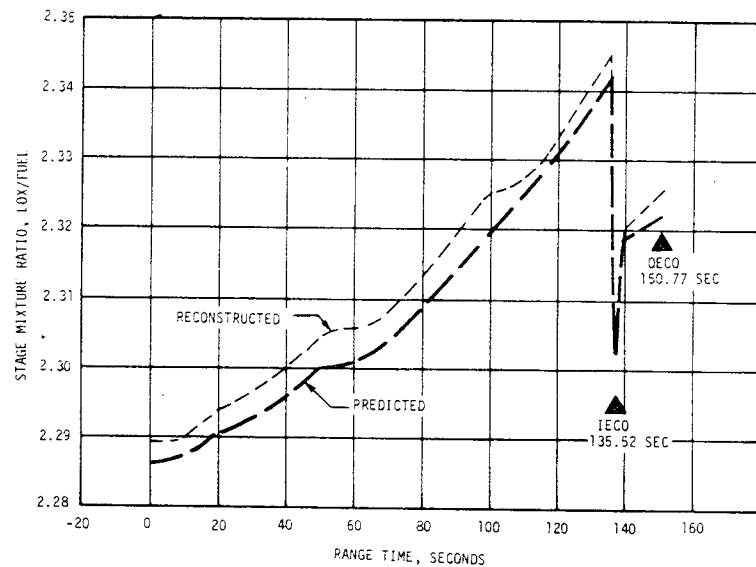
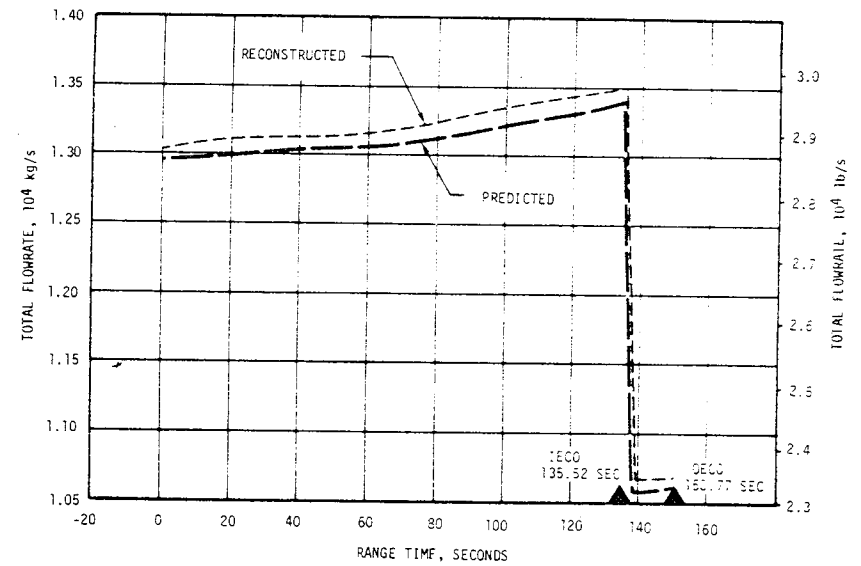
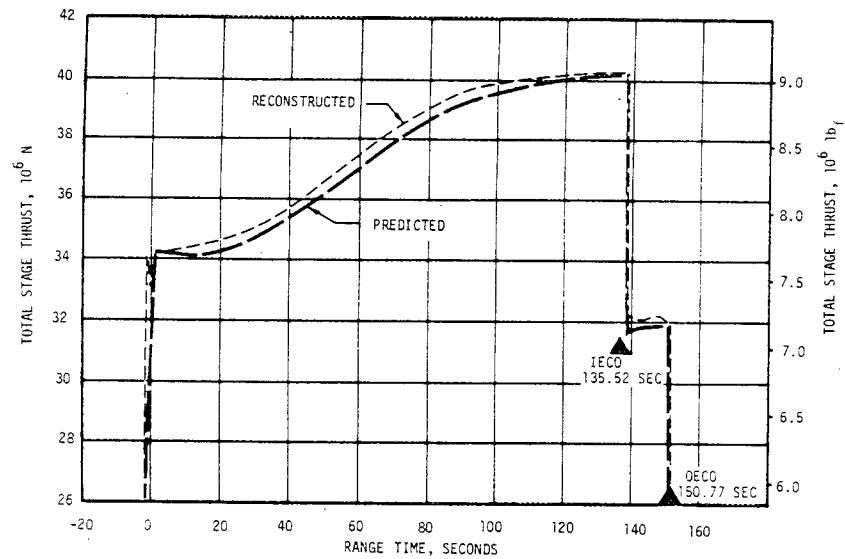


Figure 5-3. S-IC Steady State Operation

Table 5-1. S-IC Engine Performance Deviations

PARAMETER	ENGINE	PREDICTED	RECONSTRUCTION ANALYSIS	DEVIATION PERCENT
Thrust $10^3$ N ( $10^3$ lbf)	1	6766 (1521)	6735 (1514)	-0.46
	2	6695 (1505)	6690 (1504)	-0.07
	3	6788 (1526)	6775 (1523)	-0.19
	4	6637 (1492)	6690 (1504)	+0.80
	5	6655 (1496)	6730 (1513)	+1.13
Specific Impulse N-s/kg (lbf-s/lbm)	1	2594 (264.5)	2601 (265.2)	+0.26
	2	2598 (264.9)	2593 (264.4)	-0.19
	3	2592 (264.3)	2583 (263.4)	-0.34
	4	2606 (265.7)	2595 (264.6)	-0.41
	5	2603 (265.4)	2592 (264.3)	-0.41
Total Flowrate kg/s (lbm/s)	1	2609 (5752)	2589 (5708)	-0.76
	2	2578 (5683)	2580 (5689)	+0.11
	3	2619 (5774)	2622 (5781)	+0.12
	4	2547 (5615)	2578 (5683)	+1.21
	5	2557 (5637)	2597 (5725)	+1.56
Mixture Ratio LOX/Fuel	1	2.26	2.25	-0.44
	2	2.28	2.29	+0.44
	3	2.26	2.26	0.0
	4	2.26	2.27	+0.44
	5	2.26	2.27	+0.44
Note: Analysis was reduced to standard sea level conditions at liftoff plus 35 to 38 seconds.				

Table 5-2 presents a summary, reduced to sea level conditions, of the average values and deviations of longitudinal thrust, propellant flowrate, and vehicle longitudinal specific impulse. Also included in this table are vehicle mass at first motion (-0.48 seconds). Values from the flight simulation method are compared with postflight reconstruction and the predicted.

The S-IC stage received outboard engine cutoff signal 1.13 seconds earlier than predicted. The total earth fixed velocity at OECO was 17.33 m/s lower than predicted. The flight simulation results were used in an attempt to explain the time and velocity deviations. To explain the velocity deviation an error analysis was made to determine the contributing parameters and the magnitude of the velocity deviation caused by each of these parameters. Table 5-3 lists the various error contributors and the cutoff velocity deviations associated with each.

Table 5-2. Comparison of S-IC Stage Flight Reconstruction Data  
With Trajectory Simulation Results

PARAMETERS	UNITS	PREDICTED	RECONSTRUCTION	FLIGHT SIMULATION	DEVIATION FROM PREDICTED	DEVIATION FROM RECONSTRUCTION
Average sea level longitudinal thrust	N (lbf)	34,177,915.0 7,683,500.9	34,379,124.0 7,728,734.5	34,318,323.0 7,715,065.9	+ 0.41%	- 0.18%
Vehicle mass at first motion	kg (lbm)	2,777,734 6,123,855	2,784,090 6,137,868	2,784,090 6,137,868	+ 0.26%	0.0%
Average propellant flow rate	kg/s (lbm/s)	13,134.01 28,955.54	13,238.52 29,185.94	13,238.52 29,185.94	+ 0.80%	0.0%
Average sea level specific impulse	N-s/kg (lbf-s/lbm)	2602.2 265.36	2596.9 264.81	2596.9 264.34	- 0.39%	- 0.18%

Since outboard engine cutoff signal was given by a LOX level switch, the only quantities which affected the cutoff time are those which altered the level of LOX in the tank. Table 5-3 also lists the parameters which contributed to the deviation between the predicted and actual cutoff time and the " $\Delta t$ " contributions made by each. The "difference" noted in Table 5-3 is probably due to accuracy of data used in the analysis.

#### 5.4 S-IC ENGINE SHUTDOWN TRANSIENT PERFORMANCE

Cutoff signal to the inboard engine was received from the IU at 135.52 seconds. Cutoff signal to the outboard engines was initiated by LOX depletion and occurred at 150.77 seconds. This was 1.13 seconds earlier than the predicted time of 151.90 seconds. Time base three in the LVDC, which was initiated by the engine cutoff signal, was started at 150.77 seconds. The early OEEO was caused by thrust, specific impulse, and residual deviations.

Thrust decay of the F-1 engines is shown in Figure 5-4. The decay transient was nominal. The oscillations which occur near the end of "tailoff" are characteristic of the engine shutdown sequence.

The total outboard engine cutoff impulse from the engine cutoff signal to separation signal was indicated by engine analysis to be 11,660,568 N-s (2,621,400 lbf-s) compared to the predicted impulse of 10,108,584 N-s (2,272,500 lbf-s). Telemetered propulsion data indicated the cutoff impulse was greater than expected, however the guidance velocity integrator data showed the change in velocity was less than that predicted. The velocity increase was 9.1 m/s (29.9 ft/s) compared to the predicted of 11.0 m/s (36.1 ft/s). With the accuracy of determination of the above parameters and the actual occurrence of OEEO with respect to range time, the above cutoff impulse and equivalent velocity increase were within the expected values. The propellant consumption for LOX and fuel during cutoff was 2.4 percent and 4.17 percent greater respectively than the predicted.

Table 5.3 Velocity and Time Deviation Analysis at OECO  
(Simulation Versus Predicted)

VELOCITY DEVIATION	
CONTRIBUTING ERROR FACTORS	DEV. (ACT-PRED) $\Delta V$ (m/sec)
Liftoff Weight Increase (0.23%)	-15.80
Total Thrust Increase (0.41%)	+15.63
Total Propellant Flowrate Increase (0.80%)	+25.14
Axial Force Coefficient Difference	+ 1.23
Meteorological Data Difference	- 3.02
Late IECO (0.45 sec)	+ 3.38
Early OECO (-1.13 sec)	-40.62
Effect of Extrusion Rods	-3.24
Total Contribution	-17.30
Observed	<u>-17.33</u>
Difference (Observed - Total Contribution)	- 0.03
TIME DEVIATION	
CONTRIBUTING ERROR FACTORS	DEV. (ACT-PRED) $\Delta t$ (sec)
Initial LOX Load Increase (0.14%)	+ 0.48
LOX Flowrate Increase (0.80%)	- 1.20
Late CECO (0.45 sec)	- 0.11
Short Timer Setting (0.35 sec)	- 0.35
Total Contribution	- 1.18
Observed	- 1.13
Difference	+ 0.05

#### 5.5 S-IC STAGE PROPELLANT MANAGEMENT

The LOX propellant loaded was in close agreement with the predicted, but the fuel loaded was approximately 1436 kilograms (3167 lbm) less than predicted. This fuel load was 0.10 percent low, which is well within the predicted three sigma limits of  $\pm 0.5$  percent.

The S-IC does not have a closed loop propellant utilization system. Minimum residuals are obtained by attempting to load the mixture ratio of propellants which is expected to be consumed by the engines, plus the predicted unusable residuals, plus a small additional amount of usable fuel (fuel bias

This fuel bias lowers the probability of large usable LOX residuals. The usable residual deviations are a measure of the performance of the propellant utilization system. Table 5-4 shows propellant consumption throughout the flight and Table 5-5 shows the residuals after the burn portion of flight. The deviations of the usable residuals on this flight were caused by loading and engine consumption deviations along with the timer setting in the LOX level cutoff system. This timer setting was 1.2 seconds which was the conservatively predicted time between level sensor gas detection and the time when the LOX level reached the desired cutoff level in the suction ducts. It appeared that bubble ingestion due to fluid level dropout occurred earlier than predicted. This phenomenon will be evaluated again on AS-502 to determine repeatability and if it is repeatable the S-IC-3 timer settings will be re-evaluated.

## 5.6 S-IC PRESSURIZATION SYSTEM

### 5.6.1 S-IC Fuel Pressurization System

The helium pressurization system satisfactorily maintained the required ullage pressure in the fuel tank during flight. The helium flow control valves opened as programmed and the fifth flow control valve was not required. The heat exchangers performed as expected.

The low flow prepressurization system was commanded on at -97.658 seconds and performed satisfactorily. However, the ullage pressure increased approximately 0.5 N/cm<sup>2</sup> (0.7 psi) above the maximum switch actuation pressure of 19.99 N/cm<sup>2</sup> (29.0 psia) at approximately -63 seconds as shown in Figure 5-5. The low flow was not required again during countdown.

Table 5-4. S-IC Propellant Consumption\*

EVENT	PREDICTED		LEVEL SENSOR DATA		RECONSTRUCTED		BEST ESTIMATE	
	LOX	FUEL	LOX	FUEL	LOX	FUEL	LOX	FUEL
Master Ignition kg (lbm)	1,421,113 3,133,018	616,309 1,358,729	1,421,144 3,133,087	614,279 1,354,254	1,421,434 3,133,726	614,873 1,355,562	1,421,434 3,133,726	614,873 1,355,562
Liftoff -0.148 sec. kg (lbm)	1,385,429 3,054,348	607,104 1,338,435	1,388,857 3,061,906	604,554 1,332,814	1,388,704 3,061,568	605,526 1,334,956	1,389,147 3,062,545	605,148 1,334,122
IECO kg (lbm)	141,010 310,874	69,033 152,192	131,910 290,811	62,178 137,079	132,074 291,174	63,167 139,260	132,517 292,151	62,789 138,426
OECD kg (lbm)	15,271 33,667	14,854 32,747		18,271 40,280	17,761 39,157	13,987 30,836	18,200 40,124	14,281 31,485
Separation kg (lbm)	13,058 28,788	13,778 30,375			15,494 34,159	12,866 28,365	15,933 35,126	13,161 29,014
*Values do not include pressurization gas (GOX) so they will compare with level sensor data.								

Table 5-5. S-IC Residuals at Outboard Engine Cutoff Signal

PROPELLANTS	PREDICTED	ACTUAL	DEVIATION
LOX RESIDUALS			
*Usable Mainstage	0 kg (0 lbm)	3,597 kg ( 7,929 lbm)	+3,597 kg (+7,929 lbm)
Thrust Decay And Unusable	17,491 kg (38,561 lbm)	17,856 kg (39,365 lbm)	+ 365 kg (+ 804 lbm)
FUEL RESIDUALS			
Usable Mainstage	**2,419 kg ( 5,333 lbm)	1,916 kg ( 4,224 lbm)	-503 kg (-1,109 lbm)
Thrust Decay And Unusable	12,390 kg (27,315 lbm)	12,365 kg (27,261 lbm)	-25 kg (-54 lbm)
*Includes GOX pressurization gas. **Fuel bias.			

The fuel high flow prepressurization valve of the ground support equipment was commanded on at -4.192 seconds and maintained the ullage pressure within the band. At launch commit the number 1 helium flow control valve (HFCV) of the onboard pressurization system was commanded on and increased the ullage pressure to 20.33 N/cm<sup>2</sup> (29.5 psia) at umbilical disconnect. The combination of the ground pressurization system and the onboard pressurization system operating simultaneously resulted in a helium flowrate to the tank of 2.85 kg/s (6.4 lbm/s)

The prepressurization low flow and the supplemental flow are controlled by the prepressurization switch with specification limits of 18.96 to 19.99 N/cm<sup>2</sup> (27.5 to 29.0 psia). At termination of low flow prepressurization (-63.514 seconds), the switch actuated at 20.20 N/cm<sup>2</sup> (29.4 psia) which is 0.21 N/cm<sup>2</sup> (0.3 psi) above the maximum specification limit. The pressure switch failed to actuate, and the supplemental flow did not terminate before umbilical disconnect even though the pressure had increased to 20.34 N/cm<sup>2</sup> (29.5 psia). In this case either the switch actuation pressure drifted higher or the switch failed.

The onboard helium pressurization system performed satisfactorily and maintained ullage pressure within the required limits. The number 1 helium flow control valve (HFCV) was signaled to open at launch commit. Since flow was still provided from the prepressurization system, flowrates and system duct pressures were higher than the specification limits.

The highest pressures in the ducting system downstream of the HFCV manifold were seen at the inlet to the duct (Reference 60B49029 drawing). Figure 5-6 shows the pressure exceeded the duct specification design, proof pressures, and the range of the transducer during the time period of flow overlap. The peak pressure was calculated to be about 344.7 N/cm<sup>2</sup> (500 psia) for the 2.85 kg/s (6.4 lbm/s) flow. The high flowrates and system pressures were not detrimental to the stage ducting for AS-501 flight. During qualification testing, the duct demonstrated that it could withstand an excess of 483 N/cm<sup>2</sup> (700 psi) above the specification burst requirements. This operation was expected and no action was taken prior to AS-501 launch because of qualification test results. An Engineering Change Proposal (ECP) is being processed to eliminate the flow overlap by opening the number 1 HFCV at umbilical disconnect.

During flight the HFCVs 2, 3, and 4 were commanded open at 49.723, 95.519 and 133.75 seconds, respectively, which held the ullage pressure within the predicted band as shown in Figure 5-7. The number 5 HFCV was not required to operate since ullage pressure was maintained above the 5th HFCV switch actuation pressure. Helium bottle pressure as shown in Figure 5-8 stayed within expected limits.

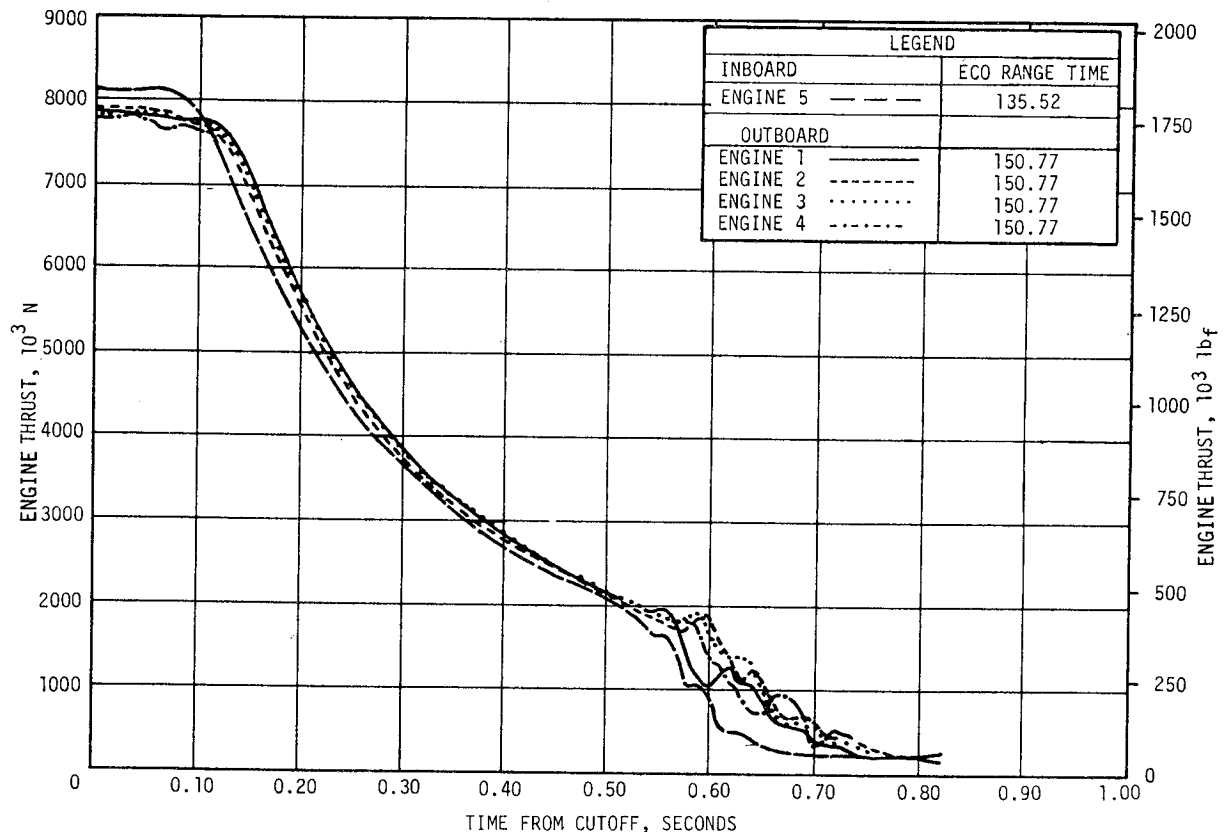


Figure 5-4. S-IC Engine Shutdown Transient Performance

The heat exchangers performed within the expected performance limits with the exception of one sampled data point. This particular data point was just outside the expected performance band with no adverse effects on stage performance.

#### 5.6.2 S-IC LOX Pressurization System

The LOX pressurization system performed satisfactorily and all performance requirements were met. The ground prepressurization system maintained ullage pressure within acceptable limits until launch commit. The onboard pressurization system subsequently maintained ullage pressure within the GOX Flow Control Valve (GFCV) band during the flight. The heat exchangers formed as expected.

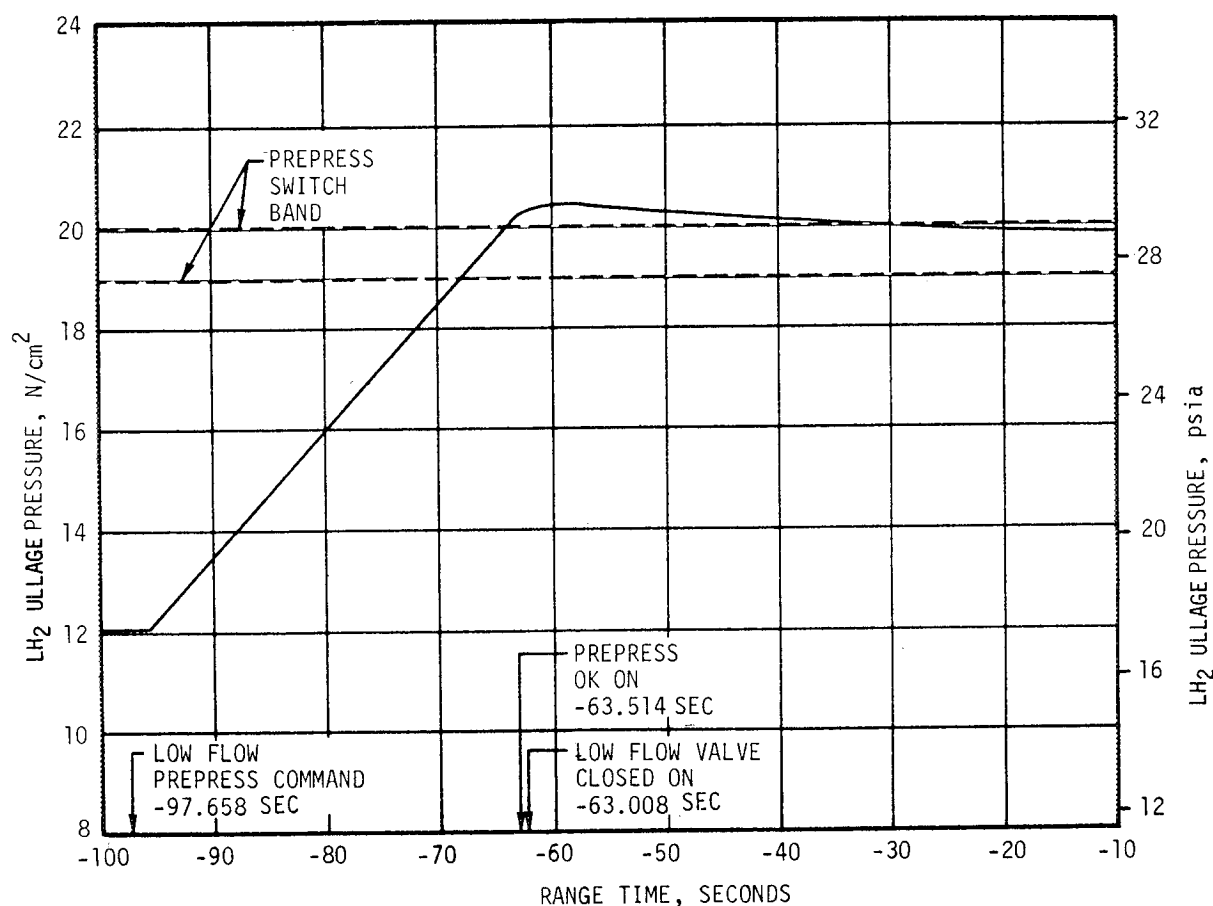


Figure 5-5. S-IC Fuel Ullage Pressure During Countdown



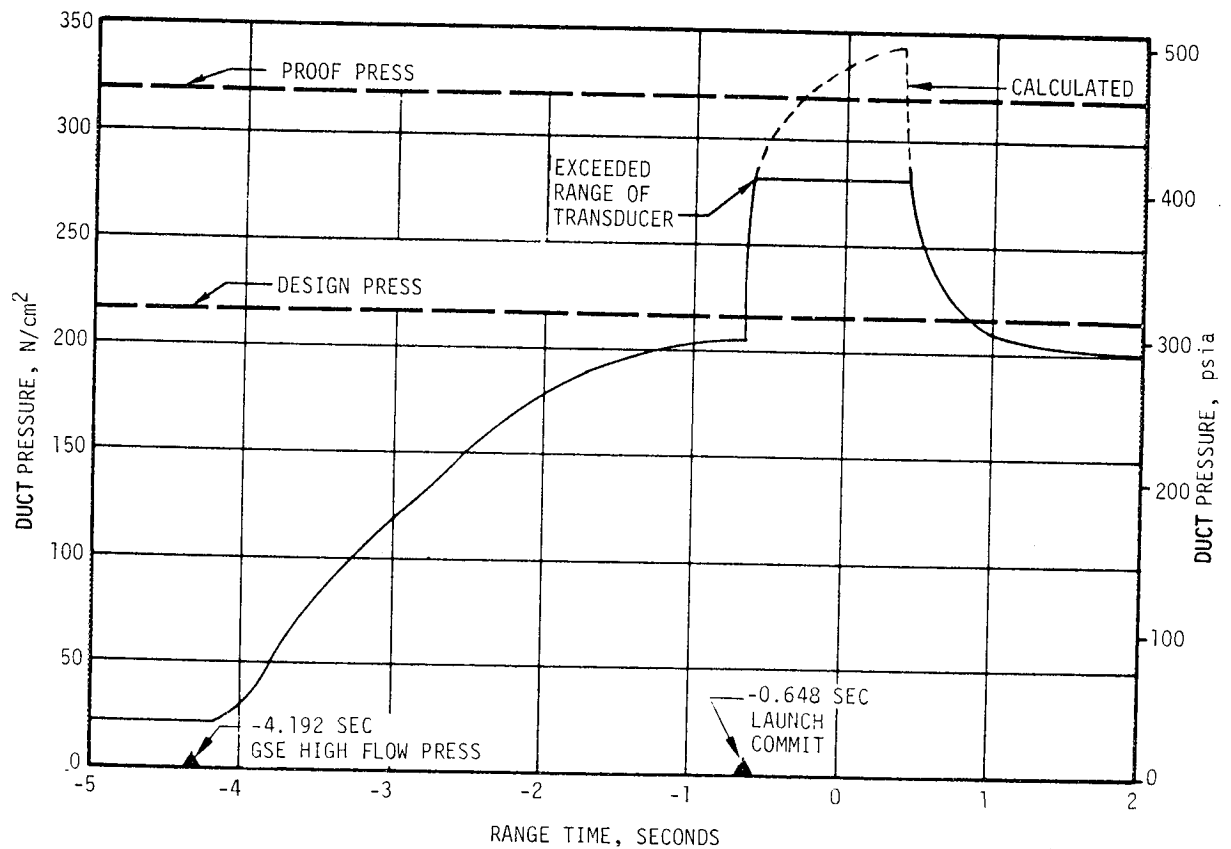


Figure 5-6. S-IC Helium Pressurization System  
(Inlet to 60B49029 Duct)

The prepressurization system was initiated by opening of the ground supply valve at -69.226 seconds. The ullage pressure increased until it entered the switch band zone which resulted in terminating the flow at approximately -61 seconds. The ullage pressure increased approximately 1.17 N/cm<sup>2</sup> (1.7 psi) above the prepressurization switch setting of 17.93 N/cm<sup>2</sup> (26.0 psia). This overshoot was caused by the closing response time of the GSE valve and the high pressure helium in the GSE supply system that "blows down" into the tank after the valve is closed. The pressure increased into the relief switch band by 0.14 N/cm<sup>2</sup> (0.2 psi), but did not exceed the minimum switch actuation pressure of 19.31 N/cm<sup>2</sup> (28.0 psia). The higher ullage pressure overshoot was expected to occur on S-IC-1 and subsequent vehicles. However, because of the smaller ullage volume on S-IC-4 and subsequent vehicles, some hardware changes may be required. The ullage pressure decay after initial pressurization occurred as the ullage gases cooled down. This caused the prepressurization valve to open at -25.254 seconds. This is typical of the system performance as seen during static firing.

The LOX tank ullage pressure during flight is shown in Figure 5-9. The ullage pressure was maintained within required limits by the GFCV throughout the flight and followed the anticipated trend. The GFCV reached full open at +120 seconds until the end of flight. The maximum GOX flowrate

during full open position of the valve was 24.4 kg/s (54 lbm/s). The GOX flow requirements for the remaining four engines increased after inboard engine cutoff until outboard engine cutoff. The heat exchanger performance showed some of the outlet temperature data points were above the expected performance limits; however, these temperatures did not exceed design limits of the ducting.

#### 5.7 S-IC PNEUMATIC CONTROL PRESSURE AND PURGE SYSTEM

The control pressure system on the S-IC stage performed satisfactorily during the 152-second flight. The functions of the system are:

- a. Close LOX and fuel prevalues after engine cutoff.
- b. Open LOX and fuel tank vent and relief valves if required.
- c. Hold LOX interconnect valves closed.
- d. Hold helium fill valve closed.

The actual pneumatic control regulator outlet pressure measured 520 N/cm<sup>2</sup> (755 psia) as shown in Figure 5-10. The control pressure system succeeded in actuating the prevalues after engine cutoff. All instrumented prevalues indicated closed positions. A slight drop in regulator outlet pressure was observed when engine number 5 prevalues were closed at approximately +136 seconds and again when engines number 1 through number 4 prevalues were closed at approximately +151 seconds. This is also shown in Figure 5-10 of outlet pressure trace.

The turbopump LOX seal gas generator actuator housing, and radiation calorimeter purge systems performed satisfactorily during the 152 second flight. The LOX Dome and GG LOX Injector Purge System also met all requirements.

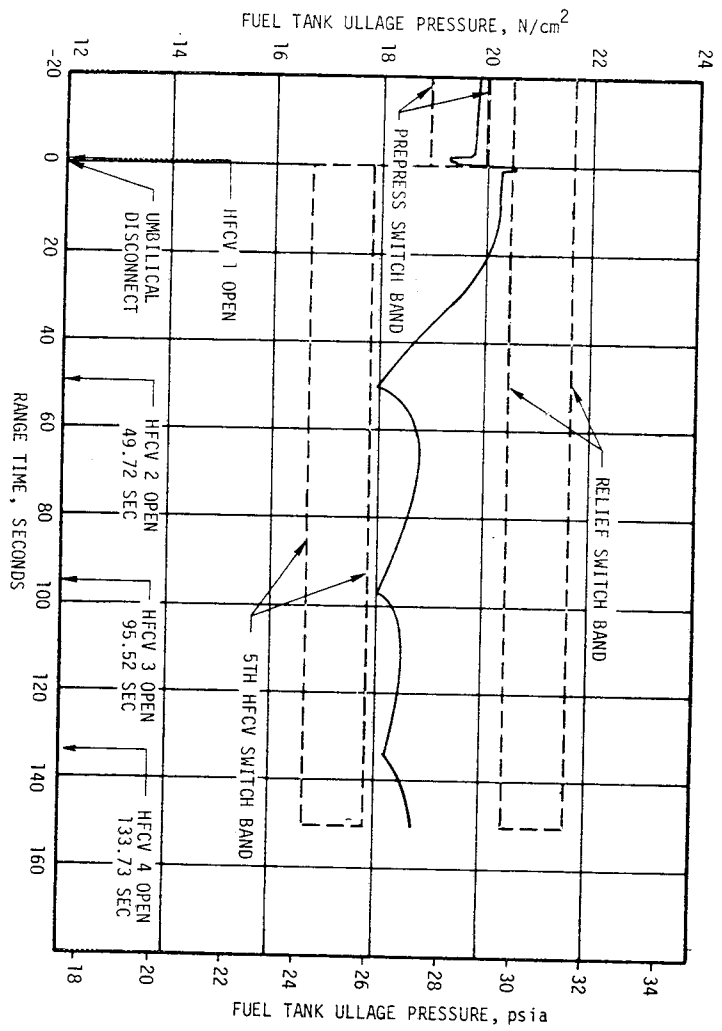


Figure 5-7. S-IC Fuel Ullage Pressure During Boost

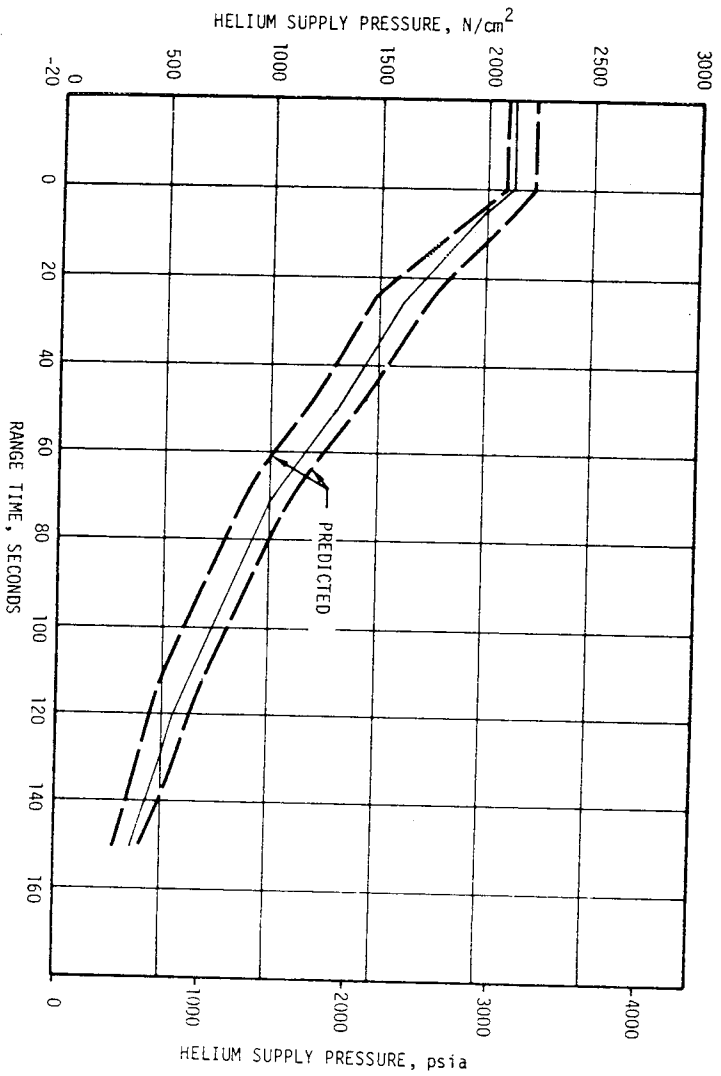


Figure 5-8. S-IC Helium Bottle Pressure for Fuel Pressurization

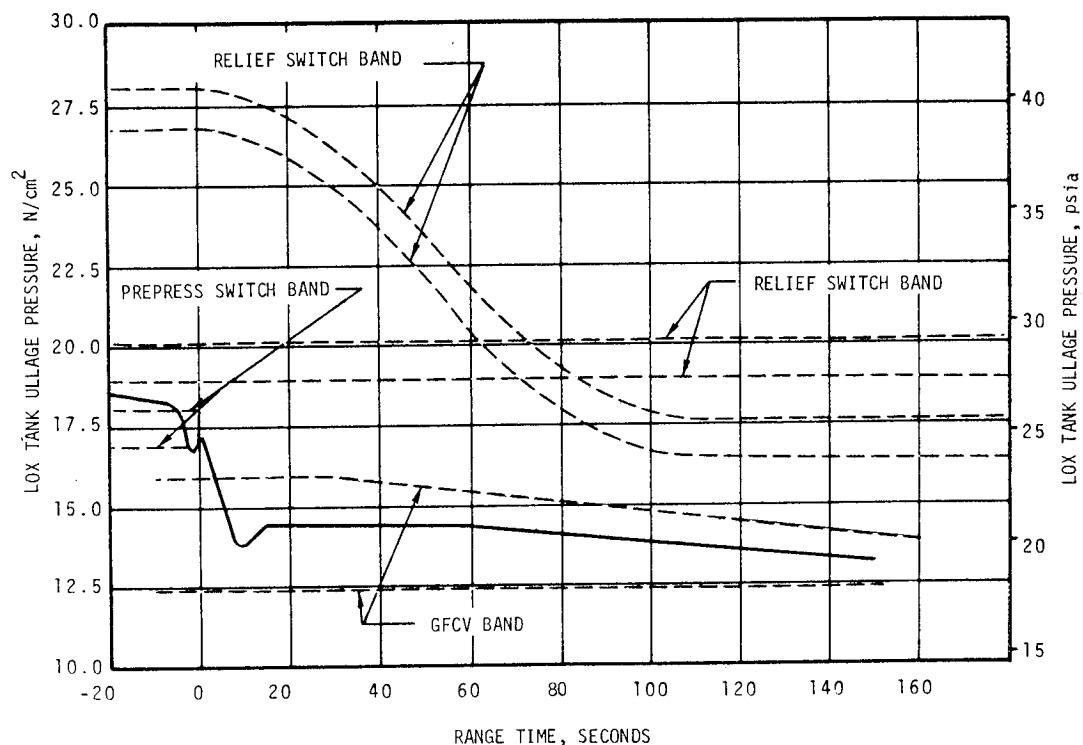


Figure 5-9. S-IC LOX Ullage Pressure

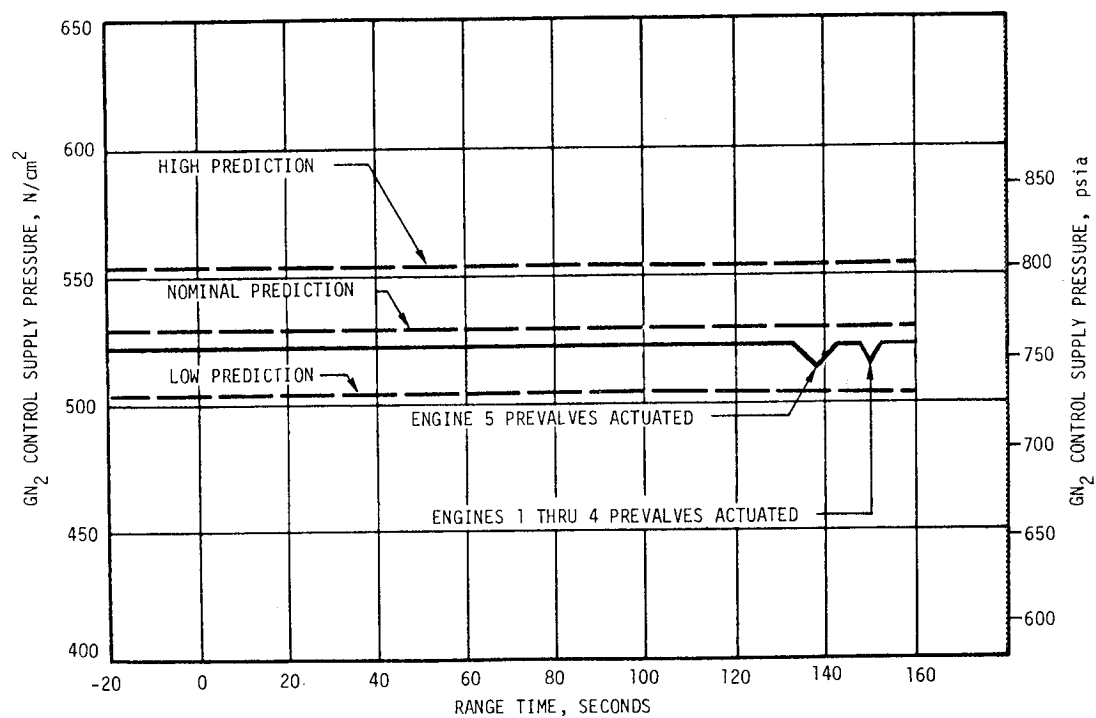


Figure 5-10. S-IC Pneumatic Control Regulator Outlet Pressure

## SECTION 6 S-II PROPULSION

### 6.1 SUMMARY

The S-II propulsion system operation during flight was satisfactory. The S-II stage performance was lower than predicted by very small percentages. Stage thrust as determined by telemetered propulsion measurements at 60 seconds of mainstage operation was 1.4 percent below the prediction value. At the same time period, total vehicle flowrate was 1.7 percent below prediction while the specific impulse exceeded the predicted level by 0.23 percent.

On the basis of flight simulation, the overall average S-II stage thrust and mass loss rate were 1.17 percent and 1.30 percent lower than predicted respectively. The specific impulse was higher by 0.14 percent during high mixture ratio operation.

The lower performance was attributed to engines numbers 2, 3, and 5, which required replacement of LOX turbopump assemblies after stage acceptance. The effects of these changes were not incorporated into the flight prediction, however the effects of these changes were within the predicted limits. Performances of engines 1 and 4 were very close to predicted.

Engine performance repeatability at 60 seconds from Engine Start Command (ESC) was within the allowable stage acceptance range. Engine thrust, mixture ratio and specific impulse were within 1.0 percent for all engines except number 3, which deviated by -2.6 percent on thrust and -1.5 percent on mixture ratio. The allowable engine acceptance performance variations are 3.0 and 2.0 percent for thrust and Engine Mixture Ratio (EMR) respectively, at rate conditions.

The propellant utilization system performed satisfactorily. Because of lower than predicted propellant flowrates and mixture ratios during the high EMR portion of S-II operation, PU step time was later than predicted by 15 seconds, but well within the allowable of  $\pm 50$  seconds. S-II burn time was approximately five seconds longer than predicted due to low propellant flowrates and a lower than predicted reference mixture ratio (RMR) setting. Propellant loadings were 0.173 percent less than predicted for LOX and 0.221 percent less than predicted for LH<sub>2</sub>. Residuals (propellant mass at S-II engine cutoff [ECO] in tanks only) were 1905 kilograms (4200 lbm) for LOX and 2148 kilograms (4735 lbm) for LH<sub>2</sub> versus the predicted 1458 kilograms (3210 lbm) LOX and 1936 kilograms (4268 lbm), LH<sub>2</sub>.

The subsystems operationally met all performance requirements, however, some out-of-band behaviors did occur and are discussed in the following paragraphs. The LH<sub>2</sub> stage fill valve closed slower than expected but within allowable tolerances. Changeout of the lip seal is being considered at this time.

The engine servicing system performed satisfactorily during prelaunch operations. At liftoff and S-II ESC, the engine start tank, the helium tank, and the thrust chamber conditions were within the required limit. In order to improve the performance margins of this system, recommendations are being considered to modify the start tank and thrust chamber redlines and to reduce the Ground Support Equipment (GSE) regulator pressure supplying GH<sub>2</sub> to the start tanks.

The LH<sub>2</sub> pressurization system supplied more than adequate Net Positive Suction Pressure (NPSP) to the engines at start and throughout mainstage. An LH<sub>2</sub> tank ullage pressure decay of 0.689 N/cm<sup>2</sup> (1.0 psi) occurred between end of pressurization on the ground to S-II ESC versus a predicted rise of 0.345 N/cm<sup>2</sup> (0.5 psi). This was of no consequence for AS-501 but may be of concern for AS-502 due to lower LH<sub>2</sub> ullage pressure. It has been recommended that a LH<sub>2</sub> "hi-press" operation like that implemented for the LOX tank on AS-501 be included after initial pressurization. This will provide the additional margin required to meet engine inlet pressure requirements on AS-502.

A high LH<sub>2</sub> bulk temperature resulted in slightly higher than predicted pump inlet temperatures at S-II ESC. This high LH<sub>2</sub> bulk temperature was caused by a high prelaunch vent stack back pressure. A modification to the Facility Hydrogen Disposal System is expected to reduce this high vent stack back pressure.

The LOX pressurization system supplied more than adequate NPSP to the engine at start and throughout mainstage. At liftoff minus 19 seconds, the LOX ullage pressure was marginal with respect to the requirement. To prevent this potential launch-abort condition from occurring on future flights the following recommendations are under consideration:

- a. Evacuate the common bulkhead, which will greatly reduce LOX tank ullage gas heat loss to the LH<sub>2</sub> tank.
- b. Eliminate LOX "hi-press" since it would not be necessary with a common bulkhead vacuum.
- c. Reduce the redline from 26.9 N/cm<sup>2</sup> (39 psia) to 25.2 N/cm<sup>2</sup> (36.5 psia).

At approximately 300 seconds after S-II ESC the LOX tank ullage pressure dropped out of the GOX regulator band. This was the result of an abnormally low GOX volumetric flow from the engine 4 heat exchanger and was possibly due to an obstruction in the heat exchanger flow path. No changes were recommended for the AS-502 flight. However, the possibility of opening up a redundant coil in the engine heat exchanger on later stages is being considered. This change will require investigation by the engine contractor and possible testing on the S-II battleship.

A greater than expected helium pneumatic gas usage occurred at ESC. This was caused by a slow closing helium purge valve on engine 2. Contamination of this valve was suspected and a modified valve including a filter has been implemented for future vehicles.

## 6.2 S-II CHILLDOWN AND BUILDUP TRANSIENT PERFORMANCE

The thrust chamber temperatures at prelaunch were satisfactory although they were on the low side of the predicted range. These temperatures ranged from 108.8 °K (-264 °F) to 100.8 °K (-278 °F) as shown in Figure 6-1. Engine number 3 showed 115.9 °K (-251 °F) which was well below the maximum redline of 144.3 °K (-200 °F).

The thrust chamber warmup rates of 22.8 °K to 33.9 °K (41 °F to 61 °F) exceeded the predicted 16.7 °K (30 °F) rise due to a warmer than expected engine environment. The high warmup rates coupled with the low chill resulted in nominal conditions at engine start. This greater than expected heatup rate resulted in thrust chamber temperatures at ESC of 141.5 °K to 125.7 °K (-206 to -233 °F), which was well within the maximum allowable of 161 °K (-170 °F).

This high thrust chamber heatup rate could result in exceeding the maximum allowable temperature at ESC if combined with a chilldown condition in the upper portion of the predicted band. This could then result in a engine/pump stall condition or "no start". Consequently, it was recommended that the prelaunch redline be reduced by 17.7 °K (30 °F) which shifts the requirements from 144.3 °K to 127.5 °K (-200 to -230 °F). To ensure meeting the new redline, the auto sequence permissive temperature should be reduced from 161 °K to 150 °K (-170 to -190 °F). Because of changes to engine thrust chamber temperature start requirements (raised from 161 °K to 172 °K [-170 °F to -150 °F]) and pending verification of the thrust chamber temperature rise rates, further changes to redline requirements may be expected. GSE and stage systems can meet the new redline and permissive temperatures as demonstrated on the AS-501 flight.

Both pressure and temperature results of the J-2 engine start tanks were within the required prelaunch and engine start box conditions. These start tank conditions occurred near the cold side of the box as shown in Figure 6-2. This start tank condition was caused by pressurization from a high chill pressure of 506 to 827 N/cm<sup>2</sup> (735 to 1200 psia) and a different than expected environment in the S-IC/S-II interstage. This pressurization procedure was different from the lower pressurization conducted during static testing at Mississippi Test Facility (MTF). This higher pressurization results in an extended chilldown time which causes slightly higher pressures at prelaunch. If the allowable two minute hold occurs between start of pressurization (from liftoff -277 seconds to liftoff -187 seconds) the maximum heatup rates will cause the start tank relief valve to open. This mode of operation is undesirable and the following recommendations are under consideration:

- a. Revise start tank prelaunch and engine start box conditions.

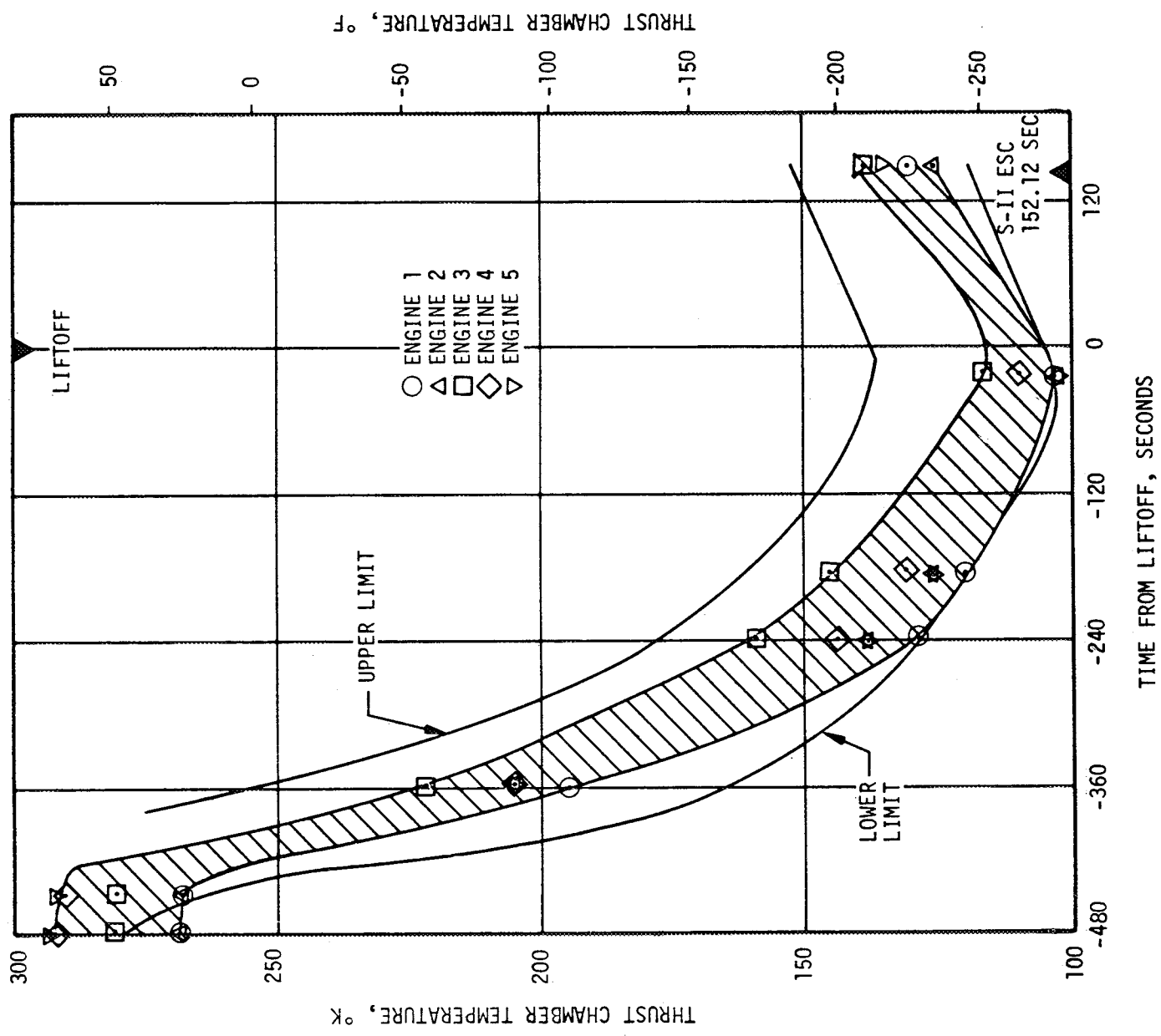


Figure 6-1. S-II Thrust Chamber Temperatures



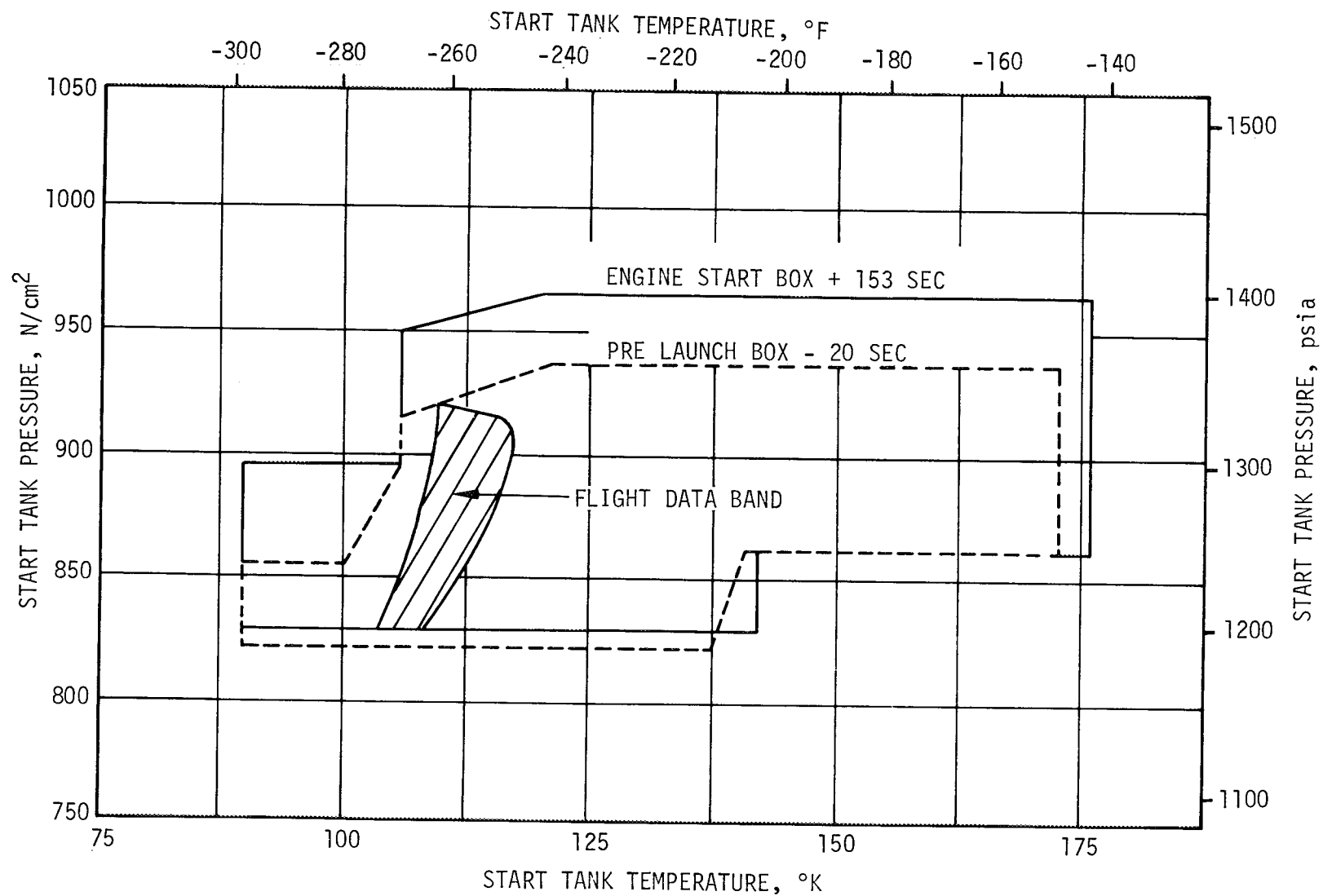


Figure 6-2. S-II Engine Start Tank Performance

- b. Revise the pressurization regulator setting from  $830 \pm 10.3 \text{ N/cm}^2$  ( $1205 \pm 15 \text{ psia}$ ) to  $808 \pm 10.3 \text{ N/cm}^2$  ( $1175 \pm 15 \text{ psia}$ ).
- c. Reorifice the GSE heat exchanger to provide warmer chill gas for the start tank.

The engine helium tank pressures were within the required prelaunch and engine start limit of  $2376 \text{ N/cm}^2$  ( $3446 \text{ psia}$ ), however, the tank pressure at ESC was above the predicted band. Engine number 3 had the highest pressure of  $2352 \text{ N/cm}^2$  ( $3411 \text{ psia}$ ). This was caused by the ground regulator pressure setting being high. A greater than expected helium pneumatic gas usage occurred at ESC which was caused by the slow closing of the helium purge valve on engine number 2. The closure of this valve occurred 4 seconds after ESC. Contamination of this valve was suspected and a modified valve including a filter has been implemented for future vehicles.

Prepressurization of the propellant tanks was performed during the prelaunch automatic sequence, attaining an LH<sub>2</sub> ullage pressure of  $22.4 \text{ N/cm}^2$  ( $32 \text{ psia}$ ) and a LOX ullage pressure of  $26.6 \text{ N/cm}^2$  ( $38 \text{ psia}$ ). LOX tank ullage pressure was further increased to  $28.0 \text{ N/cm}^2$  ( $40 \text{ psia}$ ) at liftoff minus 30 seconds. The LH<sub>2</sub> and LOX ullage pressures at ESC command were  $21 \text{ N/cm}^2$  ( $31 \text{ psia}$ ) and  $24.0 \text{ N/cm}^2$  ( $34.8 \text{ psia}$ ), respectively, well within the required limits.

Both the LH<sub>2</sub> and LOX recirculation systems performed satisfactorily giving satisfactory pump inlet conditions as shown in Figure 6-3. However, the LH<sub>2</sub> temperature was greater than predicted. This higher LH<sub>2</sub> pump inlet temperature was greater than expected due to a high LH<sub>2</sub> bulk temperature. This high bulk temperature, as shown on Figure 6-4, was caused by a high prelaunch vent stack back pressure. A modification to the Facility Hydrogen Disposal System is expected to reduce this high vent stack back pressure. The S-IVB stage experienced the same condition.

Individual J-2 engine thrust buildups were completely satisfactory. Figure 6- shows that each engine lies within the required envelope. The slowest thrust buildup was exhibited by engine number 3 which repeated its performance during stage acceptance. The most rapid buildup occurs on engine number 4. As expected, all buildup rates were faster and more uniform than those measured during stage acceptance at sea level.

The small disturbance apparent in the buildup of engine number 4 approximately three seconds after S-II engine start, was attributed to the action of the main LOX valve. Main thrust chamber pressure and main LOX valve position are shown on a common time axis in Figure 6-6. The initial second position ramp rate for the valve is quite slow, resulting in a more rapid than normal engine buildup. After the excess hydraulic forces on the valve gate are relieved, the valve moves rapidly to the full open position and the system returns to its normal operating level.

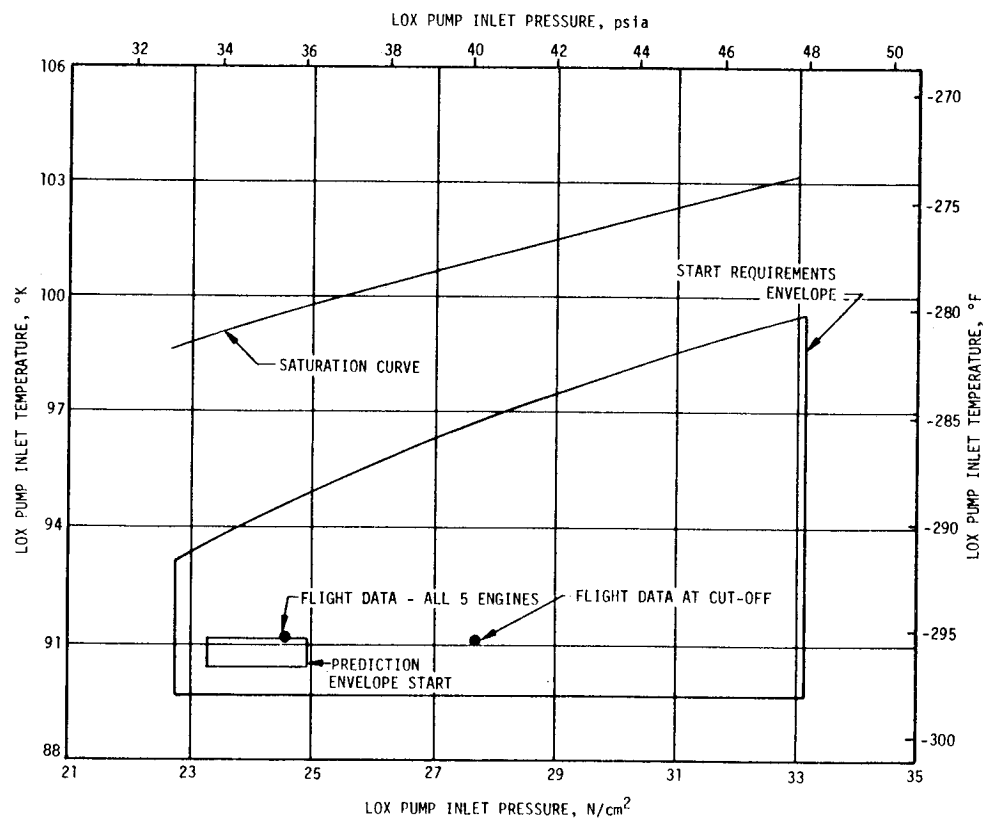
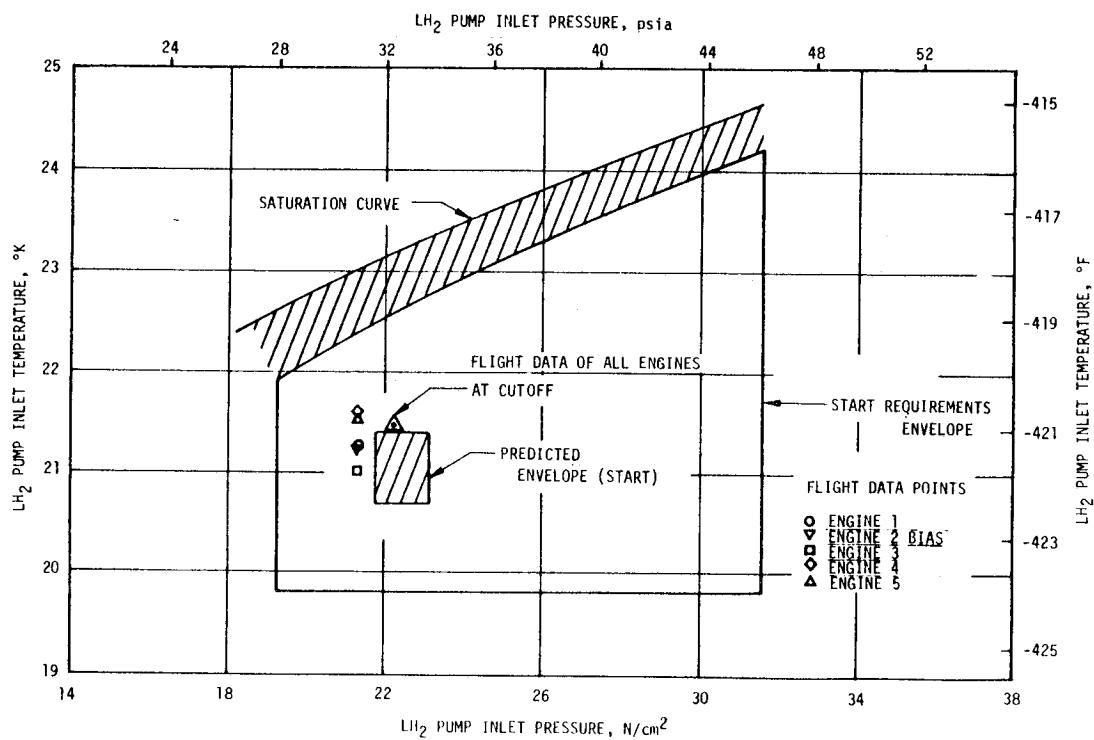
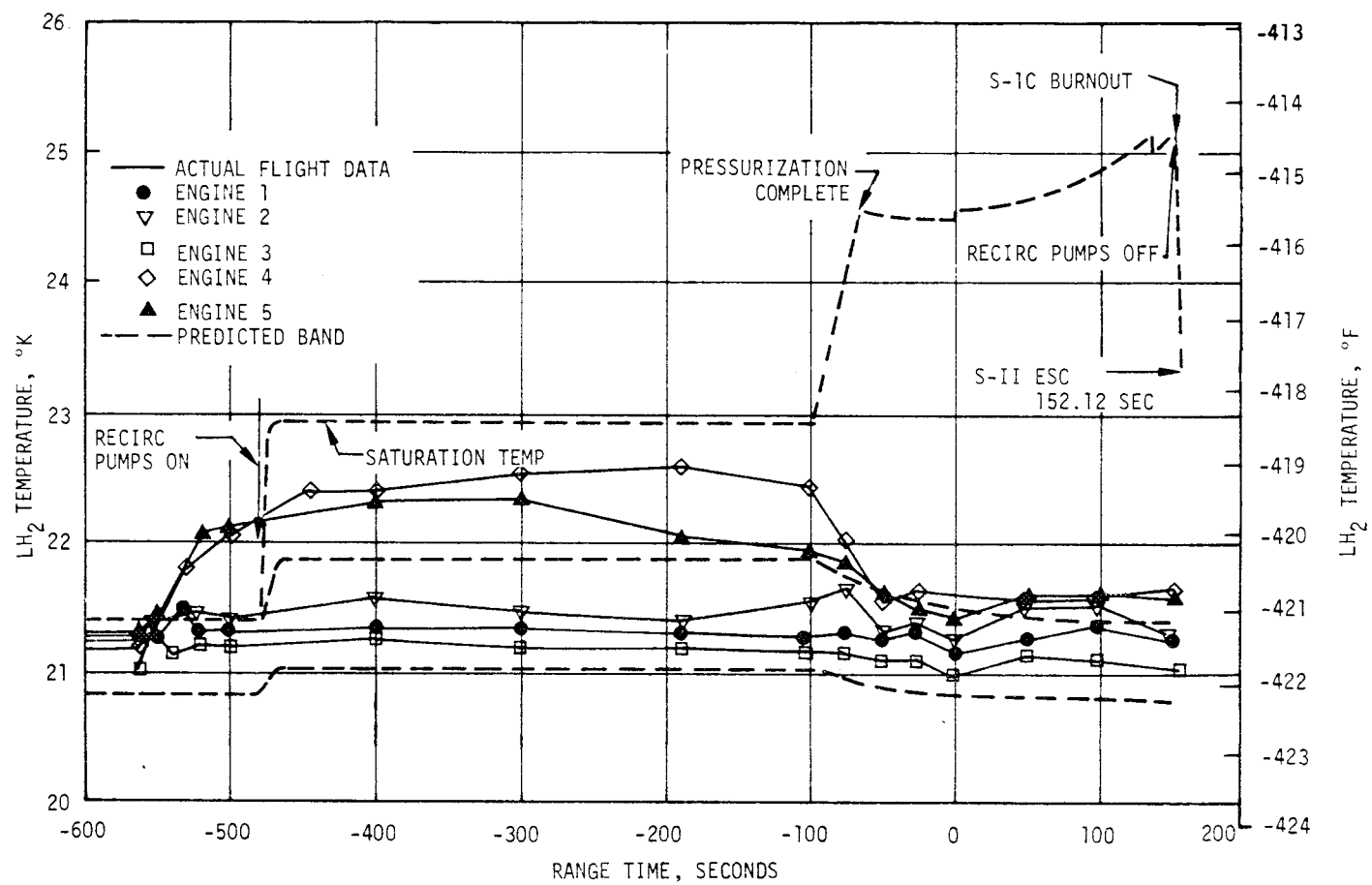
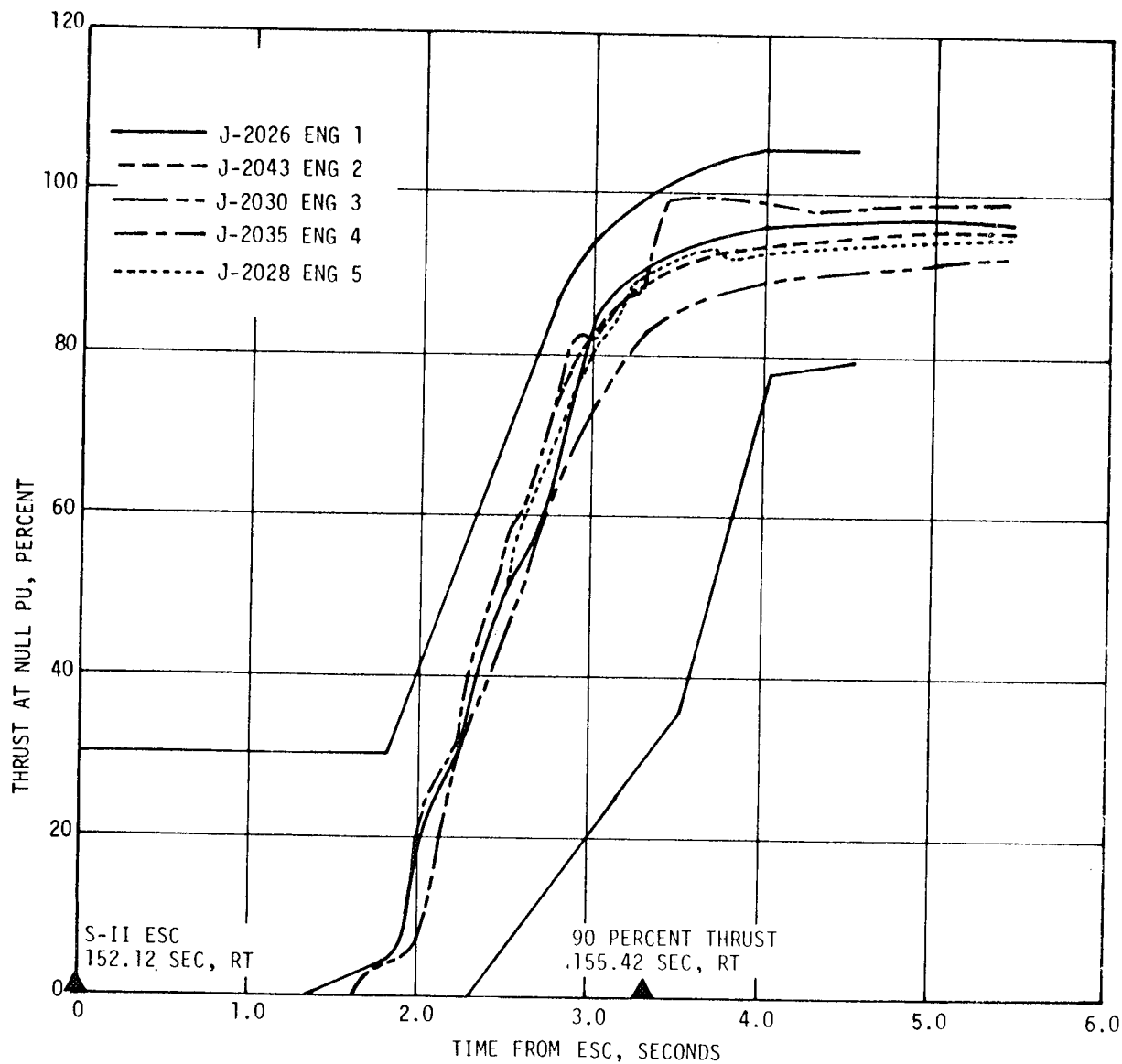


Figure 6-3. S-II Start Box Requirements

Figure 6-4. S-II LH<sub>2</sub> Recirculation System Performance



NOTE: 100 PERCENT THRUST BASED ON ENGINE THRUST AT 60 SECOND TIME SLICE.

Figure 6-5. S-II Engine Thrust Buildup

6-10

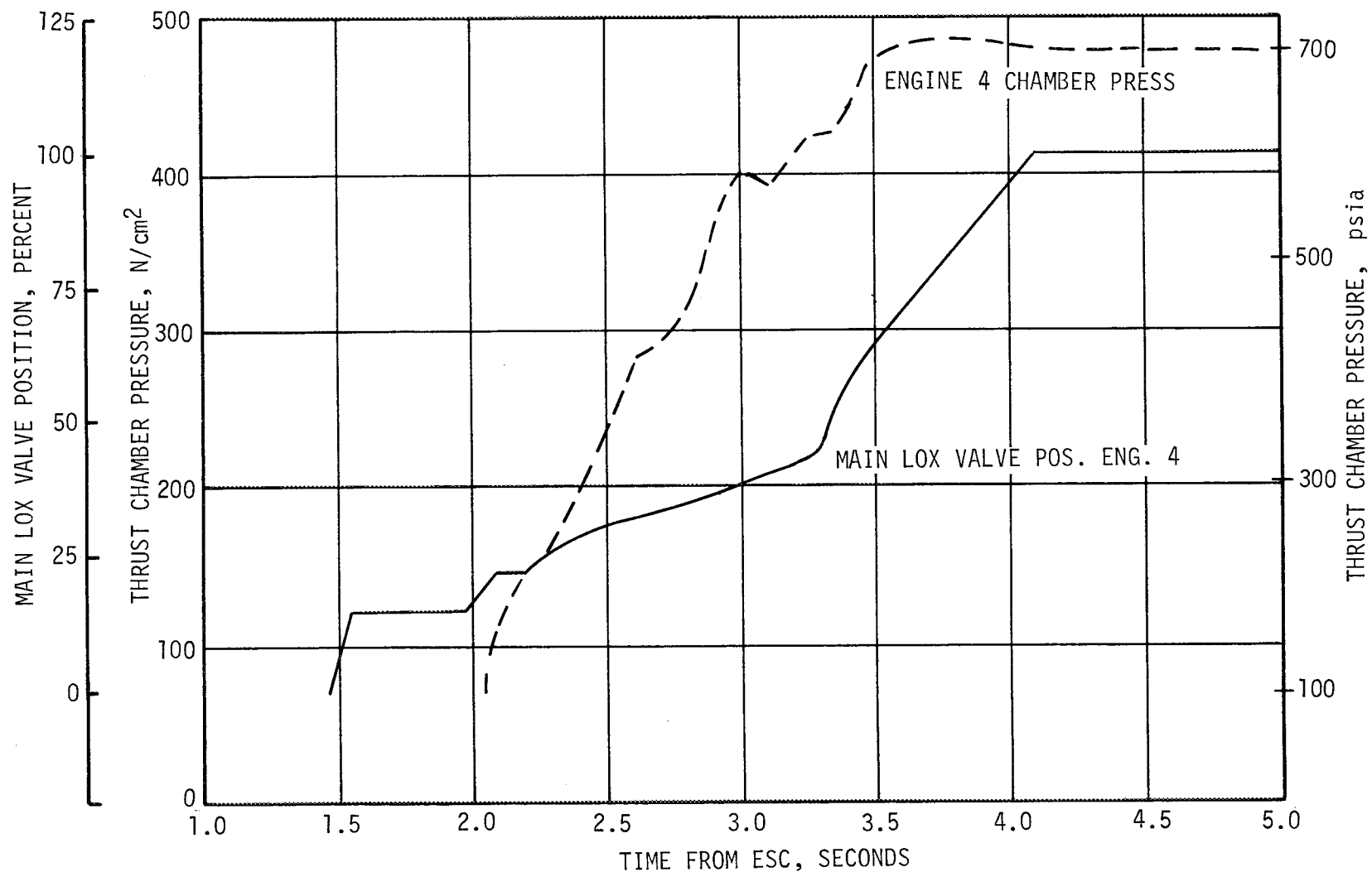


Figure 6-6. S-II Chamber Pressure Buildup on Engine Number 4

Similar operating characteristics were observed during stage acceptance testing of S-II-3 at MTF and have occurred many times during engine acceptance. The engine manufacturer does not consider this characteristic to be detrimental to engine reliability. No problems resulted in mainstage operation as a result of the small disturbance in thrust buildup.

### 6.3 S-II MAIN STAGE PERFORMANCE

The stage performance during mainstage operation was satisfactory, but slightly below the predicted performance. A comparison of predicted and actual performance of thrust, total flowrate, specific impulse, and mixture ratio is shown in Figure 6-7. The deviations in predicted performance on the individual engines ranged from a -2.6 percent to + 0.2 percent thrust as shown in Table 6-1. This table also shows the specific impulse, total flowrate and mixture ratio deviation from the predicted.

The total stage thrust at 60 seconds after ESC was 5,056,695 Newtons (1,136,847 lbf) as compared to a predicted of 5,128,544 Newtons (1,153,000 lbf). The stage specific impulse, propellant flowrate, and mixture ratio was 4180 N-s/kg (426.2 lbf-s/lbm), 1210.0 kg/s (2667.5 lbm/s) and 5.53 (LOX/Fuel), respectively. This stage performance was in close agreement with the predicted of 4170 N-s/kg (425.2 lbf-s/lbm), 1230.8 kg/s (2713.5 lbm/s), and 5.57, respectively.

Two separate analyses were employed in reconstructing S-II stage propulsion system performance. The first method, propulsion reconstruction analysis, utilized telemetered engine and stage data to compute longitudinal thrust, specific impulse, and stage mass flowrate. In the second method, flight simulation, a six-degree-of-freedom trajectory simulation was utilized to fit propulsion reconstruction analysis results to the trajectory. Using a differential correction procedure, this simulation determined adjustments to the reconstruction analysis of thrust and mass flow histories to yield a simulated trajectory which closely matched the observed mass point trajectory. These results were obtained by an iterative adjustment procedure which resulted in an increase of 0.14 percent and 0.45 percent to the total average thrust and flowrate respectively. The resulting decrease in specific impulse was 0.3 percent. A comparison of the predicted, reconstructed and simulated propulsion performance is given in Table 6-2.

The fit of the simulated trajectory to the observed trajectory was very good with the maximum deviations occurring near S-II ECO. The deviations in velocity and acceleration were 1.0 m/s and 0.1 m/s<sup>2</sup>.

### 6.4 S-II SHUTDOWN TRANSIENT PERFORMANCE

Engine cutoff signal was received 367.624 seconds after S-II start (519.76 seconds range time). At this time the total stage thrust was 4,084,883 Newtons (918,364 lbf) and the average EMR was 4.52. The stage thrust decayed to 5.0 percent of this level in approximately 410 milliseconds. The J-2 engine shutdown transient band as shown in Figure 6-8 was within the model specification limits.

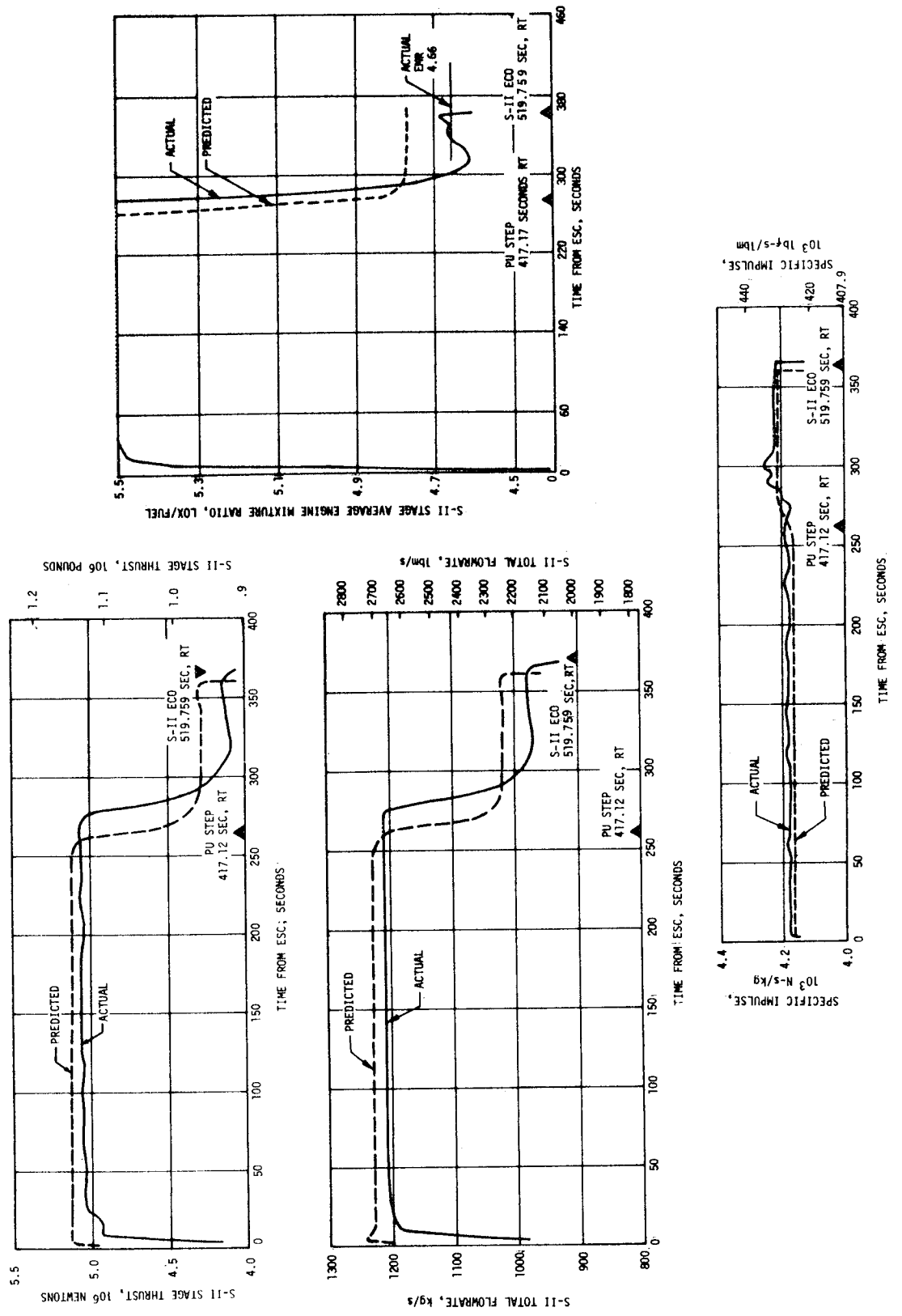


Figure 6-7 S-II Steady State Operation



Table 6-1. S-II Engine Performance Deviations

PARAMETER	ENGINE	PREDICTED	RECONSTRUCTION ANALYSIS	DEVIATION PERCENT
Thrust N (lbf)	1	1,033,270 (232,288)	1,035,726 (232,852)	+0.24
	2	1,033,270 (232,288)	1,006,965 (226,386)	-2.55
	3	1,019,926 (229,288)	993,163 (223,283)	-2.62
	4	1,019,926 (229,288)	1,021,626 (229,682)	+0.17
	5	1,020,371 (229,388)	999,216 (224,644)	-2.07
Specific Impulse N-s/kg (lbf-s/lbm)	1	4179.9 (426.23)	4188.3 (426.19)	+0.20
	2	4156.3 (423.82)	4195.7 (428.27)	+0.95
	3	4162.9 (424.50)	4164.2 (424.63)	+0.03
	4	4171.5 (425.37)	4180.1 (426.25)	+0.21
	5	4159.7 (424.17)	4166.9 (424.91)	+0.17
Flowrate kg/s (lbm/s)	1	247.2 (545.0)	247.3 (545.2)	+0.04
	2	248.6 (548.1)	240.0 (529.1)	-3.46
	3	245.0 (530.1)	238.5 (525.8)	-2.65
	4	244.5 (539.0)	244.4 (538.8)	-0.04
	5	245.3 (540.8)	239.8 (528.7)	-2.12
Mixture Ratio LOX/fuel	1	5.63	5.64	+0.18
	2	5.61	5.48	-2.32
	3	5.44	5.37	-1.29
	4	5.46	5.53	+1.28
	5	5.46	5.51	+0.92

NOTE: Analysis is at ESC plus 60 seconds.

Table 6-2. S-II Flight Reconstruction Comparison With Simulation Trajectory Match Results

PARAMETERS	UNITS	PREDICTED			RECONSTRUCTION ANALYSIS			PERCENT DEV. FROM PRED. (4)		
		HIGH MIXTURE RATIO (1)	REFERENCE MIXTURE RATIO (2)	TOTAL FLIGHT AVERAGE (3)	HIGH MIXTURE RATIO (1)	REFERENCE MIXTURE RATIO (2)	TOTAL FLIGHT AVERAGE (3)	HIGH MIXTURE RATIO (1)	REFERENCE MIXTURE RATIO (2)	TOTAL FLIGHT AVERAGE (3)
Average Longitudinal Stage Thrust	N (1b <sub>f</sub> )	5,114,023 (1,149,678)	4,293,659 (965,253)	4,900,993 (1,101,787)	5,058,360 (1,137,165)	4,118,900 (925,966)	4,832,528 (1,086,396)	-1.09	-4.10	-1.40
Average Vehicle Mass Loss Rate	kg/s (1bm/s)	1226.86 (2704.77)	1018.96 (2246.42)	1172.87 (2585.74)	1209.9 (2667.4)	974.5 (2148.4)	1153.7 (2543.5)	-1.38	-4.36	-1.77
Average Stage Longitudinal Specific Impulse	N-sec/kg 1b <sub>f</sub> -s/1bm	4168.4 (425.06)	4213.8 (429.69)	4178.6 (426.10)	4181 (426.3)	4227 (431.0)	4188 (427.7)	+0.29	+0.31	+0.38
		SIMULATION-TRAJECTORY MATCH			PERCENT DEV. FROM PRED. (5)			PERCENT DEV. FROM RECONSTRUCTION (6)		
PARAMETERS	UNITS	HIGH MIXTURE RATIO (1)	REFERENCE MIXTURE RATIO (2)	TOTAL FLIGHT AVERAGE (3)	HIGH MIXTURE RATIO (1)	REFERENCE MIXTURE RATIO (2)	TOTAL FLIGHT AVERAGE (3)	HIGH MIXTURE RATIO (1)	REFERENCE MIXTURE RATIO (2)	TOTAL FLIGHT AVERAGE (3)
Average Longitudinal Stage Thrust	N (1b <sub>f</sub> )	5,065,322 (1,138,730)	4,125,862 (927,531)	4,839,490 (1,087,961)	-0.95	-3.90	-1.25	+0.14	+0.17	+0.14
Average Vehicle Mass Loss Rate	kg/s (1bm/s)	1215.2 (2679.0)	979.8 (2160.0)	1157.4 (2555.1)	-0.10	-3.84	-1.32	+0.44	+0.54	+0.46
Average Stage Longitudinal Specific Impulse	N-sec/kg 1b <sub>f</sub> -s/1bm	4168.8 (425.1)	4211.1 (429.4)	4175.7 (425.8)	+0.01	-0.07	+0.07	-0.28	-0.37	-0.30
(1) FROM 90% THRUST TO PU CUTBACK (2) FROM PU VALVE CUTBACK +50 SEC TO J-2 CUTOFF (3) FROM 90% THRUST TO J-2 CUTOFF (4) RECONSTRUCTED MINUS PREDICTED IN PERCENT (5) FLIGHT SIMULATION MINUS PREDICTED IN PERCENT (6) FLIGHT SIMULATION MINUS RECONSTRUCTION IN PERCENT					NOTE: RESULTS ARE AVERAGE INFIGHT VALUES REDUCED TO VACUUM CONDITIONS.					

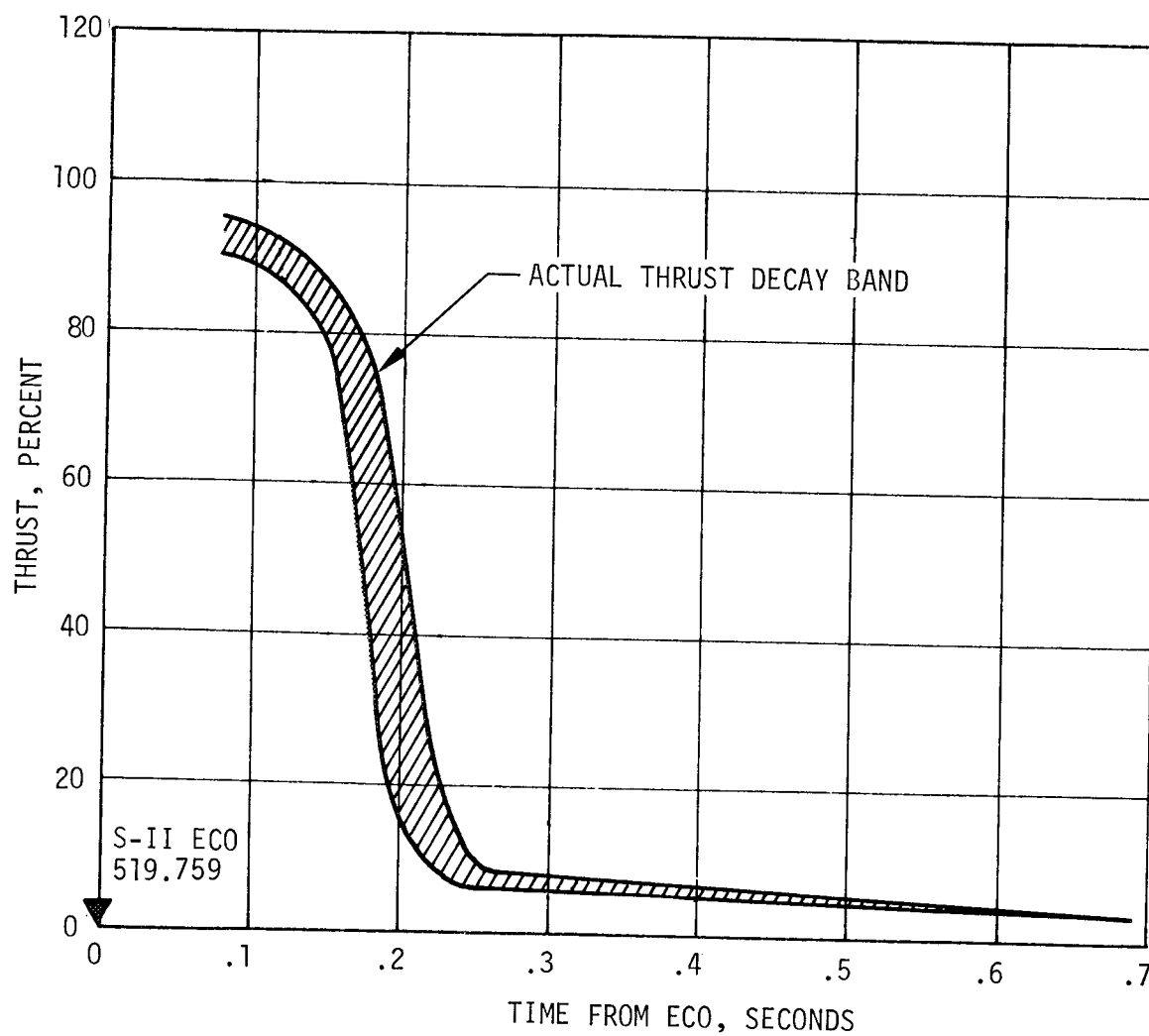


Figure 6-8. S-II Engine Shutdown Transient

The total engine cutoff impulse from engine cutoff signal to zero thrust was 923,552 N-s (207,633 lbf-s) compared to a predicted cutoff impulse of 1,012,860 N-s (227,700 lbf-s). This greater-than-expected cutoff impulse resulted in a velocity increase of 4.7 m/s (15.42 ft/s) compared to the predicted of 4.2 m/s (13.8 ft/s). The velocity increase had good correlation with the cutoff impulse change from predicted.

#### 6.5 S-II PROPELLANT MANAGEMENT

The propellant management system satisfactorily performed the functions of propellant loading, mass indication, point sensor level indication and propellant utilization.

The LOX tank was filled through the 15.2 cm (6 inch) replenish line at a slow rate of 0.0574 m<sup>3</sup>/s (900 gpm) maximum as a result of problems encountered with the fast-fill system during countdown demonstration tests. The facility Propellant Tanking Control System (PTCS) functioned satisfactorily during S-II loading and replenishing. The best estimates of propellants loaded were 69,416 kilograms (153,036 lbm) LH<sub>2</sub> and 358,416 kilograms (790,171 lbm) LOX based on flowmeter integration from the 3.0 percent LH<sub>2</sub> point sensor indicated mass and the 2.0 percent LOX point sensor indicated mass. This compares to predicted values of 69,569 kilograms (153,375 lbm) LH<sub>2</sub> and 359,037 kilograms (791,542 lbm) LOX.

At 5.5 seconds after ESC, the "PU activate" command was received and the PU valves stepped from the nominal engine start position of 5.0 EMR to the full-closed position, providing a nominal EMR of 5.5 for the first phase of S-II Programmed Mixture Ratio (PMR). The PU valves moved off the high EMR stop at 265 seconds compared to the predicted of 250 ± 50 seconds as shown in Figure 6-9. This PU step resulted in a thrust drop of 971,812 Newtons (218,483 lbf). The later than nominal step time was attributed to a lower than predicted RMR setting. The EMR started to decrease at 277 seconds, gradually moving towards a time averaged value of 4.66 EMR versus the predicted value of 4.77 EMR. Oscillations about this average were due to probe nonlinearities. A minimum value of 4.62 EMR occurred at 325 seconds and a maximum value of 4.68 EMR occurred at 357 seconds. Figure 6-10 shows the probe/tank mismatch as determined by comparison of mass data from the point sensors, PU probes, and flowmeters. The PU system error at cutoff signal was + 116 kilograms (+255 lbm) of LH<sub>2</sub> relative to that predicted at the actual LOX cutoff level. This was well within the allowable error of ± 664 kilograms (± 1465 lbm) LH<sub>2</sub>.

LOX depletion cutoff signal was received at 519.76 seconds, resulting in 367.624 seconds S-II burn time at which time the LOX remaining in the tanks and sump was 1905 kilograms (4200 lbm) versus 1458 kilograms (3210 lbm) predicted. The LH<sub>2</sub> remaining in the tank was 2147 kilogram (4735 lbm) versus 1936 kilograms (4268 lbm) predicted. This was determined by extrapolation

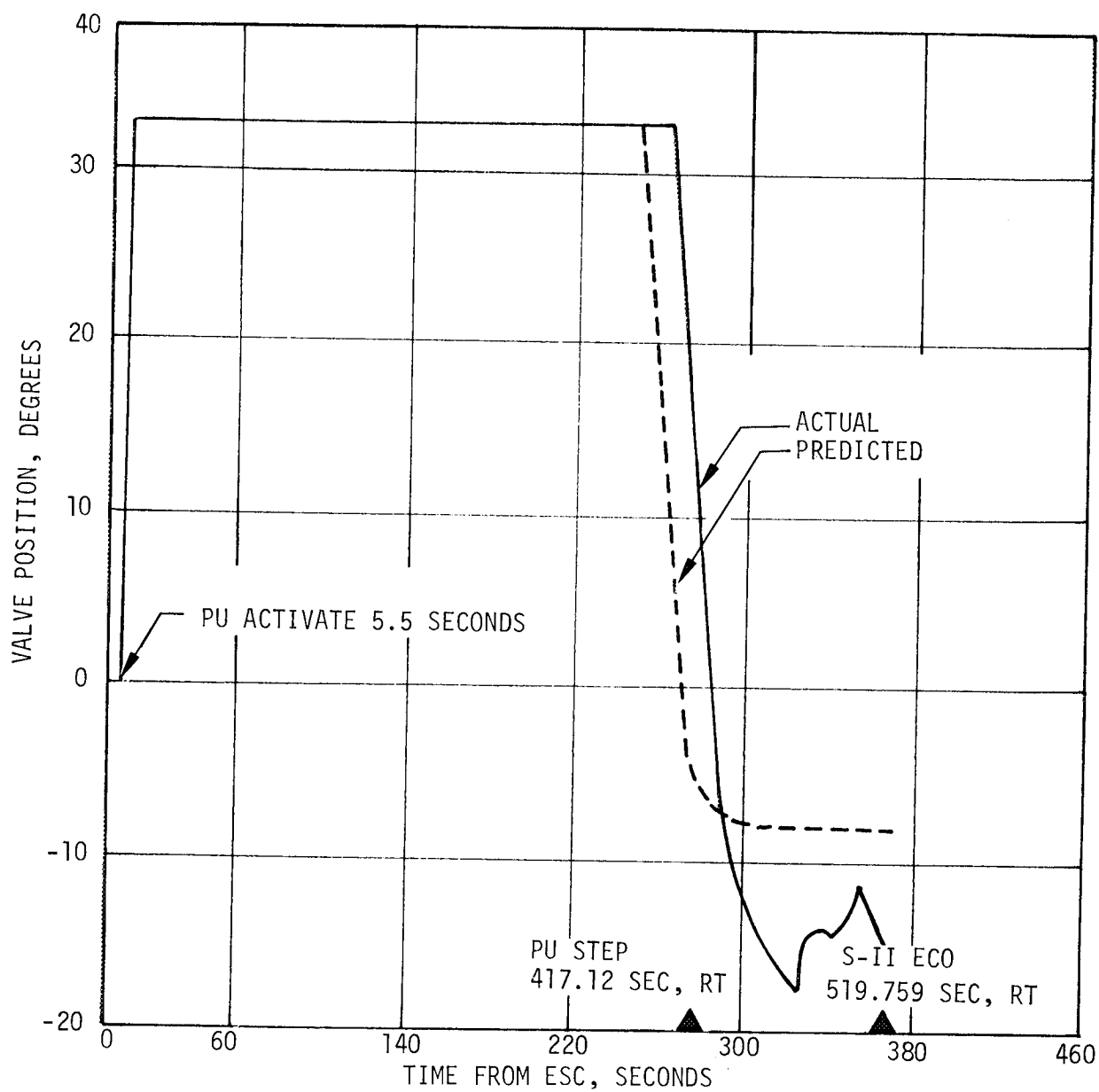
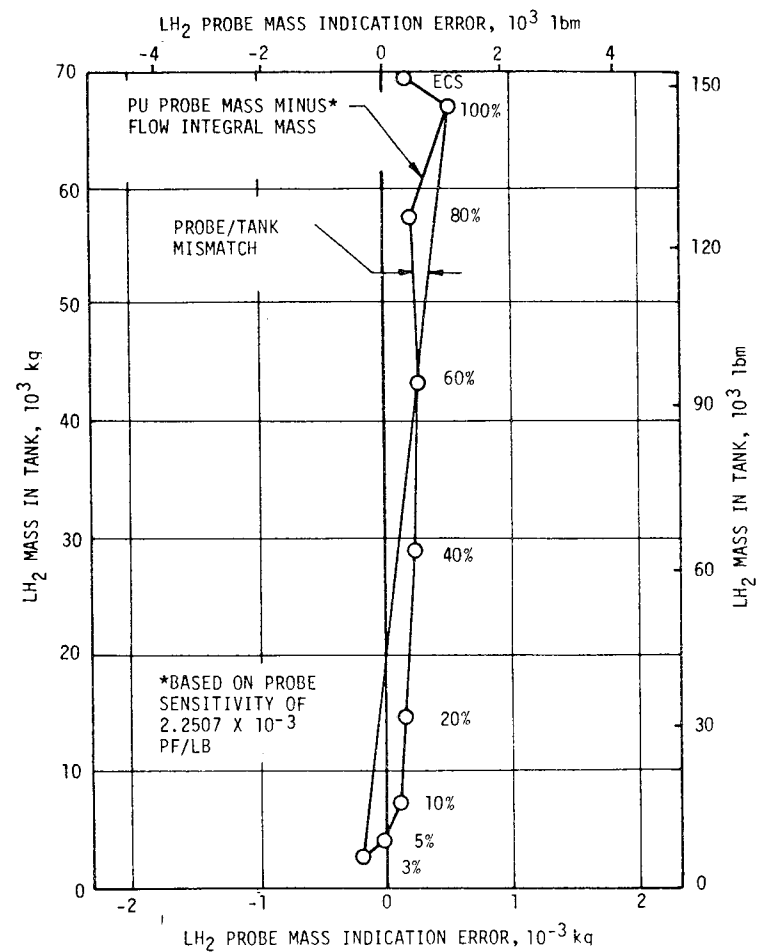
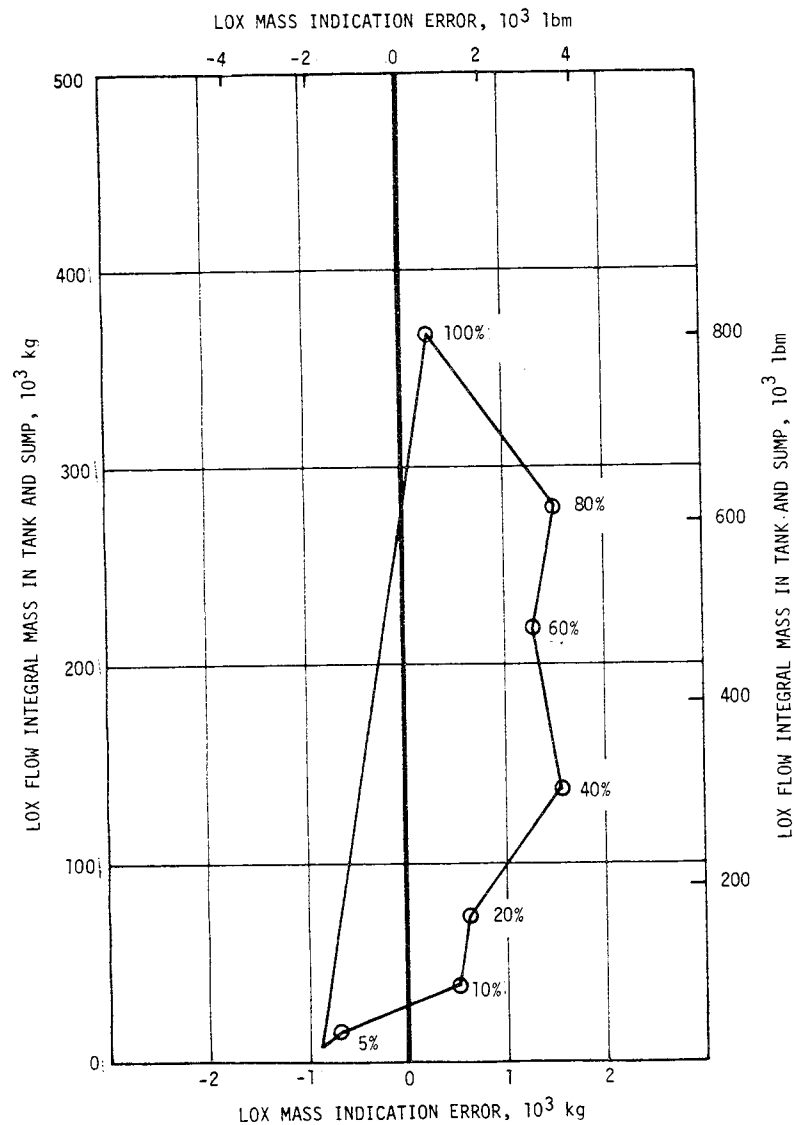


Figure 6-9. S-II PU Valve Position

Figure 6-10. S-II LOX and LH<sub>2</sub> Probe/Tank Mismatch

of point sensor data from the 2.0 percent LOX level and the 3.0 percent LH<sub>2</sub> level to the time of cutoff signal. The higher than predicted residuals were due to deletion of a 0.5 second time delay originally planned.

A comparison of propellant masses measured by the flowmeters, point sensors, and PU probes is given in Table 6-3. The best estimate mass at S-II ignition and cutoff, as determined from capacitance probe point level sensors, flow meters and the trajectory simulation was 642,079 kilograms (1,415,542 lbm) and 210,967 kilograms (465,103 lbm) respectively as shown in Figure 6-11.

The propellant slosh frequencies during S-IC and S-II burn were approximately two radians per second. The slosh effects were significantly attenuated by the electronic filters and PU system performance was stable throughout S-II stage flight. Further slosh analysis is being conducted.

## 6.6 S-II PRESSURIZATION SYSTEM

### 6.6.1 S-II Fuel Pressurization System

During prepressurization, the LH<sub>2</sub> tank was pressurized to the pressure switch setting of 22 N/cm<sup>2</sup> (32 psia). No helium makeup was required. During S-IC boost, the LH<sub>2</sub> tank pressure decayed 0.69 N/cm<sup>2</sup> (1.0 psi). It was predicted that the ullage pressure would decay midway through S-IC boost and then increase again for a net gain of 0.34 N/cm<sup>2</sup> (0.5 psi) over the pressure switch setting as shown in Figure 6-12. The ullage pressure at engine start was 21.4 N/cm<sup>2</sup> (31.0 psia) compared to the predicted pressure of 22.4 N/cm<sup>2</sup> (32.5 psia). Consequently, the LH<sub>2</sub> ullage pressure at ESC was 1.0 N/cm<sup>2</sup> (1.5 psia) lower than predicted. This pressure decay was probably lower than predicted due to a higher than expected heat loss from the ullage gas to the LH<sub>2</sub>. Since the pressurization control bands were lowered 1.7 N/cm<sup>2</sup> (2.5 psi) for structural reasons on AS-502 only, it is recommended that the LH<sub>2</sub> prepressurization sequence be changed to assure colder ullage and/or to

Table 6-3. S-II Propellant Consumption

EVENT	UNITS	PREDICTED		PU SYSTEM		ENGINE FLOW INTEGRAL		LEVEL SENSORS ANALYSIS		BEST ESTIMATE	
		LOX	LH <sub>2</sub>	LOX	LH <sub>2</sub>	LOX	LH <sub>2</sub>	LOX	LH <sub>2</sub>	LOX	LH <sub>2</sub>
Engine Start Command	kg	359,037	69,569	359,037	69,596	358,415	69,416	358,608	69,739	358,415	69,416
	lbm	791,542	153,375	791,489	153,432	790,171	153,036	792,800	153,750	790,171	153,036
PU Activate	kg	356,412	68,879	356,941	69,079	355,790	68,726	357,113	69,264	355,790	68,726
	lbm	785,754	151,852	786,921	152,293	784,383	151,516	787,300	152,700	784,383	151,516
Mixture Ratio Step	kg	76,884	21,772	77,657	18,264	77,053	18,030	76,884	18,144	77,053	18,030
	lbm	169,500	47,998	171,205	40,266	169,874	39,749	169,500	40,000	169,874	39,749
*Residuals	kg	1677	1952	1488	1975	1920	2073	1728	2076	1728	2076
	lbm	3698	4303	3281	4355	4233	4571	3810	4578	3810	4578
*Residual at end of thrust decay in tank and sump.											

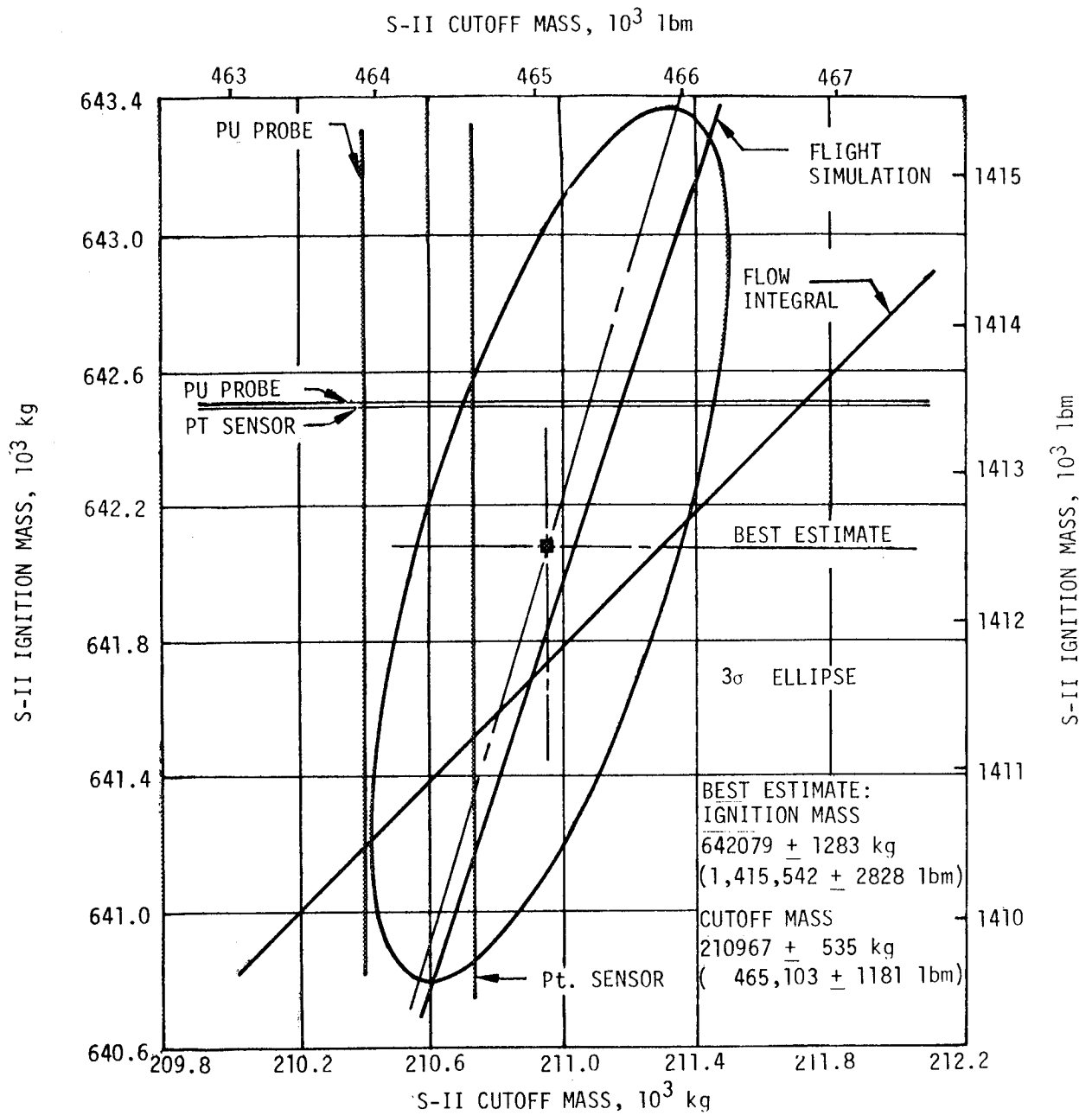


Figure 6-11. Stage Mass at S-II Ignition and Cutoff



include a "hi-press" mode of operation after initial pressurization. This change is required to insure that engine start NPSP requirements are met.

LH<sub>2</sub> tank pressurization during flight was normal. The regulator controlled the ullage pressure within the control band up to the time step pressurization was initiated at 320 seconds from engine start. The ullage pressure increased after step pressurization and at cutoff was at 22.1 N/cm<sup>2</sup> (32.0 psia) which agrees with the prediction as shown in Figure 6-13.

No fuel pressurization venting was experienced and pump inlet conditions were met as shown in Figure 6-14.

#### 6.6.2 S-II LOX Pressurization System

Prepressurization of the S-II stage LOX tank was normal. Approximately 60 seconds were required to prepressurize the LOX tank to the pressure switch setting. Several helium makeup cycles were required to maintain LOX tank pressure within the pressure switch settings. At -40 seconds "hi-press" was initiated increasing the LOX ullage pressure to the vent valve cracking pressure of 27.58 N/cm<sup>2</sup> (40.0 psia). The vent valve reseated at 27.23 N/cm<sup>2</sup> (39.5 psia). At -19 seconds, just prior to liftoff, the S-II stage LOX ullage pressure approached the redline value of 26.89 N/cm<sup>2</sup> (39 psia) which was probably due to LOX tank vent valves reseating at 27.23 N/cm<sup>2</sup> (39.5 psia) during the "hi-press" operation. In addition, the measurement being monitored by the redline observer was probably reading somewhat lower than actual. Ullage pressure was within limits at J-2 start. To prevent this potential launch-scrub condition from occurring on future flights the following recommendations are under consideration:

- a. Evacuate the common bulkhead, which will greatly reduce LOX tank ullage gas heat loss to the LH<sub>2</sub> tank.
- b. Eliminate LOX "hi-press" since it would not be necessary with a common bulkhead vacuum.
- c. Reduce the redline from 26.9 N/cm<sup>2</sup> (39 psia) to 25.2 N/cm<sup>2</sup> (36.5 psia).

During S-IC boost the LOX tank ullage pressure decayed 3.2 N/cm<sup>2</sup> (4.7 psi). Predicted decay was 2.6 to 3.5 N/cm<sup>2</sup> (3.7 to 5.1 psi). LOX tank ullage pressure at engine start was 24.0 N/cm<sup>2</sup> (34.8 psia). Figure 6-15 shows the LOX tank ullage pressure during prepressurization and S-IC boost. The LOX tank pressure exhibited its characteristic drop of about 2.1 N/cm<sup>2</sup> (3.0 psi) during the first 15 seconds from engine start. The regulator controlled the ullage pressure within its control band up to approximately 300 seconds at which time the pressure dropped below the control band of 24.8 N/cm<sup>2</sup> (36.0 psia) as shown in Figure 6-16. During the same period of time, all S-II heat exchangers experienced a decrease in outlet temperature as shown in Figure 6-17. The decrease in outlet temperature was expected at EMR step,

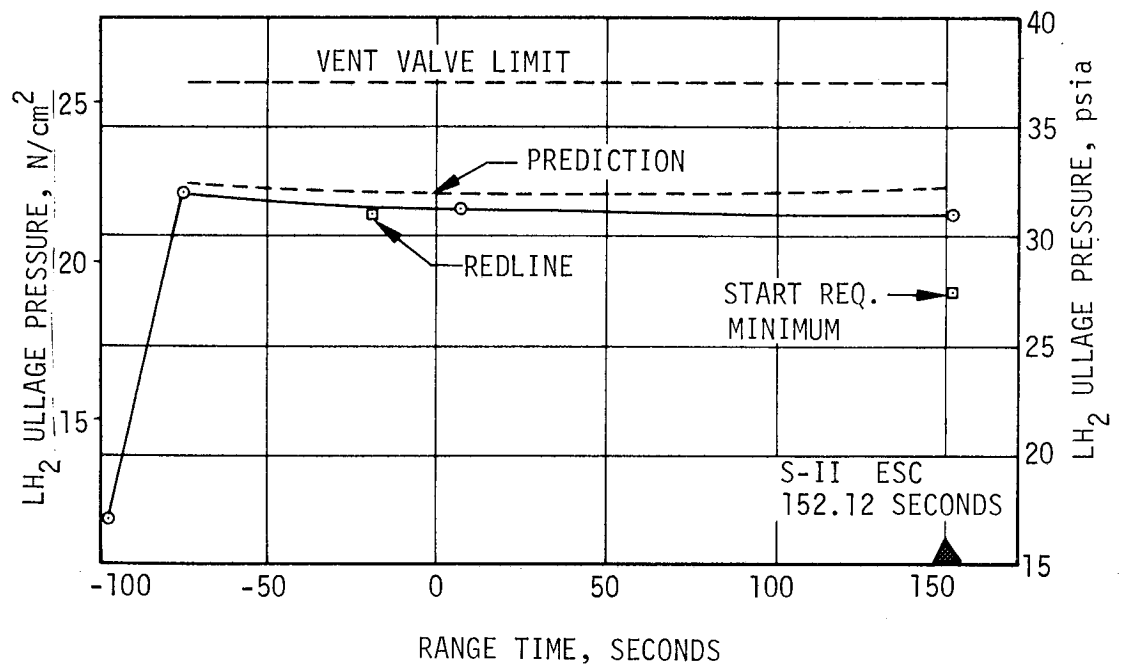


Figure 6-12. S-II LH<sub>2</sub> Tank Ullage Pressure During Prepress and S-IC Boost

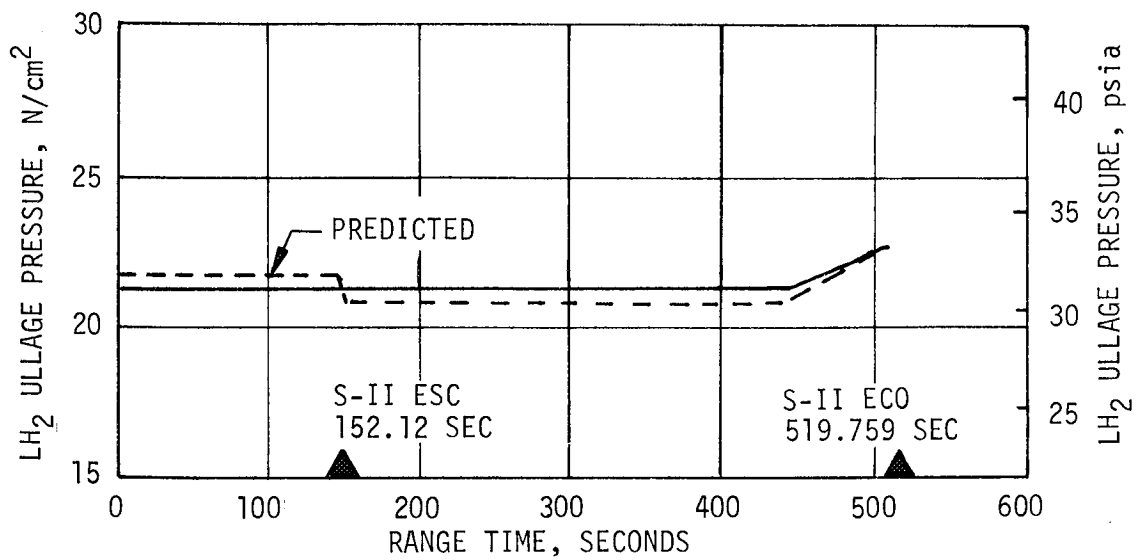


Figure 6-13. S-II LH<sub>2</sub> Ullage Pressure During S-II Burn

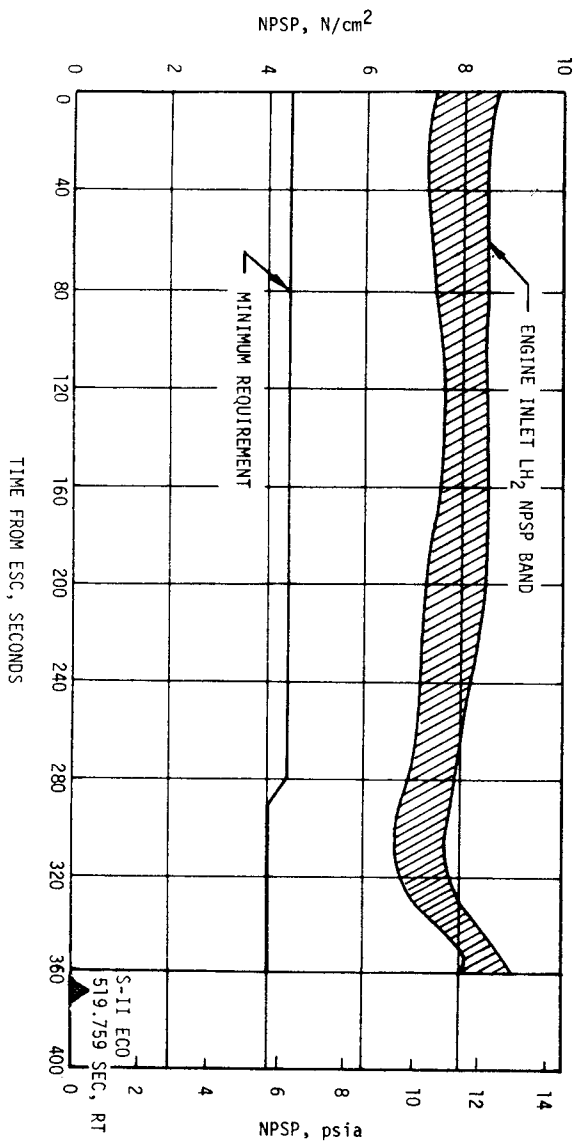
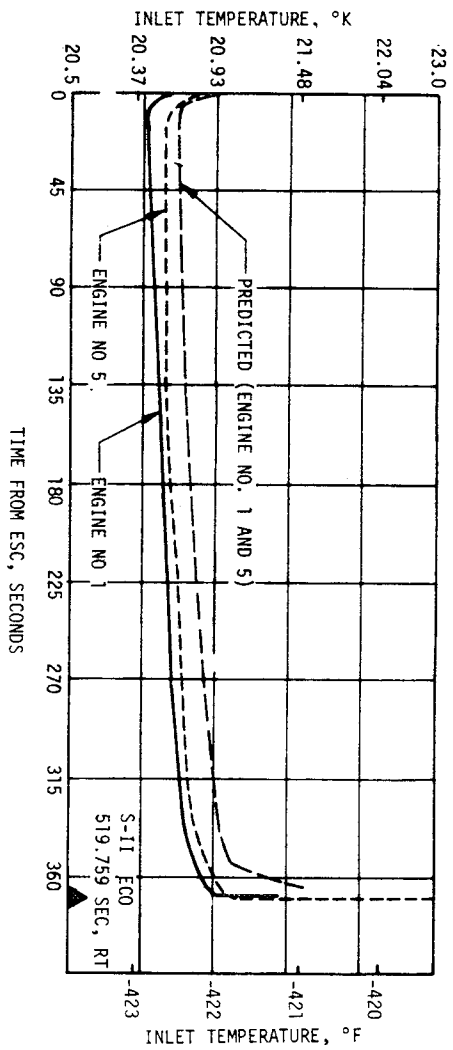
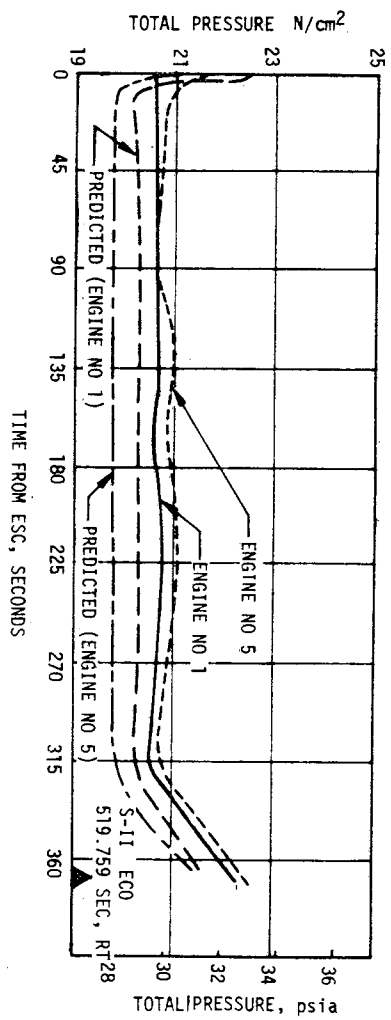


Figure 6-14. S-II Fuel Pump Inlet Conditions

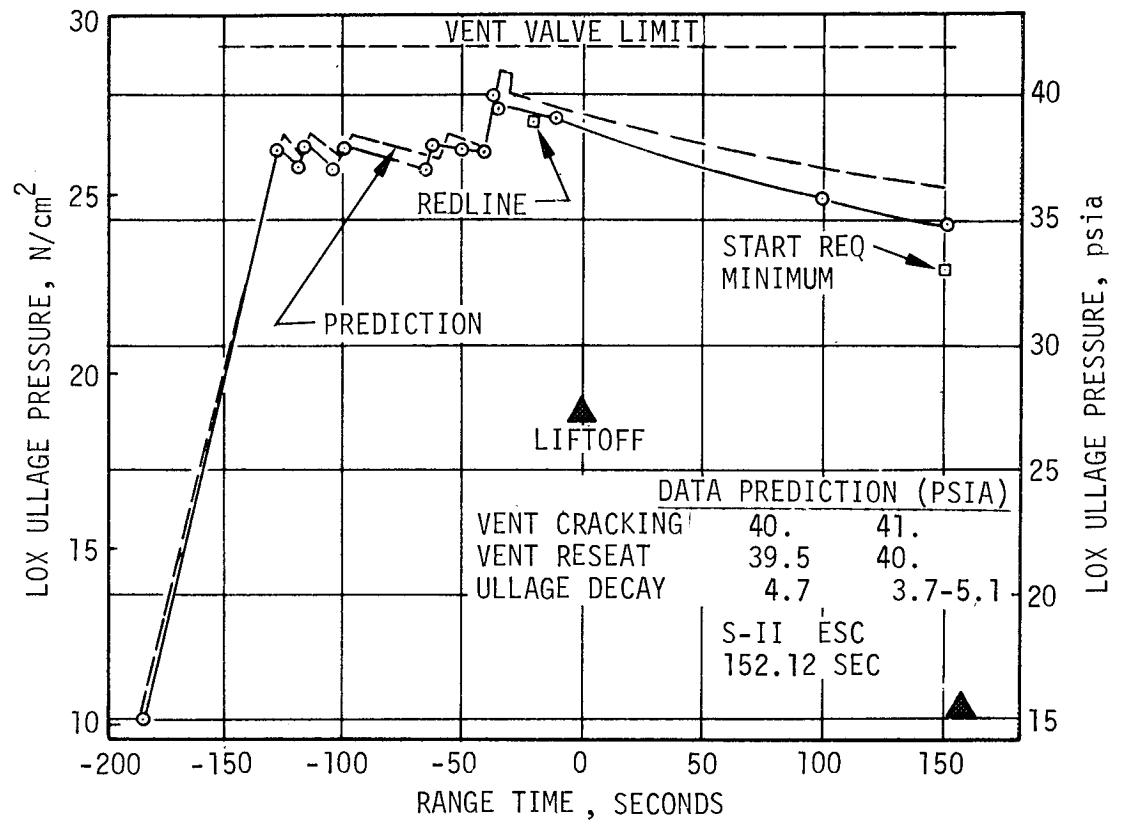


Figure 6-15. S-II LOX Ullage Pressure During Prepress and S-IC Boost

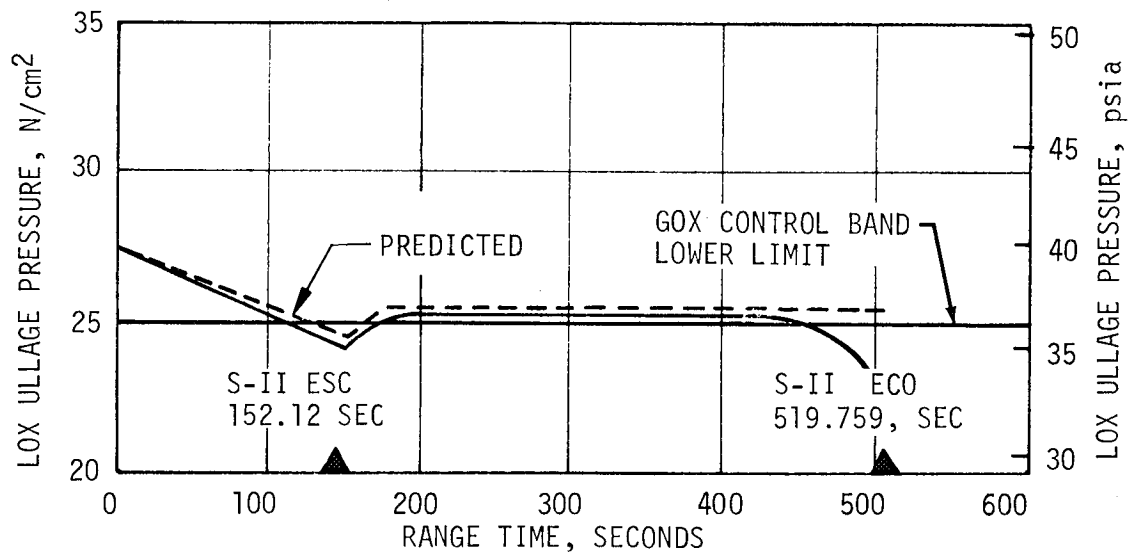


Figure 6-16. S-II LOX Ullage Pressure During Burn

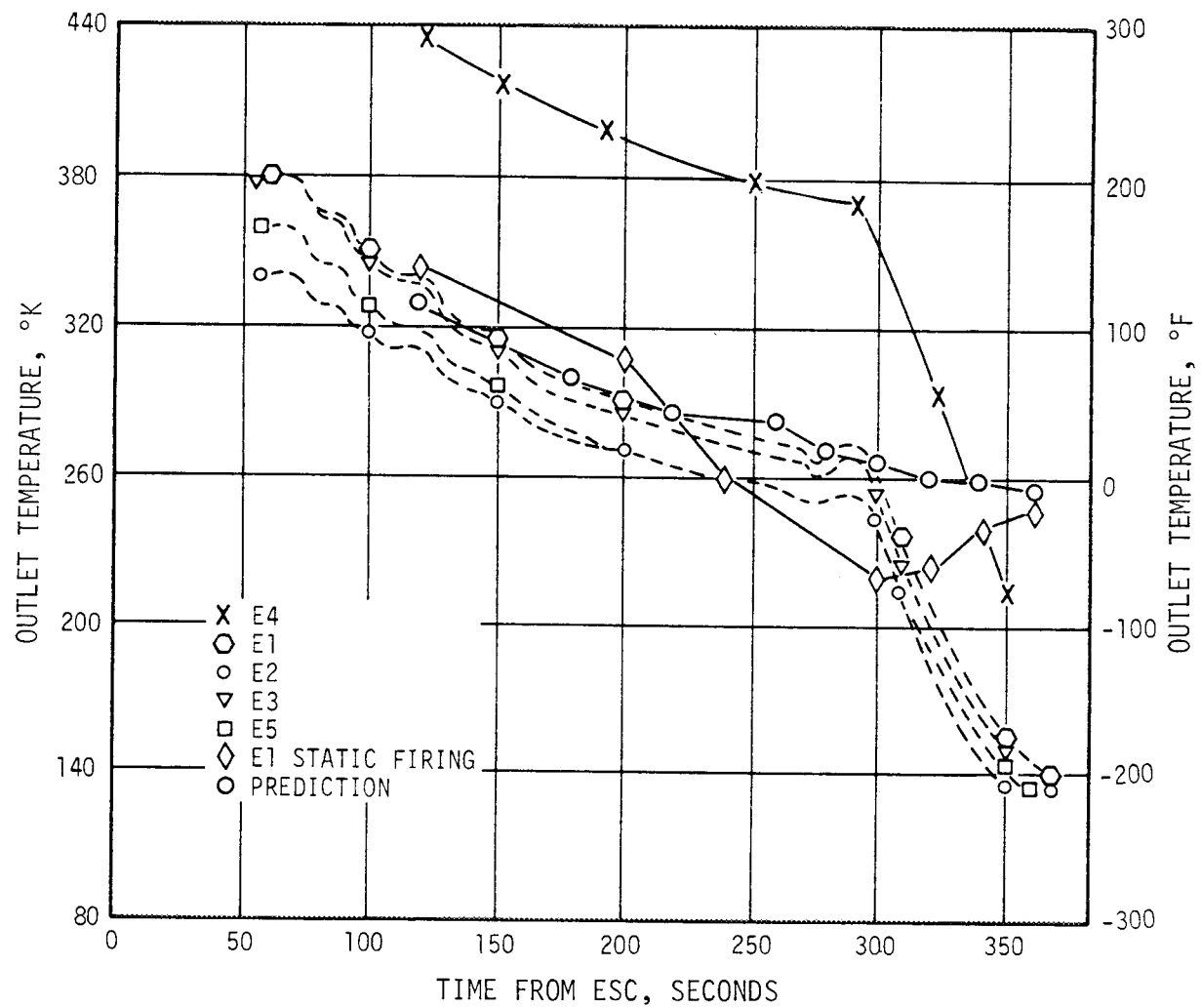


Figure 6-17. S-II Heat Exchanger Performance

but was expected to recover as noted during static firings. Engine 4 heat exchanger experienced a higher outlet temperature than predicted, possibly due to a restriction in the heat exchanger which caused an overall loss in exchanger efficiency. This decrease in heat exchanger efficiency probably caused the decrease in ullage pressure. However, LOX pump inlet conditions were met as shown in Figure 6-18.

#### 6.7 S-II PNEUMATIC CONTROL PRESSURE SYSTEM

Valve actuations in both the LH<sub>2</sub> and LOX circulation systems are controlled by a subsystem of the pressurization system. Helium gas at an initial temperature of  $294.3 \text{ }^{\circ}\text{K} \pm 16.7 \text{ }^{\circ}\text{K}$  ( $70 \pm 30 \text{ }^{\circ}\text{F}$ ) is used as the pressurant. The gas enters the subsystem through a disconnect and is stored at  $2068.4 \text{ N/cm}^2$  (3000 psig) nominal, in the main receiver. The gas then flows through a pressure regulator. Check valves downstream of the regulator prevent the loss of helium stored in surge chambers in the event of line breakage upstream of the check valves. Relief valves operate at  $551.6 \text{ N/cm}^2$  (800 psig) and prevent over-pressurization of the system as a result of increased gas temperature or regulator seat leakage.

The pneumatic control system on AS-501 functioned satisfactorily as shown in Figure 6-19. Table 6-4 shows the S-II helium mass used by the pneumatic control or valve actuation system.

Table 6-4. S-II Helium Mass

LAUNCH SEQUENCE	PNEUMATIC CONTROL PRESSURE SYSTEM HELIUM MASS READINGS (AS 501)	
	ACTUAL	PREDICTED
Liftoff Minus 30 Seconds	1.76 kg (3.88 lbm)	1.62 kg (3.58 lbm)
S-II Engine Start Command	1.76 kg (3.88 lbm)	1.60 kg (3.52 lbm)
S-II Engine Cutoff Command	1.57 kg (3.46 lbm)	1.33 kg (2.93 lbm)

NOTE: Helium mass does not include engine control bottle gas.

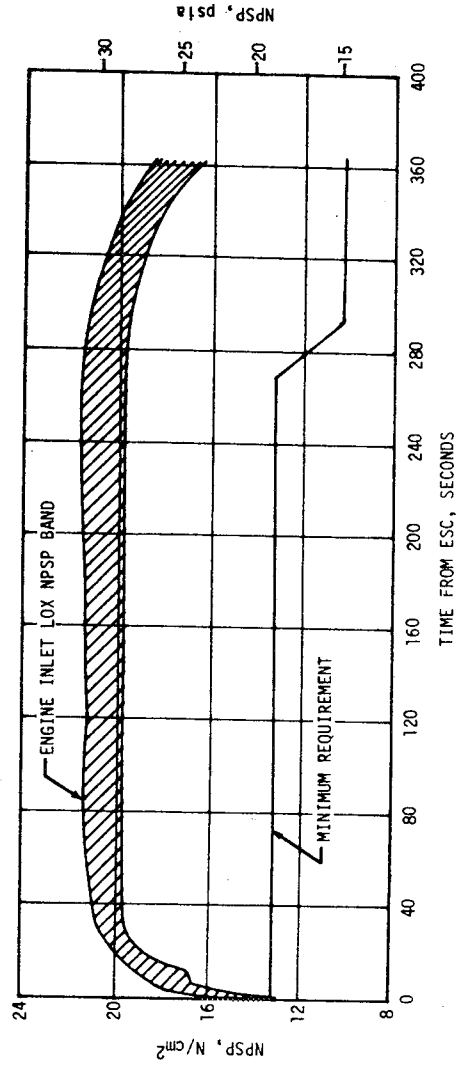
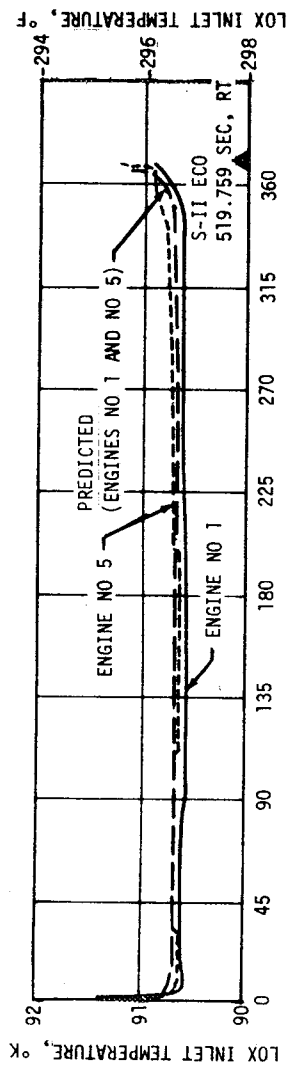
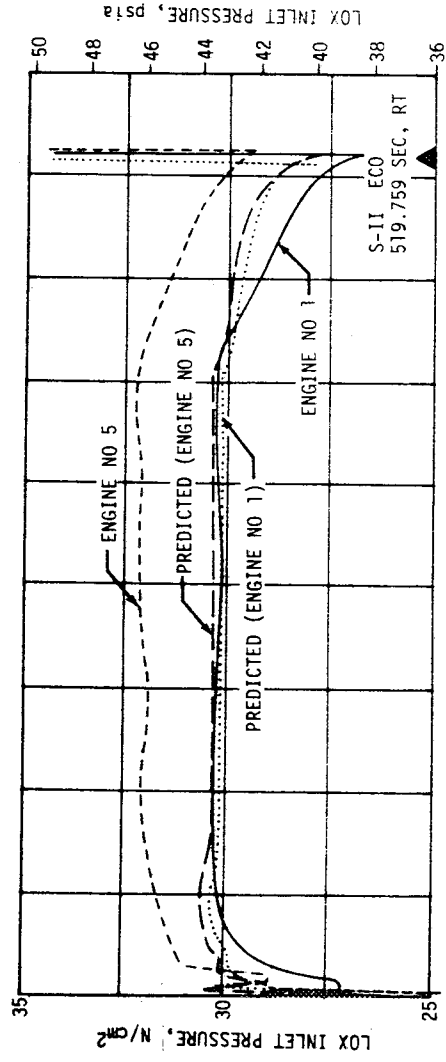


Figure 6-18. S-II LOX Pump Inlet Conditions

## 6.8 CAMERA EJECTION SYSTEM

The camera ejection subsystems performed satisfactorily and functioned as designed. The cameras were programed for ejection to start at 37.7 second after S-II engine start and actually ejected at the predicted time.

Figure 6-20 compares the two pneumatic subsystems. It appears that both subsystems leaked and a greater leak existed in the position III subsystem as evidenced by the lower storage bottles pressure, however, sufficient pressure was available to provide positive ejection. Both subsystems show the same ejection characteristics based on an approximate pressurization decay of 137.9 N/cm<sup>2</sup> (200 psi) during ejection.

Table 6-5 shows the initial helium mass in the system and the mass decay that occurred due to the ejection of the camera capsule.

## 6.9 HELIUM INJECTION SYSTEM

The inflight helium injection system supplements natural convection recirculation in the LOX recirculation line. This system injects ambient helium in the bottom of the return lines to decrease the return line fluid density, and thereby increasing the recirculation driving force.

Performance of the helium injection system was satisfactory. Requirements were met and parameters were in good agreement with predicted values. Pressurization of the helium supply bottle was normal but the end pressures were slightly higher than predicted. The supply bottle was loaded with 1.50 kilograms (3.3 lbm) and by ESC was .95 kilograms (2.1 lbm). This usage of helium mass resulted in a helium injection flow rate of 1.53 SCMM (54 SCFM).

Table 6-5. S-II Camera Ejection System Helium Mass Usage

LAUNCH SEQUENCE	ACTUAL		PREDICTED	
	Position I	Position III	Position I	Position III
Storage Bottle, Mass, at Fill Valve Closure	0.39 kg (0.86 lbm)	0.39 kg (0.86 lbm)	0.37 kg (0.81 lbm)	0.37 kg (0.81 lbm)
Leakage Loss, Fill Valve Close to Camera Eject	0.03 kg (0.07 lbm)	0.05 kg (0.11 lbm)	0.00 kg (0.00 lbm)	0.00 kg (0.00 lbm)
Camera Ejection Usage	0.02 kg (0.04 lbm)	0.02 kg (0.04 lbm)	0.02 kg (0.04 lbm)	0.02 kg (0.04 lbm)



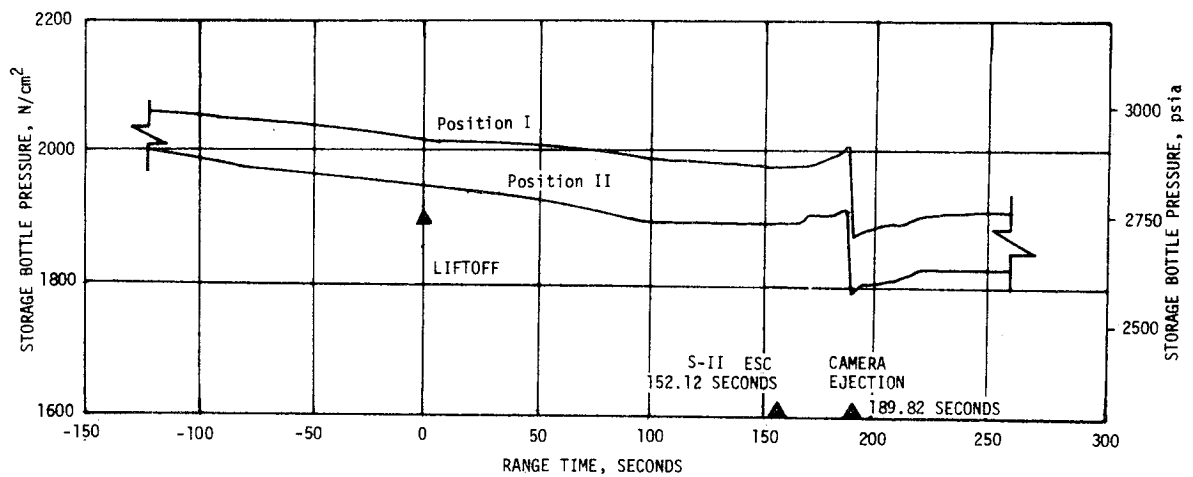
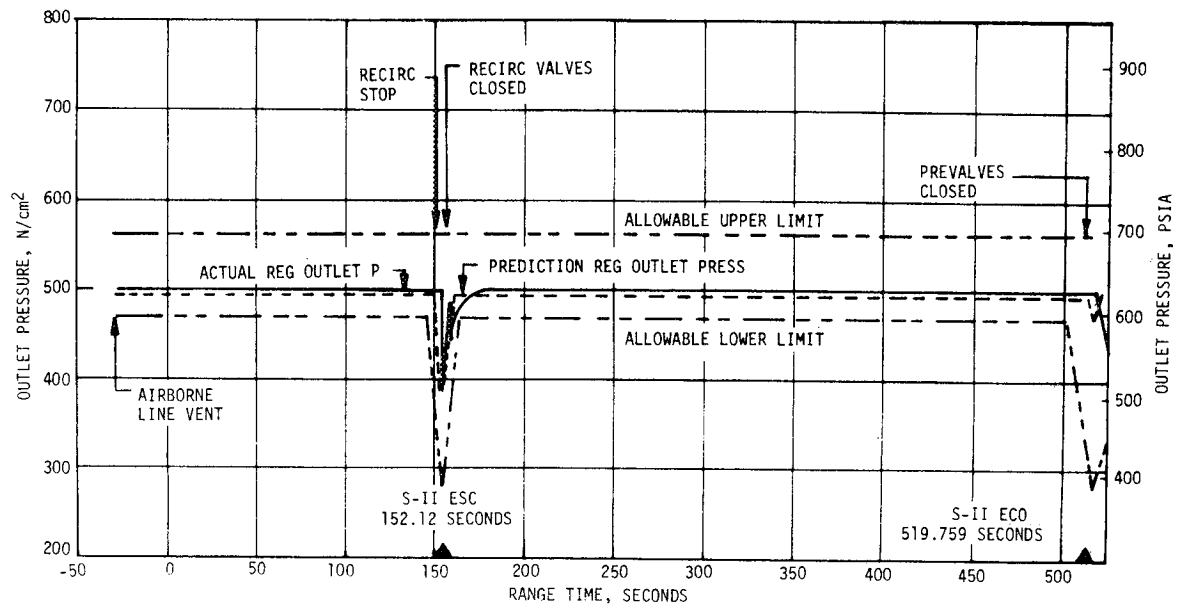


Figure 6-20 S-II Camera Ejection System Pressures



## SECTION 7 S-IVB PROPULSION

### 7.1 SUMMARY

The J-2 engine performance was satisfactory throughout the operational phase of the S-IVB/501 flight. The J-2 engine was successfully restarted in space following the two revolution coast period. The average stage performance percent deviations from the predicted are summarized below:

	First Burn	Second Burn
a. Thrust	-0.91	+1.68
b. Specific Impulse	-0.11	-0.42

The postflight performance simulation-trajectory match results for first burn showed a 0.21 percent increase in thrust over propulsion reconstruction while the mass flowrate had an increase of 0.08 percent. The first burn time was 6.2 seconds longer than predicted. This longer burn time can be attributed to lower thrust, lower mass flowrate, lower separation velocity combined with a higher initial weight, and a higher separation altitude. Specific impulse was 0.14 percent greater than reconstruction results.

The second burn simulation-trajectory match compared to propulsion reconstruction indicated a 0.67 percent increase in thrust and 0.49 percent increase in mass flowrate. A 15.18-second shorter burn time was primarily due to a high EMR operation for the first 55 seconds of mainstage. Specific impulse was 0.096 percent greater than reconstruction results.

Extrapolation of propellant flowrates to depletion indicates that a LOX depletion would have occurred approximately 38 seconds after second burn velocity cutoff with a usable LH<sub>2</sub> residual of 40 kilograms (89 lbm). This yielded a Propellant Utilization (PU) efficiency of 99.96 percent.

The subsystems operationally met all performance requirements. However, out-of-band behavior occurred on some systems as discussed in the following paragraphs.

A high LH<sub>2</sub> bulk temperature resulted in slightly higher than predicted pump inlet temperatures at S-IVB Engine Start Command (ESC). This high LH<sub>2</sub> bulk temperature was caused by a high prelaunch vent stack back pressure. A modification to the facility hydrogen disposal system is expected to reduce the high vent stack back pressure on future flights.

The Continuous Vent System (CVS) performed satisfactorily, but had an erroneous telemetered transducer output of the vent pressure during orbital coast and second burn operation. This erroneous transducer output was probably caused by thermal environment and precipitated the premature termination of the repressurization procedure by a ground command. This type of occurrence with similar action from a ground command on future flights could result in a "no start" for second burn operation. Investigations revealed that the pressure transducers were mounted directly on the vent line, and hence were subjected to the 25° K (-144.7° F) gas temperature. This temperature far exceeded the qualified operating range for these transducers. Remote location of the transducers will be accomplished for AS-502 and subsequent launch vehicles.

The pneumatic control system performed satisfactorily during boost and first burn operations. During orbital coast a system leak developed, but sufficient helium supply pressure was available to complete all second burn operations. This leak continued during the third revolution and resulted in the supply pressure eventually dropping below the regulator setting after the end of the S-IVB mission. The exact cause of the leak has not yet been determined. The leak is probably associated with one or more of the seven actuation control modules, or the regulator backup calips switch. Corrective action is being taken in both areas.

The cold helium supply for LOX tank pressurization was more than adequate to meet flight requirements. During orbital coast the pressure in the spheres apparently decreased indicating a leak. However, supporting analyses indicating leakage did not occur and that the pressure reading is in error.

An unexpected decay of LH<sub>2</sub> ullage pressure was experienced after termination of the repressurization procedure. The lower than predicted ullage pressure can probably be attributed to a malfunction of the diffuser. Premature termination of the ambient repressurization operation, a cooler blowdown of the repressurization bottles, and an energy loss from the ullage gas resulting from interaction with the liquid bulk added to the problem. Corrective action is in progress.

The Auxiliary Propulsion System (APS) performed satisfactorily with less than 75 percent consumption of the propellants. However, a marked deterioration in thrust for APS engines I<sub>IV</sub> and I<sub>II</sub> may have been experienced after spacecraft separation. APS engine I<sub>II</sub> exhibited an apparent chamber pressure decrease to 55 percent of nominal which may have been caused by a restriction of propellant flow to the engine. This is still under investigation.

## 7.2 S-IVB CHILLDOWN AND BUILDUP TRANSIENT PERFORMANCE FOR FIRST BURN

The propellant recirculation systems performed satisfactorily, meeting start and run box requirements for fuel and LOX as shown in Figure 7-1. The thrust chamber at liftoff was well below the maximum allowable redline limit of 147° K (-195° F). At S-IVB first burn ESC, the temperature was 145° K (-199° F), which is within the requirement of  $183 \pm 28^\circ \text{K}$  ( $-160 \pm 50^\circ \text{F}$ ) as shown in Figure 7-2.

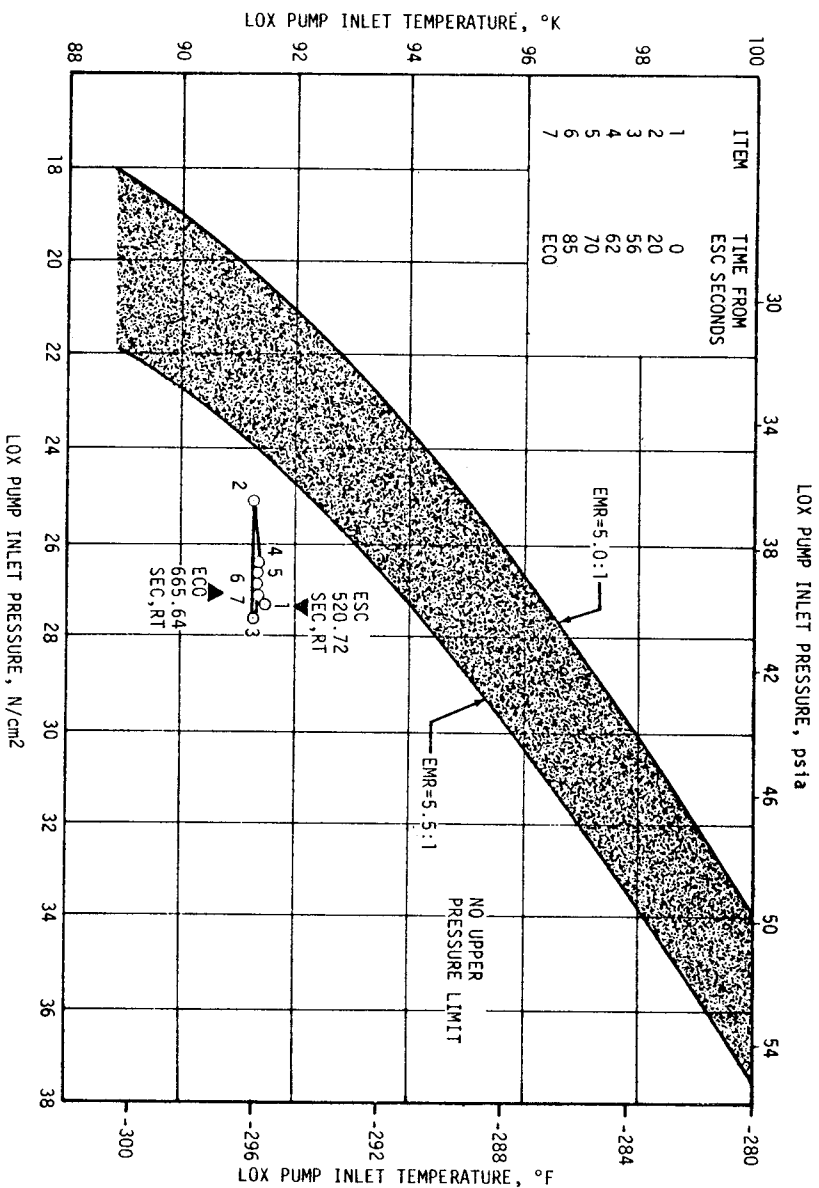
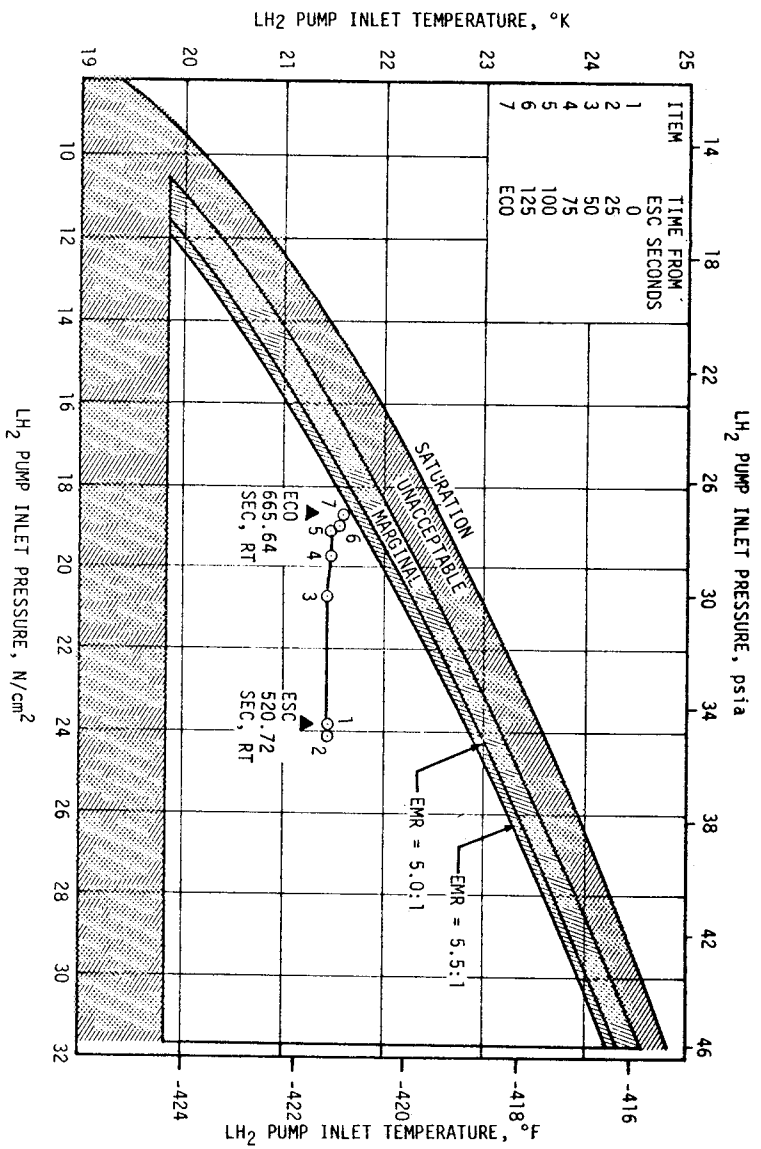


Figure 7-1. S-IVB Start Box and Run Requirements - First Burn

The chilldown and loading of the engine GH<sub>2</sub> start sphere and pneumatic control spheres prior to liftoff were satisfactory. Figure 7-3 shows the start tank performance from first burn ESC. At first burn start command the start tank conditions were within the required S-V/S-IVB region for initial start ( $913.56 \pm 51.71$  N/cm<sup>2</sup>,  $161 \pm 16.7^\circ$  K ( $1325 \pm 75$  psia,  $169.7 \pm 30^\circ$  F)). The discharge was completed and the refill initiated by S-IVB first burn ESC + 3.88 seconds. The refill was satisfactory and in good agreement with the acceptance test. The control bottle pressure and temperatures at liftoff were 2126 N/cm<sup>2</sup> (3010 psia) and 150° K (-189.7° F). Nominal chilldown system performance levels were observed during the chilldown operation. LOX system chilldown, which was continuous from before liftoff until just prior to S-IVB first burn ESC, was satisfactory. At ESC the LOX pump inlet temperature was 91.4° K (-295.2° F). Nominal chilldown system performance levels were observed during the chilldown operation.

The first burn start transient was satisfactory. The thrust buildup was within the limits set by the engine manufacturer. The PU system provided the proper null setting of the PU valve during the start transient until system activation. The thrust buildup to 90 percent performance (Start Tank Discharge Valve (STDV) + 2.5 seconds) was faster than during the acceptance test as expected. The total impulse from STDV to STDV + 2.5 seconds was 829,451 N-s (186,468 lb<sub>f</sub>-s) compared to 547,149 N-s (123,004 lb<sub>f</sub>-s) during the same interval for the acceptance test. The thrust during first burn start is shown in Figure 7-4.

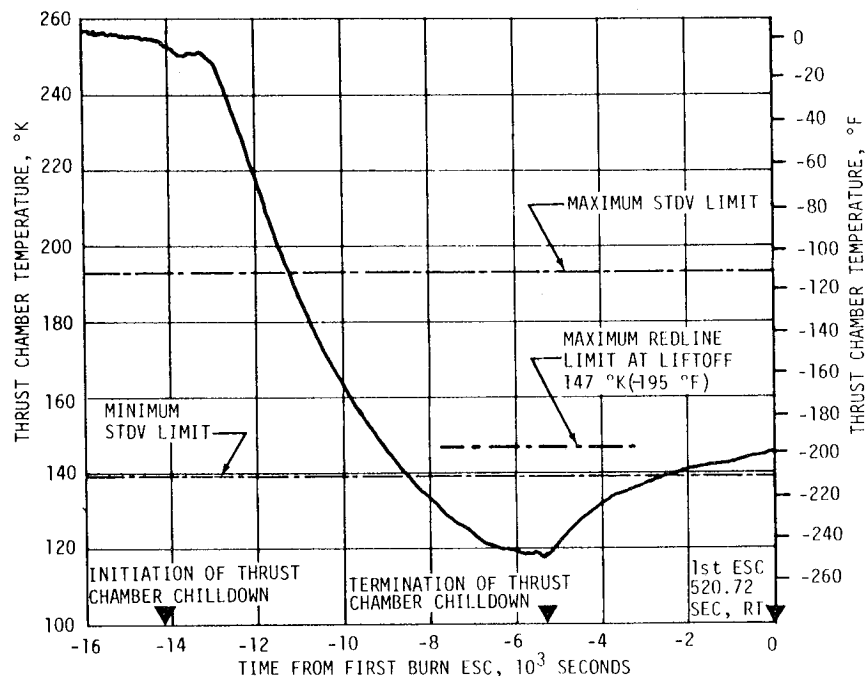


Figure 7-2. S-IVB Thrust Chamber Temperature - First Burn

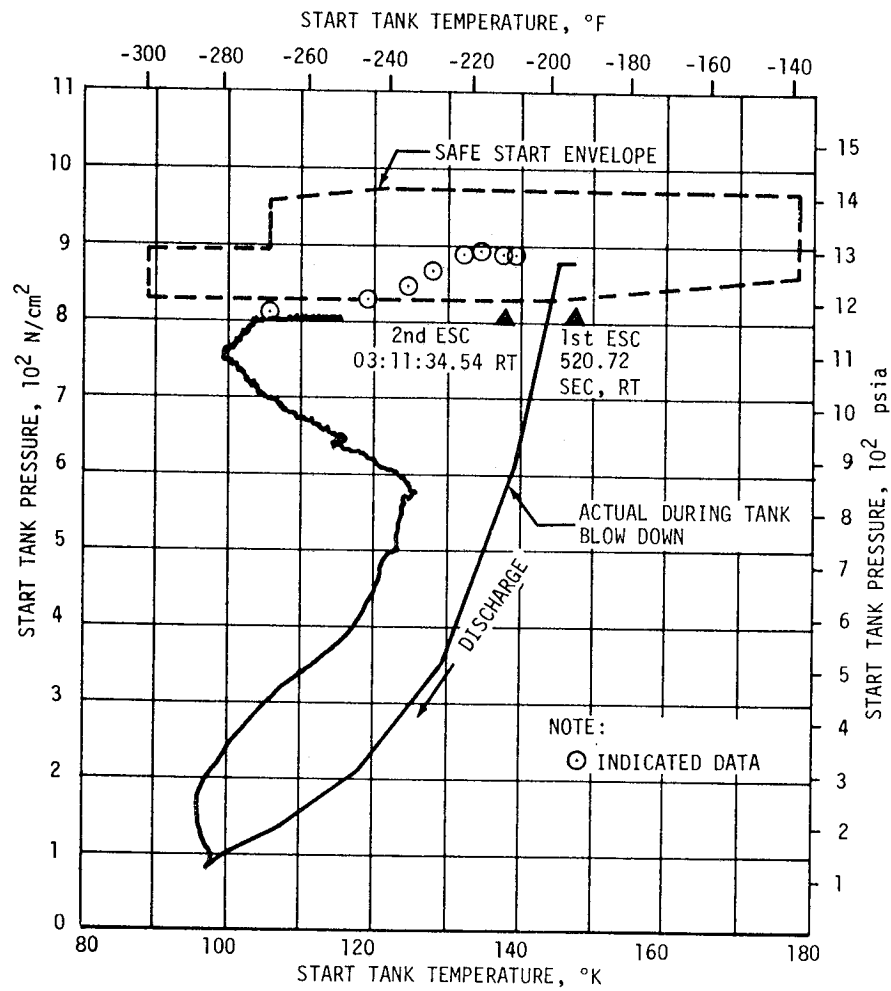


Figure 7-3. S-IVB Start Tank Performance

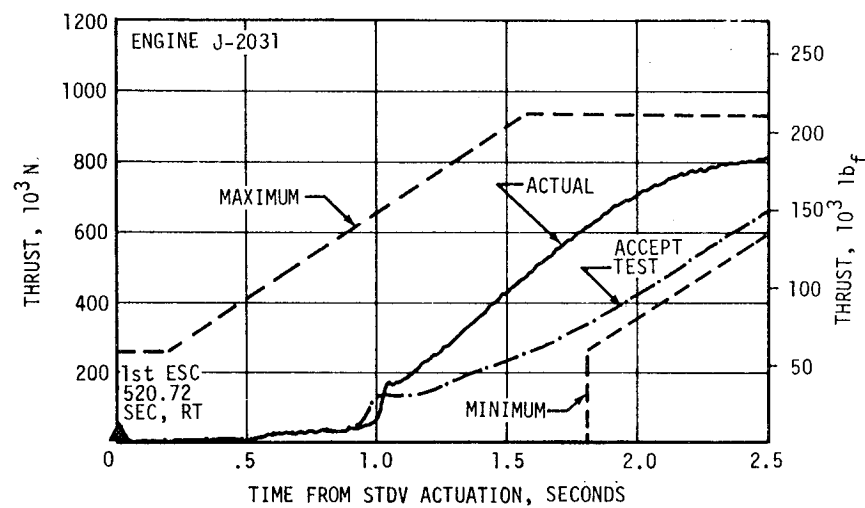


Figure 7-4. S-IVB Buildup Transient - First Burn

### 7.3 S-IVB MAINSTAGE PERFORMANCE FOR FIRST BURN

J-2 engine steady state first burn performance is presented in Figure 7-5. The PU valve was maintained at the full closed position during the mainstage period as planned. The overall performance level was satisfactory, however, the thrust and oxidizer flowrate were lower than predicted. The lower oxidizer flowrate resulted in a lower than predicted engine mixture ratio. The steady state performance deviations at standard altitude conditions are presented in Table 7-1.

Table 7-1. S-IVB Steady State Performance - First Burn

PARAMETER *	PREDICTED	RECONSTRUCTION	FLIGHT DEVIATION	% DEVIATION FROM PREDICTED
Thrust N (lb <sub>f</sub> )	1,001,490 (225,144)	989,213 (222,384)	-1228 (-2760)	-1.2
EMR LOX/Fuel	5.562	5.495	-0.067	-1.20
ISP N-s/kg (lb <sub>f</sub> -s/lbm)	4152 (423.4)	4148 (423.0)	-3.9 (-0.40)	-0.094
LOX Flowrate kg/s (lbm/s)	204.44 (450.71)	201.73 (444.74)	-2.711 (-5.977)	-1.32
Fuel Flowrate kg/s (lbm/s)	36.76 (81.04)	36.71 (80.94)	-0.043 (-0.095)	-1.23
*Reduced to standard altitude conditions at mainstage +60 seconds.				

A trajectory simulation using a differential correction procedure determines adjustments to the reconstructed engine thrust and flowrate to yield a simulated trajectory which closely matched the observed mass point trajectory. The results obtained indicated an increase over reconstructed values of 0.21 percent in thrust and 0.08 percent in mass flowrate and 0.14 percent in specific impulse for first burn as shown in Table 7-2. The S-IVB first burn time was 6.2 seconds longer than predicted. This longer burn time was accounted for as follows:

<u>Contributor</u>	<u>Deviation</u>		<u>Burn Time Delta (sec)</u>
S-IVB Thrust	-6846 N	-1539 lb <sub>f</sub>	+0.8
S-IVB mass flow	-2.09 kg/s	-4.6 lbm/s	+0.0
Initial mass	+433 kg	+965 lbm	+1.0
Separation Velocity	-134.186 ft/s	-40.9 m/s	+5.2
Separation Altitude	+1.404 n mi	+2.6 km	-1.1
Total Explained			+5.9
Unexplained			+0.3



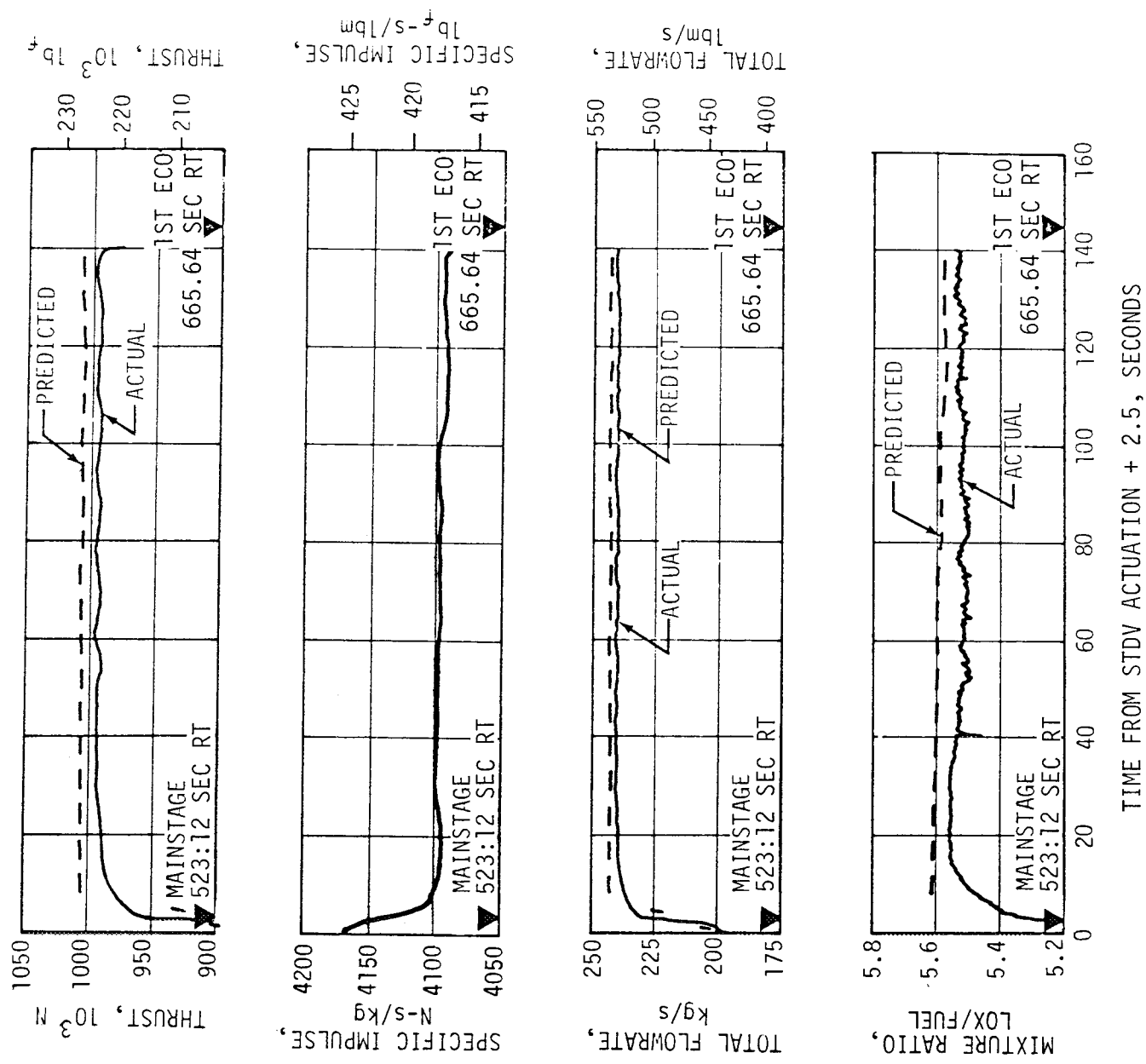


Figure 7-5. S-IVB Steady State Operation - First Burn

Table 7-2. Comparison of S-IVB Stage Flight Reconstruction Data - First Burn

PARAMETERS	UNITS	PREDICTED		FLIGHT RECONSTRUCTION		% DEV. FROM PRED.	
		HIGH MIXTURE RATIO	FIRST BURN FLIGHT AVERAGE	HIGH MIXTURE RATIO	FIRST BURN FLIGHT AVERAGE	HIGH MIXTURE RATIO	FIRST BURN FLIGHT AVERAGE
Longitudinal Vehicle Thrust	N (lb <sub>f</sub> )	1,002,723 (225,421)	1,002,723 (225,421)	993,648 (223,381)	993,648 (223,381)	-0.91	-0.91
Vehicle Mass Loss Rate	kg/s (lbm/s)	241.55 (532.52)	241.55 (532.52)	239.61 (528.25)	239.61 (528.25)	-0.80	-0.80
Longitudinal Vehicle Specific Impulse (lb <sub>f</sub> -s/lbm)	N-s/kg	4151.3 (423.31)	4151.3 (423.31)	4146.9 (422.87)	4146.9 (422.87)	-0.11	-0.11
PARAMETERS	UNITS	FLIGHT SIMULATION		% DEV. FROM PRED.		% DEV. FROM RECONST.	
		HIGH MIXTURE RATIO	FIRST BURN FLIGHT AVERAGE	HIGH MIXTURE RATIO	FIRST BURN FLIGHT AVERAGE	HIGH MIXTURE RATIO	FIRST BURN FLIGHT AVERAGE
Longitudinal Vehicle Thrust	N (lb <sub>f</sub> )	995,743 (223,852)	995,743 (223,852)	-0.70	-0.70	+0.21	+0.21
Vehicle Mass Loss Rate	kg/s (lbm/s)	239.81 (528.68)	239.81 (528.68)	-0.72	-0.72	+0.081	+0.081
Longitudinal Vehicle Specific Impulse (lb <sub>f</sub> -s/lbm)	N-s/kg	4152.5 (423.44)	4152.5 (423.44)	+0.02	+0.02	+0.14	+0.14

#### 7.4 S-IVB SHUTDOWN TRANSIENT PERFORMANCE FOR FIRST BURN

The S-IVB engine cutoff was initiated at 665.64 seconds by guidance command which was 6.2 seconds later than predicted for first burn. The engine cutoff transient was satisfactory and agreed closely with the acceptance test and predictions. The total cutoff impulse to 5 and zero percent of rated thrust was 210,423 N-s (47,305 lb<sub>f</sub>-s) and 232,197 N-s (52,200 lb<sub>f</sub>-s), respectively. Cutoff occurred with the PU valve in the fully closed position (high Engine Mixture Ratio (EMR)). The main oxidizer valve (MOV) actuator temperature was 180° K (-136° F) at cutoff. The cutoff impulse was adjusted from these conditions to standard conditions for comparison with the log book values at null PU valve position and 255.5° K or 0° F MOV actuator temperature. After these adjustments, the flight values were near the log book values. The thrust during cutoff is shown in Figure 7-6. A comparison of the predicted and actual velocity increases due to the cutoff impulse are presented in Table 7-3. This table shows a 9.5 percent decrease in velocity change for the engine flight results over predicted while the guidance data indicated a 19.0 percent decrease.

Table 7-3. S-IVB Cutoff Impulse - First Burn

PARAMETER	PREDICTED	FLIGHT		% DEVIATION FROM PREDICTED	
		ENGINE	GUID. DATA	ENGINE	GUID. DATA
Cutoff N-s Impulse ( $1b_f$ -s)	214,435 (48,207)	232,740 (52,200)	233,038 (52,389)	+8.5	+8.8 (approx)
Velocity m/s Increase (ft/s)	2.1 (6.9)	1.9 (6.2)	1.7 (5.6)	-9.5	-19.0

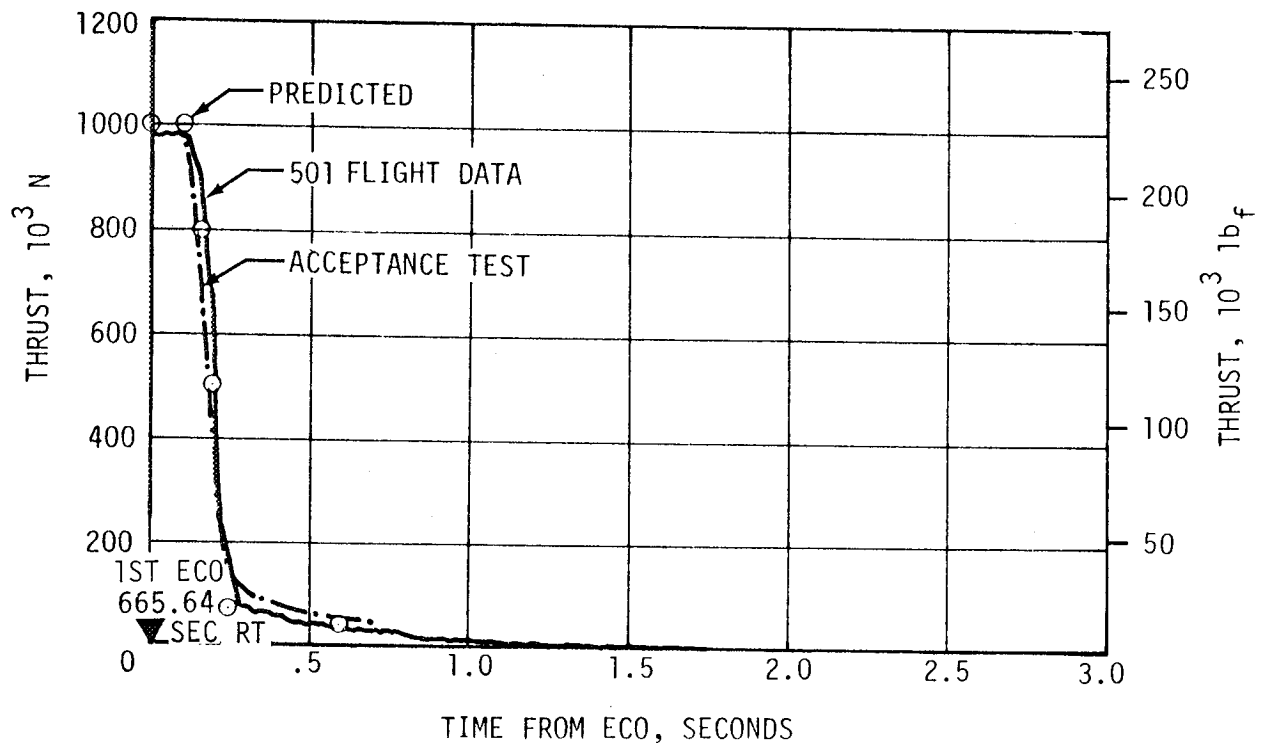


Figure 7-6. S-IVB Shutdown Transient Performance - First Burn

## 7.5 S-IVB COAST PHASE CONDITIONING

The continuous vent system shown schematically in Figure 7-7 performed satisfactorily, maintaining the fuel tank ullage pressure at an average level of  $13.4 \text{ N/cm}^2$  (19.5 psia). Nozzle pressure data, thrust, and acceleration levels for first and second orbits are presented in Figure 7-8. Ullage conditions during coast are shown in Figure 7-9.

The continuous vent regulator was activated at 724.8 seconds range time. The tank ullage pressure dropped from 20.3 to  $15.4 \text{ N/cm}^2$  (29.4 to 22.4 psia) in 152 seconds, and then gradually leveled off to  $13.4 \text{ N/cm}^2$  (19.5 psia). Regulation at this level continued, with the expected operation of the main poppet periodically opening, cycling, and reseating (see Figure 7-8). Continuous venting was terminated at 11,168.54 seconds, which was 326 seconds before second burn ESC.

Shortly after the initiation of continuous venting, the nozzle pressures began diverging as shown in Figure 7-8. By the end of the first revolution this discrepancy was a constant  $2.1 \text{ N/cm}^2$  (3.0 psi). However, the response characteristics were still the same. These transducers were mounted directly on the CVS manifold and were subjected to the extremely cold  $\text{GH}_2$  temperature of  $25^\circ \text{ K}$  ( $-414.7^\circ \text{ F}$ ). The divergence was attributed to these thermal effects, as presented in the S-IVB data and paragraph 19.2.3 of this report on vehicle measurement evaluation. Following the closure of the continuous vent regulator by preprogrammed command, the nozzle pressure data indicated a normal decrease in pressure for 1 second, a sharp pressure rise, and a long period of gradual drop (see Figure 7-8). The nozzle temperatures indicated no flow after closure.

Fuel tank ullage conditions during orbital coast are shown in Figure 7-9. Ullage temperature sensors indicated much colder temperatures than anticipated and appeared wet throughout most of the coast period, except for the 101-percent sensor. These liquid indications were probably caused by a higher wall boiloff rate than anticipated, which resulted in a greater volume of liquid droplets in the ullage space. Stage contractor contends that vapor entrapment in the liquid causes the liquid surface to rise and cover the liquid level sensors. However, this theory is inconsistent with AS-203 flight. The higher boiloff is also reflected in the total mass vented through the continuous vent. The best estimate total mass vented was calculated to be 1300 kilograms (2865 lbm). Since the ullage mass at continuous vent termination cannot be readily determined, no final boiloff mass is available. However, 1365 kilograms (3010 lbm) of  $\text{LH}_2$  boiloff is a definite maximum value.

The engine control bottle temperature was  $124^\circ \text{ K}$  ( $-236.7^\circ \text{ F}$ ) at the start of the orbital coast period which was higher than predicted, and the orbital heat up was lower than predicted. The average leakage rate of  $2.26 \times 10^{-4} \text{ kg/s}$  (0.3 lbm/hr) was comparable to that of the AS-203 flight data. The combined effect produced a flat pressure curve at about  $1282 \text{ N/cm}^2$  (1870 psia) as measured during the 3-hour coast period.

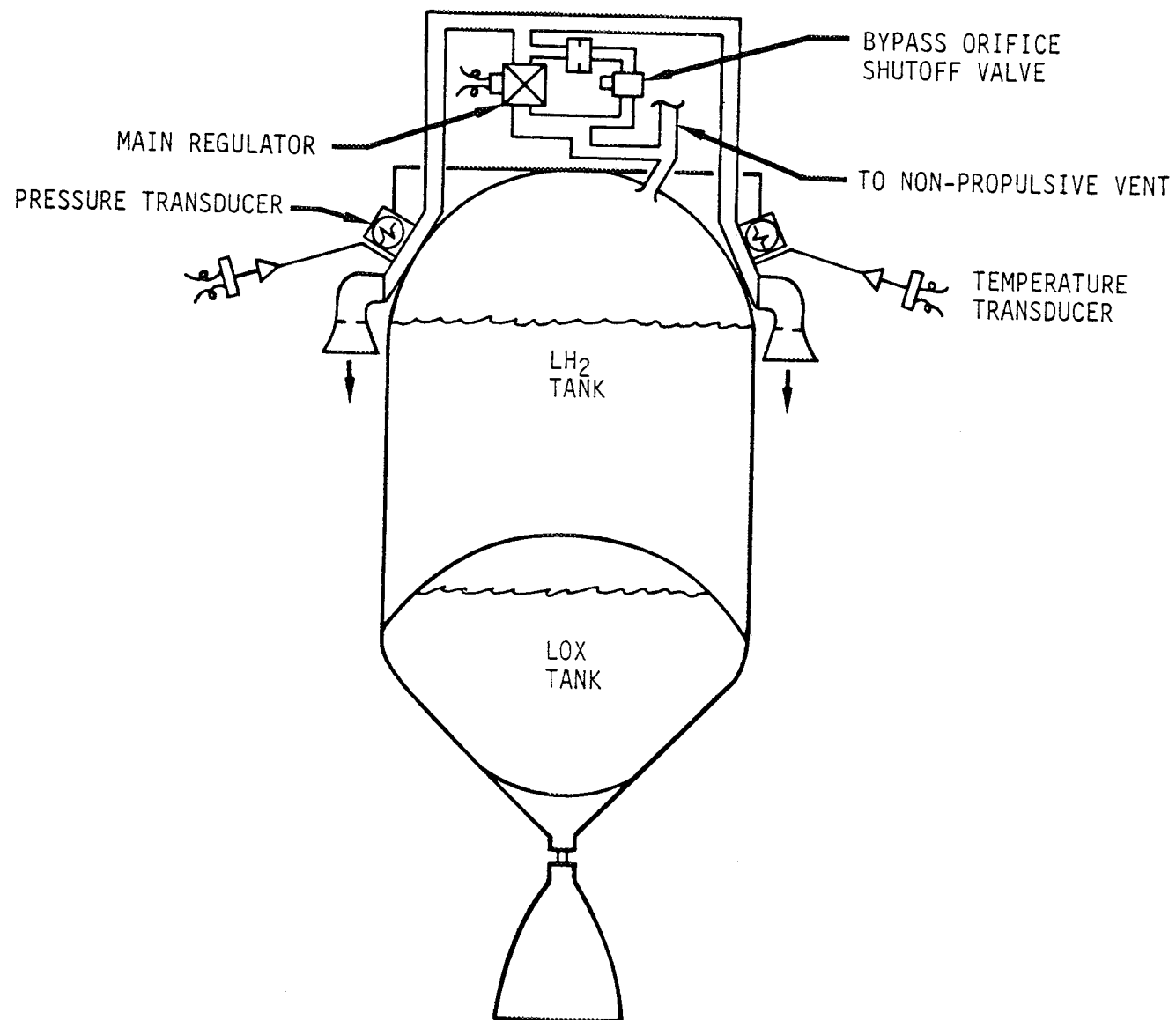


Figure 7-7. S-IVB Continuous Vent System Schematic

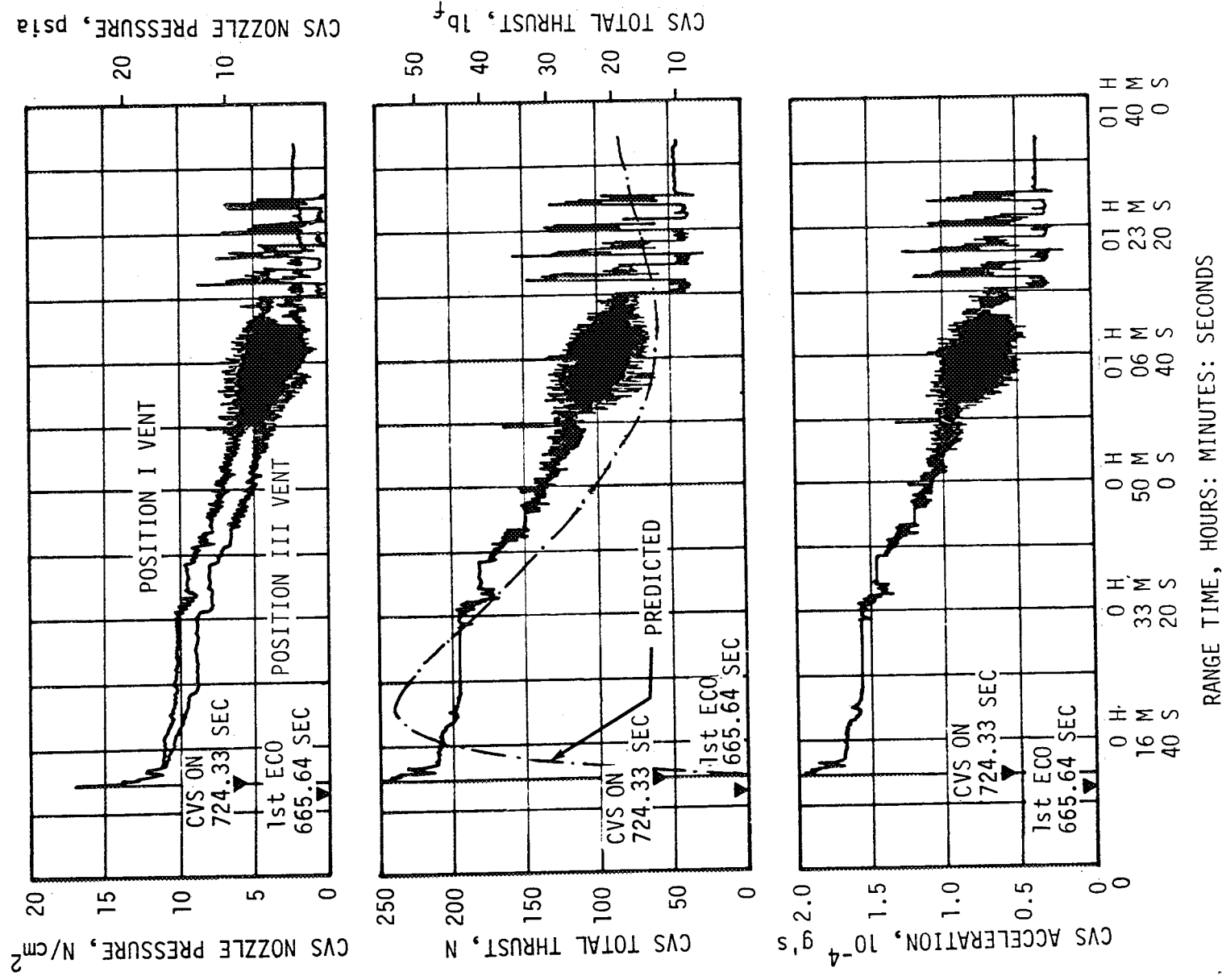


Figure 7-8. S-IVB CVS Performance - Coast Phase, Sheet 1 of 2

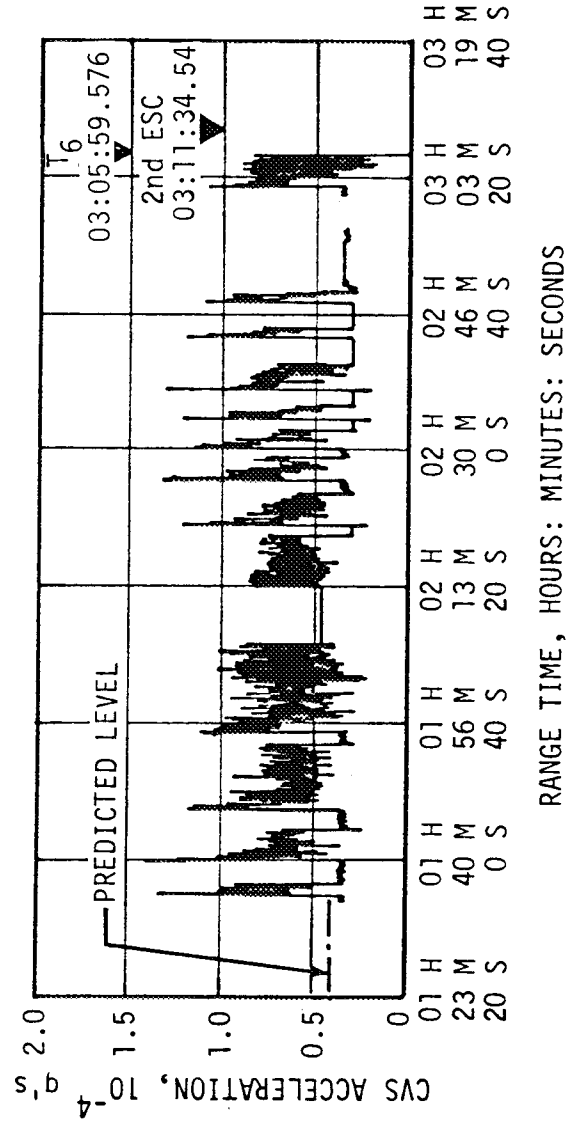
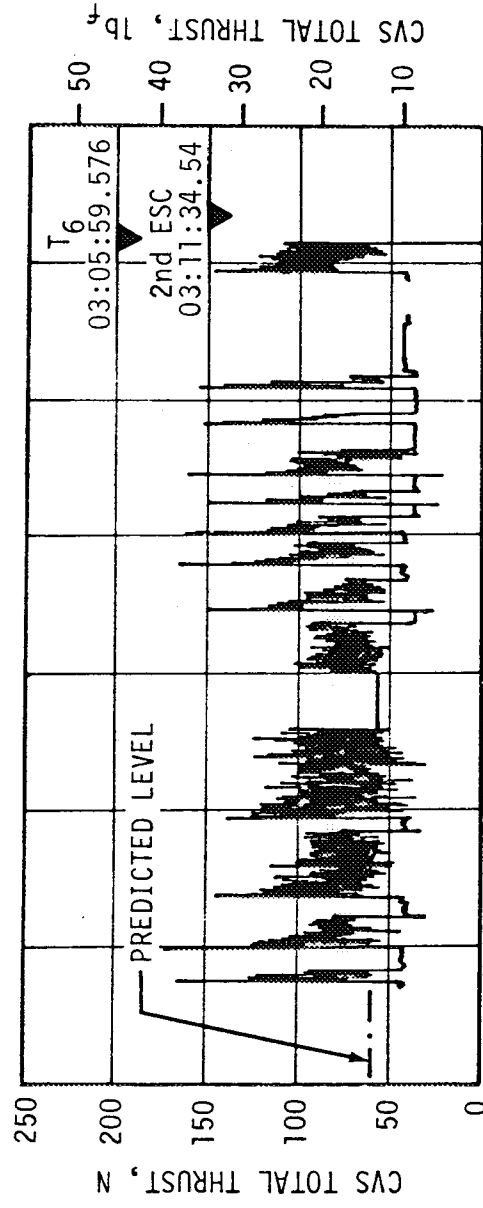
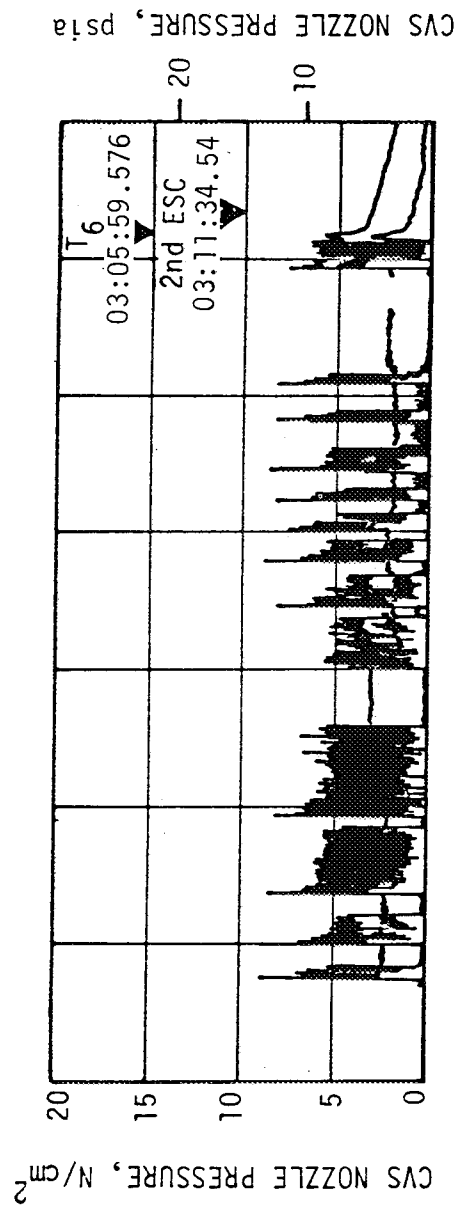
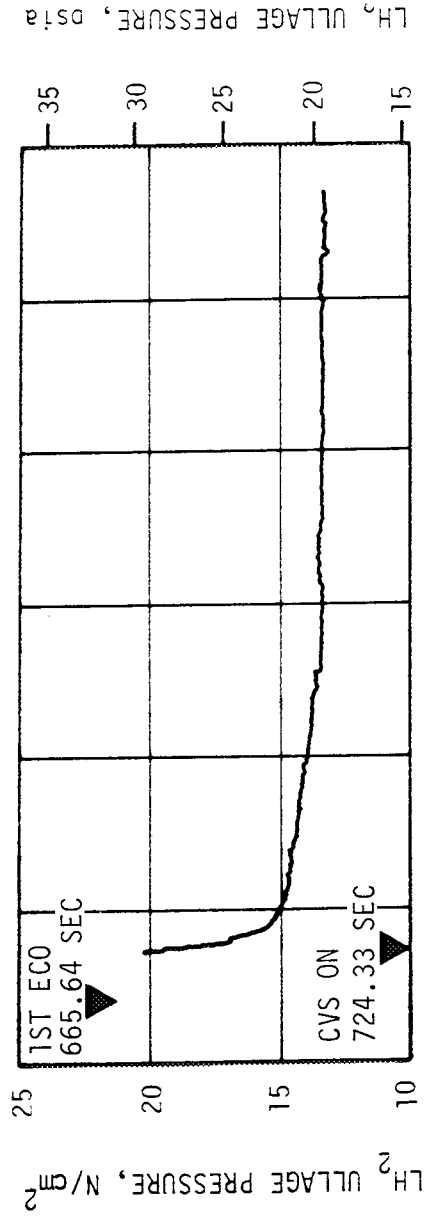
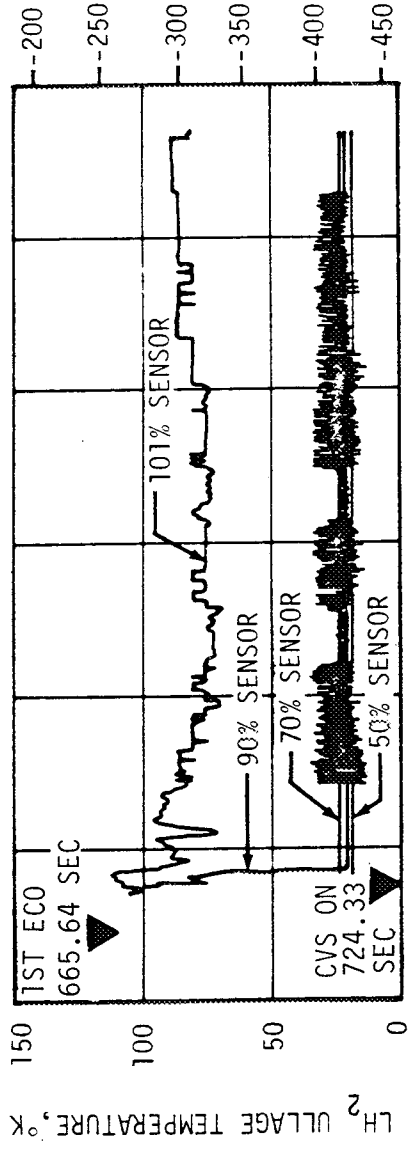


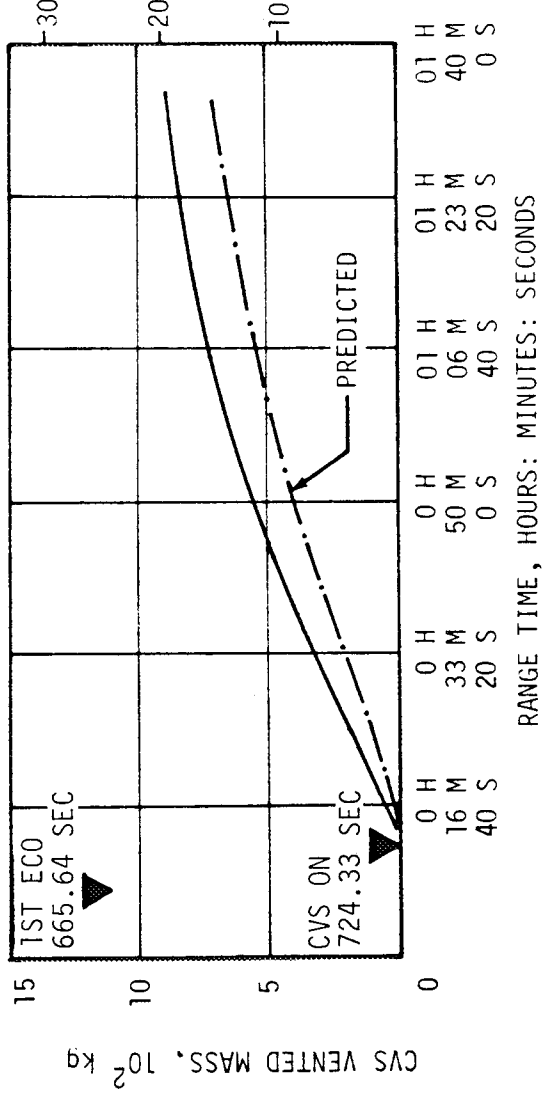
Figure 7-8. S-IVB CVS Performance - Coast Phase, Sheet 2 of 2



LH<sub>2</sub> ULLAGE PRESSURE, psia



LH<sub>2</sub> ULLAGE TEMPERATURE, °F



CVS VENTED MASS, 10<sup>2</sup> lbm

Figure 7-9. S-IVB LH<sub>2</sub> Ullage Conditions - Coast Phase, Sheet 1 of 2



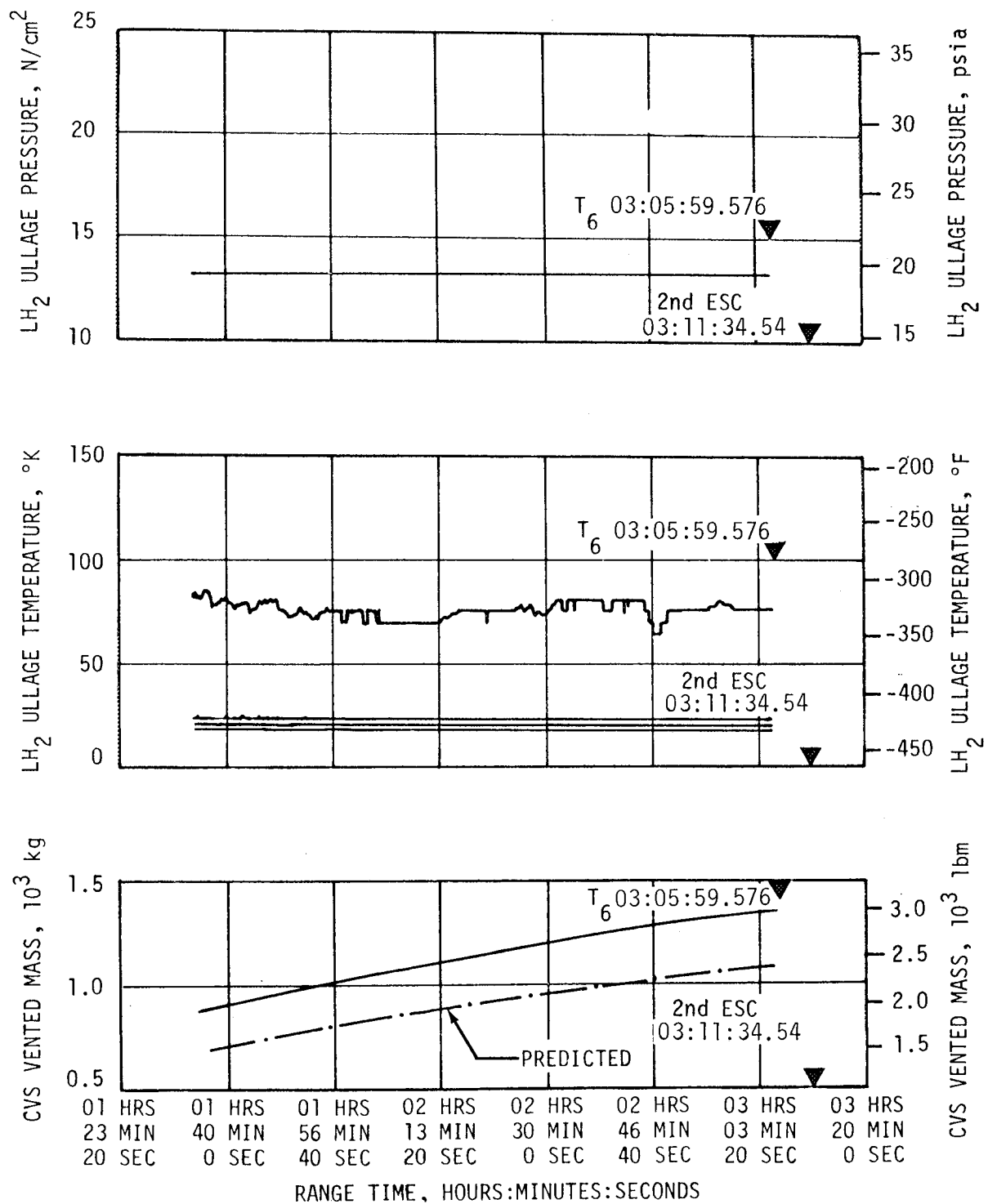


Figure 7-9. S-IVB LH<sub>2</sub> Ullage Conditions - Coast Phase, Sheet 2 of 2

The start tank pressure rise attendant with the orbital heat input was such that the conditions were within the restart envelope approximately 735 seconds after cutoff. The flowrate through the start tank relief valve balanced the pressure rise due to the tank heat up which thereby terminated the pressure rise at 889.42 N/cm<sup>2</sup> (1290 psia) at approximately 2835 seconds after cutoff. The indicated orbital temperature data as shown in Figure 7-3 deviates from the anticipated isochoric line due to local heat effects at the transducer. However, the indicated data of 889.42 N/cm<sup>2</sup> (1290 psia), 137° K (-212.7° F) at second burn start was within the predicted band.

#### 7.6 S-IVB CHILLDOWN AND BUILDUP TRANSIENT PERFORMANCE FOR SECOND BURN

The propellant recirculation systems performed satisfactorily meeting start and run box requirements for fuel and LOX as shown in Figure 7-10. The LH<sub>2</sub> bulk temperature was greater than predicted due to high vent stack back pressure and ullage gas entrapment in the liquid bulk. However, second burn fuel lead generally followed the predicted pattern and resulted in satisfactory conditions as indicated by the thrust chamber temperature in Figure 7-11. The LH<sub>2</sub> injector temperature at STDV opening during second burn were 22.9 to 90° K (-418.4 to -297.7° F), respectively. The LH<sub>2</sub> injector temperature at second burn STDV opening was near the mid-point of the 22.2 to 167° K (-419.7 to -159° F) fuel injector temperature range presently considered to be acceptable for mainstage start. The 90° K (-297.7° F) temperature at the end of the 8-second fuel lead was above the temperature that would be predicted from AEDC tests.

The AS-501 flight thrust chamber bulk temperature at the beginning of second burn fuel lead was considerably less than that used for the AEDC tests. Therefore, the high injector temperature was not explained by the thermal environment and neither was it explained by tank pressure differences. An effort is underway to reconcile the differences between the actual flight environment and the assumed environment used during AEDC testing.

The LH<sub>2</sub> chilldown system performance for second burn was satisfactory. The pump inlet temperature at second burn ESC was 22.4° K (-419.3° F). At second burn ESC -10 seconds, the pump inlet pressure was 23.6 N/cm<sup>2</sup> (34.3 psia) and the temperature was 21.8° K (-420.4° F), which yielded a Net Positive Suction Pressure (NPSP) of 8.0 N/cm<sup>2</sup> (11.6 psi).

Immediately after pre valve opening, the pump inlet temperature was 22.2° K (-419.8° F). During the 10-second interval between pre valve opening and second burn ESC, the pump inlet temperature rose because chilldown effectively ended with pre valve opening.

Second burn LOX pump chilldown was also satisfactory. At S-IVB second burn ESC the LOX pump inlet temperature was 92.1° K (-294° F). At second burn ESC -282 seconds, a perturbation occurred in the LOX chilldown system. At the end of second burn between ESC -282 and -263 seconds, the chilldown pump

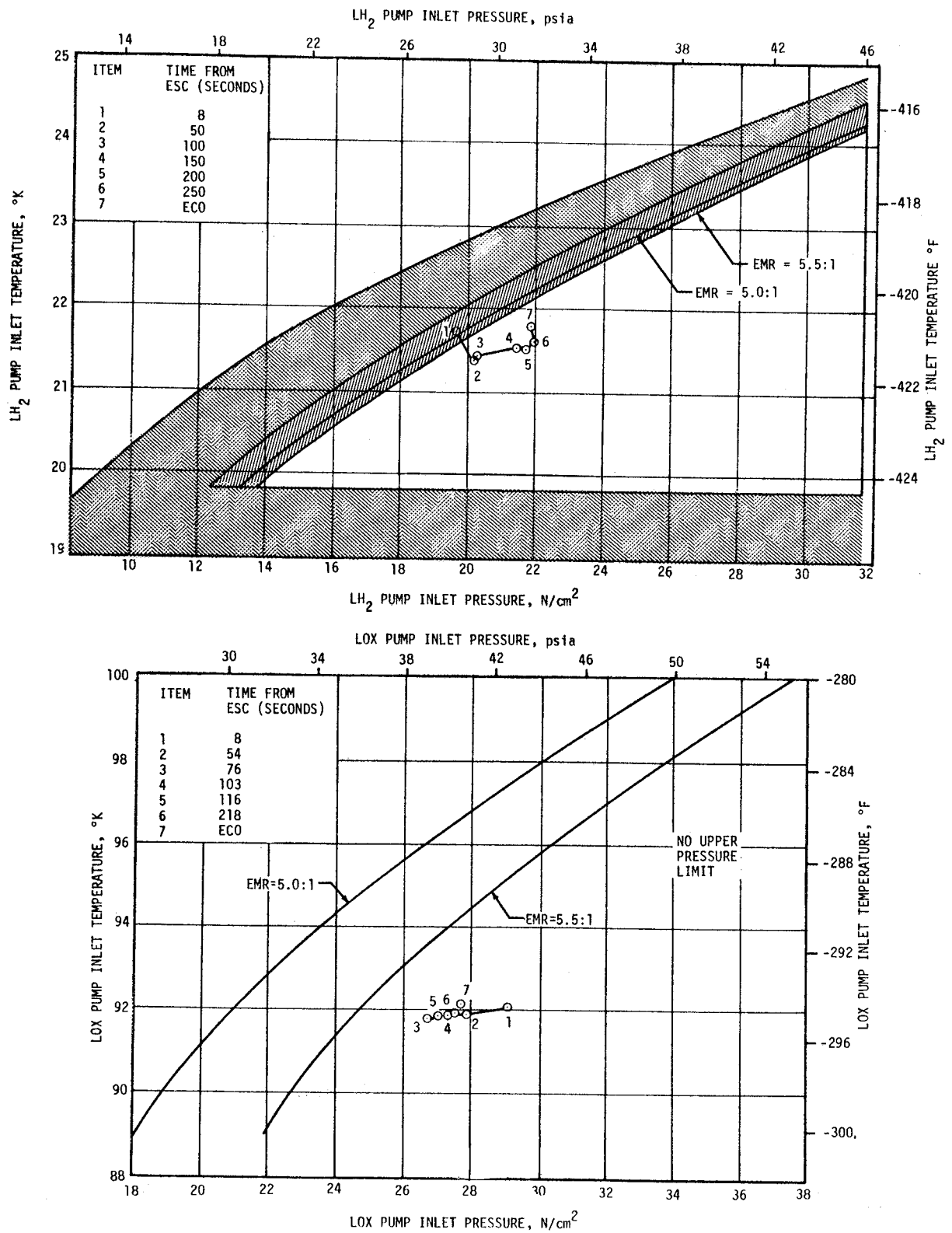


Figure 7-10 S-IVB Start Box and Run Requirements - Second Burn

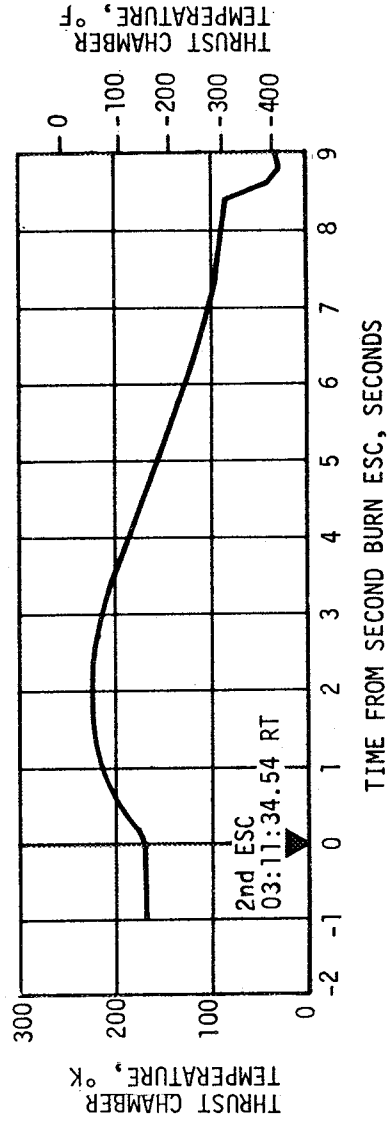


Figure 7-11. S-IVB Thrust Chamber Temperature - Second Burn

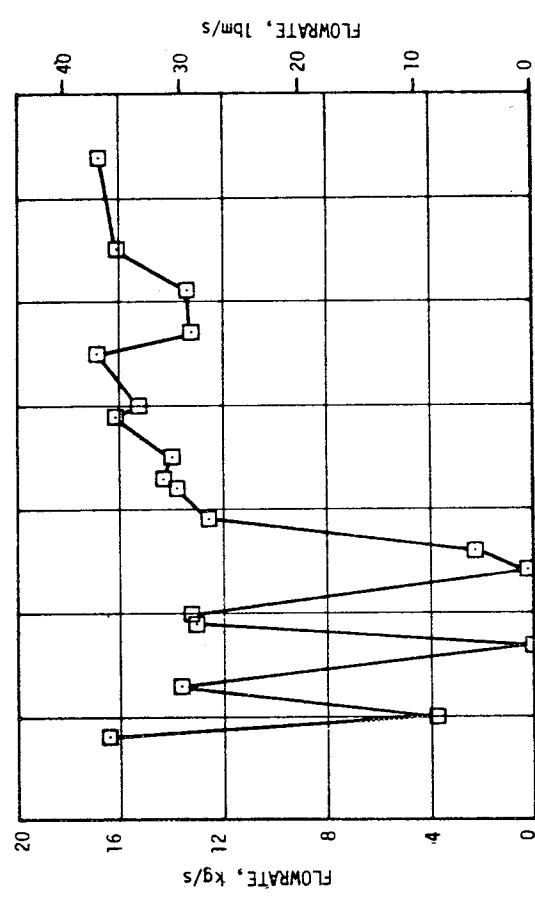


Figure 7-12. S-IVB LOX Pump Chillydown Performance - Second Burn

differential pressure and flowrate dropped from nominal to near zero and recovered three times as shown in Figure 7-12. This was caused by GOX bubble formation on the bottom of the tank. The GOX bubble formation is attributed to heat leaks through the aft LOX dome during coast. APS ullage acceleration forces resulted in the detachment of the bubble formation from the bottom of the LOX tank. As the bubbles slowly rose from the bottom of the tank and passed the chilldown pump inlet, some of the bubbles entered the LOX chilldown system. Since the chilldown system recovered to its previous level of performance, this two-phase flow disruption did not degrade the chilldown.

The engine control bottle pressure of  $1282 \text{ N/cm}^2$  (1870 psia) was lower than the predicted level of 1440 to  $1852 \text{ N/cm}^2$  (2100 to 2700 psia) due to leakage in orbit. The measured fuel level blowdown time at second burn start was 8.55 seconds. The amount of helium consumption during second burn was about the same as first burn but the pressure drop was considerably less than predicted. This pressure drop was about  $137 \text{ N/cm}^2$  (200 psi). The pressure drop during the fuel lead was  $617 \text{ N/cm}^2$  (900 psi) compared to  $754 \text{ N/cm}^2$  (1100 psi) predicted. During the engine shutdown operation and the 1-second cutoff LOX dome purge, the pressure drop was  $68.6 \text{ N/cm}^2$  (100 psi) as predicted. The control bottle pressure at second burn ECO was  $568.8 \text{ N/cm}^2$  (825 psia) and was within the predicted band of 206 to  $617 \text{ N/cm}^2$  (300 to 900 psia). The minimum control bottle pressure requirement at this time was  $206 \text{ N/cm}^2$  (300 psia).

The start tank performed satisfactorily during the initiation of second burn providing the proper energy input to the turbines for a smooth start. The lower tank temperature at second burn start command contributed to the second burn start transient being faster than the first burn transient as expected.

The second burn engine start transient was satisfactory. The PU system provided the proper fully open (low EMR) PU valve position during the restart transient until system activation. There was no evidence of observed propellant capillary action in zero gravity affecting the engine PU valve. The transition to active control was smooth and as predicted.

The thrust buildup was within the limits set by the engine manufacturer. The thrust buildup to 90 percent performance (STDV + 2.5 seconds) was faster than during the acceptance test as expected. The faster buildup was caused by the engine being warmer at ESC due to the absence of convective cooling in space. The thrust during second burn buildup transient is shown in Figure 7-13.

#### 7.7 S-IVB MAINSTAGE PERFORMANCE FOR SECOND BURN

The overall engine performance level was satisfactory. J-2 engine steady-state second burn performance is presented in Figure 7-14. A major deviation in the second burn average performance was due to the PU system commanded

Table 7-4. S-IVB Steady State Performance - Second Burn

PARAMETER *	PREDICTED	RECONSTRUCTED	FLIGHT DEVIATION	% DEVIATION FROM PREDICTED
Thrust N ( $1b_f$ )	1,001,490 (225,144)	966,400 (224,001)	-5080 (-1143)	-0.507
EMR LOX/Fuel	5.562	5.601	+0.039	+0.701
Specific Impulse N-s/kg ( $1b_f$ -s/ $1bm$ )	4152 (423.4)	4138.6 (422.02)	-13.4 (-1.4)	-0.33
LOX Flowrate kg/s ( $1bm/s$ )	204.44 (450.71)	204.28 (450.37)	-0.157 (-0.347)	-0.0769
Fuel Flowrate kg/s ( $1bm/s$ )	36.73 81.04	36.47 80.41	-0.283 -0.625	-0.77

\*Reduced to standard altitude conditions at 60 second time slice.  
Predicted is based on high step operation.

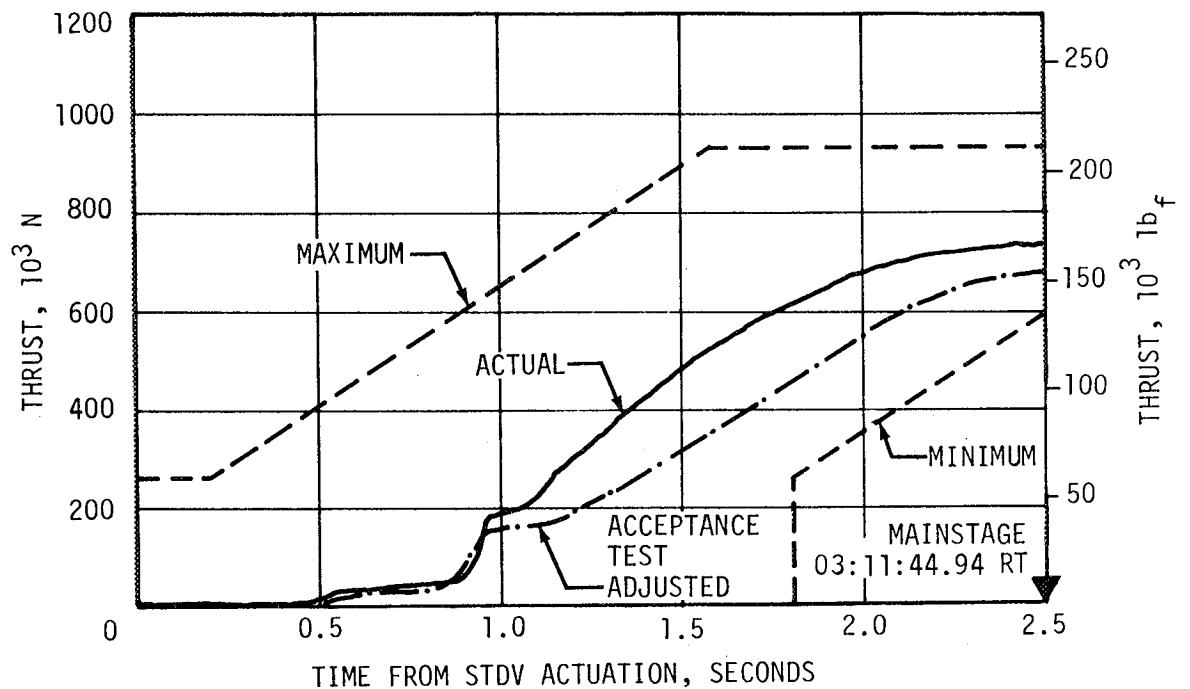


Figure 7-13. S-IVB Buildup Transient - Second Burn

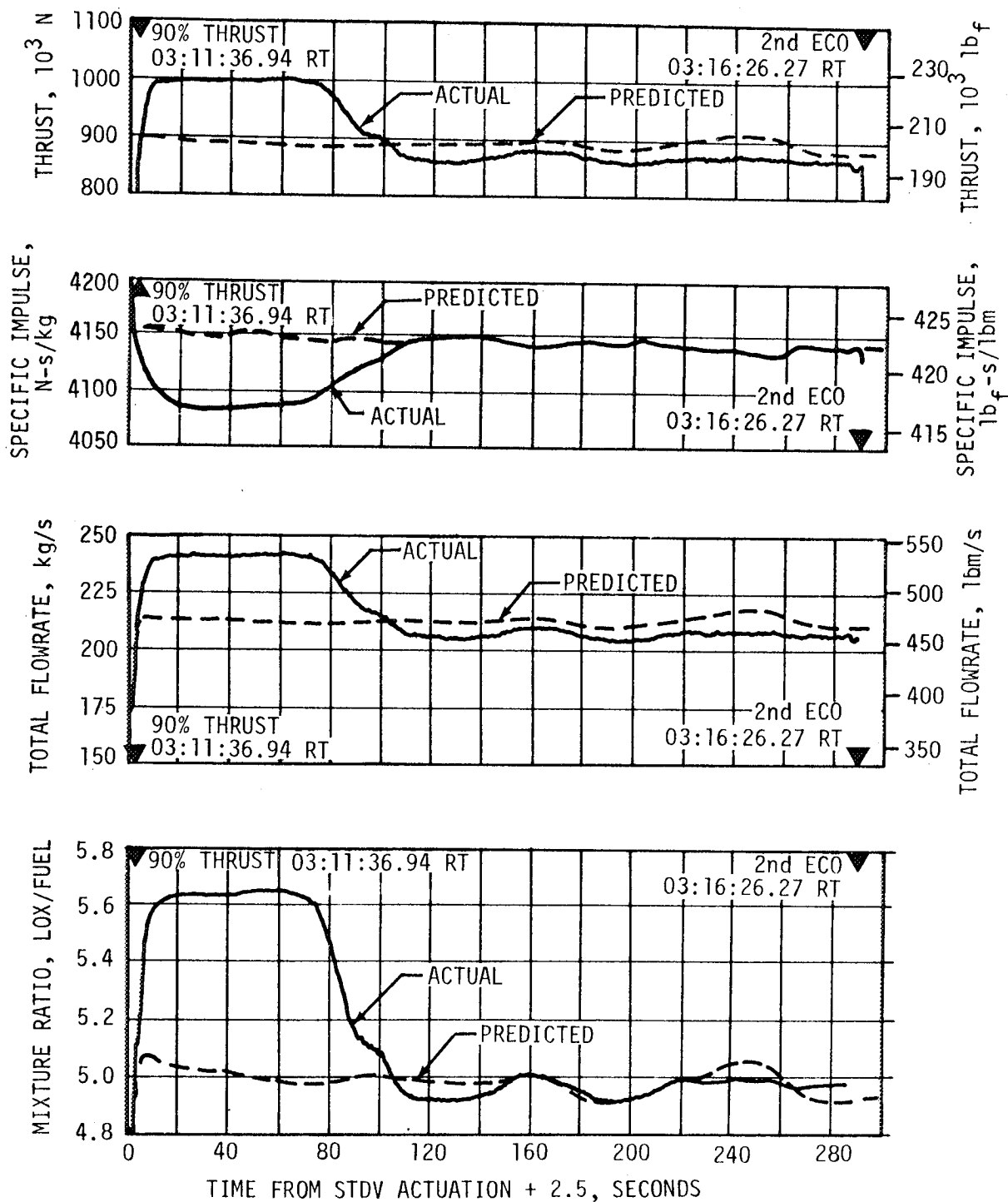


Figure 7-14. S-IVB Steady State Operation - Second Burn

high mixture ratio excursion during the first 85 seconds. The high mixture ratio excursion was mainly due to the combined effects of the first burn low engine performance and the higher than predicted fuel loss in orbit. This performance deviation contributed to the departure from the predicted nominal mixture ratio during the second burn. A velocity commanded engine cutoff command was earlier than predicted.

The PU system commanded the PU valve to fully closed (high EMR) position, upon system activation, in order to remove the excess oxidizer mass error caused by the off nominal engine performance during first burn, and the increased fuel boiloff in orbit. The PU system maintained the engine at high thrust until the error was eliminated, and engine performance cutback occurred at approximately ESC +85 seconds.

The level of engine performance during the high thrust period of second burn was closer to the predicted high level performance than during the first burn. This is demonstrated in Table 7-4 which shows that all performance parameters at standard altitude conditions agreed more closely with the prediction.

All average performance values were within 1 percent of predicted during the high mixture ratio portion of the burn. The deviations during the Reference Mixture Ratio (RMR) portion were within 3 percent. The overall average performance values are compared to the nominal prediction which operated at 5.0 RMR throughout the burn. The variations for overall average performance were within 3 percent for all parameters.

A minor perturbation in performance was also induced by the PU valve responding to a guidance commanded maneuver at approximately ESC +100 seconds

A trajectory simulation using a differential correction procedure determines adjustments to the reconstructed engine thrust and flowrate to yield a simulated trajectory which closely matched the observed mass point trajectory. The results obtained indicated an increase over reconstructed average flight values of 0.67 percent in thrust and 0.488 percent in mass flowrate and 0.096 percent in specific impulses for second burn as shown in Table 7-5. The S-IVB second burn time was 15.18 seconds shorter than predicted. This shorter burn time was accounted for as follows:

<u>Contributor</u>	<u>Burn Time Delta (sec)</u>
High Stop EMR Operation	-17.0
Low RMR Thrust Following Cutback	+ 1.0
Unexplained	+ 0.8
Total	-15.2



Table 7-5. Comparison of S-IVB Stage Reconstruction Data - Second Burn

PARAMETERS	UNITS	PREDICTED*			FLIGHT RECONSTRUCTION			% DEV. FROM PRED.		
		HIGH MIXTURE RATIO	REFERENCE MIXTURE RATIO	SECOND BURN FLIGHT AVERAGE	HIGH MIXTURE RATIO	REFERENCE MIXTURE RATIO	SECOND BURN FLIGHT AVERAGE	HIGH MIXTURE RATIO	REFERENCE MIXTURE RATIO	SECOND BURN FLIGHT AVERAGE
Longitudinal Vehicle Thrust	N (lb <sub>f</sub> )	892,122 (200,557)	892,122 (200,557)	892,122 (200,557)	999,515 (224,700)	870,961 (195,800)	907,126 (203,930)	+12.04	-2.37	+1.68
Vehicle Mass Loss Rate	kg/s (lbm/s)	212.84 (469.23)	212.84 (469.23)	212.84 (469.23)	242.17 (533.90)	208.61 (459.90)	217.34 (479.16)	+13.78	-1.99	+2.11
Longitudinal Vehicle Specific Impulse	N-s/kg (lb <sub>f</sub> -s/lbm)	4191.5 (427.42)	4191.5 (427.42)	4191.5 (427.42)	4124.8 (420.87)	4172.5 (425.74)	4171.2 (425.60)	-1.53	-0.39	-0.42
PARAMETERS	UNITS	FLIGHT SIMULATION			% DEV. FROM PRED.			% DEV. FROM RECONSTRUCTED		
		HIGH MIXTURE RATIO	REFERENCE MIXTURE RATIO	SECOND BURN FLIGHT AVERAGE	HIGH MIXTURE RATIO	REFERENCE MIXTURE RATIO	SECOND BURN FLIGHT AVERAGE	HIGH MIXTURE RATIO	REFERENCE MIXTURE RATIO	SECOND BURN FLIGHT AVERAGE
Longitudinal Vehicle Thrust	N (lb <sub>f</sub> )	1,005,698 (226,090)	877,994 (197,381)	913,220 (205,300)	+12.73	-1.58	+2.36	+0.617	+0.807	+0.672
Vehicle Mass Loss Rate	kg/s (lbm/s)	242.902 (535.507)	209.288 (461.401)	218.405 (481.50)	+15.12	-1.67	+2.61	+0.301	+0.326	+0.488
Longitudinal Vehicle Specific Impulse	N-s/kg (lb <sub>f</sub> -s/lbm)	4137.8 (422.20)	4192.6 (427.79)	4178.8 (426.38)	-1.22	+0.02	-0.24	+0.315	+0.490	+0.096

\* Predicted was for a nominal EMR throughout second burn.

## 7.8 S-IVB SHUTDOWN TRANSIENT PERFORMANCE FOR SECOND BURN

The S-IVB Engine Cutoff (ECO) was initiated by guidance cutoff which was 15.18 seconds shorter than predicted for second burn. The second burn engine cutoff transient was satisfactory and agreed closely with the acceptance test and predictions. The thrust decreased to 5 percent of the rated thrust which was 50,042 Newtons (11,250 lbf). This occurred 437 milliseconds after engine cutoff was received at the engine, while zero thrust occurred 2.31 seconds after engine cutoff. The total cutoff impulse to 5 and zero percent rated thrust was 190,072 N-s (42,730 lb-s) and 216,980 N-s (48,779 lb-s), respectively. These were less than the corresponding first burn values since second burn cutoff occurred with the PU valve below the null position (-2.5 degrees) as compared to the first burn cutoff occurring at high EMR. The MOV actuation temperature was 166° K (160.7° F) at cutoff. When the cutoff impulse was referred to standard conditions (null PU valve position and 255.5° K (460° F) MOV actuator temperature), it was in good agreement with the first burn cutoff impulse at standard conditions and with the log book value. The thrust during cutoff is shown in Figure 7-15. The second burn cutoff impulse to zero percent thrust resulted in a velocity increase of 3.41 m/s (11.2 ft/s) which correlates satisfactorily with predictions shown in Table 7-6.

## 7.9 S-IVB STAGE PROPELLANT UTILIZATION

The propellant utilization system successfully accomplished the requirements associated with propellant loading and management during burn. The best estimate propellant mass values at liftoff were 88,141 kilograms (194,318 lbm) LOX and 18,656 kilograms (41,130 lbm) LH<sub>2</sub> as compared to predicted mass values of 87,667 kilograms (193,273 lbm) LOX and 18,698 kilograms (41,222 lbm) LH<sub>2</sub>. These values were well within required loading accuracies. The best estimate S-IVB stage and payload liftoff mass was 160,122 kilograms (353,011 lbm).

A comparison of propellant mass values at critical flight events as determined by various analyses is presented in Table 7-7. In addition to the data listed, simulation-trajectory match results were included in the best estimate value. The best estimate full load propellant masses were 0.54 percent higher for LOX and 0.22 percent lower for LH<sub>2</sub> than the predicted values, as shown in Table 3-3 of Launch Operations, Section 3. This deviation was well within the required loading accuracy.

Best estimate mass values at first burn ECO and second burn ECS, shown in Table 7-7, were the statistical results of the methods listed, but their difference does not represent the most accurate measure of actual orbital boilloff. The values for orbital boilloff, as determined by independent methods, were 66 kilograms (146 lbm) LOX and 1300 kilograms (2865 lbm) LH<sub>2</sub>. Figure 7-16 presents the S-IVB best estimate ignition and cutoff masses for first and second burns. This figure includes simulation-trajectory data and values in addition to the other measurement systems listed in Table 7-7.

Table 7-6. S-IVB Cutoff Impulse - Second Burn

PARAMETER	PREDICTED	FLIGHT		% DEVIATION FROM PREDICTED	
		ENGINE	GUID. DATA	ENGINE	GUID. DATA
Cutoff N-s Impulse ( $1b_f$ -s)	185,126 (41,618)	216,980 (48,779)	210,480 (47,318)	+13.7	--
Velocity m/s Increase (ft/s)	3.08 (10.1)	3.5 (11.5)	3.41 (11.2)	+13.86	+10.8

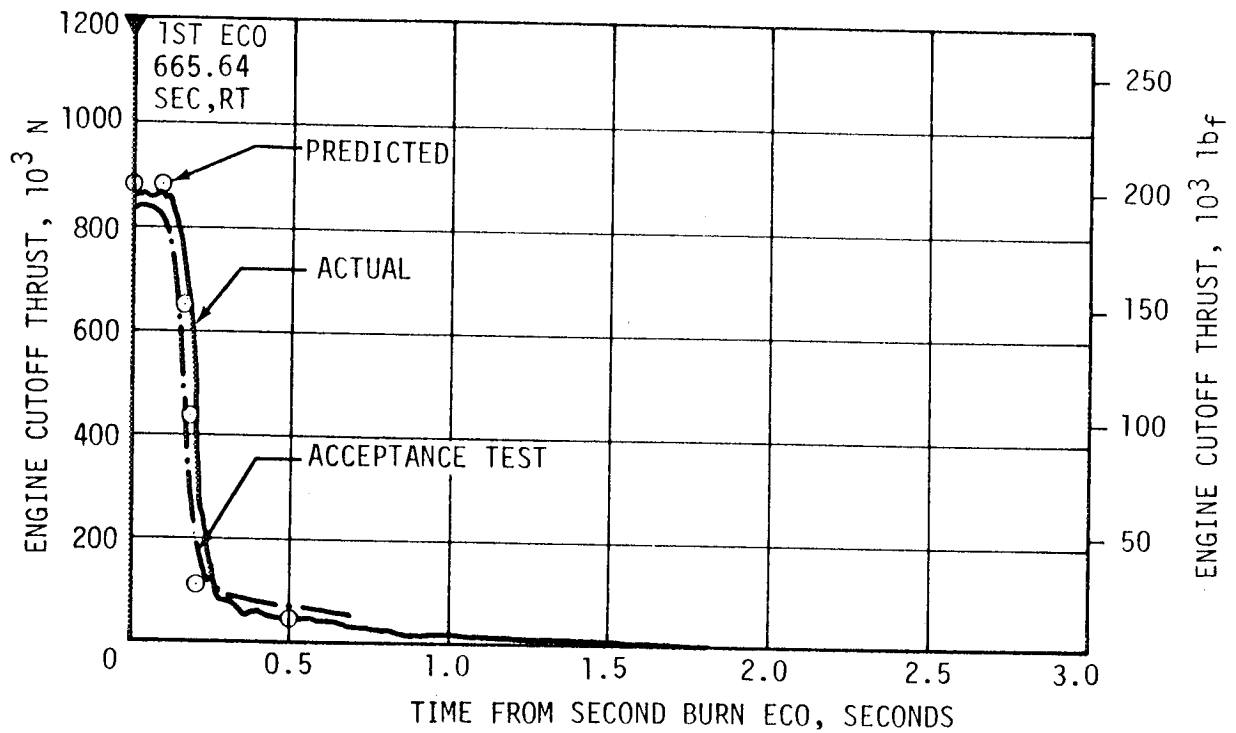


Figure 7-15. S-IVB Shutdown Transient - Second Burn

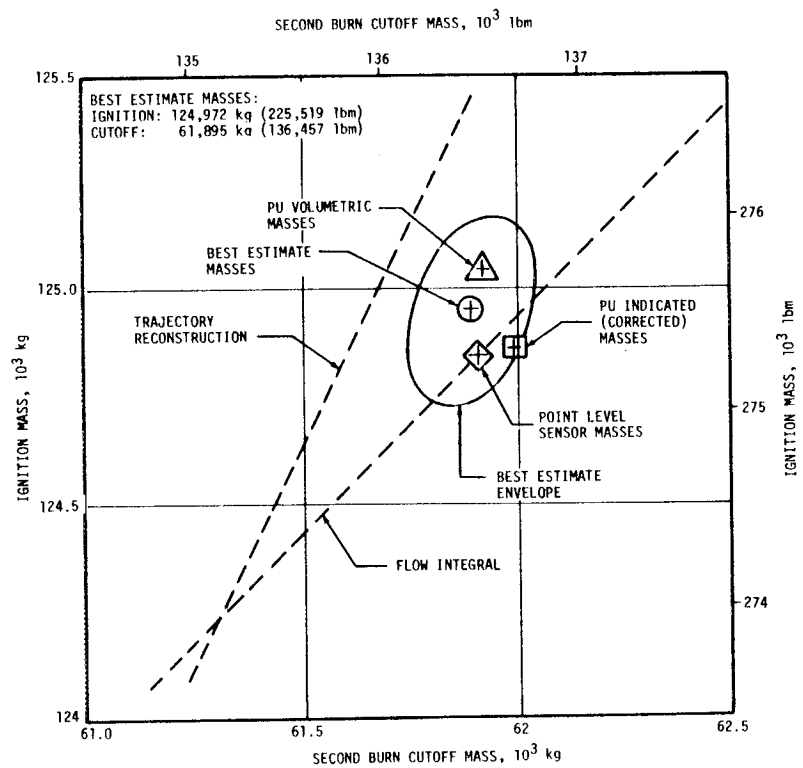
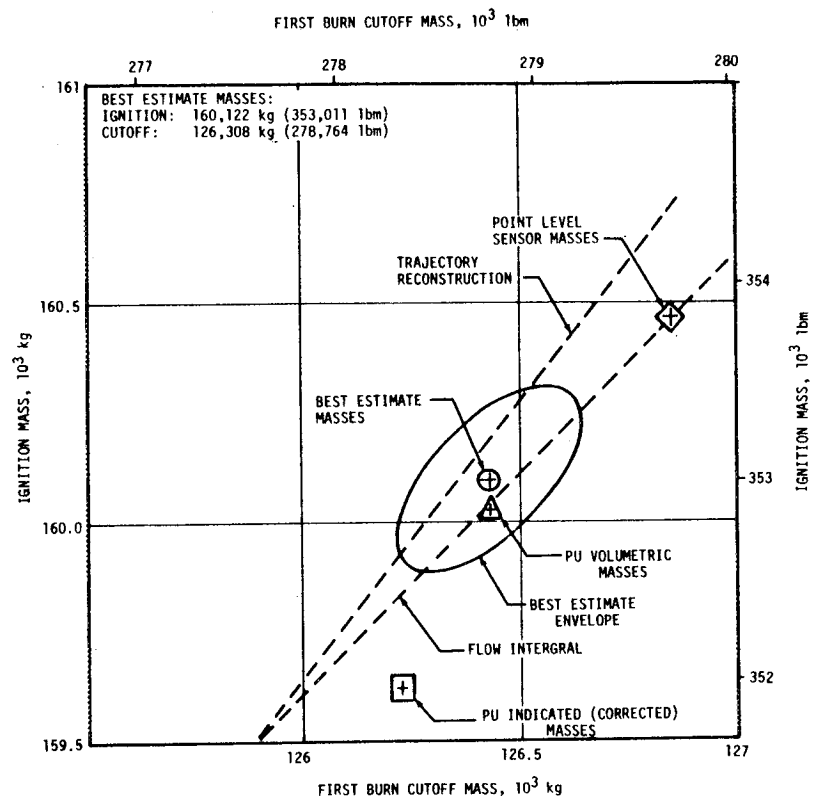


Figure 7-16. S-IVB Ignition and Cutoff Best Estimate Masses

Table 7-7. S-IVB Stage Propellant Mass History

EVENT	PREDICTED		P.U. INDICATED (CORRECTED)		P.U. VOLUMETRIC		LEVEL SENSOR (EXTRAPOLATED)		BEST ESTIMATE		FLOW INTEGRAL	
	LOX	LH2	LOX	LH2	LOX	LH2	LOX	LH2	LOX	LH2	LOX	LH2
S-IC L/O kg (lbm)	87,666 193,273	18,697.9 41,222	87,678 193,299	18,672 41,164	88,127 194,289	18,619 41,049	88,399 194,887	18,770 41,381	88,141 194,318	18,656 41,130	87,976 193,954	18,660 41,139
1ST ESC kg (lbm)	87,666 193,273	18,697.9 41,222	87,683 193,380	18,646 41,107	88,132 194,300	18,594 40,994	88,399 194,887	18,770 41,381	88,141 194,318	18,656 41,130	87,976 193,954	18,660 41,139
1ST ECO kg (lbm)	60,226 132,777	13,716.1 30,239	59,508 131,193	13,433 29,614	59,738 131,700	13,407 29,557	60,028 132,340	13,544 29,860	59,767 131,765	13,489 29,650	59,574 131,338	13,465 29,685
2ND ESC kg (lbm)	60,044 132,376	12,477.4 27,508	59,459 131,085	12,121 26,723	59,689 131,592	12,079 26,631	59,561 131,310	12,010 26,479	59,607 131,411	12,070 26,611	59,539 131,262	12,079 26,629
PU CUT- BACK kg (lbm)	----- -----	----- -----	48,994 108,013	10,100 22,266	49,034 108,103	10,064 22,187	----- -----	----- -----	----- -----	----- -----	49,046 108,128	10,141 22,357
2ND ECO kg (lbm)	5,482 12,087	1,484.6 3,273	6,864 15,133	1,730 3,815	6,831 15,059	1,689 3,723	6,860 15,123	1,648 3,634	6,801 14,994	1,676 3,696	6,843 15,087	1,723 3,798

Extrapolation of propellant-level sensor data to depletion, using the propellant flowrates to depletion, indicated that a LOX depletion would have occurred approximately 38 seconds after second burn velocity cutoff with a usable LH2 residual of 40 kilograms (89 lbm). This yielded a PU efficiency of 99.96 percent.

The first and second burn PU valve positions are illustrated in Figure 7-17. During first burn the PU valve was positioned at null for start and remained there until PU activate at first burn ESC + 8 seconds. The PU valve was then commanded to the fully closed (high EMR) position at activation and it remained there throughout first burn.

For second burn, the PU valve was successfully commanded to the fully opened (low EMR) position at second burn ESC -20 seconds to satisfy engine restart requirements. The PU valve remained there until second burn ESC +13 seconds when the fully opened (low EMR) position command was removed. At this time system dispersions caused the PU valve to travel to the fully closed (high EMR) position.

The PU valve reached the fully closed (high EMR) position at second burn ESC +25 seconds and remained there until ESC +63.5 seconds. The system dispersions, that caused the PU valve fully closed (high EMR) position operation during second burn, are nearly equally divided between propellant boiloff during orbit and the combination of PU system calibration and first burn engine performance deviation.

The engine performance deviation was caused primarily by a low LOX flowrate during first burn. The calibration deviation resulted from a combination of a LOX overload and an LH2 underload. Variations in PU system nonlinearities also added to the LOX rich conditions. The actual LOX mass, which boiled

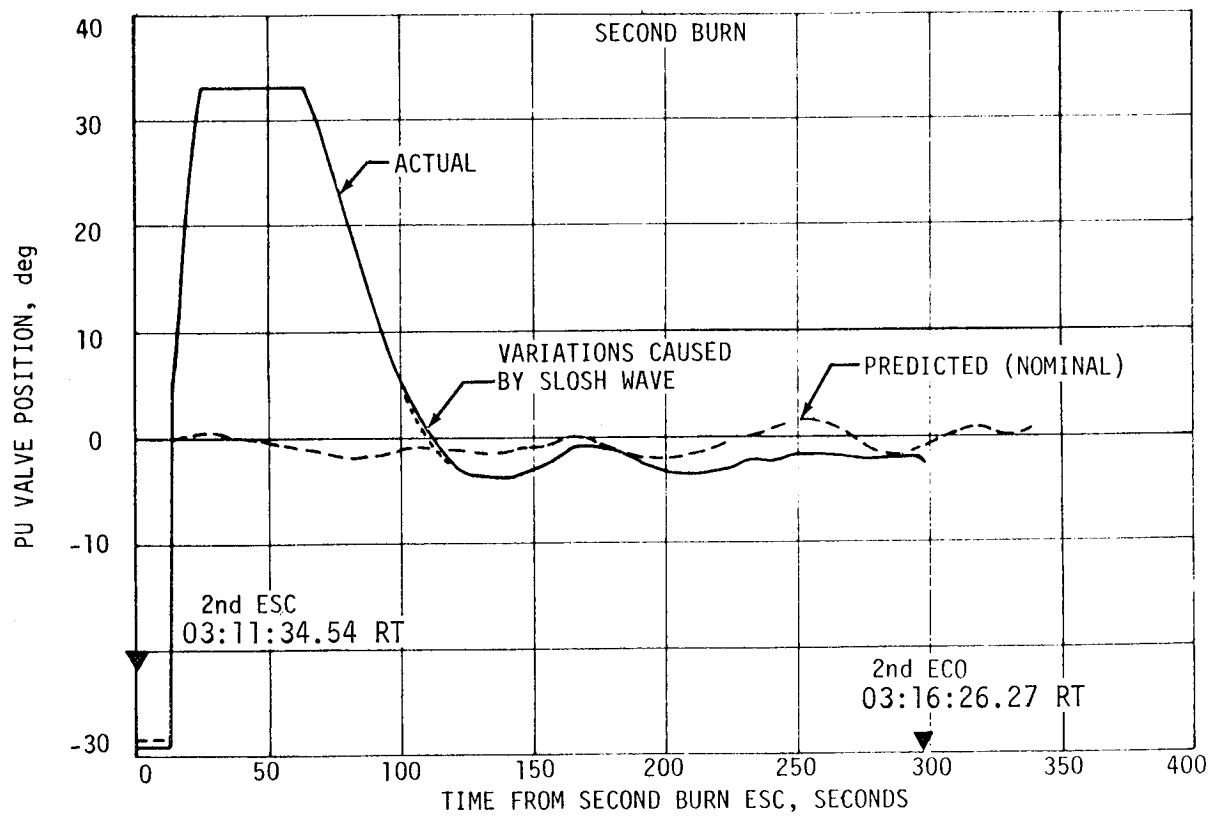
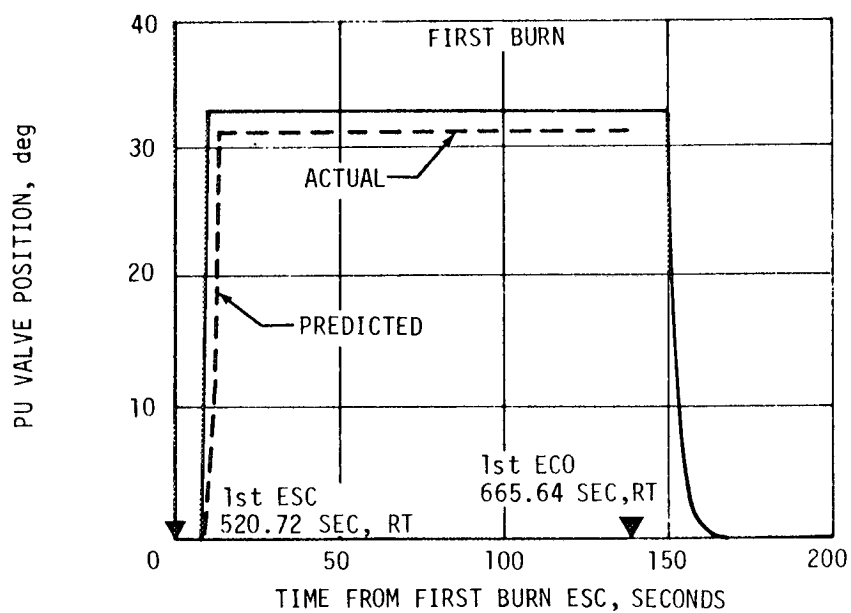


Figure 7-17. S-IVB PU Valve Positions

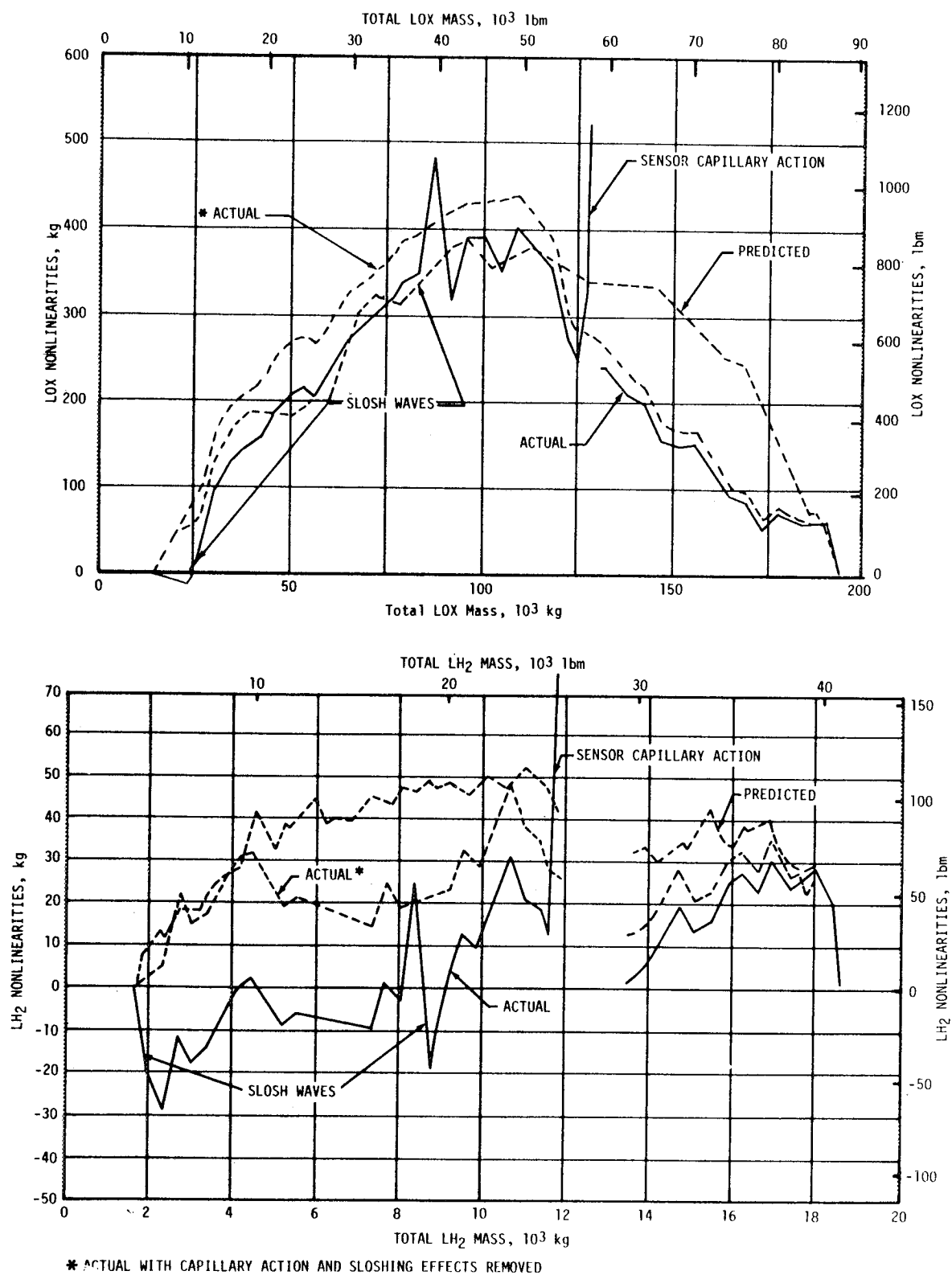


Figure 7-18. S-IVB PU System Nonlinearities

off during coast, and the LOX consumed during the first burn cutoff transient were less than predicted and added to the LOX rich condition.

The PU system tank-to-sensor mismatch nonlinearities are presented in Figure 7-18. The combination of sensor capillary action at the start of second burn and two slosh waves, caused by vehicle attitude transients during burn, caused large variations in the indicated mass data used to determine these nonlinearities. The actual PU system tank-to-sensor nonlinearities, with the sloshing and capillary effects removed, compared favorably with the predicted values adjusted for actual flight dynamics effects. Inflight LH2 tank geometry variations deviated from the predicted during first burn. The mismatch error at PU cutback was zero for LOX and -30 kilograms (-66 lbm) LH2.

Figure 7-19 shows how capillary action in the sensors affected the fine and coarse mass readings, and for comparison the engine flowmeter mass data is also shown. Due to the fully open (low EMR) valve command and associated grounding of the forward shaping network filters for the first 33 seconds of PU system activation, the effect of the capillary action on the valve itself was negligible.

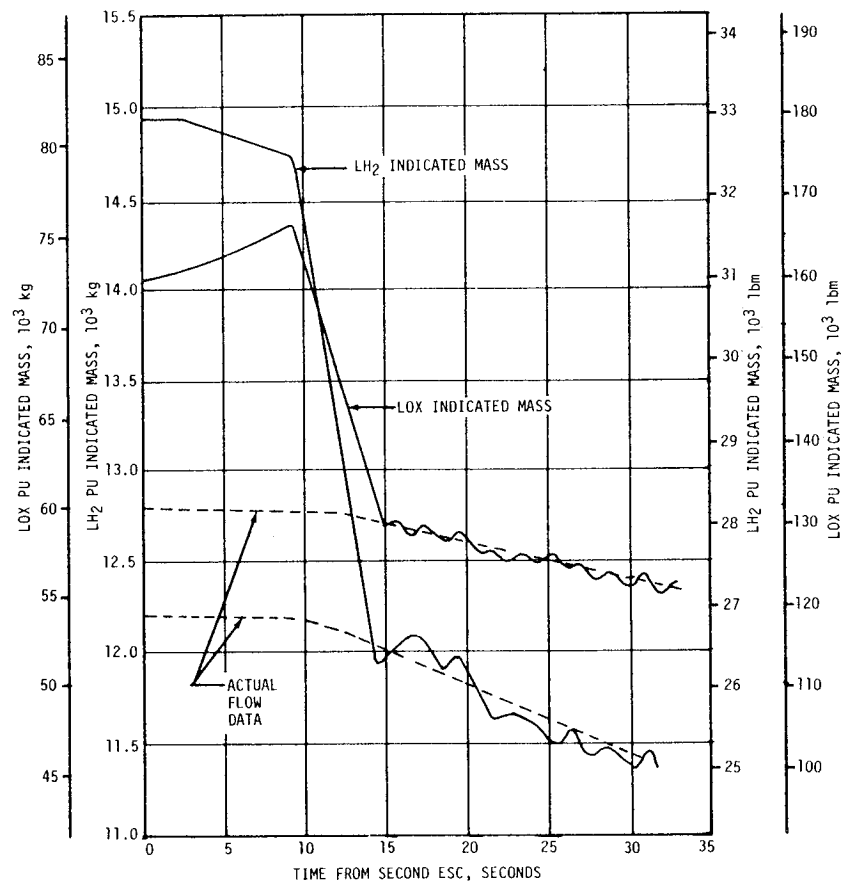


Figure 7-19. S-IVB PU Indicated Mass - Second Burn



Vehicle attitude transients resulted in two large low-frequency propellant slosh waves. The first slosh wave appeared between second burn ESC +100 seconds and ESC +120 seconds. This slosh wave was set off by a vehicle attitude transient following artificial tau mode. The PU valve was raised approximately 1 degree by this disturbance and resulted in a corresponding shift in engine performance parameters. The second low-frequency slosh wave occurred approximately 5 seconds before second burn ECO. This wave was also caused by a vehicle attitude transient and occurred at the same time the chi freeze guidance mode was applied. This disturbance resulted in a 1 degree valve tailoff and corresponding thrust variation.

The redesigned forward shaping network (slosh filter) successfully attenuated the effects of propellant sloshing on the PU valve. Propellant sloshing within a 0.2 to 0.6 hertz range was present in the mass signals and the PU summing point error signal. However, the added filter attenuated the slosh effects on the signal fed to the PU valve servo.

The actual first burn EMR was lower than predicted LOX flowrates, while the second burn EMR variations follow the PU valve history. The thrust level change from EMR cutback to the EMR position was 989,314 Newtons (224,430 lbf) to 870,961 Newtons (195,800 lbf). This resulted in a thrust level change of 118,353 Newtons (28,630 lbf).

## 7.10 S-IVB PRESSURIZATION SYSTEM

### 7.10.1 S-IVB LH<sub>2</sub> Tank Pressurization

The LH<sub>2</sub> pressurization system operationally met all engine performance requirements. However, the LH<sub>2</sub> pressurization system indicated possible deviations from the predicted during S-IVB first burn, coast phase, and second burn operations. The pressure measurement deviations, within the continuous vent system and LH<sub>2</sub> pressurization system, during orbital coast resulted in ground command activities necessitated by the mission rules. The sequence of events and associated system performances are discussed in the following paragraphs.

The LH<sub>2</sub> tank prepressurization command was received at -96.5 seconds. The LH<sub>2</sub> tank pressurized signal was received 21.5 seconds later when the LH<sub>2</sub> tank ullage pressure reached 23.3 N/cm<sup>2</sup> (33.8 psia). The ullage pressure continued to increase, reaching 24.8 N/cm<sup>2</sup> (35.9 psia) at S-IVB first burn ESC as shown in Figure 7-20.

At S-IVB first burn ESC the LH<sub>2</sub> tank ullage pressure was 24.8 N/cm<sup>2</sup> (35.9 psia). Between S-IVB first burn ESC (520.72 seconds) and approximately 525.5 seconds, the under-control orifice and the first and second burn over-control valves were open. Pressurization flow was limited to the under-control orifice not requiring first burn over-control valve operation until first burn ECO at 665.64 seconds. The ullage pressure followed a normal decay, reaching 20.0 N/cm<sup>2</sup> (29.0 psia) at first burn ECO. The actual

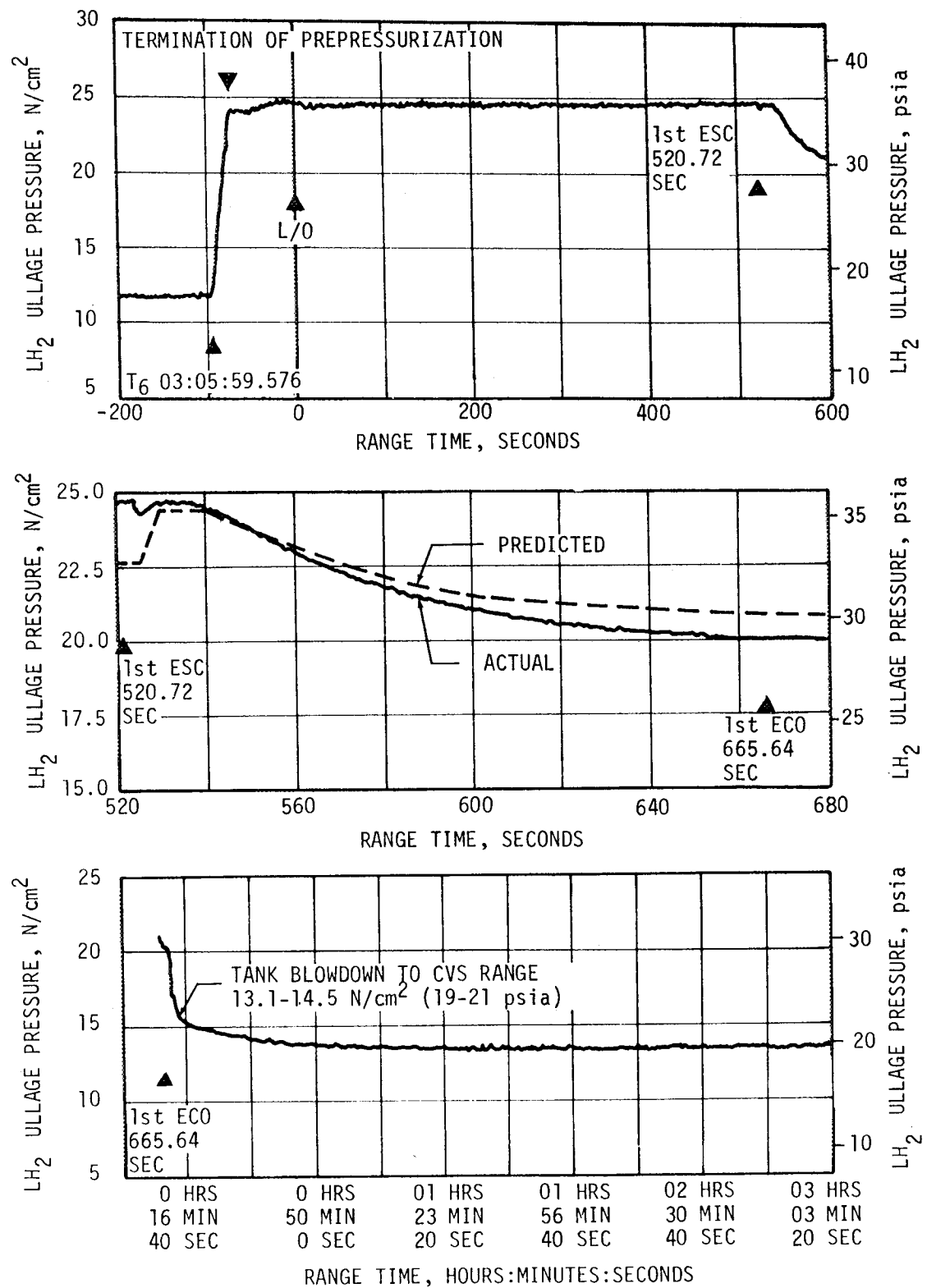


Figure 7-20. S-IVB LH<sub>2</sub> Ullage Pressure

pressure profile, while somewhat lower than predicted as shown in Figure 7-20, was satisfactory. LH<sub>2</sub> tank venting did not occur during S-IVB first burn. The GH<sub>2</sub> pressurization flowrate was approximately 0.345 kg/s (0.50 lbm/s), providing a total flow of 48.3 kilograms (70.1 lbm) during S-IVB first burn.

Following orbit insertion, the continuous vent line pressures of the LH<sub>2</sub> tank were reading approximately zero. These two line pressures are the cues on which conclusions to the open/closed condition of the continuous vent valve are made by ground control. About 1 minute after insertion, the continuous vent system was activated and displayed the expected reading on both line pressures. The system behavior as displayed on the ground was entirely normal.

During the orbital coast, with decreasing tank pressure, the line pressures steadily decayed to 13.4 N/cm<sup>2</sup> (19.5 psi) and started regular oscillations which are attributed to regulator operation. The two line pressures exhibited very similar values until the first pass over Carnarvon and at this time a pressure differential of 2.1 N/cm<sup>2</sup> (3 psi) was observed and remained for the rest of the orbital flight and the restart sequence.

Near the completion of the second revolution, Time Base 6 (T<sub>6</sub>) was initiated by onboard sequence while the space vehicle was in sight of the Guaymas station. As shown in Figure 7-21, the increase in vent line temperatures indicates a closure of the continuous vent which was scheduled to occur at T<sub>6</sub> +1.2 seconds. The two vent line pressures, still differing by approximately 2.1 N/cm<sup>2</sup> (3 psi) stopped their oscillations and then began a gradual decrease from their former peak values. This behavior was drastically different from the expected immediate pressure drop to zero. At the same time, the repressurization of the LH<sub>2</sub> tank commenced, accompanied by a corresponding decrease of the ambient helium supply pressure as shown in Figure 7-21. The rate of repressurization of the LH<sub>2</sub> tank was somewhat slower than anticipated on the basis of flight predictions. Ground control concluded that this was an additional indication of at least a partially open condition of the vent valve and took appropriate action as required by the mission rules.

Appropriate action by ground command to the switch selector consisted of four steps, three of which were made at the same time (Reference Table 2-4). First, the repressurization valve was closed, stopping the ambient helium flow into the tank. This provision was made to prevent the loss of repressurization gas through the open vent valve. The second command step attempted to close the solenoid valve electrically and at the same time applied pneumatic pressure to the pneumatic valve of the continuous vent valve assembly. The third step consisted of removing the pneumatic pressure from the valve assembly. This sequence was to be followed by an opening command to the repressurization valve at T<sub>6</sub> +256 seconds to make optimum use of the entire helium available even if the continuous vent failed completely open. The step of commanding open the repressurization valve was omitted due to additional attempts to close the valve and command handover from Texas to Cape Kennedy.

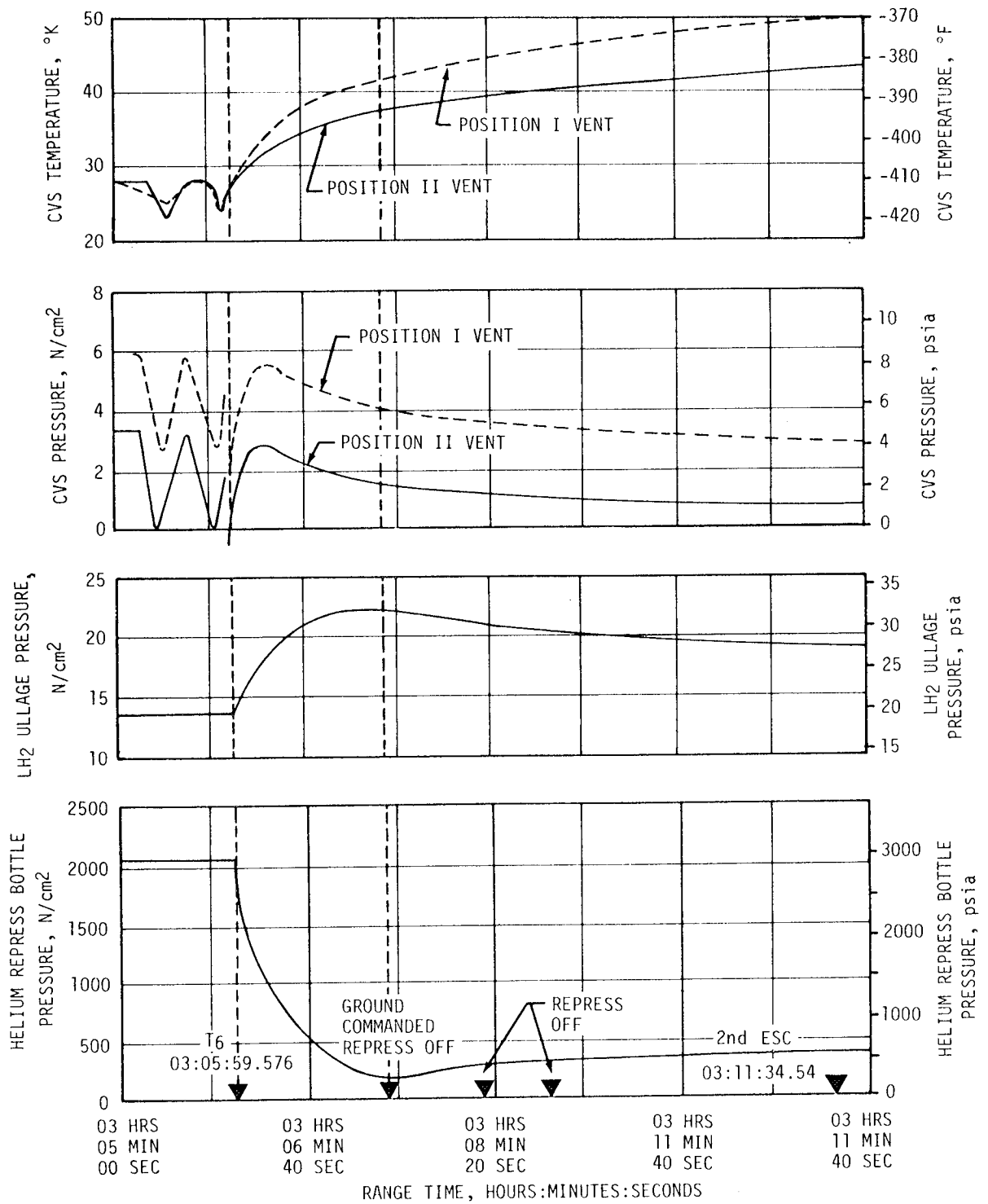


Figure 7-21. S-IVB CVS Performance - Orbital Coast

During this repressurization period the LH<sub>2</sub> tank was pressurized from 13.6 N/cm<sup>2</sup> (19.7 psia) to 22.0 N/cm<sup>2</sup> (32.0 psia). The ullage pressure subsequently decayed, reaching 19.2 N/cm<sup>2</sup> (27.8 psia) at second burn ESC as shown in Figure 7-22. Approximately 20.4 kilograms (45 lbm) of ambient helium were used in the repressurization operation, with approximately 6.4 kilograms (14 lbm) remaining in the bottles. The residual helium would have provided approximately 10.3 N/cm<sup>2</sup> (1.5 psi) additional ullage pressure. The ullage pressure of 19.2 N/cm<sup>2</sup> (27.8 psia) at second burn ESC is lower than the minimum predicted level of 21.4 N/cm<sup>2</sup> (31 psia).

The unexpected decay of LH<sub>2</sub> ullage pressure, after termination of repressurization, was probably caused by a malfunction of the diffuser or bubble formation. The corrective action presently under consideration is:

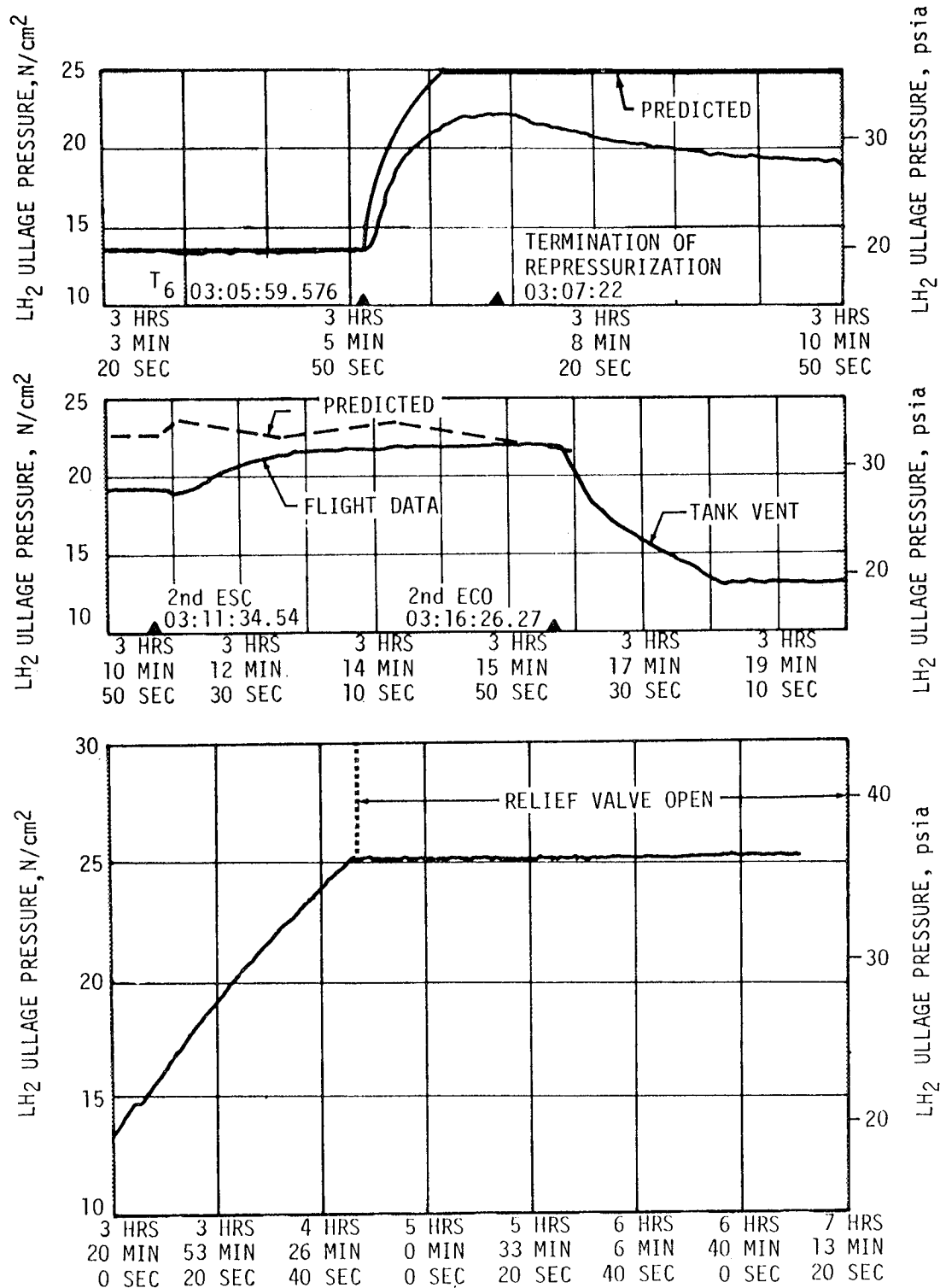
- a. Implement diffuser ground test program.
- b. Change flight sequence to optimize the repressurization cycle.
- c. Reorificing the repressurization control module.

Some other possible affects on the low LH<sub>2</sub> ullage pressure were:

- a. Premature termination of the ambient repressurization operation.
- b. A cooler than expected blowdown of the repressurization bottles (lower environmental heating of the pressurant gas resulted in a lower energy input into the ullage).
- c. A condensation of GH<sub>2</sub> bubbles into the liquid bulk (condensation of bubbles resulted in an expansion of the remaining ullage volume and a corresponding ullage pressure drop).
- d. An energy loss from the ullage gas was caused by a propellant wave induced by a significant attitude change maneuver at the start of repressurization.

Between S-IVB second burn ESC and ESC +10.6 seconds, the under control orifice, the first and second burn over-control valves were open. The first burn over-control valve closed for second burn, while the under control orifice and the second burn over-control valve remained open throughout second burn. Fuel tank ullage pressure and pressure rise rates during S-IVB second burn were lower than anticipated as shown in Figure 7-22. Preflight predictions indicated cyclic operation within the 21.4 - 23.4 N/cm<sup>2</sup> (31-34 psia) control band. The maximum pressure obtained, which occurred at second burn ECO, was 22.0 N/cm<sup>2</sup> (31.9 psia).

LH<sub>2</sub> tank venting did not occur during S-IVB second burn. The GH<sub>2</sub> pressurization flowrate ranged from 0.48 to 0.52 kg/s (0.70 to 0.75 lbm/s), providing a total flow of 142 kilograms (206 lbm) during S-IVB second burn.



RANGE TIME, HOURS: MINUTES: SECONDS

Figure 7-22. S-IVB LH<sub>2</sub> Ullage Pressure - Second Burn

In summary it is concluded that the continuous vent system operation was nominal. The vent line pressures which were nominal following CVS initiation at liftoff +751 seconds began to diverge prior to liftoff +1000 seconds. The deviation was probably transducer bias and/or inaccuracies resulting from environmental effects and had increased to 1.7 - 2.1 N/cm<sup>2</sup> (2.5 - 3.0 psi) by 00:52:04. Thermodynamic analysis has shown that the transducers at their mounting location were exposed to extreme low temperature environment and that output shifts of up to 12 percent may be experienced at these low temperatures. The oscillation of the CVS temperature and pressure prior to restart preparation initiation (03:05:59.55) indicated that the system functioned properly.

In order to prevent a reoccurrence of similar events, mission rule 5-38 is being reassessed. Recommendations presently being considered are change and/or addition of primary cues, procedural safeguards against omission of subsequent command steps, and remote location of transducers.

The LH<sub>2</sub> pump inlet NPSP was calculated from the pump interface temperature and total pressure. These values indicated that the NPSP at S-IVB first burn ESC was 9.5 N/cm<sup>2</sup> (13.8 psi). The NPSP then decreased during powered flight to a minimum value of 6.21 N/cm<sup>2</sup> (9 psi) at first burn ECO. At the minimum point the NPSP was 1.8 N/cm<sup>2</sup> (2.6 psi) above the required. Throughout the burn, the NPSP closely followed the predicted.

The NPSP at the end of fuel lead prior to second burn was approximately the same as the required level. The NPSP increased rapidly after ESC such that it was above the required level during the engine burn. At second burn ECO the NPSP was 6.0 N/cm<sup>2</sup> (8.75 psi) which was 1.97 N/cm<sup>2</sup> (2.85 psi) above the required. The pump interface total pressure at the end of fuel lead was 18.5 N/cm<sup>2</sup> (26.8 psi). The pressure continued to increase during the second burn reaching a pressure of 21.3 N/cm<sup>2</sup> (30.9 psi) at ECO. The difference between the data and the predicted was due to a lower than expected LH<sub>2</sub> tank ullage pressure.

Figures 7-23 and 7-24 summarize the fuel pump inlet conditions for first and second burns, respectively.

#### 7.10.2 S-IVB LOX Pressurization System

The oxidizer system performed adequately, supplying LOX to the engine pump inlet within the specified operating limits throughout both firings. The available NPSP at the LOX pump inlet exceeded the engine manufacturer's minimum at all times.

LOX tank prepressurization was initiated at -167 seconds and increased the LOX tank ullage pressure from ambient to 27.92 N/cm<sup>2</sup> (40.5 psia) within 15 seconds as shown in Figure 7-25. Two makeup cycles were required to maintain the LOX tank ullage pressure before the ullage temperature stabilized. The pressurization control pressure switch controlled the pressure between

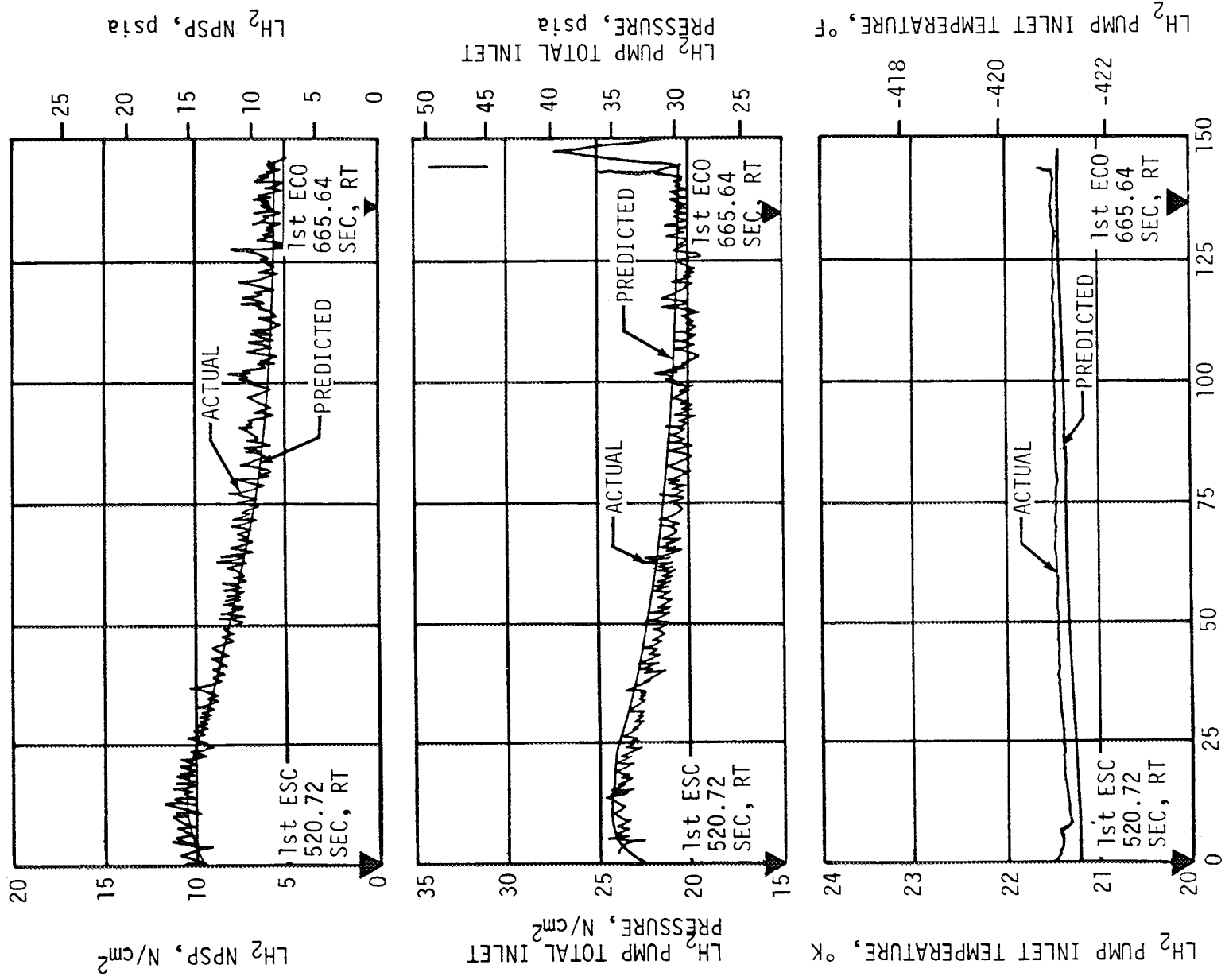


Figure 7-23. S-IVB Fuel Pump Inlet Conditions - First Burn



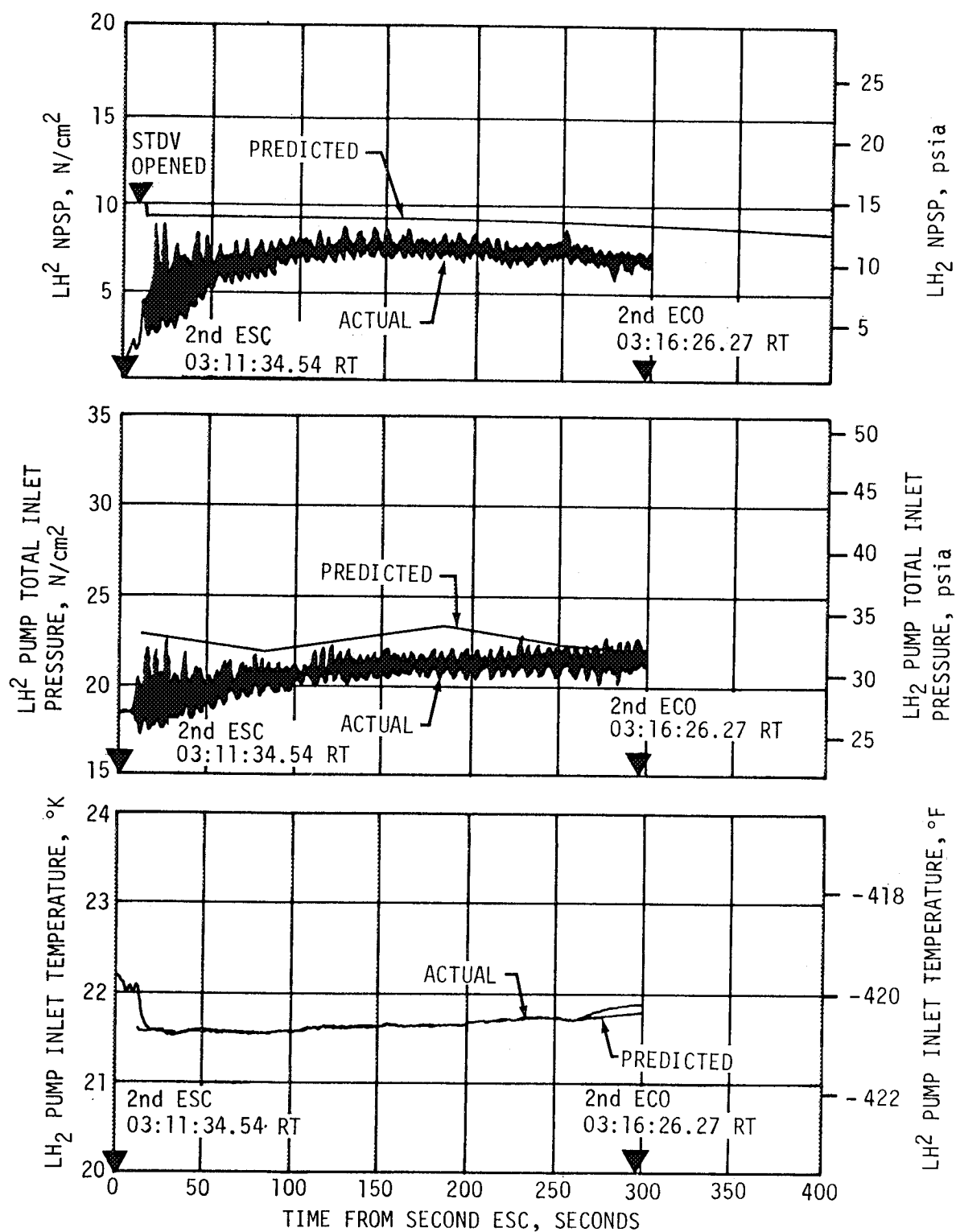


Figure 7-24. S-IVB Fuel Pump Inlet Conditions - Second Burn

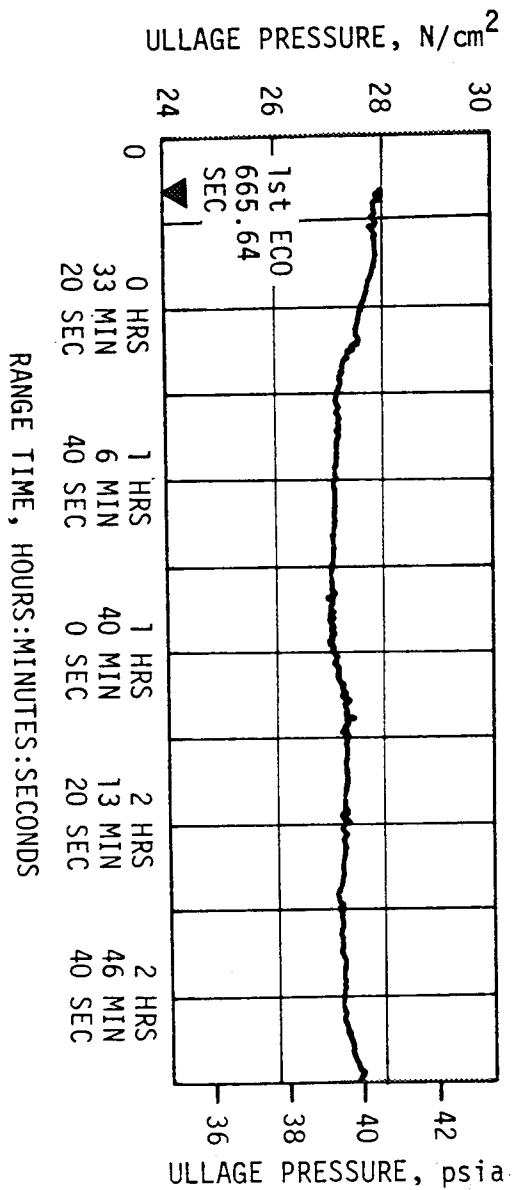
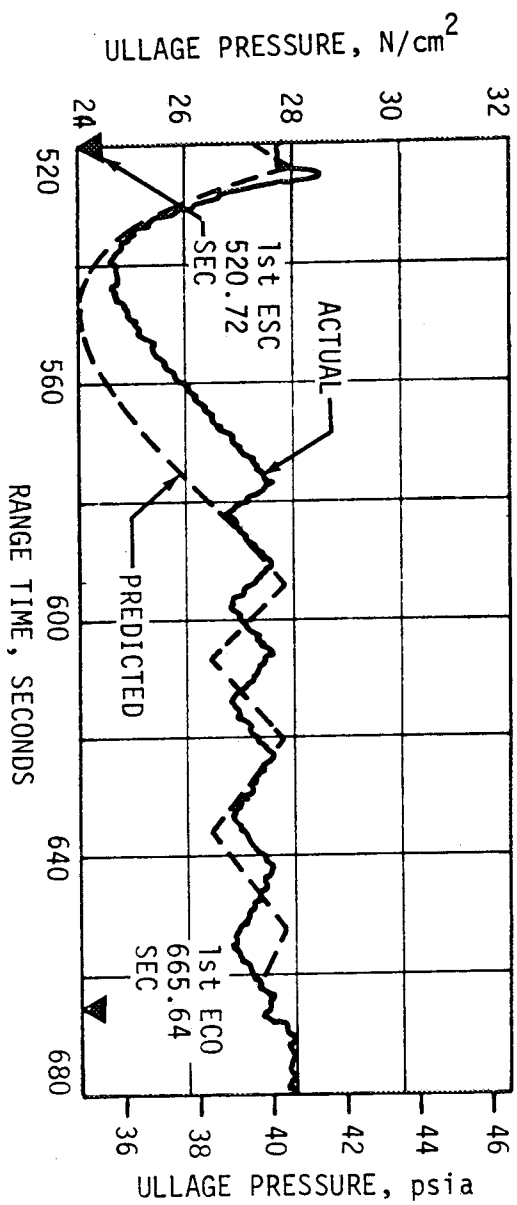
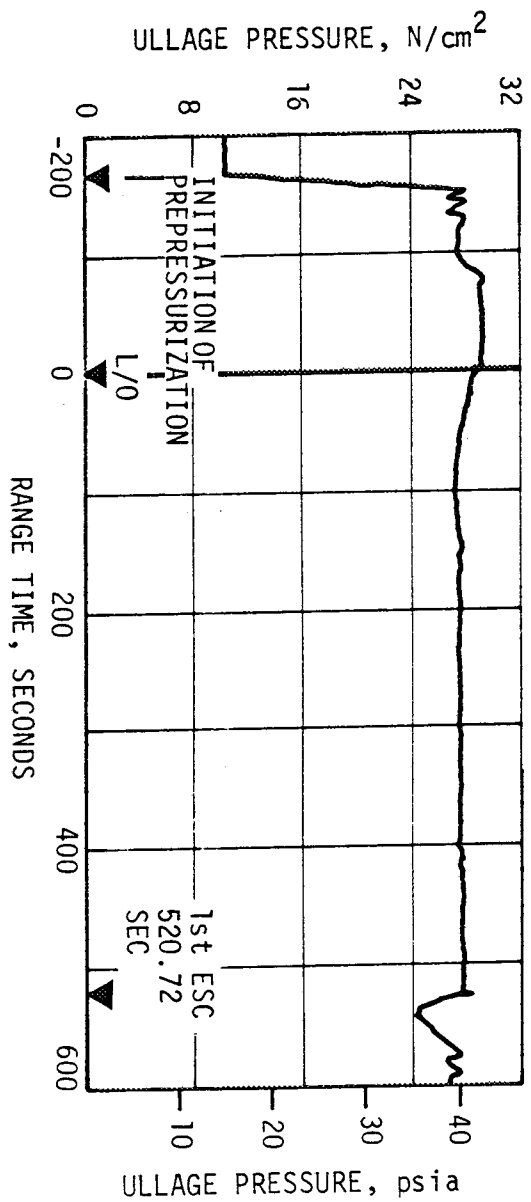


Figure 7-25. S-IVB LOX Ullage Pressure - First Burn

26.89 N/cm<sup>2</sup> (39 psia) and 27.92 N/cm<sup>2</sup> (40.5 psia). At -97 seconds the LOX tank ullage pressure increased from 27.58 N/cm<sup>2</sup> (40 psia) to 29.37 N/cm<sup>2</sup> (42.6 psia) due to fuel tank prepressurization, LOX tank vent valve purge and LOX pressure sense line purge. The LOX tank ullage pressure decreased to 27.58 N/cm<sup>2</sup> (40 psia) during S-IC boost and maintained that pressure during S-II boost.

The LOX tank ullage pressure was 27.58 N/cm<sup>2</sup> (40 psia) at ESC, satisfying the engine start requirements which is also shown in Figure 7-25. During the start transient the ullage pressure decreased to a minimum of 24.68 N/cm<sup>2</sup> (35.8 psia) before the pressurant flowrate became large enough to increase the ullage pressure. During burn the ullage pressure cycled three more times than predicted. The greater than predicted number of cycles was due to an ullage pressure drop, 0.689 N/cm<sup>2</sup> (1 psia) less than predicted during the start transient, and a smaller control band than used for the predictions. The ullage pressure was sufficient to meet the minimum NPSP requirement during powered flight.

The slight ullage pressure rise during the first few seconds after ESC is due to the pressurization system being activated at ESC, allowing gas to flow during this period.

The LOX tank pressurization flowrate variation was 0.102 to 0.191 kg/s (0.225 to 0.42 lbm/s) during over-control, and from 0.0748 to 0.136 kg/s (0.165 to 0.3 lbm/s) during under-control system operation. This variation is normal because the bypass orifice inlet temperature changes as it follows the cold helium sphere temperature. The helium used during S-IVB powered flight was 21.32 kilograms (47 lbm) (based upon flow integration) compared to 150.6 kilograms (332 lbm) loaded.

The J-2 heat exchanger outlet temperature increased to 514° K (465.3° F) by the end of the 50-second start transient period. Throughout the remainder of the first burn the temperature increased, reaching a maximum of 556° K (540.3° F) 9 seconds prior to first burn cutoff. The helium flowrate through the heat exchanger was relatively constant at 0.086 kg/s (0.019 lbm/s) during over-control and at 0.0331 kg/s (0.073 lbm/s) during under-control operation.

The oxidizer tank ullage pressure between first burn cutoff and ESC is shown by comparing Figures 7-25 and 7-26. The ullage pressure decreased from the first burn cutoff pressure of 27.58 N/cm<sup>2</sup> (40.0 psia) to a minimum of 26.95 N/cm<sup>2</sup> (39.1 psia) at 01:43:20, then increased to 27.58 N/cm<sup>2</sup> (40.0 psia) at 03:06:16 where the LOX tank ullage pressure started to increase. The increase of the ullage pressure after this time was believed to be due to bubbles of gaseous oxygen rising from the bottom of the tank to the ullage, causing approximately a 2.8° K (5° F) temperature increase of the pressurants. Because of this pressure increase, the ullage pressure at repressurization initiation was above the minimum required. The spheres were not required for repressurization. The LOX tank ullage pressure at second burn ESC was 29.37 N/cm<sup>2</sup> (42.6 psia).

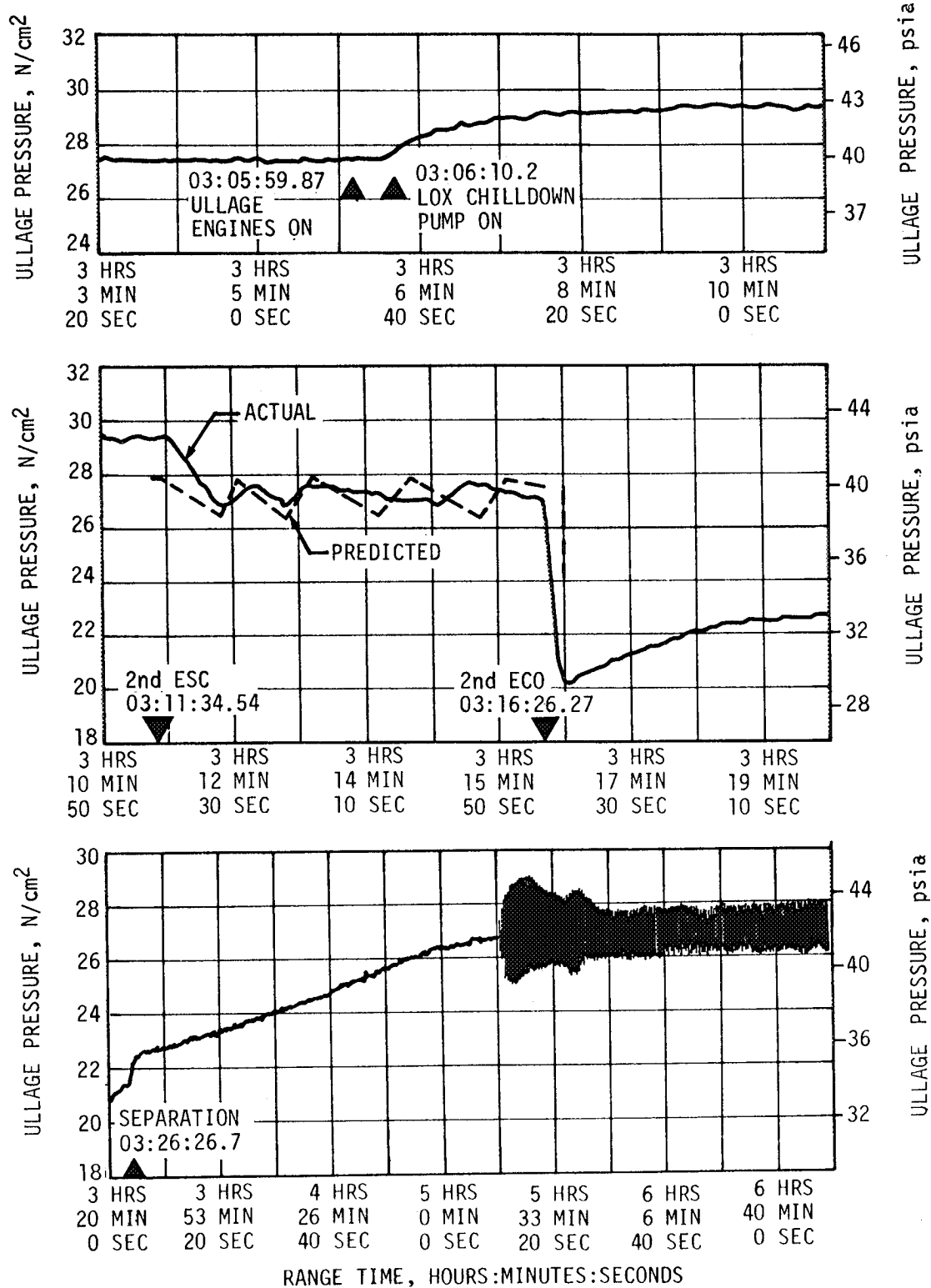


Figure 7-26. S-IVB LOX Tank Ullage - Second Burn

During orbital coast the LOX tank ullage pressure did not collapse as expected. The relative stability of the LOX tank ullage pressure is due to heating of the LOX residuals and formation of a gas pocket in the aft end of the tank. The gas pocket formation is supported by the gas and liquid temperature measurements reading above normal liquid bulk temperatures. As the gas pocket grew during orbital coast, the liquid was pushed into the ullage space thereby keeping the pressure relatively stable. The liquid agitation during ullaging caused the bubble formation to rise through the liquid to the tank ullage, thereby increasing the ullage pressure due to the mixing of relatively warm bubbles with the cold ullage.

At second burn ESC the LOX tank ullage pressure shown in Figure 7-26 was 29.37 N/cm<sup>2</sup> (42.6 psia) satisfying the engine start requirements. The ullage pressure cycled three times during the burn, one cycle less than the predicted. The fewer than predicted number of cycles was due to a narrower than predicted control band and a lower than predicted decrease during burn. During the burn, the ullage pressure was sufficient to meet the minimum NPSP requirements during powered flight.

The pressurant flowrate variation was from 0.125 to 0.15 kg/s (0.275 to 0.33 lbm/s) during under-control and from 0.181 to 0.209 kg/s (0.4 to 0.46 lbm/s) during over-control system operation. The helium usage during the second S-IVB powered flight was 43.09 kilograms (95 lbm).

The J-2 heat exchanger outlet temperature increased to 533° K (500.3° F) at the end of the 50-second start transient period. The temperature reached a maximum of 561° K (550.3° F) at 100 seconds after ESC. The temperature then cycled from 528° K (490° F) on over-control to 544° K (520.3° F) on under-control. The helium flowrate through the heat exchanger varied from 0.095 to 0.082 kg/s (0.21 to 0.18 lbm/s) during over-control and from 0.039 to 0.033 kg/s (0.085 to 0.073 lbm/s) during under-control operation.

The cold helium supply was more than adequate to meet flight requirements. At first burn ESC, the cold helium spheres contained 151 kilograms (332 lbm) of helium at a pressure of 2006 N/cm<sup>2</sup> (2910 psia). During the 144.9 seconds of first burn engine operation, the helium mass in the spheres decreased 17 kilograms (38 lbm), leaving a pressure of 1082 N/cm<sup>2</sup> (1570 psia) at first burn ECO.

During orbital coast between first burn ECO and second burn ESC, the helium mass in the spheres apparently decreased 19 kilograms (42 lbm) as indicated by the pressure trace shown in Figure 7-27. This would indicate a leakage of 0.00171 kg/s (0.00377 lbm/s). However, supporting analyses indicate that the leakage did not occur and that the pressure reading is in error.

At second burn ESC, the cold helium sphere pressure was 986 N/cm<sup>2</sup> (1430 psia). During the second burn period of 299.7 seconds, the mass in the helium spheres decreased by 28 kilograms (62 lbm) leaving 86 kilograms (190 lbm) at 552 N/cm<sup>2</sup> (800 psia) at second burn ECO.

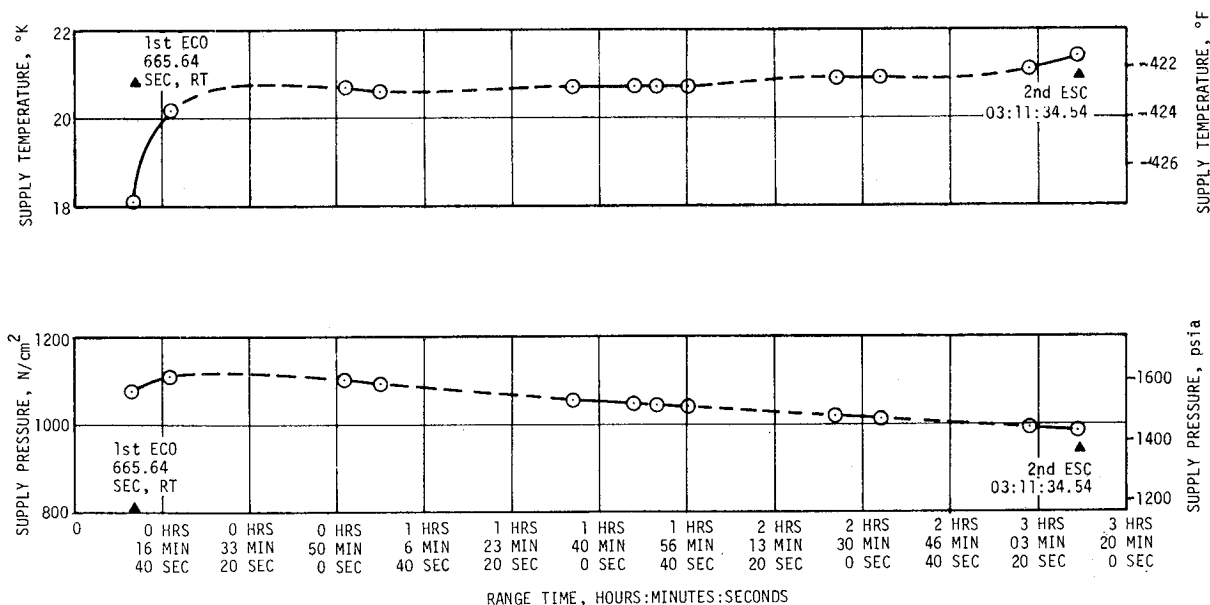


Figure 7-27. S-IVB Cold Helium Sphere Condition - Coast Phase

All values quoted were obtained through absolute mass calculations based upon bottle temperatures and pressures at the indicated times. These absolute mass calculations disagree with the values obtained through flow integration. Evaluation is continuing to resolve the discrepancy.

The NPSP calculated at the interface was  $16.3 \text{ N/cm}^2$  (23.6 psi) at S-IVB first burn ESC. The NPSP decreased after start and reached a minimum value of  $15.4 \text{ N/cm}^2$  (22.3 psi) at 25 seconds. This was  $1.15 \text{ N/cm}^2$  (1.7 psi) above the required NPSP at that time. The NPSP then increased and followed the predicted closely throughout S-IVB powered flight.

The NPSP calculated at the engine interface was  $17.24 \text{ N/cm}^2$  (25.0 psia) at S-IVB second burn ESC. At the end of fuel lead the NPSP increased rapidly to  $19.3 \text{ N/cm}^2$  (28.0 psi) then decreased to  $16.68 \text{ N/cm}^2$  (24.2 psi), cycling from this value to  $17.75 \text{ N/cm}^2$  (25.75 psi). The NPSP was close to the predicted but somewhat higher at second burn ESC and at ECO. The differences are due to a higher than expected ullage pressure at second burn ESC and a lower than expected inlet temperature at cutoff. At all times during second burn the NPSP was above the required.

The LOX pump static interface pressure during first burn followed the cyclic trends of the LOX tank ullage pressure. Values ranged from  $25.9 \text{ N/cm}^2$  (37.6 psi) at 25 seconds to  $30.8 \text{ N/cm}^2$  (44.7 psi) immediately after first burn ESC. During the remaining portion of the engine operation the pressure and the LOX pump interface temperature closely followed the predicted.

The LOX pump static interface pressure during second burn also followed the cyclic trends of the LOX tank ullage pressure. Values ranged from 32.0 N/cm<sup>2</sup> (46.4 psia) at the end of fuel lead to 29.5 N/cm<sup>2</sup> (42.8 psia) at second burn ECO. During powered flight the pressure followed closely to the predicted. The LOX pump interface temperature also closely followed the predicted.

Figures 7-28 and 7-29 summarize the LOX pump inlet conditions for first and second burns, respectively.

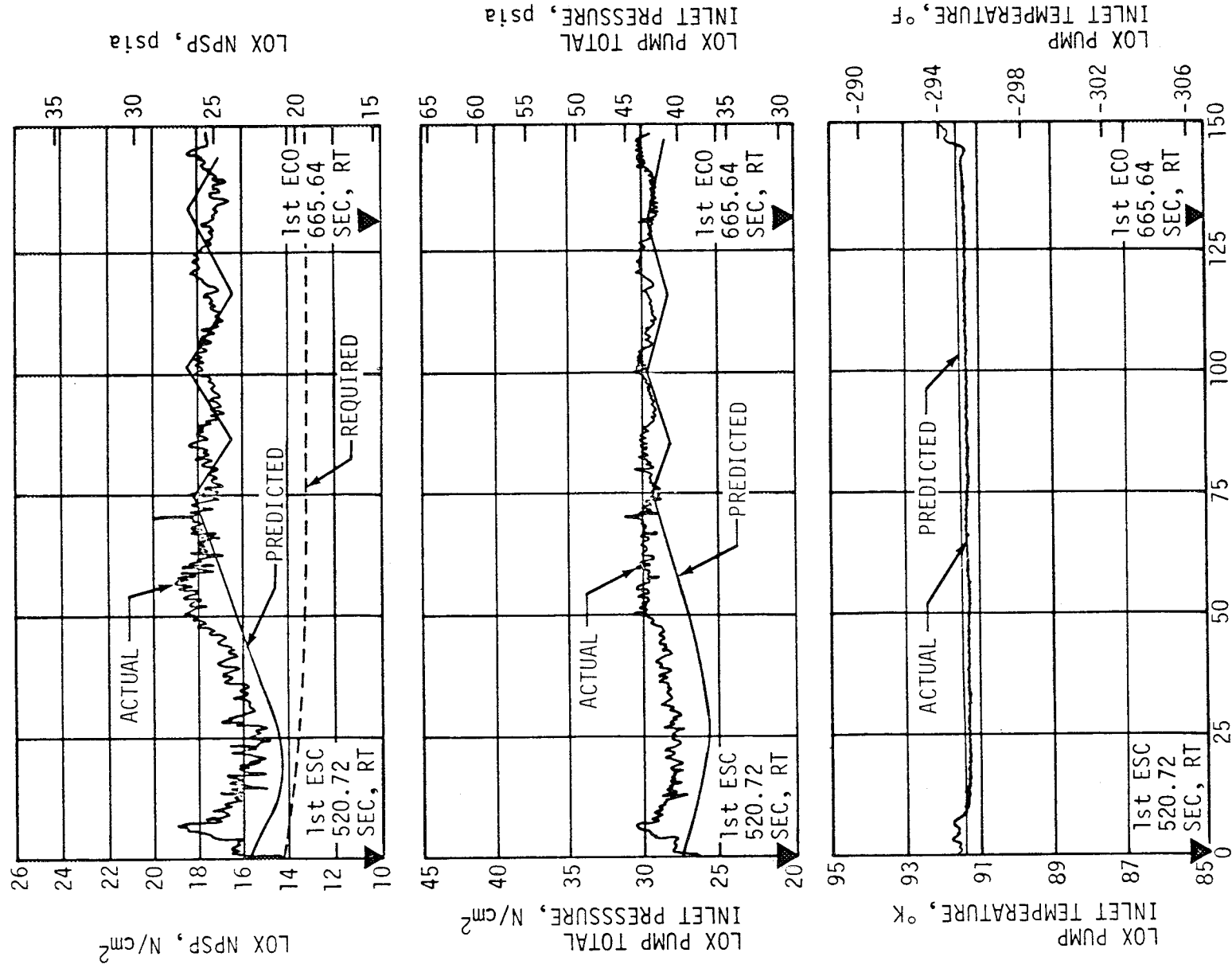
After S-IVB second burn ECO the ullage pressure remained momentarily at 27 N/cm<sup>2</sup> (39.2 psia) until the programed LOX vent occurred at 11,786.952 seconds. The pressure then decreased rapidly to 20.1 N/cm<sup>2</sup> (29.2 psia) within 10 seconds. At 03:16:36.766, the LOX vent valve was closed. By 03:20:00 the pressure had increased to 22.75 N/cm<sup>2</sup> (33 psia) due to vaporization of the residual LOX and heating of tank pressurants. At 19,100 seconds the ullage pressure had increased to 29.23 N/cm<sup>2</sup> (42.4 psia) when the sensed pressure began oscillating. The oscillations had an amplitude of 3.44 N/cm<sup>2</sup> (5.0 psi) and a period of approximately 0.5 second. Data indicates the oscillation is occurring within the sense line and not the tank ullage. Supporting data shows no change in vent valve position during this period. Sense line purge is minimal as pneumatic helium was essentially depleted by this time.

#### 7.11 S-IVB PNEUMATIC CONTROL AND PURGE SYSTEM

The pneumatic control and purge system performed satisfactorily during boost and first burn operations. During orbital coast a system leak developed, however, the helium supply pressure was sufficient to complete all second burn operations.

System performance was normal during boost and first burn operations. However, at approximately 00:58:20 the pneumatic bottle pressure began decreasing at the rate of 0.72 N/cm<sup>2</sup>/min (1.04 psi/min) as indicated in Figure 7-30. At approximately 01:48:20, the rate of pressure loss increased to 12.0 N/cm<sup>2</sup>/min (17.4 psi/min). Pneumatic control bottle temperature and regulator outlet pressure is shown in Figure 7-31. At 04:10:00 the bottle pressure had dropped to the pneumatic regulator operation band as shown in Figure 7-32. At this point the regulator poppet opened fully, and thereafter the regulator discharge pressure differed from the pneumatic bottle pressure only by the system pressure drop from the bottle through the regulator. Bottle masses at various pertinent times are shown in Table 7-8.

There is some evidence that the leak may be associated with the prevalve actuation control module of the prevalves and chilldown pump shutoff valves or the failure of a calips pressure switch diaphragm. A pneumatic control schematic is shown in Figure 7-33. The corrective actions being considered are to cap the calips port on the pressure switch to eliminate a possible leak, and a redesign of the actuation control module.



TIME FROM FIRST ESC, SECONDS

Figure 7-28. S-IVB LOX Pump Inlet Conditions - First Burn



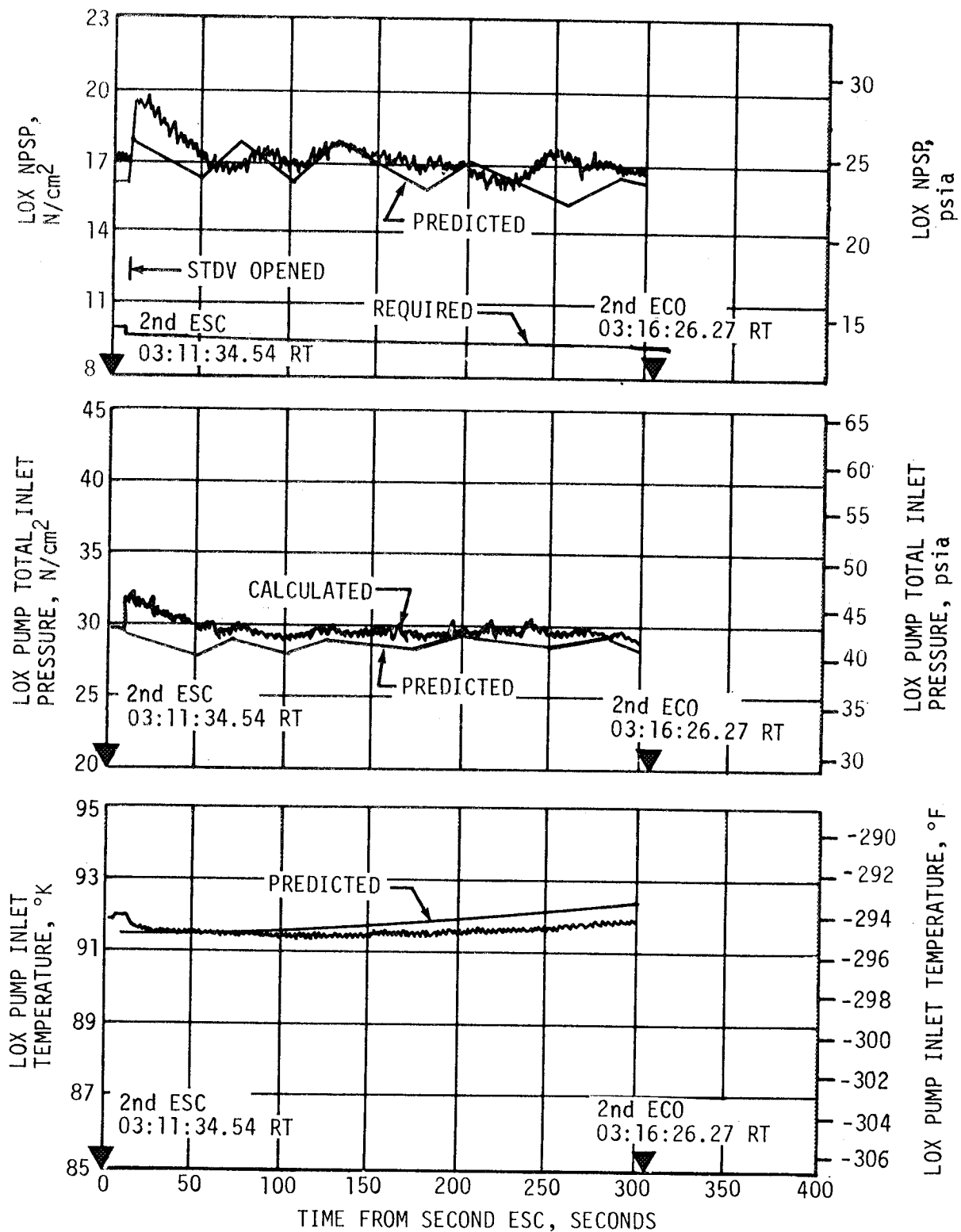


Figure 7-29. S-IVB LOX Pump Inlet Conditions - Second Burn

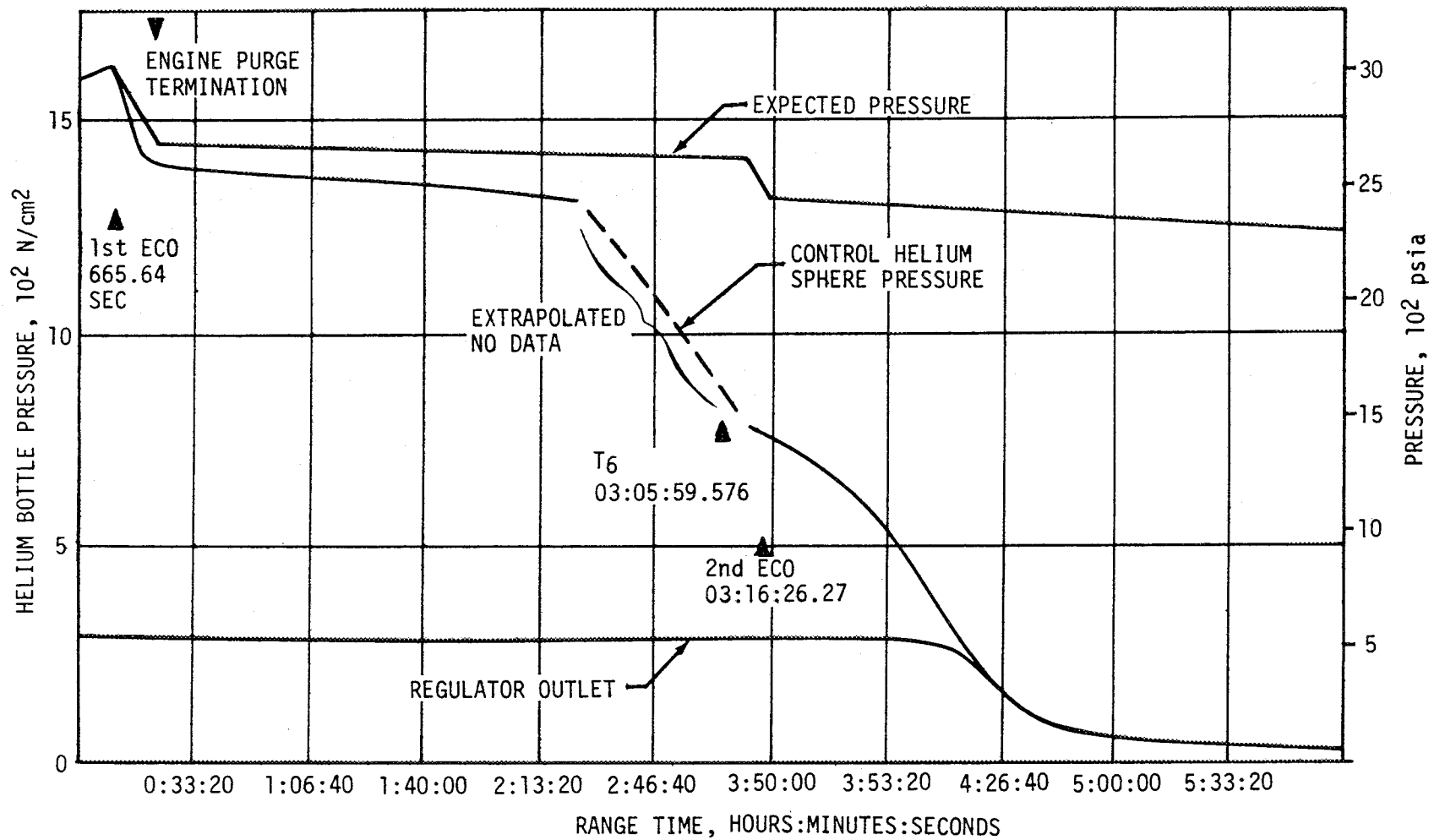


Figure 7-30. S-IVB Pneumatic Control Helium Bottle Pressure

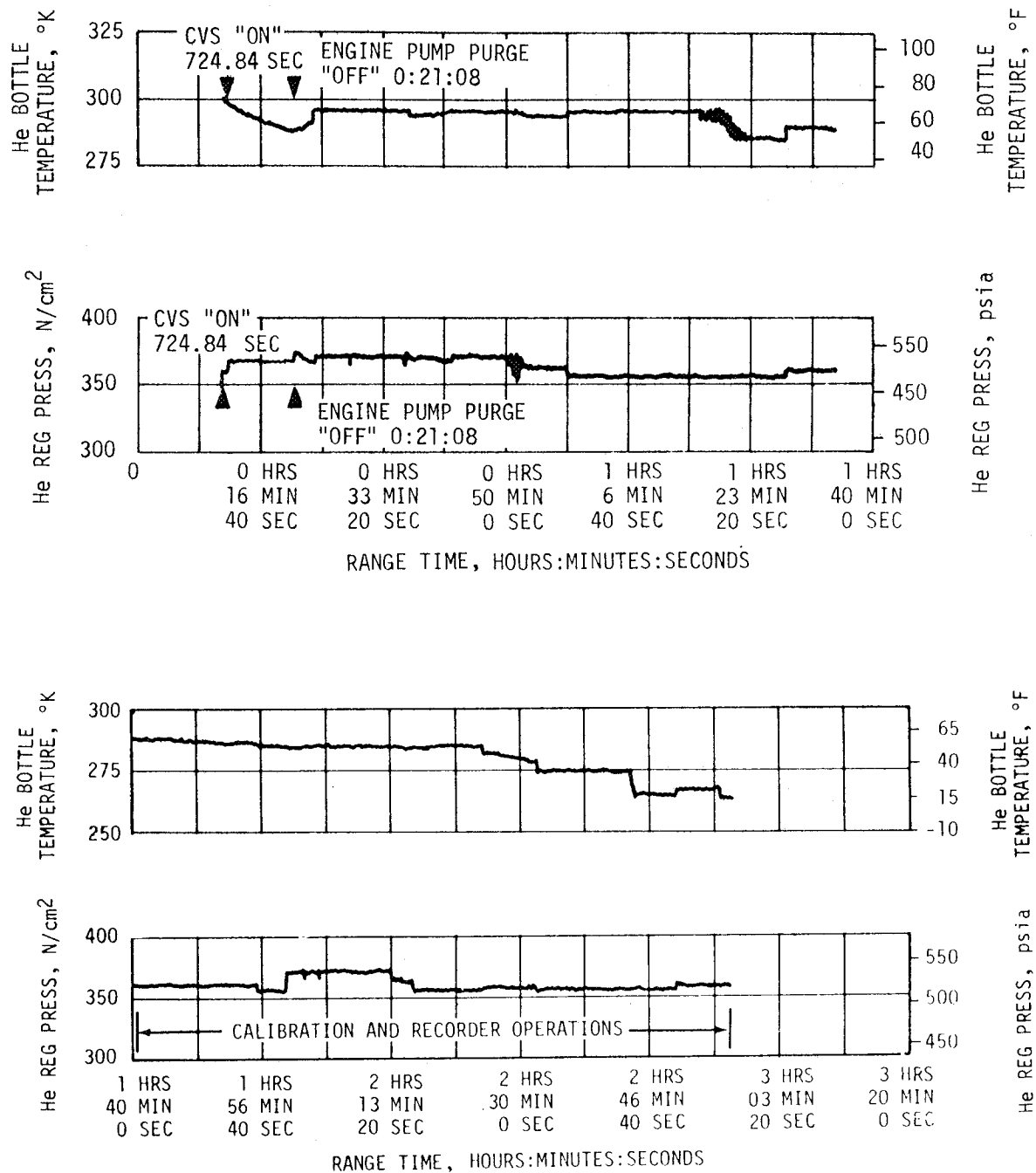
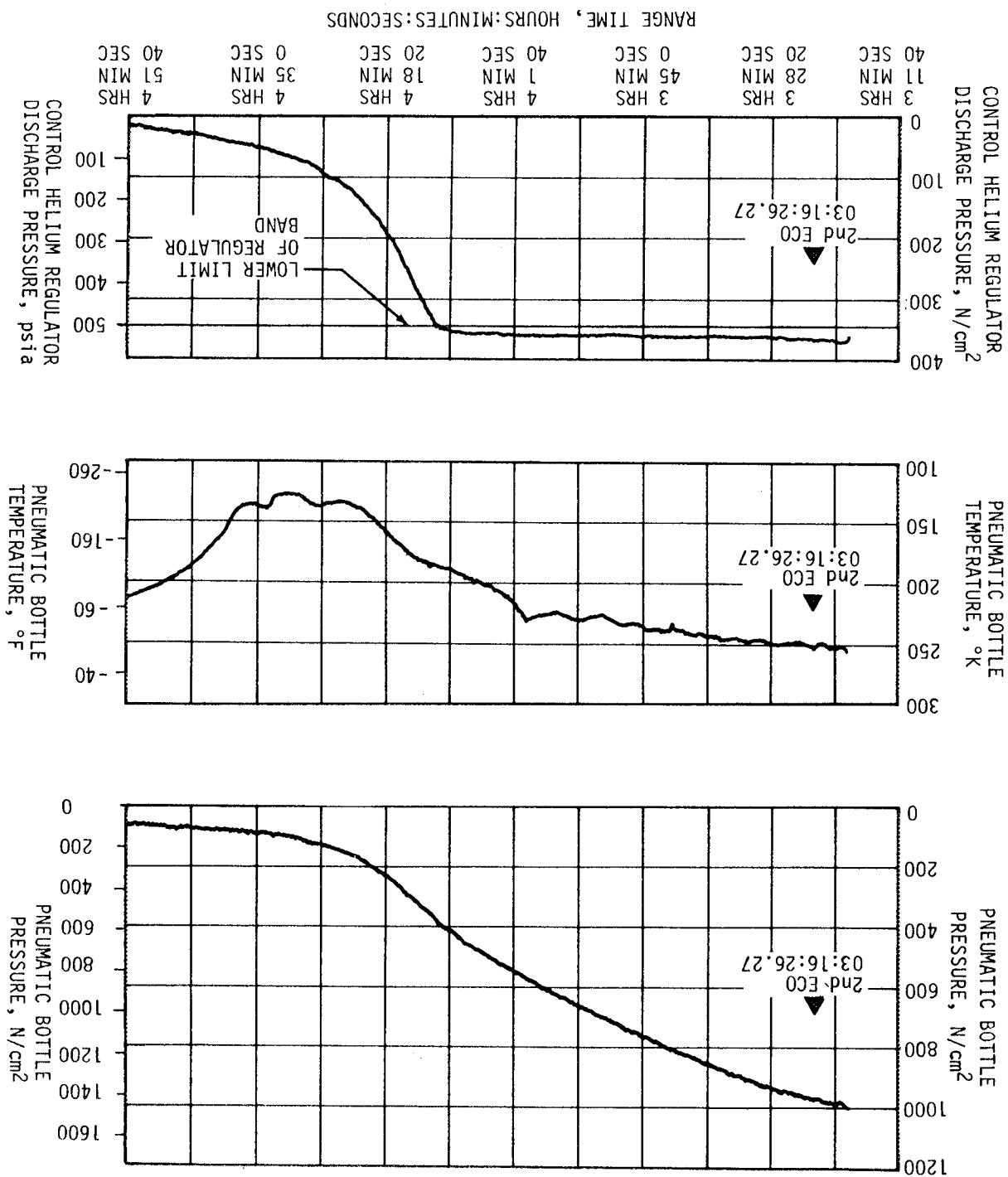


Figure 7-31. S-IVB Pneumatic Control Performance

Figure 7-32. S-IVB Pneumatic Control Performance - Second Burn



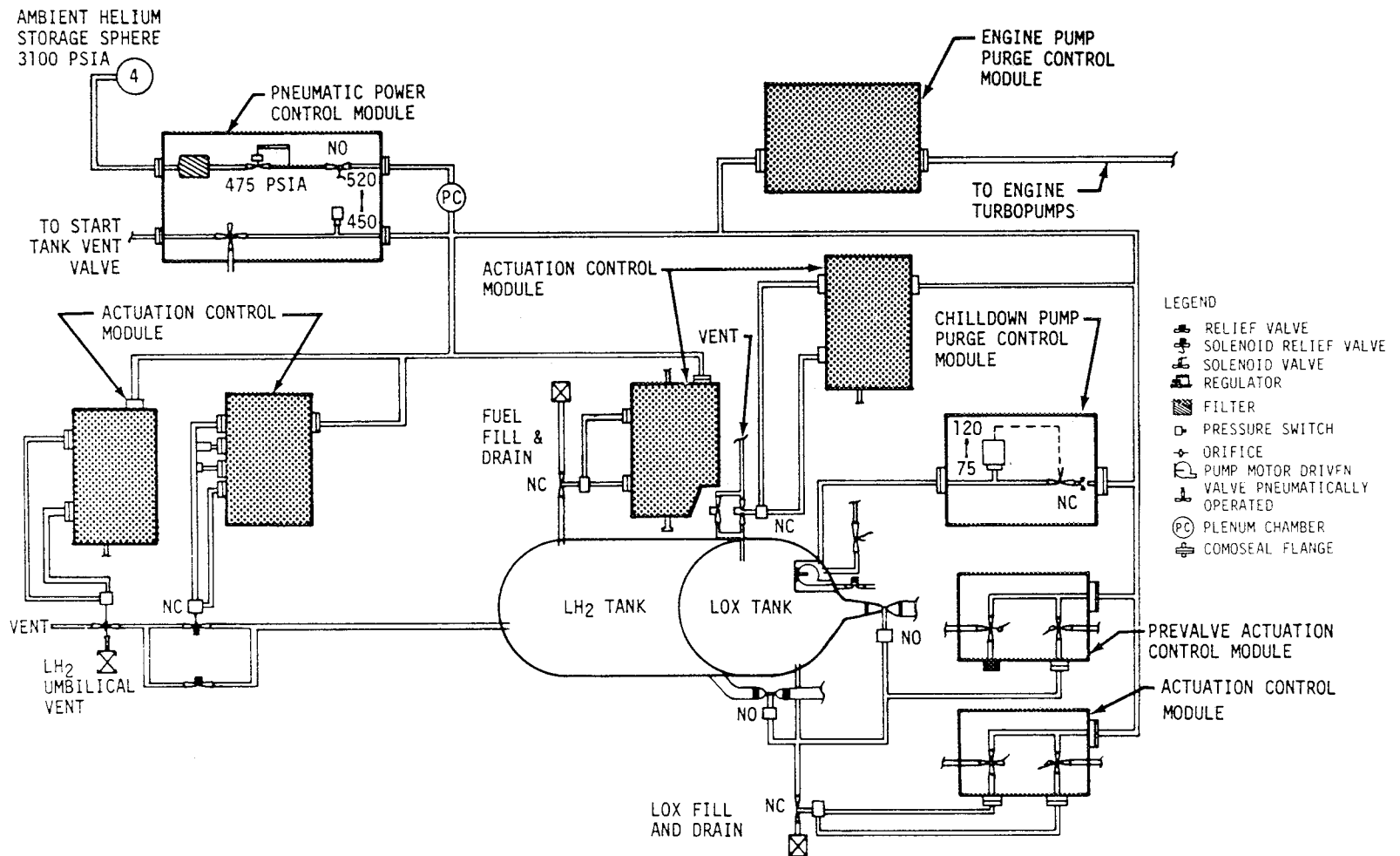


Figure 7-33. S-IVB Pneumatic Control System Schematic

Table 7-8. S-IVB Helium Bottle Mass

TIME	BOTTLE MASS	
	kg	lbm
Liftoff	3.71	8.19
First Burn ESC	3.70	8.17
First Burn ECO	3.69	8.14
3500 seconds	3.38	7.46
6500 seconds	3.37	7.43
Second Burn ESC (03:11:34.54)	2.30	5.08
Second Burn ECO (03:16:26.27)	2.29	5.05
17,500 seconds	0.19	0.42

### 7.12 S-IVB AUXILIARY PROPULSION SYSTEM

The APS pressurization systems demonstrated nominal performance throughout the flight and met control system demands as discussed in paragraph 11.1 and 11.5.4. The regulator outlet pressures were maintained at 135 N/cm<sup>2</sup> (196 psia). The APS pressures in the tanks were approximately 131 N/cm<sup>2</sup> (190 psia) as shown in Figure 7-34.

The oxidizer and fuel supply systems of the APS engines performed as expected during the flight except for the propellant temperatures measured at the propellant control modules. These temperatures were higher than expected with the oxidizer in the module at position I exceeding the transducer limit of 328° K (131.3° F). The supply pressures were nominal at approximately 131 N/cm<sup>2</sup> (190 psia) during the mission.

With the exceptions noted in the following paragraphs, the APS engine performance was as expected with a maximum propellant consumption of 65 percent as shown in Figure 7-35 and Table 7-9. Even with the anomalies noted, performance was sufficient for control throughout the mission.

During the prelaunch burp firings of the AS-501 APS engines it was noted that engine III<sub>IV</sub> did not exhibit a normal chamber pressure trace. The abnormality was attributed to the instrumentation. During the AS-501 flight, this abnormality cleared up somewhat. The chamber pressure level of engine III<sub>IV</sub> remained in the 65-70 N/cm<sup>2</sup> (95-100 psia) range throughout the flight.

Engine III exhibited normal chamber pressure during burp firings, however, during the AS-501 flight the first pulses on this engine were approximately 15 percent below the nominal 69 N/cm<sup>2</sup> (100 psia). During the latter part of the mission, after 05:00:00, the chamber pressure level decreased

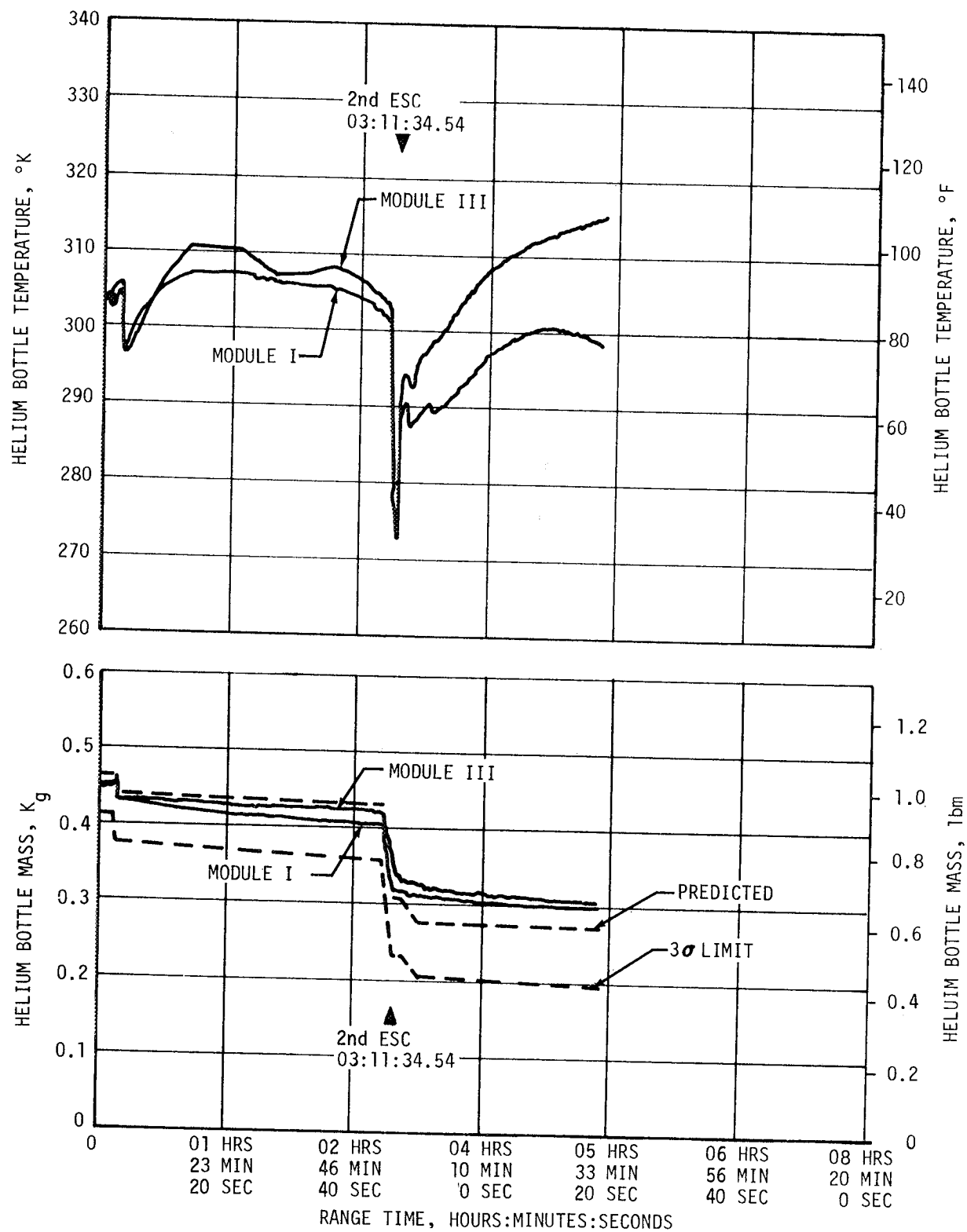


Figure 7-34. S-IVB APS Pressurization System Performance, Sheet 1 of 2

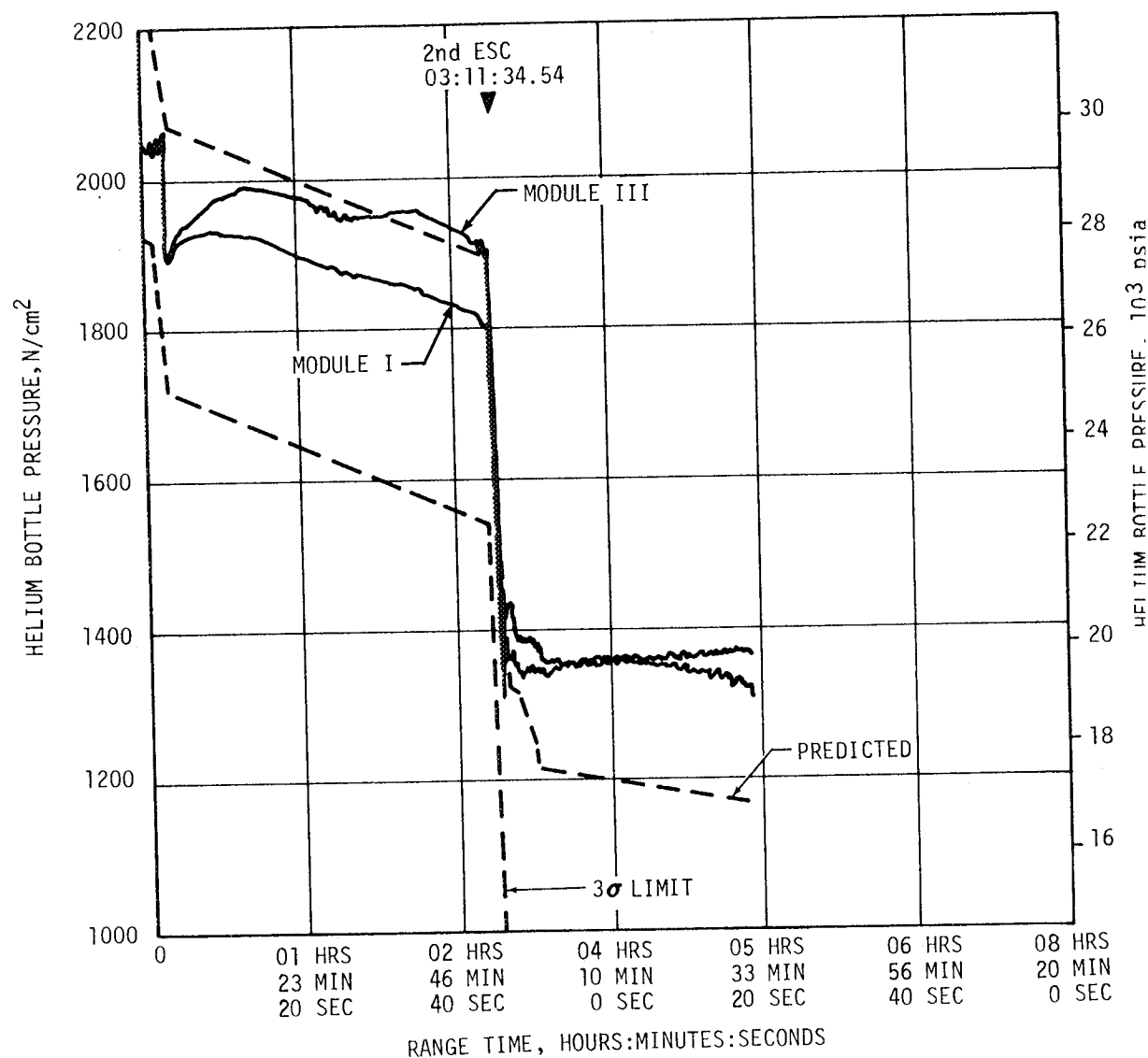


Figure 7-34. S-IVB APS Pressurization System Performance, Sheet 2 of 2

to  $38 \text{ N/cm}^2$  (55 psia). A possible cause of this anomaly was a restriction of propellant flow to the engine.

The restriction could be a result of contamination of the injector valves, orifices, or tubes by either foreign matter or precipitates from the propellants. The restriction could also be caused by vaporization of the oxidizer in the injectors or by outgassing of the helium from the propellant. The propellant temperatures (measured at the propellant control module) are shown in Figure 7-36 and it can be seen that during the period of greatest degradation, the oxidizer temperature of module at position I exceeded  $328^\circ \text{K}$  ( $131.3^\circ \text{F}$ ). The engine injector temperature was  $333^\circ \text{K}$  ( $140.3^\circ \text{F}$ ). With a chamber pressure of  $38 \text{ N/cm}^2$  (55 psia) and the recorded injector temperature, it is probable that the oxidizer will vaporize in the injector



Table 7-9. S-IVB APS Propellant Consumption

TIME PERIOD	MODULE AT POSITION I		MODULE AT POSITION III	
	OXIDIZER kg (lbm)	FUEL kg (lbm)	OXIDIZER kg (lbm)	FUEL kg (lbm)
Initial Load	82.5 (182)	56.7 (125)	84.8 (187)	56.7 (125)
First J-2 Burn Roll Control	*	*	*	*
J-2 ECO to End of First APS Ullaging	7.7 (17)	5.9 (13)	8.2 (18)	6.4 (14)
1st and 2nd Earth Revolutions	6.8 (15)	4.5 (10)	1 (2)	0.9 (2)
Restart Preparations	25 (56)	19 (41)	26 (57)	19 (42)
2nd J-2 Burn Roll Control	3 (7)	2 (4)	4 (8)	2 (5)
2nd J-2 ECO to CSM Separation	2 (5)	2 (4)	3 (7)	2 (5)
CSM Separation to Loss of Data	5.4 (12)	3 (7)	10 (22)	6 (13)
Total Usage	50.8 (112)	36 (79)	52.2 (115)	37 (81)
Residuals	38%	37%	38%	35%
* Usage not large enough to be evaluated by methods available.				

It has been noted, however, that engine I<sub>D</sub> had a higher injector temperature and exhibited normal performance. An injector valve failure could cause a degradation of chamber pressure. However, to get a degradation as great as the one observed, a combination of valves would have to fail.

Engine I<sub>IV</sub> also exhibited abnormal chamber pressures. Like engine I<sub>II</sub>, the first pulses on engine I<sub>IV</sub> were about 15 percent low. This engine did not have as great a degradation in the final phases of the mission, but during the period around 05:00:00 to 05:33:20, a chamber pressure oscillation was noted. The pressure cycled from 38 to 65 N/cm<sup>2</sup> (55 to 95 psia) at approximately 400 hertz. This frequency was near the longitudinal acoustical resonance frequency of the chamber, however, it could be due to an instrumentation problem.

The ullage engine of module at position I had abnormally long "tail-off" after each of its burns. This anomaly is under investigation and could be related to the problems of engines I<sub>IV</sub> and I<sub>II</sub>.

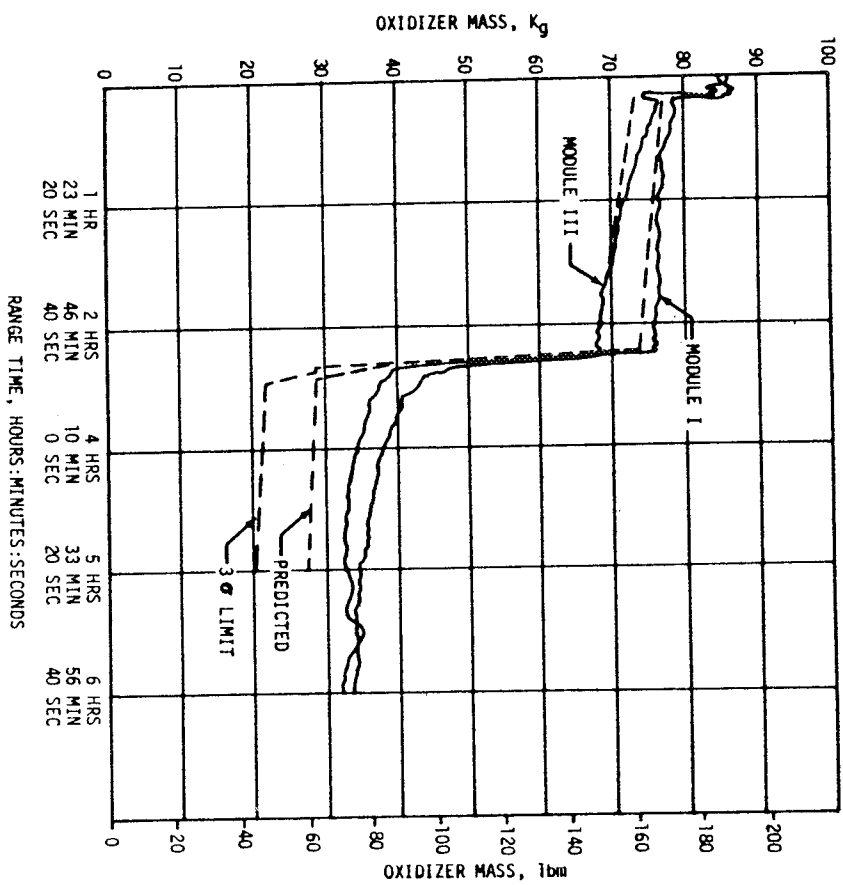
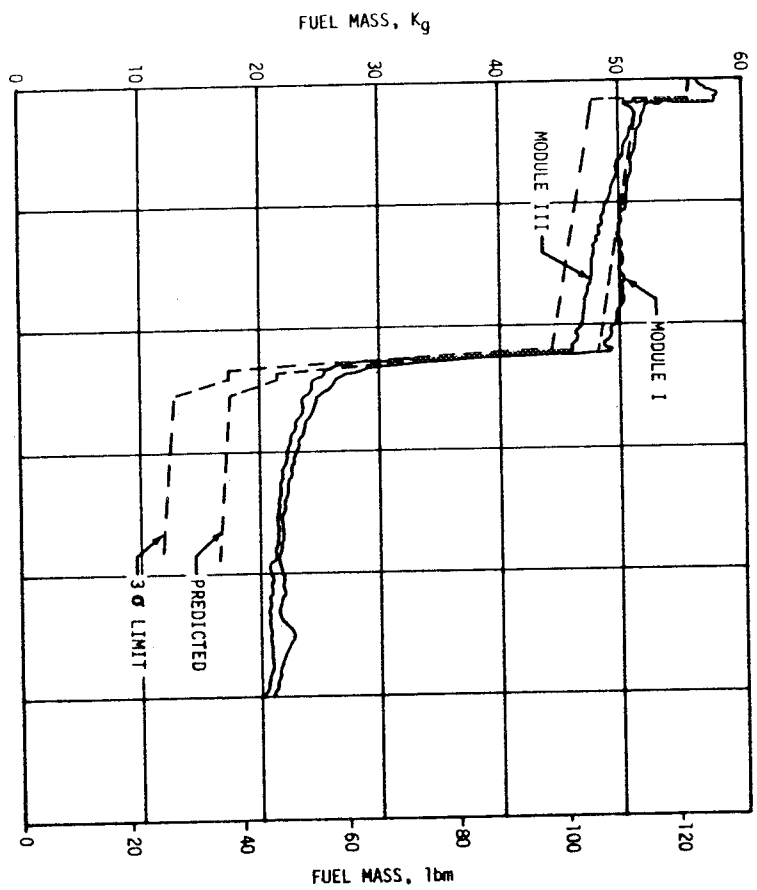


Figure 7-35. S-IVB APS Propellant Consumption

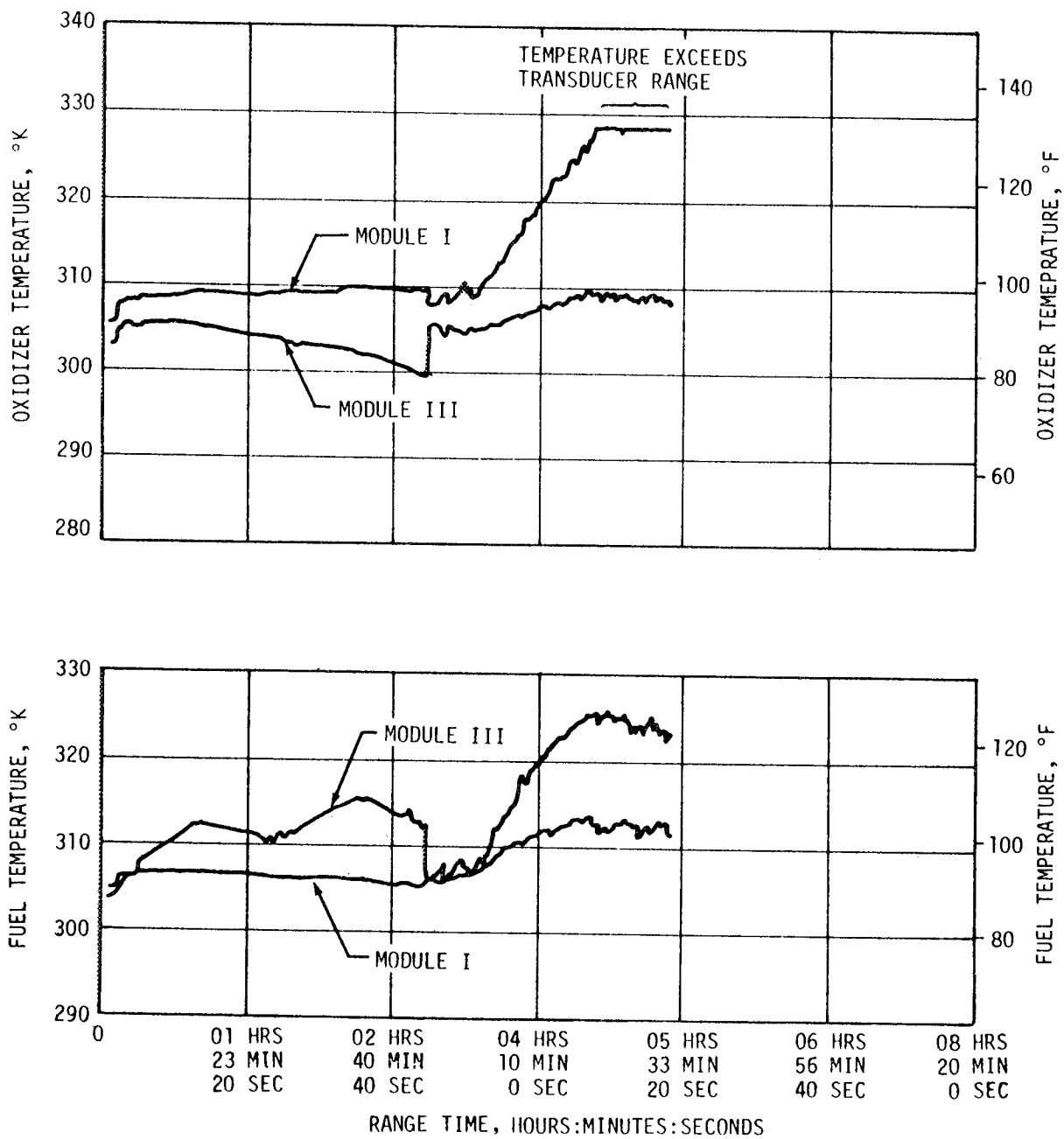


Figure 7-36. S-IVB APS Propellant Conditions



## SECTION 8 HYDRAULIC SECTION

### 8.1 SUMMARY

The S-IC, S-II, and S-IVB hydraulic systems performed within predicted limits, and the entire system operated satisfactorily throughout the flight. All parameters were within redlines by ample margins and there were no anomalies apparent during flight.

### 8.2 S-IC HYDRAULIC SYSTEM

The S-IC stage incorporated eight gimbal actuators of the Moog model and operated with fuel (RP-1) as the hydraulic medium. Analysis indicates that all actuators performed satisfactorily as commanded during the flight, as shown in Figure 8-1. The maximum actuator deflection was equivalent to 0.7 degrees engine gimbal angle at the initiation of the vehicle roll program. The average hydraulic supply pressure was  $1340 \text{ N/cm}^2$  (1944 psia), and operated in a small band within the operating limits. The temperature as depicted by the return actuator fluid was  $304^\circ\text{K}$  ( $87.8^\circ\text{F}$ ) and operated within a narrow band. The maximum hydraulic engine valve opening pressure of  $1400 \text{ N/cm}^2$  (2031 psia) was in close agreement with the maximum supply pressure of  $1380 \text{ N/cm}^2$  (2002 psia) to the actuators.

### 8.3 S-II HYDRAULIC SYSTEM

The four separate hydraulic systems on the S-II stage (one system per outboard engine) performed within normal limits with events occurring close to the predicted times. The minimum reservoir volume was 13 percent of full versus the redline of 3.0 percent and was within the nominal predicted bands. The hydraulic fluid minimum pressures and maximum temperatures were  $2400 \text{ N/cm}^2$  (3480 psia) and  $325^\circ\text{K}$  ( $125^\circ\text{F}$ ), respectively, which were well within the predicted limits as shown in Figure 8-2. The actuator forces were well below the predicted maximum of 84,500 Newtons (19,000 lb). The maximum tensile force was 46,200 Newtons (10,400 lb) which was exerted by the pitch actuator of engine number 4. The maximum force in compression was 23,100 Newtons (5200 lb) which was exerted by the pitch actuator of engine number 1. All S-II hydraulic system events occurred close to the predicted times.

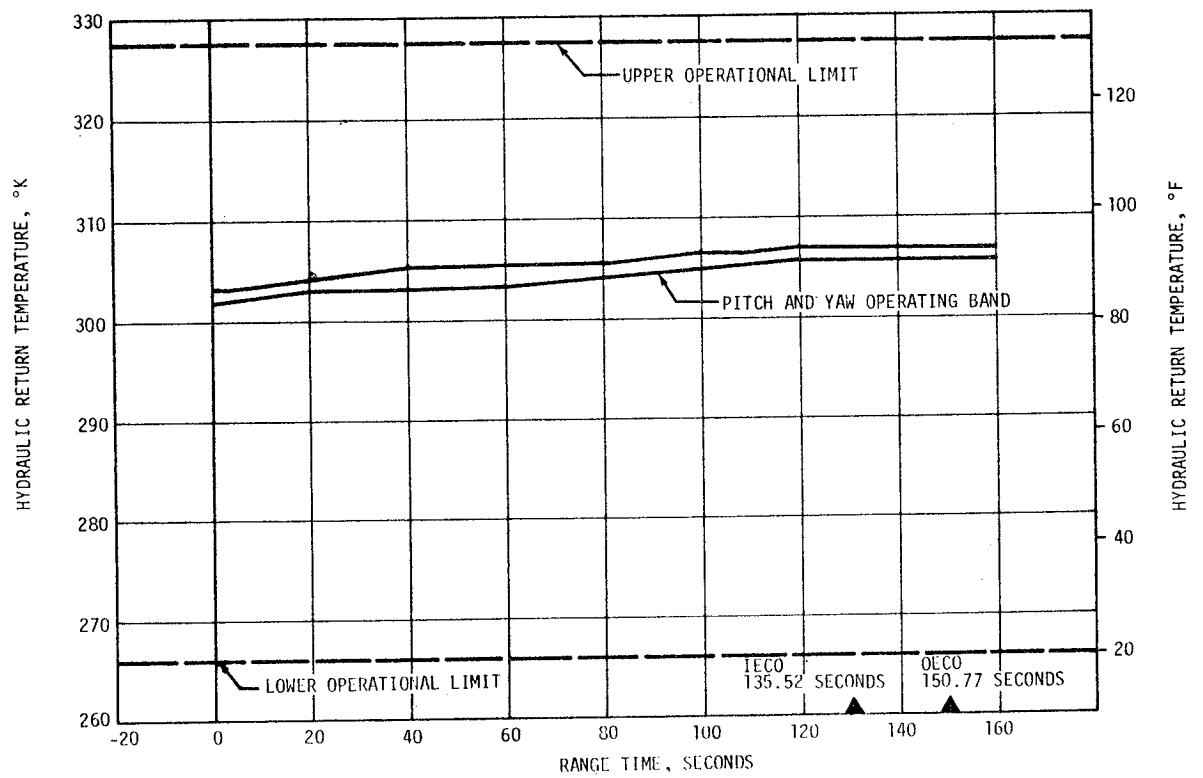
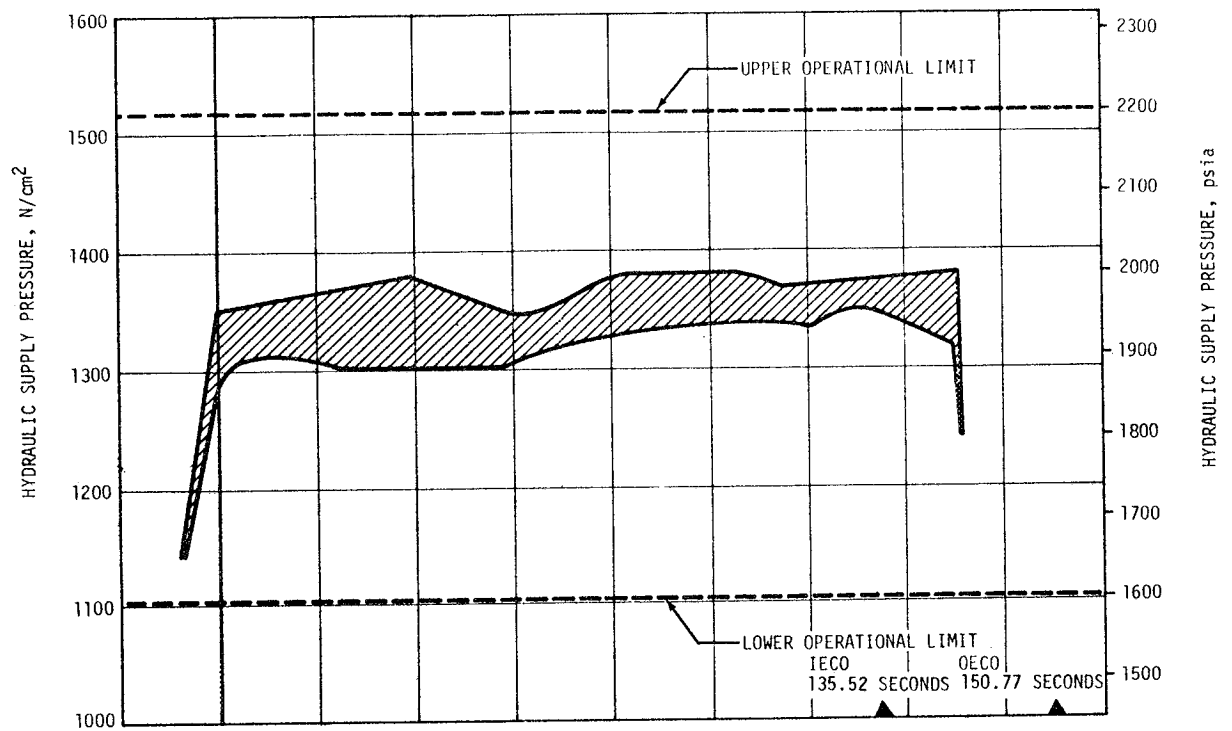


Figure 8-1. S-IC Hydraulic System Performance

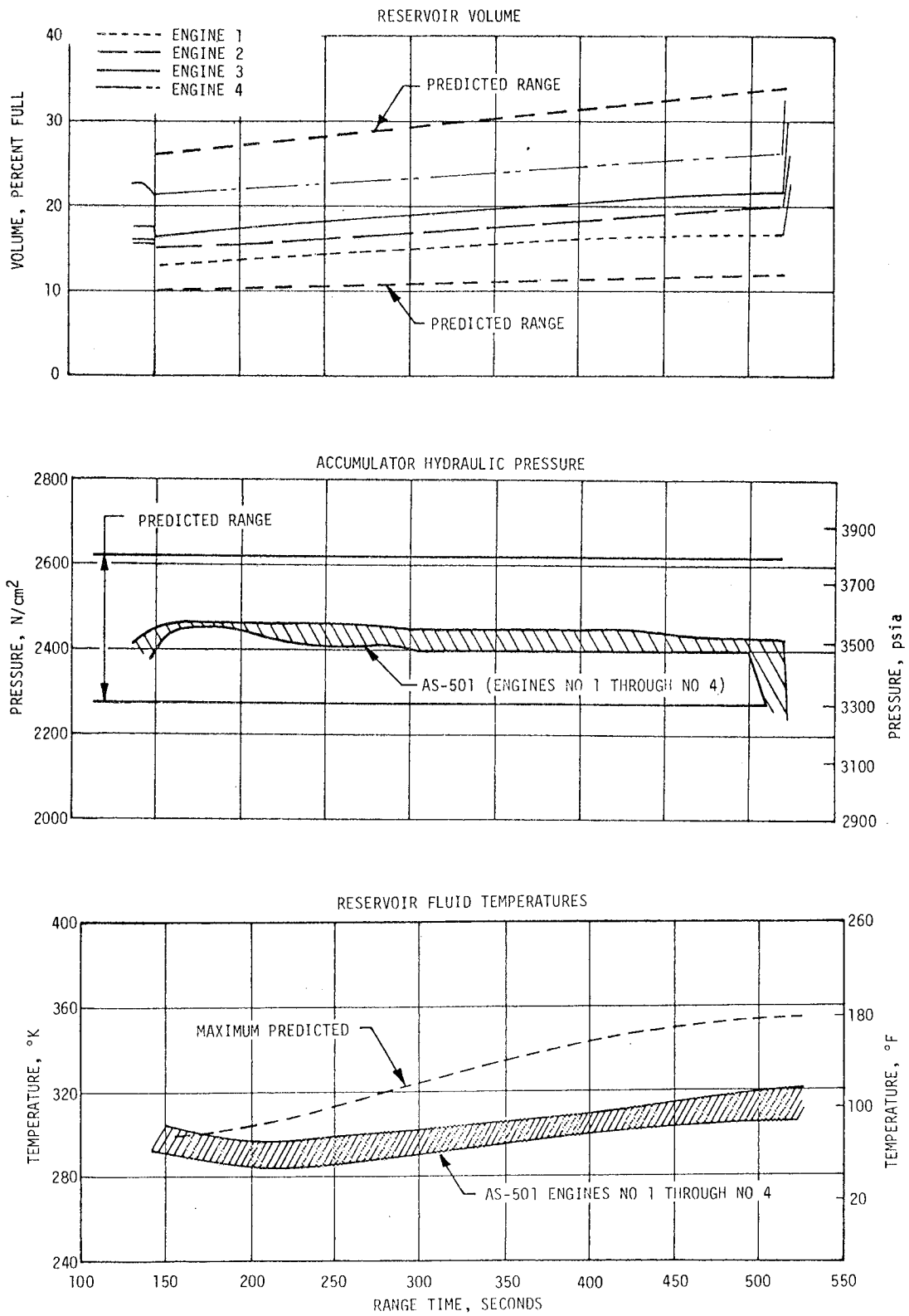


Figure 8-2. S-II Hydraulic System Performance

#### 8.4 S-IVB HYDRAULIC SYSTEM (FIRST BURN)

The S-IVB hydraulic system performed within the predicted limits after lift off with no overboard venting. However, overboard dumping did occur during prelaunch overall test operations which resulted in leaving the system at the lower reservoir limit of 85 percent at a temperature of 294°K (69.53°F). The hydraulic fluid was near 361°K (190.1°F) with the accumulator gas temperature reaching 270°K (26.3°F) which reduced the GN<sub>2</sub> precharge pressure. These conditions resulted in an oil level of 22 percent when the system was activated; however, the accumulator piston was not bottomed. Table 8-1 shows minor pressure level variations and compares the liftoff, first burn, parking orbit, and second burn system pressures.

During boost all system fluid temperatures rose steadily as the auxiliary pump was operating and convection cooling was decreasing as shown in Figure 8-3. Accumulator gas and actuator cylinder temperatures remained low since they are located on the extreme ends of the system. The main pump output pressure setting was higher than the auxiliary pump by 10.3 N/cm<sup>2</sup> (15 psi) to 24.1 N/cm<sup>2</sup> (35 psi). The main pump flange temperature rose sharply during first burn because of heat transfer from the engine. Reservoir oil level rose to 25 percent at the end of first burn due to the increased oil temperature. After engine cutoff, an increase to the 90 percent level occurred after the auxiliary pump "off" command. The supply pressure during both burns was 2413 N/cm<sup>2</sup> (3500 psia) to 2517 N/cm<sup>2</sup> (3650 psia) as compared to the allowable of 2344 N/cm<sup>2</sup> (3400 psia) to 2517 N/cm<sup>2</sup> (3650 psia). The maximum actuator torque resulting from the vehicle attitude command during first burn was in yaw at 7586 N-m (67,146 in-lb) and was well within design limits for the components.

Table 8-1. S-IVB Hydraulic System Pressures

PRESSURES	LIFTOFF N/cm <sup>2</sup> (PSIA)	FIRST BURN N/cm <sup>2</sup> (PSIA)	PARKING ORBIT N/cm <sup>2</sup> (PSIA)	SECOND BURN N/cm <sup>2</sup> (PSIA)	ALLOWABLE DURING BURN N/cm <sup>2</sup> (PSIA)
System Oil	2482 (3599.8)	2503 (3630.3)	-	2496 (3620.1)	2416 to 2516 (3504.1 to 3649.1)
Accumulator GN <sub>2</sub>	2493 (3615.8)	2503 (3630.3)	1651 (2394.6)	2496 (3620.1)	2416 to 2516 (3504.1 to 3649.1)
Reservoir Oil	119 (172.6)	125 (181.3)	47 (68.2)	123 (178.4)	94.5 to 137.9 (137.1 to 200.0)
Aux. Pump Air Tank	255 (369.8)	255 (369.8)	262 (380.0)	262 (380.0)	-----
Aux. Pump Motor Air	22 (31.9)	23 (33.4)	17 (24.7)	16 (23.2)	-----

The values have been corrected to the 293 °K ( 67 °F. )



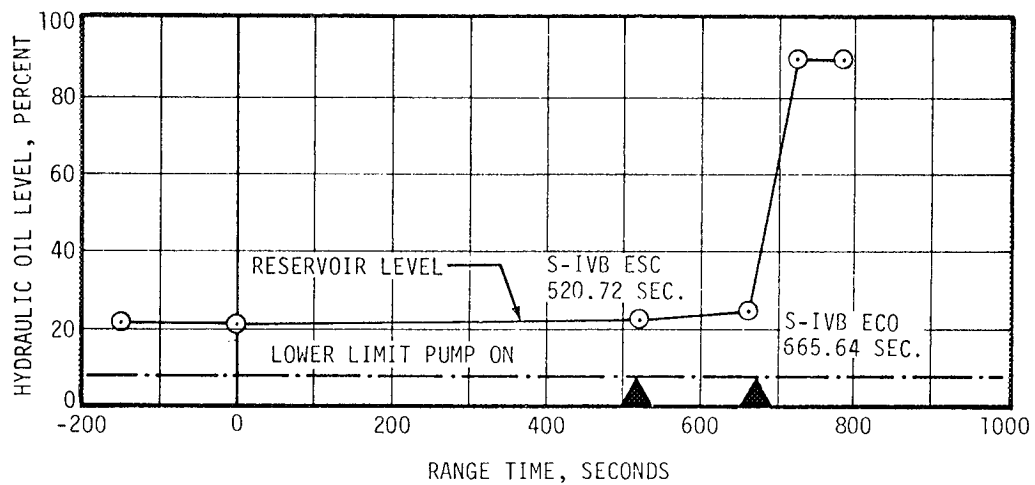
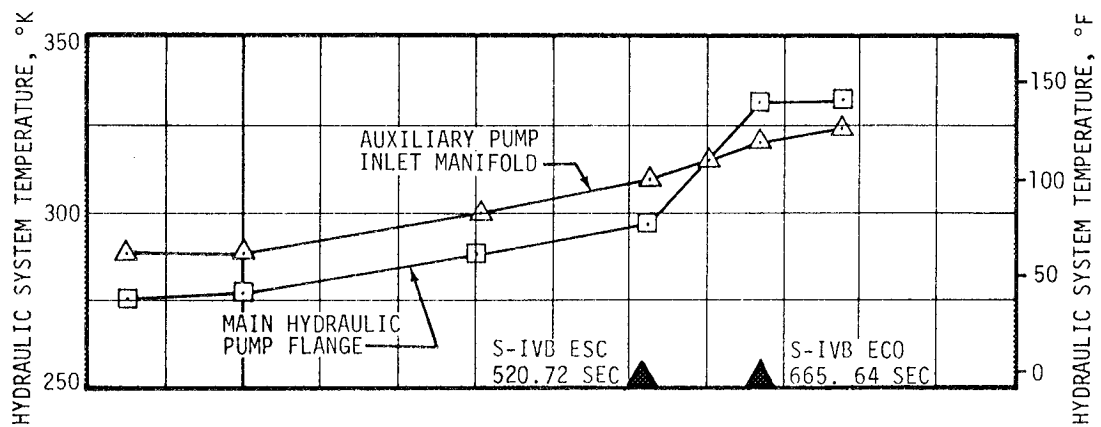
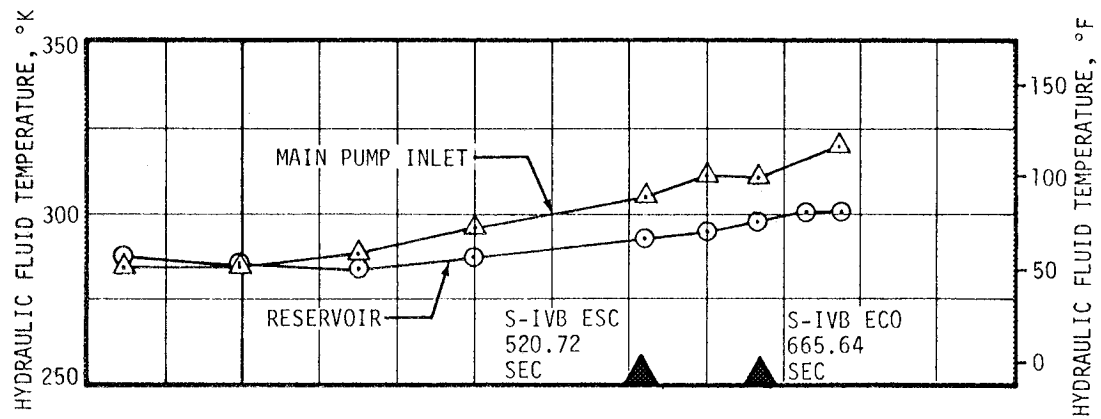


Figure 8-3. S-IVB Hydraulic System Performance - First Burn

## 8.5 S-IVB HYDRAULIC SYSTEM (COAST PHASE)

During orbital coast there were no thermal cycles of the auxiliary hydraulic pump. During a period of 50 minutes after engine cutoff, the pump inlet temperature increased from 321 to 349 °K (118.1 to 168.5 °F) due to continued heat transfer from the LOX turbine dome to the pump as shown in Figure 8-4. During remainder of the coast period this temperature decreased gradually along with other system temperatures. System bleeddown required 57 seconds and system pressure stabilized at 46.9 N/cm<sup>2</sup> (68 psia).

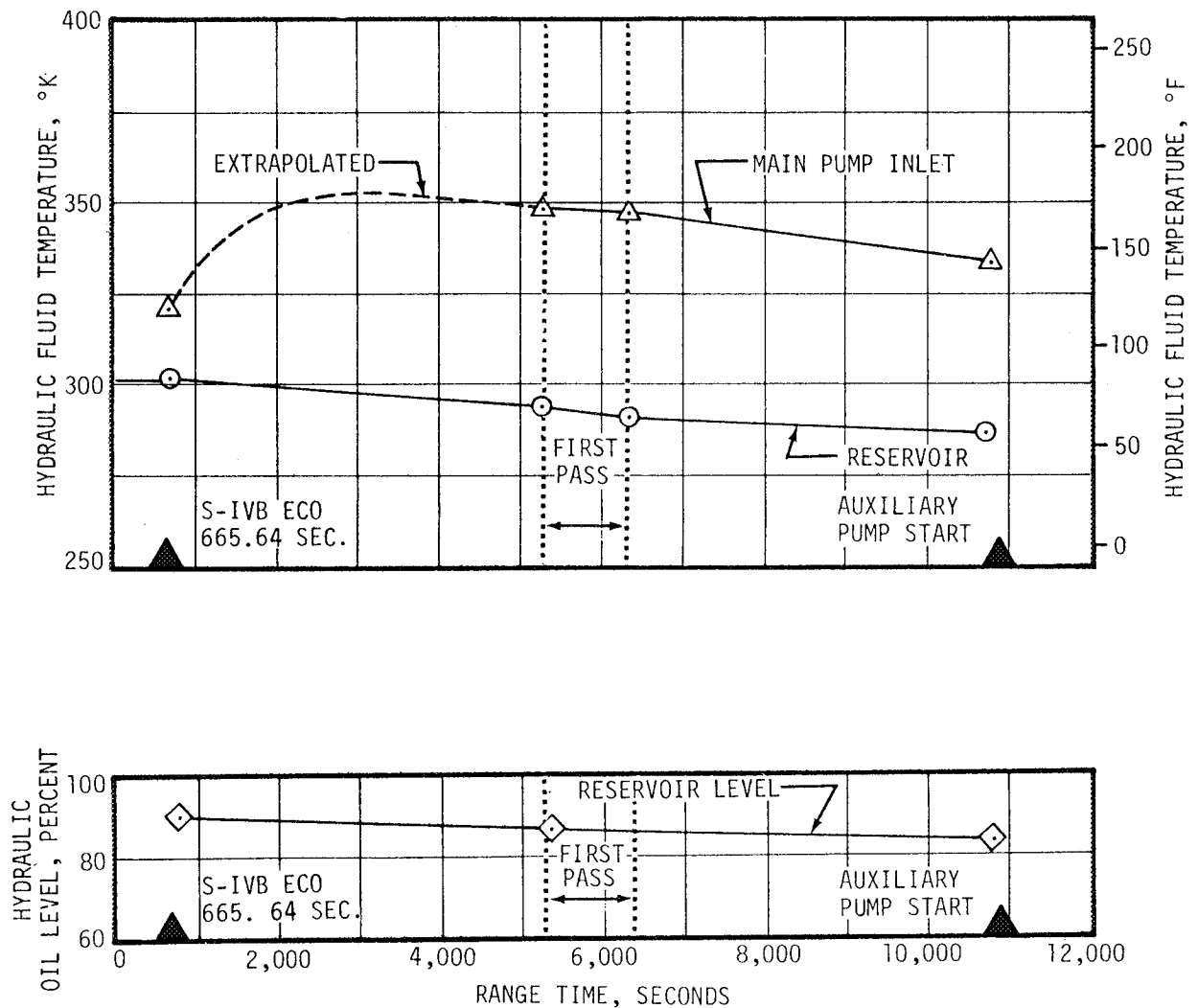


Figure 8-4. S-IVB Hydraulic System Performance - Coast Phase

## 8.6 S-IVB HYDRAULIC SYSTEM (SECOND BURN)

The auxiliary pump was activated to the flight mode at 10,914 seconds (580 seconds prior to second burn). System operation was normal through restart operation and during burn. During restart preparation the pump inlet oil temperature rose from 289°K to 309°K (60.53 to 96.53°F) at restart as shown in Figure 8-5. System pressure stabilized at 49 N/cm<sup>2</sup> (71 psia) following a 52-second bleeddown.

The maximum actuator torque resulting from the vehicle attitude command during second burn was in yaw at 11,380 N-m (100,719 in-lb) and was well within the design limit for the component.

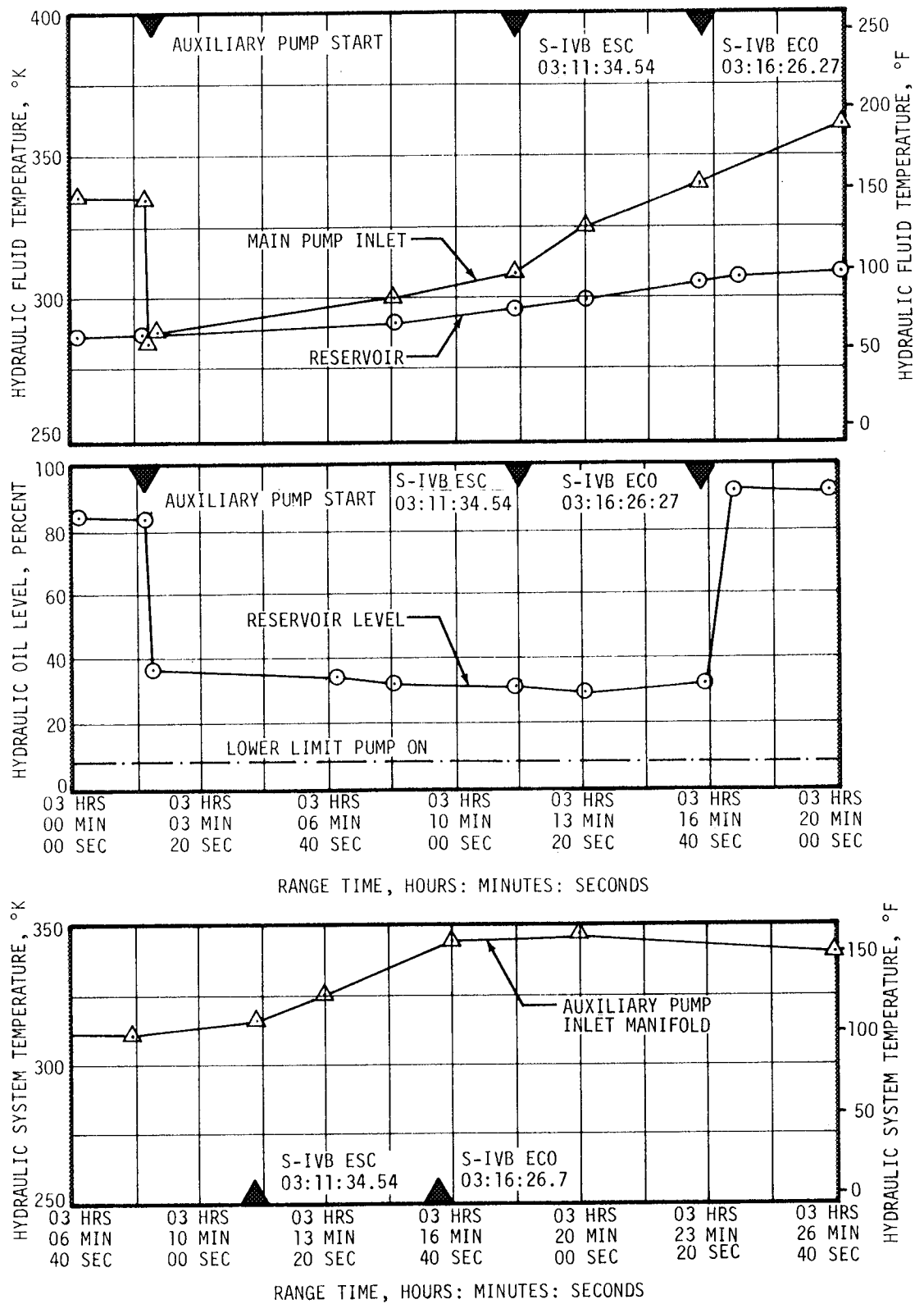


Figure 8-5 S-IVB Hydraulic System Performance - Second Burn

## SECTION 9 STRUCTURES

### 9.1 SUMMARY

The structural loads and dynamic environment experienced by the AS-501 launch vehicle were well within the vehicle structural capability. Vehicle loads, due to the combined rigid body and dynamic longitudinal load and bending moment, were well below limit design values. Tank pressures, compartment pressures, and structural temperatures also remained within limit design values.

The transients, due to thrust buildup and vehicle release, resulted in maximum longitudinal and lateral dynamic load factors of  $\pm 0.2$  g and  $\pm 0.08$  g (simulated) respectively at the command module. The maximum bending moment condition,  $5.72 \times 10^6$  N-m ( $4.22 \times 10^6$  lb-ft) in the S-IC LOX tank, was experienced at 78.70 seconds. The maximum longitudinal loads were experienced at 135.52 seconds (IECO) at a rigid body acceleration of 4.15 g's. The maximum longitudinal dynamic load factor,  $\pm 0.9$  g, occurred subsequent to OECO at the command module.

Vehicle dynamic characteristics followed the trends established by preflight analyses. As predicted prior to launch, small thrust oscillations of magnitudes less than 0.1 percent of total thrust occurred in the 4.5 to 5.5 hertz frequency range and excited the first longitudinal mode to small amplitudes. However, no longitudinal instability phenomenon occurred.

Fin bending and torsional modes compare well with analytical predictions. No fin flutter occurred. S-IC, S-II, and S-IVB stage vibrations were as expected. IU vibrations were as expected except for the inertial platform input vibrations which exceeded the random test specification at liftoff. No adverse effects were noted in platform performance.

### 9.2 TOTAL VEHICLE STRUCTURES EVALUATION

#### 9.2.1 Longitudinal Loads

The vehicle longitudinal dynamic response, due to thrust buildup and release, was determined by dynamic simulation and review of measured accelerations. The simulation utilized the individual F-1 engine thrust buildup and ignition

sequencing and holddown arm release times as determined from measured data. Predicted slow release device characteristics were used due to lack of measured data (refer to paragraph 11.3.1). Figure 9-1 shows the results of the simulation as compared to measured strain gage and accelerometer data. The upper two stations, where astronaut comfort is of prime concern, are presented in terms of acceleration and the lower two stations, where loads are the main consideration, in terms of load. In general, the measured and simulated data agree well considering that the strain gage frequency response was limited to 2.4 hertz or less. The pre-release (cantilevered) mode of approximately 2.0 hertz can be seen in both the strain data and the simulated data, while the post liftoff modes have been effectively filtered from the strain data. The predominant frequencies after release were approximately 3.8 and 4.4 hertz, corresponding to the first two longitudinal modes. The noticeable beat pattern, with a period of approximately 1.5 seconds, is due to the superposition of these two fundamental oscillations. During thrust buildup and release the maximum longitudinal dynamic load factor, approximately  $\pm 0.2$  g (simulated), occurred at the command module. The longitudinal dynamic response, shown in Figure 9-1, is well within the allowable limits when applied in conjunction with the lateral dynamic response (see Figure 9-4) and rigid body loads which existed during thrust buildup and release.

The longitudinal loads experienced during the time of maximum aerodynamic loading (maximum bending moment) and at maximum compression (IECO) are shown in Figure 9-2. The postflight calculated longitudinal loads were computed using the measured accelerations recorded during S-IC stage burn, and the predicted mass characteristics of AS-501. The measured loads from strain gage data show excellent correlation with the postflight calculated loads.

The vehicle longitudinal dynamic response experienced during S-IC OECO and S-IC/S-II separation is shown in Figure 9-3. The maximum longitudinal dynamic load factor during this period of flight, approximately  $\pm 0.9$  g, occurred at the command module. This load factor is well within allowable limits. The excellent correlation between the measured data and the response simulated by using measured forcing functions is shown in Figure 9-3.

#### 9.2.2 Bending Moments

The vehicle lateral dynamic response due to thrust buildup and release was determined by dynamic simulation and review of measured accelerations. The simulation utilized the individual F-1 engine thrust buildup and ignition sequencing, and holddown arm release times as determined from measured data. A steady 8 m/s (15.6 knots) wind was used. Predicted slow release device characteristics were used due to lack of measured data (refer to paragraph 11.3.1). Figure 9-4 shows the results of the simulation compared to measured strain gage data. For compatibility with Figure 9-1, the upper two stations are presented in terms of acceleration and the lower two in terms of bending moment. In general, considering that the filtered

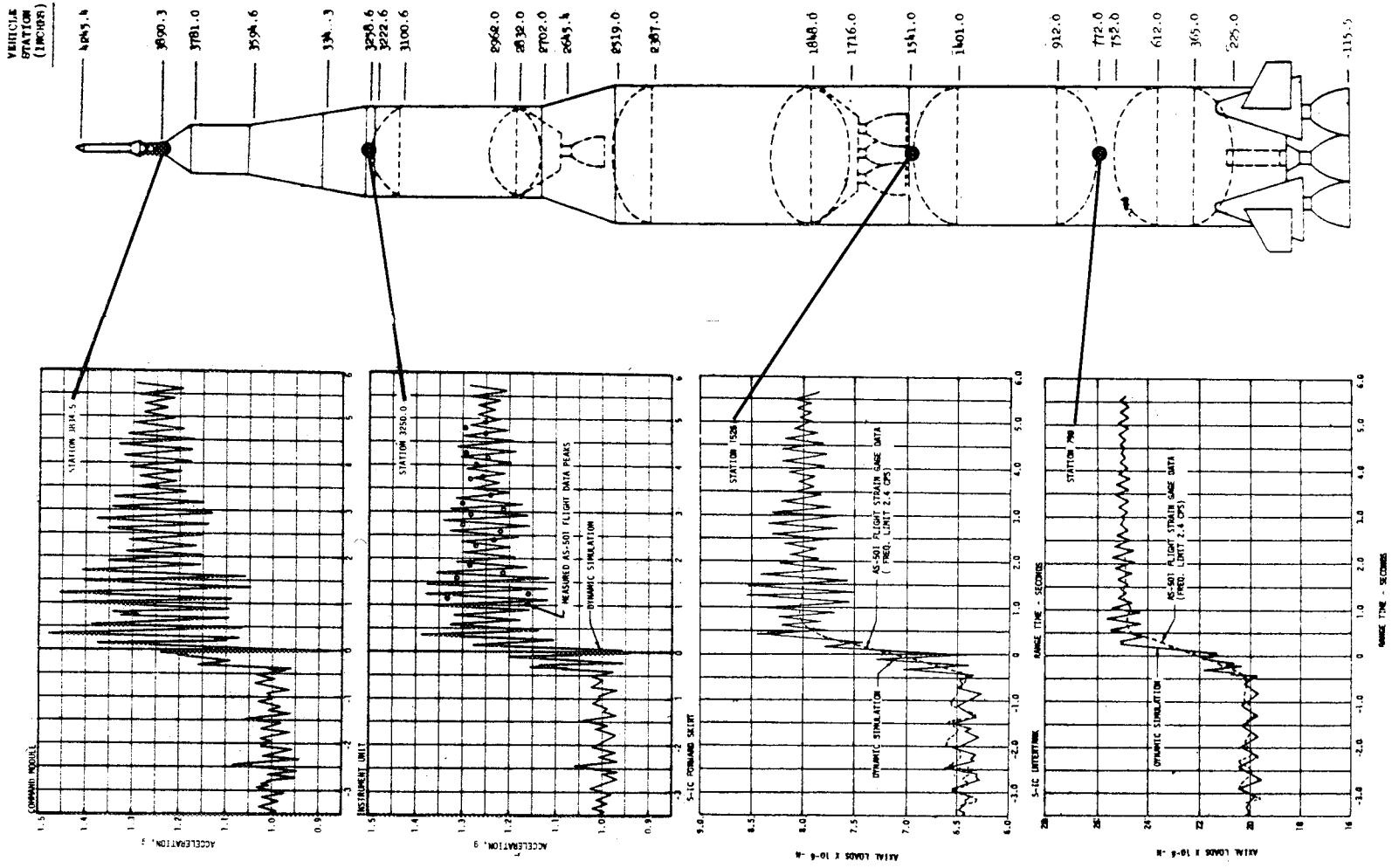


Figure 9-1. Longitudinal Structural Dynamic Response Due to Thrust Buildup and Release

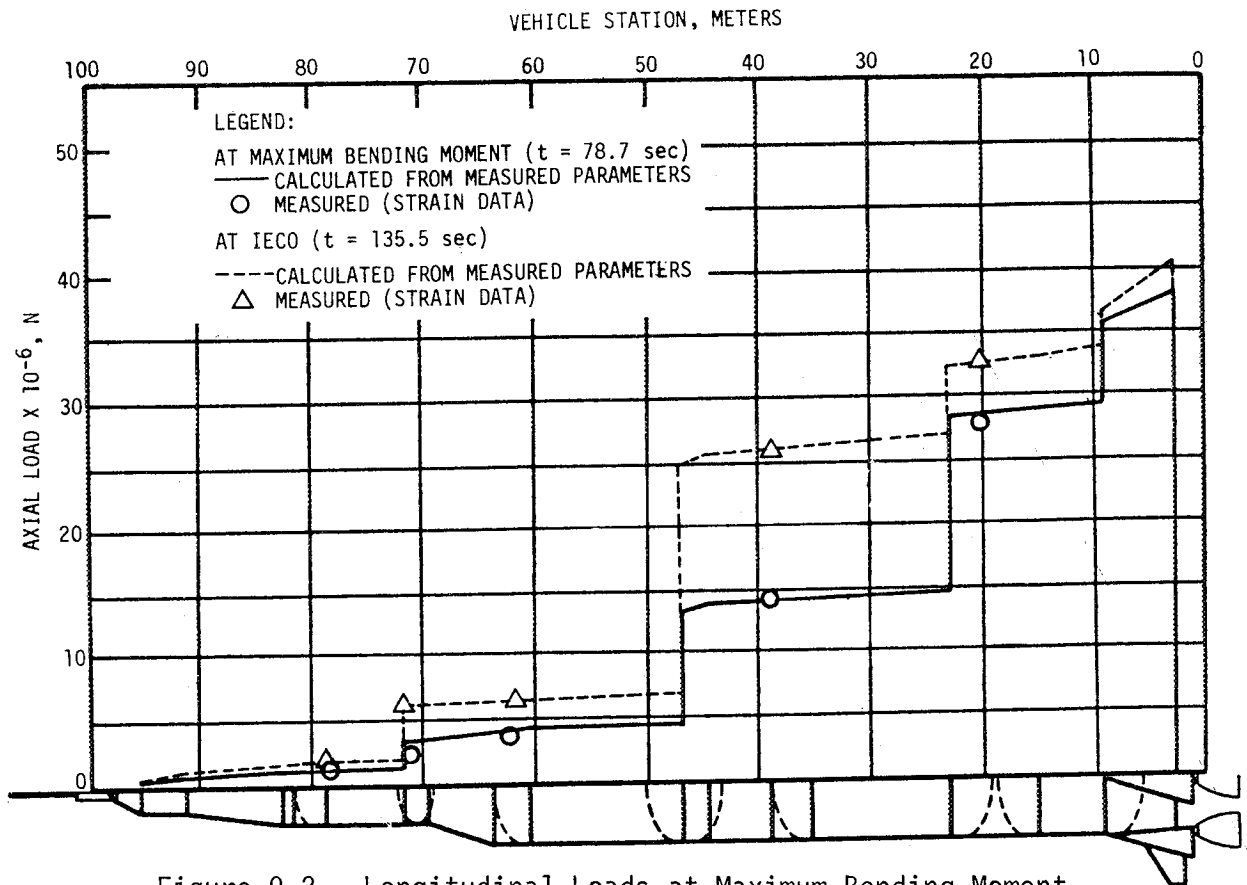


Figure 9-2. Longitudinal Loads at Maximum Bending Moment and Inboard Engine Cutoff

strain gage data includes only the rigid body load, the measured and simulated data agree very well up to liftoff. The deviations after liftoff can be attributed to strain gage unreliability at these low bending moments. During this period the maximum lateral dynamic load factor, approximately  $\pm 0.08$  g (simulated); was noted at the command module. The response shown in Figure 9-4 is well within the allowable when applied with the longitudinal dynamic response (see Figure 9-1) and the rigid body loads which exist during thrust buildup and release.

The maximum bending moment was experienced during S-IC powered flight at 78.70 seconds. The distribution of this bending moment, as a function of vehicle station, is shown in Figure 9-5 along with the normal load factor and the design bending moment. The bending moment diagram (solid line) is computed from measured thrust, gimbal angle, dynamic pressure, angle-of-attack, and modal acceleration. The bending moments indicated by circles were derived from strain gage data. The results of the two methods show excellent agreement and both are well below the design curve. Lateral load due to vehicle dynamics were insignificant at this time.



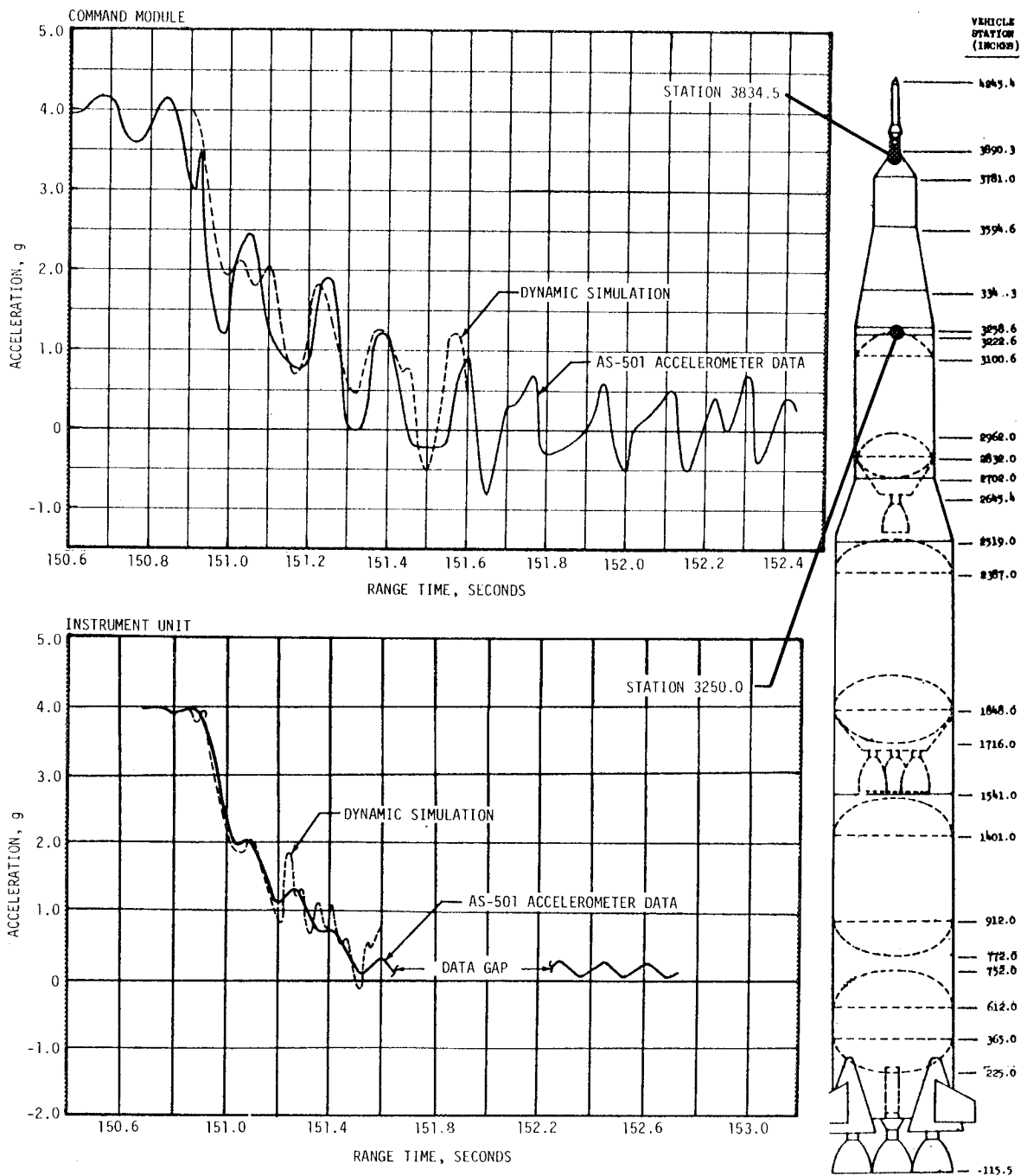


Figure 9-3. Longitudinal Structural Dynamic Response at the Instrument Unit and Command Module During S-IC/S-II Separation

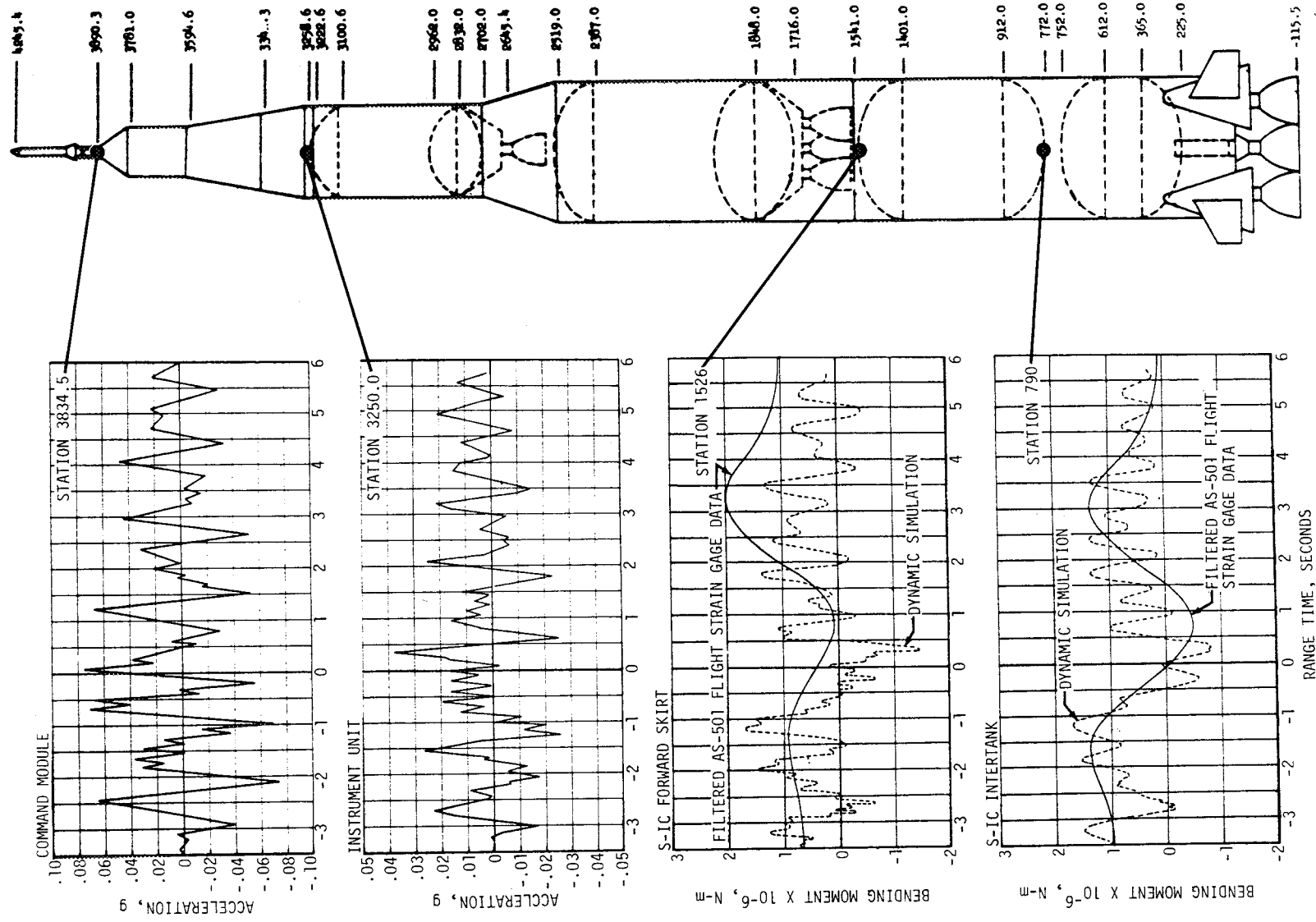


Figure 9-4. Lateral (Pitch) Structural Dynamic Response During Thrust Buildup and Release

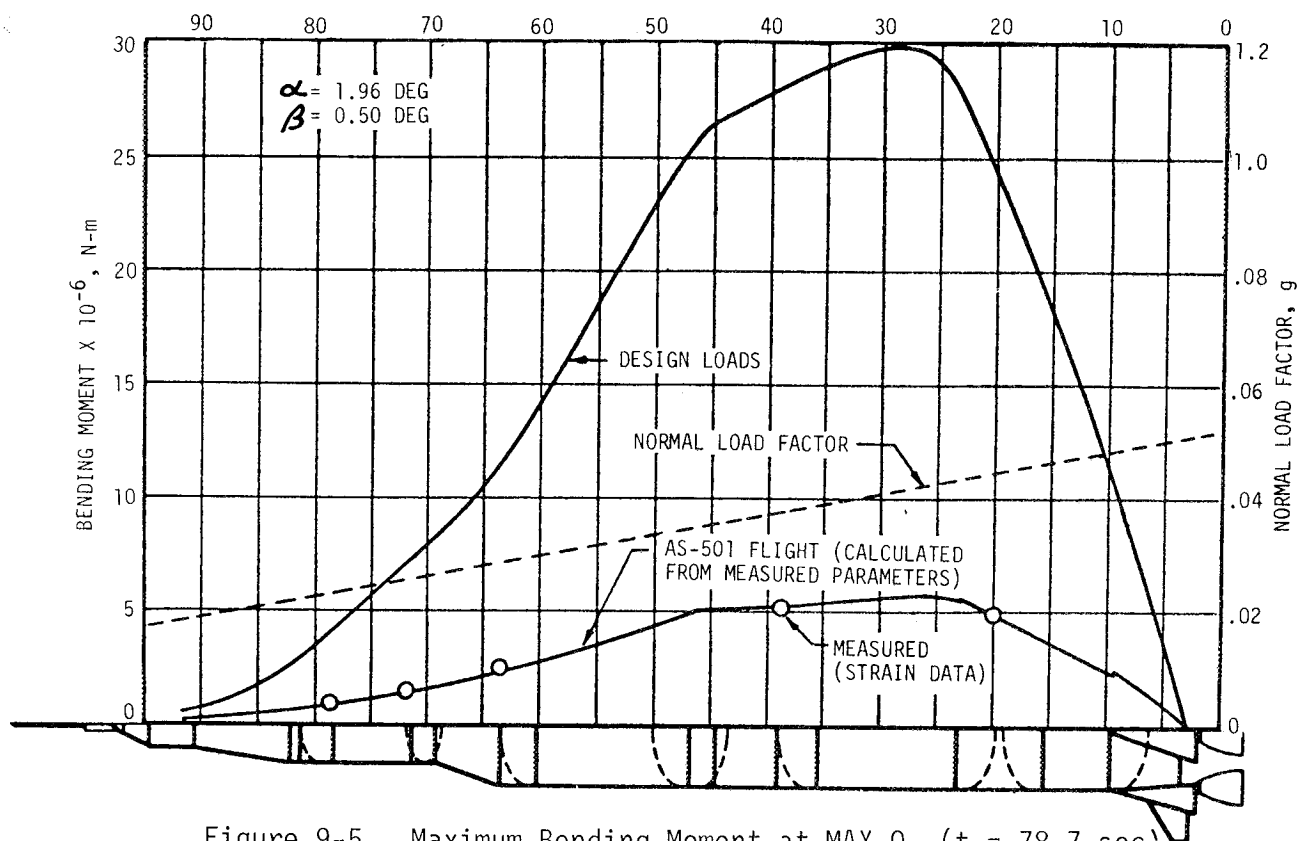


Figure 9-5. Maximum Bending Moment at MAX Q ( $t = 78.7 \text{ sec}$ )

### 9.2.3 Vehicle Dynamic Characteristics

9.2.3.1 Longitudinal Dynamic Characteristics - The predominant longitudinal frequencies and amplitudes at specific time points during S-IC stage powered flight were determined by a 0.4 hertz bandwidth spectral analysis, using selected longitudinal measurements which had suitable response. Figure 9-6 presents the results of this analysis. The frequencies recorded correlate very closely with the analytical and dynamic test results for the first longitudinal mode. The tank bulging mode, shown as a dashed line, disappears after 15 seconds as sufficient propellant is consumed. The amplitude of the first mode, as recorded at the instrument unit, peaks between 10 and 20 seconds and again between 100 and 120 seconds. The amplitude at these peaks is approximately 0.027 Grms.

Oscillograms were inspected and a spectral analysis of pump inlet and chamber pressures was accomplished to determine if any longitudinal instability phenomenon occurred due to thrust oscillations coupling with the longitudinal structural dynamics. Throughout S-IC powered flight the combustion chamber pressures exhibited small amplitude thrust oscillations varying within a 4 to 5.5 hertz frequency range. These frequencies apparently

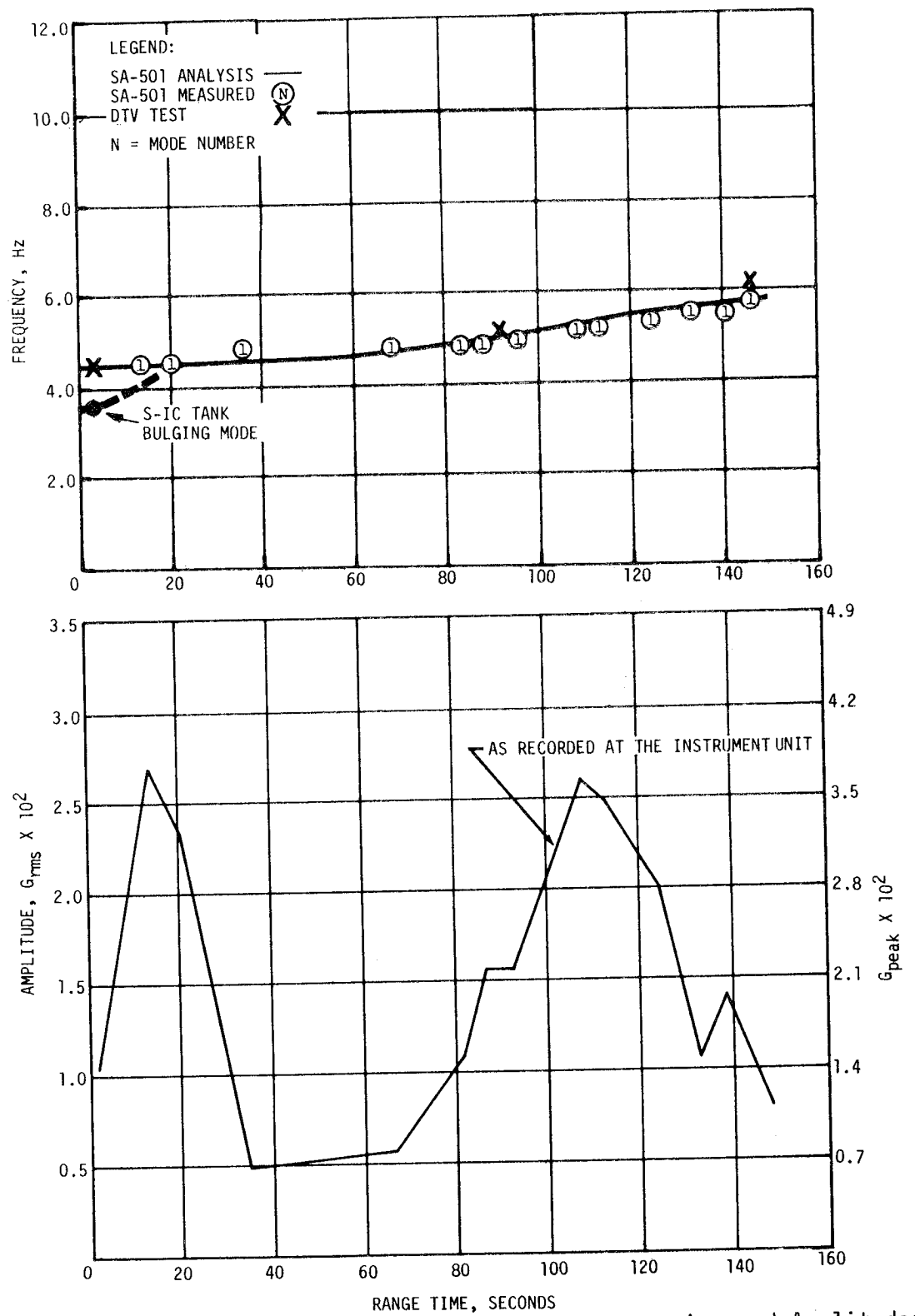


Figure 9-6. First Longitudinal Modal Frequencies and Amplitudes During S-IC Powered Flight

coincided with the frequency of the vehicle first longitudinal mode for a sufficient length of time to cause the two small amplitude peaks observed in Figure 9-6. However, the structural oscillations did not feed back into the thrust and cause a longitudinal instability. The observed longitudinal oscillations were as predicted.

Figure 9-7 shows a comparison of normalized flight data with analytically predicted longitudinal mode shapes. Mode shape data from the dynamic test have been included on one of the shapes for comparison purposes. Since the largest amplitudes obtained from the spectral analysis represent only 1 percent of the full scale range of the accelerometers, the magnitudes are difficult to establish with any degree of accuracy. Therefore, the normalized amplitudes of the measured data points in Figure 9-7 are questionable and it is believed that the true amplitudes are in close agreement with the analytical mode shapes.

9.2.3.2 Lateral Dynamic Characteristics - Low level oscillations in both pitch and yaw were detectable throughout S-IC powered flight. The frequencies of these oscillations as determined from a 0.33 hertz bandwidth spectral analysis, agree very well with the analytical predictions and dynamic test results as shown in Figure 9-8. In general, the modal amplitudes were higher in the yaw plane than in the pitch plane. The first three yaw modes and the first two pitch modes were evident, at various times, throughout first stage boost. The third pitch mode appeared only during the first 107 seconds of flight. Figure 9-8 presents the analytical and dynamic test modal frequencies versus time compared to the frequencies recorded by accelerometers at various stations.

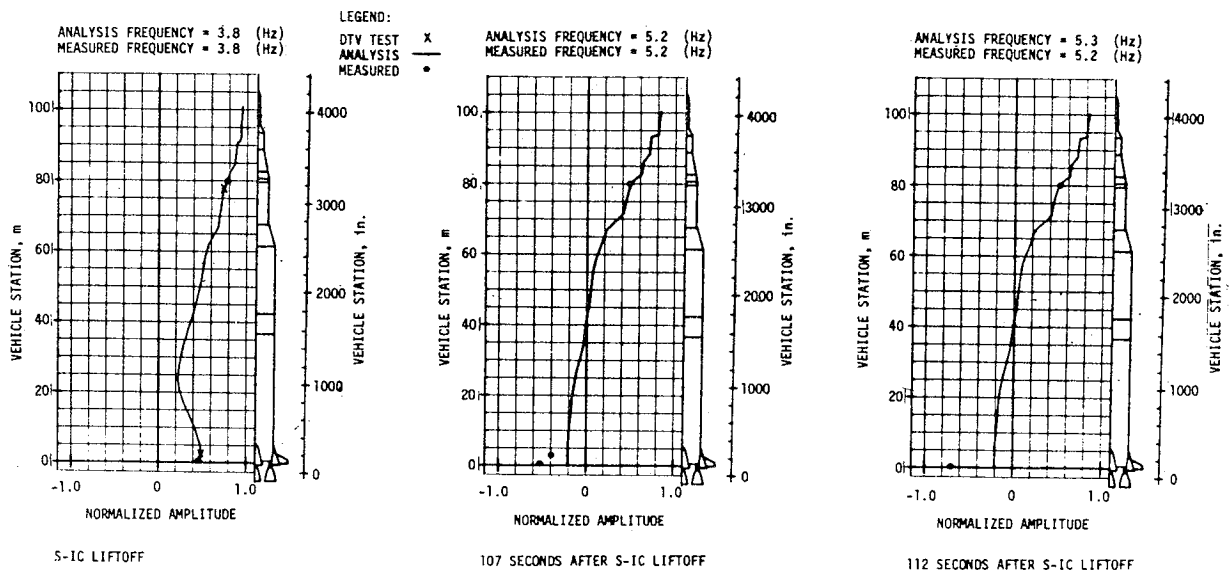


Figure 9-7. First Longitudinal Mode Shapes During S-IC Powered Flight

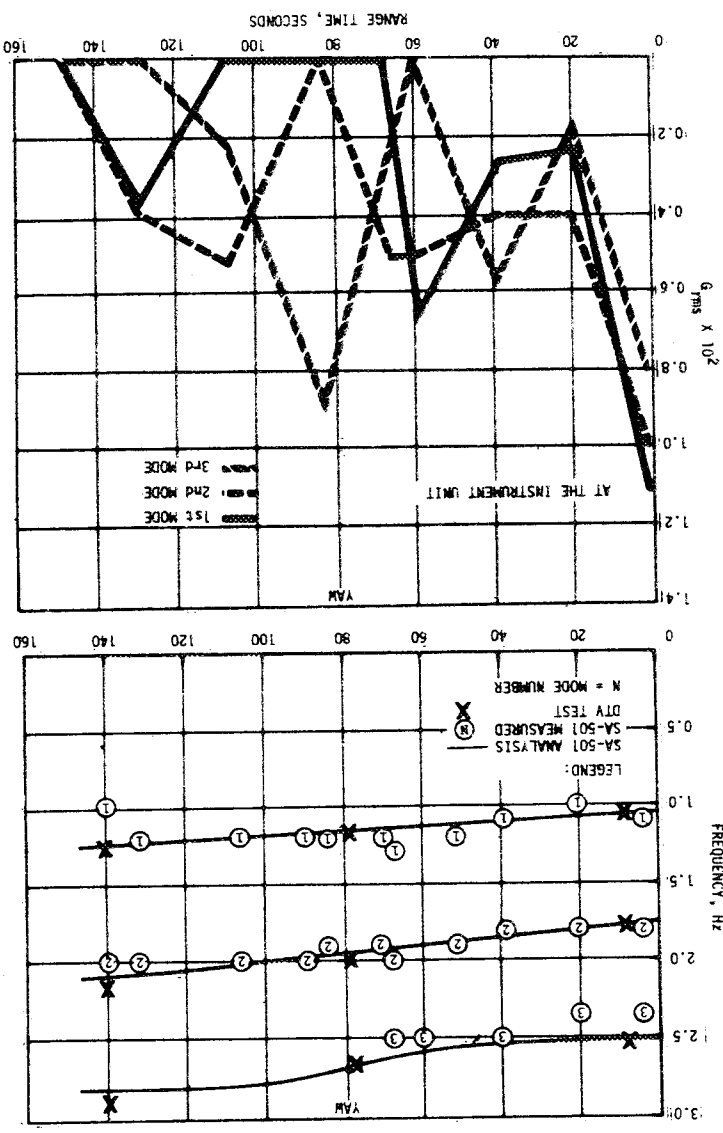
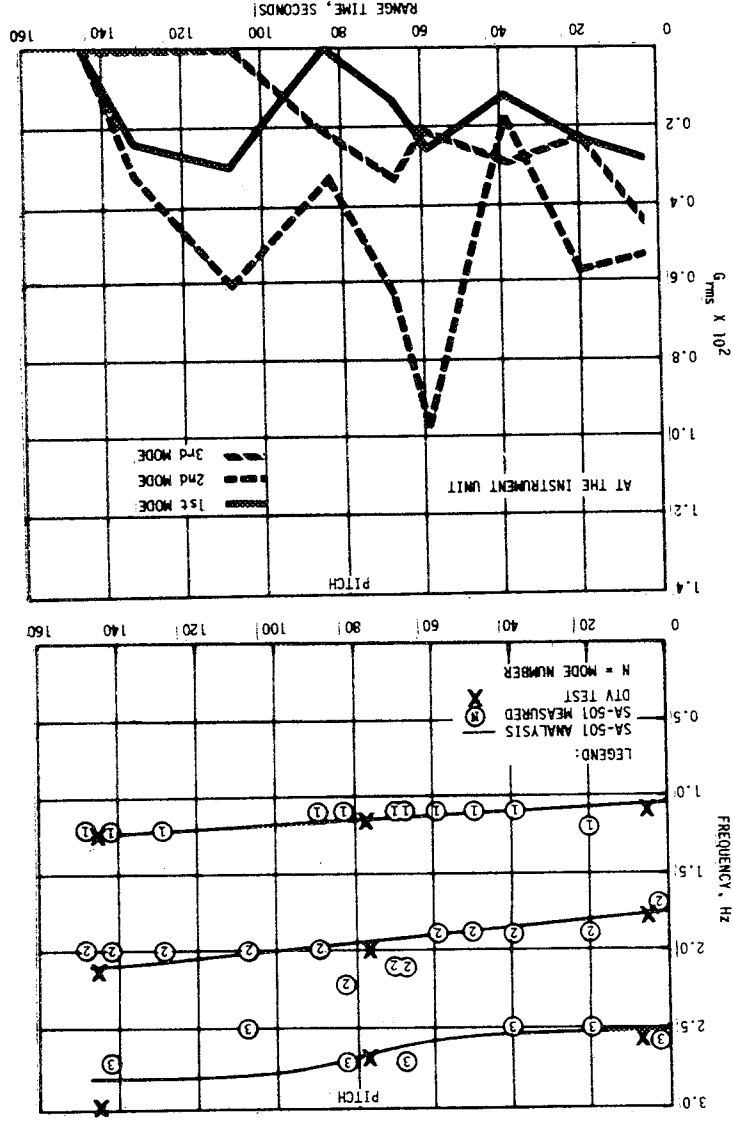


Figure 9-8. Lateral Modal Frequencies and Amplitudes During S-IC Powered Flight

Figure 9-8 also shows the amplitudes of the observed modes at the instrument unit versus time. The maximum modal amplitude observed was 0.011 Grms in the first yaw mode during liftoff at the instrument unit. It appears that the first mode phase stabilization used in the flight control system is particularly effective in damping out the first mode response. A comparison of normalized flight data with analytically predicted pitch mode shapes is presented in Figure 9-9. Mode shape data from the dynamic test have been included on two of the shapes for comparison purposes. Yaw mode shapes are identical to the pitch shapes and, therefore, are not shown.

#### 9.2.4 S-IC Fin Dynamics

Fin lateral vibration levels, as measured at fin station 132, are plotted versus vehicle velocity in Figure 9-10 for the S-IC stage powered flight. Acceleration levels were highest at liftoff and maximum dynamic pressure. At these times the levels exceeded the  $\pm 10$  g calibrated range of the accelerometers and it was not possible to determine the actual levels. At maximum dynamic pressure the level of the 25 hertz bending mode was significantly above the levels of all other modes noted.

In-flight measured values of S-IC stage fin bending and torsional mode frequencies are also shown in Figure 9-10. Dynamic test vehicle measured frequencies and analytically predicted frequencies are shown for comparison. Flight measured frequencies of 25, 38, 55, 65, and 78 hertz remained approximately constant with velocity. The 25 hertz frequency was identified as corresponding to a fin bending mode. The remaining frequencies were identified as corresponding to fin torsion or chord bending modes. Note that the fin modal frequencies did not coalesce. This data confirms that no fin flutter conditions existed for AS-501.

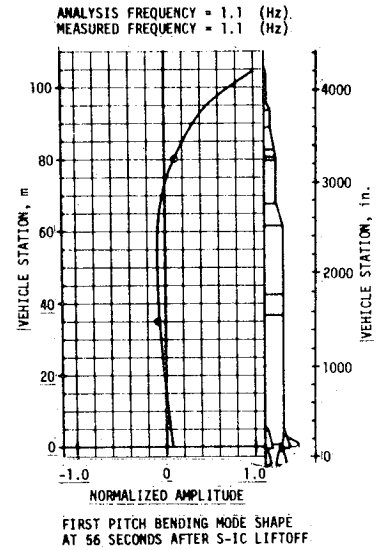
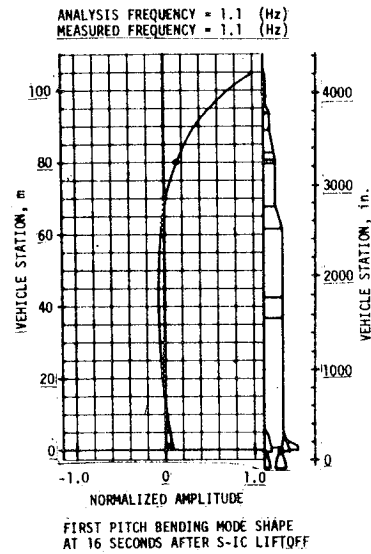
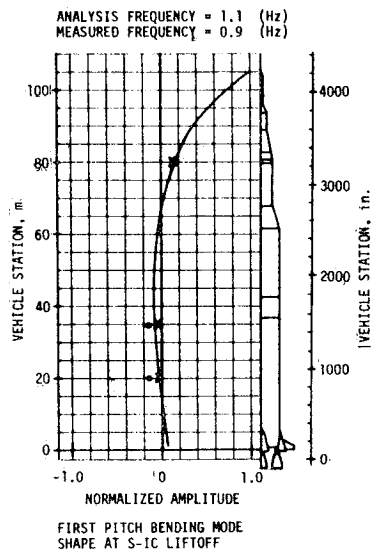
The bending moments on S-IC stage fins were well below design capability, since winds encountered in flight were well below design winds.

### 9.3 VIBRATION EVALUATION

#### 9.3.1 S-IC Stage and Engine Evaluation

The S-IC structure, engine, and component vibration measurements taken on the S-IC stage are summarized in Figures 9-11 through 9-13 and Table 9-1. A total of 51 single sideband vibration measurements were taken of which 33 yielded usable data. The acoustic environment reported in paragraphs 16.4.1 and 16.4.2 of this document correlate well with these vibration data.

9.3.1.1 S-IC Stage Structure - Measurements taken on the stage structure are summarized in Figure 9-11 and Table 9-1. Amplitudes at the thrust structure are similar to static firing levels at liftoff and are lower during the remainder of the flight. Two measurements at the thrust structure exceeded static firing levels at liftoff, but are generally within design levels. The intertank structure and forward skirt structure show vibration levels considerably less than static firing during liftoff and throughout flight.



LEGEND:  
DTV TEST x  
ANALYSIS —  
MEASURED •

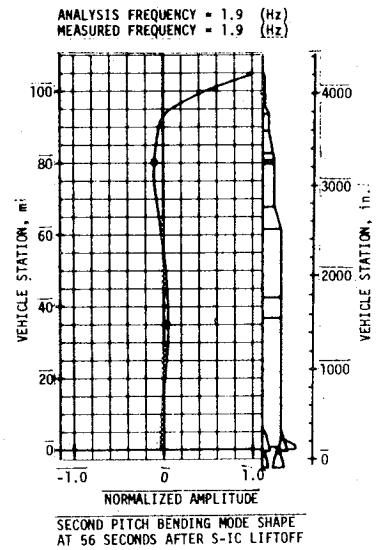
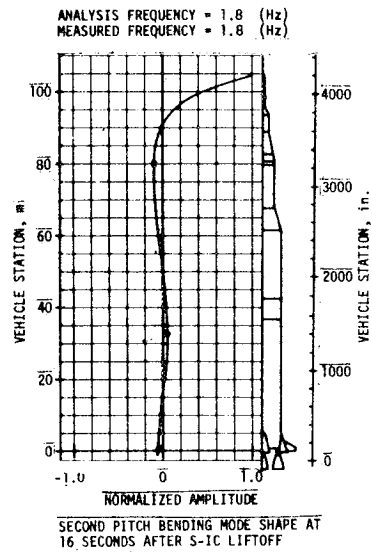
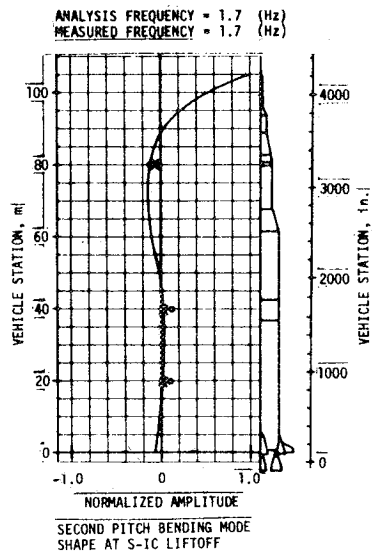


Figure 9-9. Pitch Mode Shapes During S-IC Powered Flight



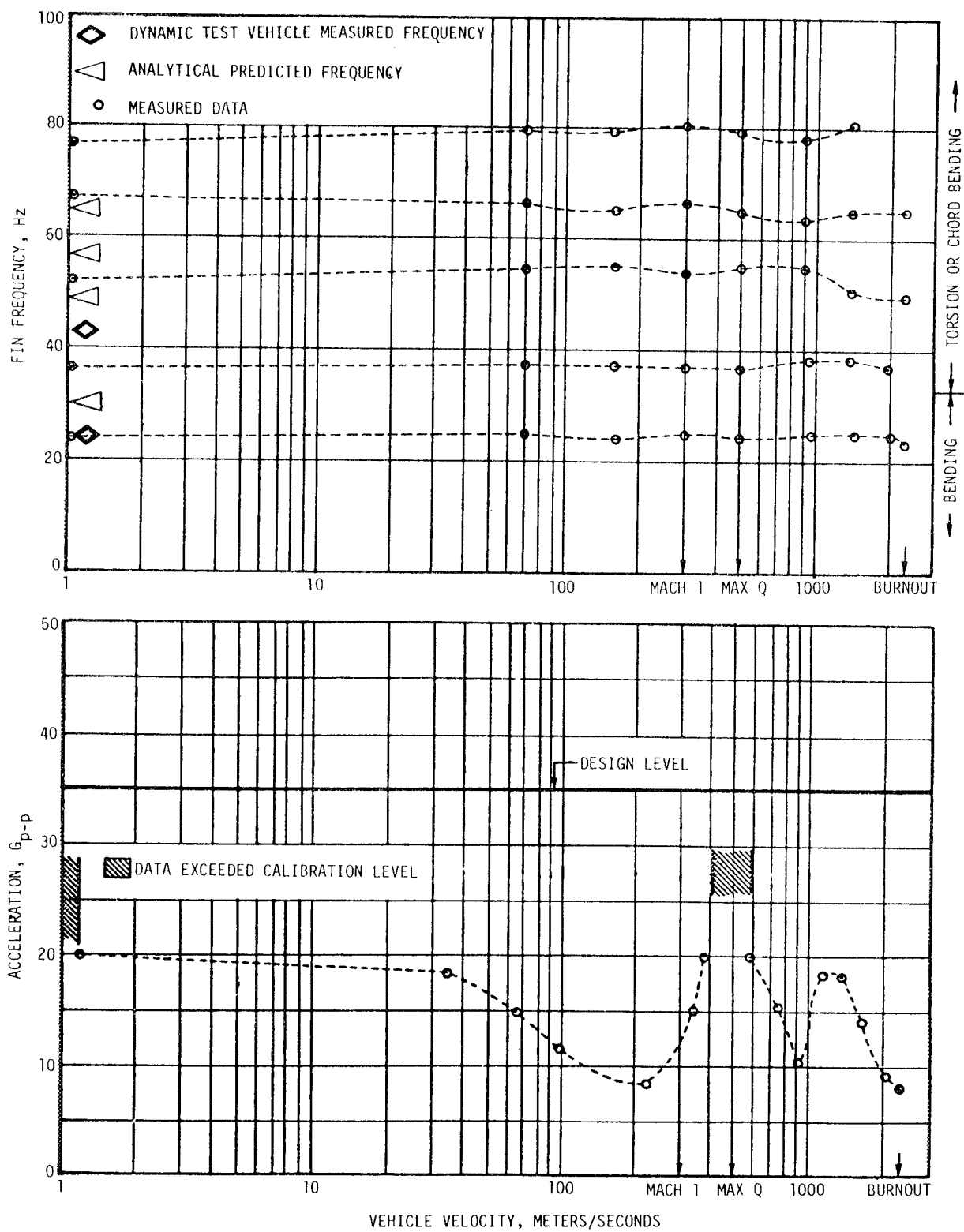


Figure 9-10. S-IC Fin Vibration Response and Bending and Torsional Modal Frequencies

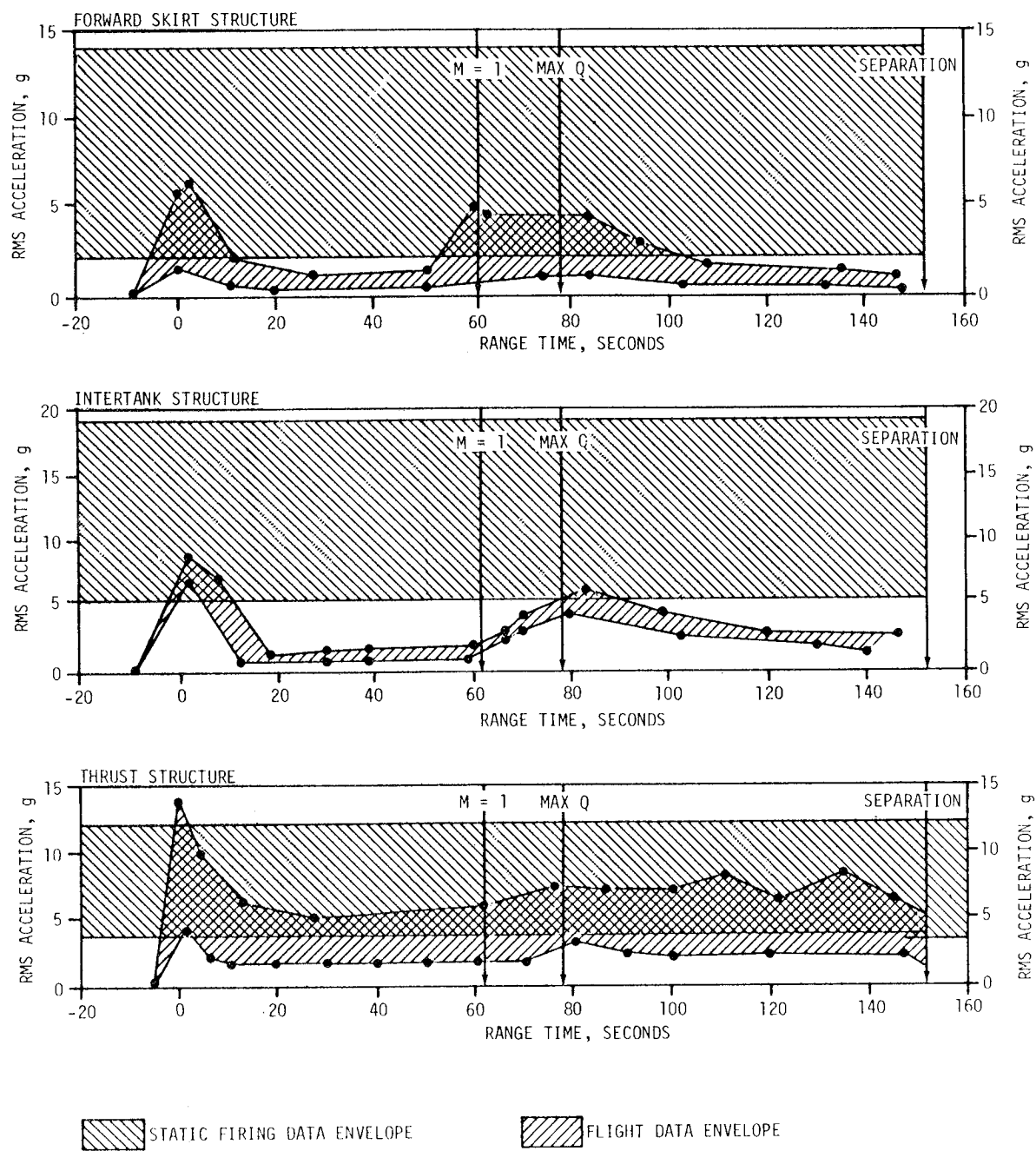


Figure 9-11. S-IC Stage Structure Vibration Envelopes

Table 9-1. S-IC Stage Vibration Summary

	AREA MONITORED	MAX LEVEL Grms	RANGE TIME (SEC)	REMARKS
Structure	Forward Skirt E18-120, E19-120, E47-120	6.8	2.9	The max Grms level of 6.8 is approximately 7.4 Grms lower than static firing levels.
	Intertank Structure E20-118, E21-118	9.1	4.0	The max Grms level of 9.1 is approximately 9.7 Grms lower than static firing levels.
	Thrust Structure E23-115, E24-115, E48-115, E49-115, E53-115, E54-115, E79-115, E80-115	13.9	0.5	The max Grms level of 13.9 is approximately 1.8 Grms higher than static firing levels but the spectra are very similar. E79 and E80 taken only from 145.1 to separation.
	Engine			
	Turbopump E39-101, E41-103, E42-101, E42-103	26.5	125.0	The max Grms level of 26.5 is approximately 11.0 Grms lower than static firing levels.
Components	LOX Feed Line E25-118, E26-118, E27-115, E28-115	10.4	-0.5	The max Grms level of 10.4 is approximately 4.3 Grms lower than static firing levels.
	Cold Helium Line E50-116, E51-116	14.0	0	The max Grms level of 14.0 is approximately 1.0 Grms lower than static firing levels.
	Engine Actuator E30-101, E30-102, E31-101, E31-102, E32-101, E32-102, E34-101, E34-102, E35-101, E35-102	6.2	123.0	The max Grms level of 6.2 is approximately 31.0 Grms lower than static firing levels.

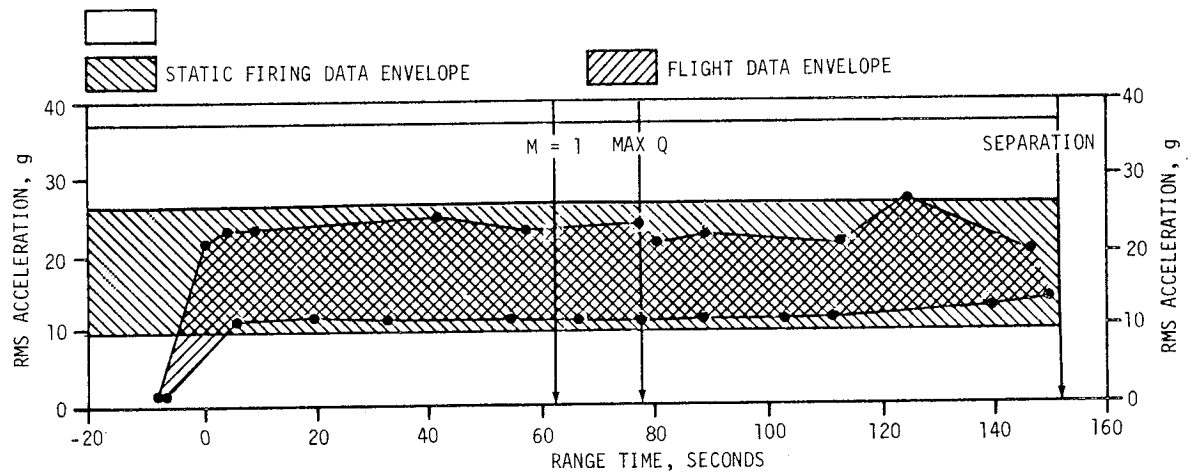


Figure 9-12. S-IC Stage Engine Vibration Envelopes (Turbopump)

9.3.1.2 F-1 Engines - Measurements on the F-1 engine combustion chamber produced insufficient data to construct an overall Grms level versus flight time plot. All five vibration measurements on the combustion chamber are considered invalid. Four measurements of 14 on the turbopump produced data sufficiently valid to indicate the levels on the F-1 engine turbopump. The Grms levels are similar to static firing throughout flight. Turbopump measurements are summarized in Figure 9-12 and Table 9-1.

9.3.1.3 S-IC Stage Components - The responses of three components on the S-IC: the servoactuators, the cold helium line, and the LOX feed line are summarized in Figure 9-13 and Table 9-1. The engine actuator measurements showed amplitudes much lower than static firing. The cold helium line showed levels similar to maximum levels measured during static firing. The higher levels at liftoff reflect the difference in deflector location relative to the cold helium line between the static firing stand and the LUT. Measurements taken on the LOX feed line show data throughout flight similar to static firing data. The constant level throughout flight indicates that the vibration is a result of engine and flow dynamics and is not affected by acoustics.

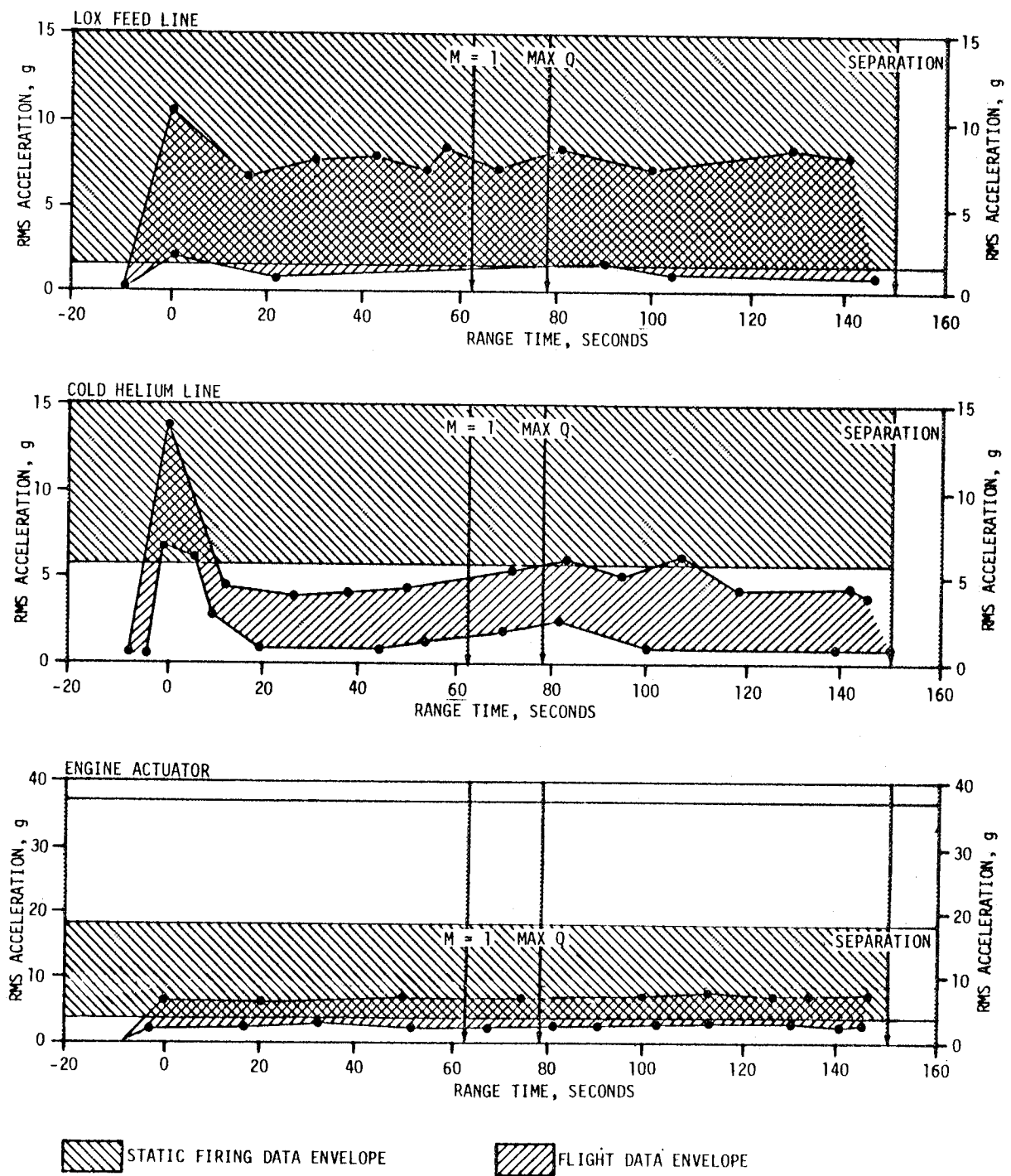


Figure 9-13. S-IC Stage Components Vibration Envelopes

### 9.3.2 S-II Stage and Engine Evaluation

The AS-501 S-II structure, engine, and component vibration measurements evaluated on the S-II stage are summarized in Figures 9-14 through 9-16 and Table 9-2. The composite vibration response characteristics of all measurements were less than the maximum overall Grms levels expected. During S-IC powered flight these vibration responses correlate closely with the acoustic environment reported in paragraph 16.4.1 of this document.

9.3.2.1 S-II Stage Structure - The measurements taken on the stage structure are summarized in Figure 9-14 and Table 9-2. The trends were as expected and the Grms levels were less than the maximum expected. Significant peaks occur at liftoff and Mach 1/Max q at all locations. On the thrust cone the maximum levels occurred after S-II engine start as expected. On the interstage a measurable peak also occurred between S-IC/S-II separation and interstage jettison due to combined effects of ullage motor firing and S-II engine thrust buildup.

9.3.2.2 S-II Stage J-2 Engines - The measurements taken on the S-II stage J-2 engines are summarized in Figure 9-15 and Table 9-2. The trends were as expected with the maximum levels occurring after S-II engine start. The LOX pump measurements show a sharp amplitude increase at the engine mixture ratio shift time, as expected. This increased vibration results from changed flow characteristics through the LOX pump after the propellant utilization (LOX bypass) valve position is changed. All composite Grms amplitudes were lower than the maximum expected.

9.3.2.3 S-II Stage Components - S-II stage forward skirt and thrust cone container vibration levels are summarized in Figure 9-16 and Table 9-2. All composite Grms amplitude levels were lower than the maximums expected and the trends were as expected. All containers showed significant response to liftoff, Mach 1/Max q, and S-II engine start.

### 9.3.3 S-IVB Stage and Engine Evaluation

Eight structural, eighteen component, and three engine measurements were included in the vibration evaluation. The maximum composite (50 to 3000 hertz) vibration levels measured at each location are summarized in Table 9-3. Time histories of the maximum and minimum composite levels for the structural, forward skirt components, aft skirt components and engine measurements are shown in Figure 9-17. Time histories of measurements comparable to measurements made during Saturn IB flights are included for information only and are shown in Figure 9-18. Vibration levels during S-IC powered flight follow the same trend as acoustic levels reported in paragraphs 16.4.1 and 16.4.2 of this document.

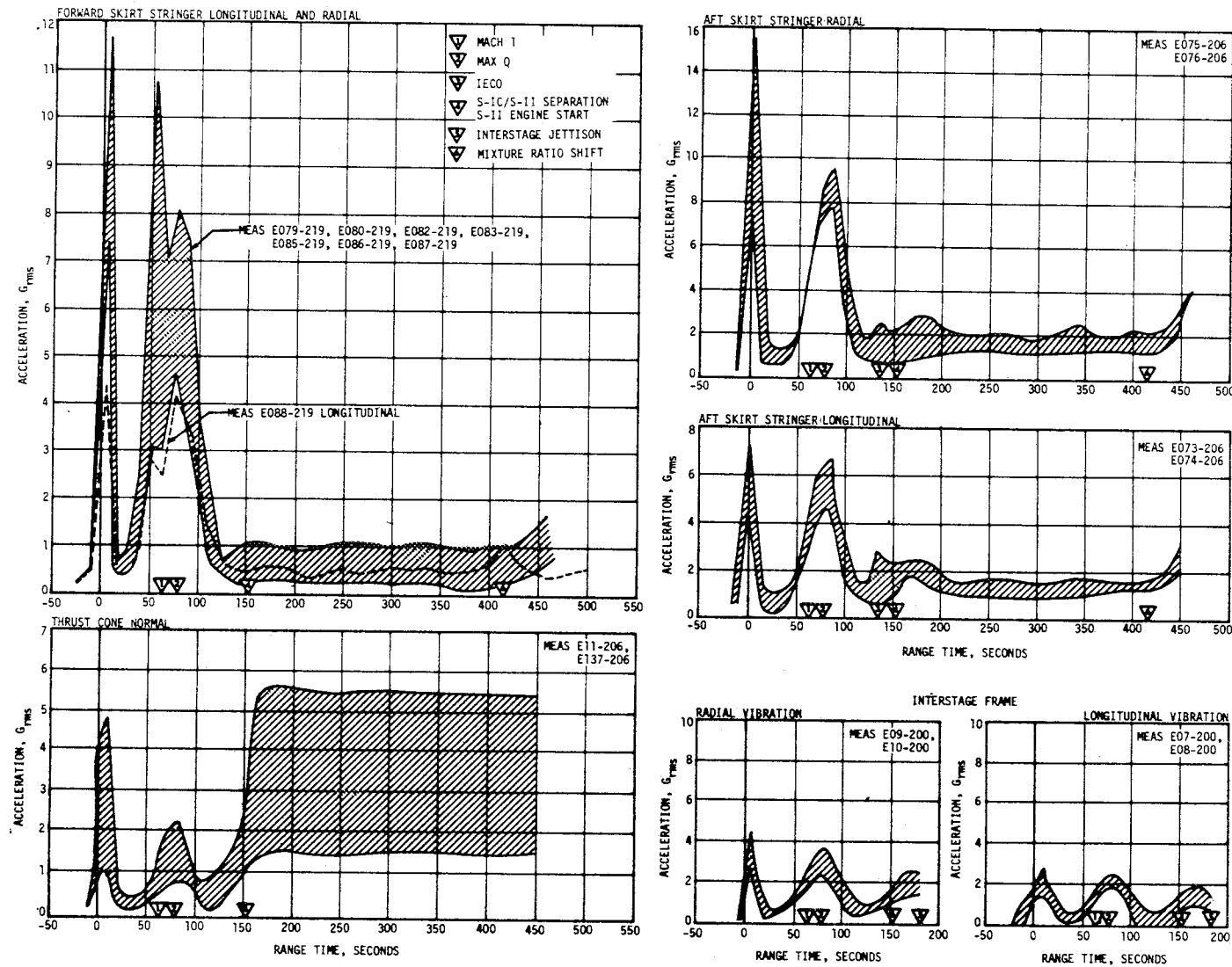


Figure 9-14. S-II Stage Structure Vibration Envelopes

Table 9-2. S-II Stage Vibration Summary

	AREA MONITORED	MAX LEVEL Grms	RANGE TIME (SEC)	REMARKS
Structure	Forward Skirt Stringer E79-219, E80-219, E82-219, E83-219, E85-219, E86-219, E87-219, E88-219	11.7 (Radial) 4.4 (Long)	8 8	
	Aft Skirt Stringer E75-206, E76-206, E73-206, E74-206	15.6 (Radial) 7.3 (Long)	2 2	
	Thrust Cone E11-206, E137-206	5.7	180	
	Interstage Frame E9-200, E10-200 E7-200, E8-200	4.4 (Radial) 2.8 (Long)	6 8	
Engines	Combustion Dome Longitudinal E1-201 through E1-205	11.0	170	The maximum Grms level of 11.0 is approxi- mately 4 Grms lower than the maximum static firing Grms level
	Fuel Pump Radial E3-201 through E3-205	14.4	170	The maximum Grms level of 14.4 is approxi- mately 2.8 Grms lower than the maximum static firing Grms level
	LOX Pump Radial E2-201 through E2-205	10.8	518	The maximum Grms level of 10.8 is approxi- mately 4.1 Grms lower than the maximum static firing Grms level
Components	Forward Skirt Containers E117-228, E118-228, E119-228, E120-228, E121-225, E122-225, E123-225, E124-225	8.8	8	
	Thrust Cone Containers E26-207 to E30-207 E17-208 to E21-208	5.2	0	



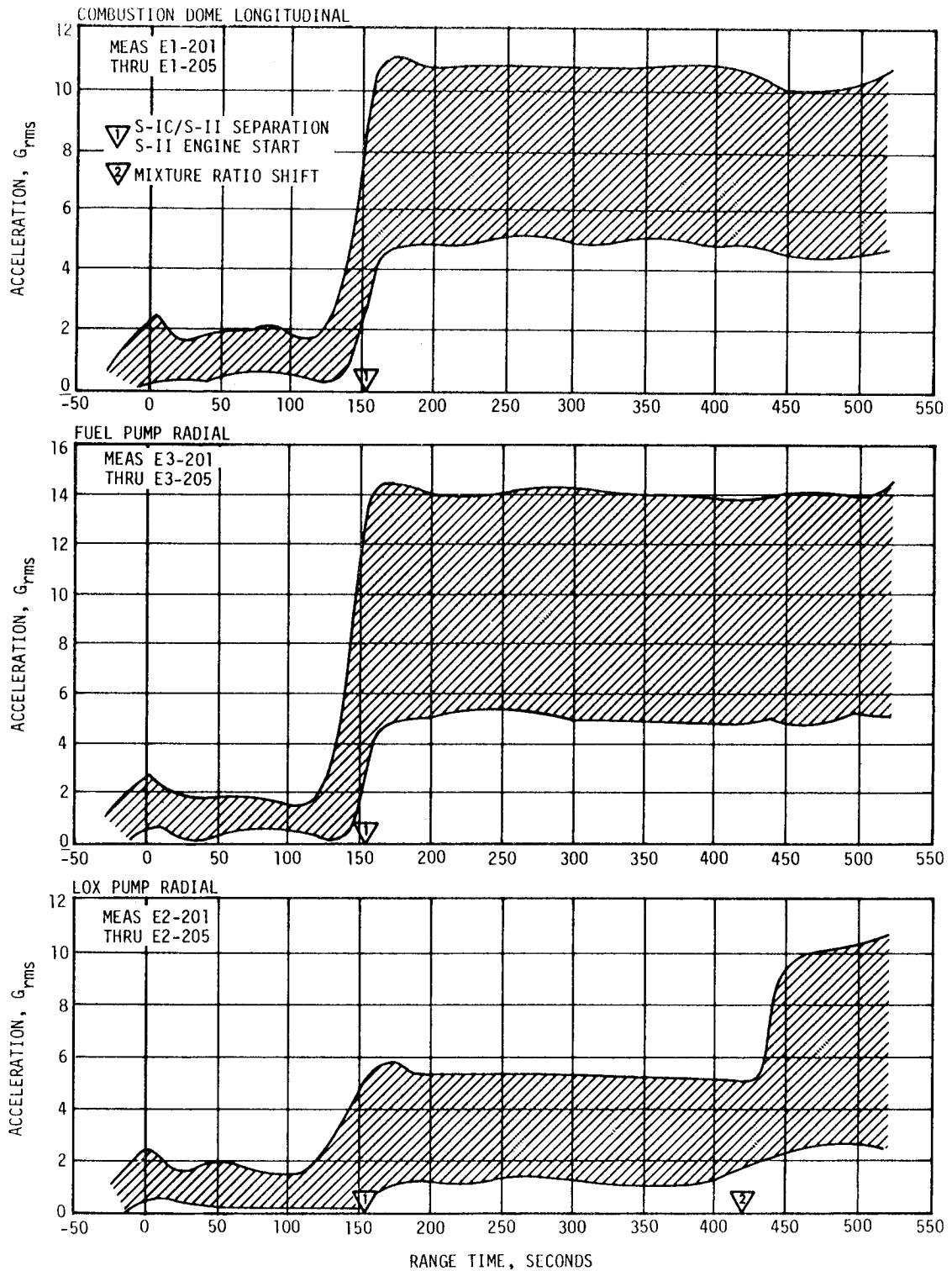


Figure 9-15. S-II Stage Engine Vibration Envelopes

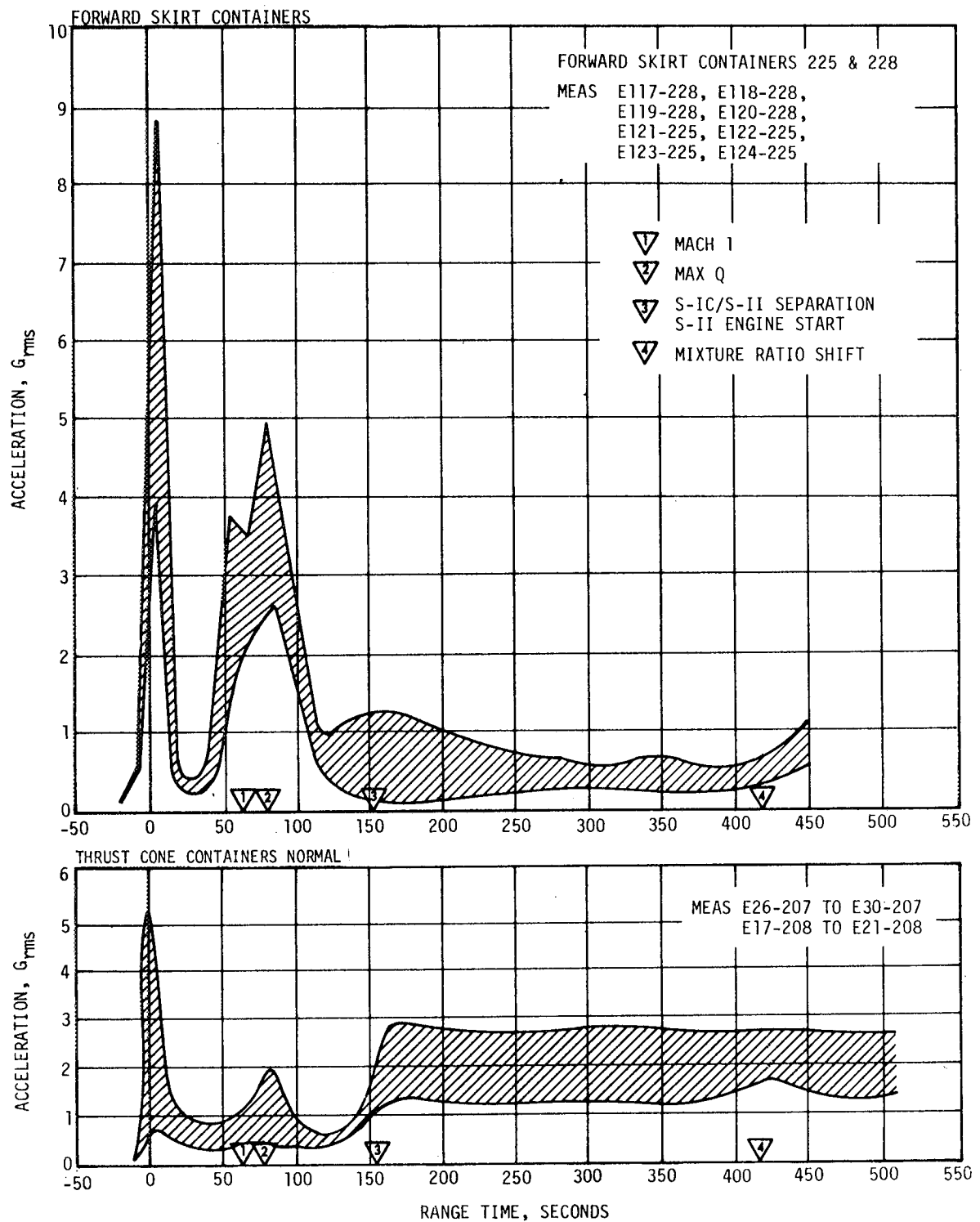


Figure 9-16. S-II Stage Component Vibration Envelopes

Table 9-3. S-IVB Vibration Summary

	AREA MONITORED	MAX LEVEL Grms	RANGE TIME (SEC)	REMARKS
Structure.	Gimbal Point-Thrust	3.5	530	(1) Prior to S-IVB burn the gimbal point and engine levels were negligible. The levels given for the time shown are applicable throughout the first and second burn of the S-IVB. The levels measured are comparable with those measured during static firing.
	Aft Separation Plane Pos II-Thrust	1.4	80	
	Forward Field Splice Pos I -Thrust	4.0	75	
	Forward Field Splice Pos I -Radial	8.0	62	
	Forward Field Splice Pos I -Tangential	2.8	62	
	Forward Field Splice Pos II-Thrust	5.0	78	
	Forward Field Splice Pos II-Radial	7.0	80	
	Forward Field Splice Pos II-Tangential	5.0	77	
Engine	Combustion Chamber Dome-Thrust	8.5	535	(2) One exception to Note 1 is the LOX turbopump. The level varied with the engine mixture ratio during the second burn, therefore, the maximum level is shown for each burn. This variation occurs during static firings also.
	LOX Turbopump-Radial	13.0	532	
	LOX Turbopump-Radial	22.0	11770	
	LH2 Turbopump-Radial	13.0	532	
Component (Fwd. Skirt)	P.U. Electronic Panel Input-Thrust	5.5	75	(3) With the exception of the gimbal point and engine measurements, all levels were negligible after the S-IC powered portion of the flight.
	P.U. Electronic Panel Input-Radial	7.5	62	
	P.U. Electronic Panel Response-Radial	4.5	2	
	E.B.W. Range Safety Panel Input-Thrust	4.0	80	
	E.B.W. Range Safety Panel Input-Radial	7.0	68	
	E.B.W. Range Safety Panel Response-Radial	2.3	68	
	Battery No. 1 Input-Thrust	3.0	78	
	Battery No. 1 Input-Radial	6.0	62	
Component (Aft. Skirt)	Battery No. 1 Input-Tangential	4.5	78	
	Sequencer Panel Input-Thrust	6.0	78	
	Sequencer Panel Input-Radial	7.5	78	
	Sequencer Panel Response-Radial	3.7	78	
	Switch Selector Panel Input-Thrust	10.0	80	
	Switch Selector Panel Input-Radial	7.5	80	
	Switch Selector Panel Response-Radial	4.0	80	
	APS MOD-1 Aft Attach Pt. Input-Thrust	3.0	78	
	APS MOD-1 Aft Attach Pt. Input-Radial	4.0	80	
	APS MOD-1 Fwd. Attach Pt. Input-Radial	5.5	0	

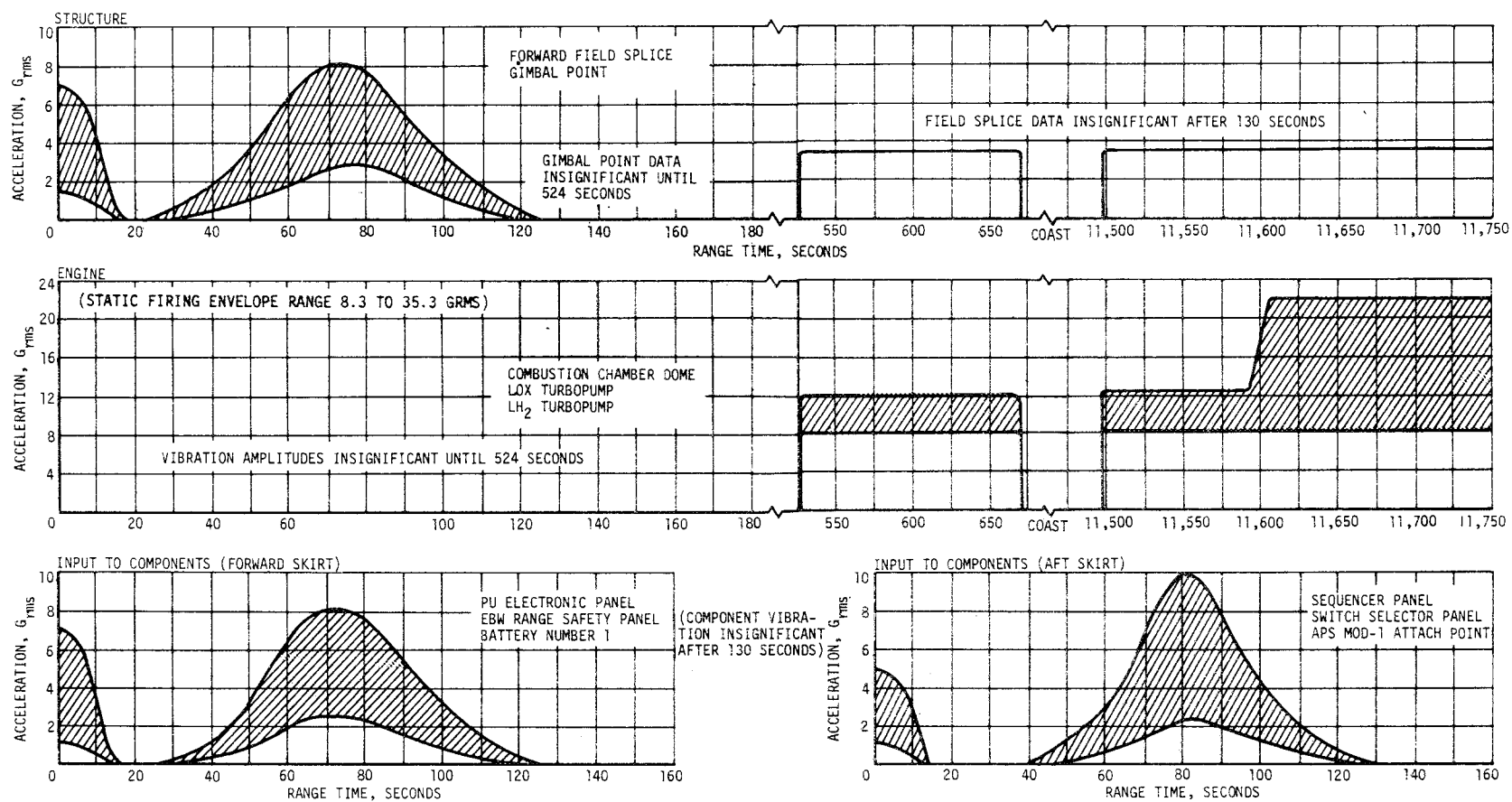


Figure 9-17. S-IVB Stage Vibration Envelopes

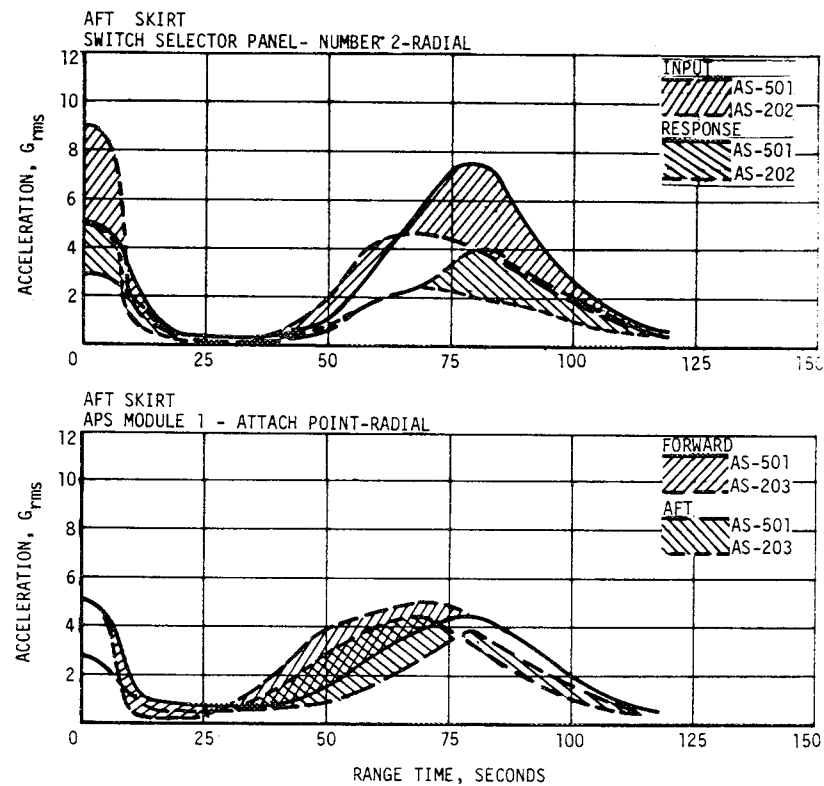
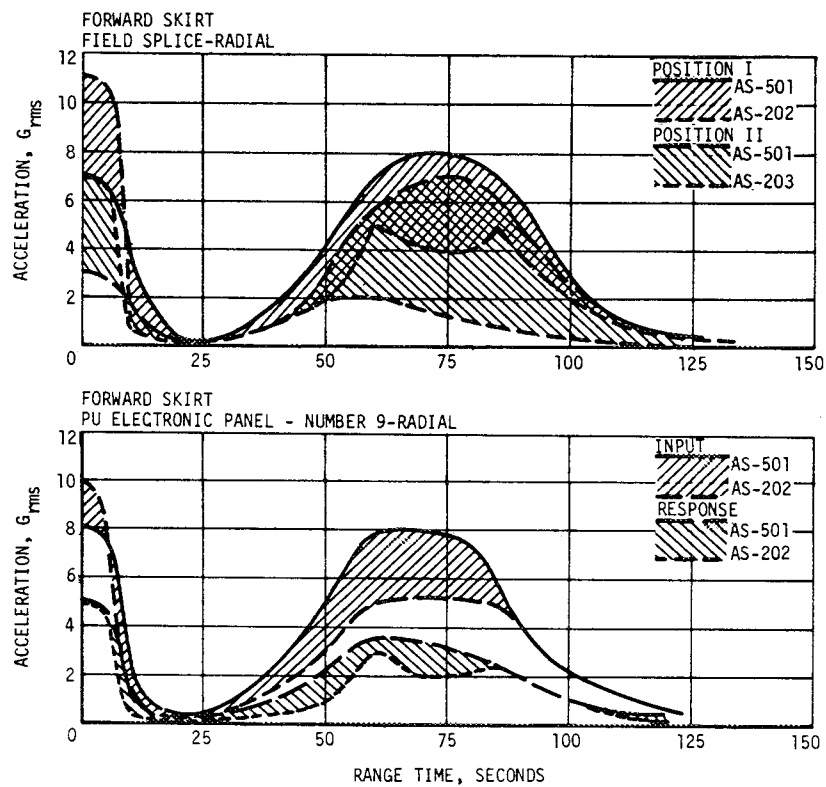


Figure 9-18. Comparison of Similar Forward and Aft Skirt Vibration Measurements (AS-501 and IB Flights)

9.3.3.1 S-IVB Stage Structure and Components - For comparison purposes the S-IVB structure and component composite vibration levels are shown with measurements taken during Saturn IB flights. The S-IVB structure and component composite vibration levels were lower at liftoff and higher in the high dynamic pressure portion of the AS-501 flight.

9.3.3.2 S-IVB Stage J-2 Engine - The J-2 engine vibration levels were insignificant during the S-IC and S-II powered portions of the flight. The levels measured during the first burn of the S-IVB were the same as levels measured during acceptance firing. No calibrations were made during the second burn and the data shown are based upon the calibrations made during the first burn. The increase in the vibration envelope part way through the second burn coincides in time with the change in engine mixture ratio. This dependency has also been noted during acceptance firings.

#### 9.3.4 Instrument Unit Evaluation

Eight measurements were used on the IU for monitoring structural vibration at the upper and lower interface rings and 20 measurements were used to monitor IU component vibration. For comparison purposes the IU structure and component measurements are shown with those taken during the Saturn IB AS-201 flight. Figure 9-19 shows the Grms time histories of these measurements. In general, higher vibration levels were experienced on AS-501 except that the component vibration was greater at liftoff on AS-202. On AS-501 the levels were generally higher at Mach 1/Max q than at liftoff and became negligible after S-IC powered flight. The external acoustics reported in section 16.4.1 follow the same trend as the vibrations.

9.3.4.1 Instrument Unit Structure - The structural vibration levels at the S-IVB/IU interface were, in general, lower than those encountered at the IU/SLA interface, but the spread of data between the interface rings was rather narrow.

9.3.4.2 Instrument Unit Components - The component vibration measurements exhibit a broader range of data than the structural measurements due to the different response characteristics of the various components. The upper portion of the component data envelopes was determined by the perpendicular measurements on the flight control computer and the gas bearing supply panel. Most of the lower portion of the envelope was determined by the three ST-124M-3 Inertial Platform gimbal measurements E1-603, E2-603, and E3-603. One anomaly was noted as a result of the component vibration evaluation. The vibration input to the ST-124M-3 Inertial Platform at liftoff exceeded the random test specification, R-P&VE-SVE-64-240, to which the platform was qualified. Power spectral density (PSD) plots for measurements E37-603, E36-603, E38-603, E43-603 and E44-603 are compared to the test specification in Figure 9-20. The measurement locations are also shown in Figure 9-20. Note that the tangential vibration is within the specification limits. However, the longitudinal and perpendicular vibrations exceed the specification

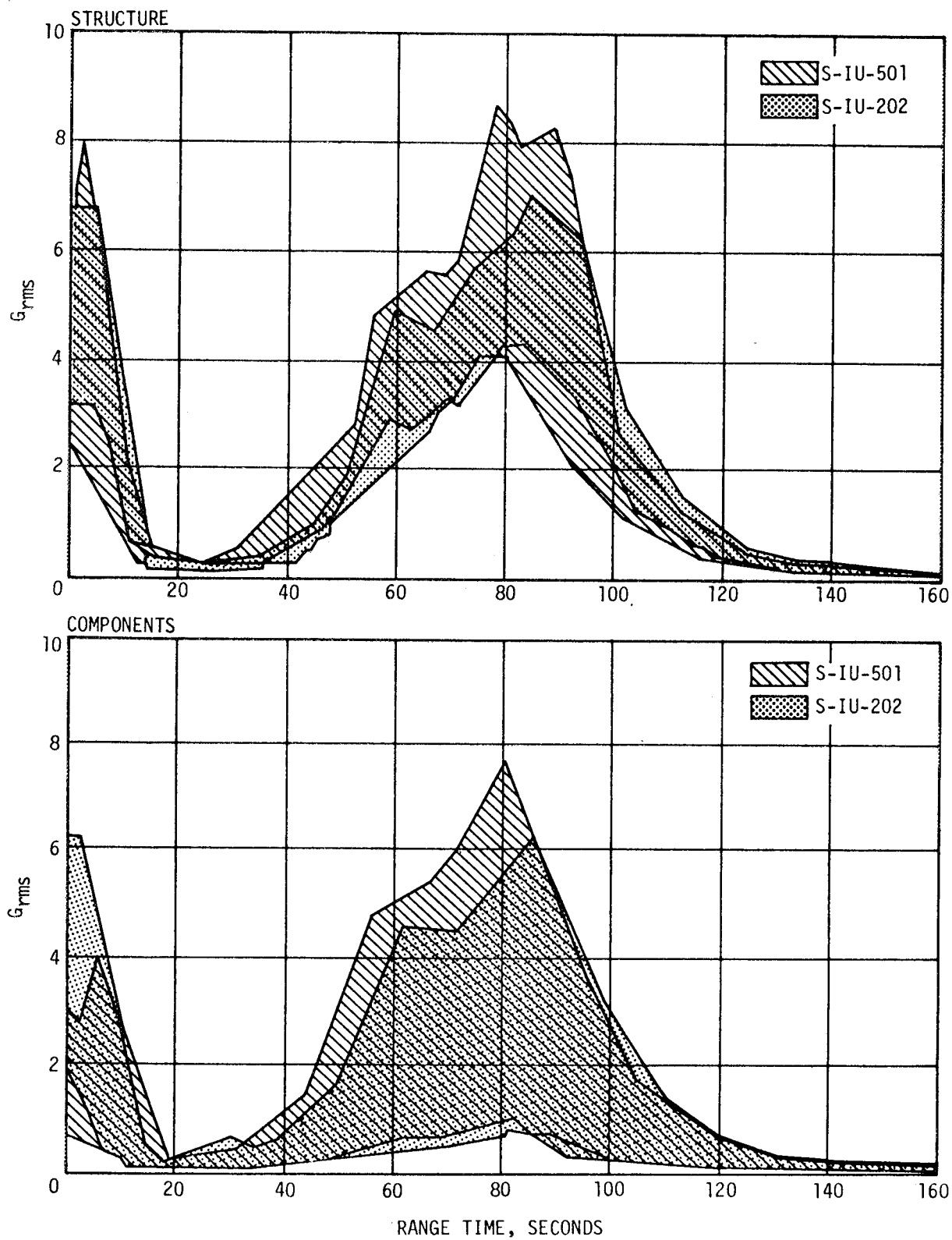
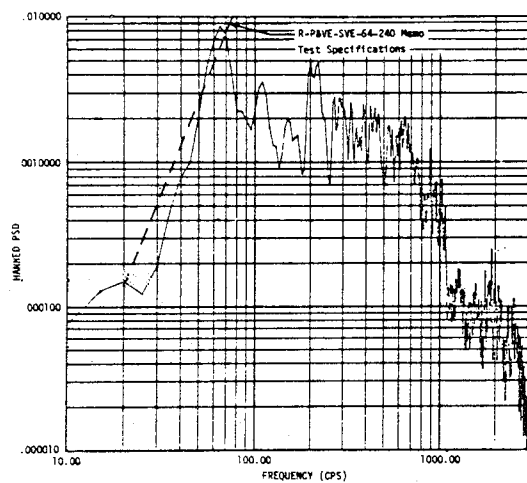
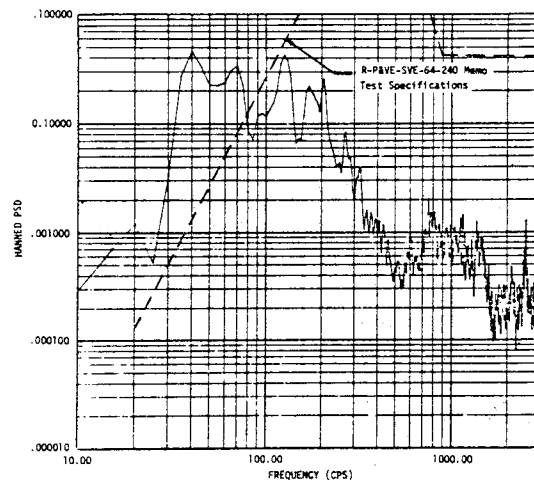


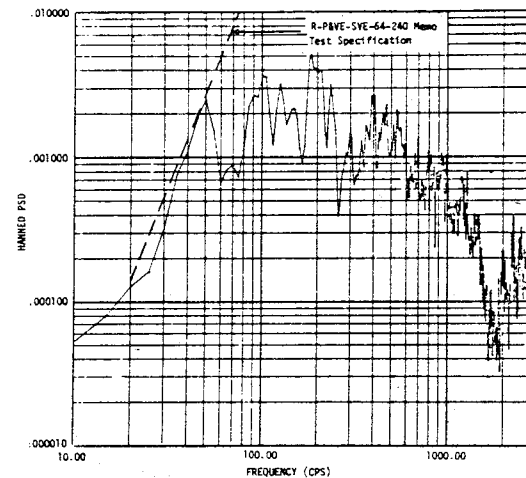
Figure 9-19. Instrument Unit Vibration Envelopes



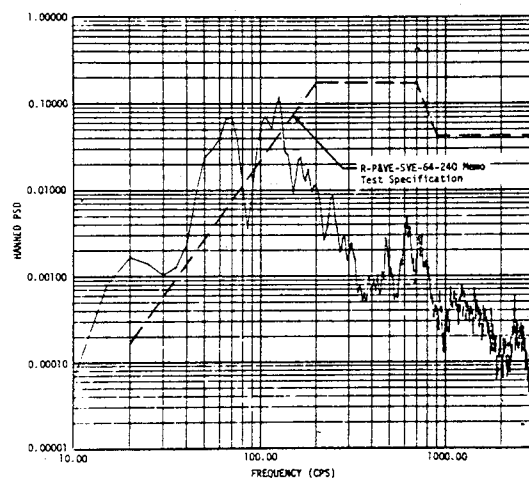
Longitudinal Vibration at the Base of the Lower Right Support Bracket (Measurement Number E37-603)



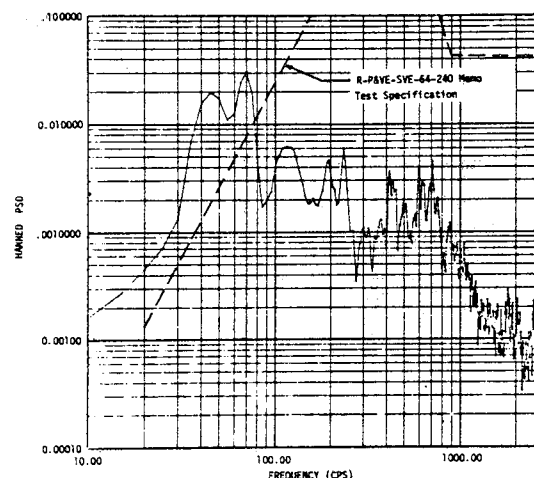
Perpendicular Vibration at the Base of the Lower Right Support Bracket (Measurement Number E36-603)



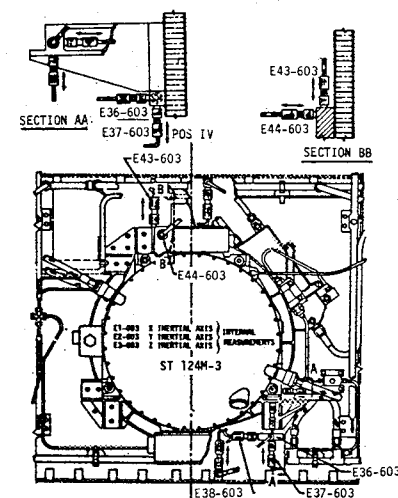
Tangential Vibration at the Base of the Lower Right Support Bracket (Measurement Number E38-603)



Longitudinal Vibration at the Base of the Upper Support Bracket (Measurement Number E43-603)



Perpendicular Vibration at the Base of the Upper Support Bracket (Measurement Number E44-603)



ST-124M-3 Vibration Measurement Numbers and Transducer Locations

Figure 9-20. Power Spectral Densities of Inertial Platform Input Vibration



at the lower frequencies. No adverse effects were noted in the performance of the inertial platform due to vibration (refer to paragraphs 10.2 and 10.5.1), however, specification changes are under consideration to bring the test spectra more in line with the observed liftoff environment.



## SECTION 10 GUIDANCE AND NAVIGATION

### 10.1 SUMMARY

The Navigation and Guidance System of AS-501 performed satisfactorily throughout boost phase of flight. The accumulation of velocity pulses near liftoff which occurred in the Z (cross range) axis during the AS-202 flight, did not occur in the X, Y, or Z axes during the AS-501 flight. Gimbal angle reasonableness test failure, as observed in the X gimbal angle on the AS-202 flight, did not occur on the AS-501 flight. Initial pitch, yaw, and roll maneuvers were performed as expected. The yaw maneuver was initiated at 1.26 seconds and terminated at 10.16 seconds.

Shortly after S-II stage ignition, a +1.3 degree ladder output was generated by the Launch Vehicle Digital Computer/Launch Vehicle Digital Adapter (LVDC/LVDA) due to a positive clockwise torque which developed a positive roll in the vehicle. The positive roll rate was nulled out by the ladder command and a +1.3 degree roll offset remained throughout S-II stage burn. Steering misalignment corrections were developed by the LVDC shortly after iterative guidance mode (IGM) initiation. At S-II stage engine cutoff, the positive clockwise roll torque was removed.

From 11,595 seconds to 11,620 seconds, commanded (CHI) rates of a maximum 1.0 degree-per-second in positive pitch and negative yaw were commanded in response to fifth phase IGM calculations. During this time, a positive roll on the vehicle was observed. The roll reached a maximum value of 2.2 degrees at 11,617 seconds and decreased to zero at 11,638.4 seconds when CHI rates reached zero.

All programmed maneuvers were completed satisfactorily during AS-501 orbital guidance.

### 10.2 GUIDANCE SYSTEM DESCRIPTION

The ST-124M Inertial Platform is a three-gimbal configuration with gas bearing gyros and accelerometers mounted on the stable element to provide a space-fixed coordinate reference frame for attitude control and for navigation measurements. Vehicle accelerations and rotation are sensed relative to this stable element. Gimbal angles are measured by resolvers, which have fine and coarse outputs, and inertial velocity is obtained from accelerometer head rotation in the form of encoder outputs, which have redundant channels.

The following changes were incorporated in the AS-501/IU platform to eliminate an accelerometer problem caused by vehicle vibration on uprated Saturn I vehicles.

- a. Three channel iron supports were placed on the outside of the AS-501/IU at the mounting points of the platform for vibration attenuation.
- b. The accelerometer float stops were changed from +3.0 and -3.5 degrees freedom to  $\pm 6$  degrees in freedom to prevent the float striking the mechanical stops during periods of high vibration levels at critical frequencies.

A block diagram of the Navigation, Guidance, and Control System is shown in Figure 10-1 and described in Appendix B.

The LVDC orbital program consists of two interruptable monitor routines. The first is the Instrument Unit Hardware Evaluation Program (HEP), and the second is the Telemetry Executive Program (TEP). Navigation, guidance, event sequencing, attitude control, and ground command processing are initiated on an interrupt basis from either HEP or TEP.

During orbital flight and when the vehicle is not over a ground station, the HEP routine is exercised. That is, the computer will be engaged in addressing the Computer Interface Unit (CIU), compressing CIU and LVDC data, and executing computer self-test.

Once the vehicle acquires a ground station, TEP is entered as the program major loop. This routine provides time sharing telemetry compressed and real time data. In addition, command system data and various special data are telemetered on an interrupt basis. Data from the LVDA is telemetered automatically.

Ground command processing is accomplished by the Command Receiver interrupt with the Digital Command System (DCS) routine. The DCS routine processes all ground commands, provides data and mode verification, and supplies the necessary information to the various affected routines.

### 10.3 GUIDANCE INTELLIGENCE ERRORS

The postflight guidance hardware error analysis is based on comparisons of the measured velocities with tracking and/or an established trajectory. Figure 10-2 presents comparisons of the platform-measured velocities with corresponding values from the final GLOTRAC data.

The accuracy of the postflight powered trajectory to parking orbit is not as good as desired. However, the excellent agreement between GLOTRAC and the postflight trajectory during S-IVB second burn indicated a very good trajectory for that portion of flight. The small velocity differences accumulated during S-IVB second burn between guidance and tracking indicated

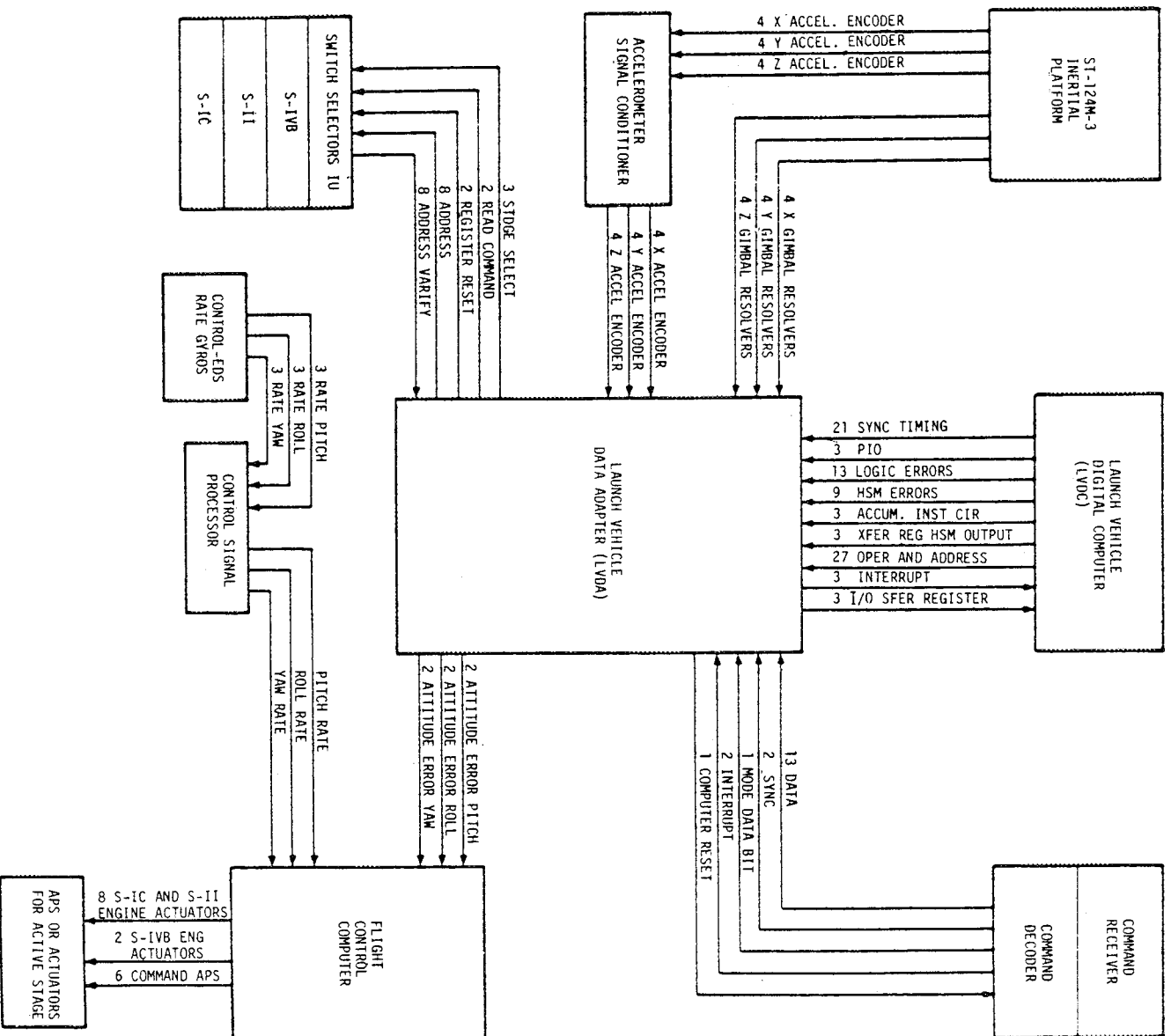


Figure 10-1. Navigation, Guidance, and Control System Block Diagram

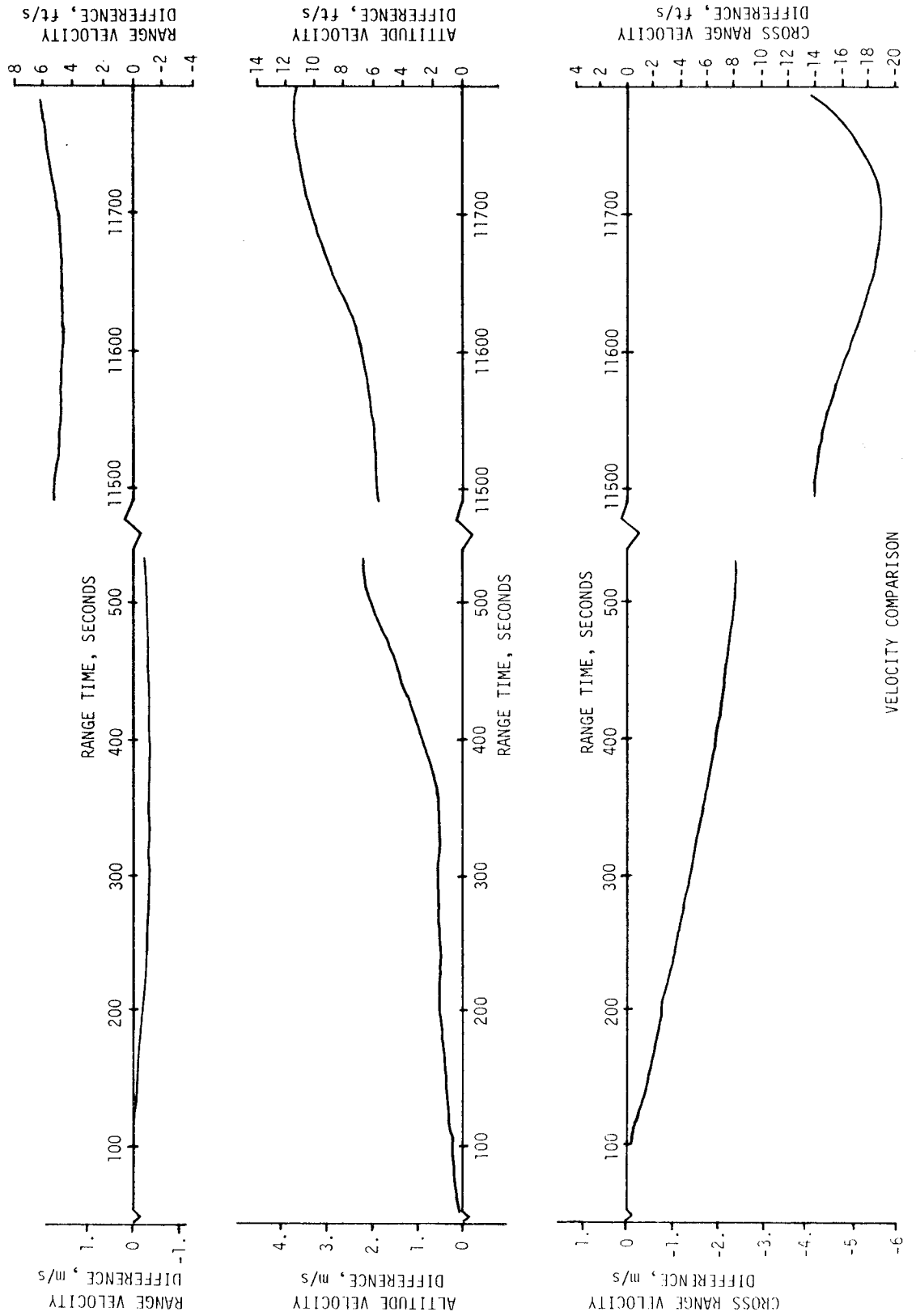


Figure 10-2. Velocity from Glotrac Minus Velocity from Guidance

very small hardware errors. No hardware error analysis is presented at this time due to late arrival of GLOTRAC data.

The bias error of each accelerometer was checked by two methods:

- a. Telemetered velocity outputs, received from the Instrument Unit after spacecraft separation, were plotted over extended periods of time to determine the acceleration during free fall. These accelerations should represent the errors due to bias. These errors were essentially the same magnitude as the preflight measurements. Any difference noted was less than  $\pm 1.0 \times 10^{-4} \text{ m/s}^2$  ( $3.3 \times 10^{-4} \text{ ft/s}^2$ ).
- b. Solutions from the postflight Orbital Correction Program (OCP) using the measured velocity changes were compatible with the bias terms shown. Curve fits of compressed telemetry of the accelerometer readings were used in the OCP.

The platform-measured velocities are shown in Table 10-1, along with values from the reference trajectory at corresponding event times. The values shown at S-IVB second burn cutoff and injection are velocities accumulated after time base 6 (11,159.58 sec). No discrepancy was noted between the data telemetered from the accelerometer pickoffs and the accumulated velocities from the LVDC. Any discrepancies between the comparisons shown in Table 10-1 and the differences shown in Figure 10-1 are due to differences between GLOTRAC and the postflight trajectory.

#### 10.4 NAVIGATION AND GUIDANCE SCHEME EVALUATION

##### 10.4.1 Guidance Comparisons

Navigation parameters at event times are shown in Table 10-2. Values from both the operational and postflight trajectories are shown for comparison with the LVDC computed values. The differences are relatively small for the launch phase events. Deviations between LVDC and postflight trajectory values reflect any errors in the guidance hardware and the accuracy of the trajectory. The differences between the LVDC and operational trajectory reflect nonstandard flight conditions and vehicle performance. The large differences noted at injection into waiting orbit are explained in the following paragraphs.

Table 10-3 presents comparisons of the postflight trajectory with the LVDC navigational parameters along with a similar comparison between the operational or preflight trajectory and predicted LVDC values. At 765.9 seconds the guidance computer went into the orbital navigation mode using a preloaded venting profile instead of the measured accelerations. The preloaded vent acceleration was intentionally held constant at a lower value (see Figure 4-6, Section 4) than the expected venting. This bias was applied to

Table 10-1. Guidance Inertial Velocity Comparisons

EVENTS	VELOCITY	TELEMETERED ACCELEROMETER m/s (ft/s)	GUIDANCE COMPUTER m/s (ft/s)	POSTFLIGHT TRAJECTORY m/s (ft/s)
S-IC OECO	$\dot{X}$	2155.6 (7072.0)	2155.6 (7072.0)	2155.5 (7071.7)
	$\dot{Y}$	2549.7 8364.1	2549.7 (8365.0)	2551.2 (8369.9)
	$\dot{Z}$	-2.6 (-8.4)	-2.6 (-8.4)	-3.0 (-9.8)
S-II Cutoff	$\dot{X}$	6641.4 (21789.2)	6641.4 (21789.2)	6641.1 (21788.2)
	$\dot{Y}$	3357.7 (11015.9)	3357.7 (11015.9)	3359.7 (11022.7)
	$\dot{Z}$	-3.6 (-11.8)	-3.6 (-11.8)	-6.3 (-20.7)
S-IVB First Cutoff	$\dot{X}$	7594.7 (24916.8)	7594.7 (24916.9)	7594.2 (24915.4)
	$\dot{Y}$	3118.0 (10229.7)	3118.0 (10229.6)	3119.9 (10235.9)
	$\dot{Z}$	2.5 (8.0)	2.5 (8.0)	-0.4 (-1.4)
Parking Orbit Insertion	$\dot{X}$	7596.8 (24923.7)	7596.8 (24923.7)	7596.3 (24922.2)
	$\dot{Y}$	3117.5 (10227.9)	3117.5 (10227.9)	3119.4 (10234.2)
	$\dot{Z}$	2.5 (8.2)	2.5 (8.2)	-0.4 (-1.2)
S-IVB Second * Cutoff	$\dot{X}$	2534.6 (8315.6)	2534.6 (8315.6)	2534.8 (8316.3)
	$\dot{Y}$	-63.2 (-207.3)	-63.2 (-207.3)	-61.8 (-202.7)
	$\dot{Z}$	-1140.8 (-3742.6)	-1140.8 (-3742.6)	-1141.0 (-3841.8)
Injection * (S-IVB CO + 10 Sec)	$\dot{X}$	2537.1 (8323.8)	2537.1 (8323.8)	2537.3 (8324.5)
	$\dot{Y}$	-66.3 (-217.4)	-66.3 (-217.4)	-64.9 (-212.8)
	$\dot{Z}$	-1142.5 (3748.4)	-1142.5 (-3748.4)	-1142.7 (-3749.1)

\*NOTE: Values represent velocity change from time base 6.  
Absolute values not applicable.



Table 10-2. Guidance Comparisons (Navigation System)

EVENT	DATA SOURCE	POSITIONS (meters) (ft)				VELOCITIES m/s (ft/s)				FLIGHT PATH ANGLE (DEG) $\gamma$
		$X_s$	$Y_s$	$Z_s$	R	$\dot{X}_s$	$\dot{Y}_s$	$\dot{Z}_s$	$V_s$	
S-IC/S-II Separation	Guidance	145710 (478051)	6435640 (21114304)	38519 (126374)	6437405 (21120095)	2542.6 (8341.8)	902.6 (2961.3)	118.6 (389.1)	2700.6 (8860.3)	NA
	Postflight Trajectory	145672 (477926)	6435810 (21114862)	38503 (126322)	6437574 (21120649)	2542.4 (8341.1)	903.5 (2964.2)	118.1 (387.5)	2700.7 (8860.6)	NA
	Preflight Trajectory	148787 (488146)	6435720 (21114566)	39161 (128480)	6437559 (21120600)	2571.4 (8436.5)	880.3 (2888.0)	133.5 (438.0)	2721.2 (8927.8)	NA
S-II/S-IVB Separation	Guidance	1716703 (5632227)	6334786 (20783418)	76976 (252545)	6563727 (21534537)	6597.8 (21646.3)	-1714.6 (-5625.2)	91.2 (299.1)	6817.6 (22367.3)	NA
	Postflight Trajectory	1716636 (5632007)	6335804 (20786758)	76257 (250187)	6564684 (21537677)	6597.5 (21645.4)	-1712.4 (-5618.2)	87.2 (286.2)	6816.7 (22364.5)	NA
	Preflight Trajectory	1711421 (5614898)	6334515 (20782529)	77468 (254160)	6562091 (21529169)	6635.1 (21768.8)	-1730.0 (-5675.9)	85.9 (281.9)	6857.5 (22498.3)	NA
S-IVB Cutoff	Guidance	2707528 (8882965)	5978208 (19613543)	89511 (293671)	6563353 (21533310)	7096.1 (23281.1)	-3215.4 (-10549.3)	82.0 (269.1)	7791.0 (25561.0)	-0.003
	Postflight Trajectory	2707505 (8882890)	5979593 (19618087)	88321 (289767)	6564595 (21537385)	7096.3 (23281.7)	-3212.0 (-10538.2)	79.2 (259.9)	7789.8 (25557.0)	0.015
	Preflight Trajectory	2663935 (8739944)	5997845 (19677969)	89010 (292028)	6563430 (21533563)	7119.4 (23357.5)	-3163.5 (-10378.8)	82.7 (271.3)	7791.0 (25561.0)	-0.001
Parking Orbit Insertion	Guidance	2778377 (9115410)	5945591 (19506532)	90327 (296348)	6563351 (21533303)	7059.4 (23160.9)	-3300.1 (-10827.1)	80.9 (265.5)	7793.1 (25568.0)	-0.002
	Postflight Trajectory	2778283 (9115101)	5946925 (19510908)	89107 (292345)	6564504 (21537086)	7059.4 (23160.8)	-3297.1 (-10817.4)	78.4 (257.3)	7791.8 (25563.7)	0.014
	Preflight Trajectory	2734965 (8972982)	5965780 (19572769)	89831 (294721)	6563431 (21533557)	7083.9 (23241.2)	-3248.7 (-10658.5)	81.6 (267.7)	7793.8 (25570.1)	0.001
Injection Second S-IVB C/O+10 Sec	Guidance	6162166 (20217080)	3172005 (10406840)	58 (190)	6930651 (22738356)	6290.0 (20636.6)	-6867.8 (-22532.1)	-1059.2 (-3474.9)	9373.0 (30751.2)	15.153
	Postflight Trajectory	6119462 (20076975)	3265209 (10712627)	-3343 (-10967)	6936095 (22756217)	6391.3 (20968.7)	-6804.1 (-22323.0)	-1058.4 (-3472.3)	9394.9 (30823.1)	15.029
	Preflight Trajectory	6168575 (20238107)	3224207 (10578107)	-11435 (-37516)	6960385 (22835909)	6355.5 (20851.3)	-6822.0 (-22381.9)	-1057.6 (-3469.8)	9383.5 (30785.8)	15.288
NA = Not Applicable										

Table 10-3. Parameter Comparisons

TIME BASE 6					ORBITAL INJECTION			
POSTFLIGHT			PREFLIGHT		POSTFLIGHT		PREFLIGHT	
PARAMETER	TRAJECTORY (OMPT)	TRAJ. MINUS GUIDANCE	TRAJECTORY	TRAJ. MINUS NAVIGATION	TRAJECTORY (OMPT)	TRAJ. MINUS GUIDANCE	TRAJECTORY	TRAJ. MINUS NAVIGATION
$x_s$ m (ft)	1998460 (6556627)	-86446 (-283615)	1972009 (6469845)	-106332 (-348858)	6119462 (20076975)	-42704 (-140104)	6188364 (20303031)	-49987 (-163999)
$y_s$ m (ft)	6264571 (20553054)	36366 (119311)	6274345 (20585121)	44175 (144931)	3265209 (10712627)	93204 (305787)	3202042 (10505387)	113943 (373828)
$z_s$ m (ft)	69595 (228330)	-2726 (-8943)	69955 (229511)	-2223 (-72933)	-3343 (-10967)	-3140 (-10301)	-13849 (-45436)	-939 (-3080)
$\dot{x}_s$ m/s (ft/s)	7415.3 (24328.4)	29.6 (97.1)	7424.7 (24359.1)	36.4 (119.5)	6391.4 (20969.1)	101.2 (332.2)	6328.0 (20761.2)	125.1 (410.4)
$\dot{y}_s$ m/s (ft/s)	-2367.8 (-7768.4)	106.2 (348.6)	-2339.0 (-7673.7)	129.5 (424.9)	-6804.1 (-22323.0)	63.7 (209.1)	-6835.5 (-22426.1)	73.4 (240.8)
$\dot{z}_s$ m/s (ft/s)	156.6 (513.9)	-1.9 (-627)	159.7 (523.8)	1.1 (3.6)	-1058.4 (-3472.3)	0.8 (2.6)	-1057.7 (-3470.2)	2.9 (9.5)
$R$ m (ft)	6575982 (21574740)	7691 (25232)	6577318 (21579127)	9234 (30300)	6936095 (22756220)	5444 (17860)	6967719 (22859970)	6861 (22510)
$v_s$ m/s (ft/s)	7785.7 (25543.7)	-4.9 (-16.2)	7786.0 (25544.6)	-5.3 (-17.4)	9394.9 (30823.1)	21.1 (69.2)	9374.8 (30757.1)	29.5 (96.8)
$\dot{x}_m$ m/s (ft/s)	8557.0 (28074.0)	8557.0 (28074.0)	7592.1 (24908.3)		11094.3 (36398.5)	8557.2 (28074.7)	10167.6 (33358.3)	
$\dot{y}_m$ m/s (ft/s)	5106.9 (16754.9)	5106.9 (16754.9)	3082.7 (10114.0)		5042.0 (16542.1)	5108.3 (16759.4)	3048.4 (10001.3)	
$\dot{z}_m$ m/s (ft/s)	27.8 (91.3)	27.8 (91.3)	3.1 (10.3)		-1114.9 (-3657.8)	27.6 (90.6)	-1140.2 (-3740.7)	
$x_g$ m/s (ft/s)	-1530.3 (-5020.7)	-1502.5 (-4929.5)	-556.1 (-1824.3)		-5091.6 (-16704.8)	-1431.1 (-4695.1)	-4228.3 (-13872.2)	
$y_g$ m/s (ft/s)	-7474.7 (-24523.3)	-7390.1 (-24245.8)	-5421.7 (-17787.7)		-11846.1 (-38865.0)	-7434.0 (-24389.8)	-9883.9 (-32427.5)	
$z_g$ m/s (ft/s)	2.50 (8.20)	3.4 (11.0)	30.2 (99.2)		-69.8 (-228.9)	6.3 (20.5)	-43.8 (-143.8)	
$\ddot{x}_g$ m/s <sup>2</sup> (ft/sec <sup>2</sup> )	-2.80 (-9.20)	0.13 (0.43)	-2.77 (-9.07)		-7.31 (-23.99)	0.068 (0.22)	-7.29 (-23.93)	0.084 (0.28)
$\ddot{y}_g$ m/s <sup>2</sup> (ft/sec <sup>2</sup> )	-8.78 (-28.82)	-0.020 (-0.066)	-8.79 (-28.84)	-0.025 (-0.082)	-3.91 (-12.81)	-0.11 (-0.34)	-3.78 (-12.40)	-0.12 (-0.41)
$\ddot{z}_g$ m/s <sup>2</sup> (ft/sec <sup>2</sup> )	-0.085 (-0.28)	0.004 (0.13)	-0.085 (-0.28)	0.004 (0.013)	0.013 (0.043)	0.004 (0.013)	0.25 (0.82)	0.001 (0.003)

obtain orbital elements which guaranteed that the spacecraft reentry path angle would not exceed -9.2 degrees for the contingency that the spacecraft propulsion system (SPS) did not ignite. A better approach to changing the orbital elements would be to retarget (i.e., change the guidance presettings). However, the retarget requirement on AS-501 came after the guidance computer flight program input deadline had passed. The decision was made to bias the vent acceleration rather than retarget because the impact was much less. Due to this biased input for orbital computations, component errors in position and velocity were large when the computer initialized for S-IVB second burn computations.

The components of acceleration due to gravity are a function of the vehicle position components. Since the components of the LVDC computed positions and velocities were significantly in error when the computer switched to the power mode of navigation for S-IVB second burn, the velocity component changes due to gravity calculations were erroneous. The predicted values in Table 10-3 were obtained by simulating a trajectory utilizing the mean expected vent profile in the trajectory model and the preloaded vent profile in the guidance computer model. The postflight orbital trajectory analysis indicates that the actual vent profile was approximately 15 percent less than the mean. Reducing the differences shown in the preflight columns by this percentage brings them into agreement with the actual differences experienced.

A study of Table 10-4 will show why the velocity differences at waiting orbit injection were considerably larger than at time base 6. The space-fixed navigational velocity is equal to the algebraic sum of the inertial guidance velocity and the gravitational velocity ( $\bar{X}_S = \bar{X}_m + \bar{X}_g$ ). The small  $\bar{X}_m$  deviations are due to postflight trajectory and guidance hardware uncertainties. The navigational velocity component deviations are due to the onboard-computer calculated gravitational velocity components. A comparison has been made with the gravity computations made by the LVDC using position components from the LVDC in the gravity equations used in the postflight and the operational trajectory programs. The points checked are at time base 6 and waiting orbit injection. The outputs of the trajectory equations are identical with the LVDC outputs to the fourth decimal place. This indicates that the guidance scheme performed properly on AS-501.

Table 10-5 presents a comparison of injection parameters computed from the LVDC data and predicted navigational values. Similar values from the postflight and operational trajectories are shown in Section 4, Trajectory.

#### 10.4.2 Evaluation of Programed Flight Maneuvers

The S-IC stage roll and yaw maneuvers were performed properly. The yaw command was set at 1.26 second and was removed at 10.16 seconds. The initial roll error of -18 degrees was removed by 31.99 seconds. The time tilt began

Table 10-4. Comparison of Velocity Changes  
Time Base 6 to Orbital Injection

PARAMETER	GUIDANCE LVDC m/s ( ft/s )	TRAJECTORY (OMPT) m/s ( ft/s )	TRAJECTORY - GUIDANCE m/s ( ft/s )
$\dot{X}_s$	-1095.7 (-3594.7)	-1024.0 (-3359.7)	71.7 (235.0)
$\dot{Y}_s$	-4393.7 (-14415.1)	-4436.2 (-14554.6)	-42.5 (-139.5)
$\dot{Z}_s$	-1217.7 (-3995.0)	-1215.0 (-3986.2)	2.7 (8.8)
$\dot{X}_m$	2537.1 (8323.8)	2537.3 (8324.5)	0.2 (0.7)
$\dot{Y}_m$	-66.3 (-217.4)	-64.9 (-212.8)	1.4 (4.6)
$\dot{Z}_m$	-1142.5 (-3748.4)	-1142.7 (-3749.1)	-0.2 (-0.8)
$\dot{X}_g$	-3632.8 (-11918.5)	-3561.3 (-11684.2)	71.4 (234.4)
$\dot{Y}_g$	-4327.5 (-14197.7)	-4371.4 (-14341.8)	-43.9 (-144.1)
$\dot{Z}_g$	-75.2 (-246.6)	-72.3 (-237.1)	2.9 (9.6)
$\dot{X}_s = \dot{X}_m + \dot{X}_g$			

Table 10-5. Injection Comparisons  
(Second S-IVB Cutoff Plus 10 Seconds)

PARAMETER	SOURCE GUIDANCE	PREFLIGHT NAVIGATION	PREFLIGHT MINUS GUIDANCE	3 SIGMA TOLERANCE
Inclination (deg)	30.172	30.171	-0.001	+0.041 -0.043
Node (deg)	135.395	135.408	0.013	+0.189 -0.193
C3 m <sup>2</sup> /s <sup>2</sup>	-27173622	-27286907	-113285	+325074 -327460
(ft <sup>2</sup> /s <sup>2</sup> )	-292494430	-293713820	-1219390	+3499070 -3524750
Eccentricity	0.57233	0.57081	-0.00152	+0.00457 -0.00457

at 11.06 seconds and was arrested at 145.07 seconds. The pitch profile was executed properly. The S-IC stage cutoff time was approximately 1.1 seconds earlier than the predicted.

The S-II stage IGM was started at 190.88 seconds and Steering Misalignment Correction (SMC) at 208.4 seconds. The initial changes in the IGM pitch and yaw commands were 6.0 and 0.3 degrees, respectively. The S-II Stage Propellant Mixture Ratio Change (PMRC) was approximately 15 seconds later than predicted. This change time is, however, well within specifications. The S-II stage IGM commands were as expected.

The first S-IVB stage IGM was started at 527.65 seconds with SMC beginning at 537.2 seconds. The change in initial pitch and yaw commands was 7.4 and 0.1 degrees, respectively. The first S-IVB stage Artificial Tau was completed at 533.4 seconds with a change in the pitch command of 2.4 degrees. Artificial Tau is a computation mode that is used to achieve a smooth transition between acceleration levels from one phase of IGM to another and is based on predicted performance. The CHI Tilde steering mode was entered at 632.25 seconds and the altitude constraint terms in the guidance steering equations, dropped at this point were less than 0.1 degree. The S-IVB stage IGM performed properly with cutoff occurring at 665.88 seconds.

The parking orbit guidance was nominal. An analysis of the accuracy of the orbital navigation is under study. Orbital guidance was initiated by 681.3 seconds. The local horizontal was achieved by 713.8 seconds.

The chilldown logic worked properly and time base 6 was started near the predicted time. The reorientation attitude for reignition was achieved with the out-of-orbit IGM beginning at 11,499.99 seconds. The initial attitude commands changed from the reoriented values by 3.8 degrees and 0.4 degree in

pitch and yaw, respectively. Comparisons of the actual F/M (thrust/mass) with the predicted F/M indicate that the Mixture Ratio (EMR) reached 5.5 soon after initiation of second S-IVB burn and changed to 5.0 approximately 85 seconds after ignition. The 5.5 EMR represents approximately 11 percent higher than nominal performance. The flight program verification effort did not cover the possibility of an initial EMR of either 5.5 or 4.5 and the corresponding shift to 5.0. The maximum perturbation considered was a 5 percent high thrust and a 5.3 percent off-load of total propellant. This combination results in an acceleration perturbation of approximately 10.9 percent, but does not consider a EMR shift. The combination was considered to test the yaw command limit of 45 degrees. The EMR shift cases were not simulated. No adverse effects resulted from the high EMR and the IGM performed correctly. Rate limiting occurred when the guidance equations were staged to use Tau 3 at 11,570.0 seconds. This is expected with the change in Tau 3 of approximately 90 seconds. Tau is the product of the average exhaust velocity and the reciprocal of acceleration; it represents the amount of time required to burn all remaining vehicle mass at a constant mass flow rate. The CHI Tilde steering mode was started at 11,758.18 seconds. The pitch command was rate limited from 11,758.18 to 11,776.10 seconds. S-IV stage cutoff occurred at 11,786.27 seconds giving a second burn time approximately 15.2 seconds shorter than predicted. The shorter burn was due to the high EMR. The attitude commands were frozen through the cutoff point.

The orbital guidance commanded the separation attitude at 11,807.2 seconds, and the vehicle was within the control system deadband by 11,955.2 seconds. The command necessary to direct position one on the vehicle toward Ascension Island was started at 12,487.1 seconds.

#### 10.4.3 Orbital Routines

Data compression performed as expected for applicable periods of flight.

A sequence of four generalized switch selector commands was transmitted by MCC-H in an attempt to close the LH<sub>2</sub> continuous vent valve. The first transmission was made at 11,242.0 seconds. This sequence was repeated at 11,295.4 and 11,325.4 seconds. All commands were received and implemented by the LVDC and proper telemetry was returned. At 11,361.4 seconds, a mode command was transmitted as shown in the telemetry data. No data transmission accompanied this mode word and no Command Receiver Pulse (CRP) was issued. The command transmitting function was transferred from Texas to the Cape at this point. At 11,441.1 seconds a mode command was transmitted. This command was rejected by the program and a 20 error code was returned. This code indicated that the program was expecting a data command and received a mode command. This occurred because no data were transmitted with the mode command at 11,361.4 seconds. Operation of the program was correct.

## 10.5 GUIDANCE SYSTEM COMPONENT EVALUATION

### 10.5.1 ST-124M-3 Inertial Platform Subsystem

The performance of the ST-124M-3 Inertial Platform and associated equipment indicated nominal performance. The accelerometer pickup and servo amplifier output signals indicated normal loop operation. The oscillations seen in the accelerometer signals were typical vibration response characteristics noted in all previous vehicles. The gyro pickup and servo amplifier output signals indicated that inertial reference was maintained throughout the entire mission. The gyro loop null voltages were at or near their specified limits ( $X = \pm 60$  millivolts,  $Y = \pm 60$  millivolts) of  $\pm 100$  millivolts. The low frequency vibration observed on the platform was greater than that seen in any previous mission. The high frequency vibration (above 120 hertz) was generally the same as that observed on AS-202-IU. Opening of the accelerometer stops to  $\pm 6$  degrees prevented the vibration induced malfunction observed in AS-202-IU from occurring on AS-501-IU as shown in Figure 10-3. The excitation voltage levels, temperatures, and pressures of the platform were within design limits; performance was as predicted.

Figure 10-4 shows a comparison of the AS-202 and AS-501 vibration levels as measured by transducers mounted on the platform inertial gimbal. This graph illustrates the higher vibration level experienced at liftoff by AS-501-IU. Further information on platform vibration is contained in structures Section 9.3.4.2.

### 10.5.2 Launch Vehicle Digital Computer and Launch Vehicle Data Adapter

The LVDA and the LVDC performed as predicted for the AS-501 flight. The occurrence of one error monitor word was observed in compressed data. This indicates a disagreement of the Triple Modular Redundant (TMR) logic channels associated with the LVDA interrupt processor during the preceding dark (no data) period. This error monitor word indicates disagreement in the TMR Computer Interface Unit (CIU) interrupt logic and did not impact mission requirements.

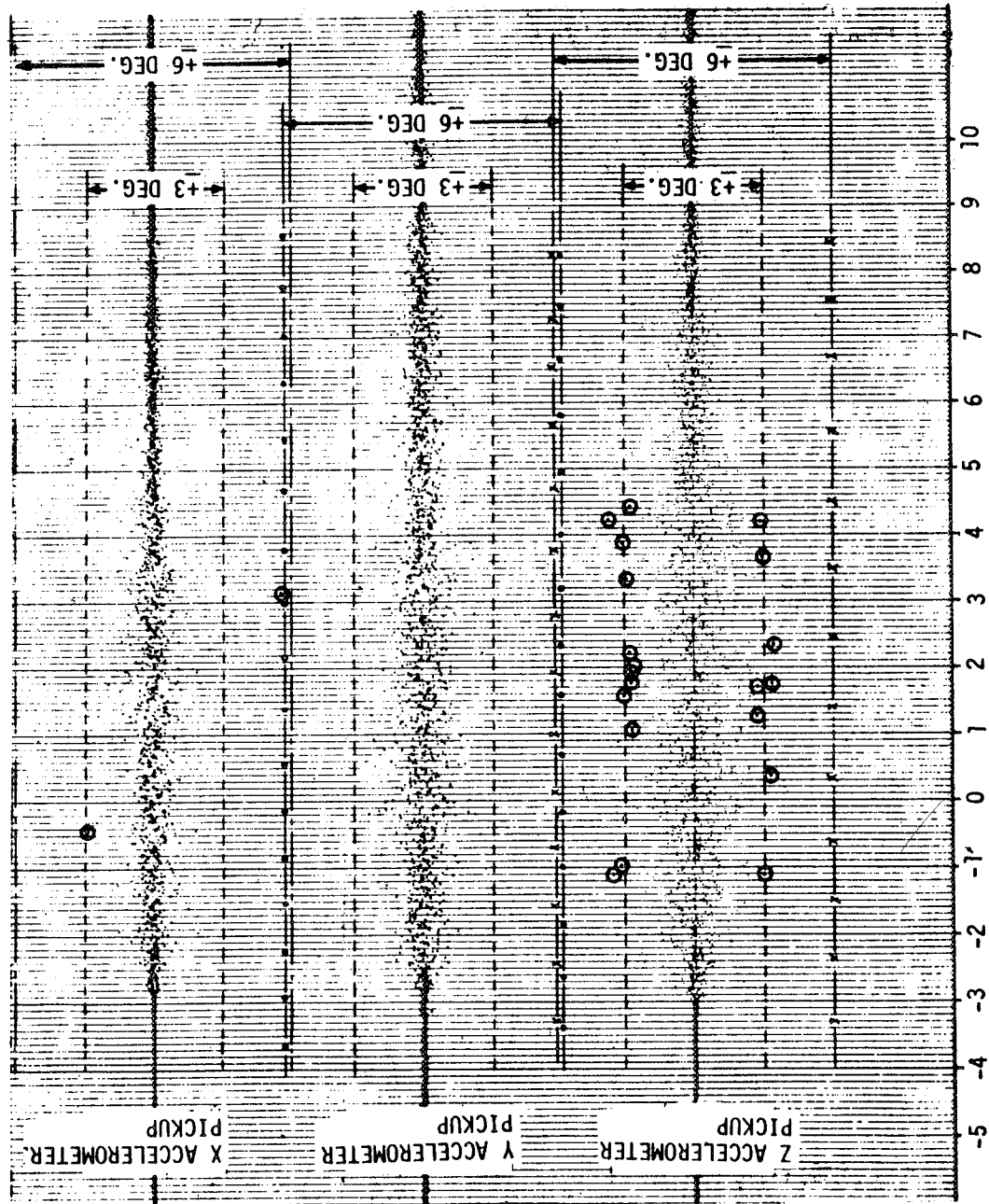


Figure 10-3. Accelerometer Pickup Outputs Vs Time (Liftoff)



10-15/10-16

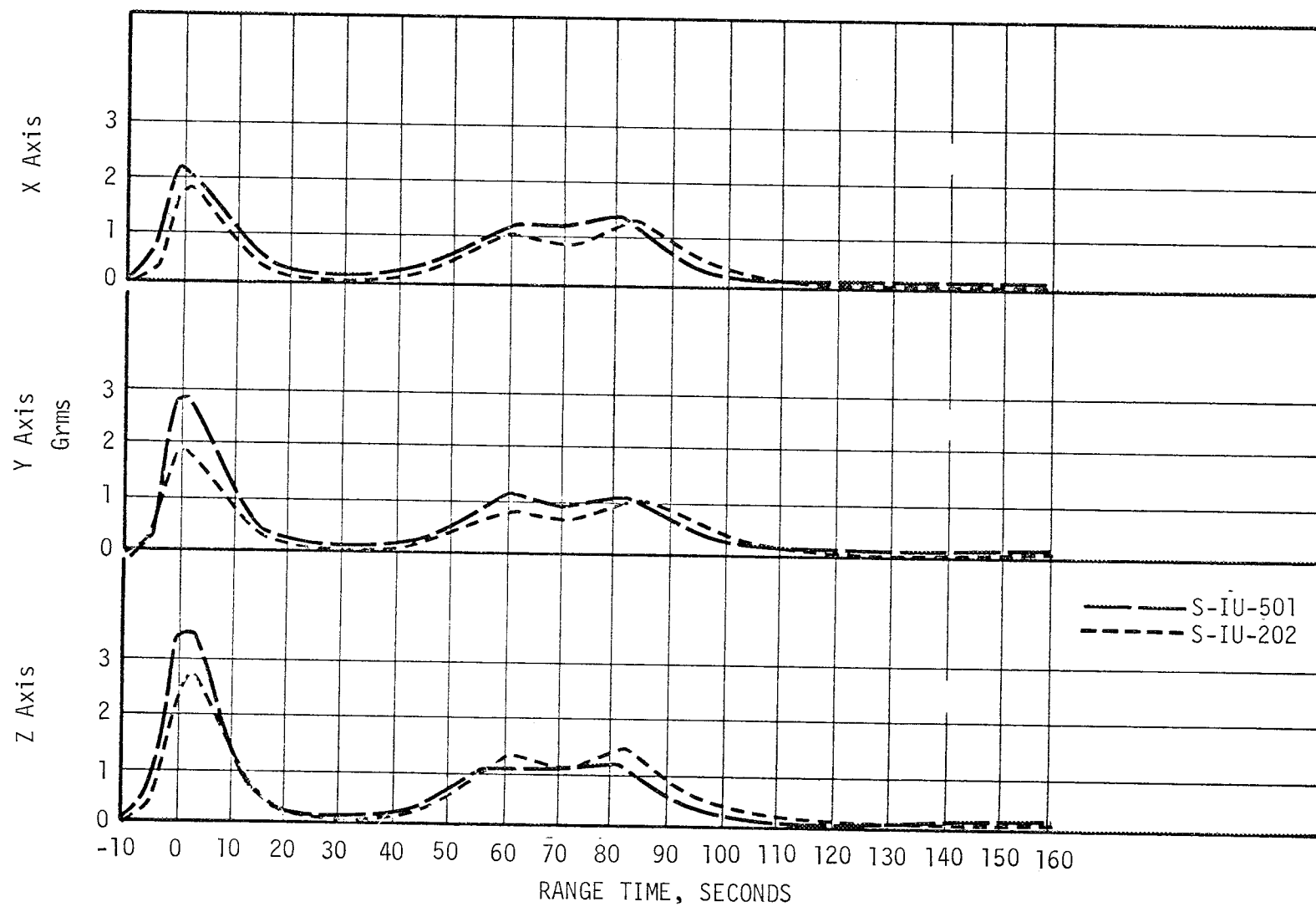


Figure 10-4. Platform Sensed Vibration for S-IU-202 and S-IU-501



## SECTION 11 CONTROL SYSTEM

### 11.1 SUMMARY

The control system performed throughout flight as expected. Liftoff transients and drift were well within expected tolerances. Vehicle liftoff acceleration, however, was substantially less than predicted apparently due to higher than expected soft release rod forces.

The maximum values of attitude errors were 1.3 degrees in pitch, and 1.0 degree in yaw and roll during S-IC powered flight.

The control system performance during S-II Stage burn was as expected. Shortly after S-II Stage ignition, a positive clockwise torque on the vehicle developed a 1.3 degree roll offset throughout the S-II Stage burn period. The roll offset was removed at S-II Stage cutoff. Cause of the roll offset may be attributed to a combination of engine misalignment and center of gravity offset.

The S-IVB stage engine control system performed normally during first and second S-IVB stage burn modes. Auxiliary Propulsion System (APS) operation was nominal throughout burn and coast periods. S-IVB control system activity during the initial portion of second burn was greater than expected due to approximately 55 seconds of J-2 engine operation at the high EMR thrust level. The S-IVB stage auxiliary propulsion system provided nominal roll control during first and second burn. It also successfully performed all required orbital maneuvers. Propellant expenditure was 62.2 percent in the module at position III and 61.8 percent in the module at position I of the APS at loss of telemetry.

Vehicle attitudes and rates were within design tolerances during S-IC/S-II, S-II/S-IVB, and S-IVB/SC separations.

### 11.2 CONTROL SYSTEM DESCRIPTION

Figure 11-1 shows the interconnection and signal flow paths for the control components. Except for attitude error commands from the guidance system, all inputs originate within the control system. A description of the control system is contained in Appendix B.

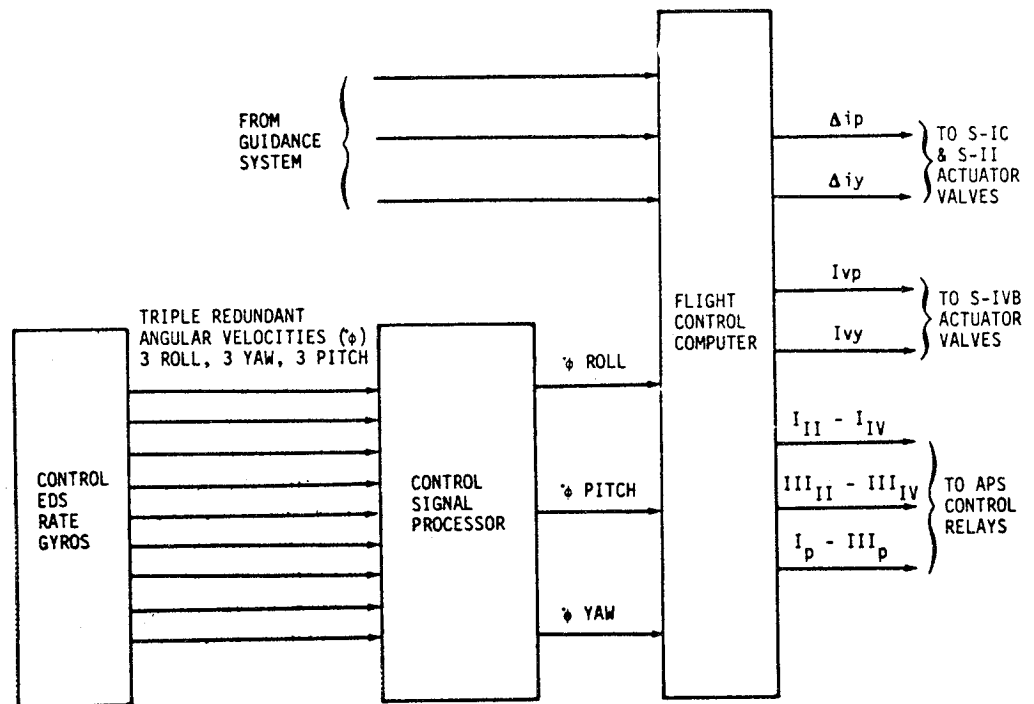


Figure 11-1. Control Components Block Diagram

Vehicle attitude correction is accomplished in accordance with the requirements of the guidance system through attitude error signals. These signals are generated by the Launch Vehicle Digital Computer (LVDC) and Launch Vehicle Data Adapter (LVDA). During S-IC stage burn attitude error commands are the result of a time tilt and roll program and occur mainly around the pitch and roll axes. At the initiation of IGM, attitude error commands become the result of guidance system computations.

Angular rate inputs are present when the control system has responded to attitude error commands and provide damping to insure that commanded changes do not occur at rates in excess of body structural limits. Vehicle attitude changes are commanded at rates of 1 degree per second or less, depending upon requirements of the guidance system.

Control system outputs are valve currents ( $I_v$ ) to first, second, and third stage engine actuators and relay currents to the APS.

### 11.3 S-IC CONTROL SYSTEM EVALUATION

This section reports the flight dynamic analysis for the SA-501 launch vehicle during S-IC flight. This includes a liftoff and tower clearance

evaluation as well as S-IC flight dynamics. Preflight dynamic analyses are contained in "Saturn V Flight Dynamics, SA-501," Boeing Document D-15509-1C. Supporting stability analysis is published in "Launch Vehicle Flight Control System Stability Analysis, SA-501," Boeing Document D5-15554-1A and updated in Boeing Memo 5-9300-H-1707 to MSFC. The update reflects the results of the Dynamic Test Vehicle Program.

The SA-501 liftoff and tower clearance is compared with the worst case preflight clearances as well as results from simulation updated with actual flight data. The S-IC dynamics are compared with updated simulation results only.

The first guidance command occurred at 1.26 seconds in the form of a 1.25 degree yaw bias returning to 0 degree in 10.16 seconds. The purpose of this command was to maneuver the vehicle away from the tower to assure tower clearance in all wind conditions.

The second guidance command was a roll command of 18 degrees that occurred at 11.06 seconds. This maneuver properly orients the vehicle along the desired launch azimuth and was completed by 31.99 seconds.

#### 11.3.1 Liftoff Clearances

Vehicle clearances of mobile launcher structure were at least 85 percent of that available. Positive clearances resulted from a favorable combination of ground wind and vehicle system misalignments. The ground wind direction was 70 degrees east of north, and the magnitude was approximately half the design wind. The combination of offset C.G., thrust unbalance, and thrust misalignment in yaw cancelled the yaw moment from center engine cant.

Table 11-1 compares the vehicle misalignments measured during flight with preflight measurements. The center engine cant calculated from flight data is 45 percent smaller than that predicted. The apparent thrust misalignment in yaw is equal to the 3 sigma value and opposes the center engine cant. As discussed below both soft release forces and the thrust-to-weight ratio are higher than anticipated. The launch ground wind is assumed to have a steady state magnitude of 8.0 m/s (26.2 ft/s). An assumed gust brings the peak to 11.5 m/s (37.7 ft/s).

Vertical motion at liftoff is shown in Figure 11-2. Although the thrust-to-weight ratio was higher than predicted, initial vertical acceleration was less. A higher-than-anticipated soft release force with an average peak value of 391,000 Newtons per rod (87,900 lb<sub>f</sub> per rod) is required to match the flight data observed by the liftoff cameras. Since the maximum values from the soft release rod force time histories are not available from the flight test data, this value cannot be confirmed.

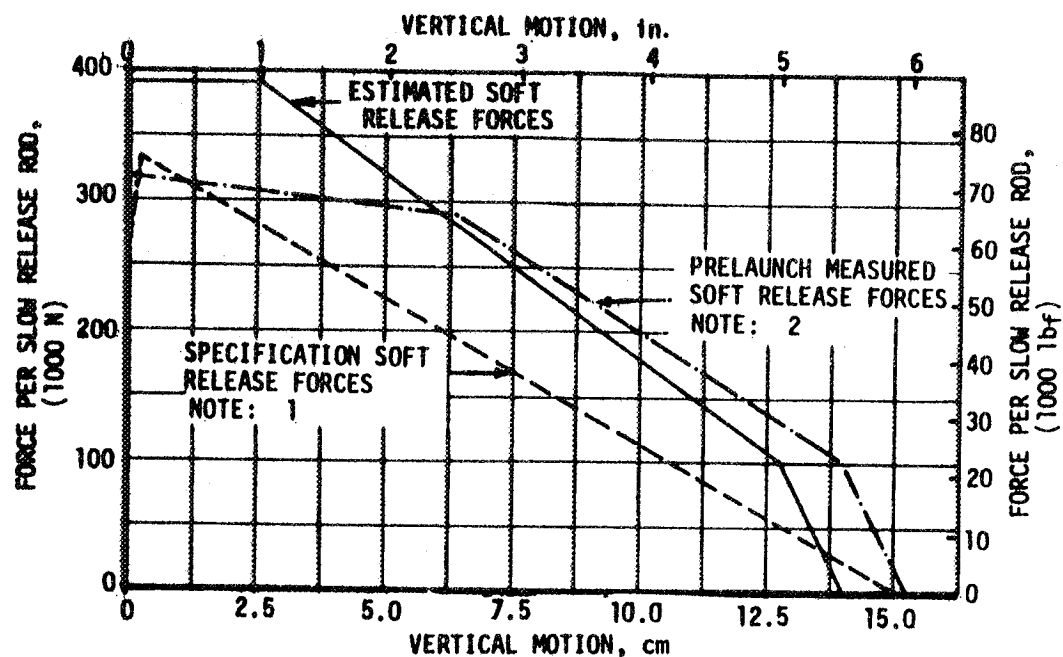
Table 11-1. SA-501 Liftoff Misalignment

	PRELAUNCH MEASURED			LAUNCH		
	PITCH	YAW	ROLL	PITCH	YAW	ROLL
Thrust Misalignment (deg)	$\pm 0.13(*)$	$\pm 0.13(*)$ (**)	$\pm 0.13(*)$	-0.07	+0.13	-0.01
Center Engine Cant (deg)	-0.56	-0.78	-	-0.31	-0.42	-
Servo Amp Offset (deg/Engine)	+0.035	-0.095	-	-	-	-
Rate Gyro Error (deg/s)	+0.03	+0.05	+0.05	-0.02	-0.00	-0.025
Platform System Errors (deg)	-0.1	-0.1	-0.25	0.0	+0.05	-0.19
Peak Soft Release Force (N/rod) (lb <sub>f</sub> /rod)		320,000 (71,940)			391,000 (87,900)	
Wind	95 Percentile Envelope			8 M/S, No Shear		
Thrust-to-Weight Ratio		1.238			1.245	

(\*) Thrust vector measurement uncertainty

(\*\*) A positive polarity was used to determine minimum fin tip/umbilical tower clearance. A negative polarity was used to determine vehicle/GSE clearances.

This uncertainty is aggravated by the momentary loss of liftoff data from measurement cameras due to a short term power failure. The indication of this trend is cause for concern. If substantially lower than predicted liftoff acceleration does exist, liftoff interference is a distinct possibility on a future vehicle with substantially less ideal combinations of wind and system misalignments. The AS-502 soft release rods should be instrumented adequately to verify this conclusion.



NOTE: 1 "CONTROLLED RELEASE MECHANISM SPECIFICATIONS FOR SATURN V, SA-501 THROUGH SA-503 VEHICLES," MSFC MEMO, R-P&VE-SLR-65-84, DATED NOVEMBER 8, 1965.

NOTE: 2 EVALUATION OF SLOW RELEASE MECHANISM AND HOLDDOWN ARMS OF SATURN V VEHICLE, BOEING DOCUMENT D5-13808, DATED SEPTEMBER 20, 1967.

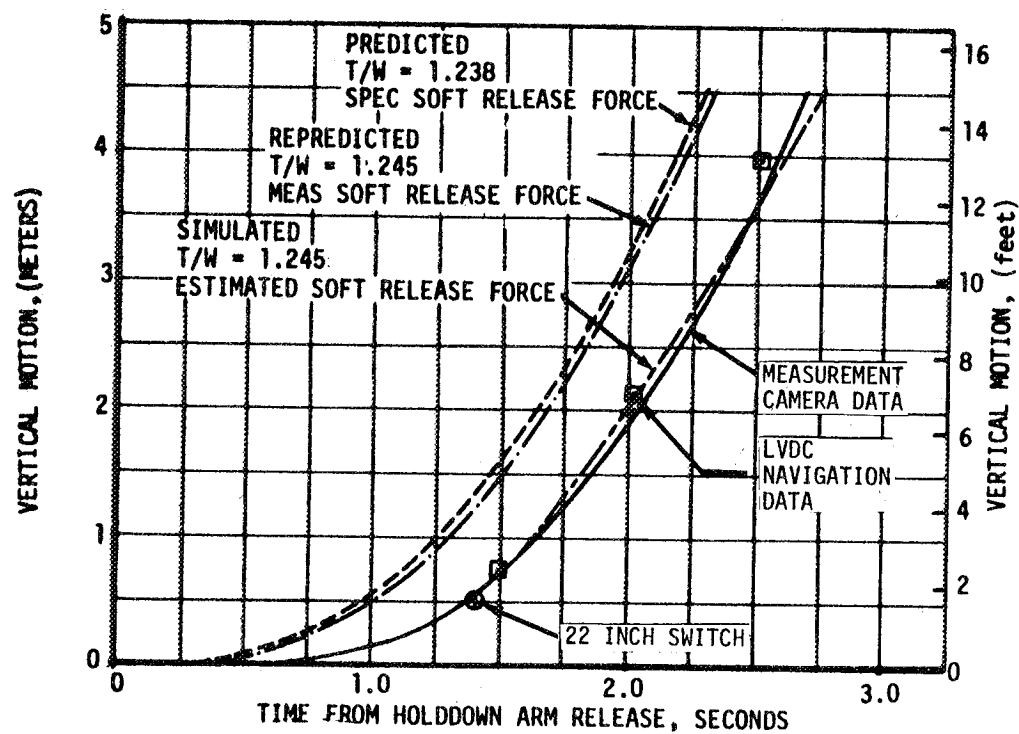


Figure 11-2. Liftoff Vertical Motion

Motion of the S-IC thrust structure and of the S-IC air scoop at position I is shown in Figure 11-3. Camera data is compared to simulated and maximum predicted clearance. Loss of camera power at liftoff caused the gap in camera data. The actual trajectory from camera data and the simulated trajectory both show nearly vertical motion of the vehicle with a maximum lateral drift of less than 2.5 centimeters (1.0 in.) after 56 centimeters (22 in.) of the vertical rise.

Clearance between the thrust structure and the protective hood at position I is presented in Figure 11-4. Only a simulated trajectory is available for this clearance. This trajectory shows very little horizontal motion, less than 2.5 centimeters (1.0 in.) in a 178 centimeter (70 in.) rise. Motion camera data showed the thrust structure was well above the hood before it closed.

Clearance between engine bell No. 4 and the holddown post at position I is shown in Figure 11-5. Only a simulated trajectory is shown for this clearance as camera data is not available. The simulated trajectory indicates a nearly vertical motion of the engine bell, traversing less than 5.1 centimeters (2.0 in.) horizontally after 610 centimeters (240 in.) of vertical rise. Motion picture camera monitoring GSE operation confirmed this conclusion.

Clearance between the tower and the S-IC fin tip is shown in Figure 11-6. Flight data was taken from a tower clearance camera located 426.7 meters (1400 ft) due west of the mobile launcher. The combination of wind blowing away from the tower and the yaw bias resulted in a clearance of 16.5 meters (54.1 ft) between the vehicle and the top of the tower. A summary of liftoff clearances is given in Table 11-2.

The exhaust plume angle of each of the five S-IC stage engines and the trajectory of the center engine gimbal are given in Figure 11-7. Translation is positive north and east. The exhaust plume angle is the angle the plume makes with the vertical at the engine gimbal point and is positive north and east.

### 11.3.2 S-IC Flight Dynamics

Time histories of conditioned vehicle attitudes compared to guidance system commands are shown in Figure 11-8. Time histories of conditioned dynamic measurements are compared with simulated results in Figures 11-9 through 11-18.

Measured and simulated vehicle attitude are shown in Figure 11-8. The yaw transient during liftoff is due to the programmed yaw maneuver which is intended to move the vehicle away from the LUT. The negative response at IECO results from removal of the center engine cant. A similar effect in pitch is not observable because of the compressed scale. The roll attitude plot illustrates the 18 degree roll maneuver that orients the vehicle pitch plane with the 72 degree launch azimuth.



YAW BIAS STARTS  
AT 1.26 SEC  
\*\* END SOFT RELEASE

PLATFORM MIS.  
PITCH .06  
YAW .04  
ROLL -.19

FLIGHT CONDITIONS

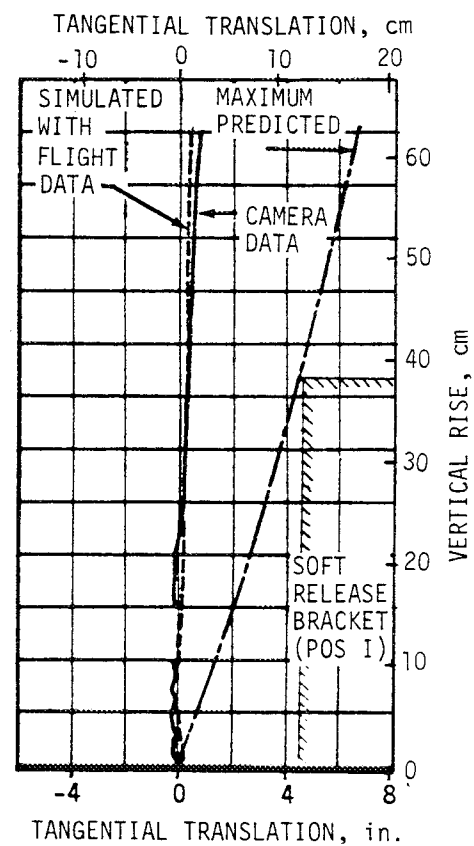
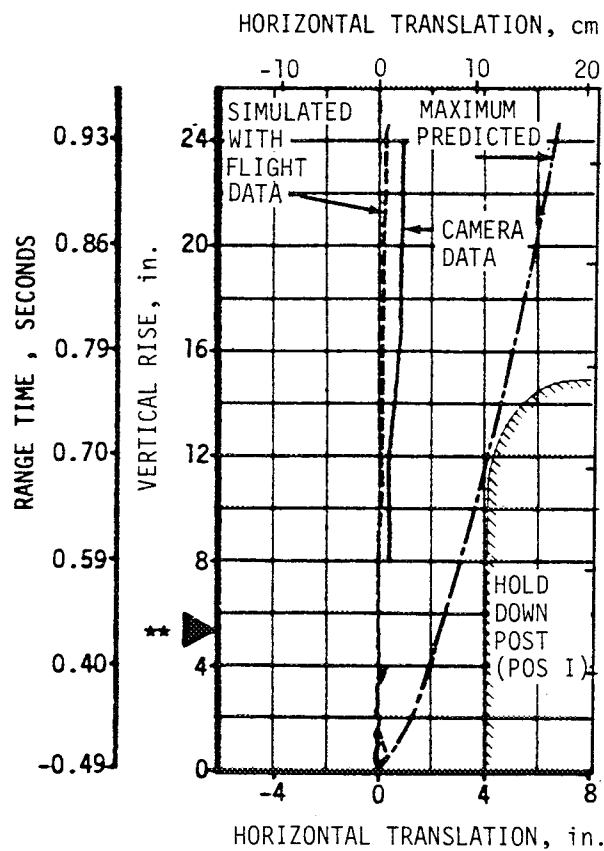
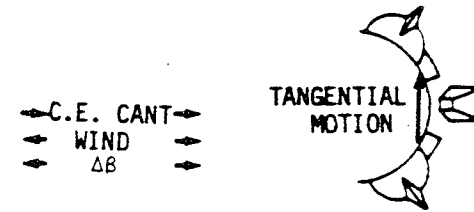
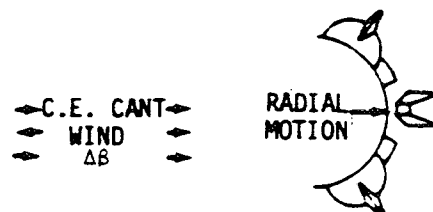
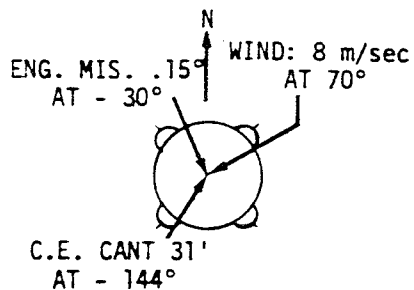


Figure 11-3. Motion at the Base of the S-IC Stage (Position I)

8-11

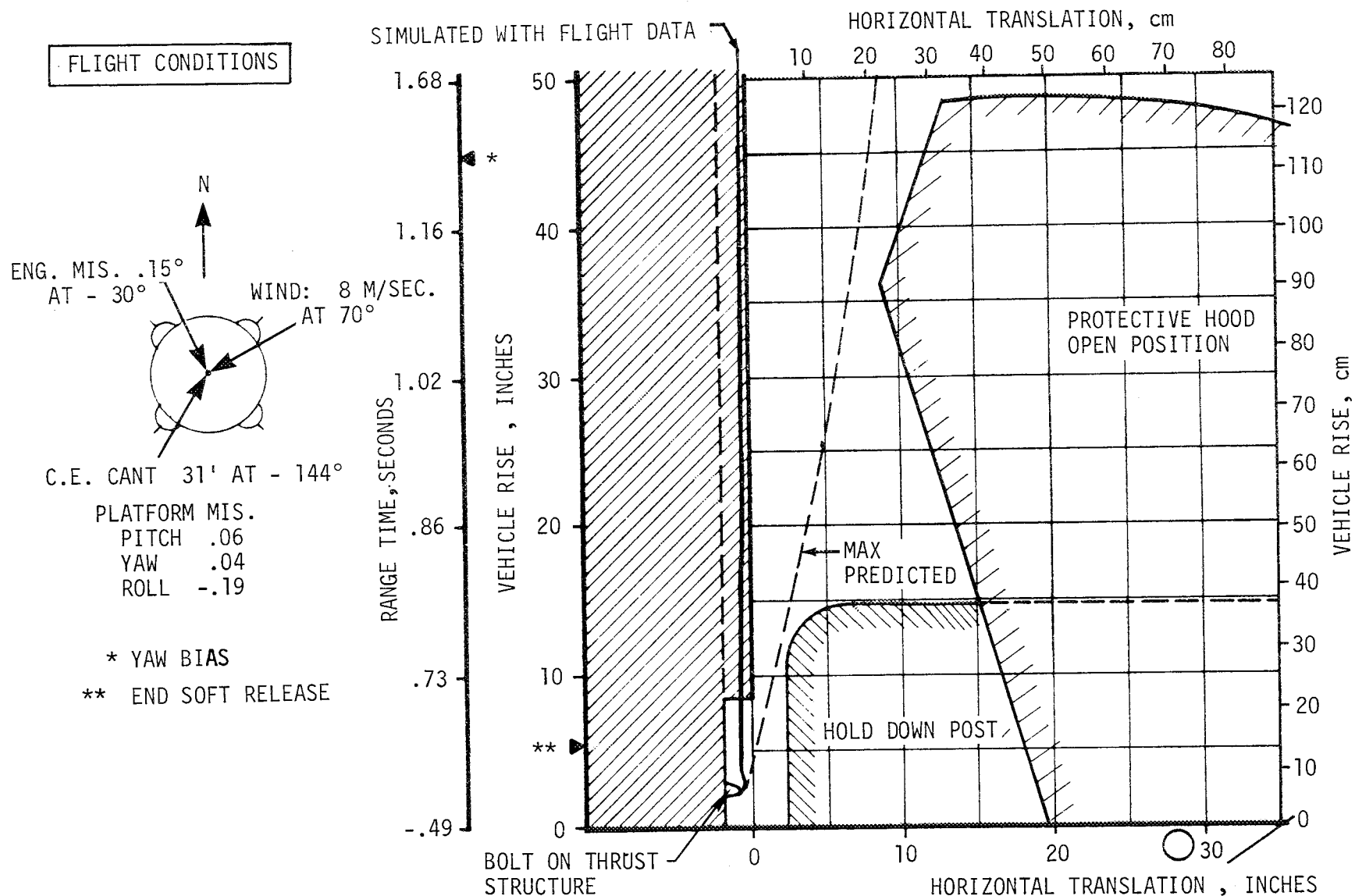


Figure 11-4. Protective Hood - Holddown Post Clearance (Position 1)

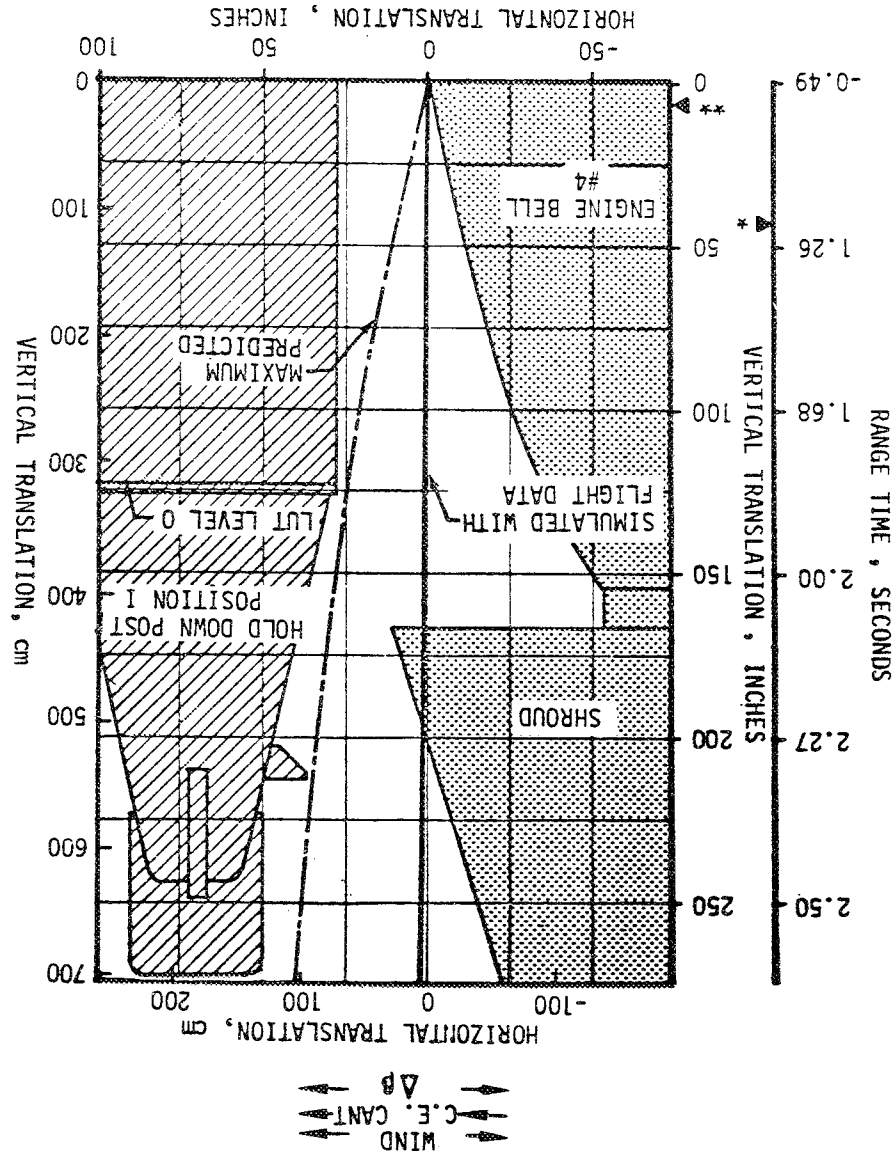
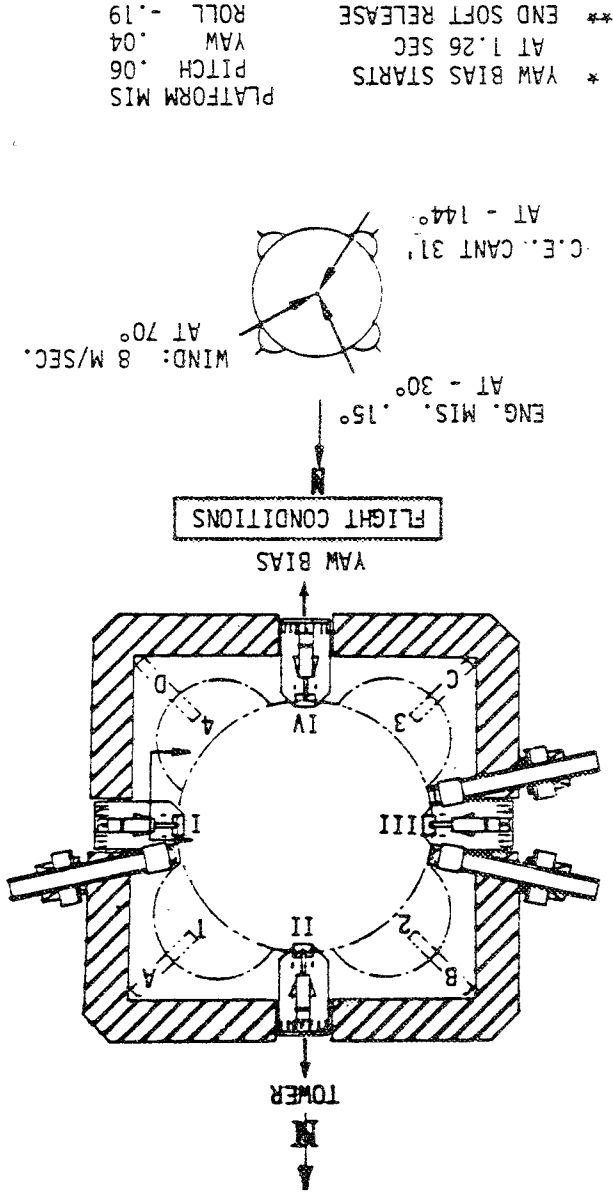


Figure 11-5. Engine Bell Clearance



11-10

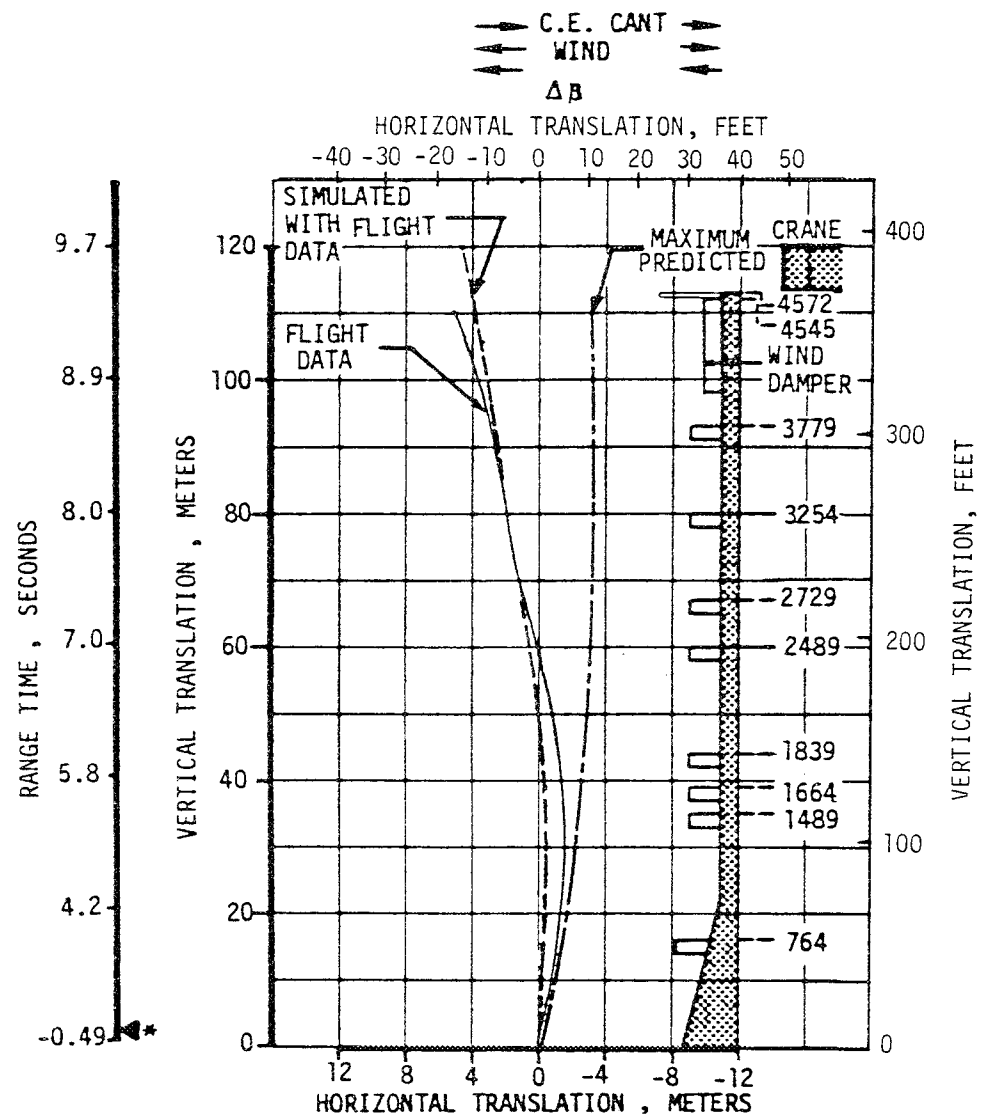
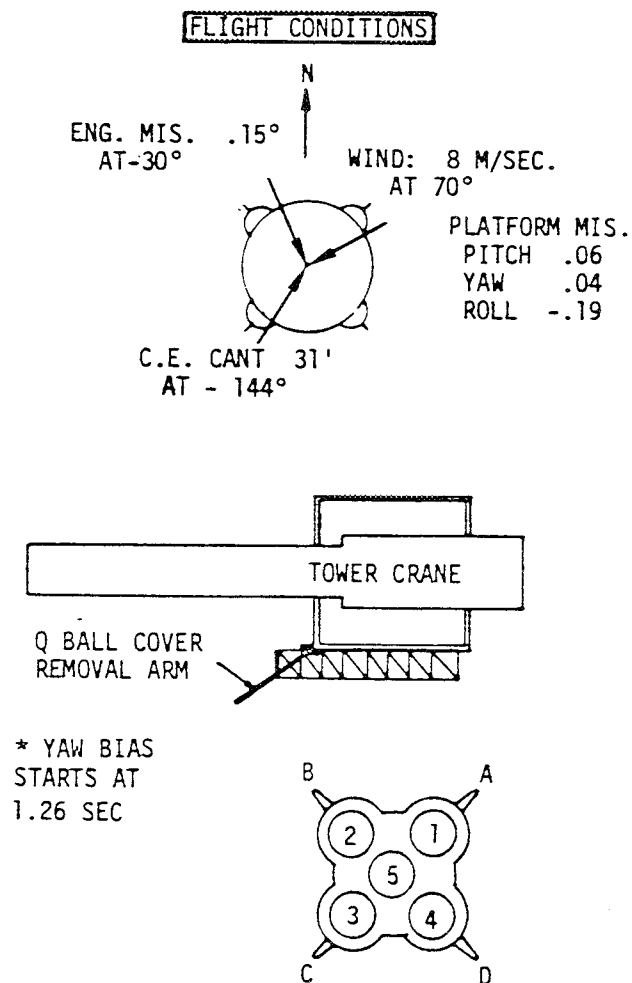


Figure 11-6. Liftoff Trajectories of Fin Tip "A"

Table 11-2. Summary of Liftoff Clearances

POTENTIAL INTERFERENCE				
VEHICLE	GROUND EQUIPMENT	AVAILABLE CLEARANCE cm (in.)	PREDICTED MINIMUM CLEARANCE cm (in.)	ACTUAL CLEARANCES cm (in.)
Thrust Structure	Holddown Post	7.75 (3.05)	1.0 (0.4)	6.9 (2.7)
Thrust Structure	Holddown Post Hood	25.40 (10.00)	7.6 (3.0)	24.1 (9.5)
Airscoops	Soft Release Bracket	11.9 (4.70)	0.3 (0.1)	10.9 (4.3)
Thrust Structure Insulation	Liftoff Switches	Variable	*	12.7 (5.0)
Airscoops	Tail Service Mast	Variable	12.7 (5.0)	**
Engine Bell	Holddown Post	96.52 (38.00)	2.5 (1.0)	94.0 (37.0)
Service Module	SM Swing Arm	Variable	101.6 (40.0)	**
S-IVB Stage	S-IVB Forward Swing Arm	Variable	101.6 (40.0)	**
S-II/S-IVB Interstage	S-IVB Aft Swing Arm	Variable	17.8 (7.0)	**
S-II Stage	S-II Forward Swing Arm	Variable	116.8 (46.0)	**
S-II Stage	S-II Intermediate Swing Arm	Variable	116.8 (46.0)	**
Fin Tip	S-IVB Aft Swing Arm	Variable	609.6 (240.0)	1117.6 (440.0)

\* Switch rolls off striker plate

\*\* Camera data indicates clearance - no quantitative data available

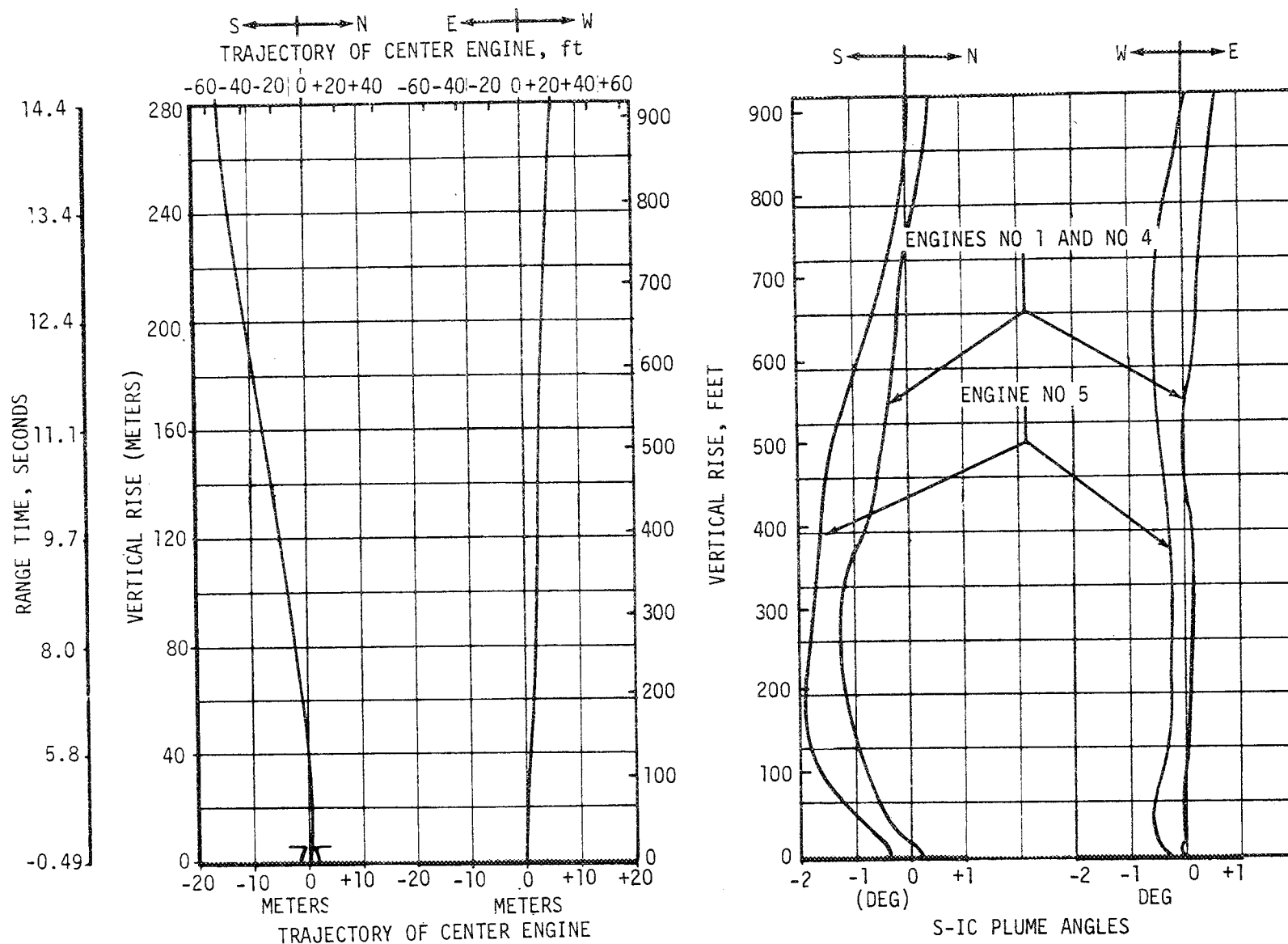


Figure 11-7. S-IC Plume Angles and Center Engine Trajectories

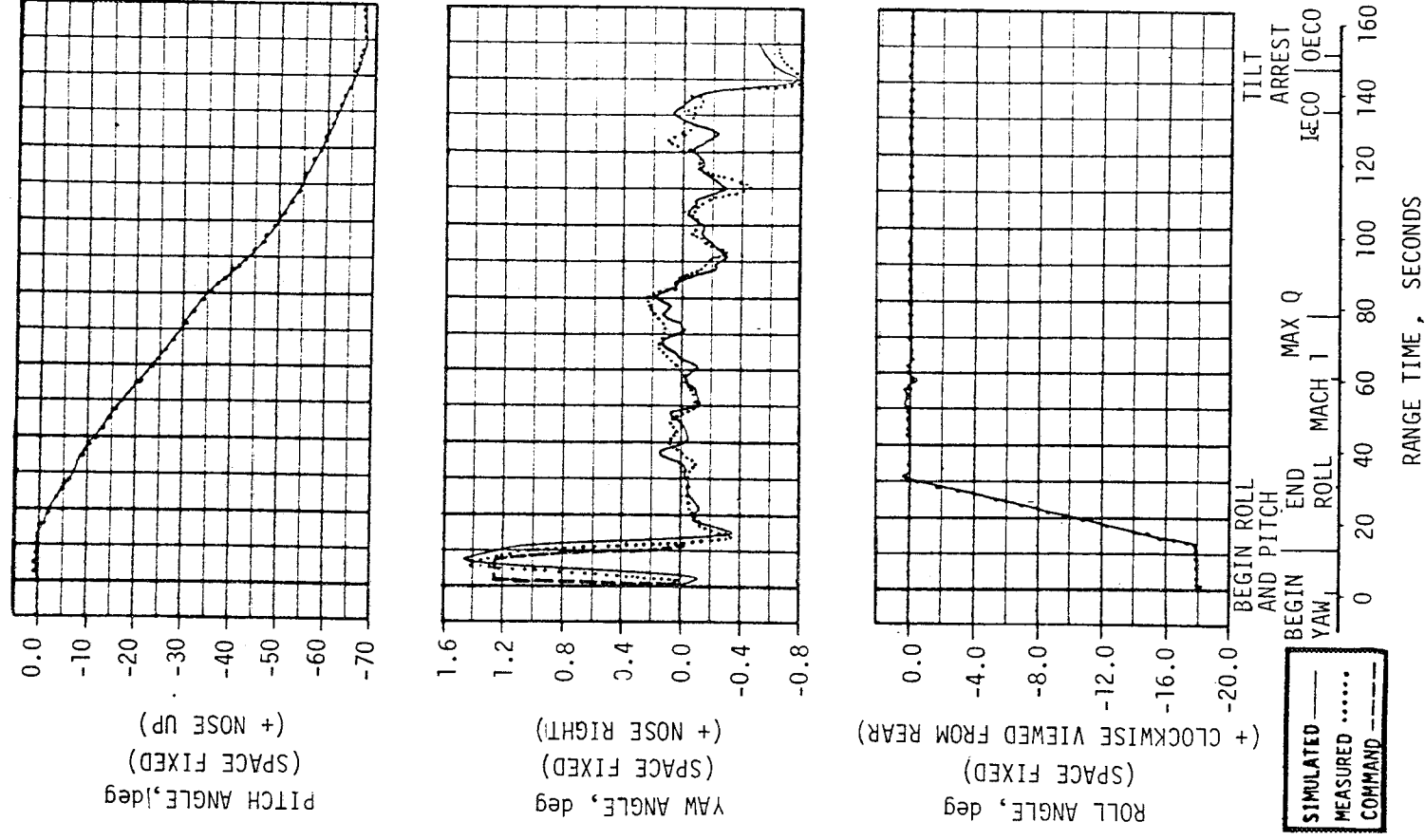


Figure 11-8. Vehicle Attitude During S-IC Burn

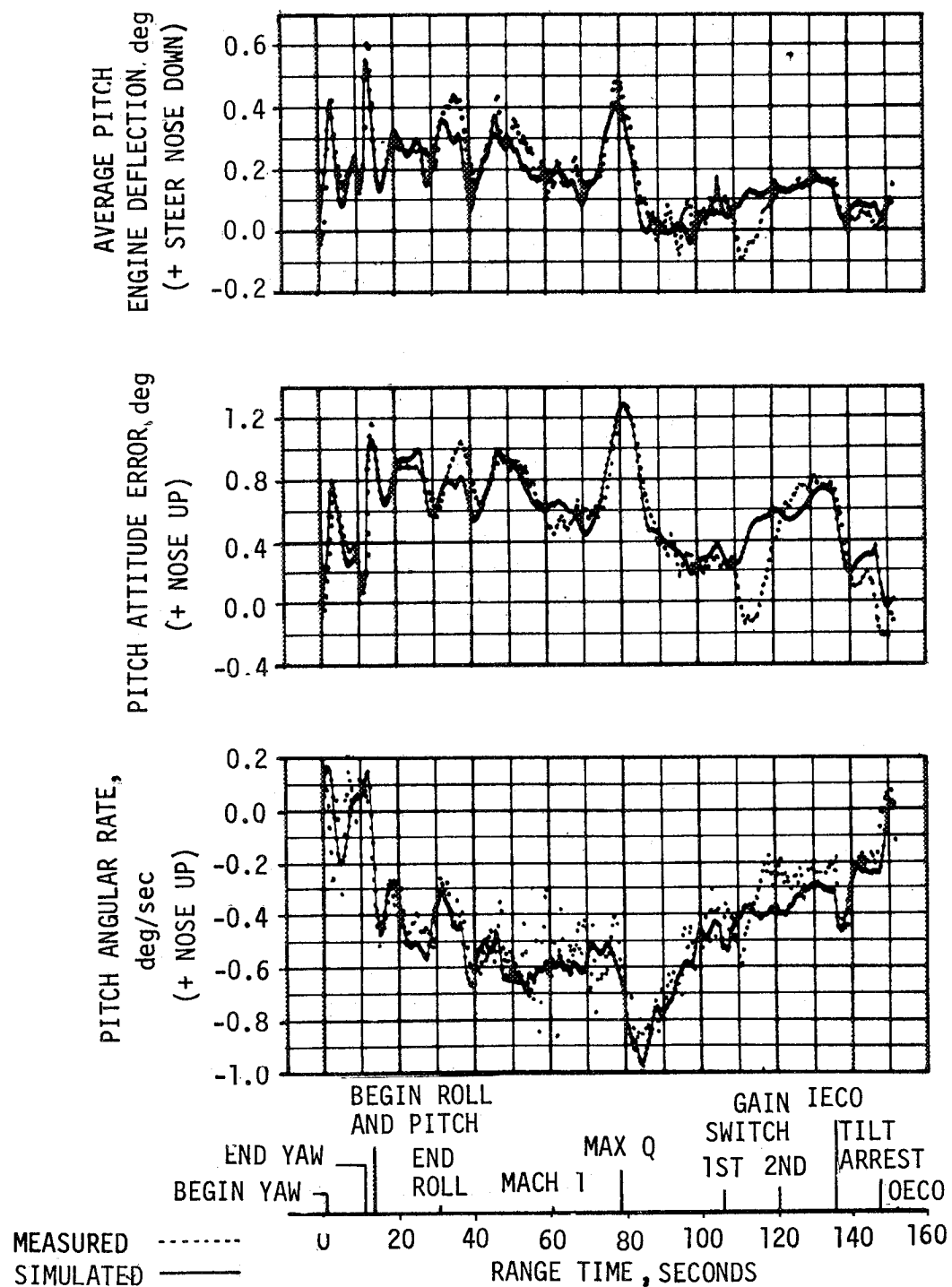


Figure 11-9. Pitch Plane Dynamics During S-IC Burn



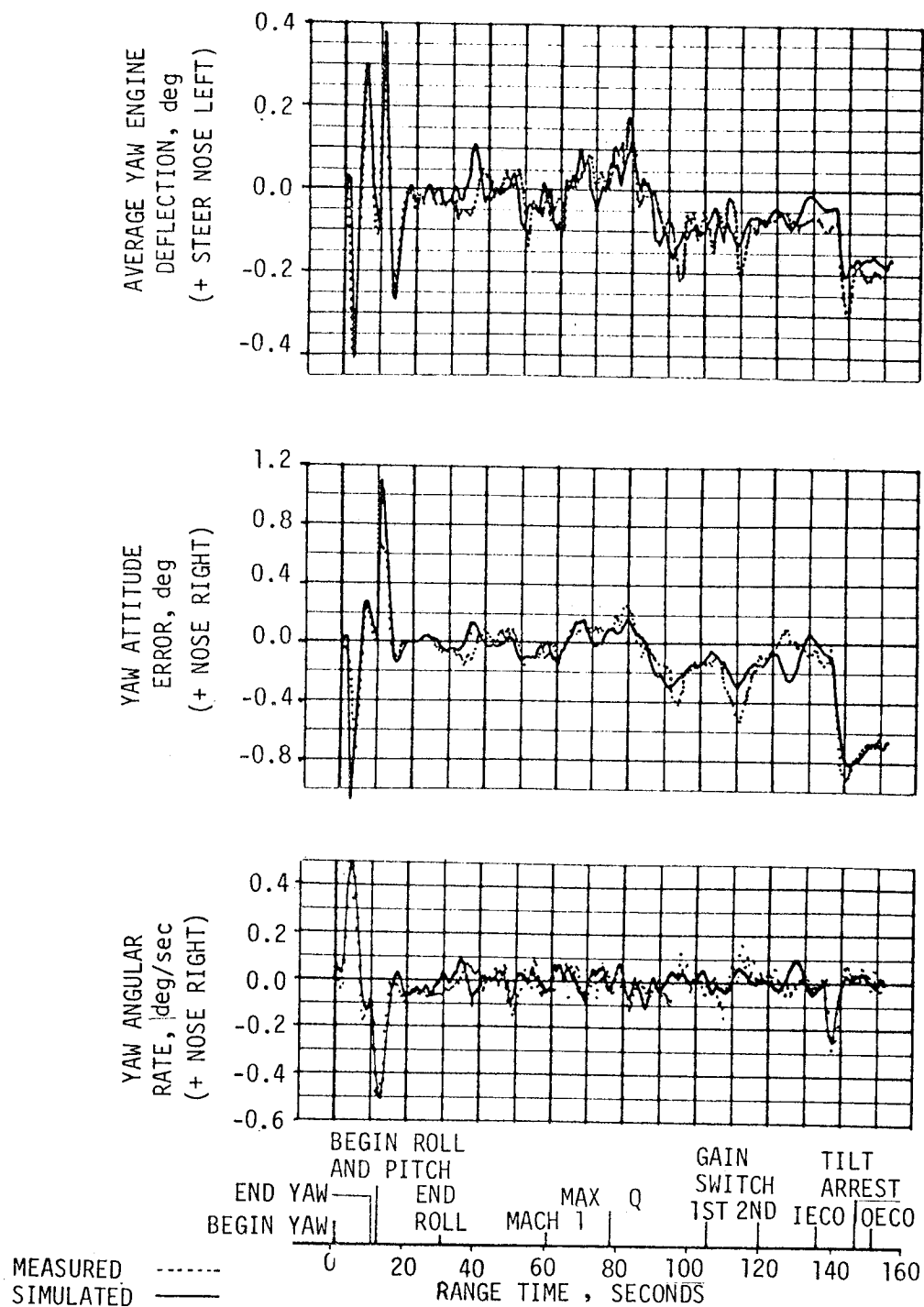
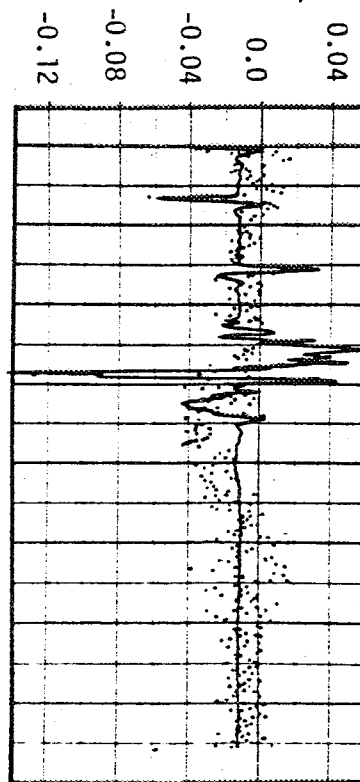
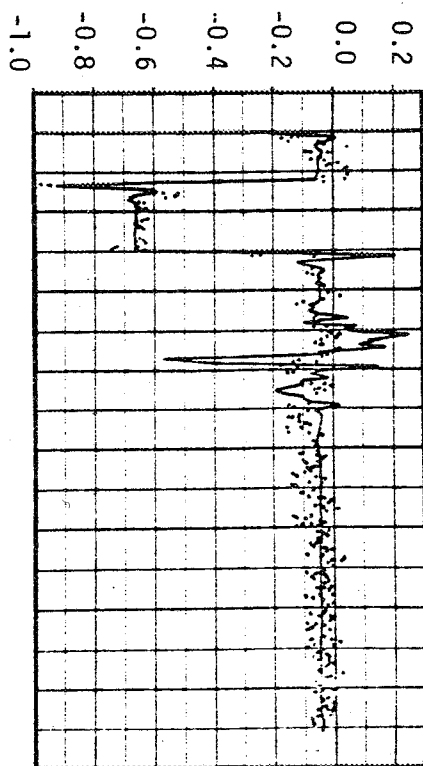


Figure 11-10. Yaw Plane Dynamics During S-IC Burn

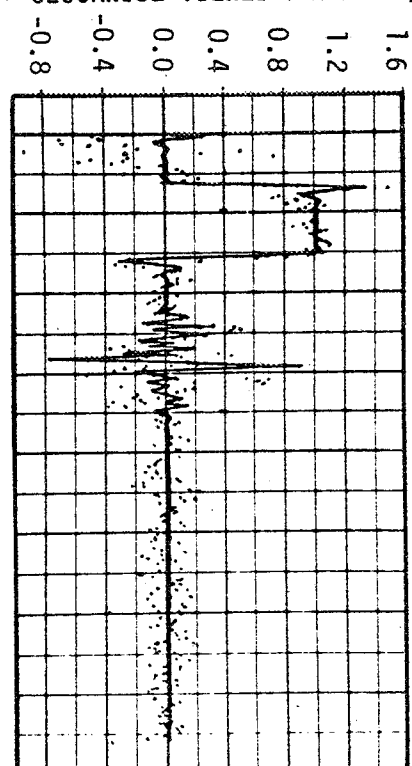
AVERAGE ROLL  
ENGINE DEFLECTION, deg  
(+ STEER COUNTERCLOCKWISE  
VIEWED FROM REAR)



ROLL ATTITUDE ERROR, deg  
(+ CLOCKWISE VIEWED FROM REAR)



ROLL ANGULAR RATE, deg/sec  
(+ CLOCKWISE VIEWED FROM AFT)



SIMULATED —  
MEASURED - - -

BEGIN ROLL AND PITCH  
END ROLL  
MACH 1  
MAX Q  
OECCO  
RANGE TIME, SECONDS

Figure 11-11. Roll Plane Dynamics During S-1C Burn

JIMSPHERE .....  
 DERIVED .....  
 FROM Q-BALL ———

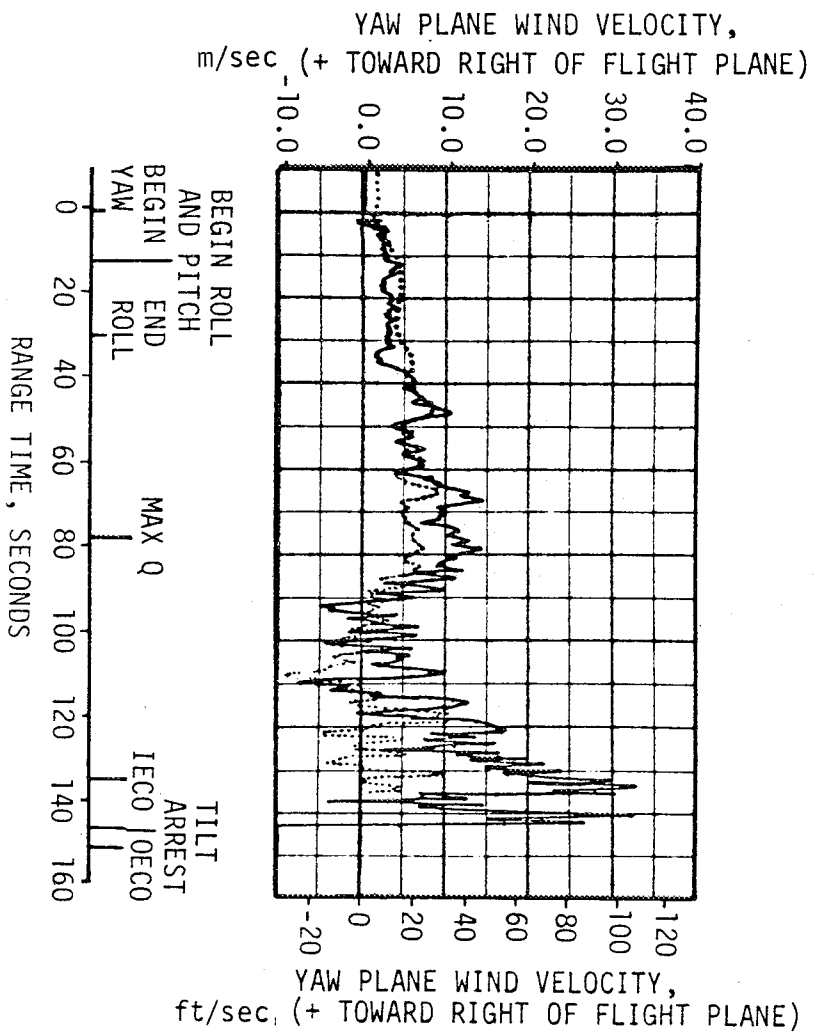
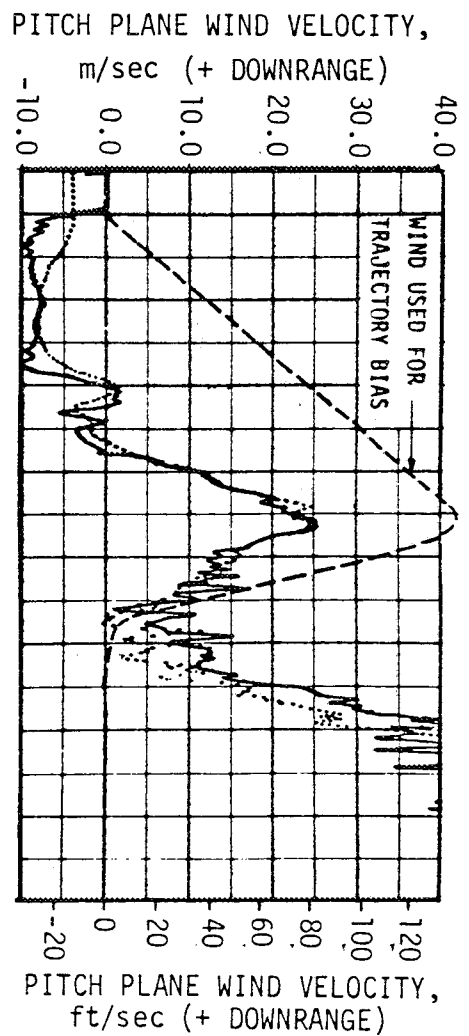


Figure 11-12. Wind Velocity During S-IC Powered Flight

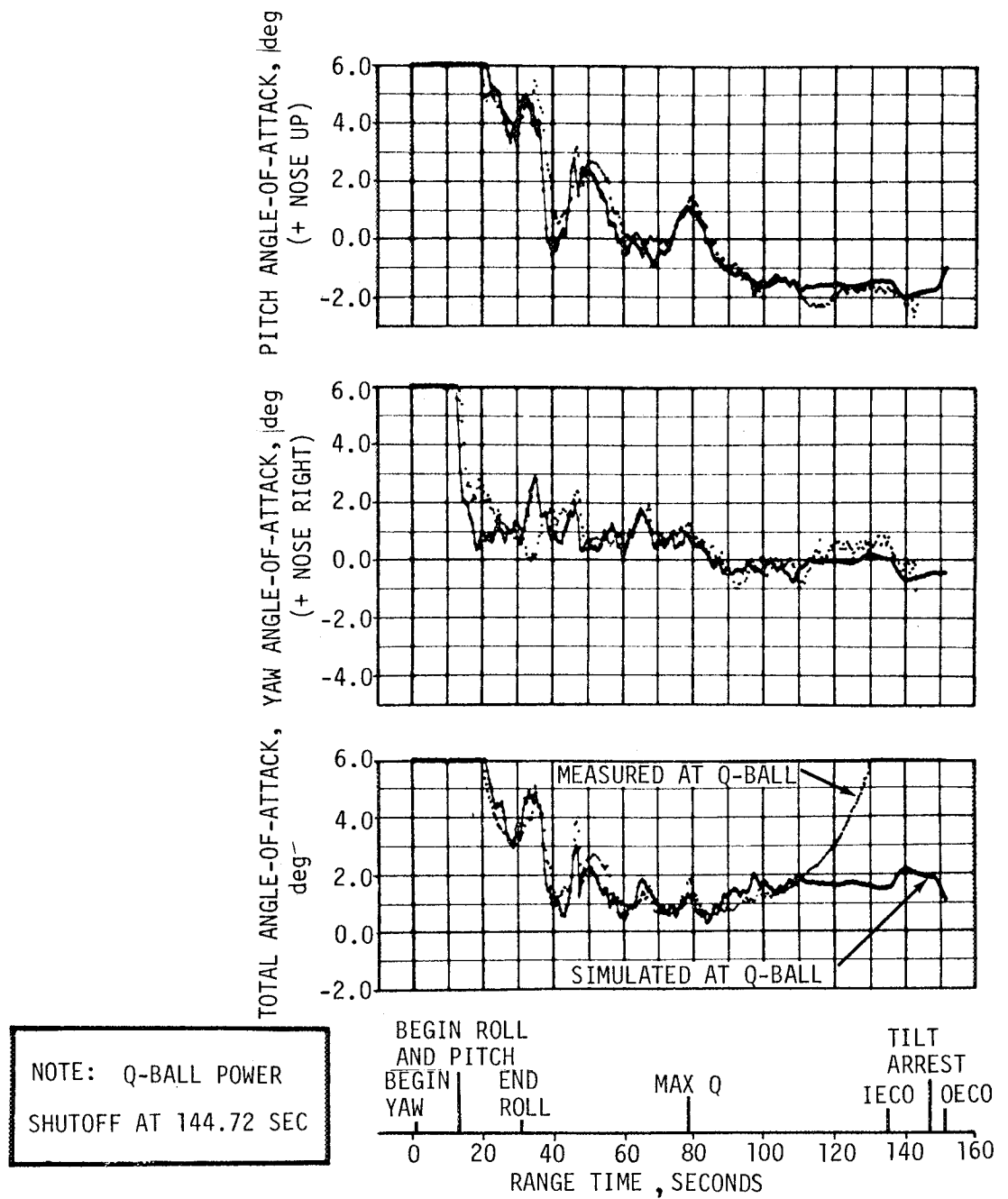


Figure 11-13. Free Stream Angle-of-Attack During S-IC Burn

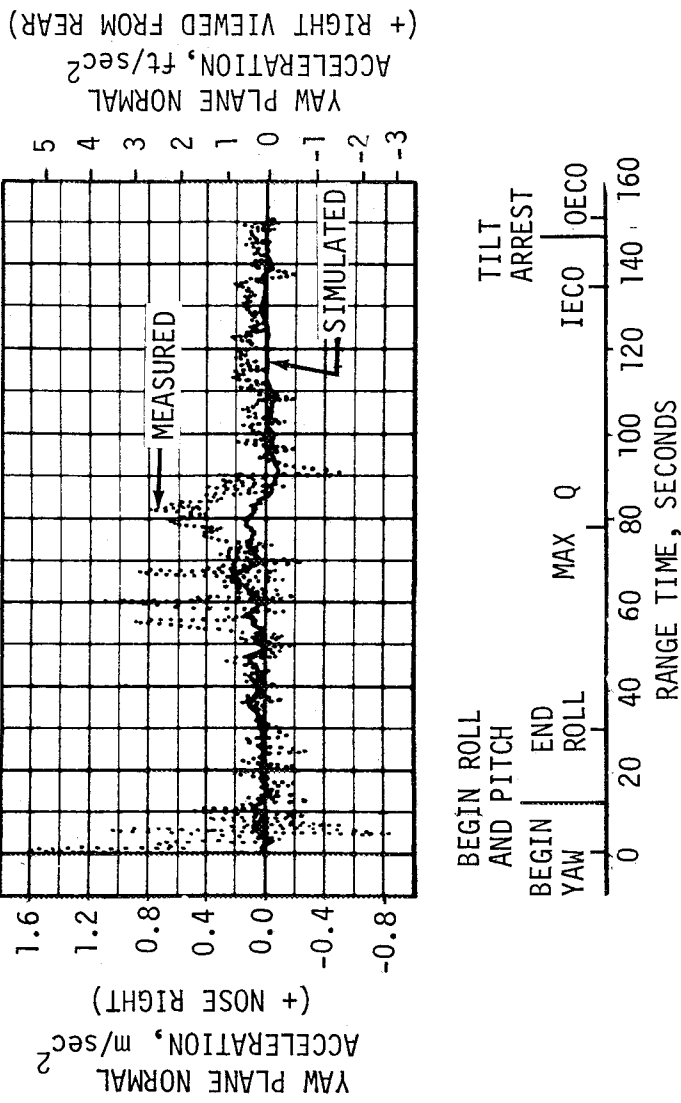
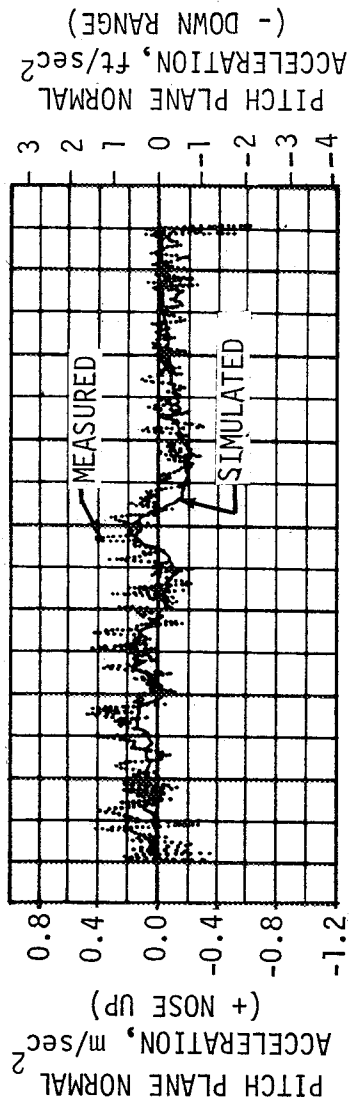
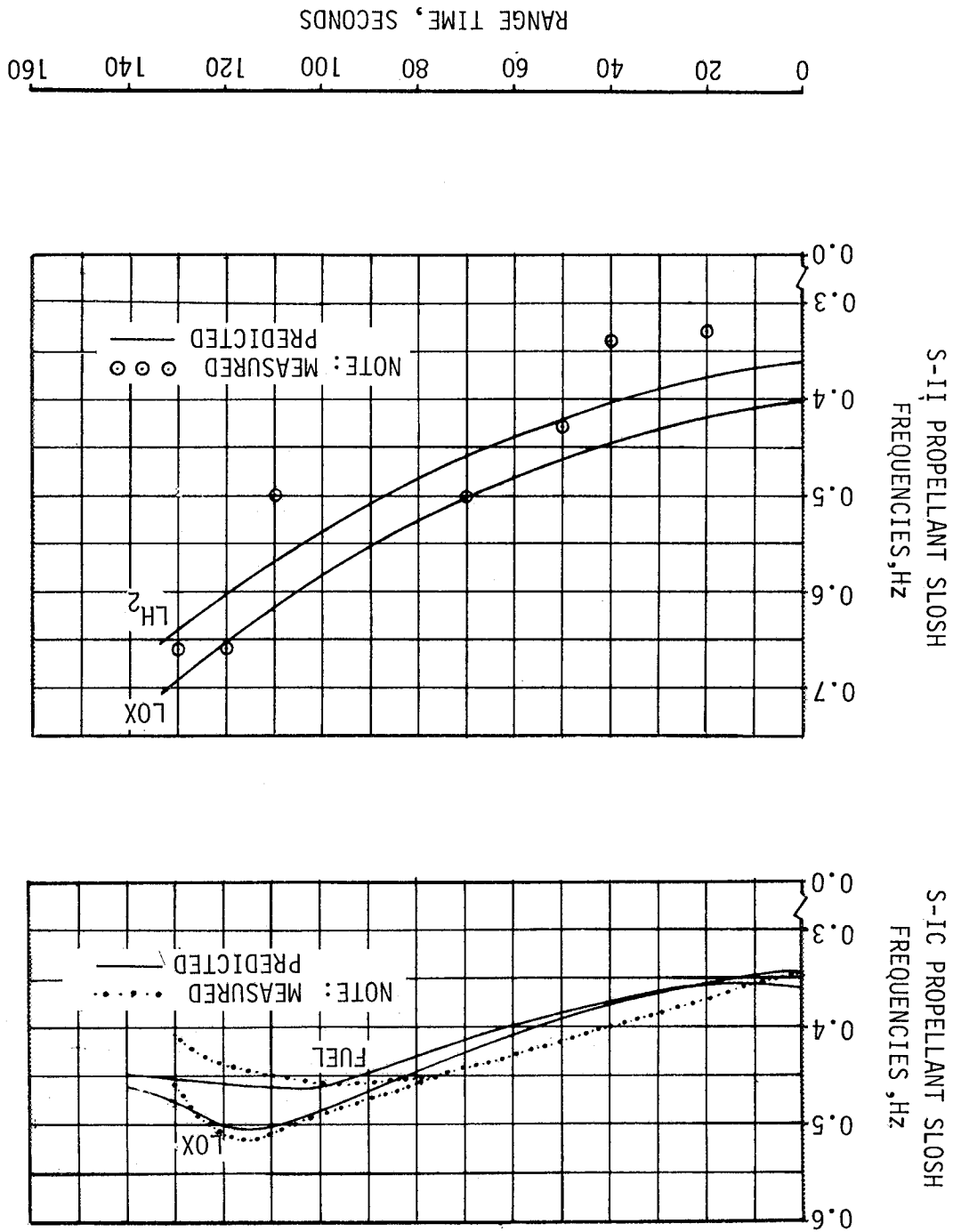


Figure 11-14. Normal Acceleration During S-IC Powered Flight

Figure 11-15. Predominant SLOSH Frequencies During S-IC Burn



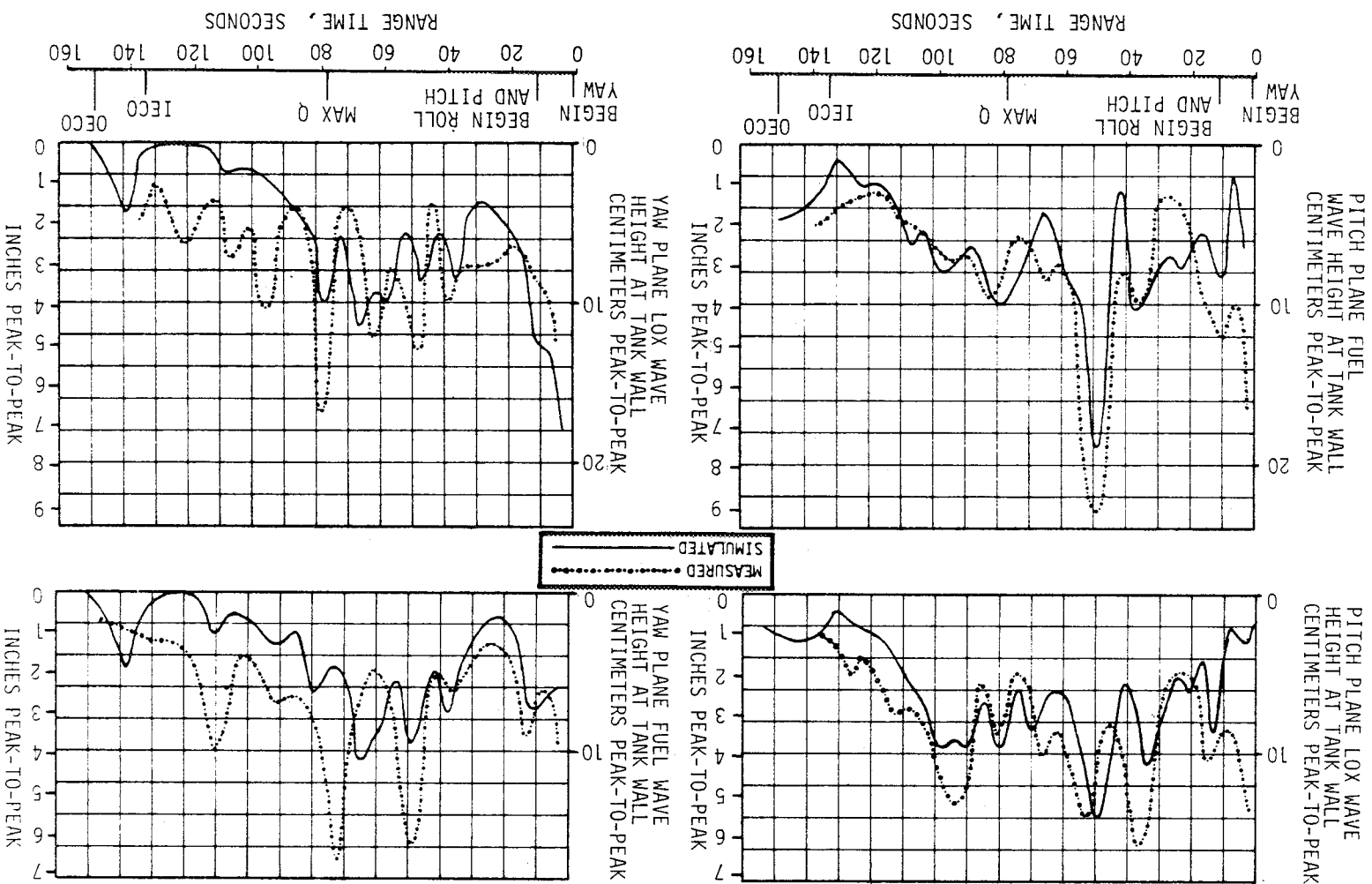
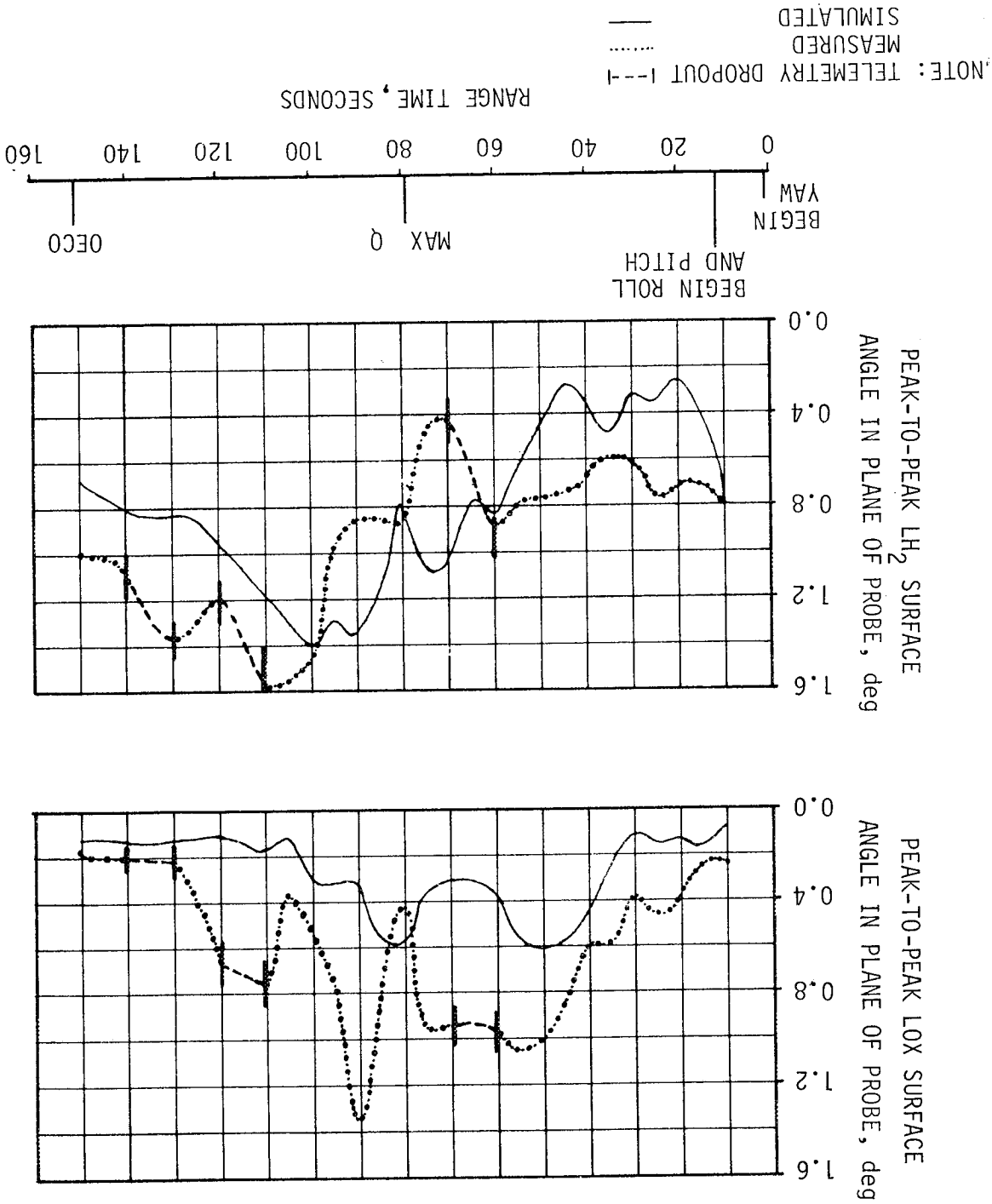


Figure 11-16. S-IC Propellant Slopsh Amplitudes During S-IC Burn

Figure 11-17. S-II Propellant SLOSH Amplitudes During S-IC Burn





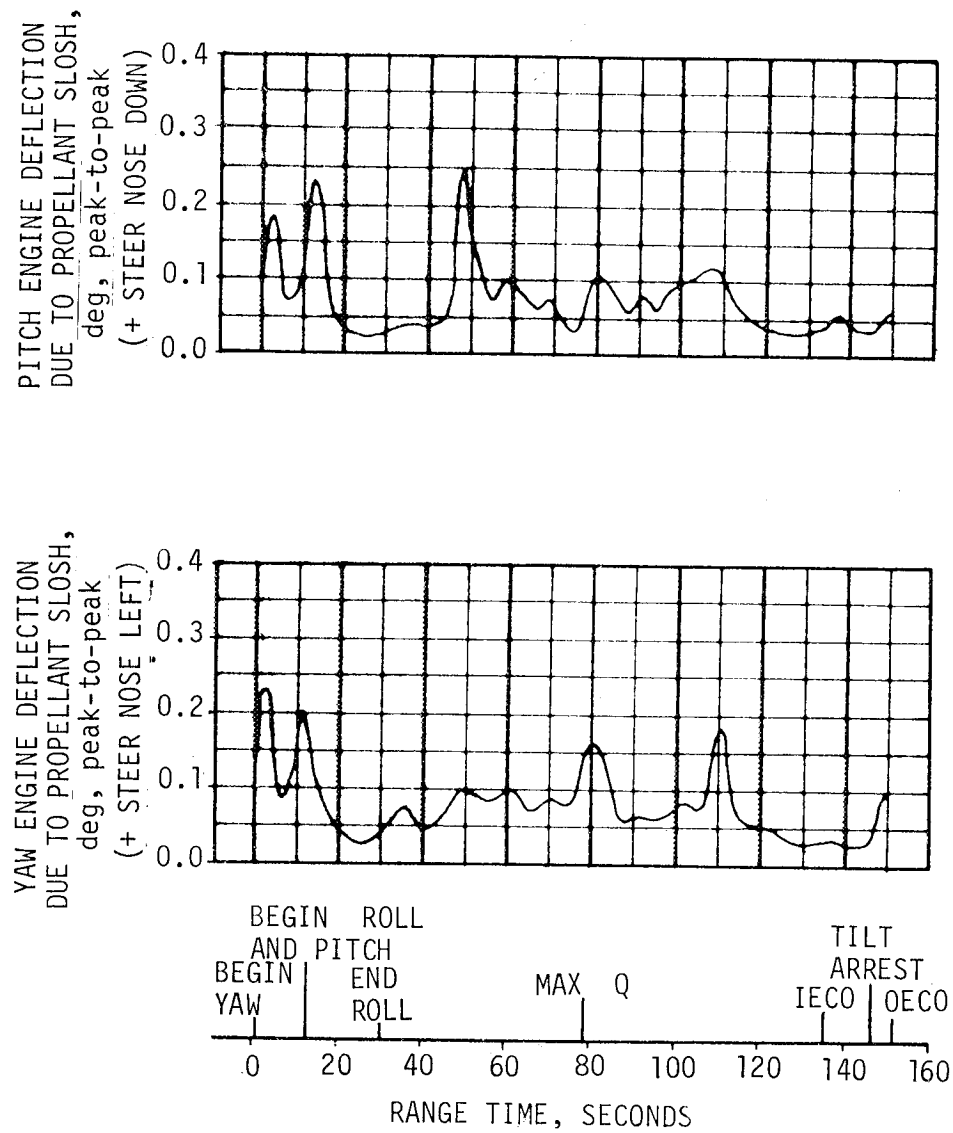


Figure 11-18. S-IC Engine Deflection Response to Propellant Slosh

The yaw maneuver is implemented as a cross range command in navigation coordinates. The initial -18 degree roll attitude causes a pitch transient from the yaw maneuver. All other pitch dynamics, as shown in Figure 11-9, result from indicated pitch plane disturbances. The large peak at 80 seconds is due to a change in slope of the tilt program. Deviations between simulated and measured dynamics beyond 114 seconds result primarily from wind uncertainties.

Since the actual wind is primarily a tail wind, major dynamics in the yaw plane, as shown in Figure 11-10, result from the yaw maneuver and the removal of the center engine cant moment at IECO.

Major roll dynamics, as shown in Figure 11-11, result from the roll maneuver from -18 to zero degrees roll attitude. The small transient following first motion results from the vehicle correcting an initial roll attitude error of -0.18 degree. Transients occurring between 40 and 70 seconds are attributed to roll aerodynamics which become prominent in the region of Mach 1. The apparent bias of the measured engine deflection and roll error can be attributed to a combination of center-of-gravity offset, roll engine misalignment, and thrust unbalance. Power spectral density analysis of the measured data reveals predominant frequencies of 0.3 and 0.9 hertz. These frequencies correspond closely to the roll control frequencies.

The launch ( $T=0$ ) wind, as shown in Figure 11-12, was essentially a tailwind with a peak magnitude of 26.5 m/s (86.9 ft/s), at 74 seconds, in the maximum dynamic pressure region. The pitch tilt program was biased for a tailwind having a peak magnitude of 42 m/s (137.9 ft/s) at approximately 79 seconds. Pitch and yaw plane components of the flight wind velocity, determined from  $T=0$  Jimsphere data, are shown. Wind is also determined by analysis using Q-Ball measured pitch and yaw angle-of-attack, post flight trajectory data, and other vehicle data. Pitch plane wind velocity plot is cut off at 40 m/s (131.2 ft/s) because of the lack of confidence in high altitude Q-Ball wind calculations beyond that point.

Pitch, yaw and total free-stream angle-of-attack are shown in Figure 11-13. Measured angle-of-attack is derived from the Q-Ball. Pitch and yaw delta pressure components are direct measurements whereas the total is calculated on board the vehicle. A breakdown in the calculation of total delta pressure appears to account for the divergence beginning at 110 seconds. Peak total angle-of-attack in the maximum dynamic pressure region reaches only 1.96 degrees. This demonstrates the effectiveness of the wind biased trajectory. Simulated angle-of-attack is derived from an analysis program using the  $T=0$  Jimsphere wind.

Normal accelerations of the vehicle center of gravity are shown in Figure 11-14.

Frequencies of predominant propellant slosh modes are shown in Figure 11-15. Frequencies are derived from probe data.

Propellant slosh amplitudes in the S-IC tanks are shown in Figure 11-16. Peak-to-peak wave heights are derived from opposing pairs of liquid level probes in the pitch and yaw planes. Figure 11-17 shows peak-to-peak propellant surface angles in the S-II tanks. These angles are in the plane of the probe and are not necessarily the maximum amplitudes since the orientation of the sloshing motion is not known. The probes are located approximately midway between the vehicle centerline and tank wall, at the liquid level assumed, and 35 degrees from position III towards position II. Excitation of slosh motion is at a level comparable to predicted values and appears to result from known disturbances. There is no evidence of slosh instability.

Peak-to-peak engine response to propellant slosh is shown in Figure 11-18. The response is derived by passing engine deflection time histories through bandpass filters, retrieving only slosh frequency components. Since the frequencies of significant slosh modes lie within a relatively narrow band, the engine responses shown are due to all tanks collectively. Peak responses correspond to peak pitch and yaw responses shown in Figures 11-9 and 11-10, respectively. The small actuator activity at slosh frequencies confirms that slosh is adequately stabilized.

Peak-to-peak engine response to first and second bending modes (not shown) was determined by passing engine deflection time histories through bandpass filters, retrieving only bending frequency components. Maximum engine response to first bending was 0.05 degrees in pitch occurring at 12.0 seconds, and 0.3 degrees in yaw occurring at 1.5 seconds. Maximum engine response to second bending was 0.045 degrees in pitch occurring at 12.0 seconds and 0.036 degrees in yaw occurring at 16.0 seconds. The evidence indicates that bending dynamics is adequately stabilized throughout flight.

The maximum values of control parameters experienced during S-IC powered flight are summarized in Table 11-3. The S-II dynamic conditions at S-IC/S-II separation are given in Table 11-4.

#### 11.4 S-II CONTROL SYSTEM EVALUATION

The S-II stage attitude control system performance was found to be satisfactory. Analysis of the magnitude of modal components in the engine deflections revealed that vehicle bending and S-II propellant sloshing had negligible effect upon the control system performance. The maximum yaw and roll attitude errors and attitude rates following S-IC/S-II separation were attributed to separation disturbances and non-uniform J-2 engine thrust buildup. The largest pitch transient attitude error occurred following iterative guidance mode (IGM) initiation. Engine deflection angles recorded during flight indicate the pitch and yaw actuators followed commands from the flight control computer within specified limits.

Table 11-3. Maximum Control Parameters During S-IC Flight

PARAMETER	UNITS	PITCH	YAW	ROLL	CONSTRAINT
Attitude Error	deg	1.3	0.98	1.0	15.3
Angular Rate	deg/s	-0.98	-0.5	1.5	10.0
Engine Deflection (Average)	deg	0.61	-0.43	-0.044	5.16
Angle-of-attack (In Max-q Region)	deg	1.48	1.29		
Normal Acceleration	m/s <sup>2</sup> (ft/s <sup>2</sup> )	0.568 (1.86)	1.60 (5.25)		
Dynamic Pressure (q)	N/cm <sup>2</sup> (lb <sub>f</sub> /in <sup>2</sup> )		3.44 (4.99)		
q $\alpha$ Product	N-deg/cm <sup>2</sup> (lb <sub>f</sub> -deg/in <sup>2</sup> )		6.27 (9.09)	Vector Sum	

Table 11-4. S-IC Dynamic End Conditions\*

PARAMETER	UNITS	PITCH	YAW	ROLL
Attitude Error	deg	-0.16	-0.56	-0.25
Attitude Rate	deg/s	0.19	0.17	-0.7
Average Actuator Position	deg	0.14	-0.35	-0.03

\* Conditions at separation command, range time 151.43 seconds

The rigid body, S-II LOX and LH<sub>2</sub> sloshing mode frequencies and the first and second bending mode frequencies are of interest from a control viewpoint. Flight control filters and gains were chosen to attenuate and/or phase shift certain modes in order to obtain acceptable control system performance.

#### 11.4.1 Attitude Control Dynamics and Stability

Vehicle attitude angles in the pitch, yaw, and roll planes are compared to the command angles in Figure 11-19. The IGM was initiated at approximately

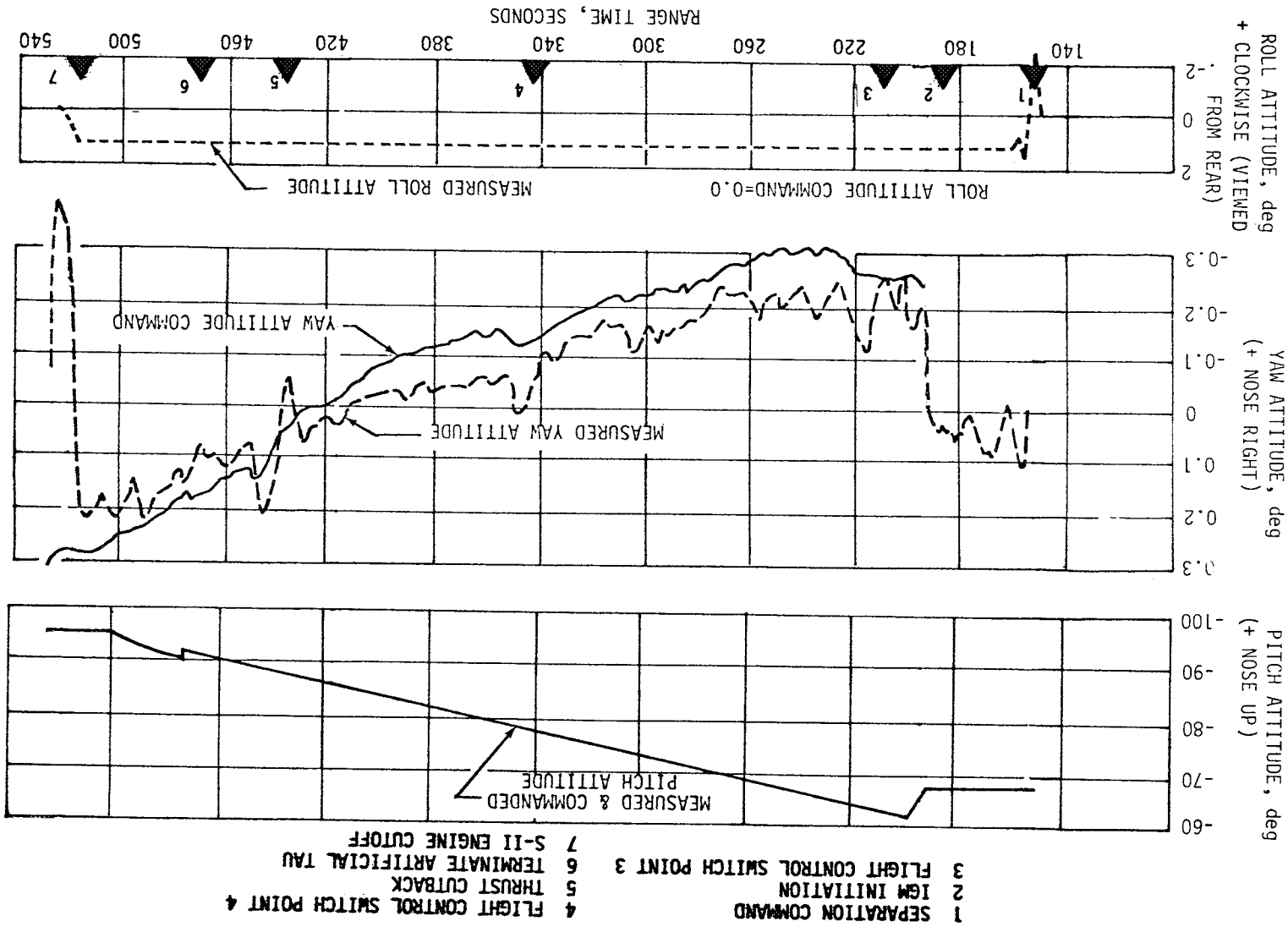


Figure 11-19. Telemetered and Command Attitude Angles

191 seconds. The principal vehicle transient during IGM operation occurred in the pitch plane. The pitch/yaw gain changes were at 212 seconds and 342 seconds. Maximum control parameters during S-II stage powered flight are summarized in Table 11-5.

Steady state attitude errors prior to guidance initiation were less than 0.12, 0.06 and 1.3 degrees for the pitch, yaw and roll axes, respectively. Measured and simulated attitude errors in pitch, yaw and roll axes are shown in Figure 11-20. A constant moment of 60,000 N-m (44,254 lb<sub>f</sub>-ft) has been added to the roll axes in the analog simulation. Addition of this moment is sufficient to account for the 1.3 degree roll error. Measured and simulated attitude rates in the pitch, yaw and roll axes are shown in Figure 11-21. Average telemetered engine gimbal angles in pitch, yaw and roll were modified by adding corrections for engine thrust misalignments, and thrust structure compliance effects as determined from static firing tests as shown in Figure 11-22.

Maximum gimbal angles of -0.08, -0.7, and -0.7 degrees occurred at 195, 154 and 155 seconds for the pitch, yaw and roll axes, respectively.

Maximum engine gimbaling capabilities are approximately 7 degrees inboard and 6 degrees outboard, measured in the pitch-yaw axes. The attitude control responses indicate that the S-II stage performed satisfactorily throughout flight.

#### 11.4.2 Liquid Propellant Dynamics and Their Effects on Flight Control

The LOX and LH<sub>2</sub> slosh amplitudes during the S-II flight were obtained by reconstruction techniques on the fine mass probe measurements as shown in Figure 11-23. The "saw-tooth" characteristics of the fine mass probes during S-II flight were filtered. The amplitude plots show periodic biasing (non sinusoidal) which should be ignored. The data shown do not reflect hydrodynamic attenuation. Analog simulation of the flight also indicated sloshing of the liquid propellants.

Slosh frequencies based on data from the fine mass probe measurement for the S-II stage LOX and LH<sub>2</sub> propellant tanks were determined using power spectral density techniques as shown in Figure 11-24. Measured LH<sub>2</sub> frequencies showed good agreement with the theoretical slosh frequencies, but the agreement between observed LOX frequencies and theoretical values was not as good. The observed LOX frequencies were in the range of 0.5 to 0.6 hertz as compared to theoretical values ranging from 0.2 to 0.4 hertz. These higher frequencies also occurred in the S-II pitch and yaw gyros. The theoretical S-IVB slosh frequencies are shown in Figure 11-24. S-IVB sloshing was not discernible during the S-II flight.

The presence of periodic sloshing modes in the engine deflections were analyzed using bandpass filtering as shown in Figure 11-25. The maximum deflections were less than 0.07 and 0.05 degrees in pitch, and yaw, respectively.

Table 11-5. Maximum Control Parameters During S-II Stage Powered Flight

PARAMETER	S-IC/S-II SEPARATION	GUIDANCE INITIATION	THRUST CUTBACK	TERMINATE ARTIFICIAL TAU	S-II CUTOFF
Pitch Attitude Error (deg)	-0.3	-1.8	0.7	0.9	0.4
Yaw Attitude Error (deg)	-0.6	0.3	-0.1	-0.1	-0.1
Roll Attitude Error (deg)	-2.0	1.5	1.5	1.4	1.3
Pitch Rate (deg/s)	0.3	1.2	-0.2	0.3	-0.2
Yaw Rate (deg/s)	0.3	-0.1	-0.1	-0.2	-0.1
Roll Rate (deg/s)	2.8	-0.2	-0.5	-0.2	-0.2
Pitch Activator Position (deg)	0.4	-0.8	0.1	0.2	0.1
Yaw Activator Position (deg)	-0.7	0.2	0.1	-0.1	-0.1
Roll Activator Position (deg)	-0.7	0.2	0.2	0.2	0.2

The J-2 engine deflection were analyzed for the presence of bending mode components. The deflection measurement data from engine No. 1 were filtered and analyzed by a spectrum analysis program. The results indicate negligible engine deflection due to bending of the vehicle.

#### 11.5 S-IVB CONTROL SYSTEM EVALUATION

The S-IVB Thrust Vector Control System (TVC) and APS provided satisfactory pitch, yaw and roll control during S-IVB first and second burns and throughout the parking and waiting orbits. The vehicle attitudes correlated well with actual commanded attitudes during each burn. Demands on the control system were well within the capabilities of the system.

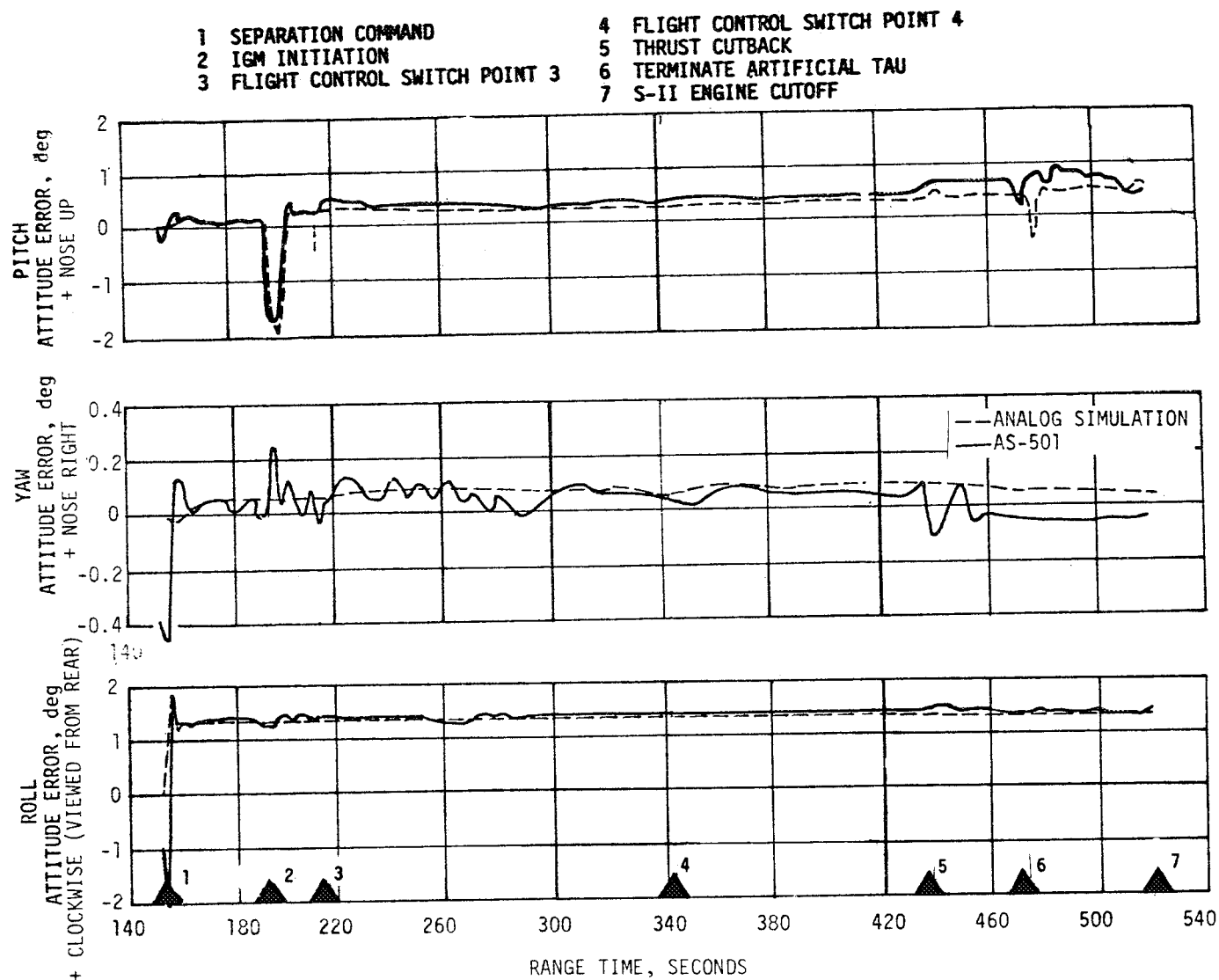


Figure 11-20. Attitude Errors During S-II Powered Flight



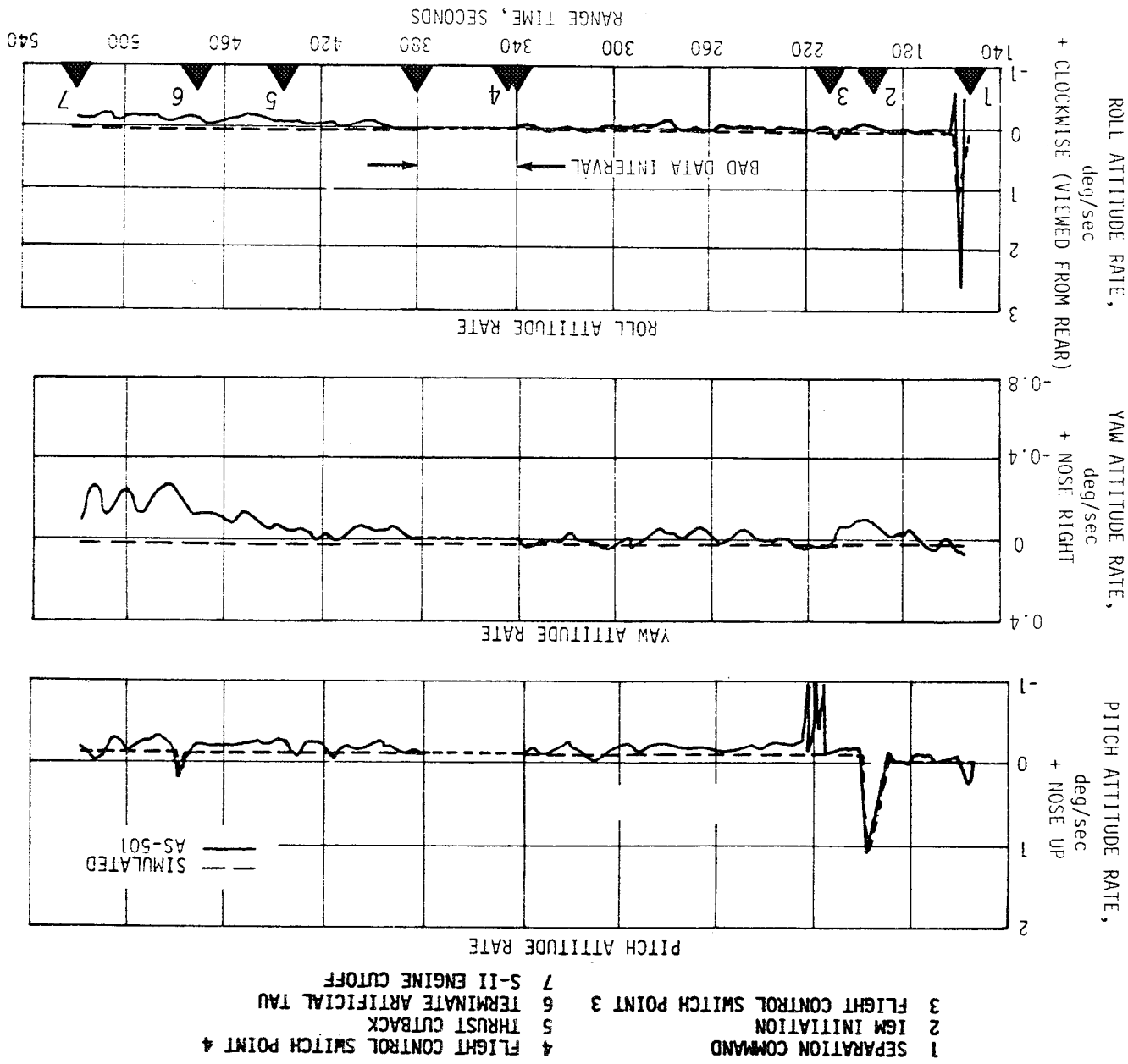
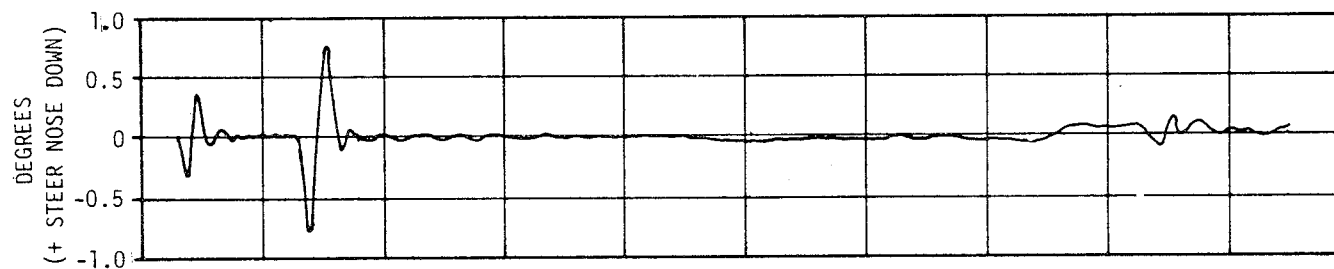


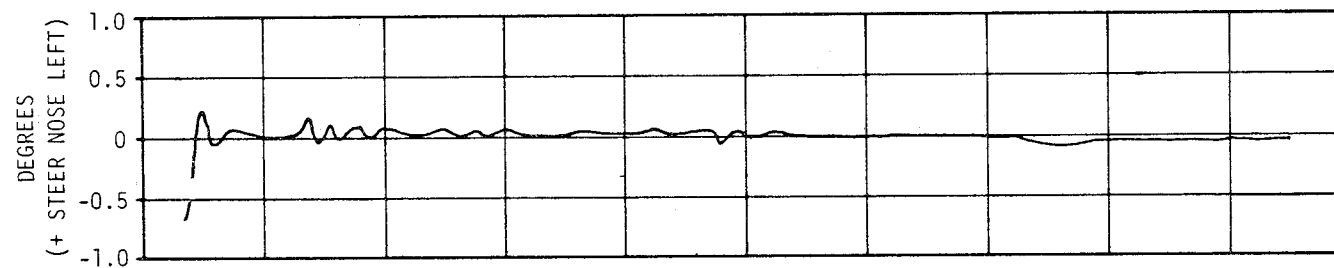
Figure 11-21. S-II Stage Attitude Rates

- |                                 |                                 |
|---------------------------------|---------------------------------|
| 1 SEPARATION COMMAND            | 4 FLIGHT CONTROL SWITCH POINT 4 |
| 2 IGM INITIATION                | 5 THRUST CUTBACK                |
| 3 FLIGHT CONTROL SWITCH POINT 3 | 6 TERMINATE ARTIFICIAL TAU      |
|                                 | 7 S-II ENGINE CUTOFF            |

## AVERAGE PITCH ENGINE DEFLECTION



## AVERAGE YAW ENGINE DEFLECTION



## AVERAGE ROLL ENGINE DEFLECTION

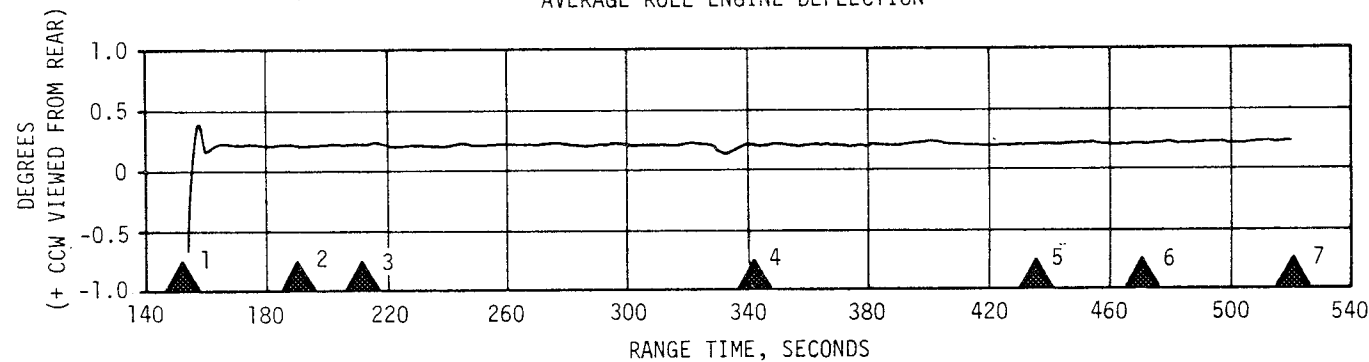


Figure 11-22. Average S-II Engine Deflections

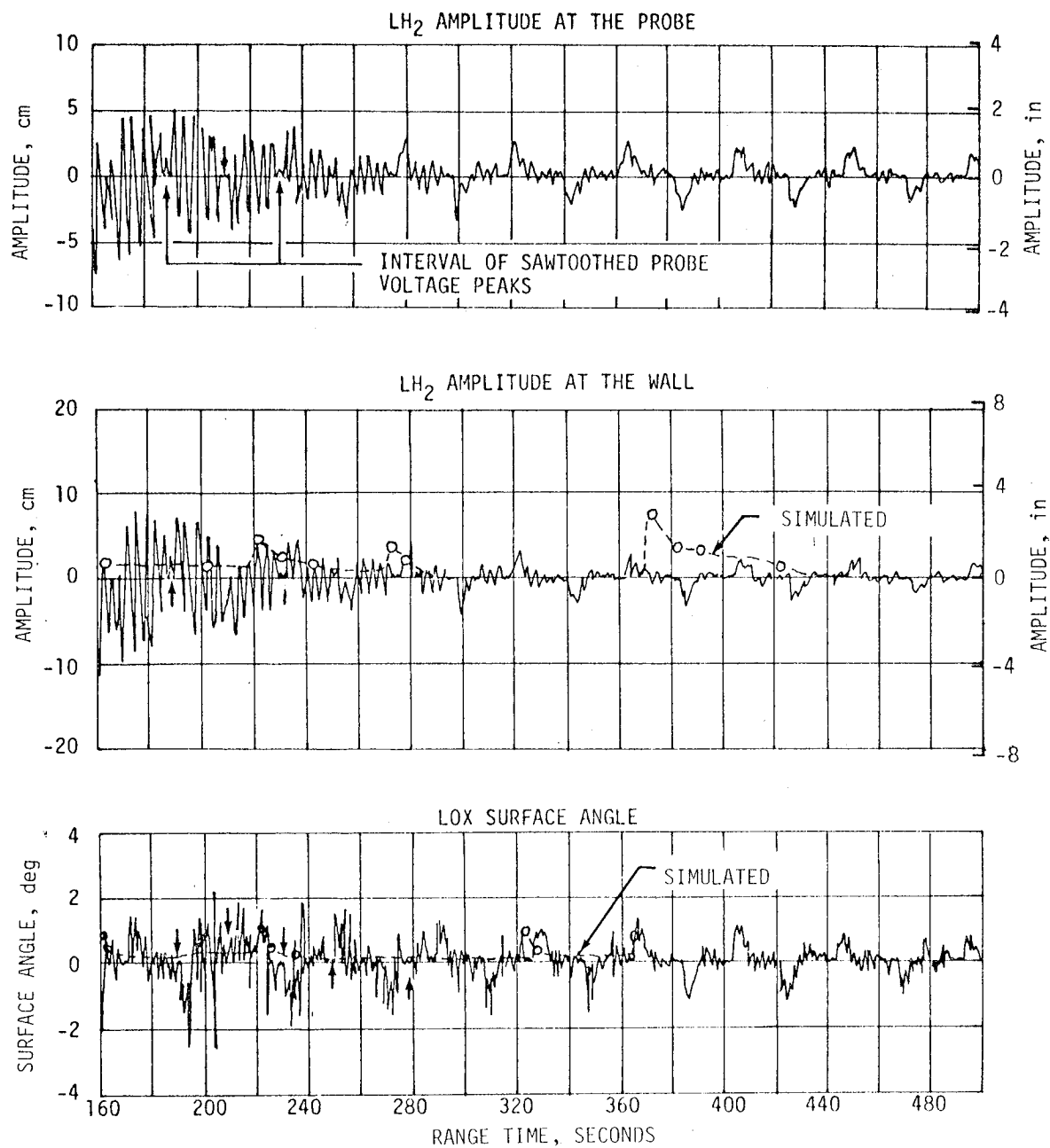


Figure 11-23. LH<sub>2</sub> and LOX Slosh Amplitudes During S-II Flight

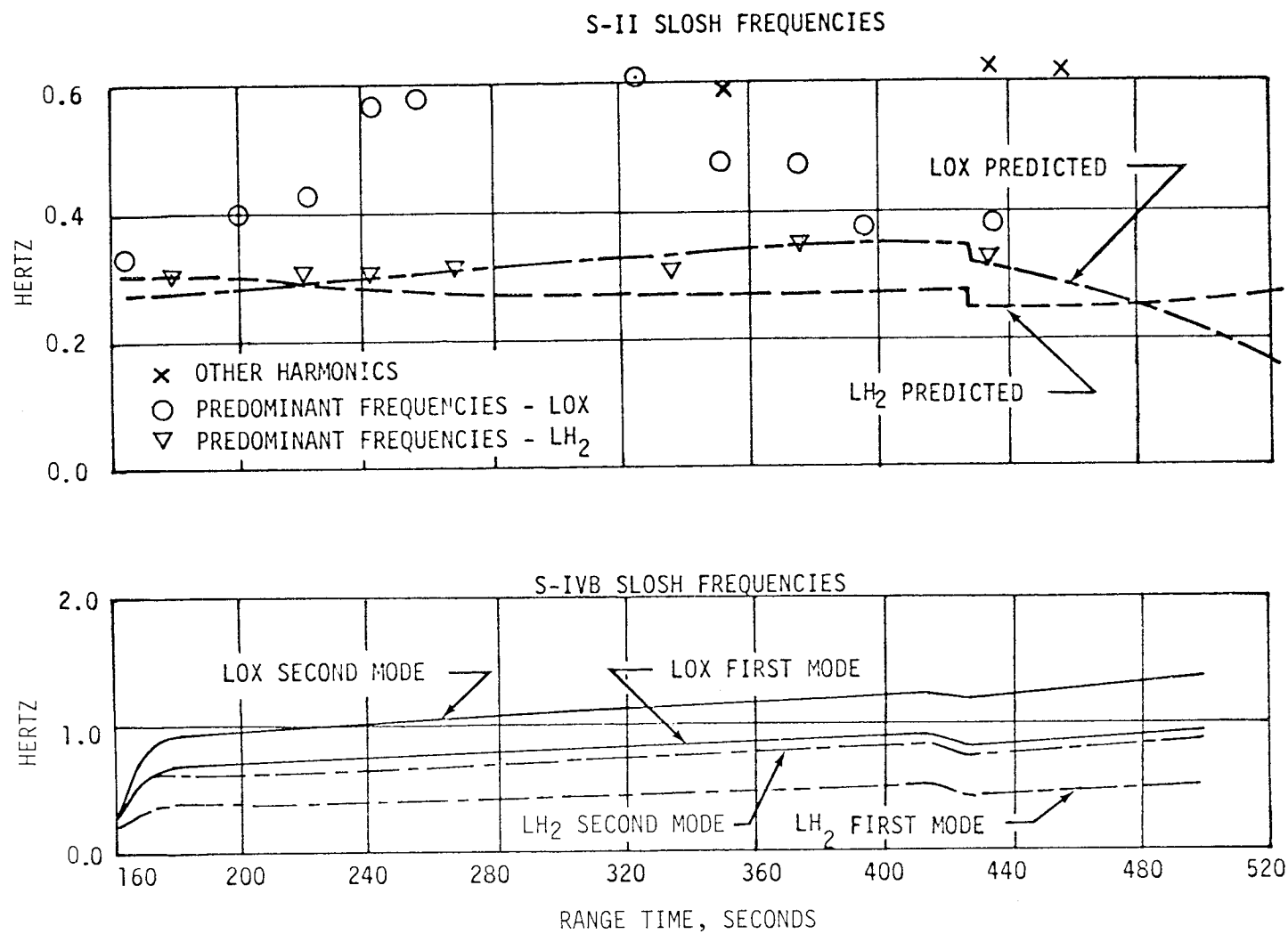


Figure 11-24. SLOSH Frequencies

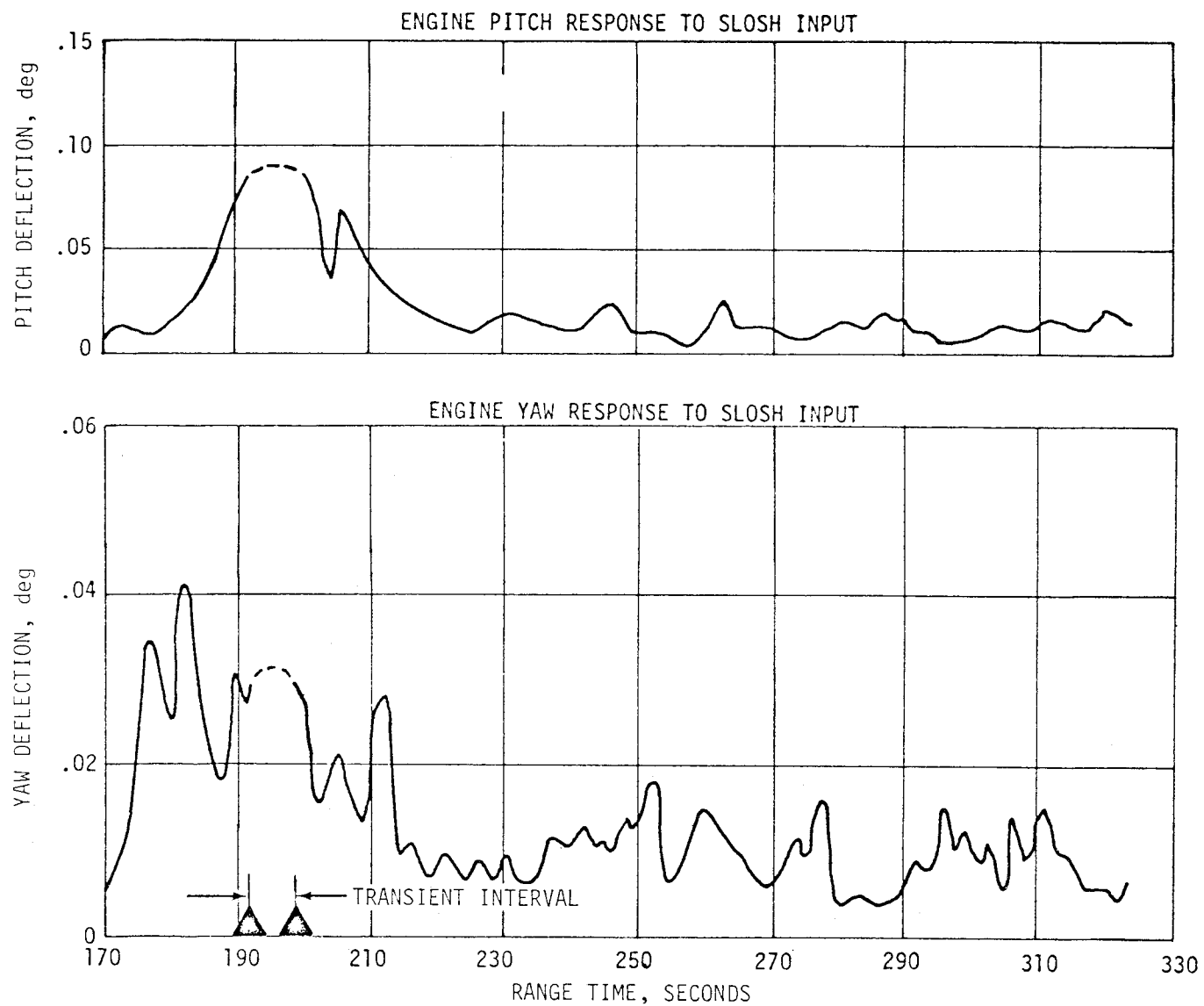


Figure 11-25. J-2 Engine Pitch and Yaw Response to S-II Stage Sloshing

### 11.5.1 Control System Evaluation During First Burn

Attitude errors, angular velocities, and engine actuator positions during first burn are presented in Figures 11-26 through 11-28, respectively. Commanded and actual pitch and yaw attitudes during first burn are presented in Figures 11-29 and 11-30, respectively. The agreement between the actuator positions computed from the control equation and the actual actuator position indicates that the steady state control gains were close to their design values. Maximum pitch, yaw and roll errors during first burn were +2.2, -0.9 and +1.2 degrees, respectively. The +1.2 degree roll attitude error existed at S-II cutoff and was removed following S-II/S-IVB separation. Maximum control system parameters are presented in Table 11-6.

APS firings for roll control are indicated at the bottom of Figure 11-26. Impulse delivered for roll control during first burn was 1085.4 N-s (244.0  $\text{lb}_f\text{-s}$ ) from the module at position I and 1184.1 N-s (266.2  $\text{lb}_f\text{-s}$ ) from the module at position III. The difference in impulse is attributed to apparent low performance for engines I<sub>II</sub> and I<sub>IV</sub> in the module at position I. This roll control was required to correct for the roll induced disturbances during S-II/S-IVB separation, guidance initiation, and a 17.6 N-m (13.0  $\text{lb}_f\text{-ft}$ ) steady state roll torque.

During first burn, following S-II/S-IVB separation, sloshing was excited but was quickly damped due to the high damping afforded by the LH<sub>2</sub> tank baffle and deflector and the LOX tank baffle. Slosh amplitudes were very small throughout the remainder of first burn, therefore, no measurable LH<sub>2</sub> slosh frequencies were obtained. LOX frequency data were obtained during first burn indicating that LOX sloshing occurred between the predicted first and second mode natural frequencies.

LOX and LH<sub>2</sub> slosh amplitudes observed on the PU probe fine mass data during first burn were well damped due to the deflector and baffle in the LH<sub>2</sub> tank and a baffle in the LOX tank.

### 11.5.2 Control System Evaluation During Parking Orbit

APS engine firing data in conjunction with commanded and actual vehicle attitudes indicate that attitude control during parking orbit was normal. Commanded and actual vehicle attitudes following first S-IVB cutoff, and during the restart orientation are shown in Figures 11-31 and 11-32. The actual vehicle attitude is seen to follow the commanded attitude very well. APS propellant usage during parking orbit was lower than expected.

Temperature sensor data in the LH<sub>2</sub> tank indicated that a slosh wave similar to that experienced on AS-203 existed following S-IVB first cutoff. Indications of the presence of this wave were apparent in the pitch plane approximately 40 seconds after cutoff. This wave covered the sensors to the deflector (vehicle station 80.031m [3150.9 in]) but appeared to subside as the sensors were dry approximately 20 seconds after being wetted.

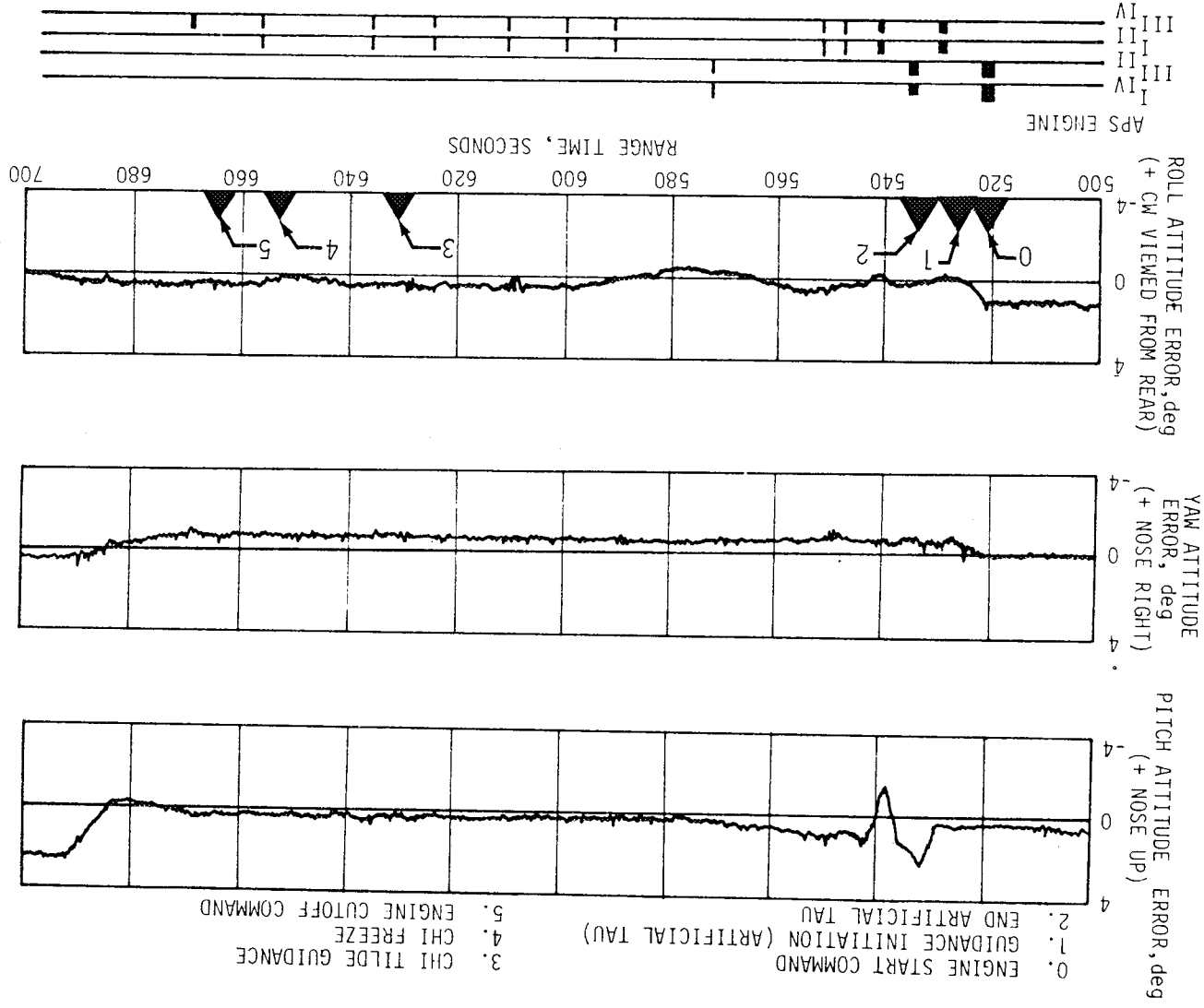


Figure 11-26. Attitude Error and Auxiliary Propulsion System Engine Firings During S-IVB First Burn

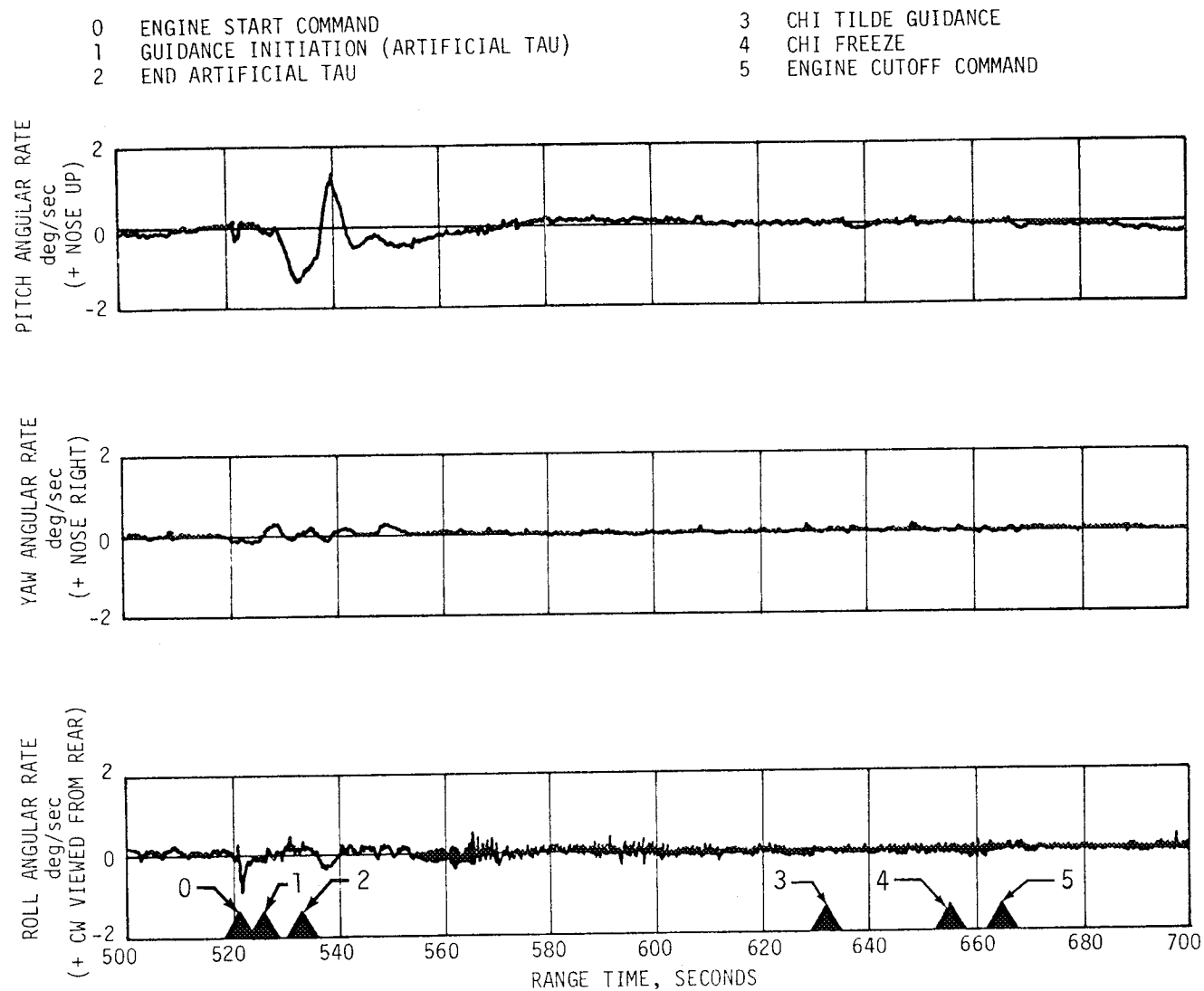


Figure 11-27. Angular Velocities During First Burn



YAW ACTUATOR POSITION (deg)  
(+ STEER NOSE LEFT)

PITCH ACTUATOR POSITION (deg)  
(+ STEER NOSE DOWN)

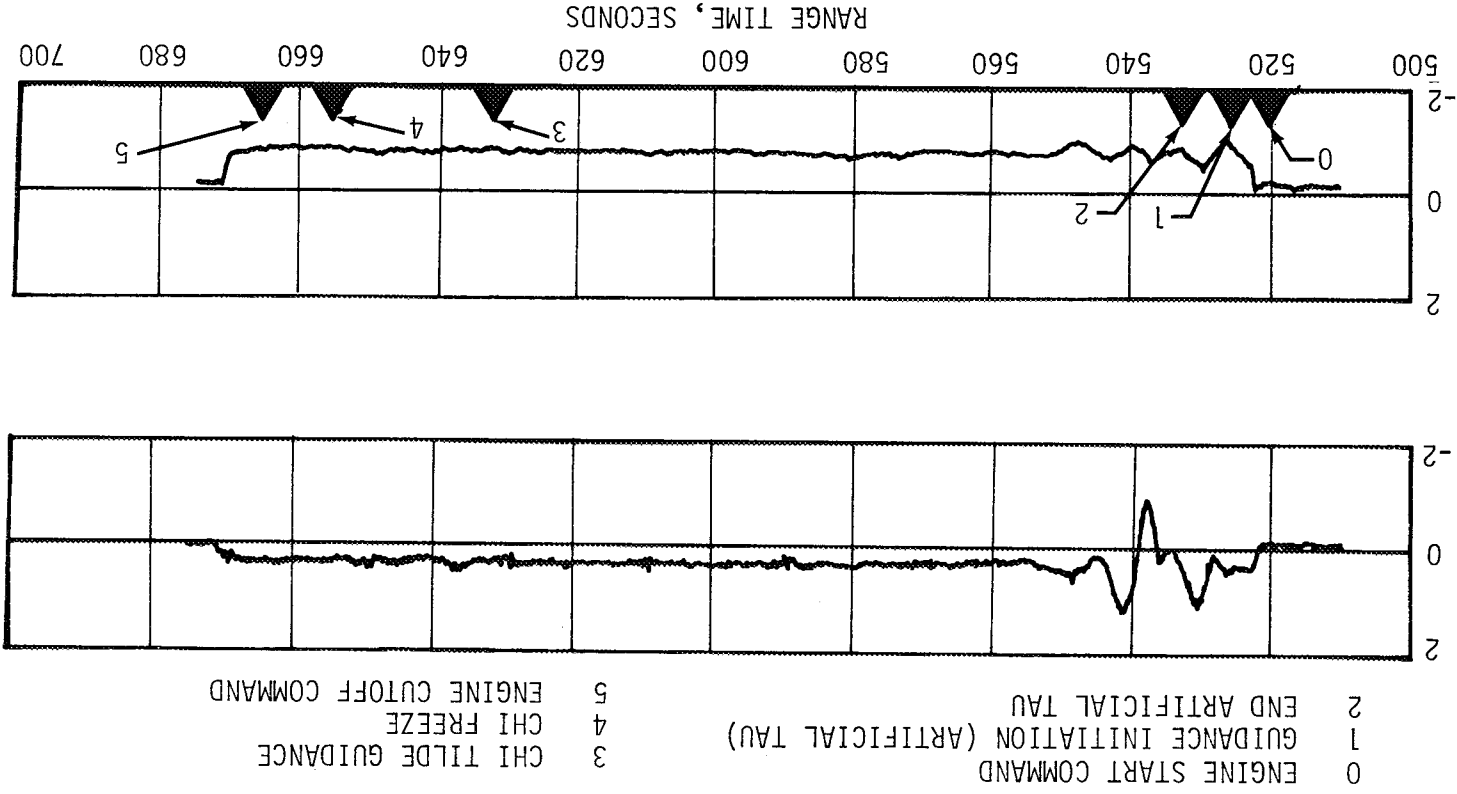


Figure 11-28. S-IVB Pitch and Yaw Actuator Positions During First Burn

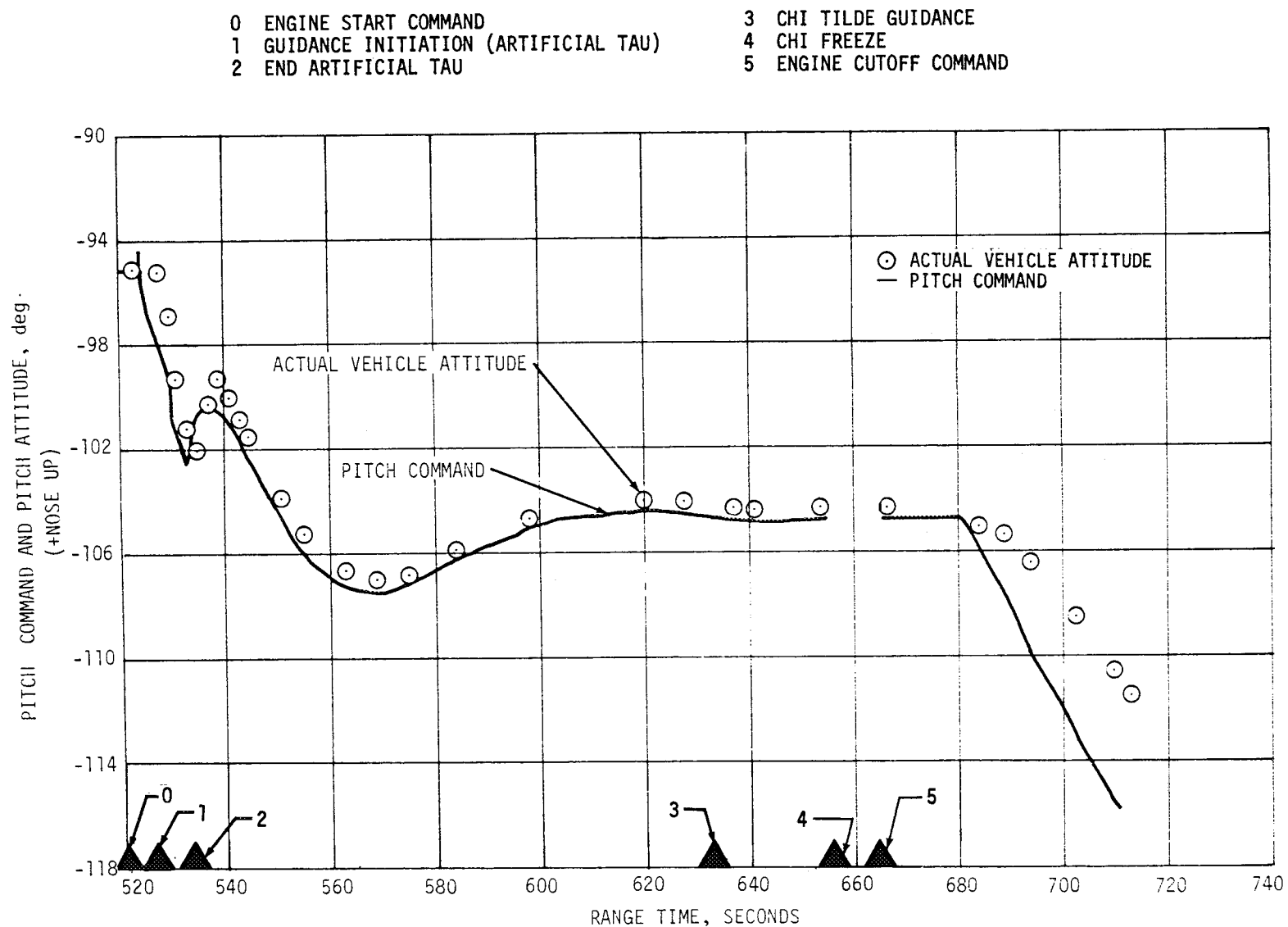


Figure 11-29. Vehicle Attitude During S-IVB First Burn

11-47

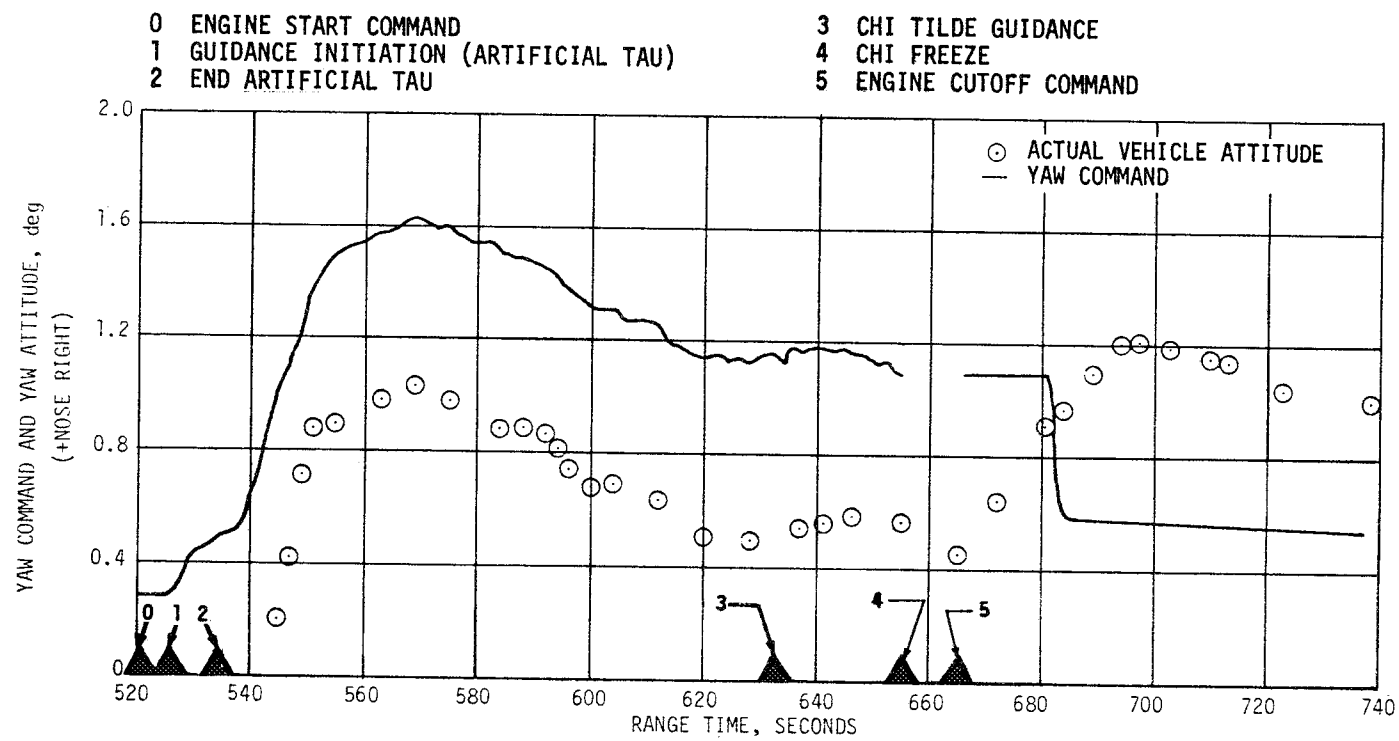


Figure 11-30. Vehicle Attitude During S-IVB First Burn

Table 11-6. Maximum Values of Critical Flight Control Parameters-First Burn

PARAMETER	*S-IVB/S-II SEPARATION AND GUIDANCE INITIATION	CHI TILDE GUID. MODE	CHI FREEZE	J-2 CUTOFF
Pitch Attitude Error (deg)	+2.2	0.7	+0.5	+0.5
Yaw Attitude Error (deg)	-0.83	-0.68	-0.7	-0.65
Roll Attitude Error (deg)	1.4	+0.72	+0.7	+0.7
Pitch Rate (deg/s)	-1.4	-0.15	0.0	-0.25
Yaw Rate (deg/s)	+0.25	0.0	0.0	0.0
Roll Rate (deg/s)	-0.5	0.0	0.0	0.0
Pitch Actuator Position (deg)	+1.13	+0.46	+0.37	+0.35
Yaw Actuator Position (deg)	-0.91	-0.8	-0.8	-0.8
* Includes effects of artificial tau guidance mode				

During parking orbit temperature patches on the tank wall indicated that the liquid level varied between vehicle station 78.634 m (3095.9 in.) and 80.031 m (3150.9 in.) (the LH<sub>2</sub> surface level at first cutoff was at approximately vehicle station 78.050 m [3072.9 in.]). However, the sensors on the instrumentation probe during this same time period indicated a higher liquid level. The probe sensor data indicated that during parking orbit the LH<sub>2</sub> surface level was above station 79.904 m (3145.9 in.).

For the entire parking orbit period, the data from sensors on the instrumentation probe always indicated liquid where as the wall temperature patches near the same station level indicated vapor. Therefore, an apparent difference exists when comparing data obtained from the wall patches and probe sensors.

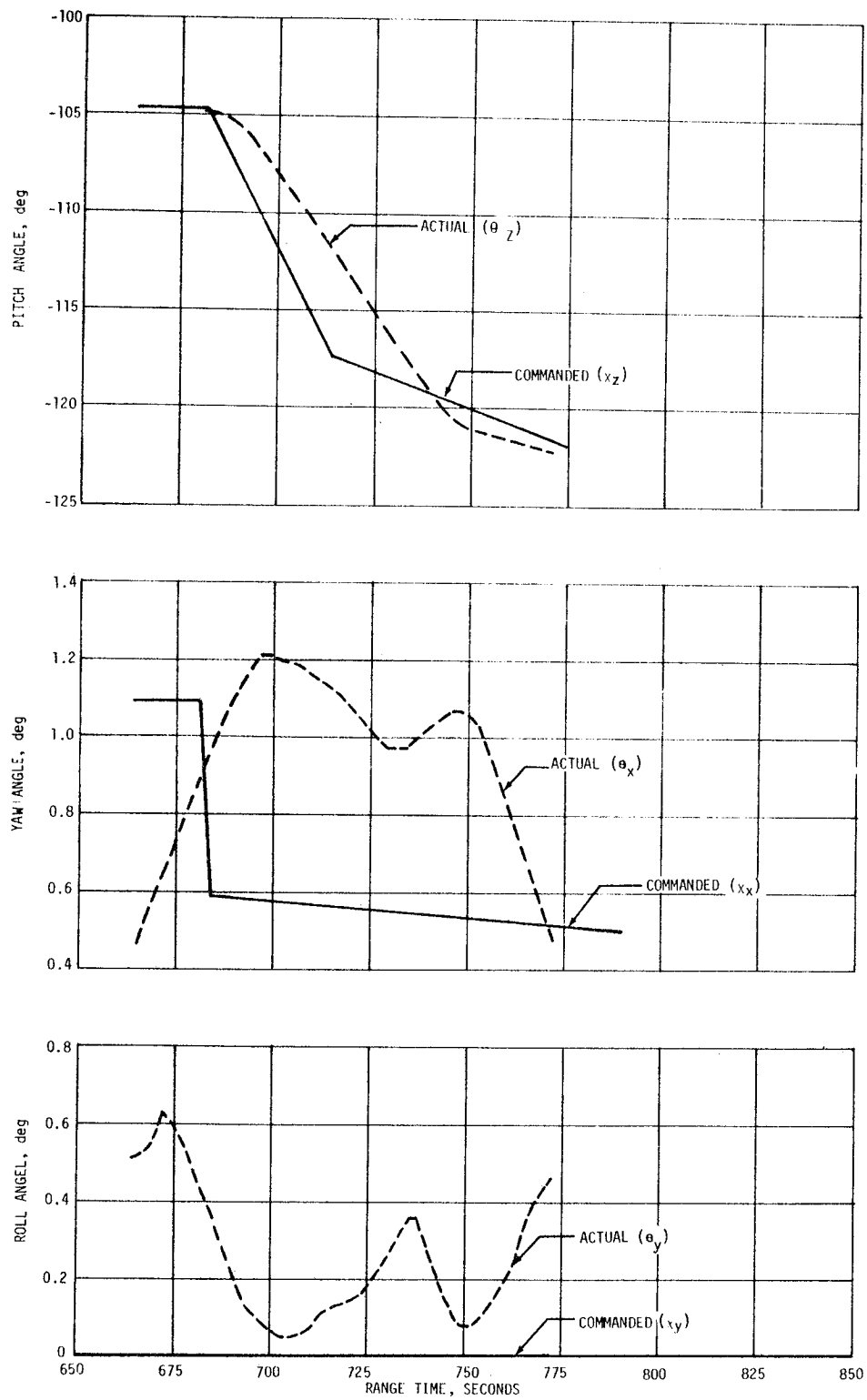


Figure 11-31. Vehicle Attitude Following S-IVB First Burn Cutoff

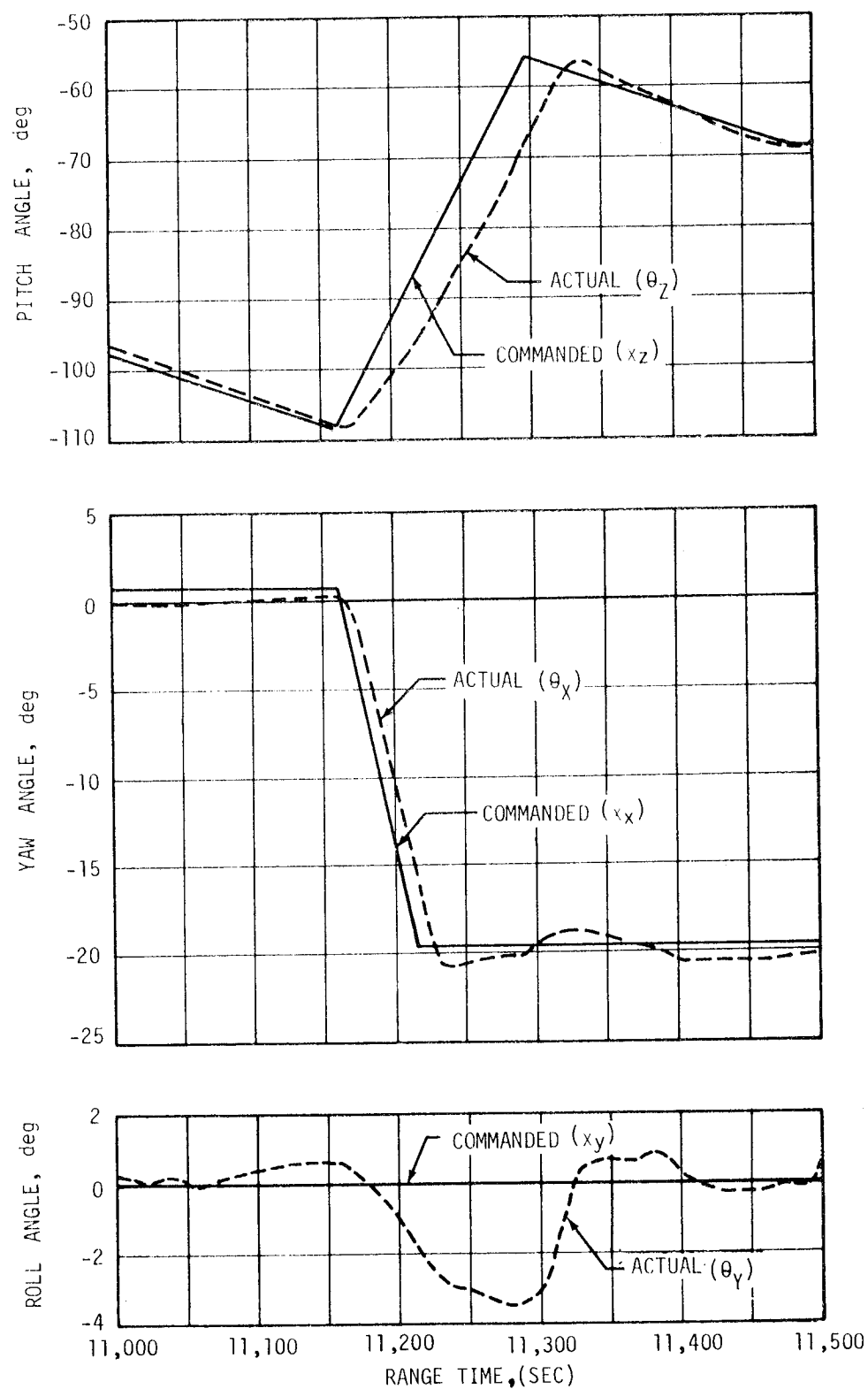


Figure 11-32: Vehicle Attitude During Restart Orientation Maneuver

At initiation of the restart maneuver, the ullage engines were ignited, the LH<sub>2</sub> continuous vent valve closed, and the LH<sub>2</sub> tank repressurization initiated. Immediately following these events, the APS engines were fired in order to align the vehicle in both pitch and yaw to the proper attitude for J-2 re-ignition. During these attitude maneuvers, the sensors on the instrumentation probe indicated LH<sub>2</sub> slosh activity above the deflector. The exact contribution of the attitude maneuver to propellant slosh activity and the attendant ullage pressure collapse problem is being investigated. Preliminary investigation indicates that the relatively high propellant surface level prior to restart coupled with the attitude restart maneuver could cause the LH<sub>2</sub> slosh as experienced by the sensors in the LH<sub>2</sub> tank forward dome area.

### 11.5.3 Control System Evaluation During Second Burn

Attitudes errors, angular velocities, and engine actuator positions during second burn are presented in Figures 11-33 through 11-35. Commanded and actual pitch and yaw attitudes during second burn are presented in Figure 11-36. The agreement between the actuator positions computed from the control equation and actual actuator positions indicates that the steady state control gains were close to their design values. Maximum pitch, yaw and roll errors during second burn were +2.0, -2.4 and +2.3 degrees, respectively. During second burn, control system transients were experienced between 11,570 seconds and 11,630 seconds as a result of the relatively large steering commands issued by the guidance system (see Figure 11-33). These control system transients appeared normal in response to the guidance commands. The maximum engine deflection during this time interval was approximately one degree. Maximum control system parameters for second burn are presented in Table 11-7.

APS firings for roll control are indicated at the bottom of Figure 11-33. Impulse delivered for roll control during second burn was 1118.3 N-s (251.4 lb<sub>f</sub>-s) and 1335.8 N-s (300.3 lb<sub>f</sub>-s) for the module at position I and the module at position III, respectively. Again, as in first burn, the difference in the impulse is attributed to apparent low engine performance. During second burn there was a steady state roll torque of 17.6 N-m (13.0 lb<sub>f</sub>-ft).

During second burn good LOX and LH<sub>2</sub> frequency data were obtained since relatively high amplitude sloshing occurred. LH<sub>2</sub> sloshing occurred primarily near to the predicted LH<sub>2</sub> first mode natural frequency. LOX sloshing, similar to first burn, occurred between the predicted first and second mode LOX natural frequencies. The observed LOX sloshing frequency as shown in Figure 11-37 was very near the LOX first mode closed loop resonant frequency which lies between the first and second mode natural frequency. The control system and vehicle dynamics cause the first mode LOX closed loop resonant frequency to increase significantly above the first mode natural frequency.

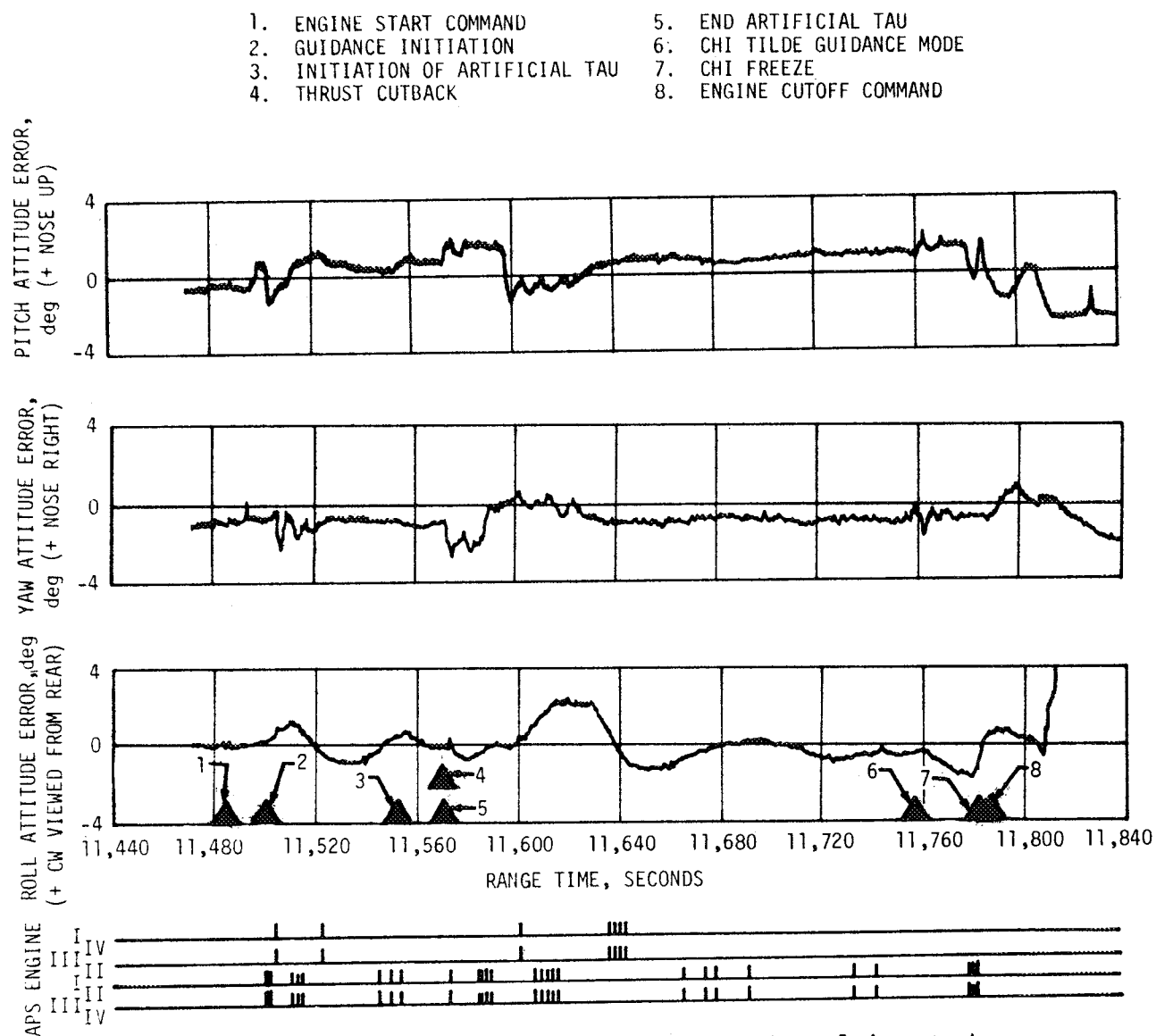


Figure 11-33 Attitude Error and Auxiliary Propulsion System Engine Firings During S-IVB Second Burn



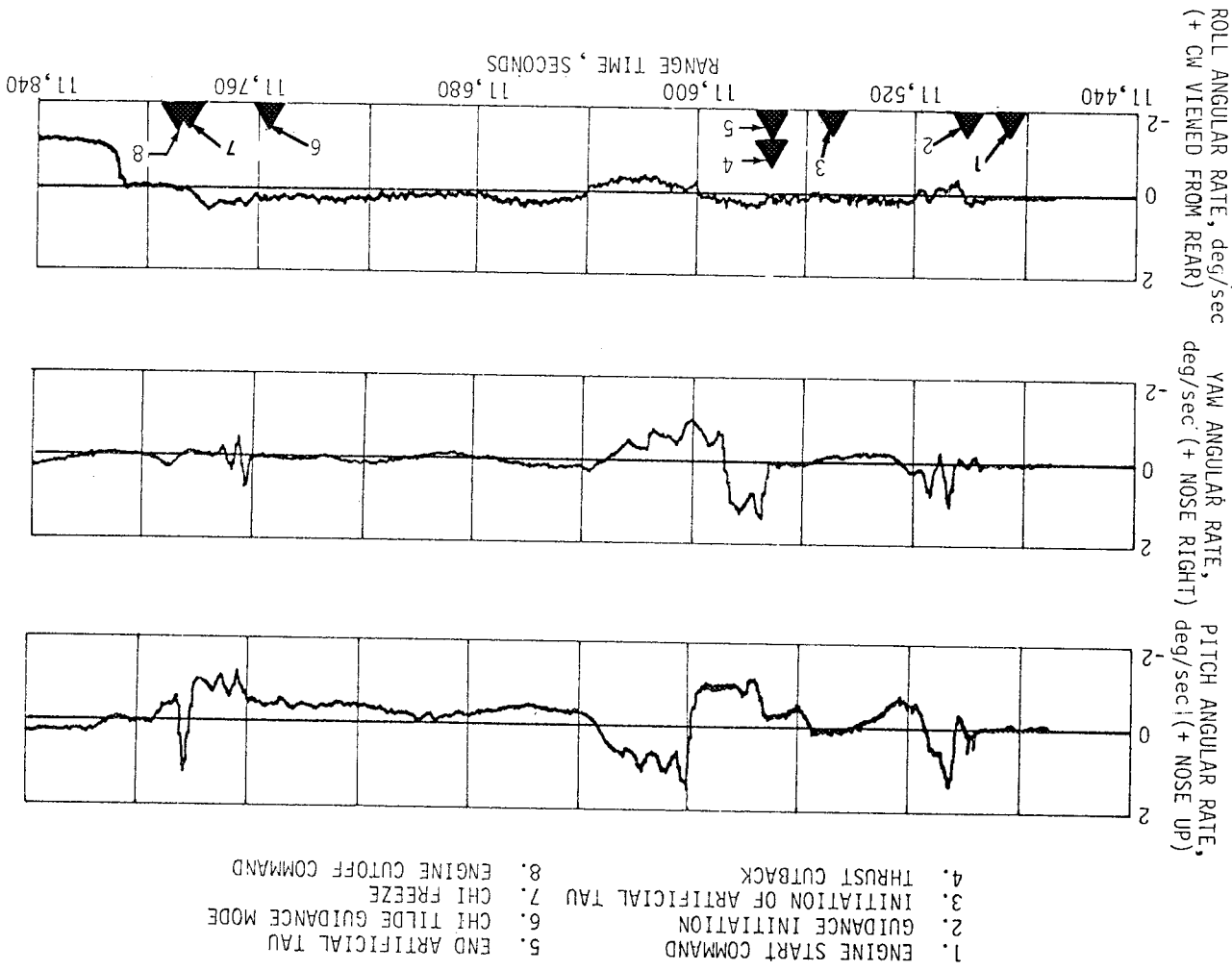


Figure 11-34 Angular Velocities During Second Burn

- |                                 |                            |
|---------------------------------|----------------------------|
| 1. ENGINE START COMMAND         | 5. END ARTIFICIAL TAU      |
| 2. GUIDANCE INITIATION          | 6. CHI TILDE GUIDANCE MODE |
| 3. INITIATION OF ARTIFICIAL TAU | 7. CHI FREEZE              |
| 4. THRUST CUTBACK               | 8. ENGINE CUTOFF COMMAND   |

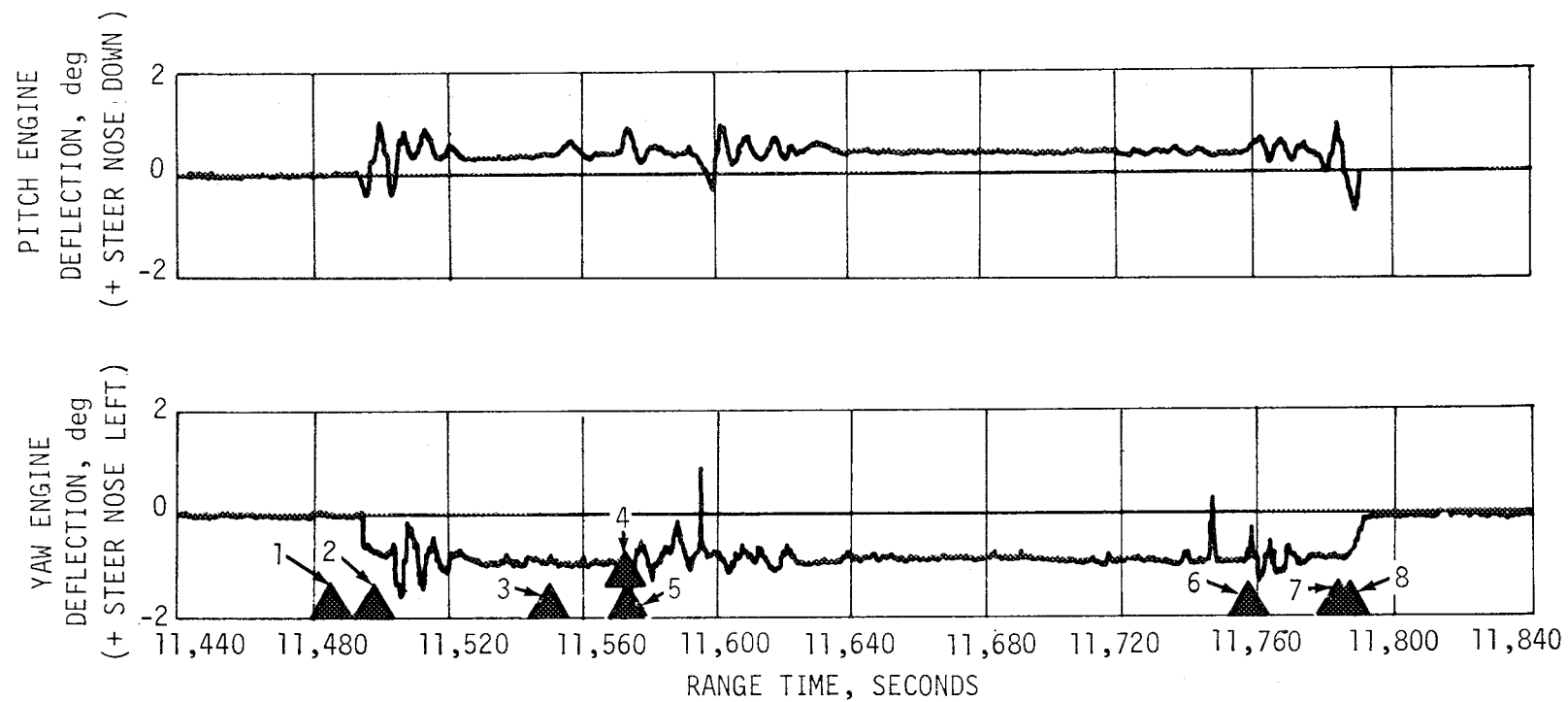


Figure 11-35 S-IVB Pitch and Yaw Actuator Positions During Second Burn

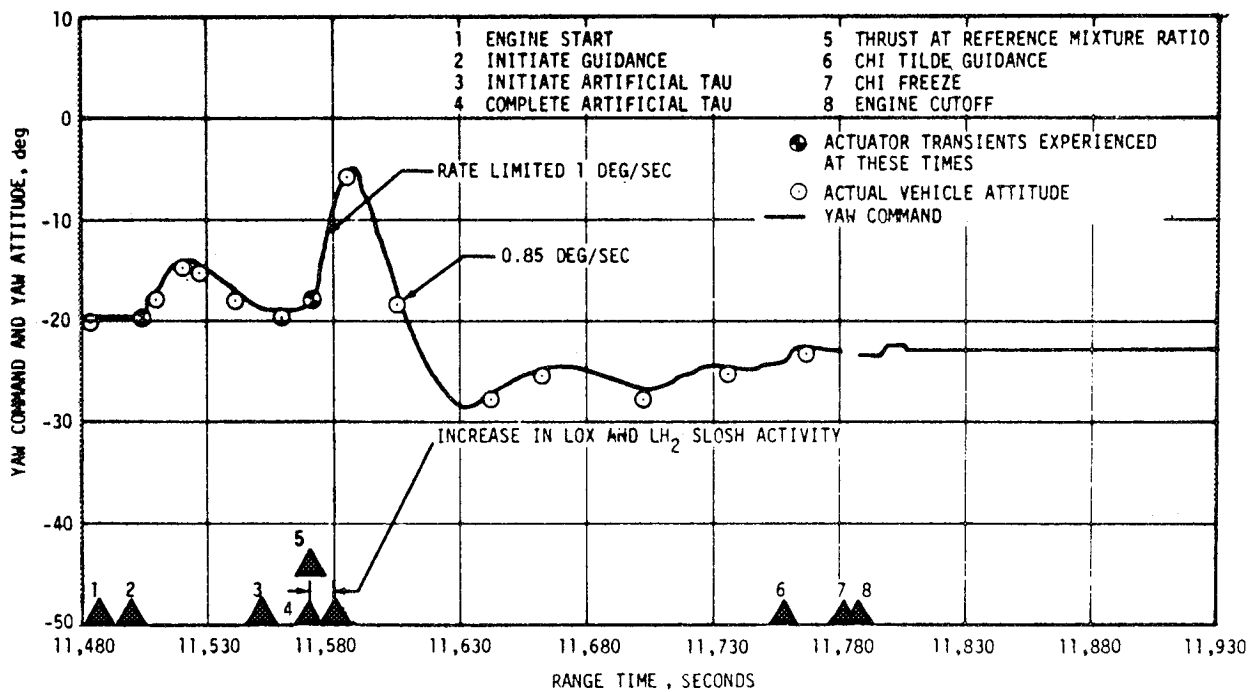
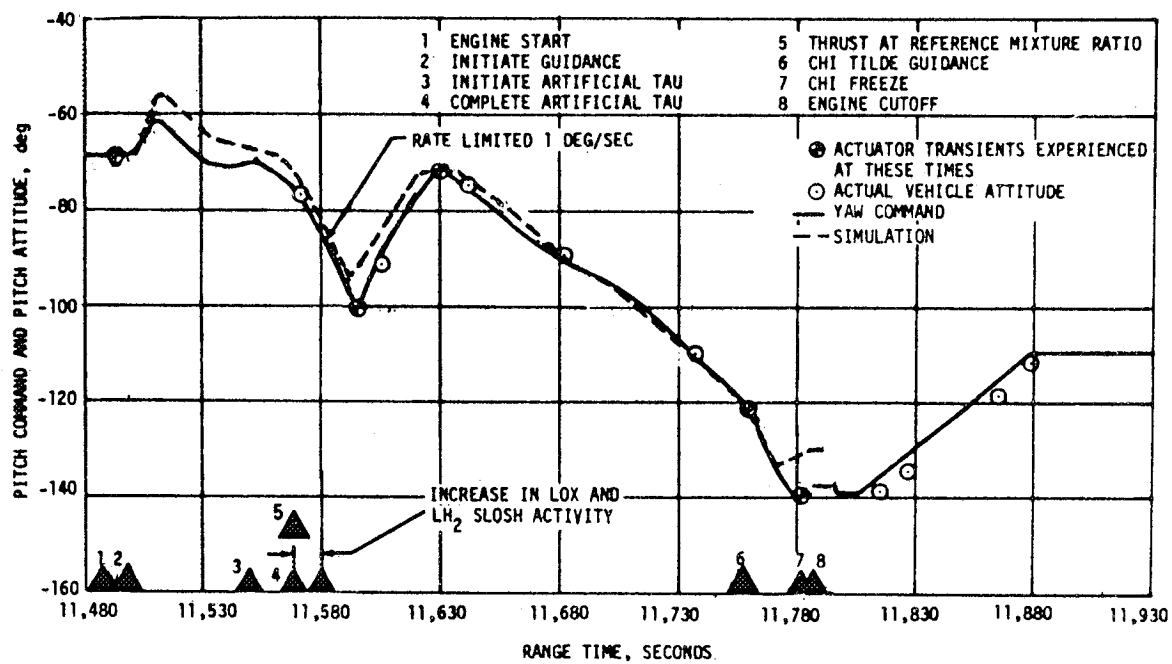


Figure 11-36. Vehicle Attitude During S-IVB Second Burn

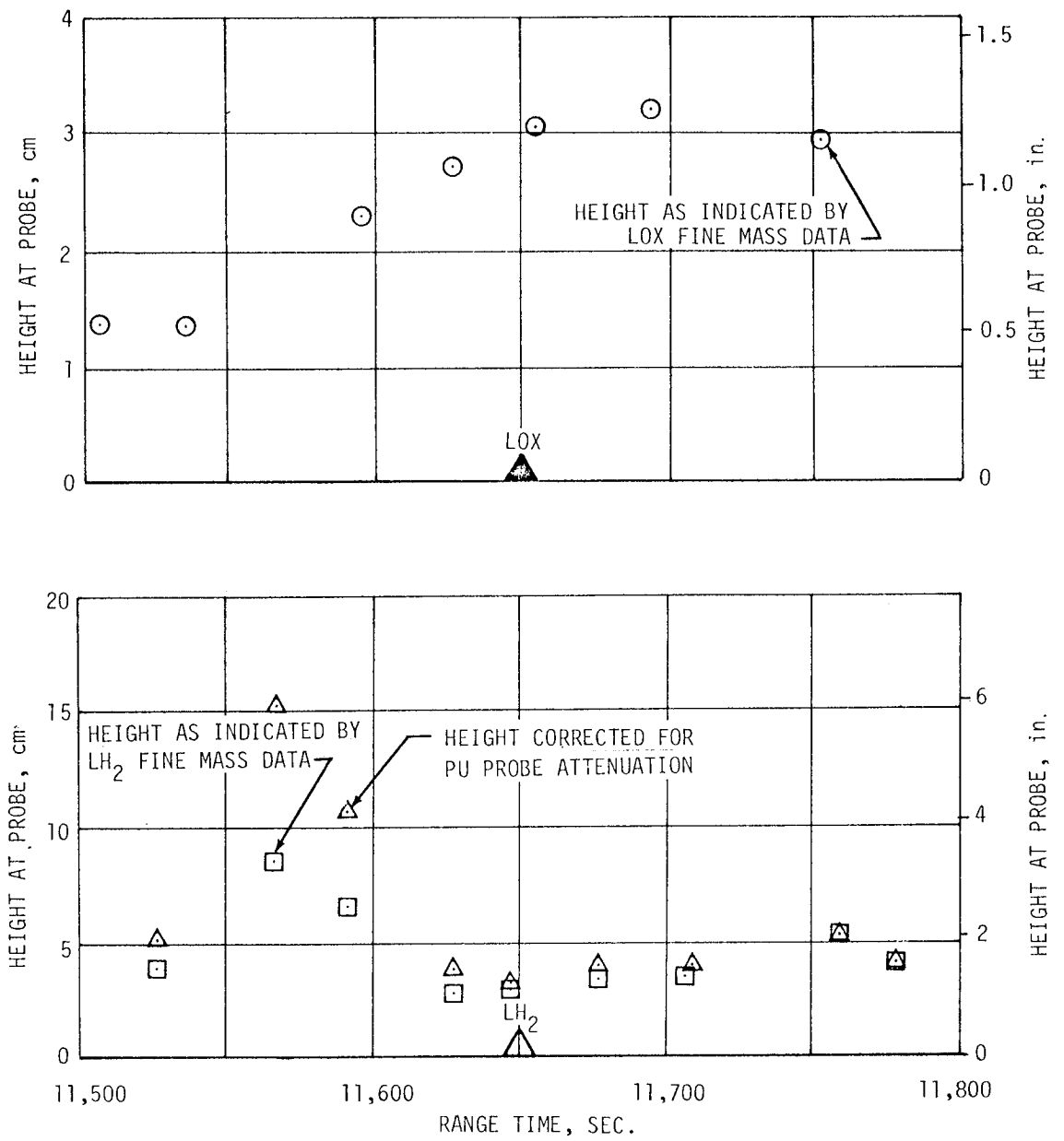


Figure 11-37. S-IVB Slosh Heights During Second Burn

Table 11-7. Maximum Values of Critical Flight Control Parameters-Second Burn

PARAMETER	ESC AND GUIDANCE INITIATION	ARTIFICIAL TAU MODE	CHI TILDE GUID. MODE	CHI FREEZE	J-2 CUTOFF
Pitch Attitude Error (deg)	1.44	2.1	1.6	1.06	-1.5
Yaw Attitude Error (deg)	-2.2	-2.4	-1.7	-0.9	0.7
Roll Attitude Error (deg)	1.5	2.5	-1.45	0.7	0.9
Pitch Rate (deg/s)	1.4	1.3	-1.2	1.1	-0.5
Yaw Rate (deg/s)	1.1	1.4	0.7	0.0	0.3
Roll Rate (deg/s)	-0.35	-0.4	0.45	0.45	-0.15
Pitch Actuator Position (deg)	0.82	0.89	0.63	0.92	-0.8
Yaw Actuator Position (deg)	-1.6	-1.52	-1.3	-1.0	-0.95

This occurred only with the first mode LOX slosh frequency due to the location and magnitude of the slosh mass. All other slosh closed loop resonant frequencies are very close to the slosh natural frequencies. Therefore, it appears that the first mode LOX sloshing frequency was as expected. However, the PU LOX mass sensor is sensitive to second mode LOX sloshing due to its location; thus it is possible that a combination of first and second mode LOX sloshing occurred.

During second burn LOX slosh amplitudes (see Figure 11-37) appeared to increase immediately following the change in guidance commands and vehicle attitude at 11,570 seconds. The maximum slosh amplitude at the probe was approximately 3.05 centimeters (1.2 in.). These increased slosh amplitudes were sustained throughout the remainder of second burn primarily because the propellant surface was below the LOX baffle and limited damping was available.

#### 11.5.4 Control System Evaluation During Waiting Orbit

APS engine firing data in conjunction with commanded and actual vehicle attitude data indicates that attitude control during waiting orbit was normal. Commanded and actual vehicle attitudes following second S-IVB cut-off, maneuver to spacecraft separation attitude, and alignment to Ascension Island are presented in Figures 11-38 and 11-39. APS propellant usage for attitude control during both parking and waiting orbits (excluding ullaging requirements) to loss of data (approximately 25,000 seconds) was 36.4 kg (80.0 lbm) for module at position I and 38.2 kg (84.0 lbm) for module at position III. This propellant usage was lower than expected for attitude control. The lower than expected usage may be attributed to lower than predicted propellant sloshing during orbit. APS usage for attitude control is being investigated further. APS impulse requirements for significant events are summarized in Table 11-8.

#### 11.6 INSTRUMENT UNIT CONTROL COMPONENTS EVALUATION

##### 11.6.1 Control-EDS Rate Gyros/Control Signal Processor Analysis

The analysis of the Control-EDS Rate Gyros/Control Signal Processor indicates that the performance of this combination was nominal. The maximum response of the rate gyros to vibration and acoustics occurred between -2.0 to +20 seconds and +55 to +80 seconds. The maximum range at +8.5 seconds was 8 deg/sec peak-to-peak in roll at a frequency of 21 hertz. A second sample at +60 seconds was 10.4 deg/sec peak-to-peak in roll again at 21 hertz. The 21 hertz values are modulated at a frequency of 1 to 3 hertz. The rate switch filters at these sample points reduced these values to less than 3 deg/sec peak-to-peak performing as designed. The maximum response to vibration was in the roll plane with reduced response in the pitch plane and practically no response in the yaw plane. These values were eliminated by filters in the FCC and did not have any effect on the control parameters.

Vehicle angular rates developed and angles commanded at significant events are tabulated in Table 11-9 and are within the predicted variations. The highest rates detected occurred at 58 seconds, about the pitch and roll axes and reached maximum amplitudes of -1.5 and +2.2 deg/sec in pitch and roll, respectively. These rates were -2.5 and -3.75 deg/sec about the pitch and roll axes, respectively, in S-IU-202.

No valid overrate conditions were observed during S-IC or S-II stage burns. However, before the analysis can be completed, additional data is required.

##### 11.6.2 Flight Control Computer Performance

The performance of the FCC was as expected during S-IC, S-II and S-IVB stage flights. Analyses of the angular velocity and attitude error signals indicated that these signals, as telemetered from the FCC, were similar to the same signals telemetered from the originating components.

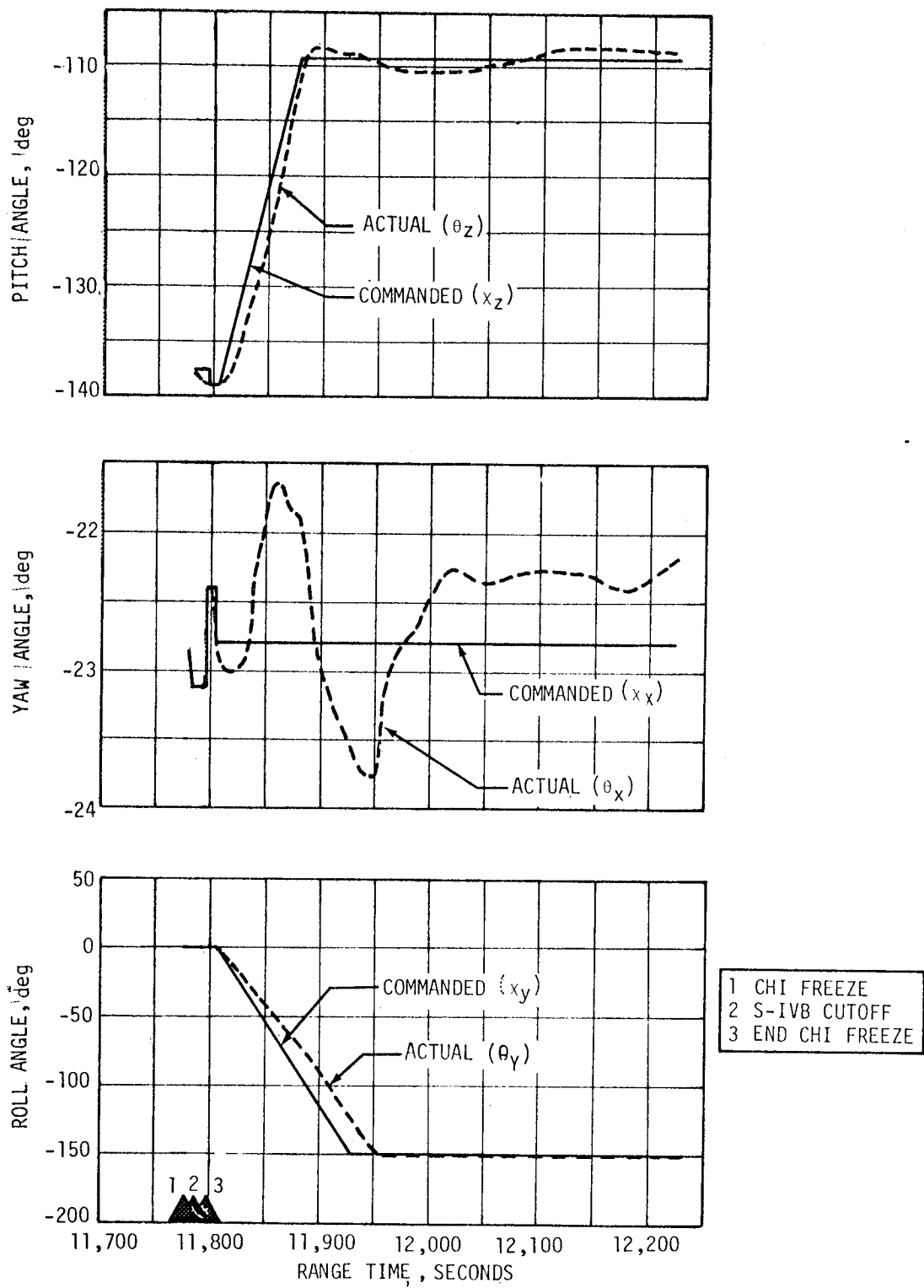


Figure 11-38 Vehicle Attitude Prior to Spacecraft Separation

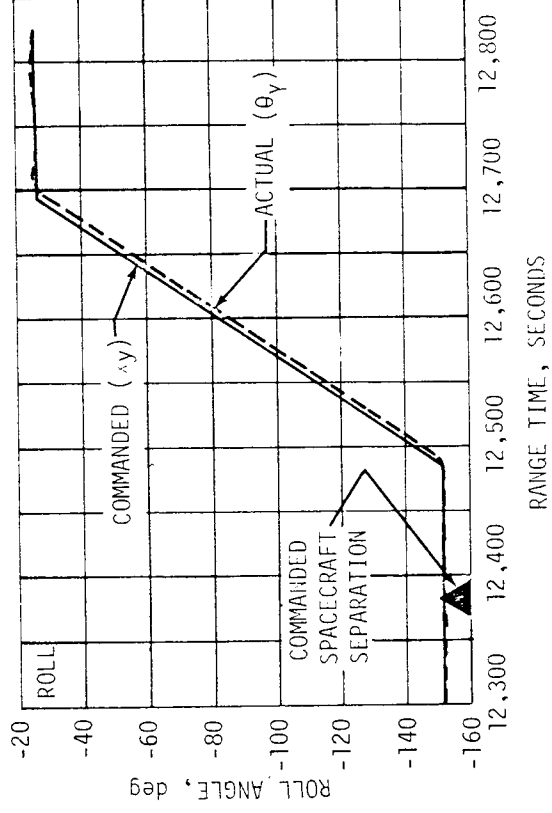
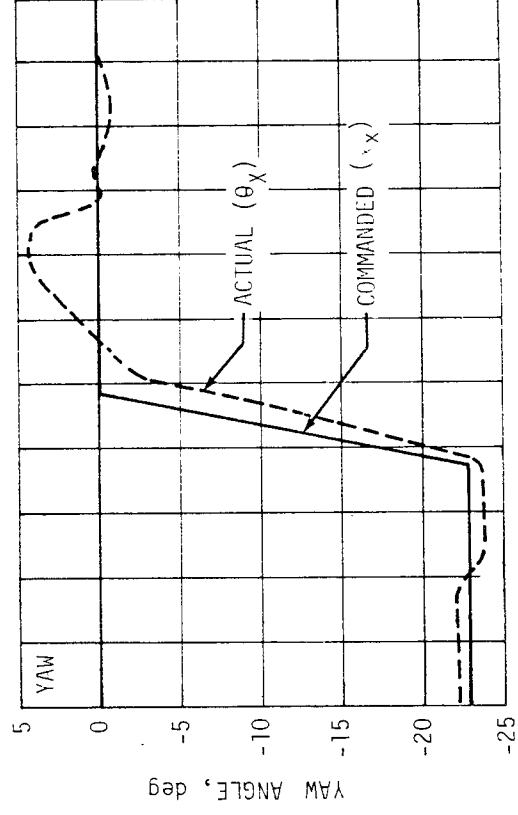
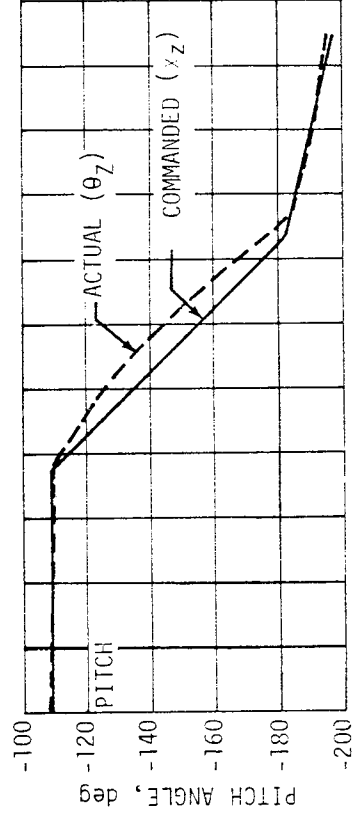


Figure 11-39 Vehicle Attitude Following Spacecraft Separation



Table 11-8. APS Impulse Requirements

EVENT	UNITS	APS ENGINE							
		MODULE AT POS. I TOTAL	MODULE AT POS. III TOTAL	I <sub>IV</sub>	I <sub>P</sub>	I <sub>II</sub>	III <sub>II</sub>	III <sub>P</sub>	III <sub>IV</sub>
S-IVB First Burn	N-s	1085.4	1184.1	652.1		433.2	672.6		511.5
	lb <sub>f</sub> -s	244.0	266.2	146.6		97.4	151.2		115.0
Maneuver to Local Horizontal Following First Cutoff (Until Loss of Data at Tape Recorder Playback)	N-s	7009.9	7055.3		6839.1	170.8	200.2	6855.2	
	lb <sub>f</sub> -s	1575.9	1586.1		1537.5	38.4	45.0	1541.1	
Orientation Maneuver for Restart	N-s	22407.0	21614.8	5460.2	11506.2	5441.1	5177.3	10753.1	5684.4
	lb <sub>f</sub> -s	5037.3	4859.2	1227.5	2586.7	1223.2	1163.9	2417.4	1277.9
S-IVB Second Burn	N-s	1118.3	1335.8	209.1		909.2	234.4		1101.4
	lb <sub>f</sub> -s	251.4	300.3	47.0		204.4	52.7		247.6
Initial Recovery Following Second Cutoff	N-s	1421.2	3741.8			1421.2	1238.4	2503.4	
	lb <sub>f</sub> -s	319.5	841.2			319.5	278.4	562.8	
Orientation Maneuver for S-IVB/CSM Separation	N-s	4252.0	7717.2	1097.8	722.8	2431.4	2418.5	4102.1	1196.6
	lb <sub>f</sub> -s	955.9	1734.9	246.8	162.5	546.6	543.7	922.2	269.0
S-IVB/CSM Separation	N-s	715.7	682.8	267.7	238.9	269.1	305.6	131.7	245.5
	lb <sub>f</sub> -s	160.9	153.5	46.7	53.7	60.5	68.7	29.6	55.2
Alignment to Ascension Following S-IVB/ CSM Separation	N-s	3110.6	6412.6		734.4	1705.4	2045.3		
	lb <sub>f</sub> -s	699.3	1441.6		165.1	383.4	459.3		

Table 11-9. Vehicle Angular Rates Developed and Angles Commanded at Significant Events

Event	Pitch		Yaw		Roll	
	RATE (deg/sec)	ANGLE (deg)	RATE (deg/sec)	ANGLE (deg)	RATE (deg/sec)	ANGLE (deg)
Tower Clearance	1.0	0.5	1.0	-1.0	1.5	Null
Roll and Pitch Program	0.5	0.5	-0.5	1.0	1.0	-0.6
Mach 1	-0.5	0.7	-0.15	Null	2.5	Null
Max Q	-1.6	1.3	0.1	0.2	0.5	-0.1
IECO	-0.5	Null	-0.26	Null	Null	Null
OECO	0.2	-0.5	0.1	-0.6	Null	Null
S-IC/S-II Separation	0.3	-0.3	0.3	-0.6	-0.4	-1.7
S-II Ignition	0.35	-0.3	0.4	-0.5	2.8	1.3
Initiate IGM	1.2	-1.7	-0.08	Null	-0.15	1.3
Second Phase IGM	-0.13	0.5	0.05	Null	±0.5	1.3
S-II ECO	Null	0.4	-0.1	-0.1	-0.2	1.3
S-II/S-IVB Separation	-1.75	2.0	0.24	-0.6	-0.4	0.5
S-IVB Ignition	1.5	2.0	0.24	-0.6	-1.0	0.5
Third Phase IGM	2.0	2.0	0.24	-0.8	-0.8	0.6
S-IVB First ECO	-0.05	0.5	Null	-0.5	Null	0.5
S-IVB Re-Ignition	0.5	-0.2	Null	-0.7	-0.3	-0.5
Fourth Phase IGM	1.2	-1.0	1.0	-2.0	-0.4	1.2
Fifth Phase IGM	-1.0	2.0	-0.9	-2.4	-0.4	2.2
S-IVB Second ECO	Null	Null	0.25	-0.8	0.3	-1.5

### 11.6.3 Gimbal Actuators Analysis

The maximum delta I currents for S-IC, S-II, and S-IVB stage first burn were -7.0, -6.0,  $\pm 6.0$  milliamperes, respectively, and each occurred in pitch actuators. These values represent approximately 13 percent of the capabilities of the 50 milliamperes servo amplifiers.



## SECTION 12 SEPARATION

### 12.1 SUMMARY

S-IC retro motor performance was satisfactory. S-IC/S-II separation and associated sequencing was accomplished as planned. Subsequent S-IC dynamics provided adequate positive clearance between the stages following separation. Performance of the S-II stage during S-IC/S-II separation was nominal with no anomalies noted. The S-II ullage motors functioned as predicted within the required limits. Photographic coverage provided evidence that S-II second plane separation was satisfactory.

The four retro motors mounted on the S-II stage performed satisfactorily in separating the S-II and S-IVB stages. All performance parameters were close to nominal. S-IVB ullage motor performance was satisfactory. Separation of the S-IVB stage from the S-II stage was accomplished satisfactorily within the desired time period.

S-IVB attitude control was normal during S-IVB spacecraft separation.

A summary of separation events and times of occurrence is given in Table 12.1.

### 12.2 S-IC/S-II SEPARATION EVALUATION

Performance of the S-IC/S-II separation system was satisfactory with no anomalies noted. The S-IC/S-II stage switch selectors which sequence the separation system responded correctly to the signals from the Instrumentation Unit. The switch selector output (28-VDC pulses) actuated the appropriate circuitry in the separation system to control the Exploding Bridgewire (EBW) firing units arm and trigger circuits. All EBW firing units responded correctly.

#### 12.2.1 S-IC Retro Motor Performance

The S-IC retro motor performance was satisfactory. The ignition signal to the retro motors occurred at 151.48 seconds. The average effective retro motor temperature was determined to be approximately 288.5°K (60°F) based on the observed effective burn times. The effective impulse, average effective thrust, and associated 3 sigma limits were dependent on the retro motor temperature. The limits and nominal values shown in Table 12-2 reflect this dependency.

Table 12.1. Commanded Separation Event Times

EVENT	ACTUAL TIME (SEC) RANGE TIME	PREDICTED TIME (SEC) RANGE TIME
S-II Ullage Motor Fire Signal	151.24	152.40
S-IC/S-II Separation Signal	151.43	152.60
S-IC Retro Motor Ignition	151.48	152.65
S-II Engine Start	152.12	153.30
S-II Second Plane Separation Signal	181.44	182.60
S-IVB Ullage Motor Fire Signal	520.44	517.02
S-II/S-IVB Separation Command	520.53	517.12
S-II Retro Motor Fire Signal	520.57	517.16
S-IVB Engine Start On	520.72	517.32
S-II/S-IVB Separation Complete	521.57	518.17
Start S-IVB-IU/CSM Separation	12,386.47	12,399.59

Table 12-2. S-IC Retro Motors System Performance

RETRO MOTOR	EFFECTIVE BURN TIME, SECONDS	TOTAL IMPULSE N-SECONDS lb <sub>f</sub> -SECONDS	PARAMETER	
			EFFECTIVE IMPULSE, N-SECONDS lb <sub>f</sub> -SECONDS	AVERAGE EFFECTIVE THRUST, N lb <sub>f</sub>
Fin A - Position I	0.6448	296,002 66,543.9	264,963 59,566.1	410,922 92,378.9
Fin A - Position II*	0.6446	281,314 63,241.9	255,733 57,491.1	396,728 89,188.0
Fin B - Position II**	0.6237	302,386 67,979.1	267,578 60,153.9	429,017 96,446.9
Fin B - Position III	0.6371	287,982 64,740.9	261,013 58,678.1	409,685 92,100.9
Fin C - Position III	0.6463	284,553 63,970.1	258,931 58,210.0	400,633 90,065.9
Fin C - Position IV	0.6375	290,242 65,249.0	260,034 58,458.0	407,893 91,698.0
Fin D - Position IV	0.6301	275,496 61,934.0	250,759 56,372.9	397,964 89,465.9
Fin D - Position I	0.6292	288,983 64,966.0	259,540 58,346.9	412,492 92,731.9
Average	0.6366	288,369 64,827.9	259,816 58,409.0	408,133 91,751.9
Nominal 288.5°K (60°F) Rocket	0.640	No Nominal or 3σ limits given	246,876 55,499.9	386,995 86,999.9
-3σ Limit 288.5°K (60°F) Rocket	0.603		242,428 54,500.0	364,754 82,000.0
+3σ Limit 288.5°K (60°F) Rocket	0.677		251,769 56,599.9	409,236 91,999.9

\* Lowest Maximum Thrust

\*\* Highest Maximum Thrust

The data received from telemetry showed chamber pressures higher than expected. Thiokol specifications predict a nominal chamber pressure of 1137.6 N/cm<sup>2</sup> (1650 psia) for a 288.5°K (60°F) grain temperature. Flight data, however, gave pressures from 1171 N/cm<sup>2</sup> (1700 psia) to 1274 N/cm<sup>2</sup> (1850 psia).

Figure 12-1 shows thrust versus time for the motor with highest maximum thrust (retro motor No. 3) and for the motor with lowest maximum thrust (retro motor No. 2). The ballistic definitions used as a basis for the retro motor performance analysis are consistent with the model specification.

As shown by Table 12-2 some of the ballistic parameters exceeded the 3 sigma maximum limits. This behavior is particularly evident for the effective impulse, and is a consequence of the high chamber pressures received from telemetry. Investigation into transducer and system accuracy has thus far disclosed no reason for the chamber pressure magnitude.

From a performance standpoint there is no concern that the pressures were higher than expected. With the exception of the apparently high combustion pressures, the retro motors functioned normally and provided a successful S-IC/S-II stage separation. From a design standpoint both the retro motors and stage attachment hardware are structurally adequate to withstand higher thrust levels. However, since the combination of motor to motor performance deviation and estimated telemetry measurement system error does not seem to account for the observed performance levels, further investigation is in order, and will be conducted to attempt to resolve this discrepancy. Initial investigation will center on the retro motor chamber pressure transducer.

#### 12.2.2 S-II Ullage Motor Performance

The S-II ullage motors functioned as predicted within the required limits. Performance parameters of the eight ullage motors are summarized in Table 12-3. Ullage motor ignition signal was given at 151.24 seconds. Ullage motor composite thrust-time curve is shown in Figure 12-2. A review of the chamber pressures showed the motor-to-motor variation was within plus or minus 3.5 percent. This variation was extremely low considering that the motors used on the AS-501 flight were from three different manufacturing lots.

#### 12.2.3 S-IC/S-II Separation Dynamics

The first plane separation was monitored by accelerometers and rate gyros on each of the two stages. Separation rate transducers (extensimeters) provided relative separation rate and distance data. In addition, motion picture film provided a visual indication of the clearance between the two stages as they separated. For evaluation purposes, first plane separation dynamics were calculated using a digital computer. These calculations were



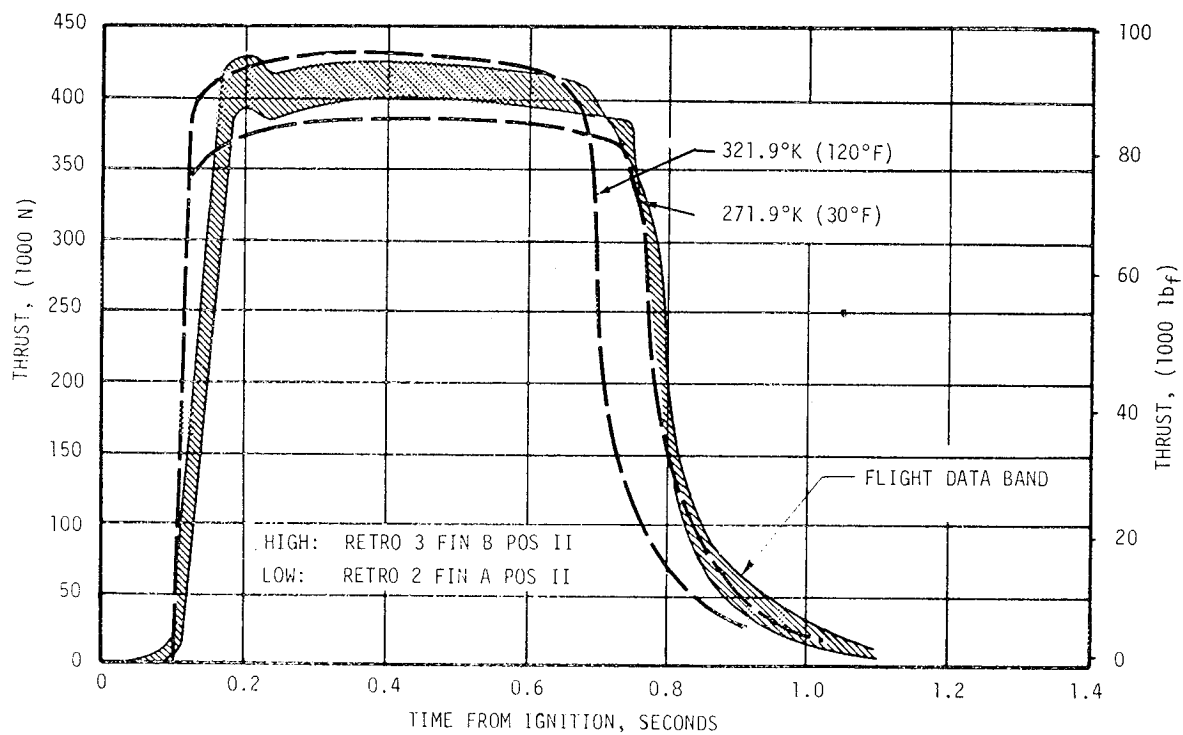


Figure 12-1. S-IC Retro Motors Thrust

Table 12-3. S-II Ullage Motor Performance

EVENTS		MOTOR								REQUIREMENTS AT 294.4 °K (70 °F)	
		1	2	3	4	5	6	7	8	MAX	MIN
Burn Time*	Seconds	3.797	3.702	3.735	3.736	3.75	3.705	3.712	3.756	4.02	3.40
Maximum Thrust	Newtons Pounds	110,858 24,922	113,807 25,585	109,972 24,723	107,988 24,277	111,449 25,055	113,220 25,453	112,784 25,355	**	115,504 25,980	100,618 22,620
Average Burn Time Chamber Pressure	N/cm2 psia	694.1 1,006.8	700.0 1,015.4	678.7 984.5	679.6 985.7	694.7 1,007.6	694.7 1,000.7	690.5 1,001.5	681.8 989.0	741.1 1,075.0	620.5 900.0
Average Burn Time Thrust	Newtons Pounds	103,006 23,157	103,883 23,354	100,725 22,644	100,854 22,673	103,087 23,175	102,379 23,016	102,455 23,033	101,347 22,748		
Burn Time Total Impulse	N-s lbf-s	391,196 87,945	384,618 86,466	376,264 84,588	376,860 84,722	387,193 87,045	379,346 85,281	380,383 85,514	380,080 85,446	404,737 90,989	341,799 76,840

\*Time between 75% Start Transient Maximum Chamber Pressure and the Decrease to 75% of Maximum Chamber Pressure

\*\*Transducer Malfunction, Data Questionable

based on flight data covering, initial trajectory conditions, thrust of the F-1 engines, retro and ullage motors, engine gimbal angles, and mass properties. The results of these calculations are presented and compared with flight test data in Figures 12-3 through 12-5.

Figure 12-3 shows relative velocity and longitudinal acceleration. The plot for relative velocity also shows the incremental velocities of the two separating stages. These are the changes in velocities from time of first motion. The relative translation of the two separating stages is shown in Figure 12-4.

The point is also indicated where the S-IC stage clears the 0.41 meters (16 in.) of the J-2 engines extending beyond the separation plane. Very close agreement between the simulated results and the actual data is indicated in this figure. The minimum clearance was calculated to be 1.31 meters (52.1 in.) between Engine No. 1 and the S-IC stage.

Flight data for the S-II attitude errors in the three axes are given in Figure 12-5. S-IC pitch and yaw dynamics following separation are shown in Figure 12-6. Attitude deviations are derived by integrating the angular rate. The significant result is that the S-IC stage pitches nose up and to the right after separation. This motion can be attributed to the higher measured tail-off thrust of the number one and two F-1 engines.

### 12.3 S-II SECOND PLANE SEPARATION DYNAMICS

Photographic coverage provides the only means of adequately monitoring second plane separation (see Figure 12-7). However, the dynamics of the second stage were calculated using a digital computer. These calculations utilized

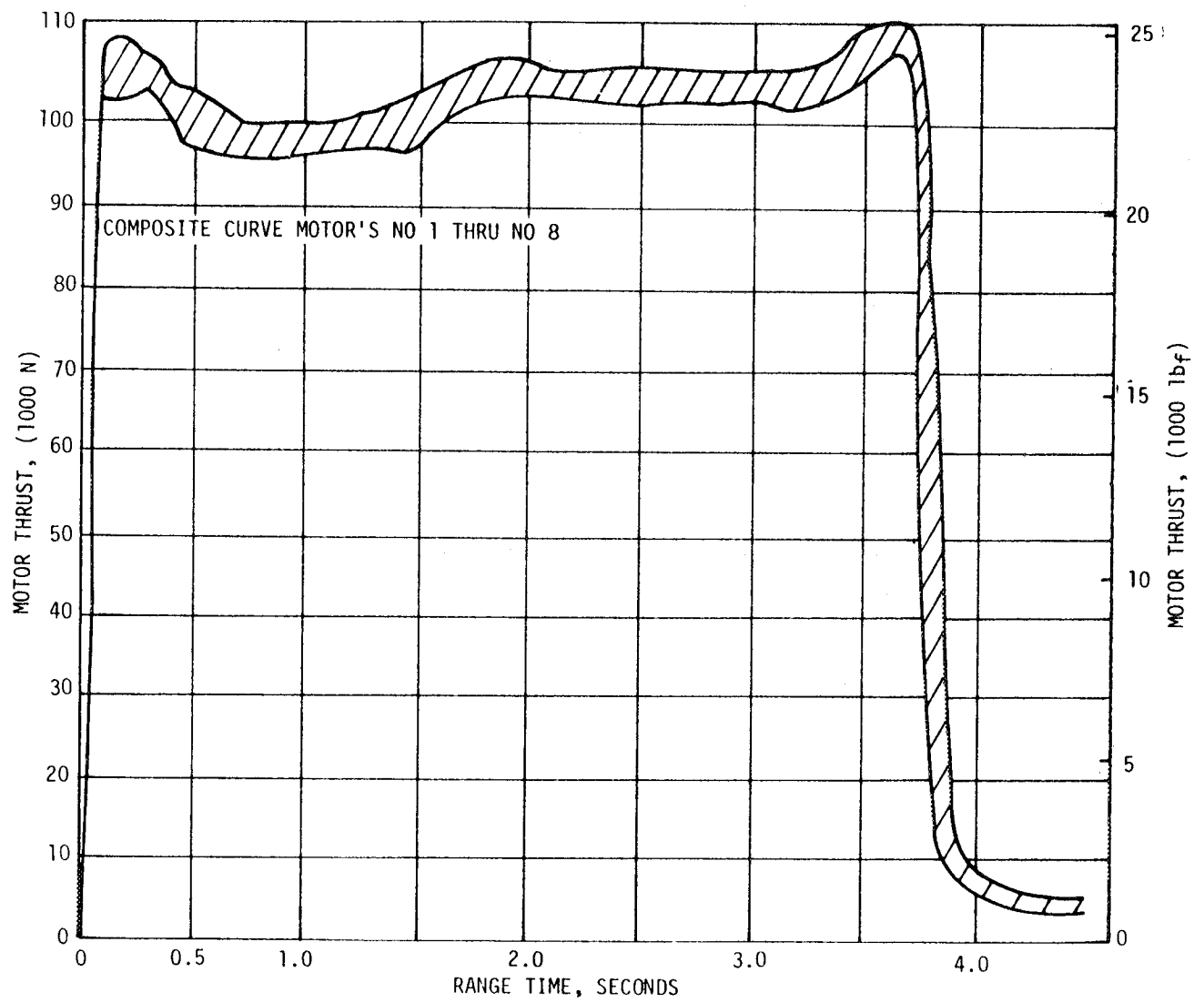


Figure 12-2. S-II Ullage Motor Thrust

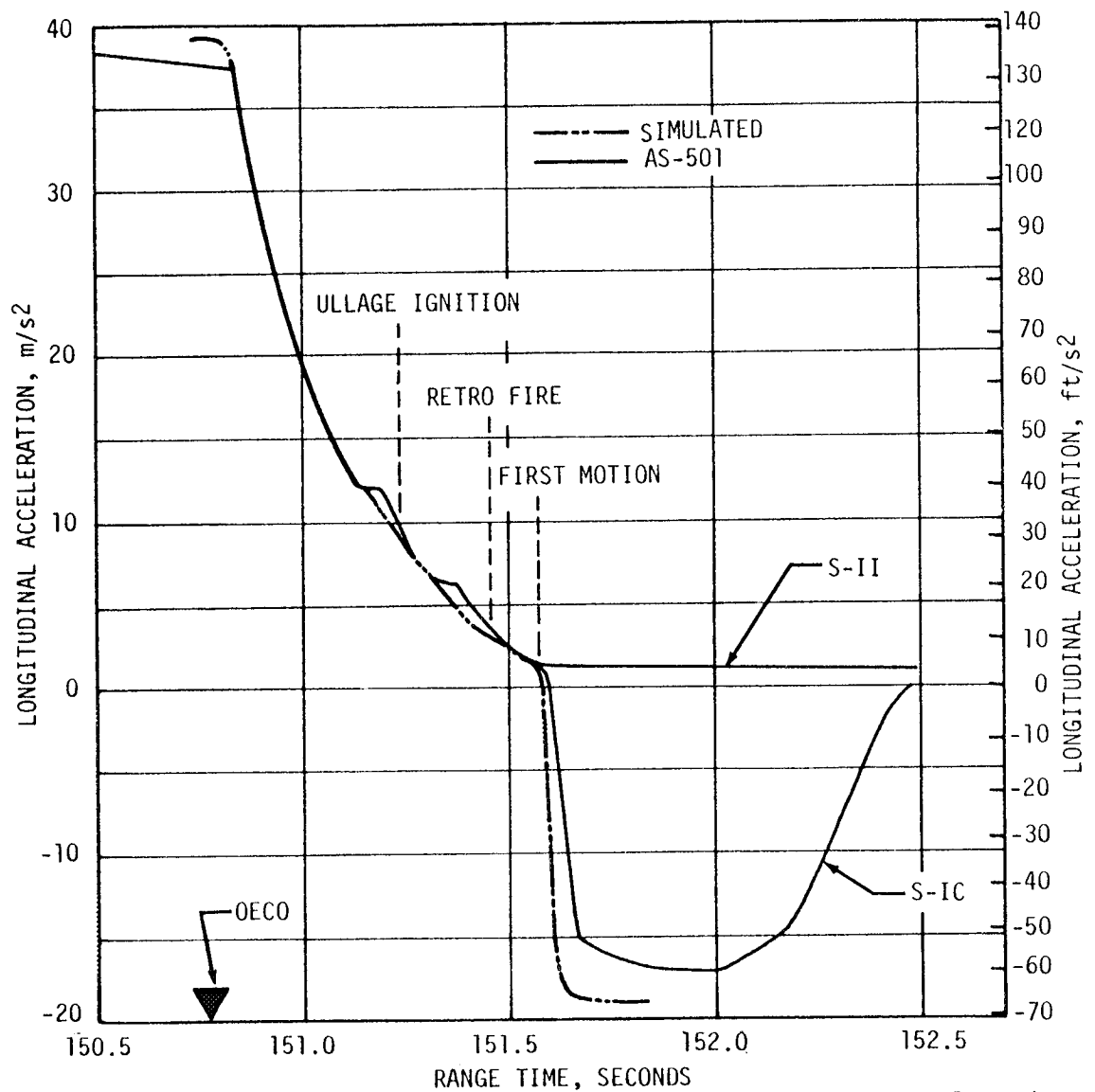
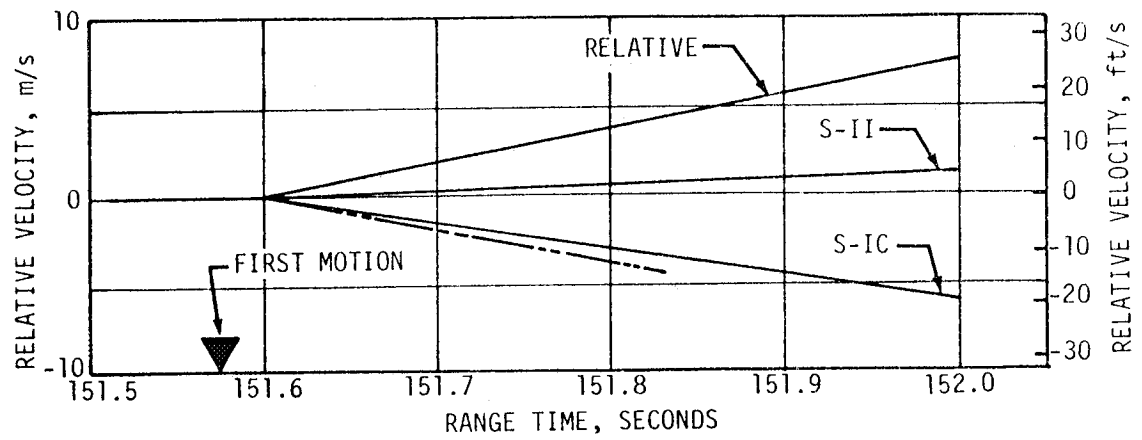


Figure 12-3. S-IC/S-II Relative Velocity and Longitudinal Acceleration

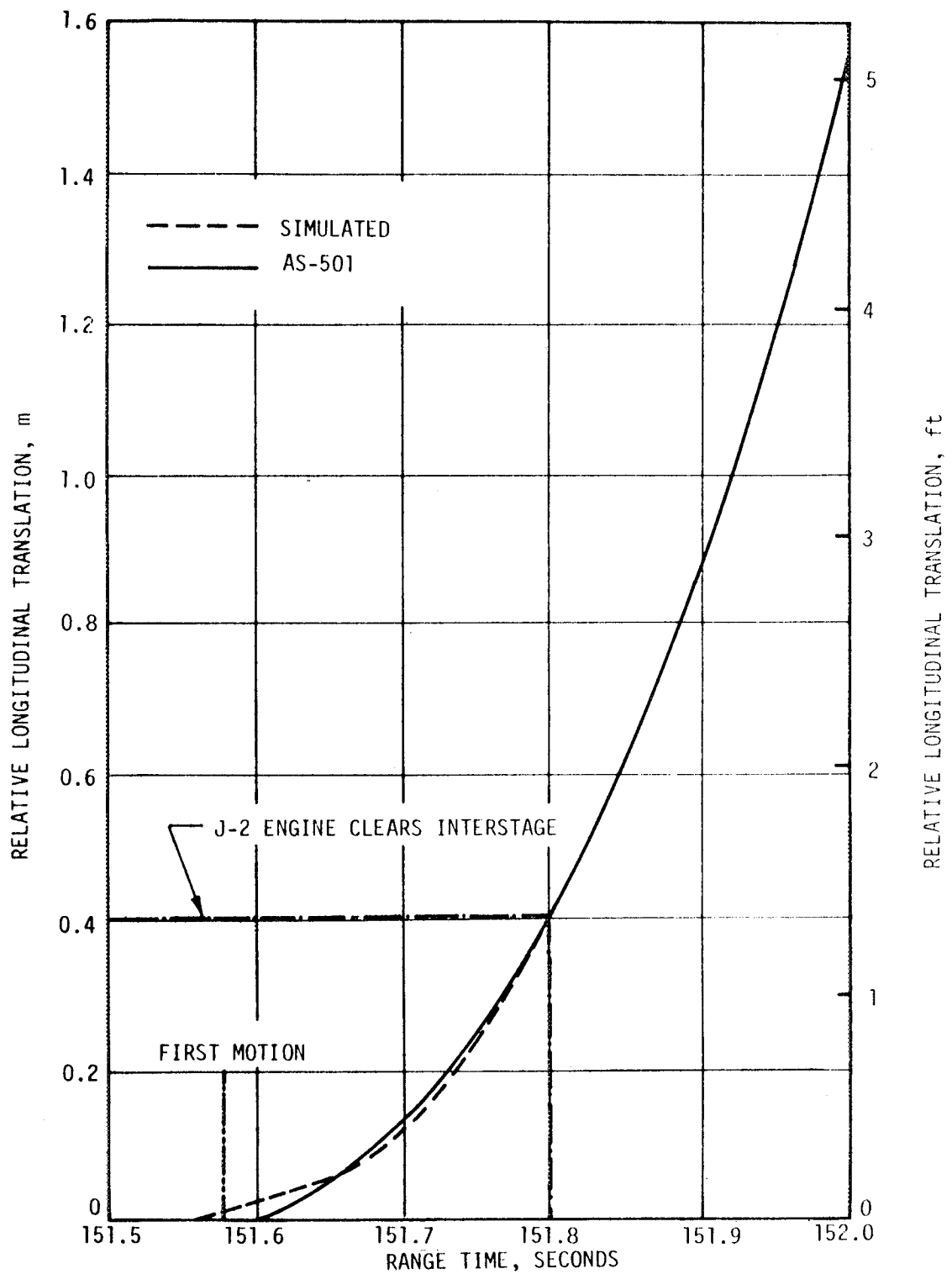


Figure 12-4. S-IC/S-II Separation Distance

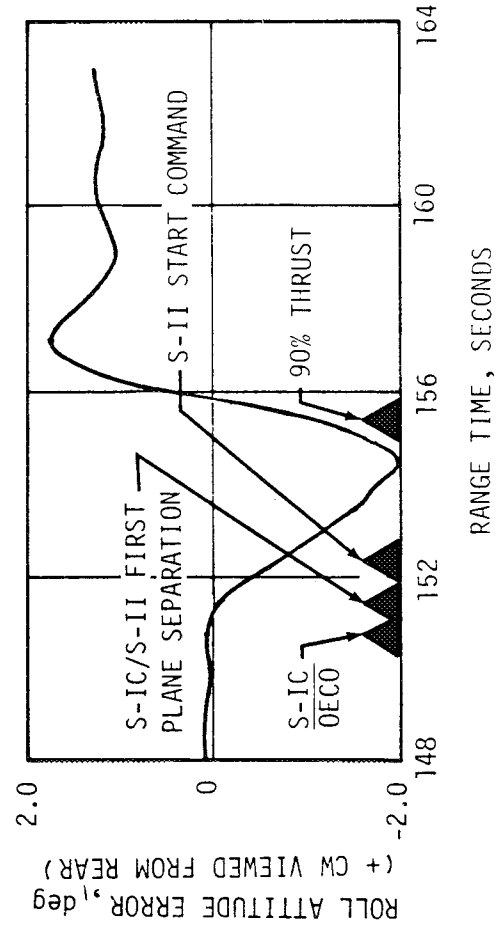
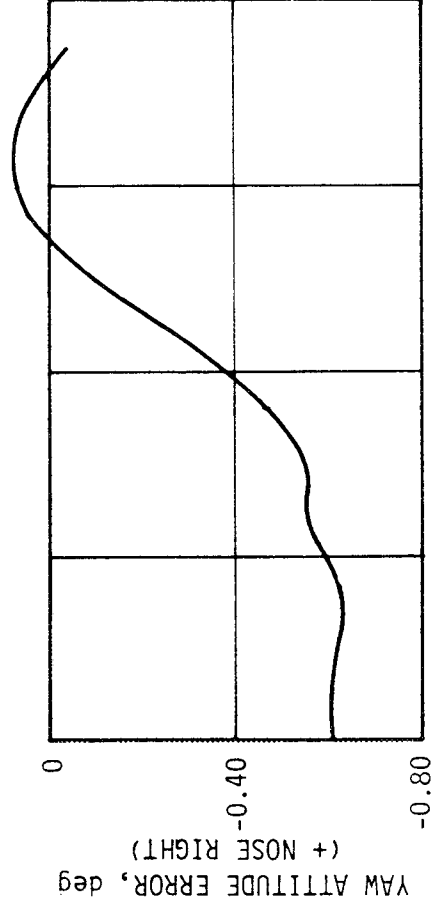
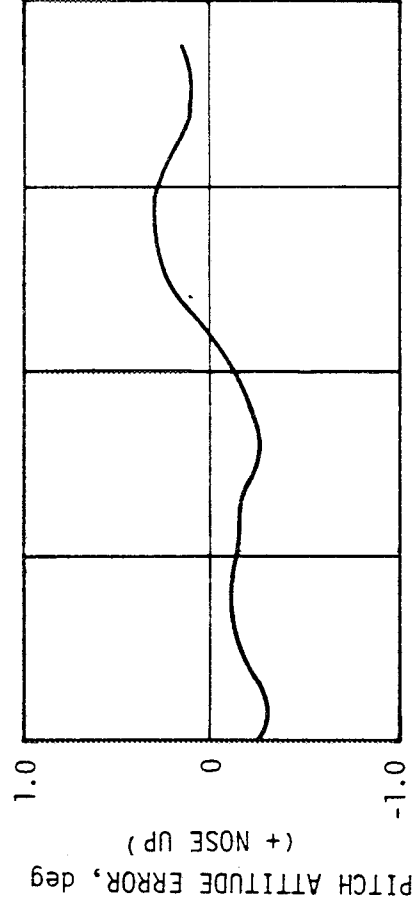


Figure 12-5. S-II Stage Attitude Errors During S-IC/S-II Separation

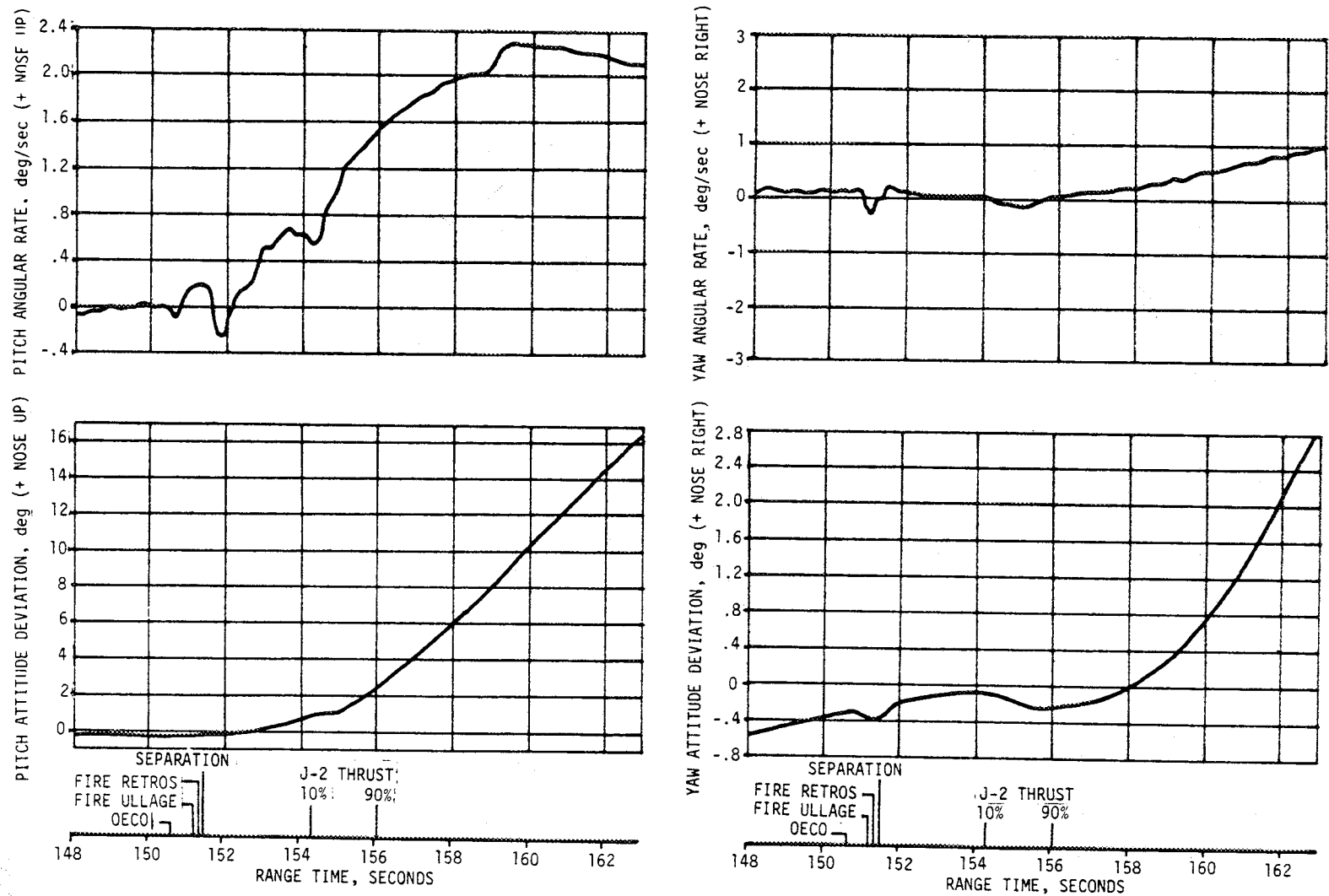


Figure 12-6. S-IC Pitch and Yaw Dynamics Following S-IC/S-II First Plane Separation

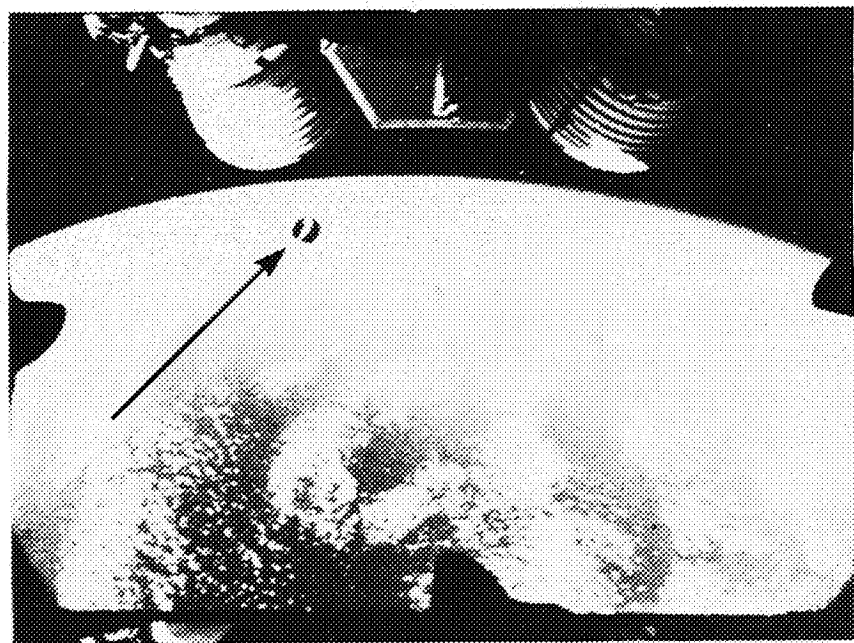
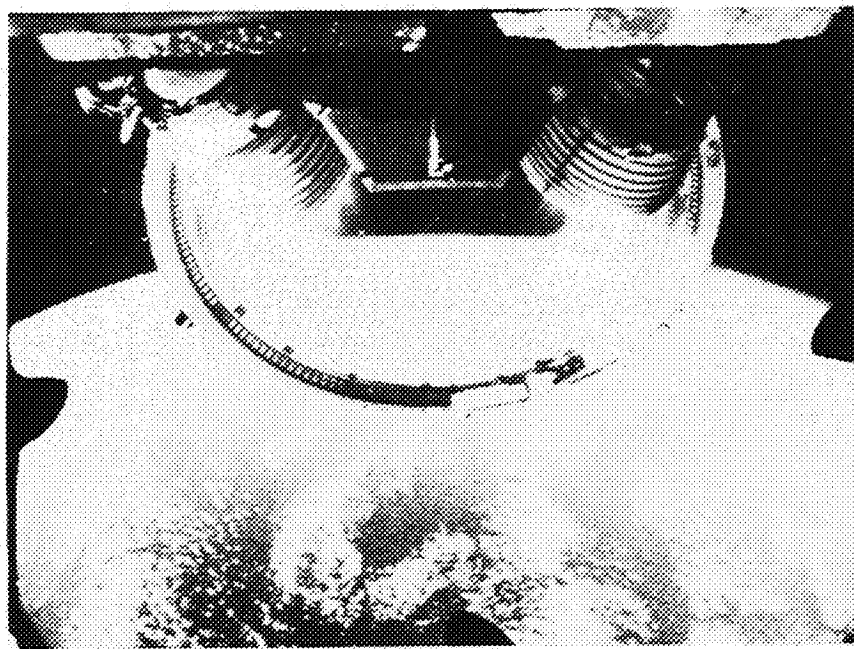


Figure 12-7. S-IC/S-II Second Plane Separation



appropriate initial trajectory data, postflight mass characteristics, and J-2 engine plume data. The only flight data from film analysis available at the time of analysis were relative velocity and relative displacement. All other data were calculated results.

The relative separation velocities between the two bodies are shown in Figure 12-8. The reduced data from the separation film were somewhat scattered but a smooth curve could be sketched through the data points. The corresponding velocities calculated by a digital program were found to be greater than flight data indicated. After reducing the electrical disconnect force used in the separation calculation, from the predicted 155 pounds to zero, the computed relative velocity falls very close to the average obtained from flight. Both sets of these calculations are shown in the figure.

The clearance between the engines and the interstage was also calculated by computer and is shown for each engine in the figure. The figure shows the lateral clearance; i.e., the clearance projected in the Y-Z plane, versus the body station on the interstage at which the closest distance occurs. To get the clearance to the inside of the interstage ring, the ring depth is subtracted. This results in a minimum clearance of 1.03 meters (41 in.).

The axial separation distance versus time is also compared to the calculated (simulation) data.

#### 12.4 S-II/S-IVB SEPARATION EVALUATION

Performance of the S-II/S-IVB separation system was satisfactory with no anomalies noted. The S-II/S-IVB stage selectors which sequence the separation system responded correctly to the signals from the Instrumentation Unit. The switch selector output (28-VDC pulses) actuated the appropriate circuitry in the separation system to control the EBW firing units arm and trigger circuits. All firing units responded correctly.

##### 12.4.1 S-II Retro Motor Performance

The four retro motors mounted on the S-II stage performed satisfactorily and separated the S-II stage from the S-IVB stage. Table 12-4 presents performance parameters for the individual retro motors. All performance parameters were close to their nominal values. Thrust profiles for the retro motors are shown in Figure 12-9.

##### 12.4.2 S-IVB Ullage Motor Performance

Ullage motor performance was satisfactory. The ullage motor ignition command was given at 520.44 seconds, with the jettison command at 532.53 seconds. These times were very close to the predicted. Table 12-5 presents the individual rocket motor performance parameters.

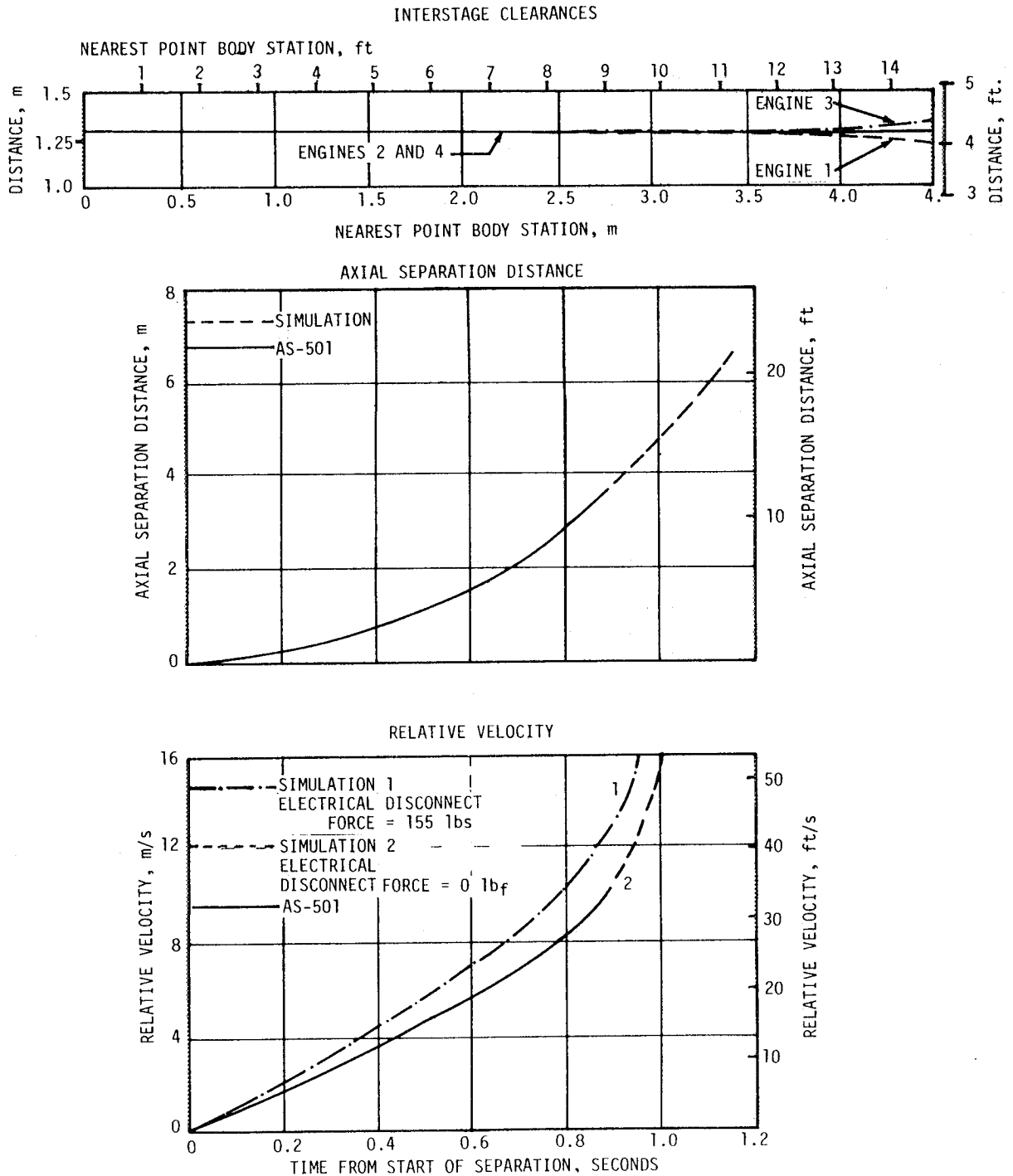


Figure 12-8. Relative Velocity, Interstage Clearance Distance and Axial Separation Distance During Second Plane Separation

Table 12-4. S-II Retro Motor Data

PARAMETER	UNITS	SPECIFICATION LIMITS AT 288.9 °K (60 °F)					
		1	2	3	4	MAXIMUM	MINIMUM
Motor Number							
Maximum Thrust	N	185,660	186,065	189,877	193,364	193,142	152,129
	lbf	41,738	41,829	42,686	43,470	43,420	34,200
Burn Time	sec	1.545	1.510	1.430	1.460	1.67	1.38
Burn Time Total Impulse	N-s	260,755	254,572	249,812	256,929	250,435	232,598
	lbf-s	58,620	57,230	56,160	57,760	56,300	52,290
Burn Time Average Thrust	N	168,766	168,588	174,682	175,972	175,416	134,292
	lbf	37,940	37,900	39,270	39,560	39,435	30,190
Burn Time Average Pressure	N/cm <sup>2</sup>	1186.3	1193.0	1236.7	1232.6	1341	1114
	lbf/in <sup>2</sup>	1731.4	1730.3	1793.7	1787.7	1945	1615

Table 12-5. S-IVB Ullage Motor Performance

PARAMETER	UNIT	MOTOR A (POS II - III)	MOTOR B (POS III - IV)	NOMINAL PERFORMANCE LIMITS	
				MAXIMUM	MINIMUM
Burn Time*	(Sec)	3.86	3.87	4.10	3.54
Average Burn Time Chamber Pressure	(N/CM <sup>2</sup> )	678	671	758	614
	(PSIA)	984	971	1,100	890
Maximum Thrust	(N)	15,466	15,297	18,460	11,565
	(lb)	3,477	3,439	4,150	2,600
Average Burn Time Thrust	(N)	15,186	15,017	16,841	13,745
	(lb)	3,414	3,376	3,786	3,090
Burn Time Total Impulse	(N-Sec)	58,628	58,112	60,451	55,603
	(lb-Sec)	13,180	13,064	13,590	12,500

\*The time interval between 10 percent of maximum chamber pressure during the start transient and 75 percent of maximum chamber pressure during the cutoff transient.

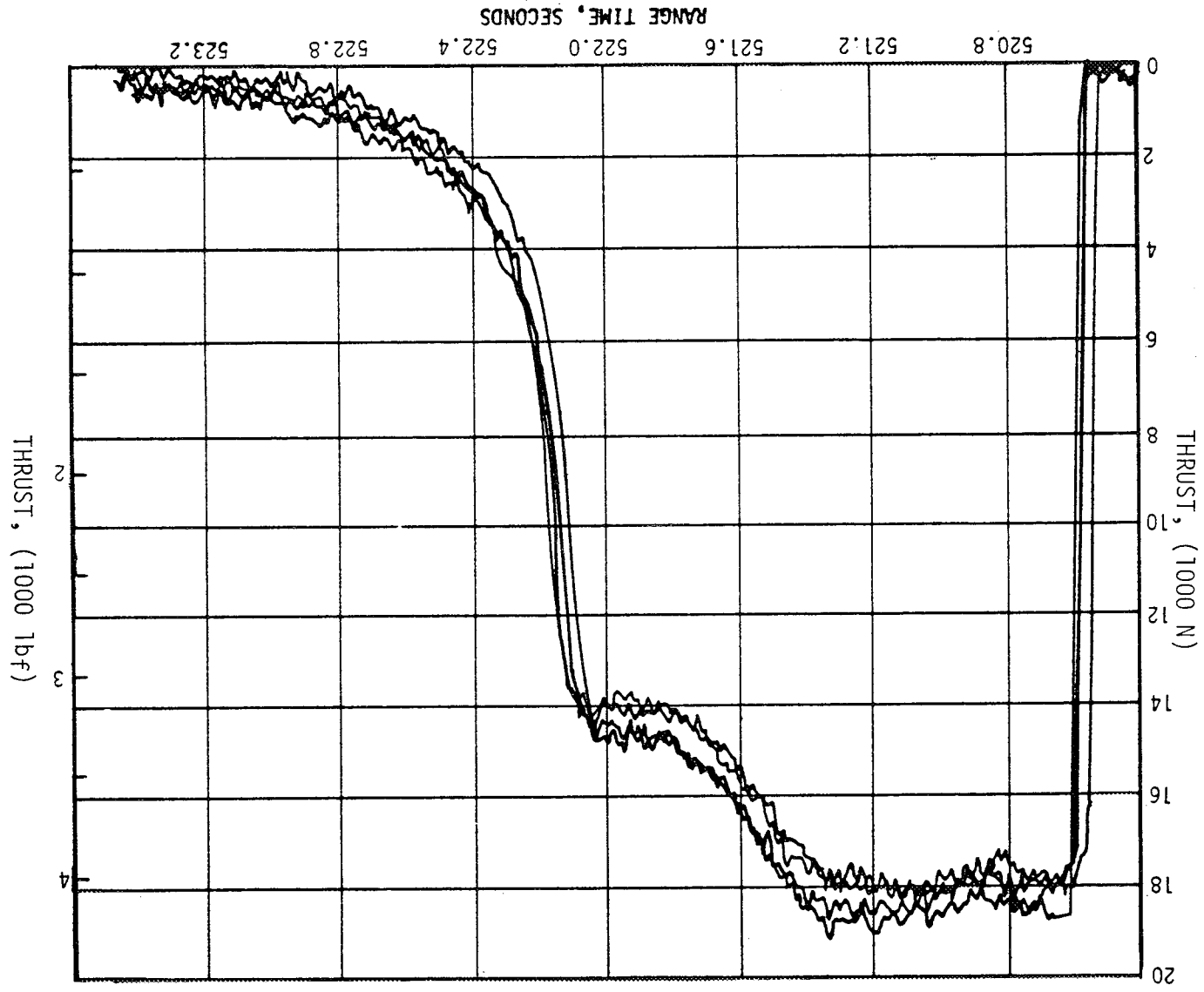


Figure 12-9. S-II Retro Motor Thrusts

A comparison of these data with nominal performance limits indicates that both motors performed within design specifications. Figure 12-10 presents the thrust profiles during firing.

#### 12.4.3 S-II/S-IVB Separation Dynamics

Separation of the S-IVB stage from the S-II stage was accomplished satisfactorily within the desired time period. S-II/S-IVB separation was initiated at 520.528 seconds and first axial motion between the stages occurred 0.052 seconds later. Complete separation occurred when the S-IVB stage engine nozzle bell cleared the S-II stage separation plane. Complete separation was accomplished 1.044 seconds after the separation command.

Small S-II and S-IVB angular velocities and lateral accelerations utilized 4.83 cm (1.9 in.) of the available 2.11 meters (83 in.) of lateral clearance. The S-II pitch, yaw, and roll rates remained between 0.0 and -0.7 deg/sec during separation, and the S-IVB rotational rates ranged between 0.0 and -0.2 deg/sec between separation command and separation complete.

The axial distance required for complete separation was 5.51 meters (217 in.). The lateral clearance available was 2.11 meters (83 in.) when the S-IVB engine was in the null position. From extensometer and acceleration data, the time of first axial motion and axial separation history was reconstructed as shown in Figure 12-11.

The longitudinal accelerations of the S-II and S-IVB stage are shown in Figure 12-12. The reconstructed acceleration histories were obtained from S-II and S-IVB accelerometer data. A time bias was applied to these acceleration histories to compensate for the time lag inherent in the accelerometer data. Retro motor chamber pressure data was used to determine the time bias.

The S-II and S-IVB stage angular velocities during separation are shown in Figure 12-13. Prior to first motion between the stages, the pitch, yaw, and roll rates were approximately zero. The S-II angular velocities during the separation interval never exceeded -0.7 deg/sec. The S-IVB angular velocities remained small during the separation interval, never exceeding -0.2 deg/sec.

The S-II and S-IVB lateral accelerations during separation are shown in Figure 12-14. These acceleration histories were obtained from the telemetered accelerometer data. The S-IVB pitch lateral acceleration varied between plus and minus 8.2 cm/s<sup>2</sup> (0.27 ft/s<sup>2</sup>). The S-II lateral acceleration during separation varied between -0.076 m/s<sup>2</sup> (-0.25 ft/s<sup>2</sup>) and -0.14 m/s<sup>2</sup> (-0.45 ft/s<sup>2</sup>) in the pitch plane; it varied between +0.046 m/s<sup>2</sup> (+0.15 ft/s<sup>2</sup>) and -0.058 m/s<sup>2</sup> (-0.19 ft/s<sup>2</sup>) in the yaw plane. Neither the ullage nor retro motor burns contributed noticeable rates during the separation sequence. Relative velocity between the S-IVB stage and S-II stage is shown in Figure 12-15.

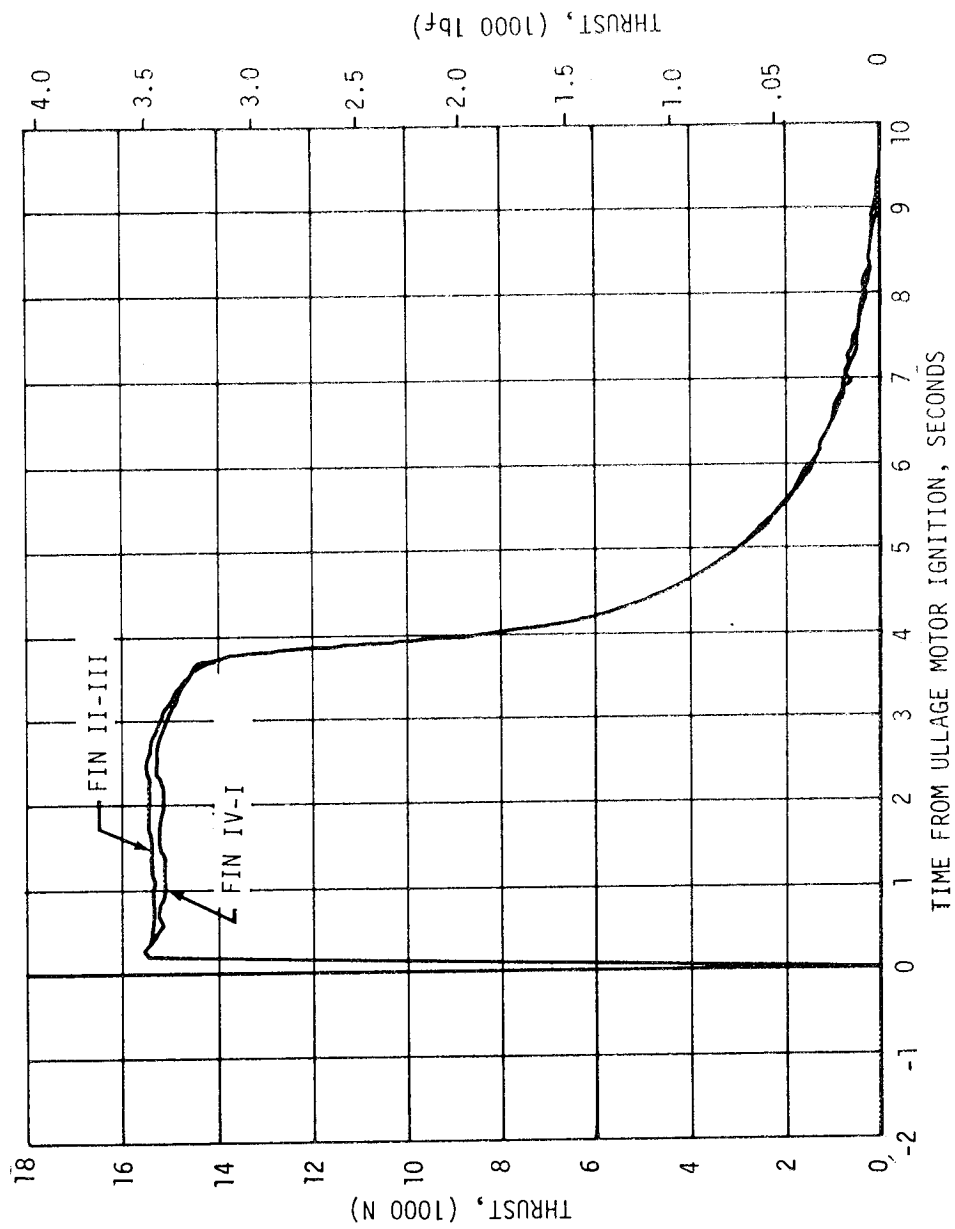


Figure 12-10. S-IVB Ullage Motor Thrust

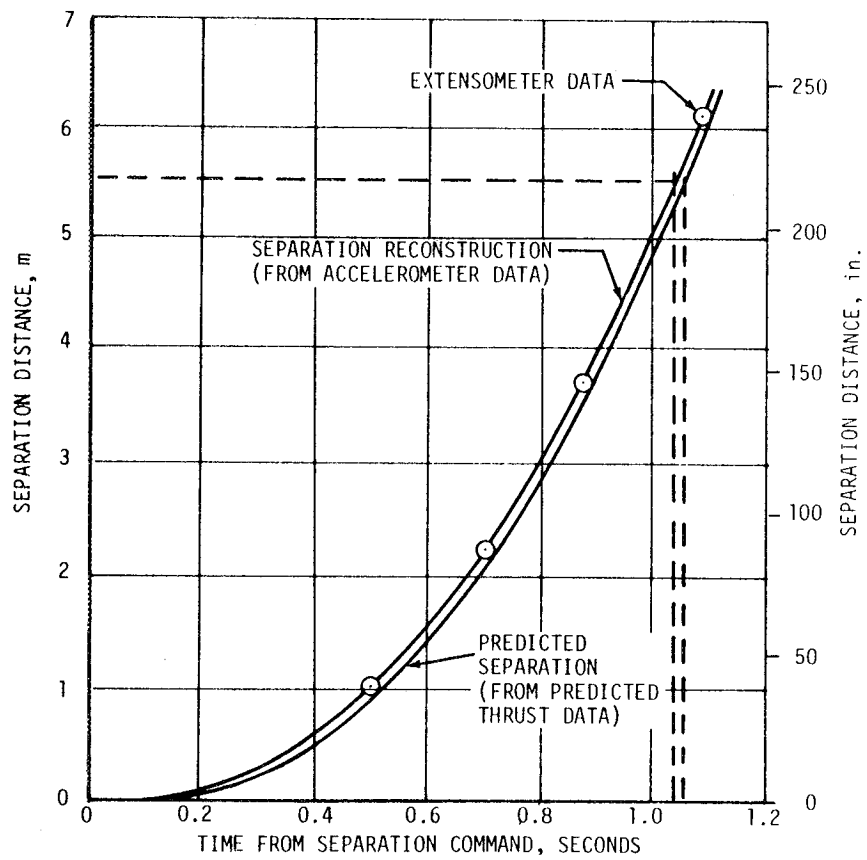


Figure 12-11. S-II/S-IVB Separation Distance

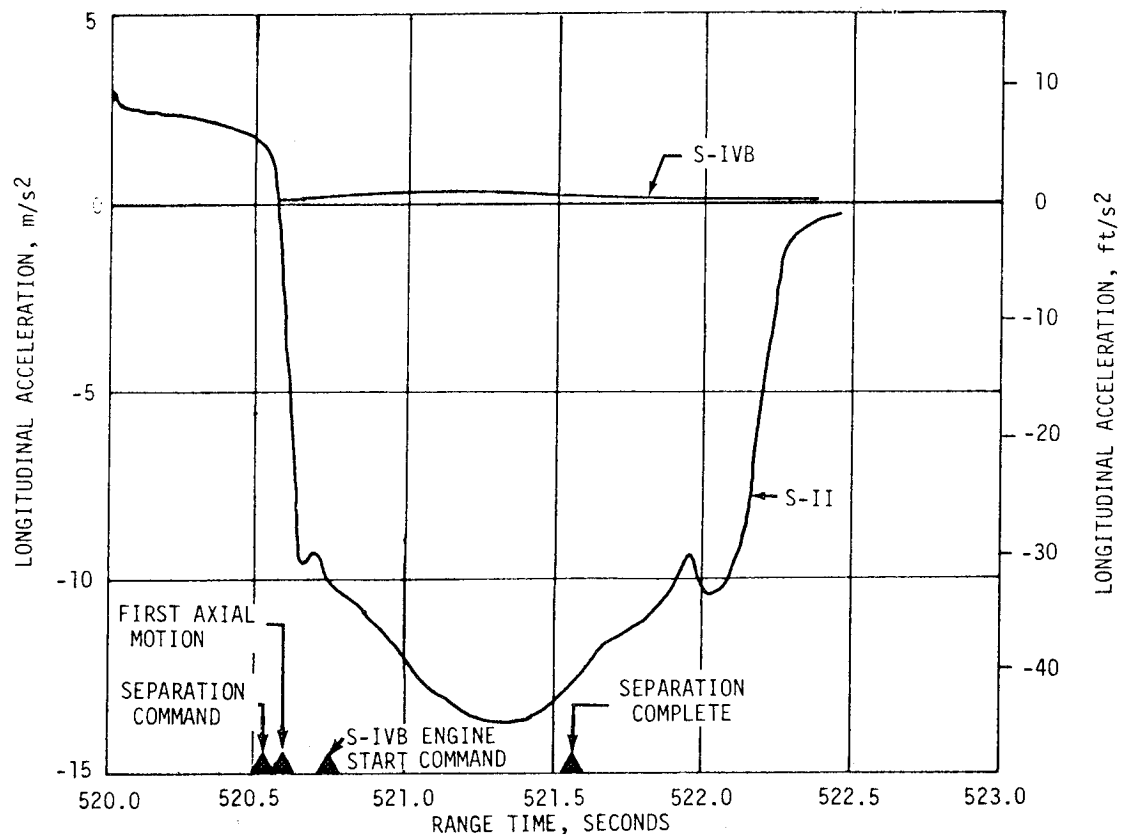


Figure 12-12. S-II/S-IVB Longitudinal Acceleration



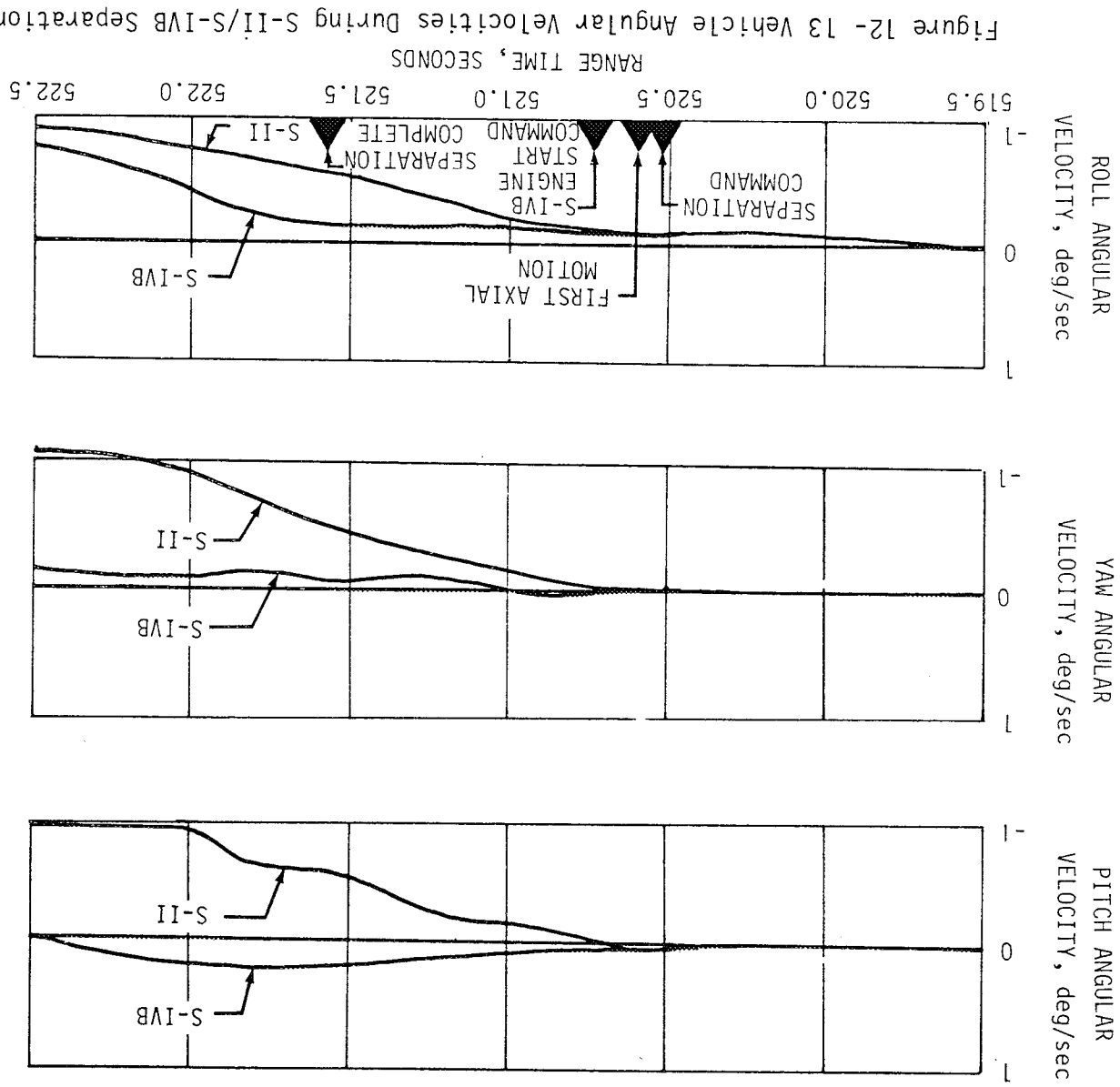


Figure 12-13 Vehicle Angular Velocities During S-II/S-IIVB Separation

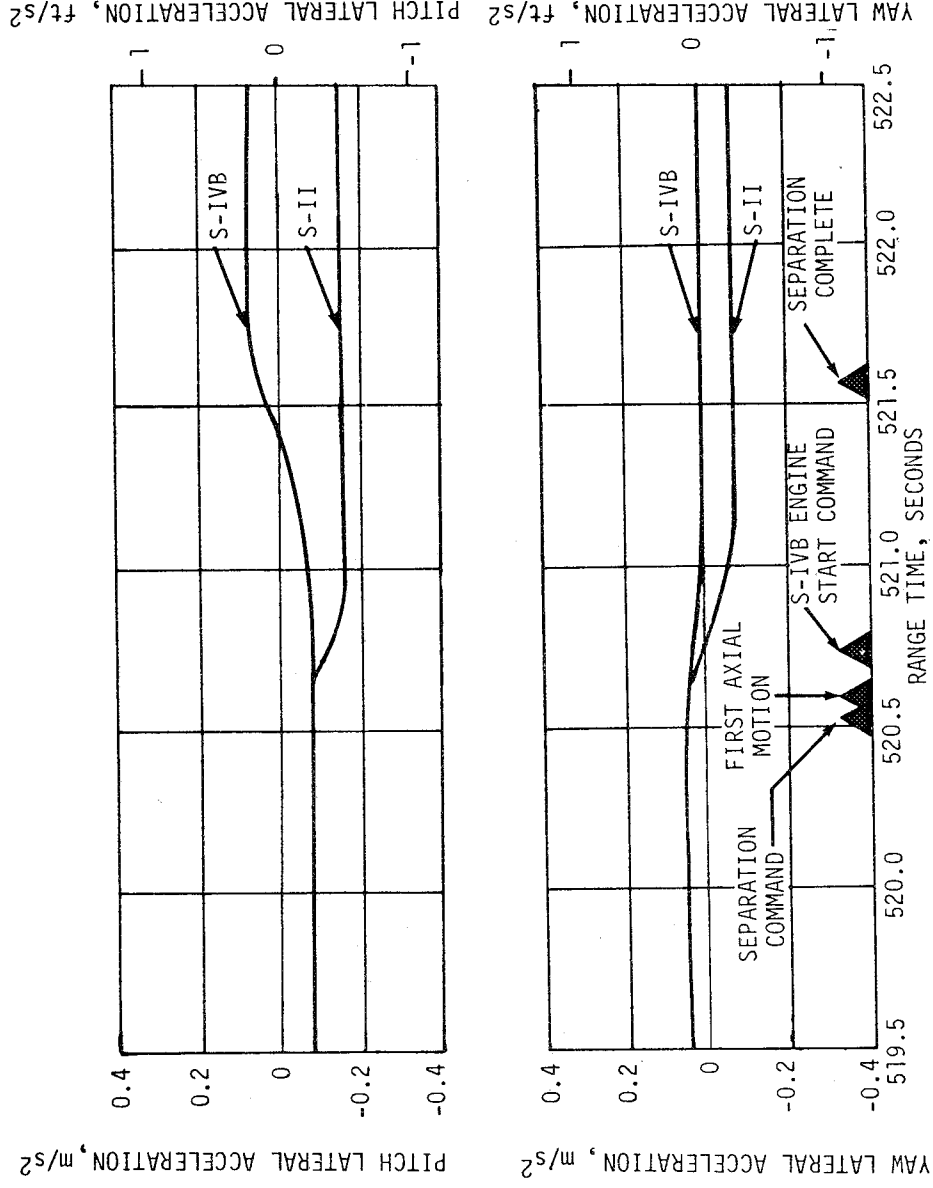


Figure 12-14. Lateral Acceleration

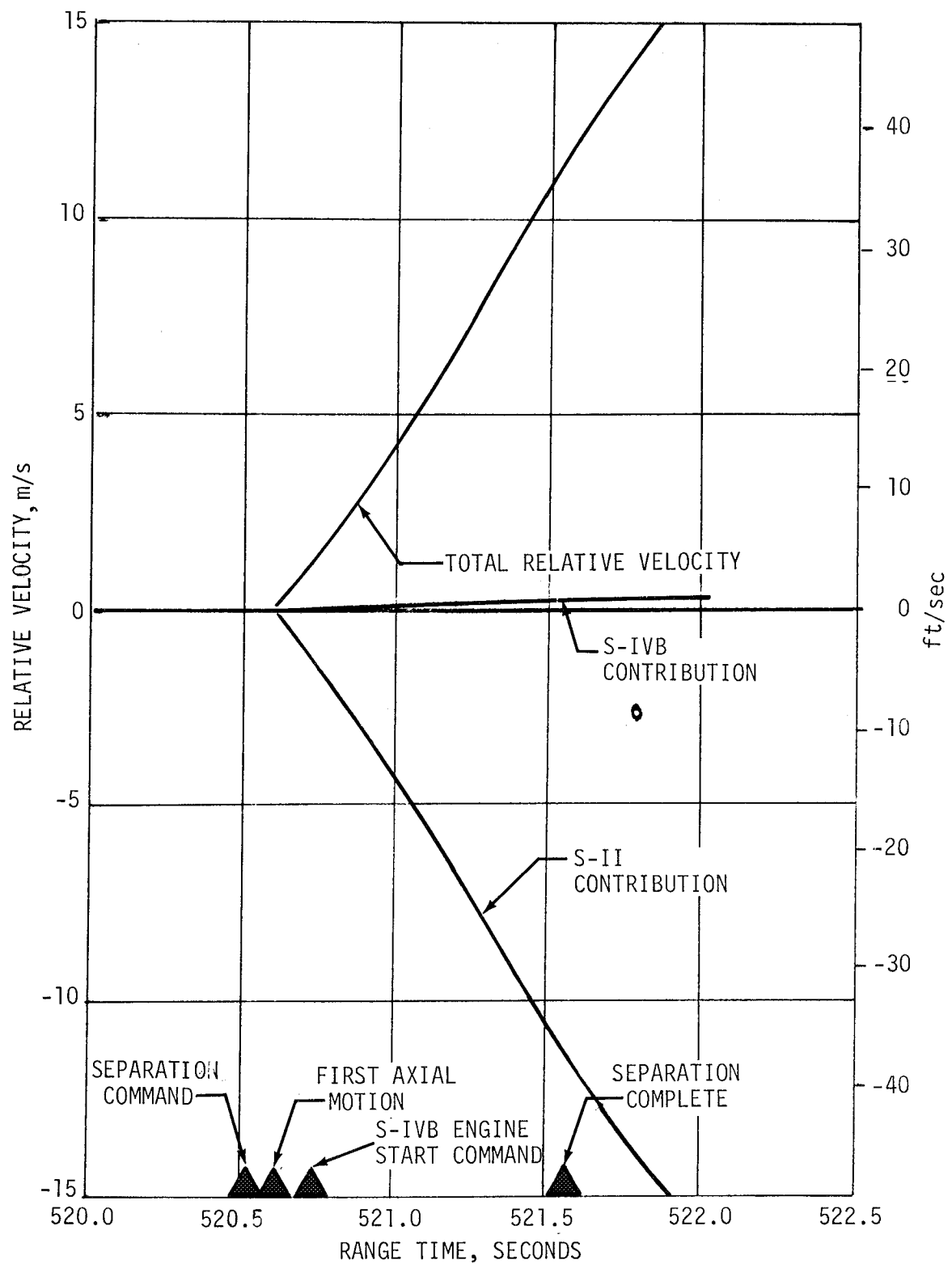


Figure 12-15. S-II/S-IVB Relative Velocity

## 12.5 S-IVB-IU/CSM SEPARATION EVALUATION

S-IVB attitude errors and angular rates during the S-IVB-IU/spacecraft separation are presented in Figures 12-16 and 12-17. The maximum pitch, yaw, and roll attitude errors following spacecraft separation were 0.9, 0.7 and 0.7 degrees, respectively. Maximum pitch, yaw, and roll rates were 0.1, 0.1, and 0.16 deg/sec respectively. S-IVB attitude control appeared normal during S-IVB-IU/spacecraft separation. Since there were no measurable forces acting on the S-IVB-IU during spacecraft separation, no incremental velocity could be determined.

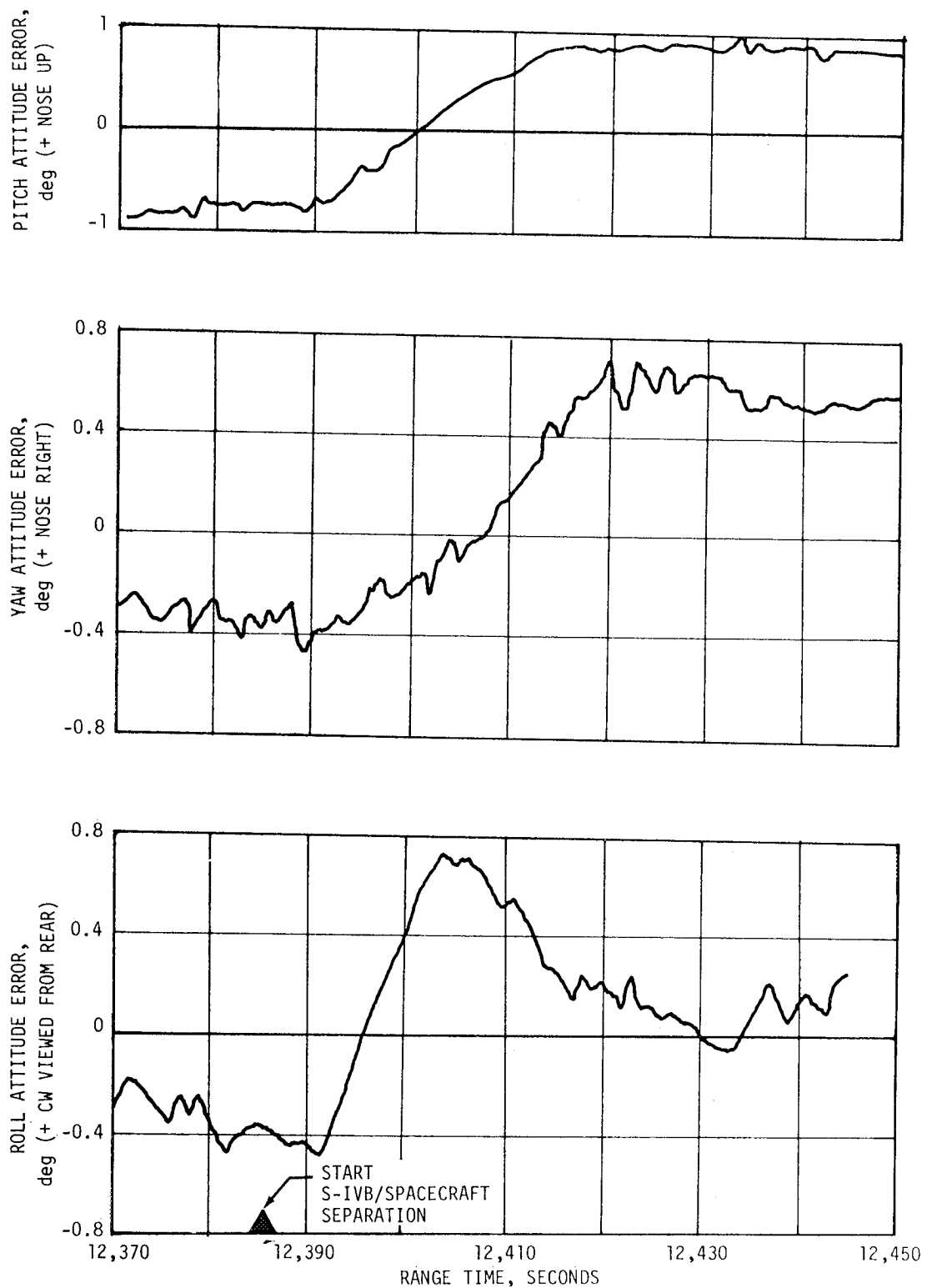
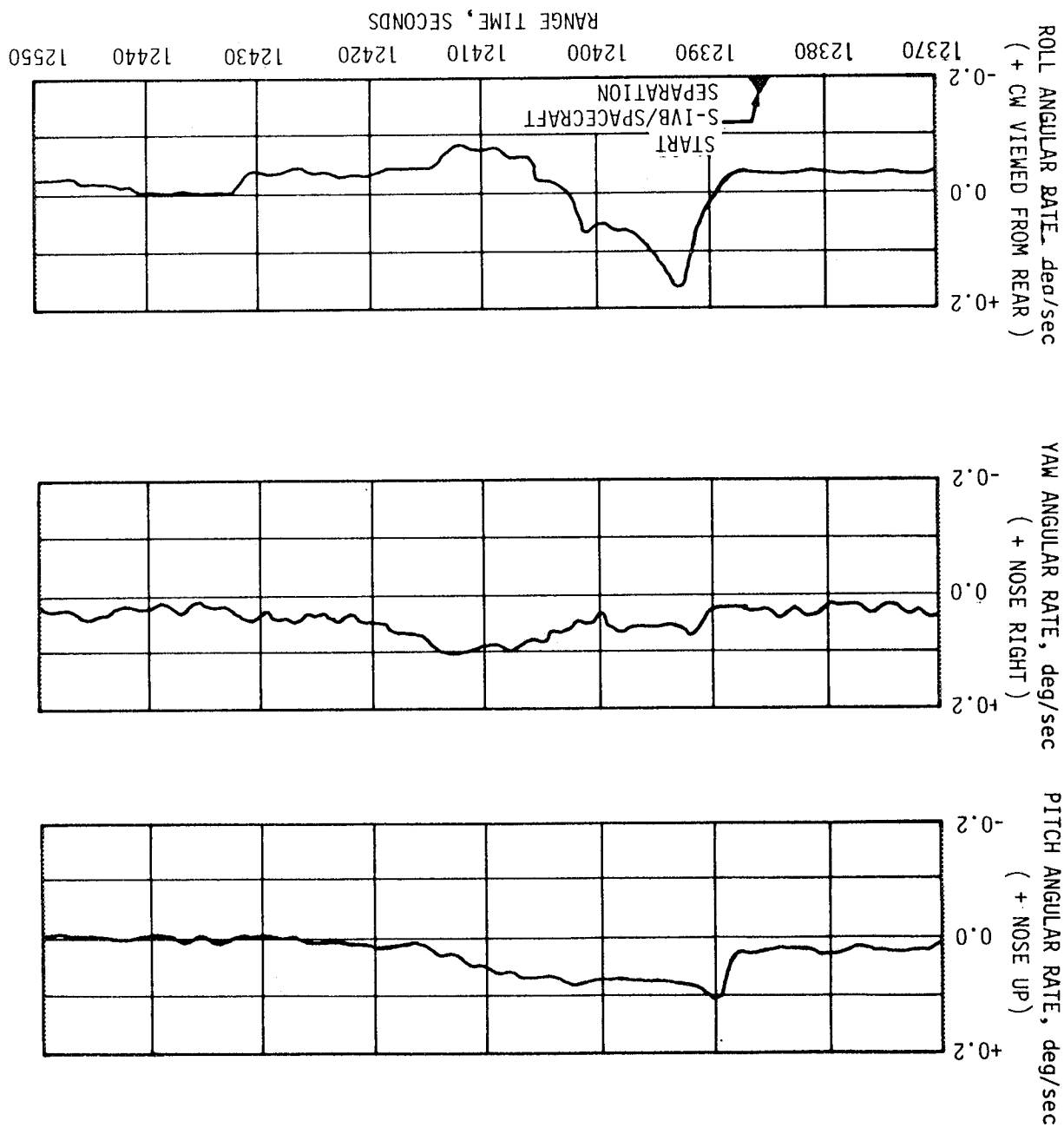


Figure 12-16. S-IVB-IU Attitude Errors During Spacecraft Separation

Figure 12-17. S-IVB Angular Rate During Separation from Spacecraft



## SECTION 13 ELECTRICAL NETWORKS

### 13.1 SUMMARY

The performance of all launch vehicle stage electrical systems was satisfactory throughout the flight period. Battery voltages and currents were satisfactory and remained within predicted tolerances. All battery temperatures were indicated as falling within acceptable limits. The Instrument Unit 6D30 battery lost the temperature measurement at approximately 90 seconds due to a transducer malfunction. Battery performance, however, indicated that temperature effects were similar to other batteries. The electrical portion of each individual stage control system responded normally. Performance of the master measuring voltage supplies was satisfactory. All Exploding Bridgewire (EBW) firing units responded correctly.

### 13.2 S-IC STAGE ELECTRICAL SYSTEM

The S-IC stage electrical system operated satisfactorily throughout S-IC powered flight and all mission objectives were attained.

Main power bus voltages and currents on busses +1D10 and +1D20 are shown in Figures 13-1 and 13-2, respectively. The battery voltages were well within requirements of 26.5 VDC to 32 VDC during S-IC powered flight. The battery currents were well within the operational limits of 64 amperes for Battery No. 1 and 125 amperes for Battery No. 2.

The range of values for the seven measuring power supplies varied from a low of 5.005 VDC to a high of 5.035 VDC, falling well within the operational limits of  $5 \pm 0.05$  VDC.

All channels of the S-IC stage switch selector functioned as programmed by the IU.

Separation and retro motor EBW firing units were armed and triggered. Charging time and voltage characteristics of the EBW firing units were within design specifications. Time between retro motor, ignition signals, and the separation firing signals was within requirements.

### 13.3 S-II STAGE ELECTRICAL SYSTEMS

The S-II stage electrical system operated satisfactorily throughout S-II flight, and all mission objectives were attained.

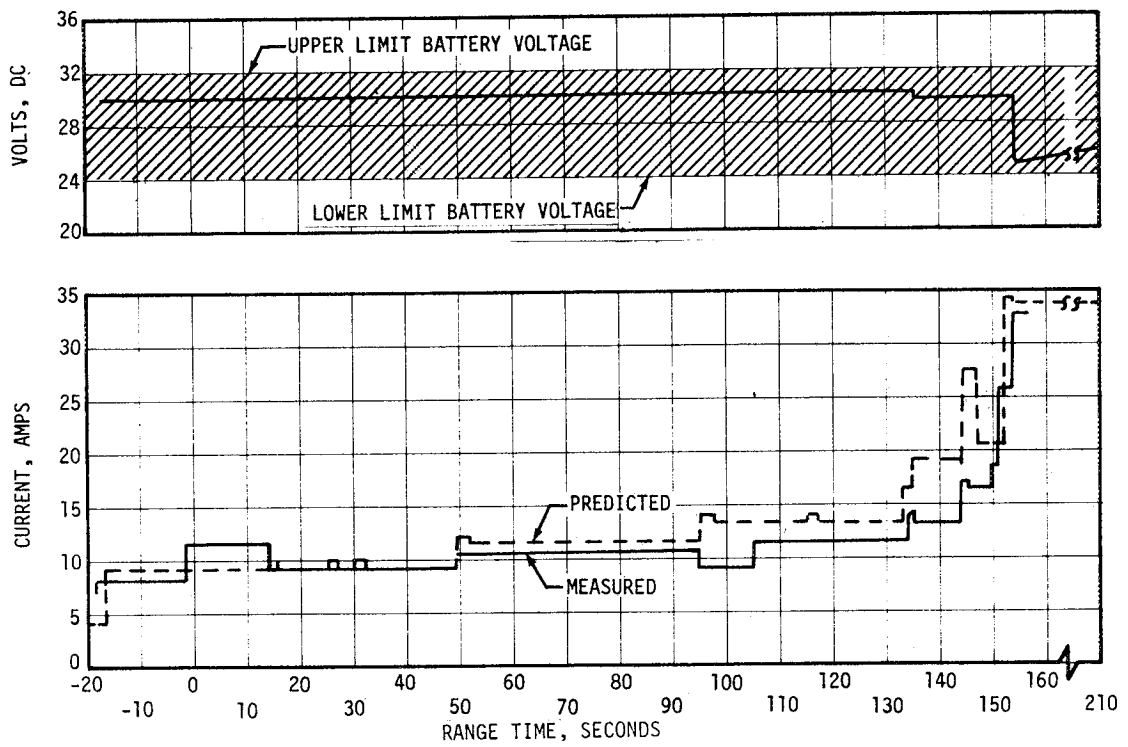


Figure 13-1. S-IC Stage Voltage and Current, Bus 1D10

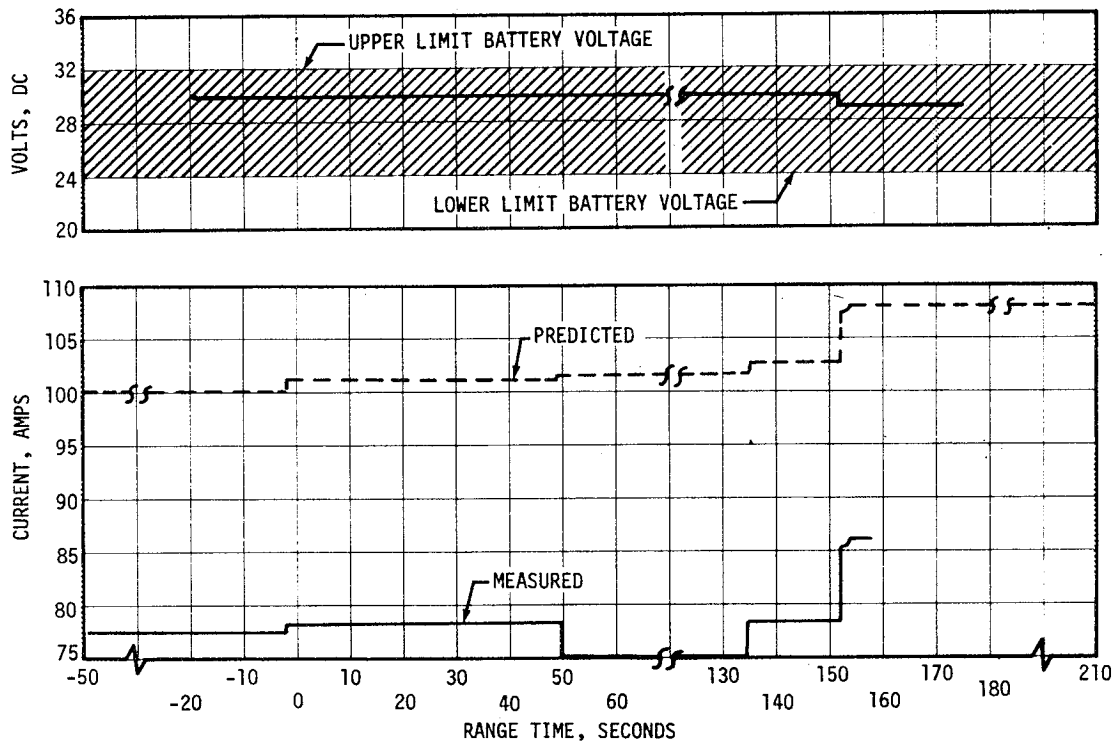


Figure 13-2. S-IC Stage Voltage and Current, Bus 1D20



Bus voltages remained within specified voltage limits throughout the pre-launch and flight periods. Main bus current averaged 33 amperes during S-IC boost and 55 amperes during S-II boost. Instrumentation bus current averaged 50 amperes during S-IC and S-II boosts. Recirculation bus current averaged 91 amperes during S-IC boost. Voltage and current profiles for the main, instrumentation, and recirculation busses are presented in Figures 13-3 thru 13-5. Predicted bus current levels were determined from maximum values of component power consumption test data. This resulted in predicted values that are somewhat higher than actual bus current measurements. The lower currents were expected and agree with CDDT data. The ignition bus voltage profile is presented in Figure 13-6. The estimated J-2 engine ignition load is 35 amperes, based upon S-II acceptance static firing data.

S-II stage battery capacity consumption in ampere hours and as a percent of rated capacity are presented in Table 13-1 along with the battery temperature extremes.

The LH2 recirculation inverters operated properly throughout the stage powered J-2 engine chilldown period. Voltages for the five inverters varied from a low of 40.3 VAC to a high of 44.5 VAC, falling within the 37 to 48 VAC range specified. Inverter frequencies ranged from a low of 399.3 hertz to a high of 403.0 hertz, falling within the 396 to 404 hertz range specified.

Table 13-1. S-II Battery Consumption

BATTERY	DESIGNATION (REFERENCE)	CAPACITY (AMP-HR)	CONSUMPTION (AMP-HR)	PERCENT CONSUMED	TEMPERATURE	
					MAX	MIN
Main	2D11	35	7.84	22.4	87°F 309°K	88°F 304°K
Instrumentation	2D21	35	8.24	23.5	99°F 310°K	89°F 305°K
Recirculation No. 1	2D51	35	5.07	14.5	80°F 300°K	75°F 297°K
Recirculation No. 2	2D51 and 2D61	35	5.12	14.6	84°F 302°K	79°F 299°K

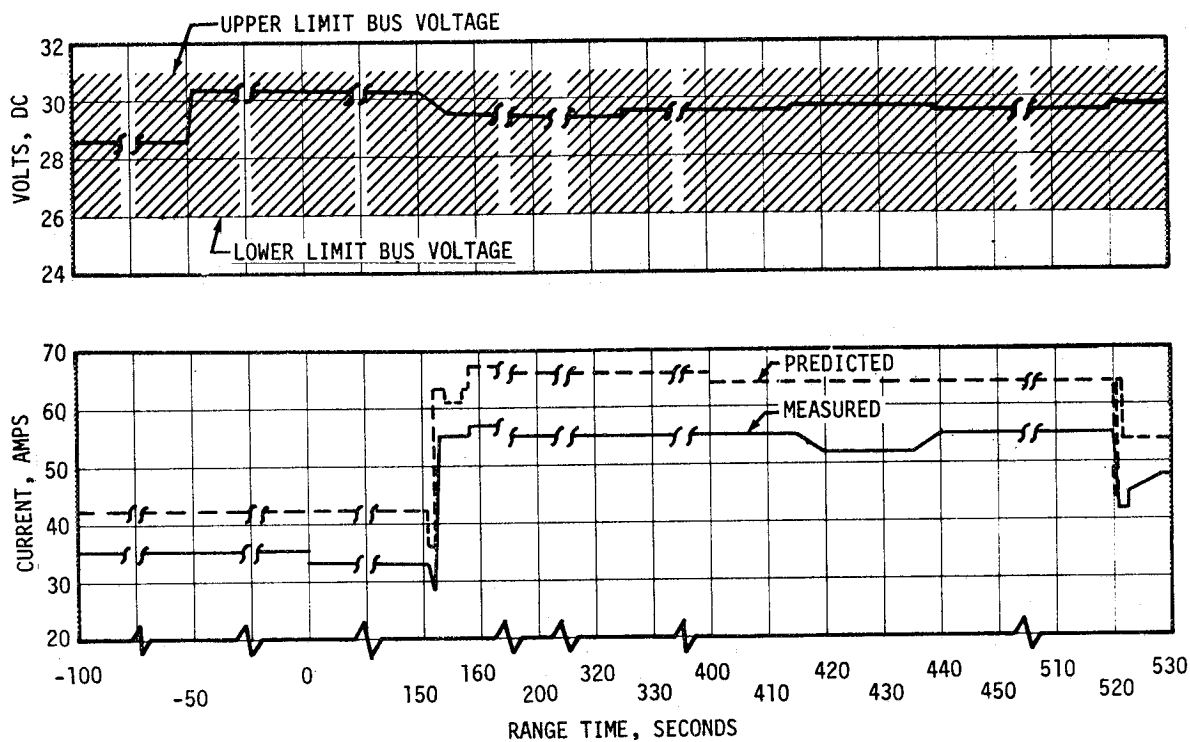


Figure 13-3. S-II Stage Main DC Bus Voltage and Current

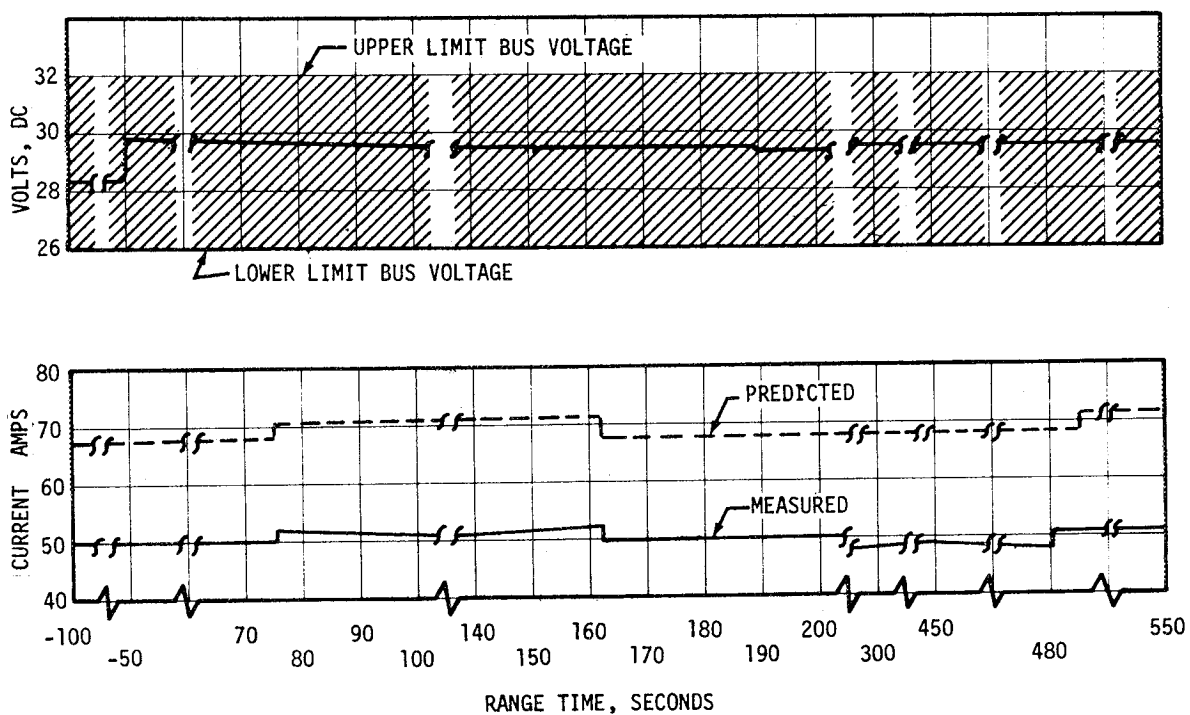


Figure 13-4. S-II Stage Instrumentation Bus Voltage and Current

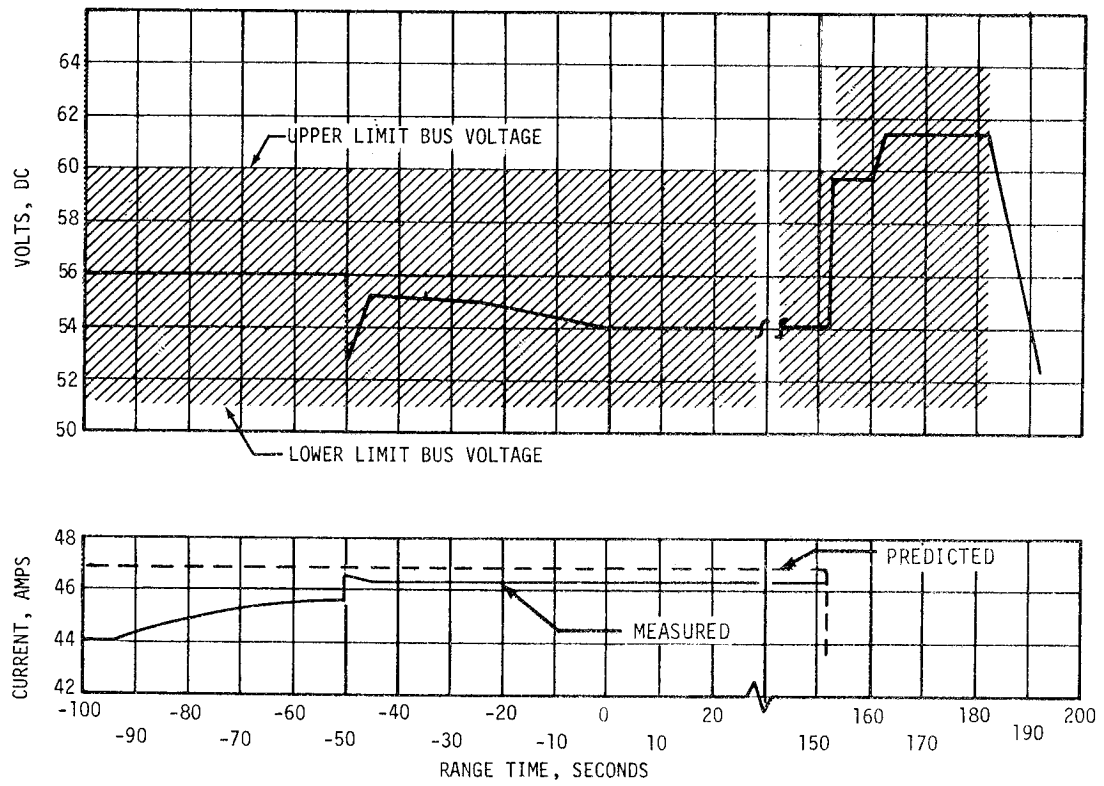


Figure 13-5. S-II Stage Recirculation DC Bus Voltage and Current

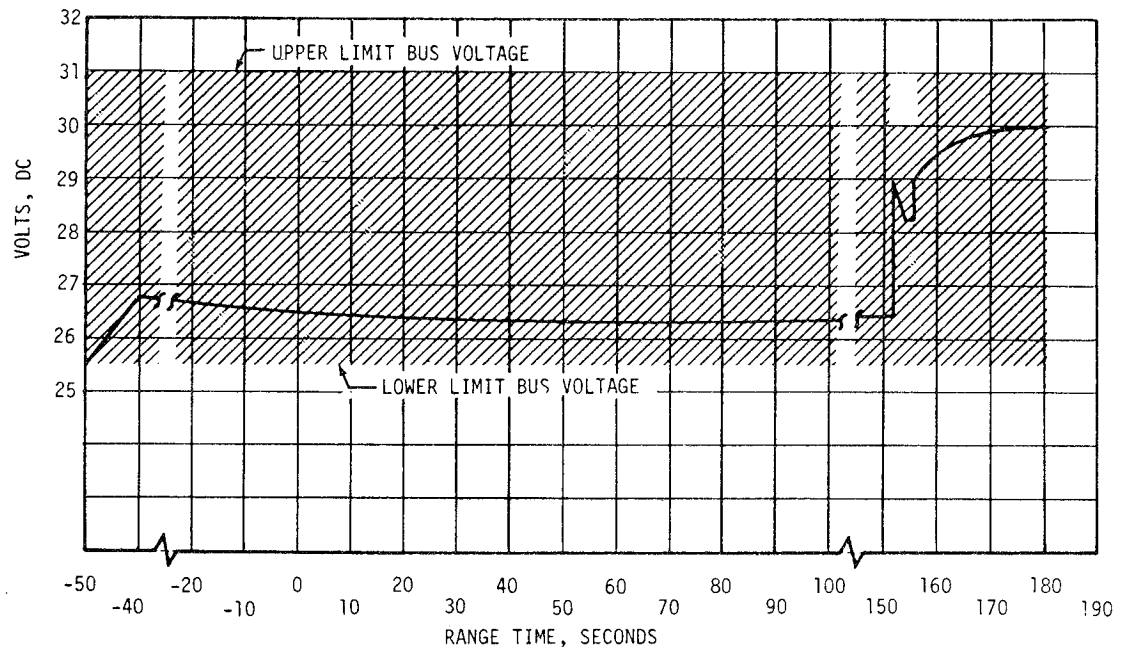


Figure 13-6. S-II Stage Ignition DC Voltage

All firing units for S-II ullage motor initiation, S-II second plane separation, S-II/S-IVB separation, and S-II/S-IVB retro motors operated within specification requirements. Review of the performance data for various systems controlled by switch selector commands indicated proper operation of the switch selector.

#### 13.4 S-IVB STAGE ELECTRICAL SYSTEM

The S-IVB stage electrical system operated satisfactorily throughout the flight, and all mission objectives were attained.

The power system of the S-IVB stage consisted of four batteries, a PU static inverter, two chilldown inverters, and smaller power supplies. These components performed satisfactorily with operating characteristics within the predicted performance.

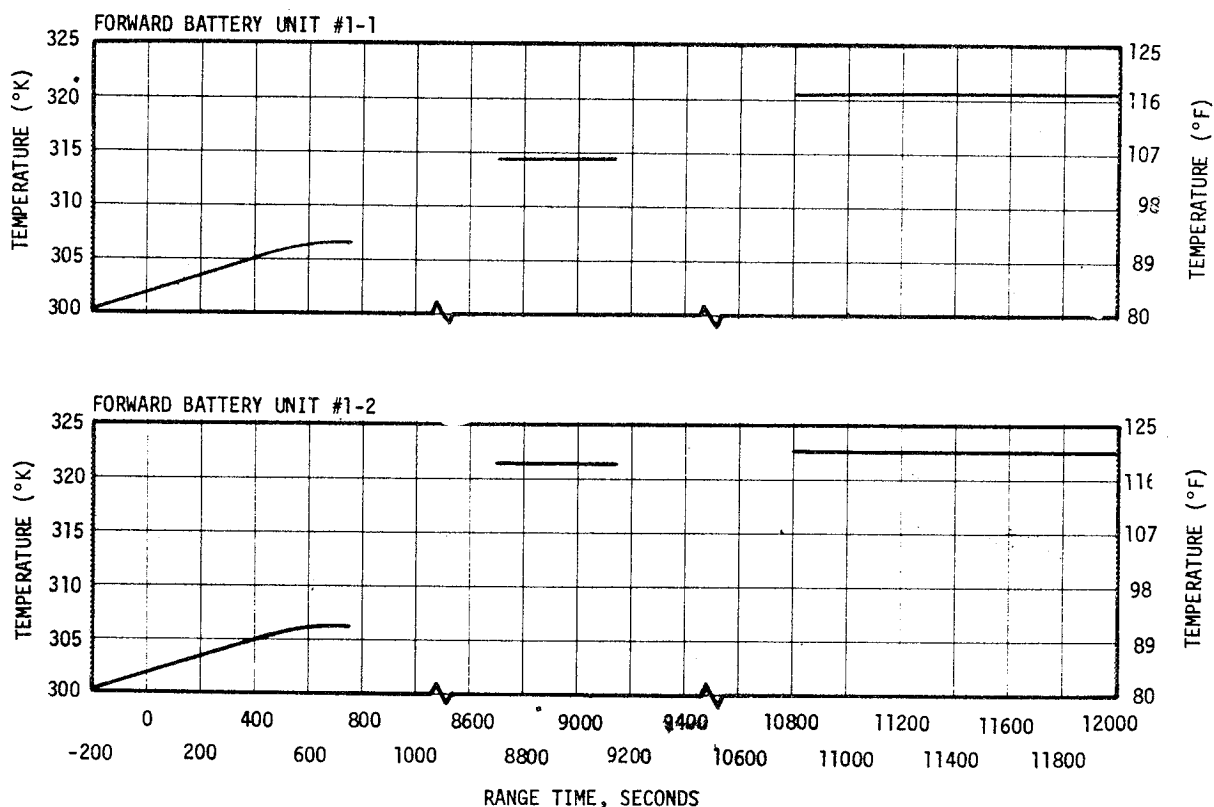
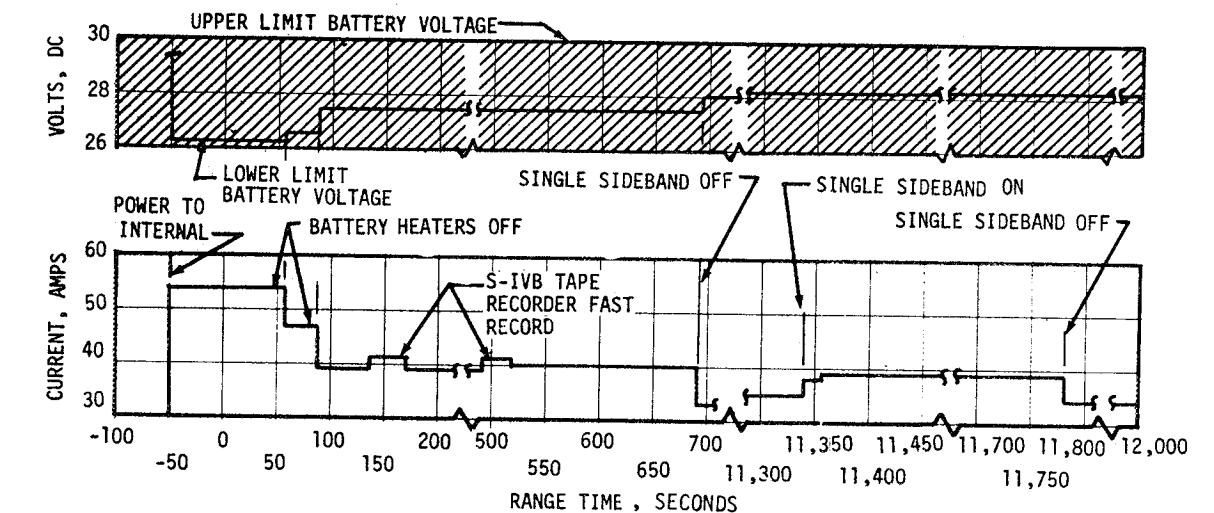
Battery voltages and currents remained within specified limits from liftoff to flight termination. First and second burn load profiles are shown in Figures 13-7 thru 13-10. Table 13-2 shows approximate power consumption of the S-IVB batteries.

Table 13-2. S-IVB Battery Consumption

BATTERY	CAPACITY (AMP-HRS)	CONSUMPTION (AMP-HRS)		PERCENT USAGE
		Maximum Expected	Actual	
Fwd. No. 1 (2 units)	350	279	128	36
Fwd. No. 2	25	13.5	13	52
Aft No. 1 (2 units)	300	59	11	4
Aft No. 2 (2 units)	80	52	27	34

Battery temperatures were well within the 347° K (165° F) limit. The highest temperature observed was 322° K (120° F) for forward battery No. 1 (Unit 2) during second burn. Figures 13-7 thru 13-10 present the battery temperature histories which indicate normal heat rise during battery loading and proper cycling of the heater circuits to maintain battery temperature.

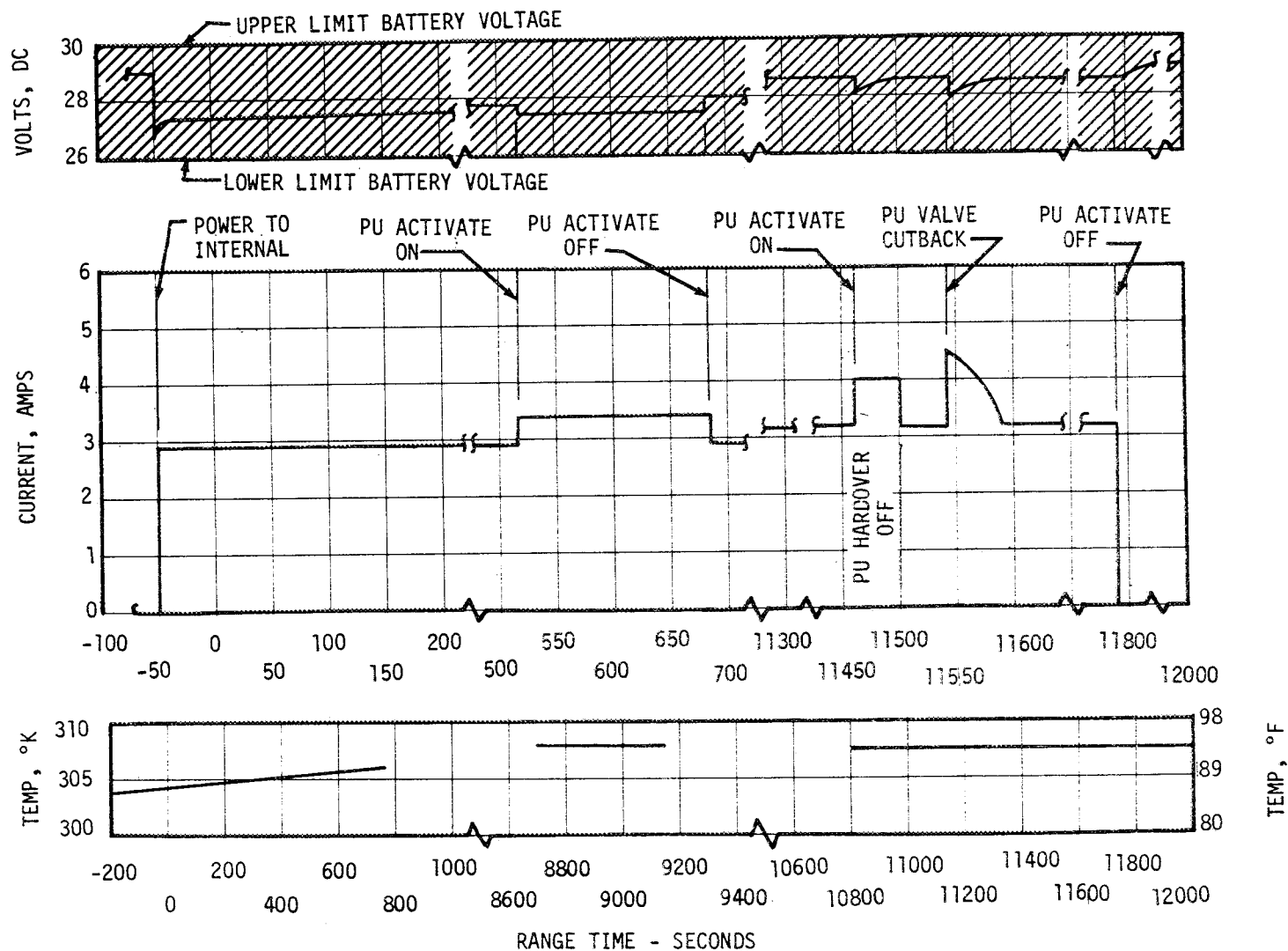
Performance of the static inverter/converter was satisfactory. At umbilical disconnect, the static inverter/converter voltage was 115 VAC. Voltage remained at this level through PU system activate and to shortly after S-IVB cutoff, when it dropped to 114.5 VAC and then remained at this level throughout the balance of flight. These voltages were well within the



NOTE: PREDICTED CURRENT WAS BASED ON MAXIMUM LOADS. VALUES ARE BEYOND THE SCALE OF THESE PLOTS AND THEREFORE NOT SHOWN. ACTUAL CURRENT FELL WELL BELOW PREDICTED.

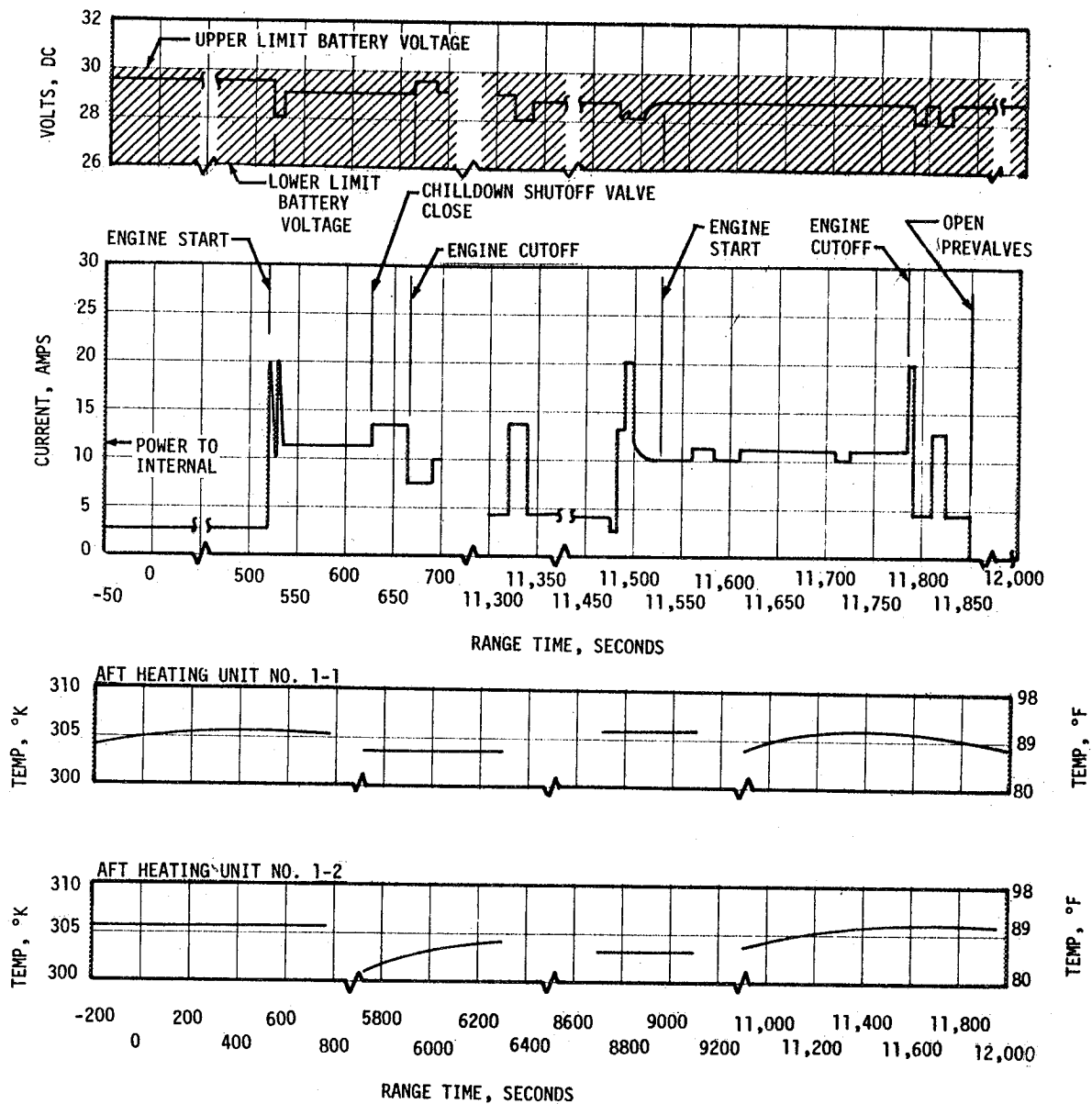
Figure 13-7. S-IVB Stage Fwd Battery No. 1 Voltage, Current, and Temperature

13-8



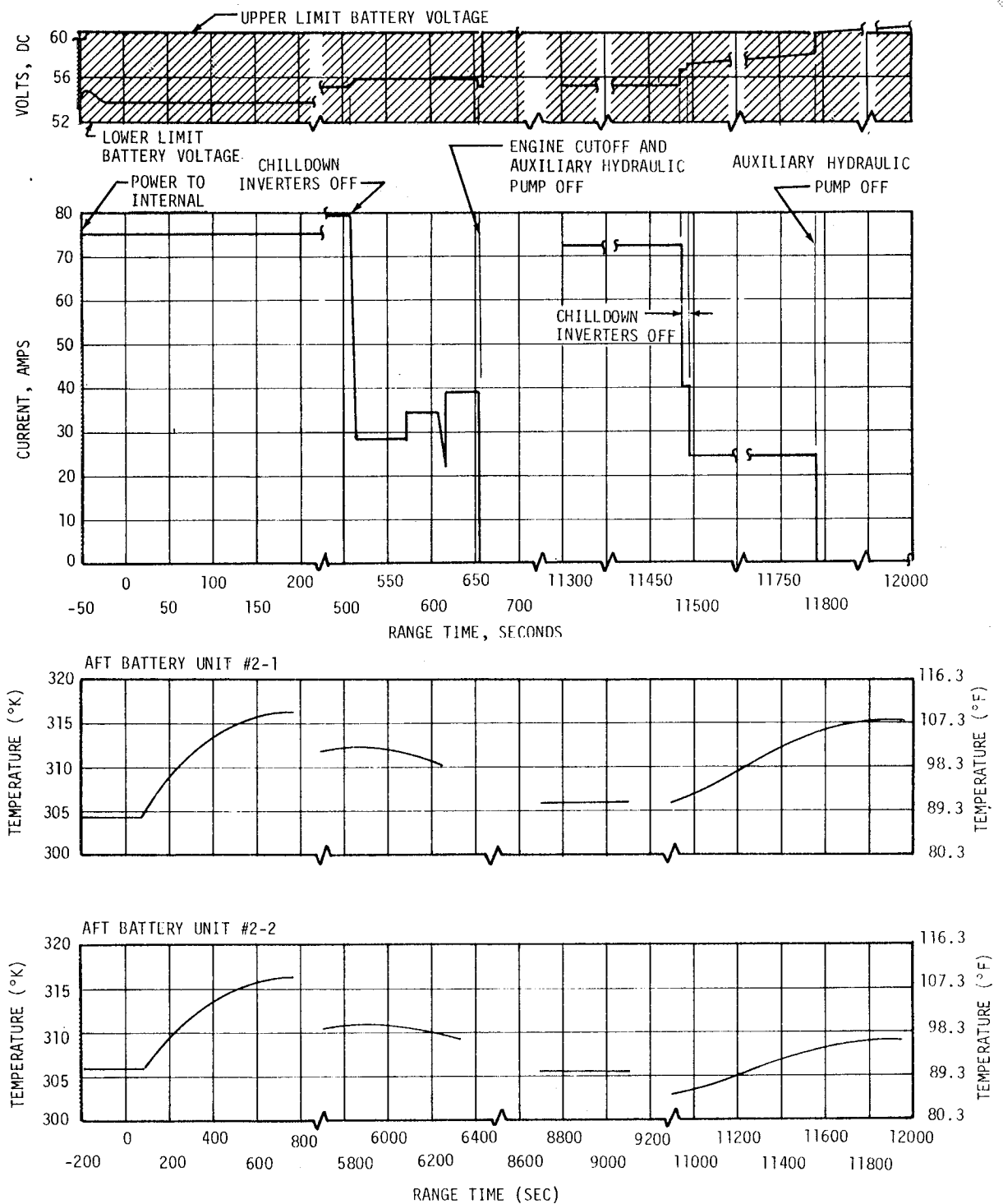
NOTE: PREDICTED CURRENT WAS BASED ON MAXIMUM LOADS. VALUES ARE BEYOND THE SCALE OF THESE PLOTS AND THEREFORE NOT SHOWN. ACTUAL CURRENT FELL WELL BELOW PREDICTED.

Figure 13-8. S-IVB Stage Fwd Battery No. 2 Voltage, Current, and Temperature



NOTE: PREDICTED CURRENT WAS BASED ON MAXIMUM LOADS. VALUES ARE BEYOND THE SCALE OF THESE PLOTS AND THEREFORE NOT SHOWN. ACTUAL CURRENT FELL WELL BELOW PREDICTED.

Figure 13-9. S-IVB Stage Aft Battery No. 1 Voltage, Current, and Temperature



NOTE: PREDICTED CURRENT WAS BASED ON MAXIMUM LOADS. VALUES ARE BEYOND THE SCALE OF THESE PLOTS AND THEREFORE NOT SHOWN. ACTUAL CURRENT FELL WELL BELOW PREDICTED.

Figure 13-10. S-IVB Stage Aft Battery No. 2 Voltage, Current, and Temperature



115  $\pm$  3.45 VAC requirement. Frequency remained well within the 400  $\pm$  6 hertz limits specified except for a brief period during the PU hardover operation when frequency rose to 406.3 hertz. The 5-volt and 21-volt supplies remained within the specified limits of 5  $\pm$  0.5 VDC and 21  $\pm$  1.5, -1.0 VDC. Internal temperature ranged between a maximum temperature of 299° K (78° F) and a minimum temperature of 297° K (75° F).

The fuel and LOX chilldown inverters ranged from a low voltage of 55 VAC to a high voltage of 57.2 VAC, falling within the 49 to 60 VAC limits specified. Inverter frequencies ranged between 399.2 to 400.4 hertz; falling well within the 400  $\pm$  10 hertz limits. Likewise, temperatures which ranged from 282° to 300° K (48° to 80° F) were within the 224° to 344° K (34° to 160° F) allowed.

The 5-volt excitation modules remained within specified limits. The S-IVB stage electrical control system responded normally to the commands which were received from the Instrument Unit. The switch selector decoded the signals properly and through the sequencer activated the desired relays, valves, etc. at the proper times.

All EBW firing units functioned as expected in response to their respective commands. The ullage motor ignition EBW's were charged at 480 seconds and were fired at 520 seconds. The ullage motor jettison EBW's were charged at 529 seconds and fired at 531 seconds, resulting in the jettison of both ullage motors. Since the flight was successful, the destruct EBW's were not charged or fired.

### 13.5 INSTRUMENT UNIT ELECTRICAL SYSTEM

The Instrument Unit electrical system operated satisfactorily throughout the flight.

Battery voltages and currents were normal throughout the flight. Battery load and temperature profiles are shown in Figures 13-11 thru 13-14. Excursions were experienced in the 6D10 battery voltage and current near liftoff and in the region of MAX Q (50 to 90 seconds). The platform 56-volt power supply showed loading during these excursion times, the 6D10 current varying as much as 4 amperes. The loads on the 56-volt power supply can vary from 1 to 6 amperes and the 28-VDC load to the platform can vary from 9 to 11 amperes. These two load limits are normally approached at times of maximum vibration of the ST-124M Inertial Platform. Since these times coincide with the excursions on the 6D11 bus, these fluctuations can be considered as normal input power variations of the ST-124M Inertial Platform. The temperature measurement of 6D30 battery was lost at approximately 90 seconds, as shown in Figure 13-11. The measured internal temperatures of the remaining batteries were seen to slowly increase with time. Concurrent with the temperature increase, the battery terminal voltage increased. Similar voltage increase in the 6D10 battery indicated that battery temperature was following the same trend as in other batteries. These increases were nominal for a silver-zinc battery.

The distributors operated nominally, as did the 5-volt measuring voltage supply.

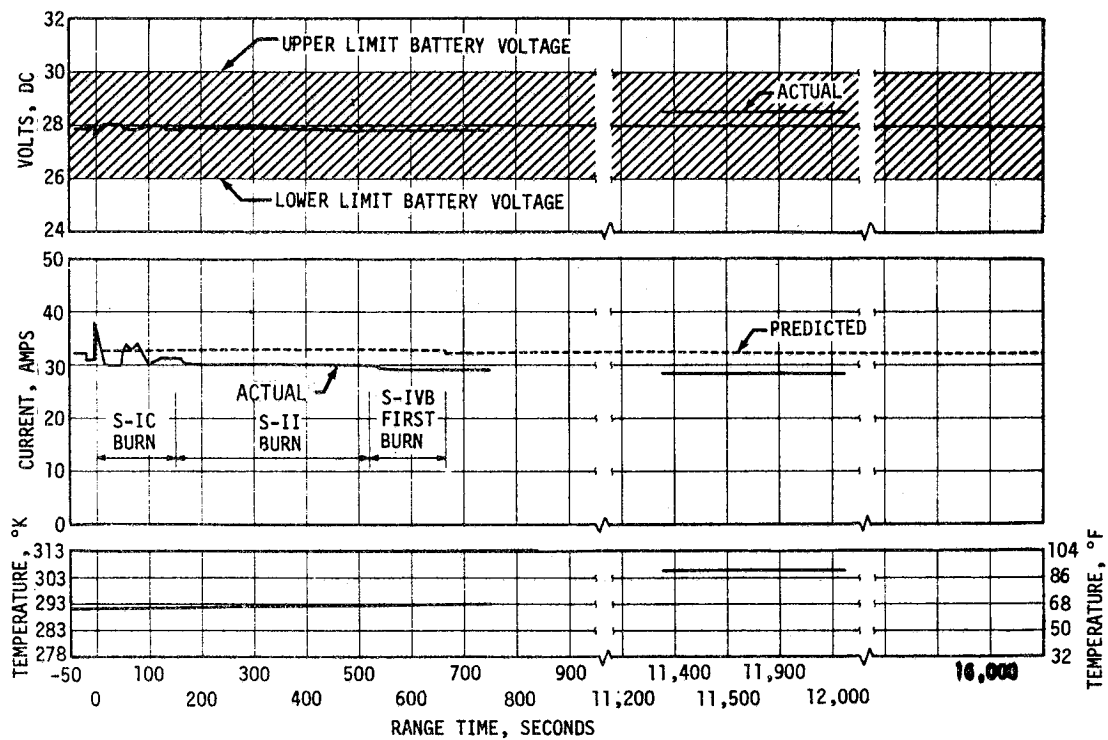


Figure 13-11. IU Battery 6D10 Voltage, Current, and Temperature

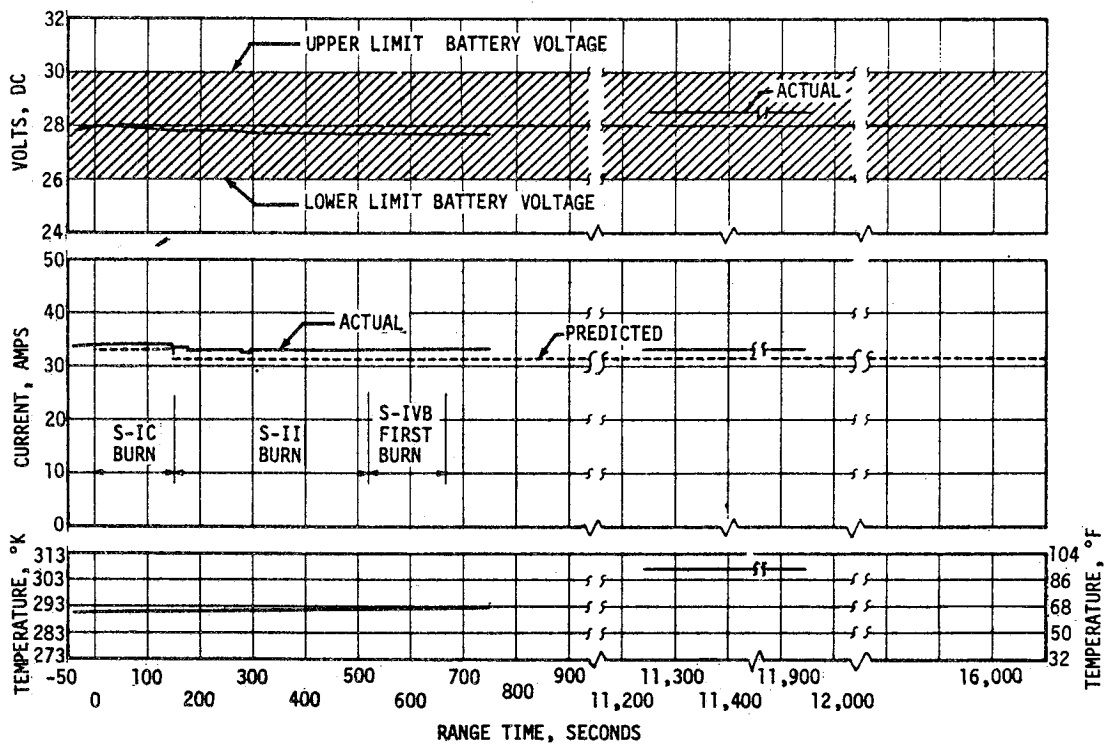


Figure 13-12. IU Battery 6D20 Voltage, Current, and Temperature

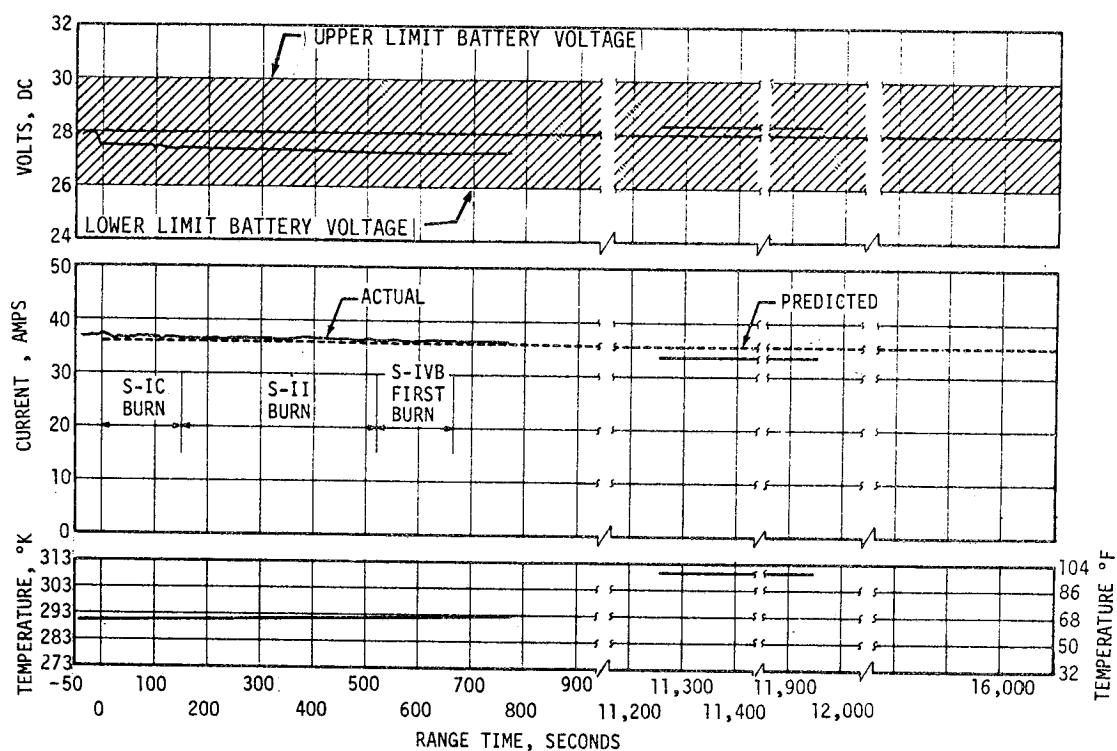


Figure 13-13. IU Battery 6D30 Voltage, Current, and Temperature

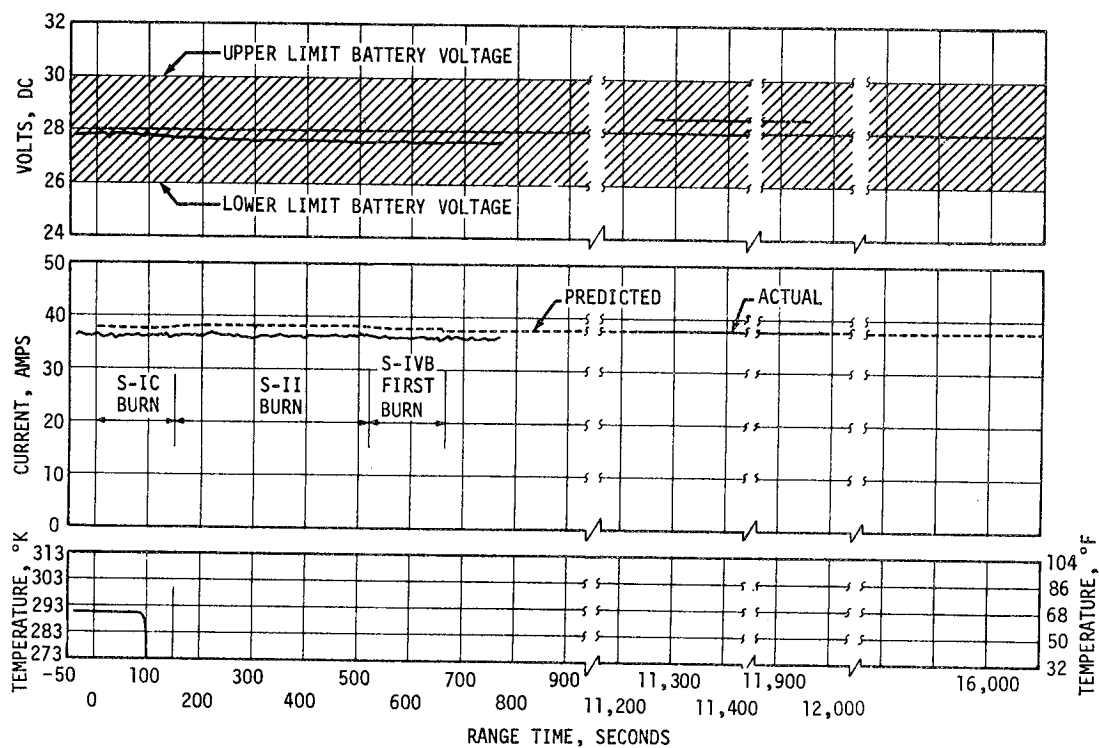


Figure 13-14. IU Battery 6D40 Voltage, Current, and Temperature



## SECTION 14 RANGE SAFETY AND COMMAND SYSTEMS

### 14.1 SUMMARY

Data indicated that the redundant Secure Range Safety Command Systems (SRSCS) on the S-IC, S-II, and S-IVB stages were ready to perform their functions properly on command if flight conditions had required and that the safe-disconnect system responded properly to command. The performance of the command and communications system in the Instrument Unit (IU) was excellent.

### 14.2 RANGE SAFETY COMMAND SYSTEMS

The SRSCS provides a means to terminate the flight of the vehicle by radio command from the ground in case of emergency situations in accordance with range safety requirements. After successful insertion into earth orbit, the system is deactivated by ground command. Each powered stage of the vehicle was equipped with two command receivers/decoders and necessary antennas. The SRSCS in each stage was completely independent of those in other stages.

Three types of SRSCS commands were required for this unmanned flight as follows:

- a. Arm/fuel cutoff - Charging of the Exploding Bridge Wire (EBW) firing unit and thrust termination.
- b. Destruct - Propellant dispersion by firing of the EBW.
- c. Safe - Command system switched off.

During flight, telemetry indicated that the command antennas, receivers/decoders, destruct controllers, and EBW units functioned properly and were in the required state of readiness if needed. Because the flight was successful no arm/cutoff or destruct commands were required; therefore, all data except receiver strength telemetry remained unchanged during the flight. At 683 seconds the safing command was initiated, deactivating the system. Both S-IVB stage systems, the only systems in operation at this time, responded properly to the safing command.

RF performance of the system is discussed in paragraph 19.5.3.1.

### 14.3 COMMAND AND COMMUNICATIONS SYSTEM

The IU Command and Communication System (CCS) is a phase-coherent receiver-transmitter capable of establishing a communication link between the unified S-band (USB) ground stations and the IU of the Saturn V launch vehicle. The operational requirements of the CCS include command up-data and down-link telemetry. Turnaround ranging is also desirable, but not mandatory. Specifically, the CCS will: receive and demodulate command up-data for the guidance computers in the IU, transmit pulse code-modulated (PCM) mission control measurements originating in the S-IVB and the IU to the USB ground stations for processing, and coherently retransmit the pseudorandom noise (PRN) range code that is received from the USB ground stations. The CCS physically consists of a transponder, power amplifier, and antenna system,

Performance of the CCS for AS-501 appeared to have been excellent. All stations obtained good data, with only minor discrepancies occurring at the MILA/USB. This station had problems maintaining phase lock due to S-IC/S-II staging and interstage jettison. RF performance of the system is discussed in paragraph 19.5.3.2.

The CCS command history is shown in Table 14-1. A total of 5622 known commands were sent. Of 5249 test commands sent, 5205 were verified as having been received, 1 was verified as lost, and 44 were not verified because the vehicle was over the horizon during these periods. All 373 operational commands were verified as having been received.

Table 14-1. CCS Command History, AS-501

STATION	PASS	TEST WORDS				FLIGHT WORDS			
		SENT	VERIFIED RECEIVED	VERIFIED MISSED	BAD TLM	SENT	VERIFIED RECEIVED	VERIFIED MISSED	BAD TLM
GMIL	Launch	--	--	--	--	--	--	--	--
	1	177	177	0	0	--	--	--	--
	2	--	--	--	--	5	5	0	0
ASC	1	--	--	--	--	--	--	--	--
	2	--	--	--	--	--	--	--	--
	3	2352	2351	1	0	119	119	0	0
CRO	1	614	576	0	38	--	--	--	--
	2	--	--	--	--	--	--	--	--
	3	1971	1971	0	0	213	213	0	0
HAW	1	--	--	--	--	--	--	--	--
	2	135	129	0	6	--	--	--	--
TEX	1	--	--	--	--	--	--	--	--
	2	--	--	--	--	36	36	0	0
Totals		5249	5204	1	44	373	373	0	0

14-3/14-4





## SECTION 15 EMERGENCY DETECTION SYSTEM

### 15.1 SUMMARY

The Emergency Detection System (EDS) was flown in the "open-loop" configuration on AS-501. The automatic abort circuit was deactivated in the spacecraft. The performance of the EDS was satisfactory. No abort limits were reached and no false indications were sensed by the system. The sequential events all occurred at the proper times.

### 15.2 SYSTEM DESCRIPTION

Figure 15-1 presents a functional diagram of the EDS. The automatic abort capability was deactivated prior to flight in the command module and the absence of a crew dictated that the manual abort loop be open. The parameters which governed automatic abort were angular overrate and two or more S-IC engines out. The automatic mode was deactivated in the launch vehicle prior to S-IC inboard engine cutoff. Angular overrate and engine thrust indications are also used for manual abort for manned flight. The other manual abort parameters were angle-of-attack dynamic pressure product ( $\Delta P$ ) and loss of launch vehicle inertial reference.

Redundant EDS transducers for fuel tank ullage pressure measurements were flown in the S-IVB and S-II stages; however, no meters were provided in the block II spacecraft. The AS-501 EDS was an extension of the Saturn IB design to provide for the additional stage.

### 15.3 SYSTEM EVALUATION

#### 15.3.1 General Performance

The excursions of the various parameters sensed by the EDS remained within acceptable limits throughout flight, and discrete sensors responded properly.

#### 15.3.2 Propulsion System Sensors

Although no display capability existed in the AS-501 command module and no abort limits were established for S-II and S-IVB fuel tank ullage pressures, the transducers in the tanks performed satisfactorily. The thrust OK pressure switches on the engines functioned properly and the output from the EDS

# SATURN V CREW SAFETY SYSTEM

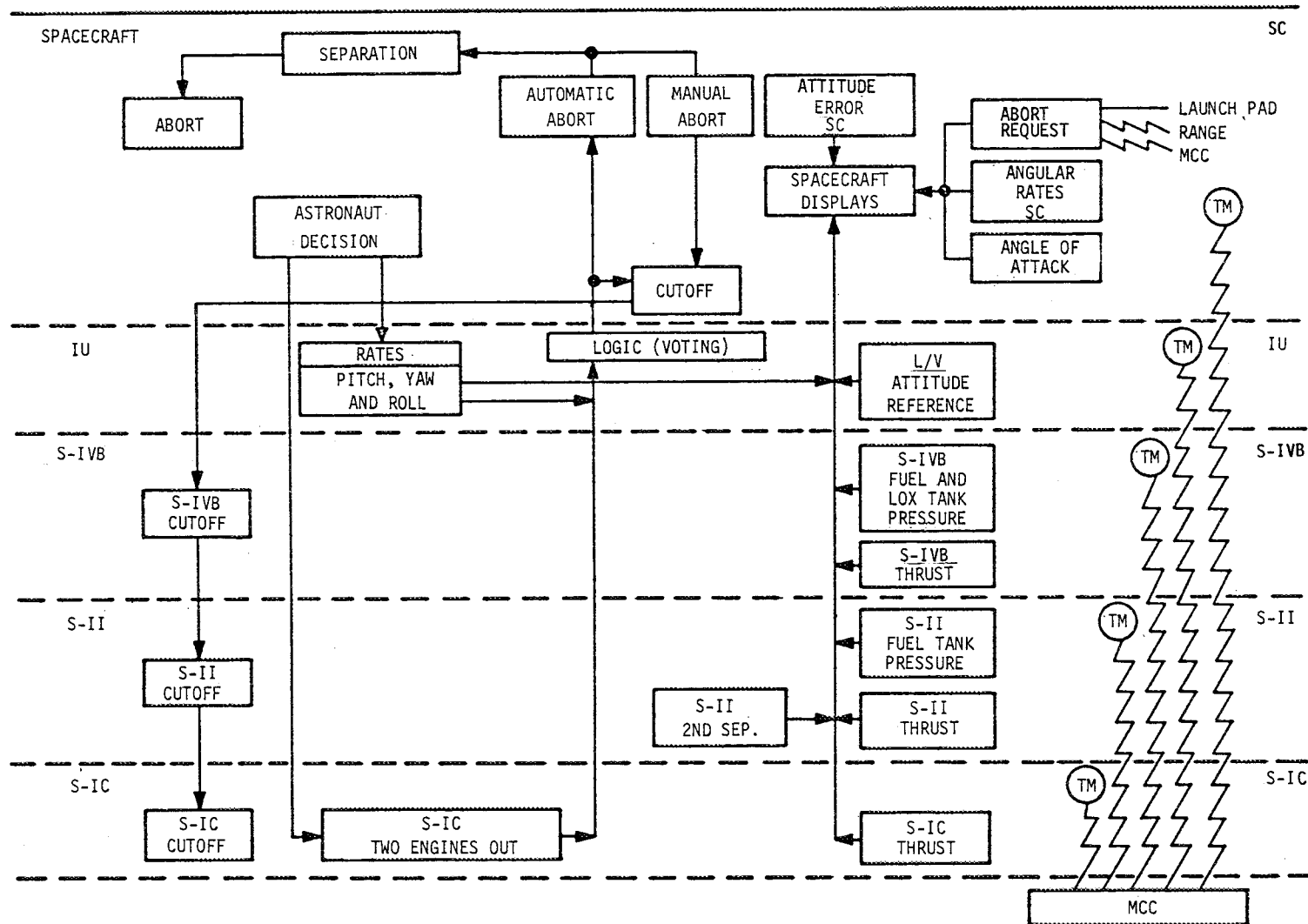


Figure 15-1 EDS Functional Diagram

logic in the IU was satisfactory. Table 15-1 is a tabulation of the performance of the thrust OK pressure switches.

### 15.3.3 Flight Dynamics and Control Sensors

The angle-of-attack dynamic pressure product is sensed by a redundant Q-Ball, and one of the outputs is displayed in the CM. The other output is telemetered from the IU. The maximum recorded on AS-501 was  $0.586 \text{ N/cm}^2$  (0.85 psid) at 46.9 seconds; peaks at  $0.407 \text{ N/cm}^2$  (0.59 psid) and  $0.386 \text{ N/cm}^2$  (0.56 psid) occurred at 35.3 and 78.8 seconds respectively. The preliminary Saturn V abort limit is a  $2.21 \text{ N/cm}^2$  (3.2 psid). Figure 15-2 gives a trace of the  $\Delta P$  versus time.

A failure of the launch vehicle inertial reference is indicated when the platform gimbal angles are displaced excessively for a given increment of time. These limits for AS-501 were set such that, before sensing is switched to the backup mode, an angular displacement in excess of 0.4 degree must occur in at least three minor computation cycles of 40 milliseconds duration, in a major computation cycle of approximately 1 second duration. Reasonableness-test failures must then occur an additional 15 times during the next second before guidance reference failure is considered to exist. The maximum angular displacement during a single minor computation cycle during powered flight of AS-501 was 0.15 degree, which represents 32.5 percent of the gimbal angular rate which must occur as stated above to result in a loss of launch vehicle guidance reference.

The abort limits in AS-501 for angular overrates were  $\pm 4$  degrees/second in the pitch and yaw axes and  $\pm 20$  degrees/second in the roll axis. During the time of automatic abort activation, the maximum rates sensed by the rate switches were: -0.9 degree/second in the pitch axis at 82.2 seconds, 0.5 degree/second in the yaw axis at 12.7 seconds, and -2.5 degrees/second at 22.8 seconds in the roll axis. As a result of the relatively low angular rate, no indication of rate-switch closures was detected.

### 15.3.4 Network Sequential Events

There were no anomalies in the performance of the EDS networks. The times for EDS associated events were nominal. Tables 15-2 and 15-3 are tabulations of the events and times of functioning.

Table 15-1. Performance Summary of Thrust OK Pressure Switches

STAGE	ENGINE	SWITCH	TIME CLOSED (SEC)	TIME OPENED (RANGE TIME, SEC)
S-IC	1	1	-2.746	150.937
	1	2	-2.694	150.945
	1	3	-2.632	150.953
	2	1	-2.402	150.937
	2	2	-2.326	150.945
	2	3	-2.300	150.978
	3	1	-2.690	150.987
	3	2	-2.702	150.994
	3	3	-2.676	151.003
	4	1	-2.450	150.928
	4	2	-2.486	150.937
	4	3	-2.402	150.945
	5	1	-2.894	135.585
	5	2	-2.966	135.585
	5	3	-2.868	135.585
S-II	1	1	154.820	519.968
	1	2	154.845	519.993
	2	1	154.895	519.960
	2	2	154.928	519.993
	3	1	154.978	520.043
	3	2	155.012	519.993
	4	1	154.820	520.051
	4	2	154.862	520.010
	5	1	154.903	519.968
	5	2	154.920	519.985
S-IVB 1ST BURN	1	1	525.481	665.842
	1	2	525.531	665.842
S-IVB 2ND BURN	1	1	11496.260	11786.415
	1	2	11496.330	11786.415

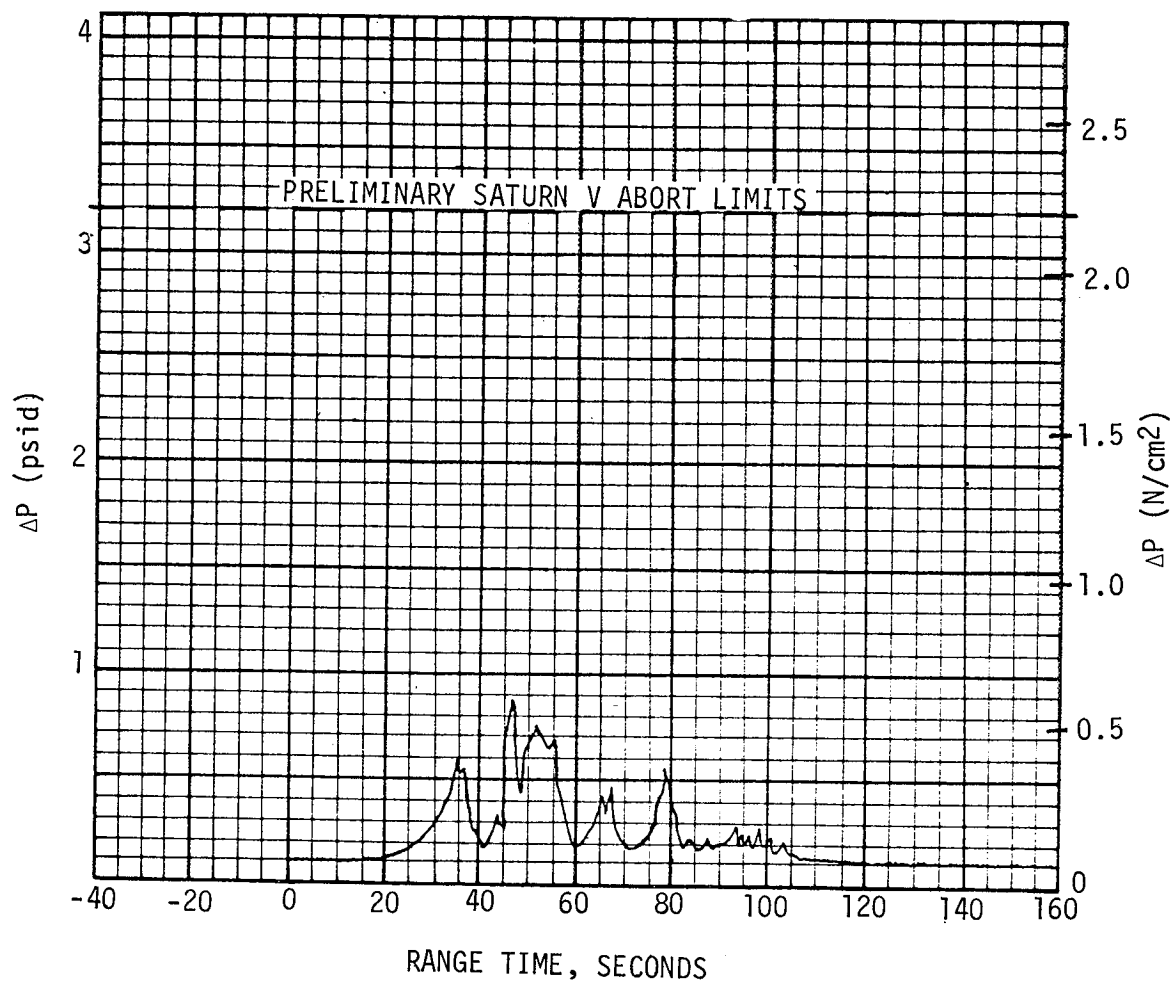


Figure 15-2. Q-Ball  $\Delta P$  Versus Flight Time

Table 15-2. Discrete EDS Events

DISCRETE MEASUREMENT	DISCRETE EVENTS	RANGE TIME (SEC)
K 73-602	Launch Vehicle EDS Cutoff Enable (Switch Selector)	30.230
K 74-602	Launch Vehicle EDS Cutoff Enable (EDS Timer No. 1)	40.979
K 81-602	EDS S-IC Stage One Engine Out	135.725
K 82-602	EDS S-IC Stage One Engine Out	135.702
K 57-603	Q-Ball Power Bus 6D31	144.751
K 58-603	Q-Ball Power Bus 6D41	144.751
K 79-602	EDS S-IC Stage Two Engines Out	150.976
K 80-602	EDS S-IC Stage Two Engines Out	150.976
K 87-602	LET Jettison A	187.142 (On) 187.182 (Off)
K 87-602	LET Jettison B	187.328 (On) 187.353 (Off)

Table 15-3. Switch Selector EDS Events

SWITCH SELECTOR FUNCTION	STAGE	RANGE TIME (SEC)	TIME FROM BASE (SEC)		
			NOMINAL	ACTUAL	DEVIATIONS
Liftoff Start TB1		0.263	$T_1+0.0$		
Auto Abort Enable Relays Reset	IU	5.216	$T_1+5.0$	4.953	-0.047
Launch Vehicle Engines EDS Cutoff Enable	IU	30.212	$T_1+30.0$	29.949	-0.050
S-IC Two Engines Out Auto Abort Inhibit Enable A	IU	134.426	$T_1+134.2$	134.163	-0.037
S-IC Two Engines Out Auto Abort Inhibit Enable B	IU	134.613	$T_1+134.4$	134.350	-0.050
Excess Rate (PYR) Auto Abort Inhibit	IU	134.818	$T_1+134.6$	134.555	-0.045
Excess Rate (PYR) Auto Abort Inhibit	IU	134.035	$T_1+134.8$	134.772	-0.028
Start TB2	S-IC	135.469	$T_2+0.0$		
Inboard Engine Cutoff	S-IC	135.518	$T_2+0.0$	0.049	-0.049
Q-Ball Power Off	IU	144.719	$T_2+9.3$	9.250	-0.505
Outboard Engines Cutoff, Start TB3	S-IC	150.769	$T_3+0.0$		
LET Jettison A	IU	187.133	$T_3+36.4$	36.364	-0.030
LET Jettison B	IU	187.319	$T_3+36.6$	36.550	-0.050





## SECTION 16 VEHICLE PRESSURE AND ACOUSTIC ENVIRONMENT

### 16.1 SUMMARY

The vehicle internal, external and base region pressure environment was monitored by a series of differential and absolute pressure gauges. These gauges were used in confirming the vehicle design external, internal, and base region pressure environments. The flight data were generally in good agreement with the predictions and well within the values to which the structure was designed.

The vehicle internal and external acoustic environment was monitored by a series of microphones positioned to measure both the rocket engine and aerodynamically induced fluctuating pressure levels. The measured acoustic levels were generally in reasonable agreement with the liftoff and inflight predictions. However, no valid internal acoustic data were obtained for the S-II stage. No detrimental effects due to the acoustic levels have been determined at this time.

### 16.2 SURFACE PRESSURE AND COMPARTMENT VENTING

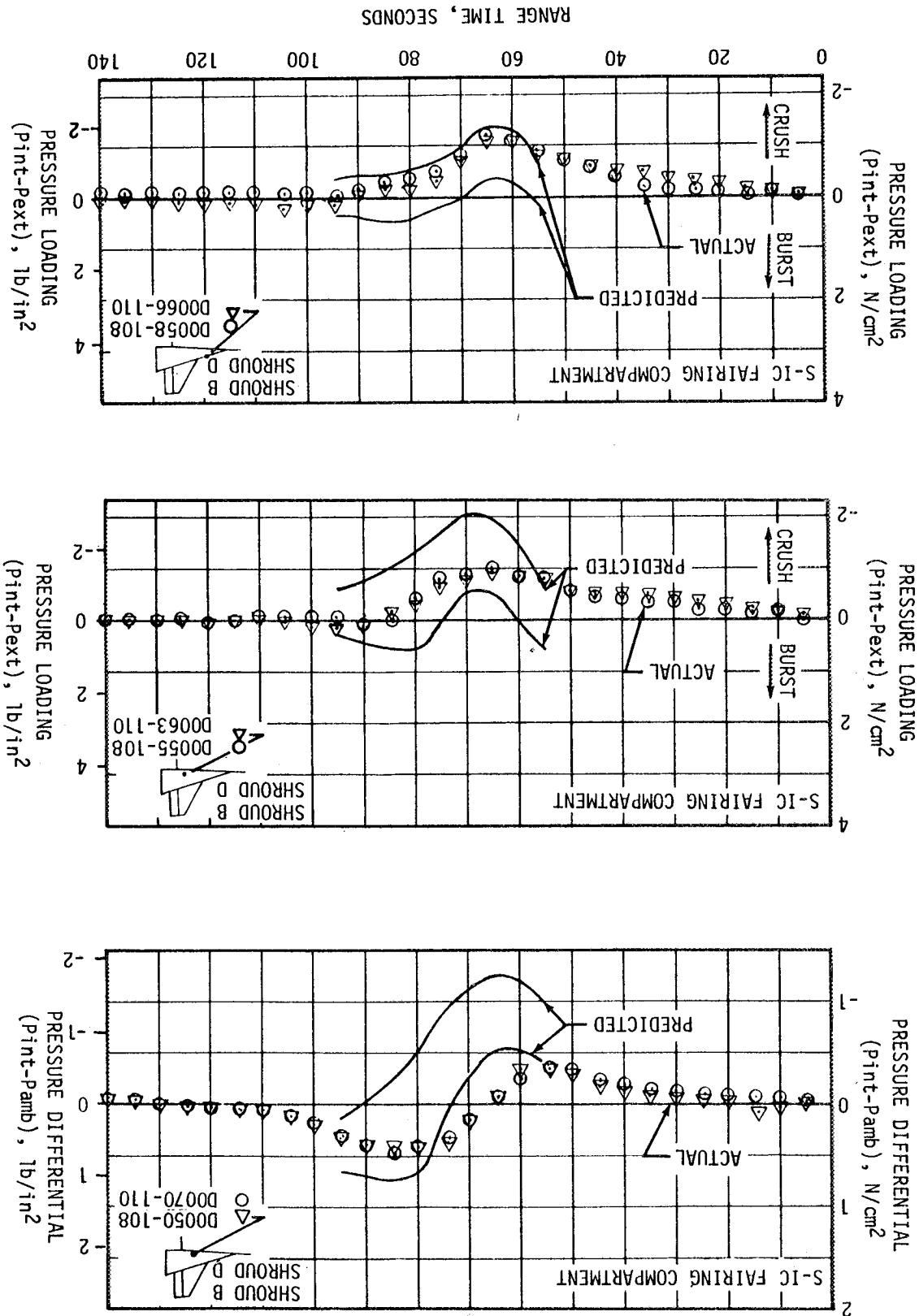
#### 16.2.1 S-IC Stage

The internal and external pressure environment on the S-IC stage was monitored by 43 pressure transducers located in and on the engine fairings, aft skirt, intertank, and forward skirt. Representative data from a portion of these instruments are compared with preflight predictions in Figures 16-1 thru 16-3. Compartment pressure histories were predicted using an analytical venting program, known vent and leakage areas, and appropriate external flow field parameters. The vehicle angle-of-attack was neglected in these analyses since the internal pressure was quite insensitive to these effects for the configuration flown. The external pressure environment was predicted using wind tunnel data for a ten degree angle-of-attack. These data were combined to provide the pressure loading ( $P_{\text{internal}}/P_{\text{external}}$ ) bands for the critical flight regions.

#### 16.2.2 S-II Stage

Differential pressures across the S-II forward skirt area, shown in Figure 16-4, were calculated by taking differences between various external static pressure measurements and one internal pressure measurement in the forward

Figure 16-1. S-1C Engine Fairing Compartment Pressure Differential and Aerodynamic Loads



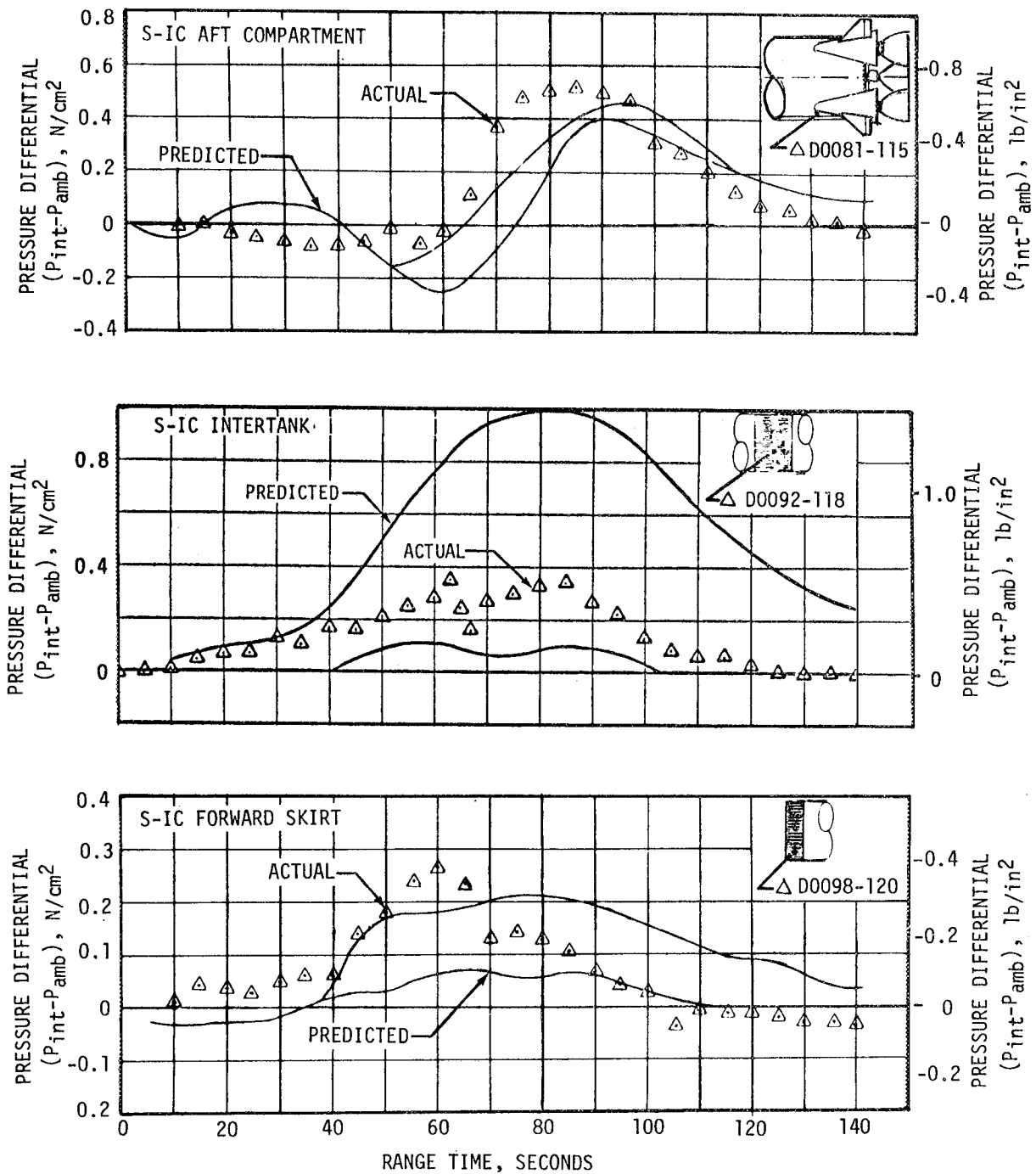


Figure 16-2. S-IC Compartment Pressure Differentials

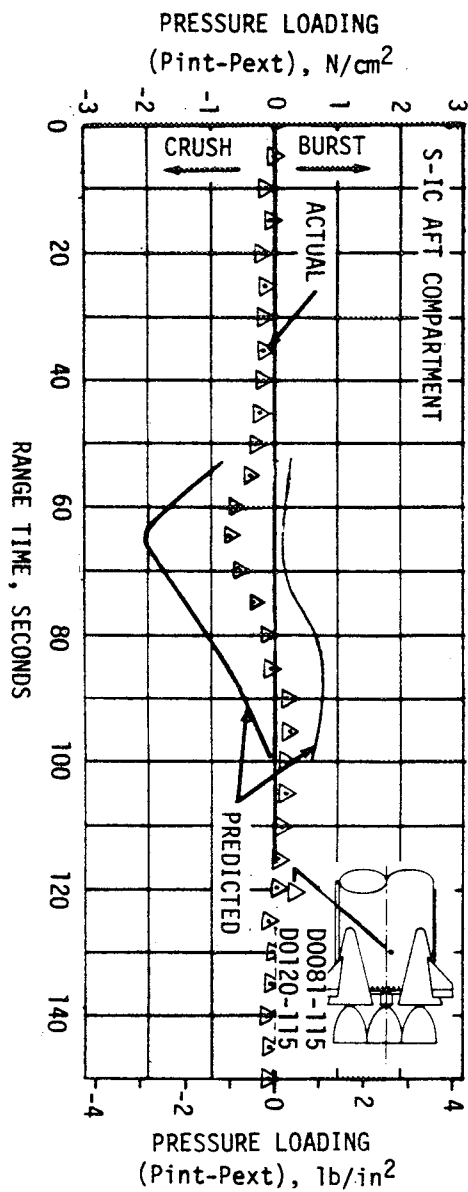
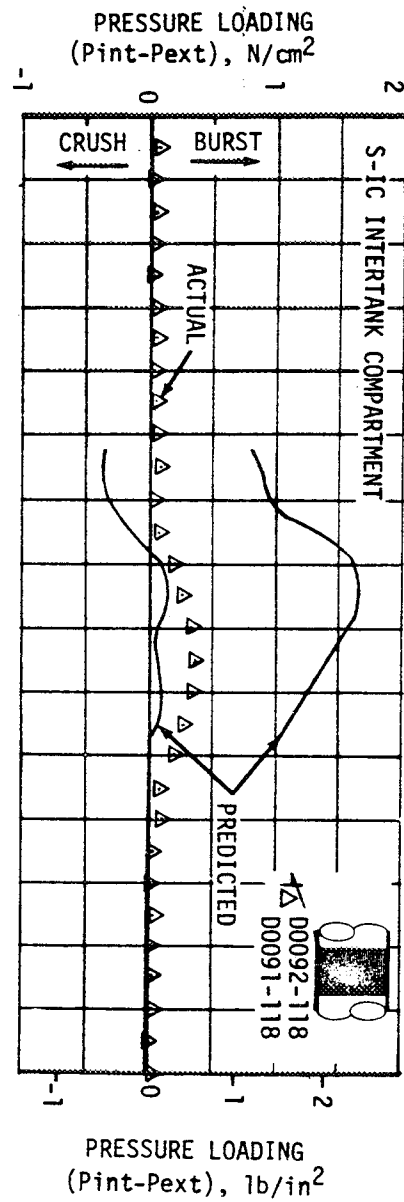
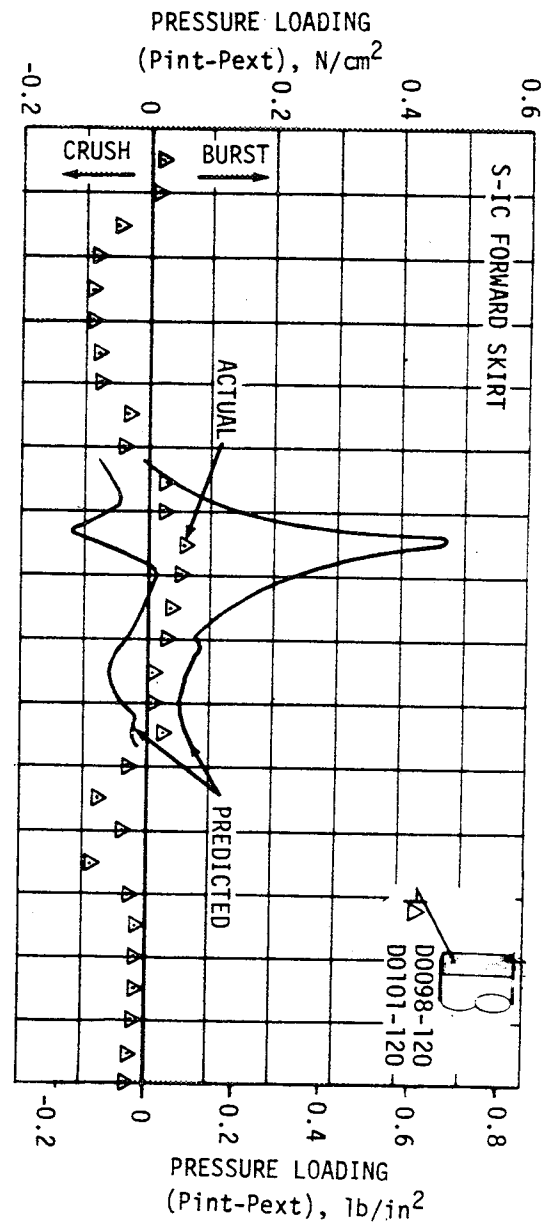


Figure 16-3. S-IC Compartment Pressure Loads

skirt compartment. A maximum bursting load of approximately  $3.5 \text{ N/cm}^2$  ( $5.08 \text{ psid}$ ) was observed at 56 seconds for the external measurement located at vehicle station 63.88 meters (2515 in.). Measured pressure loads were close to predicted and well below design limits.

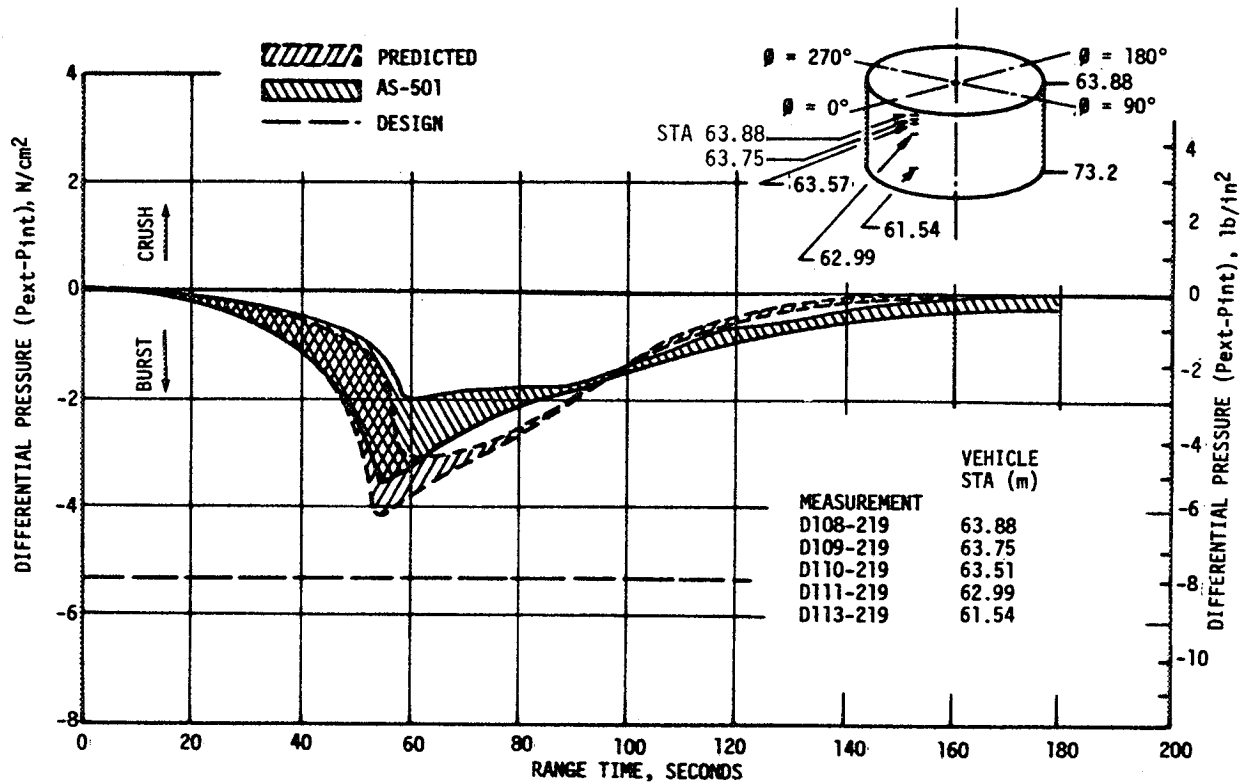


Figure 16-4. Forward Skirt Differential Pressures

Three pairs (internal/external) of absolute pressure measurements were located at vehicle stations 60.40 meters (2378 in.), 54.18 meters (2133 in.) and 48.0 meters (1890 in.) on the LH<sub>2</sub> sidewall insulation in order to measure the load across the insulation. The external pressure measurements at vehicle stations 54.18 meters (2133 in.) and 48.0 meters (1890 in.) malfunctioned. Comparison of the one external and three internal pressure measurements with postflight predicted is shown in Figure 16-5. The external pressure measured at the upper manifold location at vehicle station 60.42 meters (2378 in.) showed good correlation with the prediction. Measured internal pressures at this location were much lower than predicted, and the exact cause for this deviation has not been determined. Internal pressures measured at the other two locations at vehicle stations 54.18 meters (2133 in.) and 48.0 meters (1890 in.) were generally in good agreement with predictions. The predicted internal pressure histories were computed by means of a multiple venting digital computer program using a math model to simulate the LH<sub>2</sub> sidewall insulation. The math model was developed empirically by matching S-II-1, S-II-3, and S-II-4 ambient

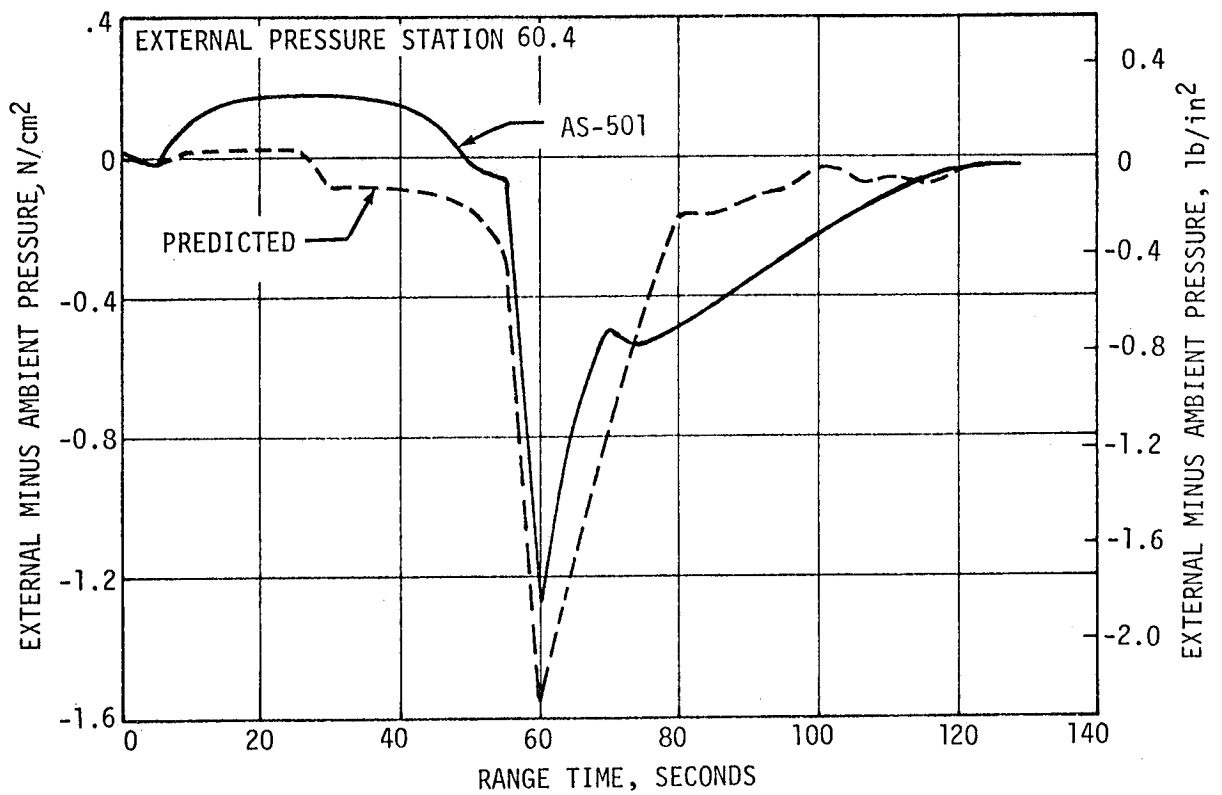
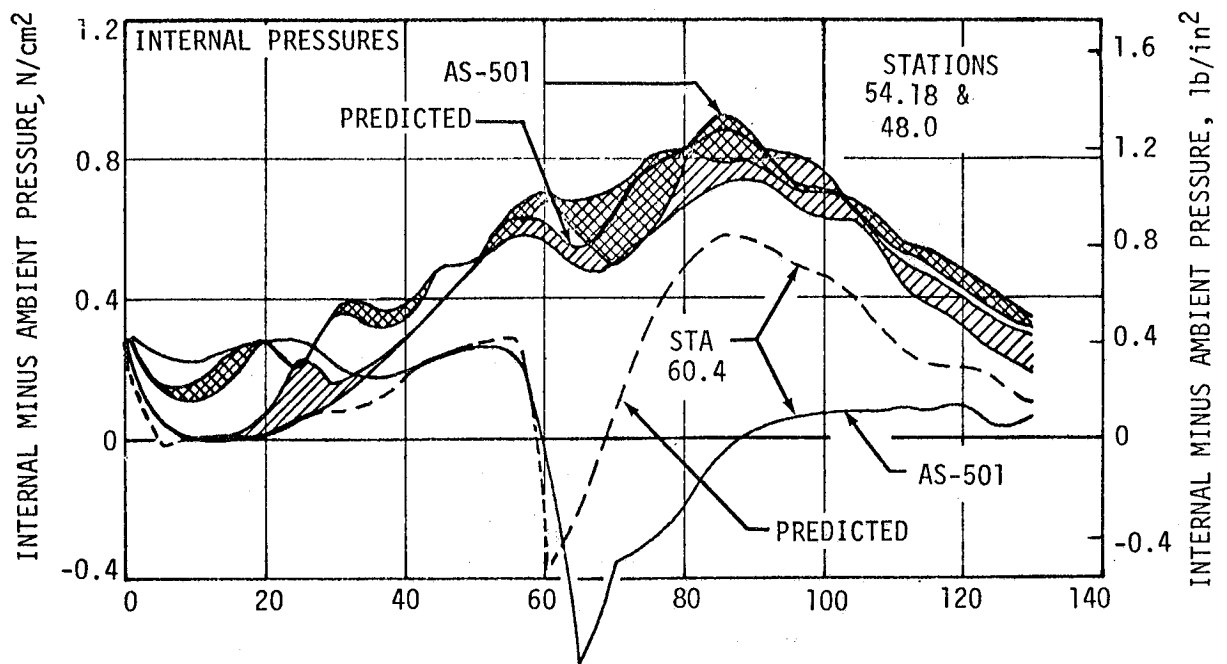


Figure 16-5. Sidewall Insulation Differential Pressures

blowdown test data. The discharge coefficient due to the pressure ratio  $P_{\text{manifold}}/P_{\text{external}}$  was not considered at vent spouts during the blowdown simulation in developing the math model and was, therefore, not included in the flight prediction. However, the discharge coefficients based on the cross-flow velocity across the vent spout were included in the prediction.

An equivalent leakage of approximately 2.0 cubic meters per minute (70 SCFM) of helium, detected during ground purging, was included in the flight predictions but its contribution to the overall internal pressure was found to be small.

Using available flight data and postflight predictions, a differential pressure profile across the insulation was constructed for the critical transonic flight phase. The sidewall insulation maximum differential pressure was calculated to be approximately  $1.9 \text{ N/cm}^2$  (2.75 psid).

### 16.2.3 S-IVB Stage

A comparison of the S-IVB aft interstage compartment pressure data with predicted values is presented in Figures 16-6 and 16-7. Figure 16-6 shows compartment pressure minus ambient pressure. The predicted values were based on a 501 nominal trajectory (M-AERO-D-1) and covered the maximum and minimum estimates. The flight data fell generally within this envelope.

Figure 16-7 shows maximum and minimum values of compartment pressure minus local external pressure. The flight data fell within the predicted envelope.

## 16.3 BASE PRESSURES

### 16.3.1 S-IC Base Pressures

Static pressures on the S-IC base heat shield were recorded by eleven measurements, two of which were heat shield differential pressures. Representative data from a portion of these instruments were compared with predictions in Figure 16-8.

The S-IC base pressure differentials are shown in the upper portion of Figure 16-8. The flight data agreed well with the predicted bands. The trends in the data were as expected. During the subsonic and transonic portion of flight (0 to 10 kilometers altitude), the base pressure was less than ambient. Between 6 and 7 kilometers, the F-1 engine exhaust plume began to increase the base pressures to a point where they exceeded ambient between 10 and 11 kilometers. The S-IC base heat shield differentials, shown in Figure 16-8, were well within the predicted values. The design differential for the heat shield was  $1.38 \text{ N/cm}^2$  (2.0 psi). Wind tunnel data and analytical predictions were used to establish the bands.

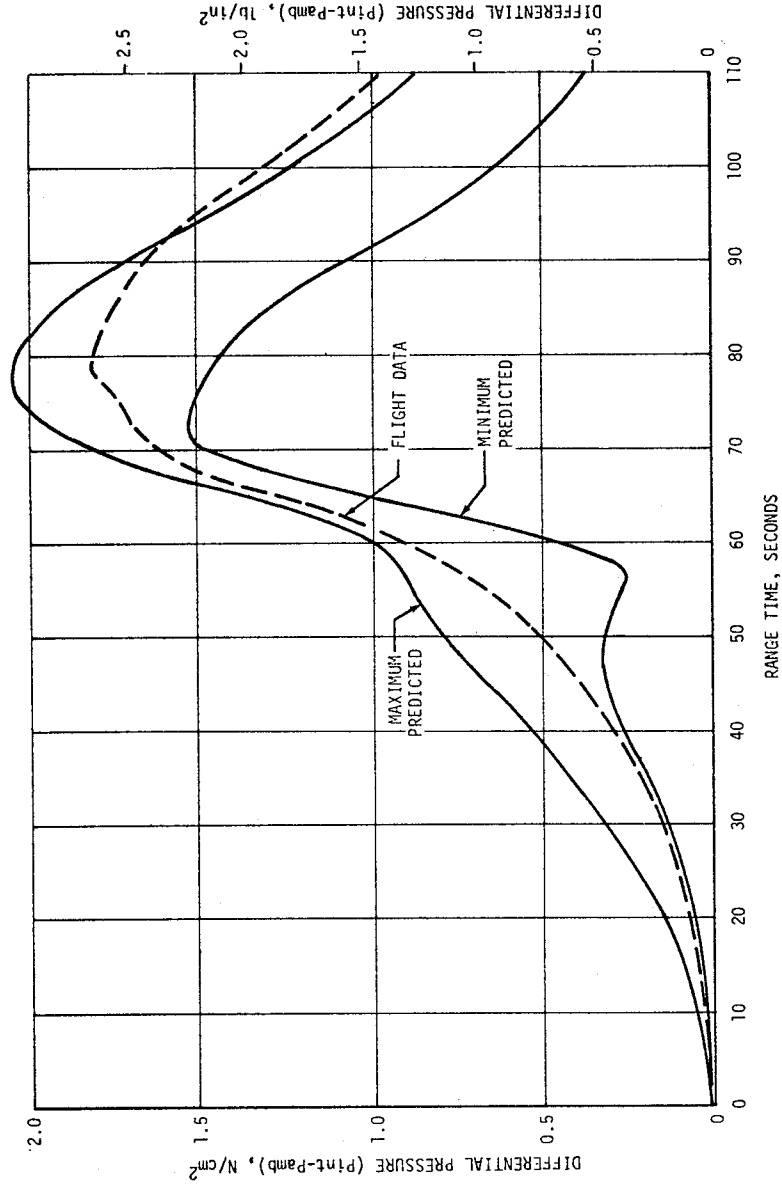


Figure 16-6. S-II/S-IVB Interstage Pressure Differential

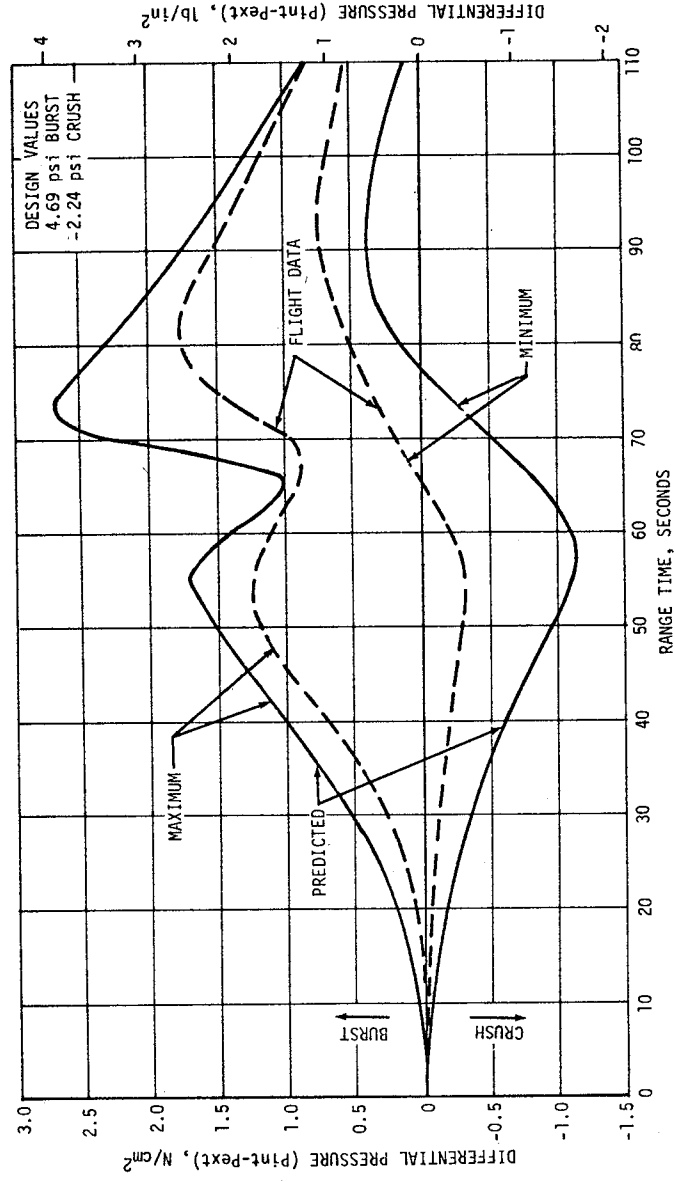


Figure 16-7. S-II/S-IVB Interstage Pressure Loading



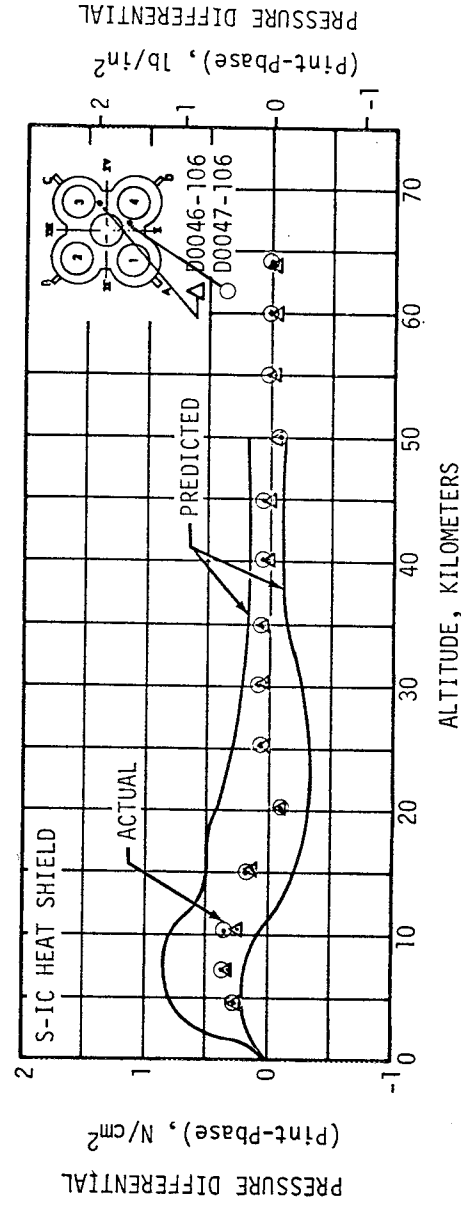
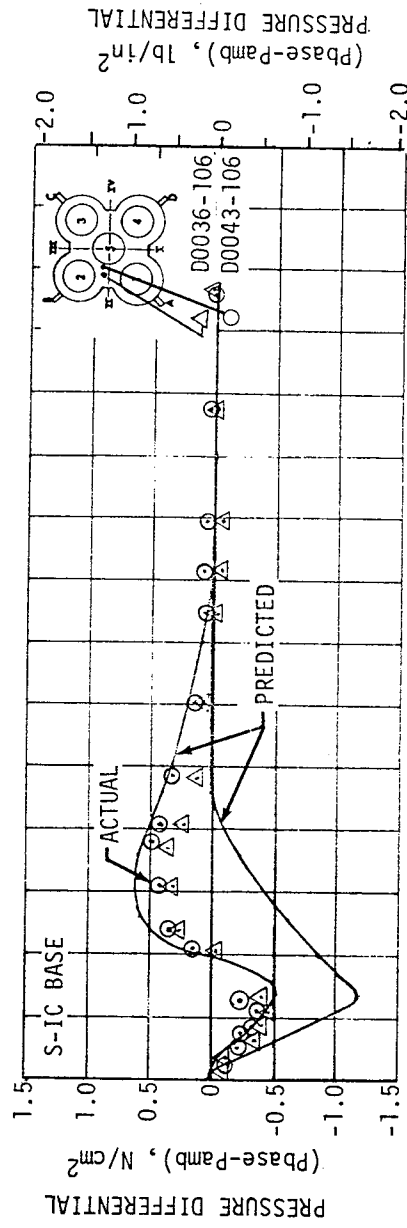
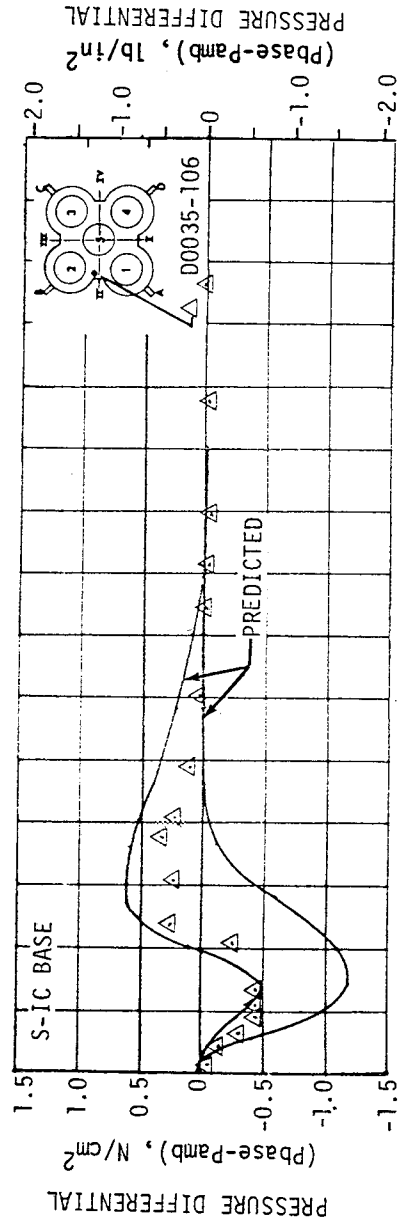


Figure 16-8. S-IC Base Heat Shield Pressure Environment

### 16.3.2 S-II Base Pressures

Maximum absolute pressures measured on the aft face of the S-II heat shield during S-II boost were approximately  $0.045 \text{ N/cm}^2$  ( $0.065 \text{ psia}$ ); this is shown in Figure 16-9. Pressures shown are for two heat shield locations representative of the overall base heat shield pressures. The difference in pressure between the two transducers may be due to engine gimbaling effects. Pressure drops were experienced at second plane separation and propellant mixture ratio step down, as expected. Measured pressures were slightly lower than the predicted values, which were based on hot flow model test results. The steady state S-II value of engine deflection was also considered in the prediction. Hot flow test results did not reflect the pressure drop which occurred after second plane separation.

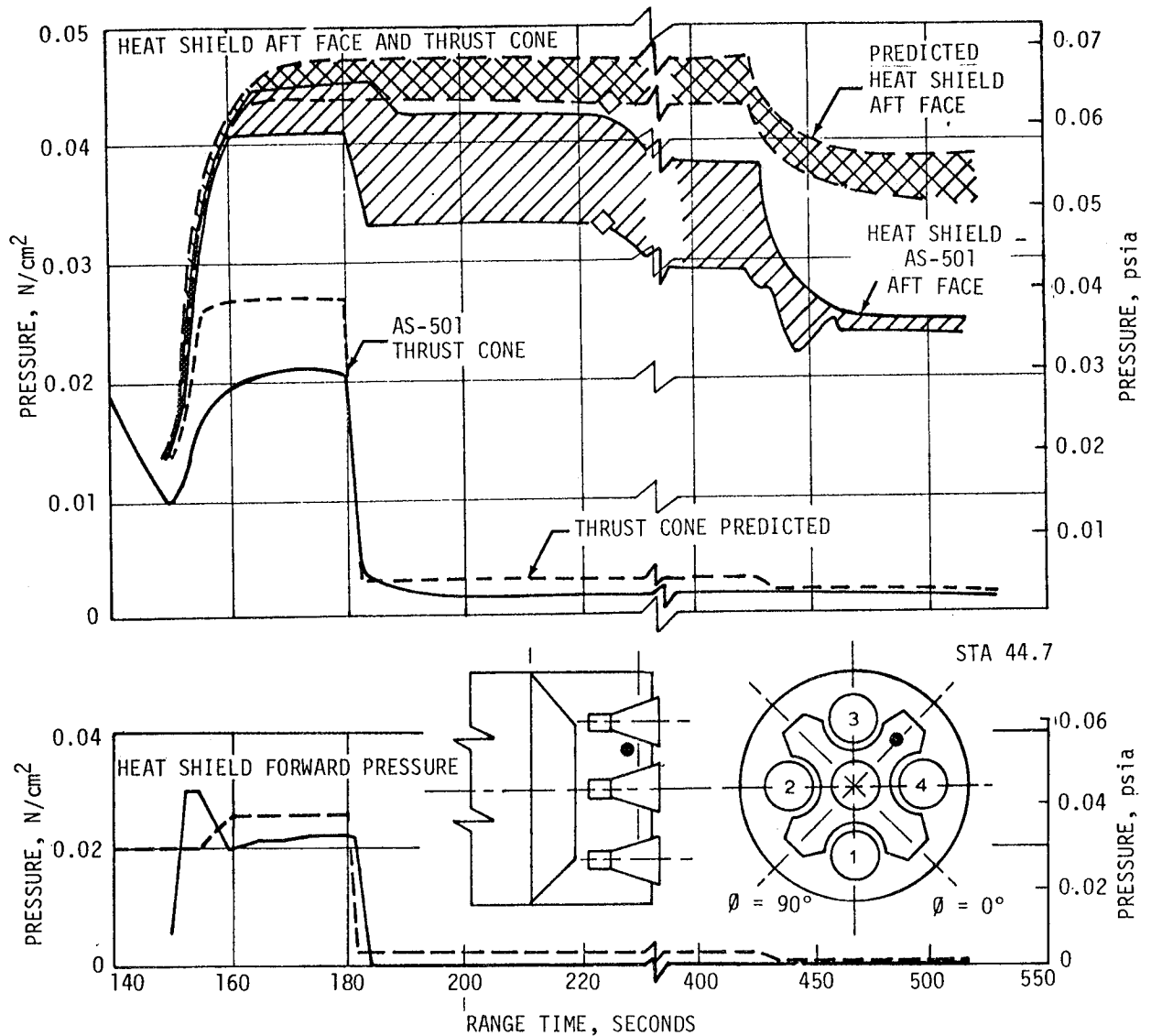


Figure 16-9. S-II Base Pressures

Pressures measured on the thrust cone and on the forward face of the heat shield were in good agreement with predicted. This is shown in Figure 16-9. In these areas the pressure drop resulting from second plane separation was more pronounced than on the aft face of the heat shield. It should be noted that the flight data were relatively constant in these regions showing that the base heat shield forward face pressures and the thrust cone surface pressure were independent of engine gimbaling effects.

#### 16.4 ACOUSTIC ENVIRONMENT

##### 16.4.1 External Acoustics

The external fluctuating pressure environments for the AS-501 vehicle were recorded by nine measurements which were located on the Instrument Unit, S-IVB forward and aft skirts, S-II forward and aft skirts, S-IC intertank and aft compartments, and fin D. Representative data for these instruments were compared with predictions in Figures 16-10 thru 16-12.

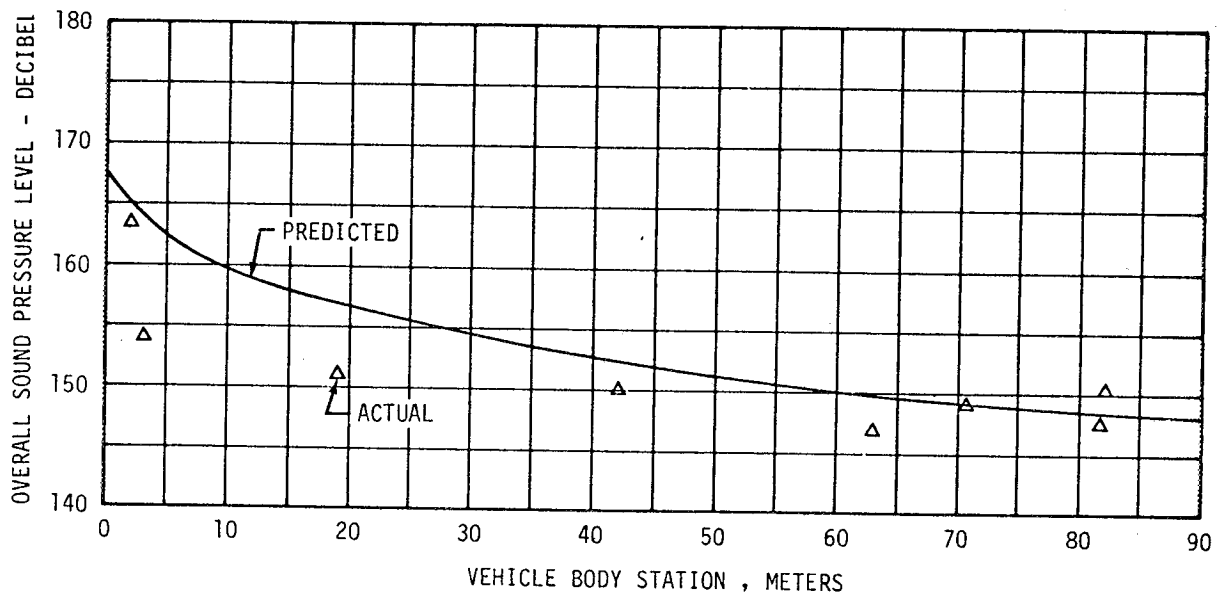


Figure 16-10. Vehicle External Overall Sound Pressure Level at Liftoff

The AS-501 external acoustic environment at liftoff is shown in Figure 16-10. The prediction curve was derived assuming a single deflector flame bucket, whereas the launch pad flame bucket was a double deflector configuration. The measured data were in reasonable agreement with the predictions.

Overall fluctuating pressure levels for vehicles AS-201, AS-202, and AS-501 are shown in Figure 16-11. Comparisons between AS-501 flight data and flight data obtained from AS-201 and AS-202 were possible for the IU location only.

16-12

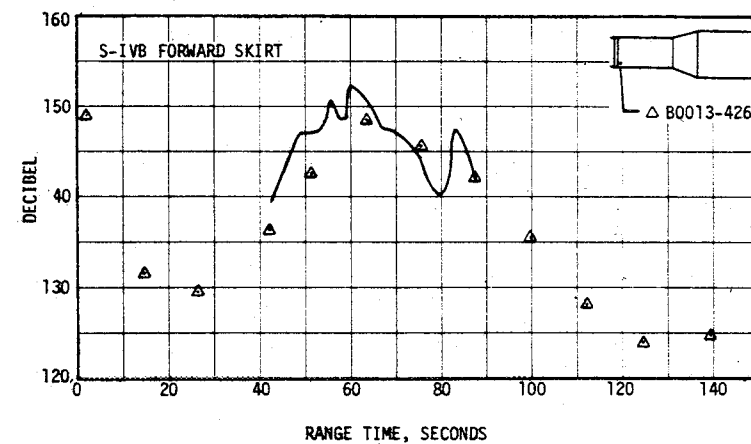
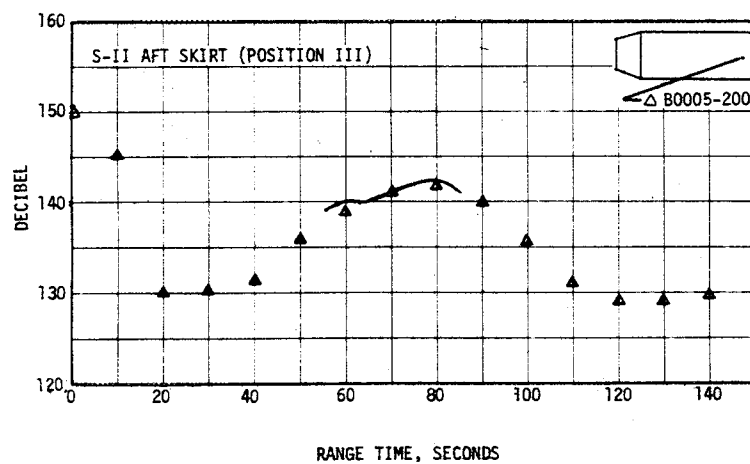
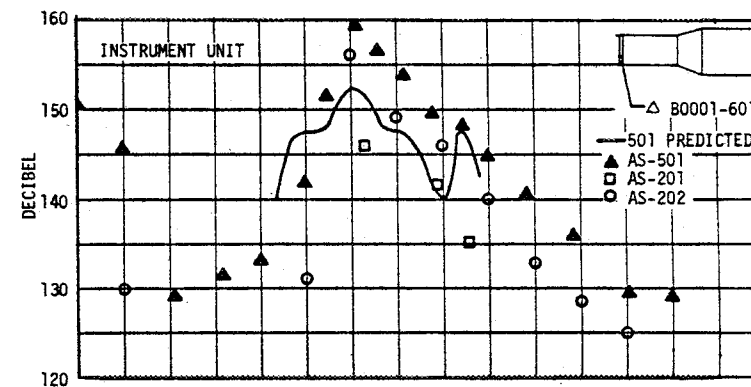
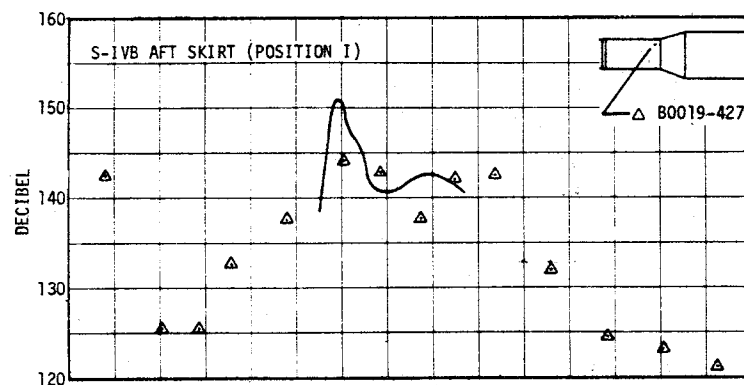


Figure 16-11. Vehicle Overall Fluctuating Pressure Level, Sheet 1 of 2

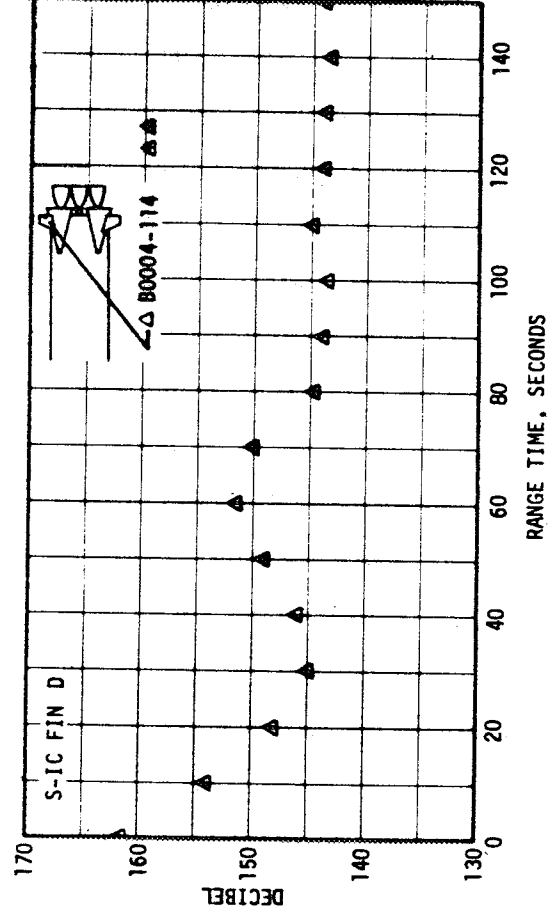
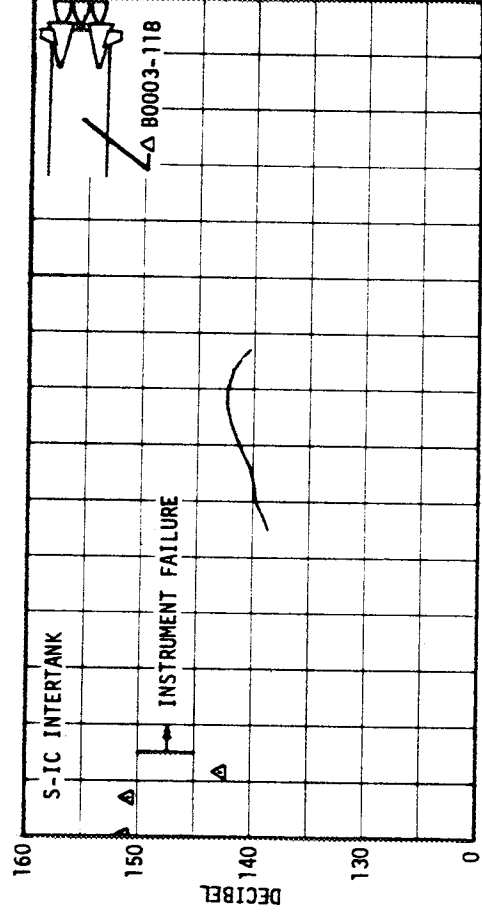
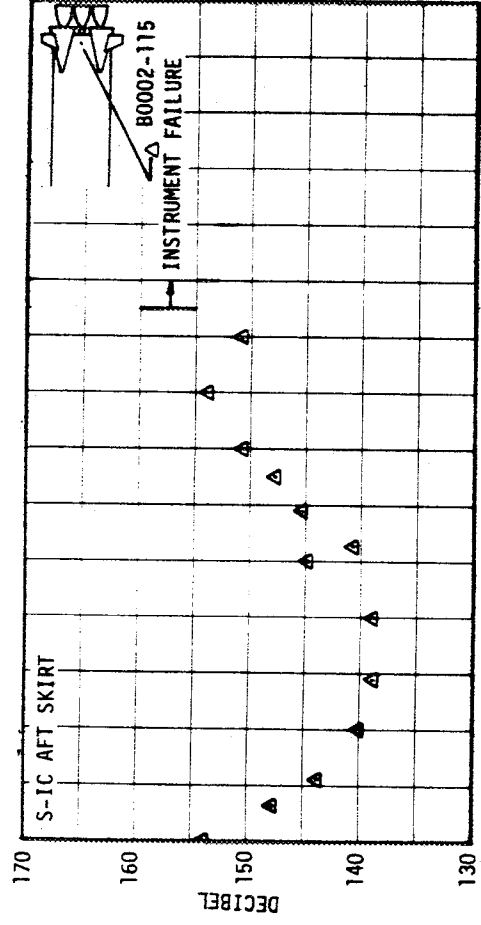


Figure 16-11. Vehicle Overall Fluctuating Pressure Level, Sheet 2 of 2

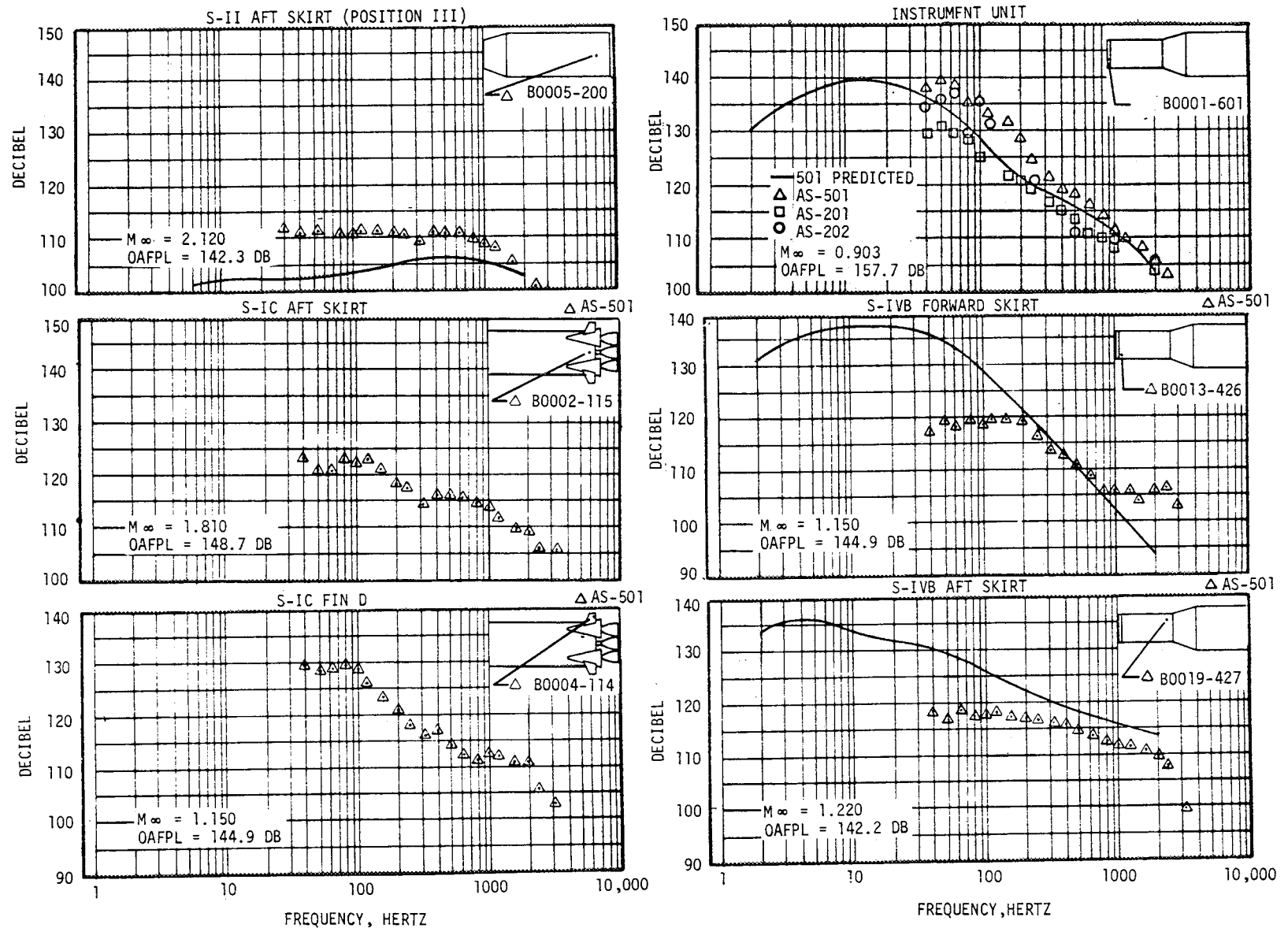


Figure 16-12. Vehicle External Fluctuating Pressure Spectral Densities

Good agreement exists between AS-501 and AS-202 flight data. Better agreement could be achieved for times greater than 60 seconds if the AS-202 flight times were increased to obtain exact matching of trajectory conditions for the vehicles. The trajectories for AS-201 and AS-202 have dynamic pressures nearly equal to those of AS-501 at equivalent Mach numbers. The data for times greater than 60 seconds does not show this behavior and is under additional investigation.

AS-201 data had the same general data trend as AS-501 but with lower overall fluctuating pressure levels. A prediction curve for AS-501 IU based on analytic methods is shown in Figure 16-11 and is in reasonable agreement with the measurements.

External fluctuating pressure spectral densities from vehicles AS-201, AS-202 and AS-501 for times near the occurrence of maximum local aerodynamic fluctuating pressures are shown in Figure 16-12. As expected from the overall fluctuating pressure plot, AS-501 and AS-202 data were in good agreement. AS-201 data has the same data trend with slightly lower spectrum levels below 100 hertz. All flight data were in good agreement with the AS-501 prediction.

All fluctuating pressure levels were referenced to  $2 \times 10^{-5} \text{ N/m}^2$  ( $0.0002 \text{ dyne/cm}^2$ ) and were obtained from root-means-square time histories. The pressure spectra were obtained from a one-third octave band analysis. The data presented do not necessarily reflect the maximum levels due to the large time interval between data points. Predictions were based on a clean configuration and do not account for local protuberance effects. Variations between the reference trajectory and the actual AS-501 trajectory and angle-of-attack effects were not reflected in the predictions.

#### 16.4.2 Internal Acoustics

The S-IC stage intertank internal acoustic data, as obtained from the one internal acoustic measurement, are shown in Figure 16-13. The level measured during liftoff was similar to that measured during static firing. The levels measured during the remainder of S-IC powered flight were much lower than static firing and lower than expected.

The S-IVB internal acoustic environment was measured in both the forward and aft skirts. The forward microphone was located near position II and 14.4 centimeters (5.7 in.) aft of the field splice. The aft microphone was located near position I, 79.3 centimeters (31.2 in.) forward of the separation plane. Time histories for the composite (50 to 3000 hertz) levels are shown in Figure 16-14 compared to levels measured at a similar location on the forward skirt of S-IVB-202 and levels measured on the aft skirt of S-IVB-203 at a location on the opposite side of the stage.

MEASUREMENT INCLUDED	MAXIMUM SPL (db) (0-3000 CPS)		REMARKS
	STATIC FIRING [1]	FLIGHT [3]	
B1-118	145.1 145.4	142.3 @ T+0.5	[2]

[1] THE TWO VALUES ARE THE AVERAGE OVERALL RMS AND THE MAXIMUM OVERALL RMS MEASURED DURING ALL THE S-IC FLIGHT STAGE STATIC FIRINGS.

[2] RISE AT T+36 SECONDS, 2.5 SECONDS DURATION, REASON UNKNOWN.

[3] DECIBEL REFERENCED TO  $2 \times 10^{-5}$  N/m<sup>2</sup>.

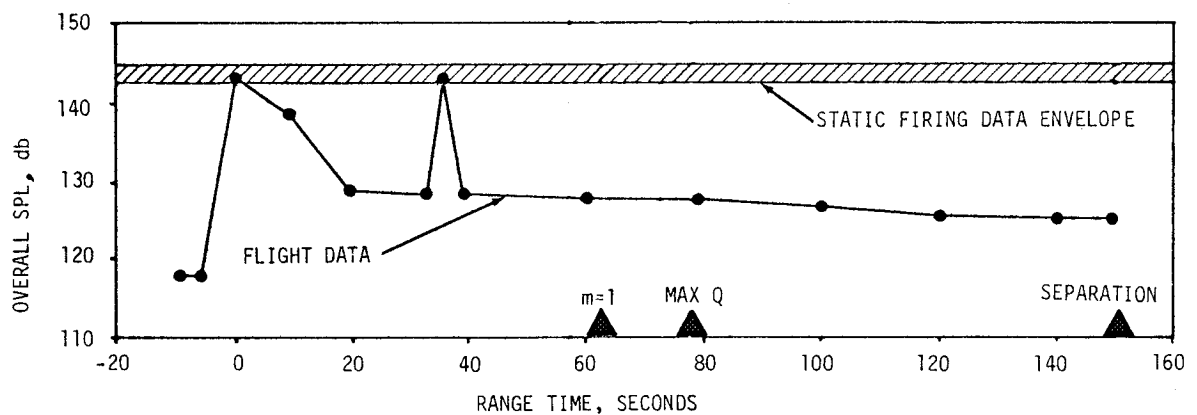


Figure 16-13. S-IC Acoustic Environment, Acoustic Measurement Summary  
- Intertank, Internal

The maximum overall internal sound pressure levels in the S-IVB stage measured during the high dynamic portion of the flight were lower than the maximum sound pressure levels measured at liftoff. The maximum sound pressure levels measured at liftoff were also lower than those measured during Saturn IB launches. However, the levels measured at the forward skirt were higher than those measured during Saturn IB flight. These higher levels are presumed to be caused by the additional turbulence generated by the antifrutter kit installation.



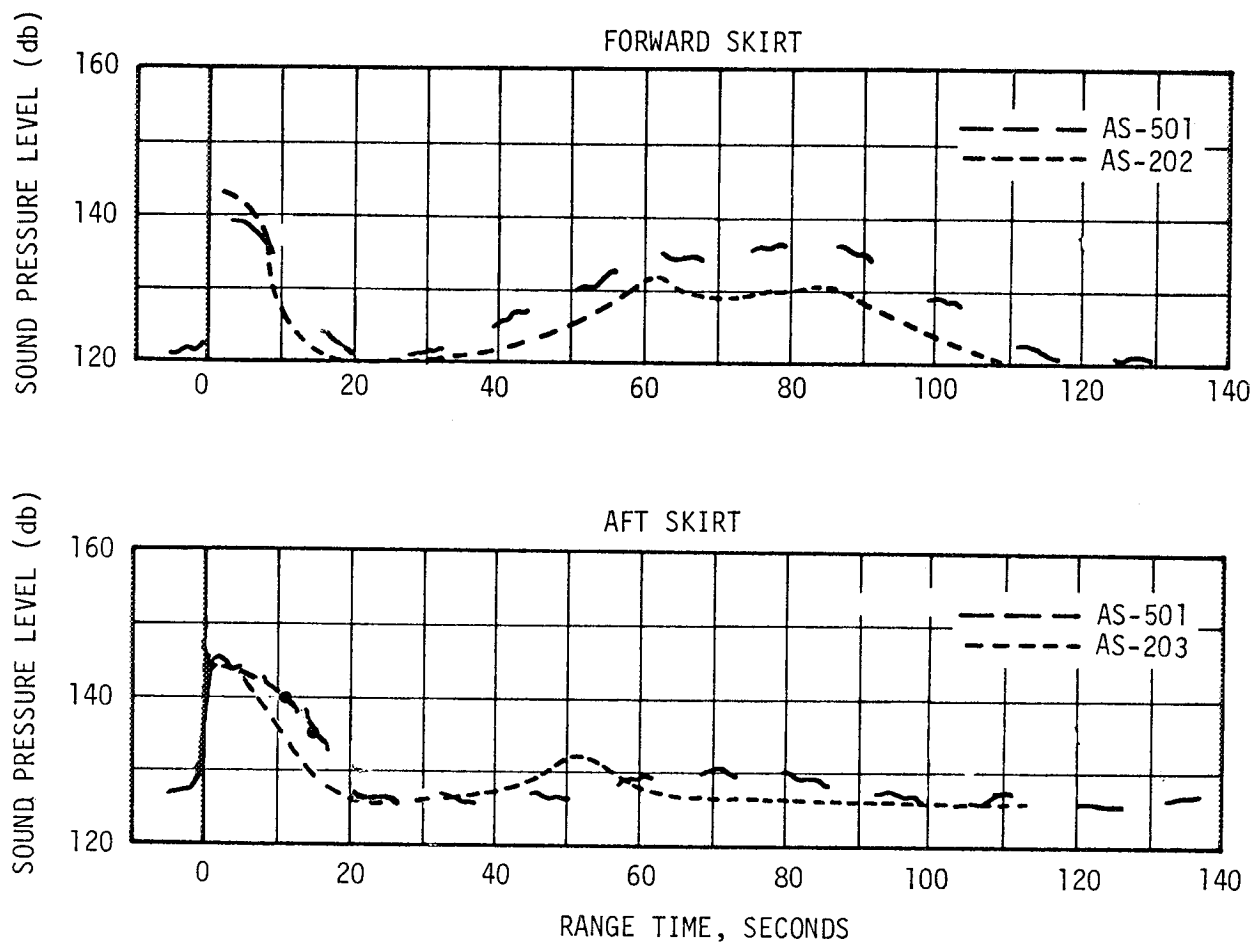


Figure 16-14. S-IVB Internal Sound Pressure Levels



## SECTION 17 VEHICLE THERMAL ENVIRONMENT

### 17.1 SUMMARY

The AS-501 vehicle thermal environment was generally less severe than that for which the vehicle was designed. Aerodynamic heating was not as severe as expected on the cylindrical portions of the vehicle for the trajectory flown and substantially below the predictions based on the MSFC maximum heating trajectory. Base heating rates were well below the maximum design heating rates for the respective stages.

Aerodynamic heating of the S-IC fins and engine fairings was about as expected for the trajectory flown. The effectiveness of the insulation on the S-IC forward skirt in reducing protuberance induced heating could not be determined due to large variations in the insulation thickness. The only suspected anomaly noted in the thermal protection system appears to be the loss of a small section of the M-31 to the level of the open face honeycomb. However, since the base region environment was substantially below the design level, temperatures in this area did not exceed design limits.

Protuberance induced heating effects on the S-II stage were generally below the design and postflight predictions. However, predictions for the undisturbed flow regions correlated well with the flight data. The measured radiative heat flux on the base heat shield was in good agreement with the postflight prediction; however, the measured total heat flux was lower than the postflight prediction and was well below the design value. While the data indicated convective heating to the base region throughout S-II boost. The data could not be correlated with the gas recovery temperature since it fell below the transducer range.

Results of the postflight studies indicate that the analytical models and prediction techniques used for AS-501 were valid and, further, that the vehicle structure was capable of withstanding the environment of the MSFC maximum heating trajectory.

### 17.2 S-IC BASE HEATING AND SEPARATION ENVIRONMENT

Thermal environments in the base region of the S-IC were recorded by 40 measurements which were located on the heat shield, F-1 engines, and base of Fin D. This instrumentation included six radiation calorimeters, 20 total asymptotic calorimeters, and 14 gas temperature probes. Representative

data from a portion of these instruments are compared with predicted and design environments in Figures 17-1 through 17-5.

Total heating rates to the base heat shield calorimeters were well below the MSFC design environment, as shown in Figure 17-1. The S-IC base heat shield thermal environment was primarily radiation heating with convective cooling, as determined from postflight studies. Radiation was about as predicted except in the 15 to 45 kilometers (49,000 ft to 148,000 ft) altitude range where radiation increased rapidly to values greater than those experienced at sea level. This increase in radiation was attributed to plume expansion and afterburning of the fuel rich exhaust products. Afterburning ceased at the higher altitudes, and a corresponding decrease in radiation was noted. The predicted radiation to the heat shield and engines was determined from an analytical plume model at sea level. Dropoff with altitude was based upon Saturn I flight data. Results from the total and radiation calorimeters indicated that a convective cooling rate was experienced on the base heat shield until an altitude of 20 kilometers (66,000 ft) and then changed to a small convective heating rate at the higher altitudes. A different trend is noted in Figure 17-2 for the F-1 engine nozzle extension near the nozzle lip, where convective heating was present from liftoff to a maximum value at an altitude of 15 kilometers (49,000 ft). Convective heating to the nozzle lip at altitudes above 25 kilometers (82,000 ft) was negligible.

The base heat shield gas temperatures were well below the design gas temperatures, as shown in Figure 17-1, and correlated well with predictions which were based on model test data. Gas temperatures measured on the engines, Figure 17-2, were greater than the heat shield gas temperatures but were well below the design environment.

Calorimeter data, Figure 17-2, have shown that the total heating rates on the nozzle lip did not exceed 25 watts/cm<sup>2</sup> (22 Btu/ft<sup>2</sup>-sec), whereas the MSFC maximum design value is approximately 38 watts/cm<sup>2</sup> (34 Btu/ft<sup>2</sup>-sec). The temperature of the air inside the cocoon was expected to reach as much as 533°K (500°F) but did not exceed 355°K (180°F). The lower hat band of engine No. 1 has an allowable temperature of 1089°K (1500°F) but did not exceed 908°K (1174°F).

The total heating rates measured on the base of Fin D are compared with the predicted environment in Figure 17-3. Flight data and prediction were in good agreement from liftoff to an altitude of 10 kilometers (33,000 ft). Plume expansion and afterburning above this altitude resulted in a similar increase in incident heating to the base of the fin as noted previously for the heat shield and engines.

The data acquired during S-IC/S-II separation were not adequate to completely describe the separation environment. As shown in Figure 17-4, the forward skirt skin was heated only slightly during separation; however, data from the LOX tank dome thermocouples indicated rather high heating rates, 33.2 watts/cm<sup>2</sup> (28.8 Btu/ft<sup>2</sup>-sec). Since the gas temperatures measured at separation were not sufficient to drive the LOX tank dome to the recorded

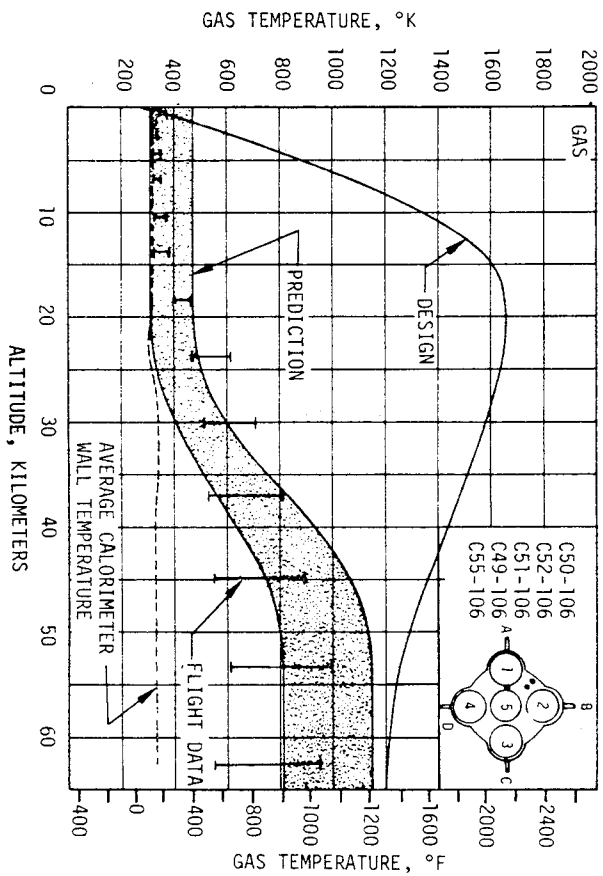
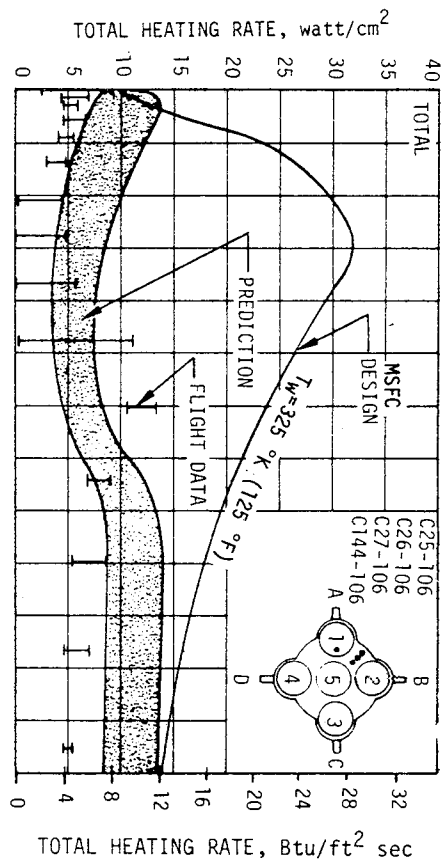
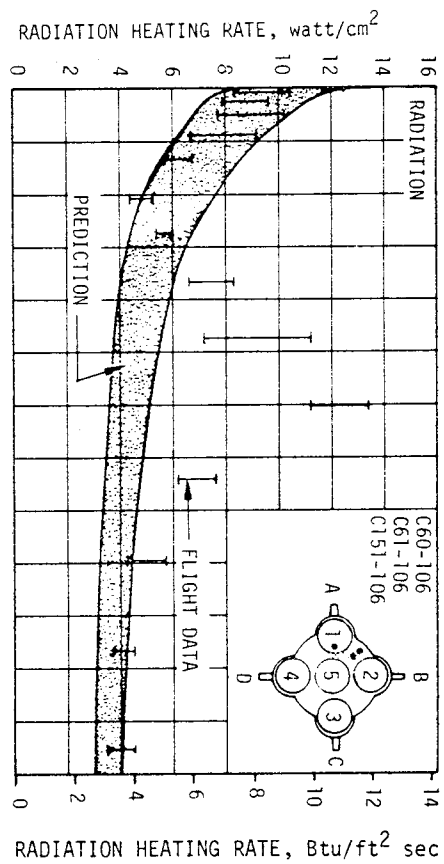


Figure 17-1. S-IC Base Heat Shield Thermal Environment

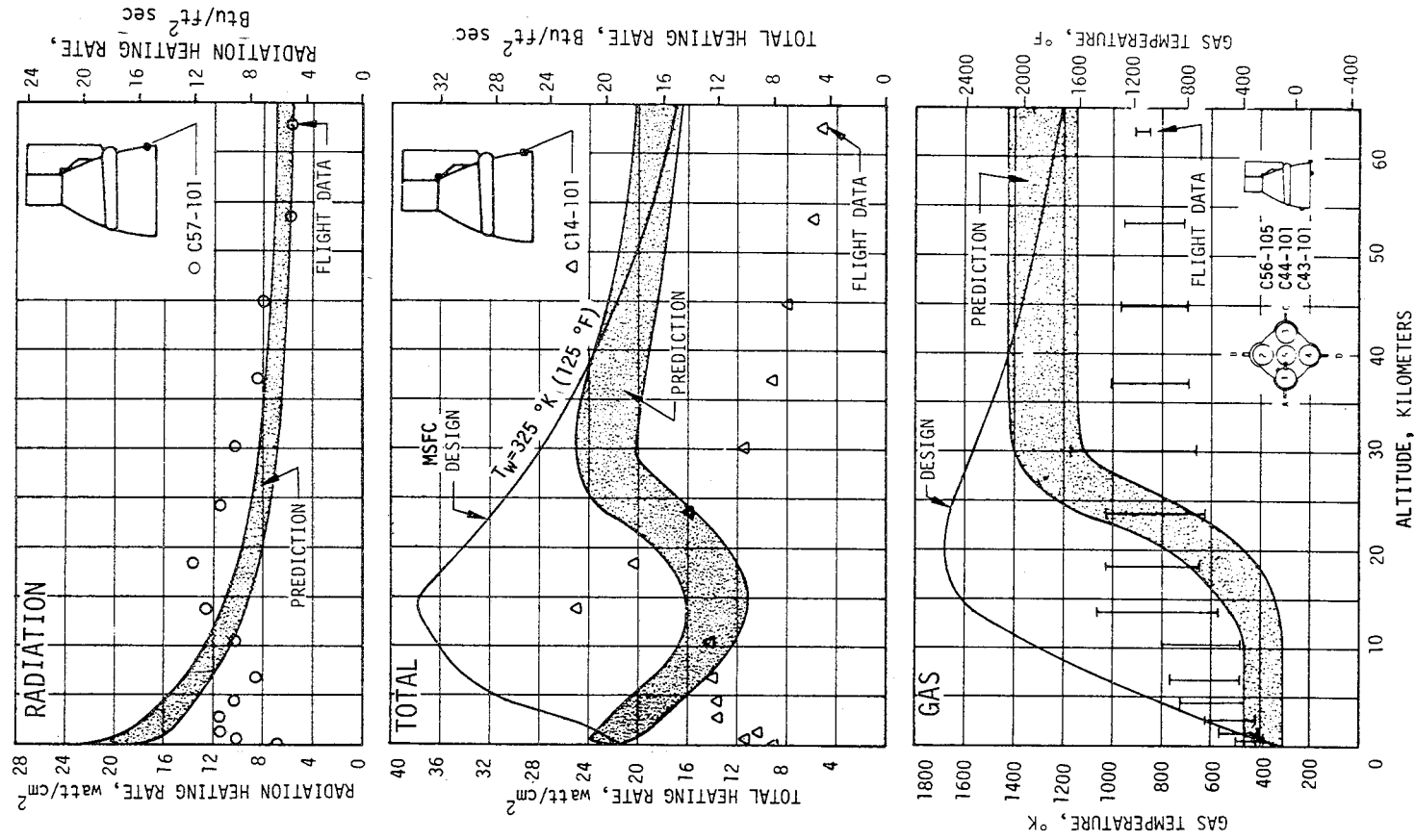


Figure 17-2. F-1 Engine Thermal Environment

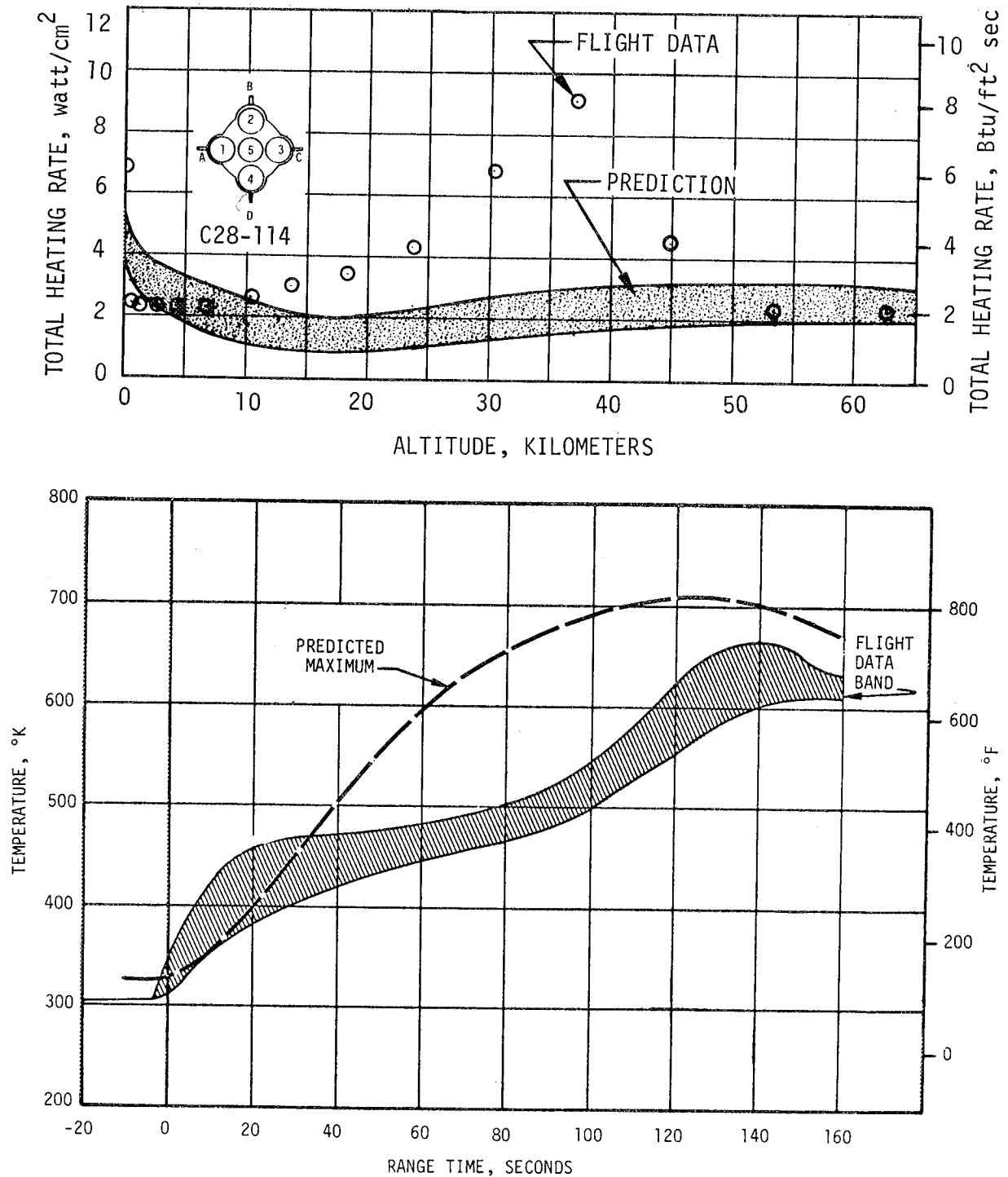


Figure 17-3. S-IC Fin Aft Face Thermal Environment

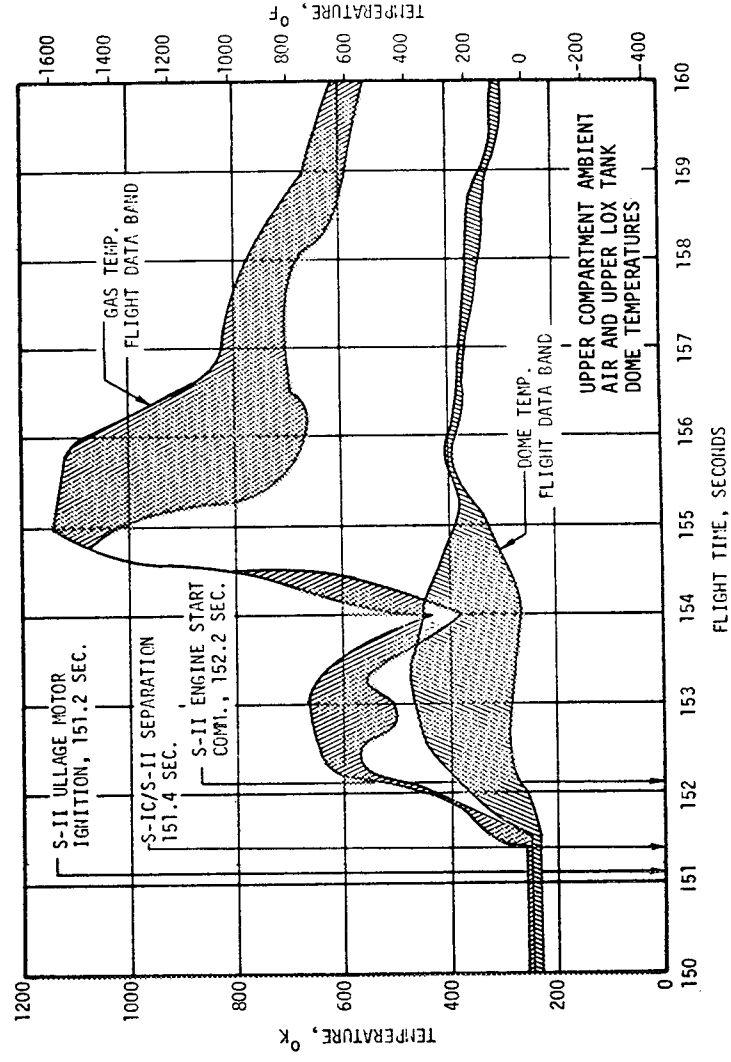
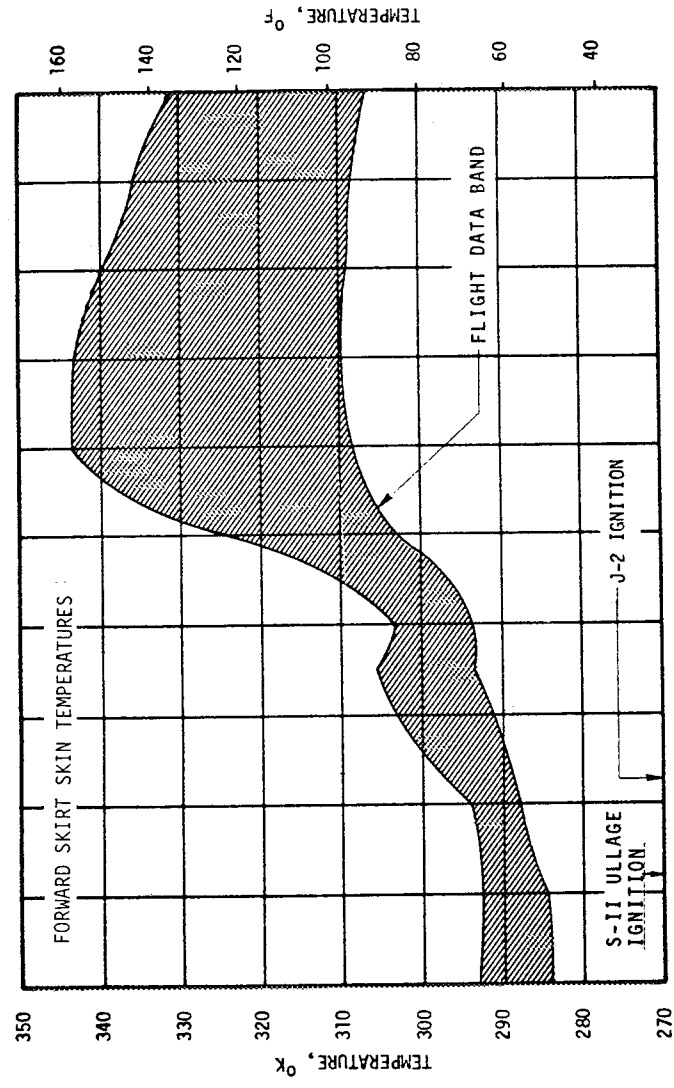


Figure 17-4. S-IC Interstage Thermal Environment During Separation



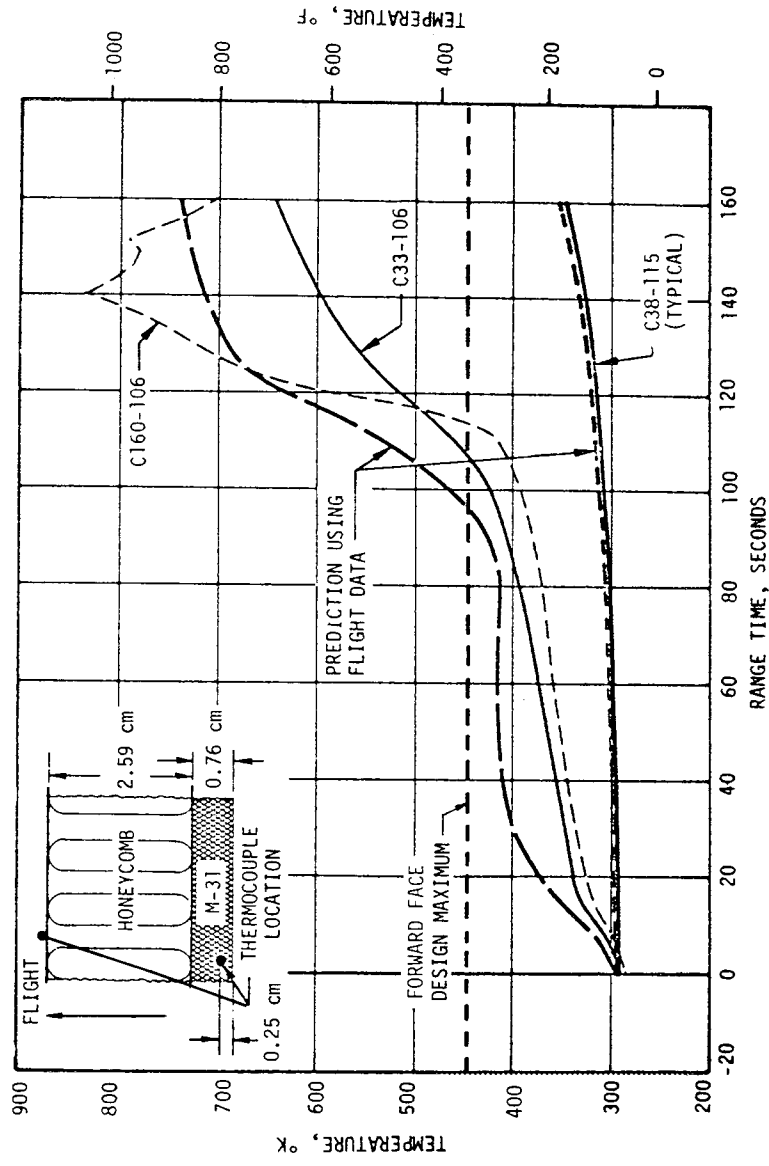
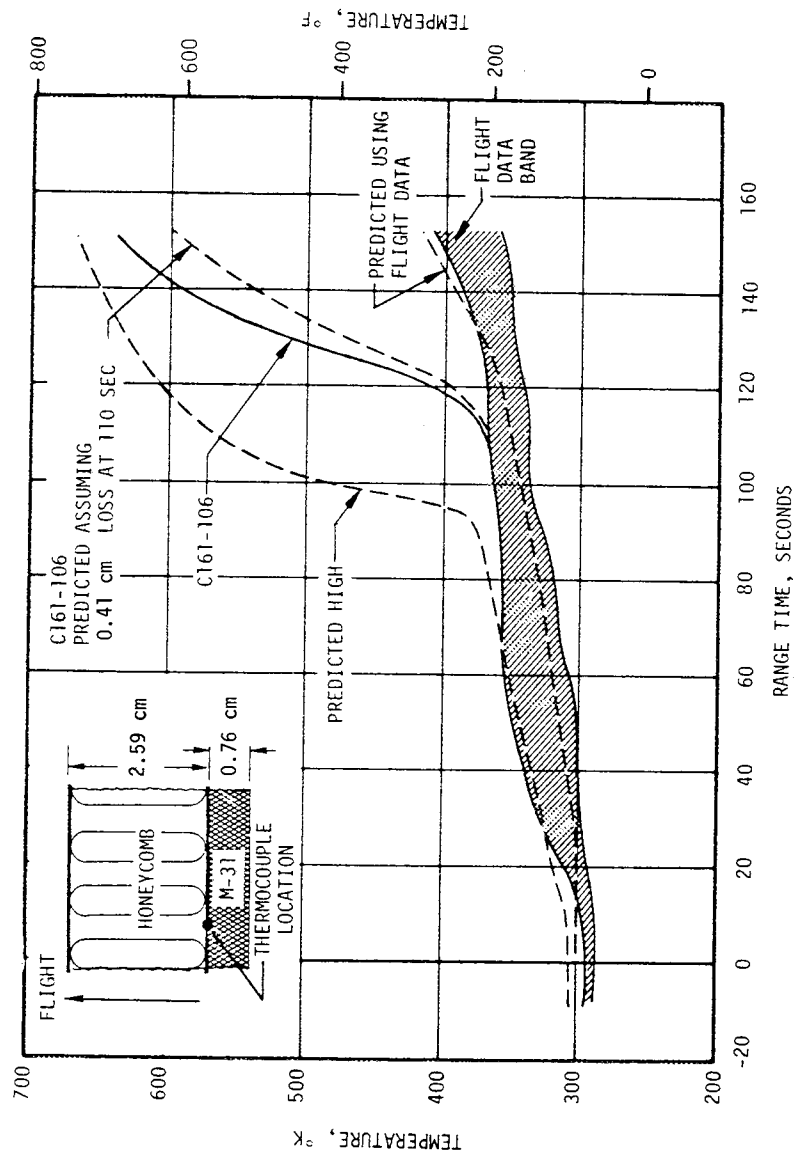


Figure 17-5. S-IC Base Heat Shield Structural Temperatures

temperatures barring unrealistically high heat transfer coefficients, and since particle impingement could not occur at the time when the temperatures started to increase, it was concluded that the thermocouples were not in good contact with the LOX tank dome and were unreliable indications of dome temperature.

Reliable gas temperatures and structural temperatures were not recorded during signal dropout which occurred from range times of 151 to 152.3 seconds and from approximately 154 to 155 seconds. Data during these time periods have been extrapolated in Figure 17-4.

Forward skirt pressure data are incomplete and prevent adequate evaluation of whether or not the forward skirt deflections resulting from differential pressures during staging will interfere with camera ejection on vehicles AS-502 and AS-503. However, fragmentary data received during staging show pressure spikes as high as  $5.19 \text{ N/cm}^2$  ( $7.52 \text{ psia}$ ) at vehicle station 37.8 meters (1488 in.). This is an area of concern inasmuch as most of the pressure data were lost due to the separation blackout, and the maximum design pressure for separation at this station number was  $2.2 \text{ N/cm}^2$  ( $3.2 \text{ psia}$ ). Action is being taken to change telemetry channels for forward skirt pressure measurements to PAM 1 or 2 to permit utilization of the onboard tape recorder for future flights.

Using measured flight data, Figure 17-1, and the design base region heat transfer coefficient, very good correlation with the measured heat shield temperatures was achieved as shown in Figure 17-5. With the exception of one measurement, all M-31 honeycomb interface temperatures fell within a narrow band of data, as shown in Figure 17-5. At about 110 seconds the data from a measurement located 3.05 meters (120 in.) from the vehicle centerline at position III diverged from this narrow band. An examination of probable instrumentation failure modes and thermocouple output led to the conclusion that the thermocouple did not fail. Further studies of known heat shield failure modes and heat shield history showed that M-31 insulation loss to the level of the open face honeycomb can occur. Using the insulation thickness available after loss of the M-31 to the open honeycomb level (at 110 seconds), a close correlation between data and computer results was achieved.

Data from two other thermocouples which were on the same heat shield panel also exhibited an unusual trend at approximately 110 seconds. As shown in lower portion of Figure 17-5, one probe measured the temperature of the forward side of the heat shield panel and at 110 seconds appeared to have separated from the panel. The second probe was buried 0.25 centimeter (0.1 in.) forward of the M-31 aft surface. At 110 seconds this thermocouple indicated a sharp rise in temperature, peaking at center engine cutoff and dropping to what appeared to be a steady state value just before outboard engine shutdown. A similarly installed thermocouple at another location showed none of these sharp temperature changes and indicated a maximum temperature about  $200^\circ\text{K}$  ( $360^\circ\text{F}$ ) lower. The resulting trends would be

seen if the M-31 had debonded at the open face honeycomb, allowing the hot gas to flow behind the insulation, heating both sides of the section. Exactly what caused the unusual results in the area of the heat shield in question was not known, but some M-31 loss and delamination was indicated.

The fact that the heat shield environment and resultant heat shield temperatures were considerably below the design values suggests that the base air scoops may not be required to lower the base region heating. Investigation to determine the effect of deleting the air scoops is being considered.

### 17.3 S-II BASE HEATING AND SEPARATION ENVIRONMENT

The postflight predictions of cold wall  $295^{\circ}\text{K}$  ( $72^{\circ}\text{F}$ ) convective heating rates to the S-II stage base heat shield and thrust cone region were based on hot flow model test data using the AS-501 flight J-2 engine performance (Propellant Mixture Ratio (PMR), chamber pressure, and temperature) and engine gimbaling histories. The radiative heating rates, emanating from the gaseous engine exhaust plumes, were computed by means of a digital computer program using the method of total hemispherical emissivity derivatives. Engine PMR, chamber pressure, and temperature effects as well as the radiation originating in the high temperature and pressure plume impingement regions were accounted for by means of the plume properties input into the program.

Figure 17-6 shows total and radiative heating rates measured on the aft face of the heat shield. A maximum total heating rate of approximately  $4.1 \text{ watts/cm}^2$  ( $3.6 \text{ Btu/ft}^2\text{-sec}$ ) was measured during S-II burn. The flight data shown have not been normalized to the cold wall conditions; however, the correction is not expected to make any appreciable difference due to the low heating rates experienced on this flight. Detailed analysis of the measured heating rates and the actual engine gimbal patterns may give improved analytical results.

Figure 17-6 also shows the measured incident radiative heat flux on the base heat shield and the postflight prediction. The postflight prediction of incident radiative heat flux was assumed to be proportional to the total engine thrust and hence showed an initial rapid increase to the constant steady state values.

The flight data, on the other hand, took a considerably longer time (approximately 83 seconds after J-2 ignition) to reach the steady state value. This difference may have been the result of condensation and ice formation on the calorimeter window due to the cold base region environment. This is substantiated by the rapid and pronounced drop in incident radiation after the PMR step down, at which time the initial base region environment would no longer affect the calorimeter. Also, it should be noted that the measured incident radiative value should be multiplied by a factor of 0.84 in order to account for the radiometer view angle and hence obtain the actual incident radiative heat flux. Including this correction, the measured heat flux of  $1.26 \text{ watt/cm}^2$  ( $1.11 \text{ Btu/ft}^2\text{-sec}$ ) was only slightly higher than the design

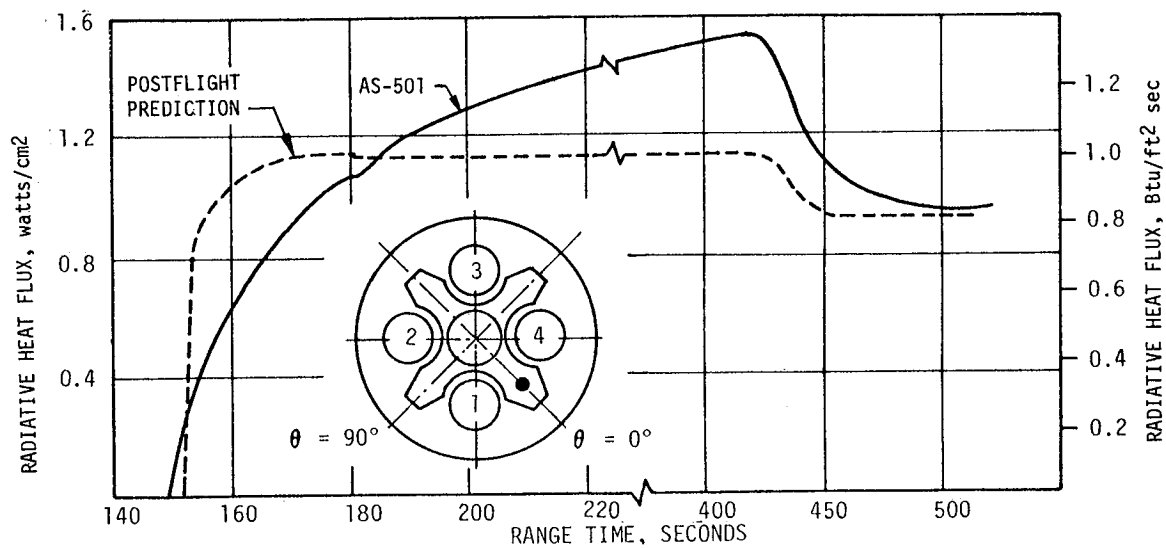
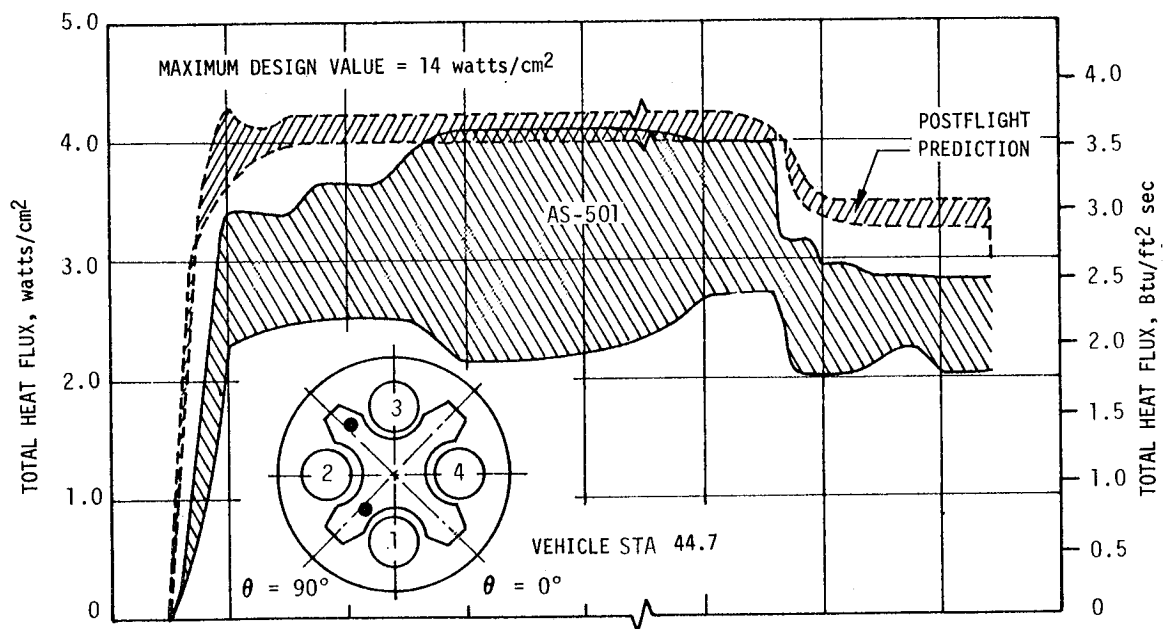


Figure 17-6. S-II Heat Shield Heating Rates

value of 1.22 watts/cm<sup>2</sup> (1.07 Btu/ft<sup>2</sup>-sec) at this location. This may be accounted for by the postflight prediction analysis using a higher PMR than the PMR used in deriving the design value.

Thrust cone total heating rates were below predicted and design limits as shown in Figure 17-7. A maximum value of 1.4 watt/cm<sup>2</sup> (1.23 Btu/ft<sup>2</sup>-sec) was recorded during the time the interstage was on. As expected, heating rates exhibited a pronounced drop to approximately 0.15 watt/cm<sup>2</sup> (0.13 Btu/ft<sup>2</sup>-sec) following interstage jettisoning. The flight data are not normalized to the cold wall conditions. Also, the model used in the hot flow tests did not accurately simulate the geometric configuration for those transducer locations which are installed on the instrumentation container; therefore, some discrepancy between the prediction and flight data should be expected.

Base heat shield temperatures were well below design and agreed well with postflight predictions, as shown in Figure 17-7. The design temperatures were calculated using the maximum design environment. Data shown indicate a maximum temperature of approximately 742°K (875°F) occurring near 300 seconds of S-II boost. In general, temperature histories corresponded to the measured heating rates.

Two of the above measurements were installed on the S-II heat shield with a special corrosion resistant steel mount. The additional capacitance from these mounts caused a temperature lag in the actual AS-501 flight temperatures compared to the design temperatures. The special mounts were included in the thermal models used to determine the postflight predicted temperatures.

Data from heat shield forward surface measurements indicated maximum temperatures during S-II boost of 269°K to 300°K (25°F to 80°F). These temperatures were considerably below the predicted preflight maximum temperatures of 478°K to 532°K (400°F to 500°F).

The forward side heating rates used for the design temperatures which occurred during the first 30 seconds after S-II engine start and before initiation of second plane separation were 0.68 watt/cm<sup>2</sup> (0.6 Btu/ft<sup>2</sup>-sec) and 0.28 watt/cm<sup>2</sup> (0.25 Btu/ft<sup>2</sup>-sec) for convective and radiant heating, respectively. These heat flux values were reduced to 0.11 watt/cm<sup>2</sup> (0.1 Btu/ft<sup>2</sup>-sec) and zero, respectively, for the postflight analysis, thus reducing the forward side temperature increases by one order of magnitude. The actual AS-501 forward side temperatures were lower than predicted, indicating that the heat shield was quite effective in deflecting the hot exhaust gases away from the base region.

Thrust cone temperatures were considerably lower than expected because of the low base heating rates, as shown in Figure 17-8. The maximum recorded temperature was 280°K (45°F). A reasonable agreement was obtained between the actual flight temperature history for this measurement and temperatures calculated using actual flight heat rates and gas recovery temperature of 500°K (440°F). This was also done for the measurement on the cover of container 208, as shown in Figure 17-8.

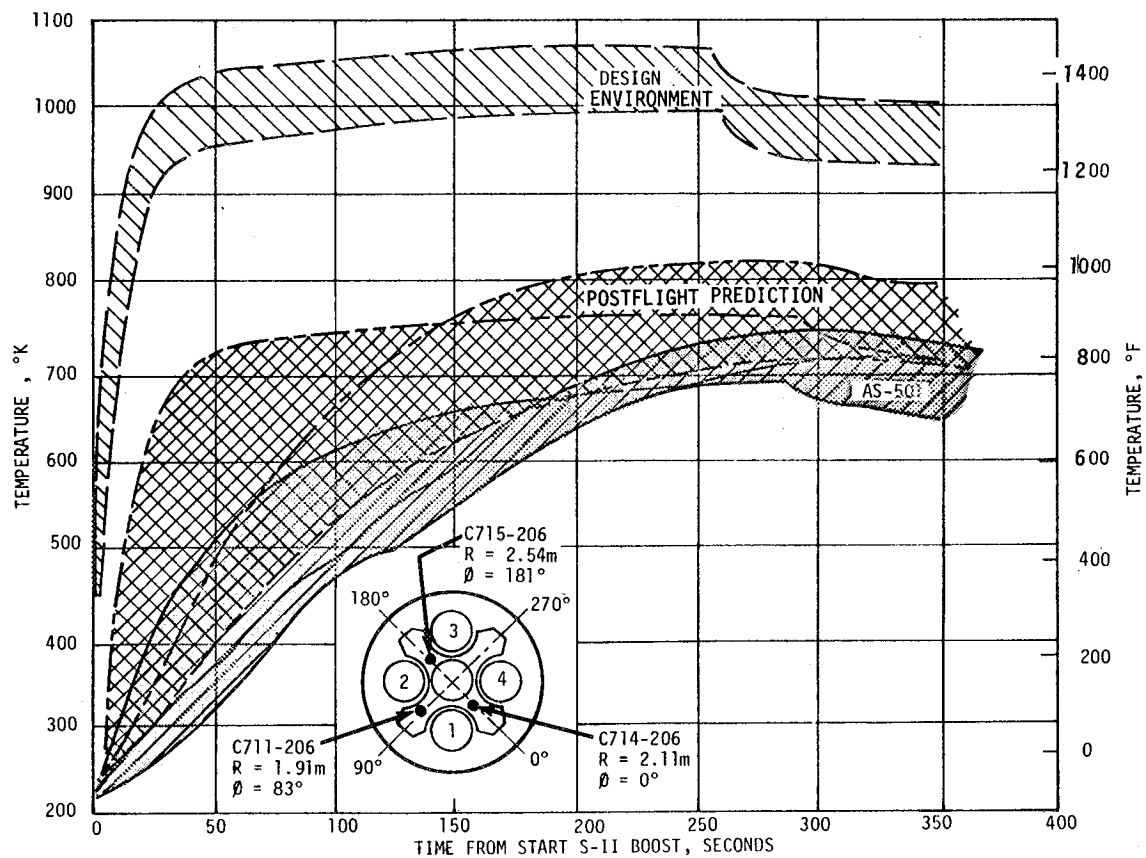
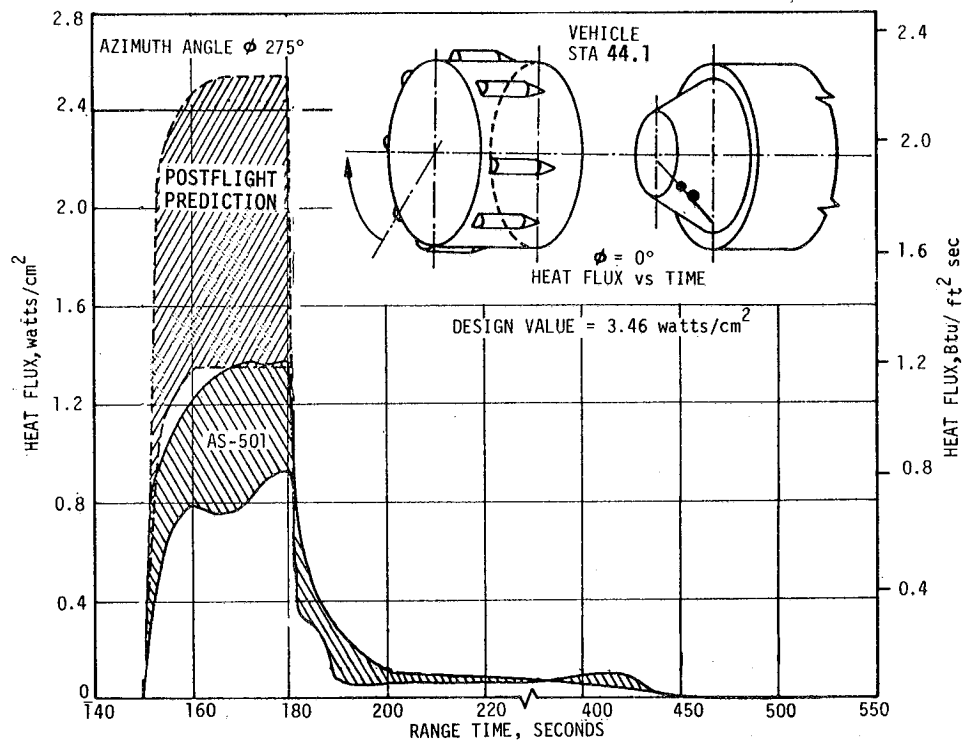


Figure 17-7. S-II Base Region Thermal Environment

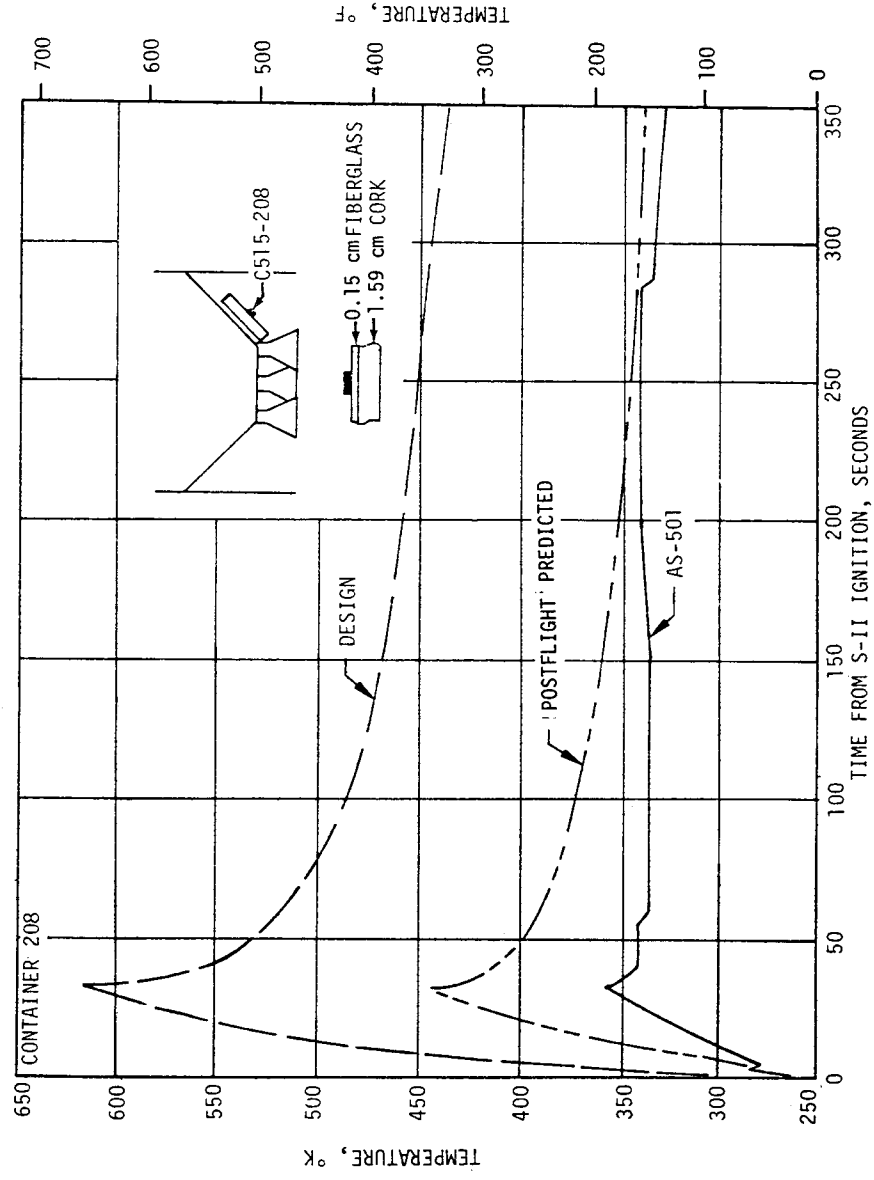
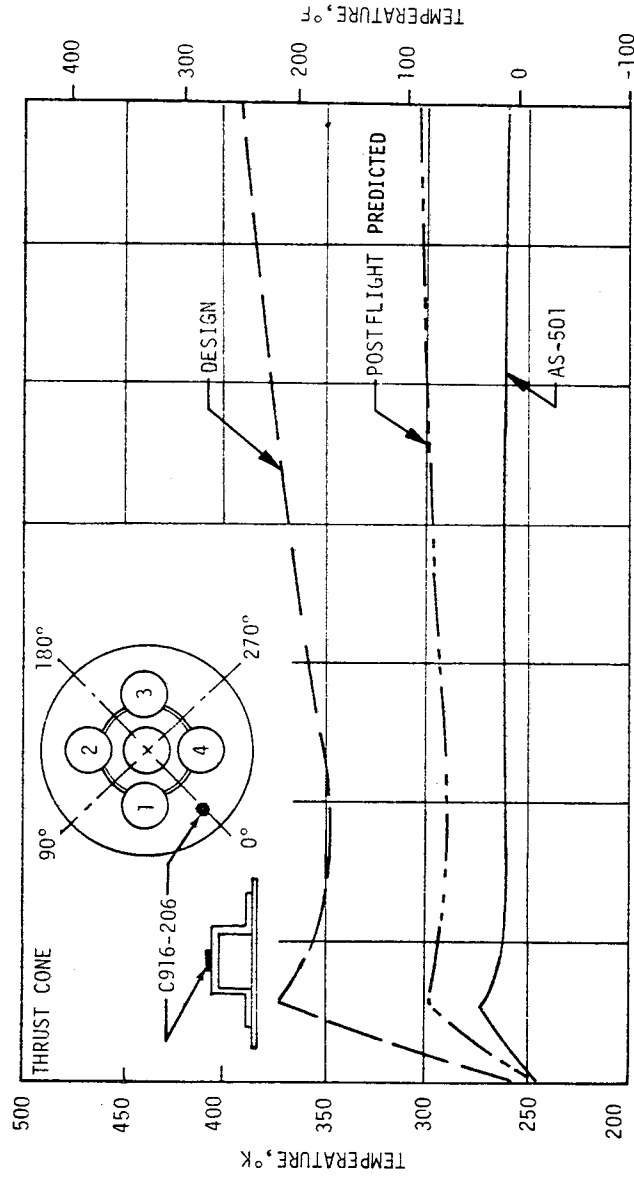


Figure 17-8. Thrust Cone Area Temperatures

Engine curtain gas recovery temperature measurements indicated a maximum gas temperature of 338°K (150°F). A maximum temperature of 625°K (665°F) was predicted prior to second plane separation, diminishing to 310°K (98°F) for the duration of S-II boost flight. However, after second plane separation, the gas temperature ranged from 265°K to 285°K (17° to 53°F). Since the gas temperatures on the thrust cone region were above the transducer range maximum of 338°K (150°F), it appears that the engines' curtains were subjected to convective cooling throughout S-II boost flight.

#### 17.4 S-II/S-IVB SEPARATION ENVIRONMENT

The heat flux on the J-2 engine bell during retro motor fire at 520.55 seconds was measured by two calorimeters. The heat flux had an initial rise to approximately 0.28 watt/cm<sup>2</sup> (0.25 Btu/ft<sup>2</sup>-sec) at 0.5 second after separation. It is suspected that this initial surge was due to the combination of solid ullage and retro motor gases filling the interstage region. The heat flux dropped to 0.16 watt/cm<sup>2</sup> (0.14 Btu/ft<sup>2</sup>-sec) at 1 second after separation, and then began rising again as a result of retro motor plume impingement. The heat flux reached a maximum value of 0.42 watt/cm<sup>2</sup> (0.37 Btu/ft<sup>2</sup>-sec) at 1.6 seconds and dropped thereafter. The heat flux data were considerably lower than the analytical prediction. The maximum heat flux that was predicted in line with the retro motor was 2.56 watts/cm<sup>2</sup> (2.26 Btu/ft<sup>2</sup>-sec). The predicted heat fluxes at 45 degrees from the centerline are 50 percent of the centerline values.

The analyses were based on a perturbed retro motor flow (flow passing through shock interactions) prior to impingement on the J-2 engine from 1.2 to 1.4 seconds after separation. Direct plume impingement on the calorimeters was considered after that time.

#### 17.5 VEHICLE AEROHEATING THERMAL ENVIRONMENT

##### 17.5.1 S-IC Stage Aeroheating Environment

The aerodynamic heating environment effects were measured using thermocouples mounted to the backside of thin structural skin on the S-IC fins, engine fairings, intertank compartment, and forward skirt. Generally, the temperatures were within the preflight prediction bands based on the MSFC design environment and were well within the maximum design capability.

Comparisons of analytically calculated heating rates for the maximum heating trajectory and postflight AS-501 trajectory indicated a 23 percent lower heat input from the postflight trajectory.

Figures 17-9 and 17-10 show the flight data compared with the preflight prediction bands for the four areas considered. The maximum expected curve on the bands represents expected temperatures based on the Saturn V maximum



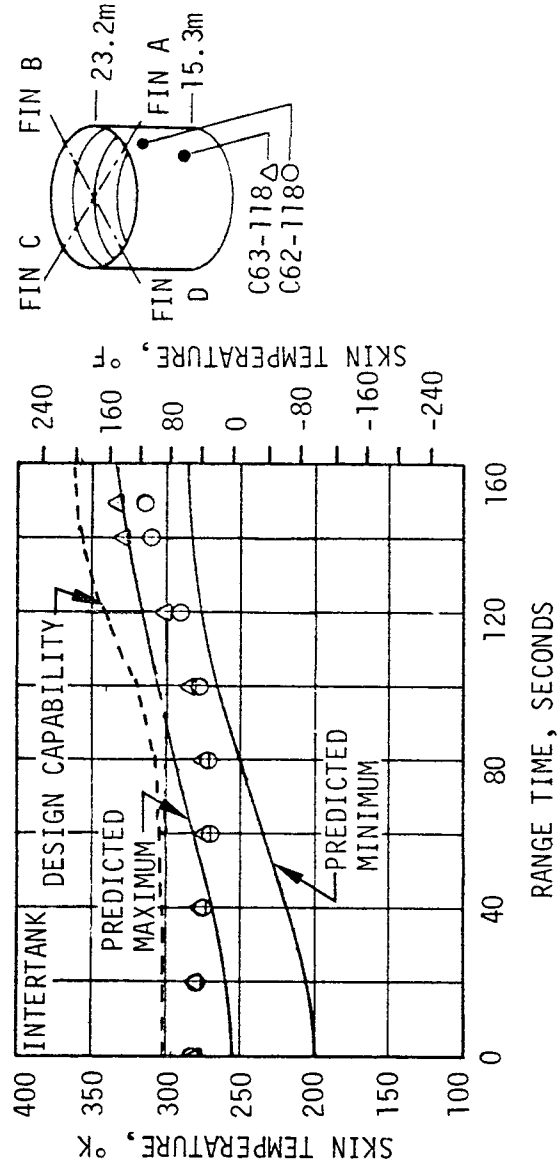
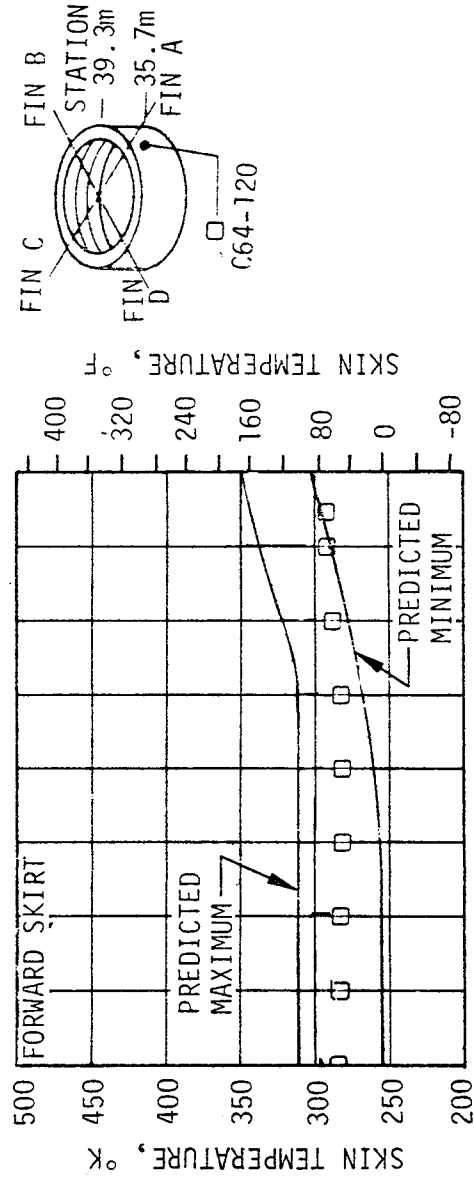


Figure 17-9. S-IC Body Aerodynamic Heating

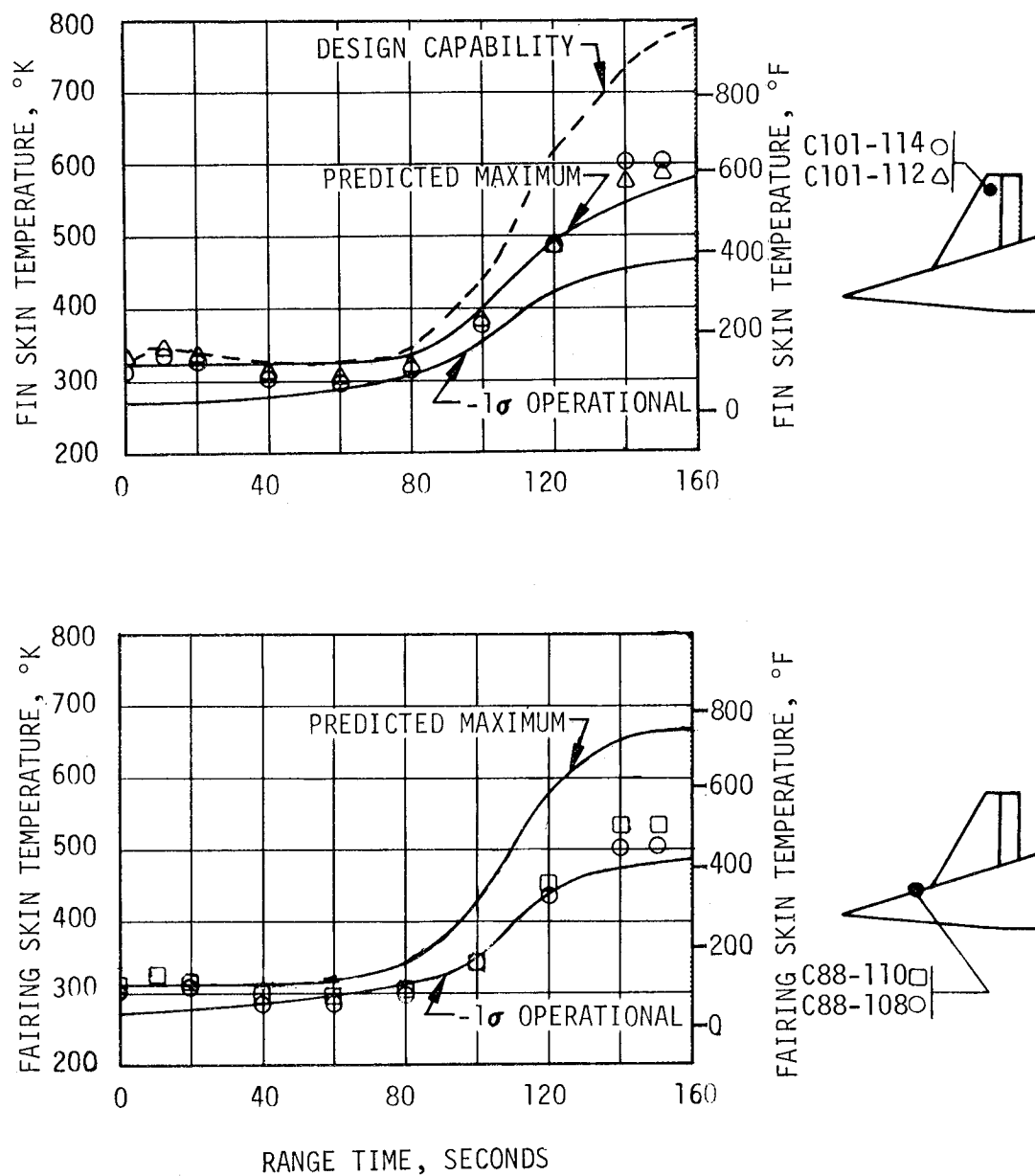


Figure 17-10. S-IC Fin and Fairing Temperature Histories

heating trajectory ( $+3\sigma$  variations on the reference trajectory parameters), while the minimum expected curve represents a  $-1\sigma$  deviation on the initial operational trajectory parameters.

The skin temperatures on the forward skirt remained at a nearly constant level throughout flight ranging from 275°K (35°F) to 294°K (70°F). A typical measurement is shown in Figure 17-9. The forward skirt was insulated with silicone rubber insulation which limited aerodynamic heating effects and kept skin temperatures at a constant level until S-IC/S-II separation where a sharp temperature rise was seen due to S-II ullage motor plume impingement. Analysis to determine forward skirt aerodynamic heating rates during powered flight was not possible with the data obtained due to the unknown insulation thickness in the areas of the instrumentation. KSC Non-Conformance Record 008224 documented the insulation thicknesses at various locations on the forward skirt and indicated that the insulation thicknesses in some areas was as much as 2.5 times the required. Action to correct this problem on AS-502 has been initiated.

The behavior of the data recorded on the fuel tank suggested that the thermocouples were poorly attached to the tank wall, and read combined tank wall temperatures and boundary layer gas temperature. Since these thermocouples were attached in the same manner as those on the LOX tank and were also found to be loosely attached on S-IC-3, -4, and -5, the data were not considered usable.

Due to the relatively good agreement between predictions and measured temperatures on the unpressurized portions of the vehicle and the erratic behavior of the LOX tank thermocouples, it was concluded that these instruments were not recording true skin temperatures. Corrective action for future stages is being initiated. Temperatures on the intertank skin were below the predicted maximum from 50 seconds until near the end of powered flight, as shown in Figure 17-9. Initial temperatures were about 39°K (70°F) higher than expected. This was probably due to the winds at the launch site.

It is also seen in Figure 17-9 that the intertank skin temperature decreased until about 70 seconds and from this point continued to increase until the end of flight, falling slightly above the predicted band. The cooling during the first 70 seconds followed the trend of ambient compartment gas temperatures which decreased from about 253°K (-4°F) to about 230°K (-45°F) during the first 70 seconds. Attempts to simulate the temperature data indicate that combined cooling of the inside of the skin and boundary layer cooling (due to air passing over the cold LOX tank wall) contributed to the cooling of the skin during the early portion of flight.

Temperatures measured on the electrical tunnel in the intertank area were well below the predicted maximum throughout flight. The maximum recorded temperature was approximately 455°K (359°F) at 150 seconds where the predicted maximum was 572°K (570°F). This was to be expected since the maximum heating trajectory was not flown by AS-501.

One measurement located on the pressure tunnel ramp at vehicle station 38.57 meters in the forward skirt area was under silicone rubber insulation and reached 316°K (110°F) at the end of powered flight. This temperature was in good agreement with those on the forward skirt skin located under insulation.

Temperatures on the thrust structure skin remained near the predicted values during powered flight except for the effect of burning exhaust gases during liftoff and a sharp increase at approximately 120 seconds. All of the temperatures measured were in a region immediately forward from a base air scoop. The sharp increase in temperatures at 120 seconds was attributed to flow of base gases forward through the scoops over the thrust structure skin. This was not considered in the preflight prediction.

The flight data indicated that only one of the four thermocouples recorded temperatures above the predicted maximum of 336°K (154°F) at approximately 145 seconds. However, the temperatures were within the capability of the structure and presented no problems.

Skin temperatures on the aluminum portion of the S-IC engine fairings were below the predicted maximum, as shown in Figure 17-10. The initial rise in temperature from 0 to 10 seconds was due to burning F-1 engine exhaust gases which enveloped this area at liftoff. This same effect was noted on all temperature measurements on the fins and thrust structure as well. The data from vehicle stations 7.75 meters and 5.52 meters showed little difference in temperature, indicating the absence of any severe temperature gradients on the forward fairing.

Skin temperatures on the titanium portion of the fairing aft of the heat shield were far below the predicted maximum throughout the flight. The maximum temperatures recorded ranged from 780°K to 855°K (944° to 1080°F) as compared to the design maximum of 1030°K (1394°F). This resulted from the fact that base radiation levels and base gas temperature were much less severe than the design values utilized for the prediction.

Skin temperatures on both the wedge and flat portions of the fins fell within a relatively narrow band and were slightly higher than the predicted maximum at the end of flight, as shown in Figure 17-10. The initial rise in temperature above the predicted values at liftoff was due to radiation and convective heating from burning F-1 engine exhaust gases which enveloped the entire base area. This effect was not accounted for in the predictions. After 120 seconds, the temperatures fell slightly above the predicted band, leveling off at 591° to 605°K (604° to 629°F) at approximately 145 seconds. However, this was well within the capability of the structures and is not expected to present any problems.

#### 17.5.2 S-II Stage Aeroheating Environment

Aerodynamic heating measurements made on the S-II stage near and on protuberances were below design limits and agreed well with postflight predictions.

The postflight heat rate predictions considered actual trajectory, angles-of-attack, and local flow properties calculated by means of a computer program. Consideration was also given to vehicle-surface-to-calorimeter mismatch effects.

A comparison of AS-501 measured, design, and postflight predicted data for locations on and adjacent to S-II protuberances is shown in Figure 17-11. Flight data show good agreement with the predictions for the fairing nose sections which were not influenced by upstream disturbances. Maximum aerodynamic heating rates of approximately  $1.38 \text{ watt/cm}^2$  ( $1.22 \text{ Btu/ft}^2\text{-sec}$ ) and  $1.20 \text{ watt/cm}^2$  ( $1.06 \text{ Btu/ft}^2\text{-sec}$ ) were obtained on the ullage motor and LH<sub>2</sub> feedline nose fairings, respectively. However, the LH<sub>2</sub> feedline fairing nose heating rate peaked about 13 seconds earlier than predicted. The calorimeter located adjacent to the ullage motor fairing, seen on the left hand plot of Figure 17-11, which was enveloped by the low shock wave, also showed good correlation with the prediction. This measurement also peaked 13 seconds earlier than predicted.

Selected structural, fairing, and surface temperature measurements influenced by aerodynamic heating for AS-501 are shown in Figures 17-12 and 17-13. Each plot gives the actual flight data along with the design, preflight, and postflight predictions. Design predictions were based on the North American Rockwell design heating trajectory. Preflight predictions were based on the AS-501 preflight trajectory aerodynamic heating rates, and the postflight predictions were based on the heating rates discussed previously.

Measured forward skirt skin temperatures, as shown in Figure 17-12 were only slightly lower than the postflight prediction and further aerodynamic heating rate refinements are expected to result in even better correlation.

LH<sub>2</sub> tank insulation surface temperature measurement data are also shown in Figure 17-12. The postflight prediction for vehicle station 58.19 meters compared well with the flight data but the predictions for vehicle station 56.92 meters and vehicle station 58.04 meters were much higher than the flight data. The wide range of flight data for the LH<sub>2</sub> tank insulation was unexpected and so far unexplained. Effects of angle-of-attack, frost, instrument mounting and operation, and refined heating rates are still being investigated as possible causes for the wide range of flight data.

Interstage stringer cap instrument temperature, shown in Figure 17-13, shows that the postflight prediction was higher than the flight data. Effort is continuing on the thermal model and heating rate changes for better interstage temperature correlation.

Internal skin temperature measurements made in the LH<sub>2</sub> feedline fairing and in the ullage motor fairing indicated values lower than postflight predictions, as seen in Figure 17-13. Effort is continuing on the thermal model, and actual heating rate refinements are expected to reduce the difference.

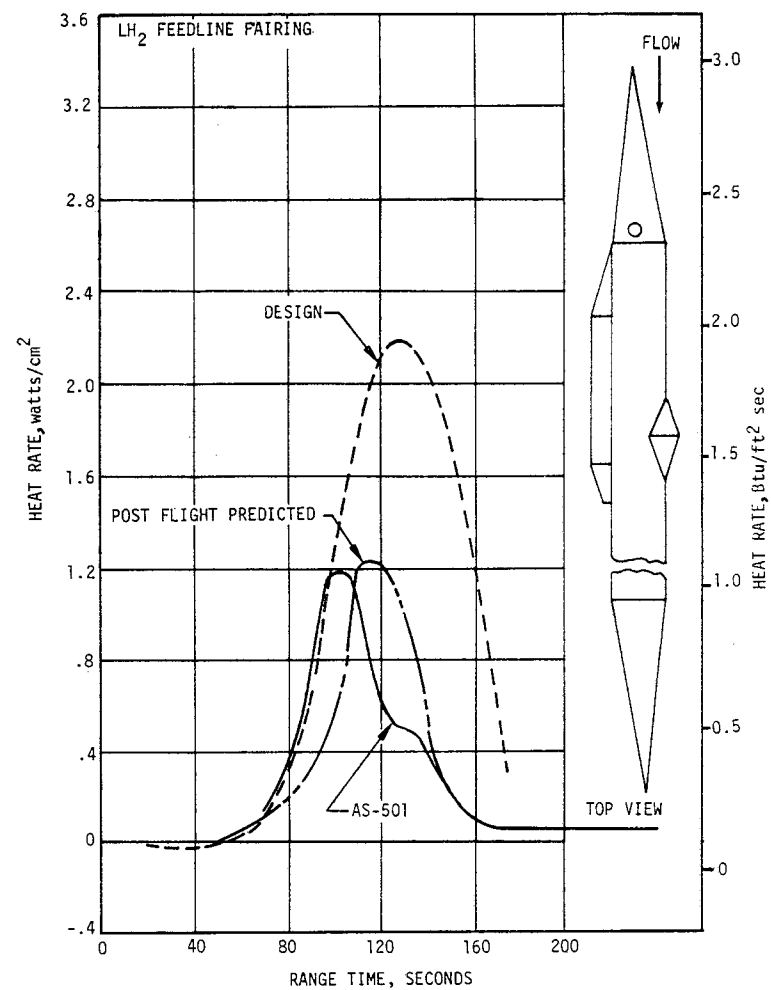
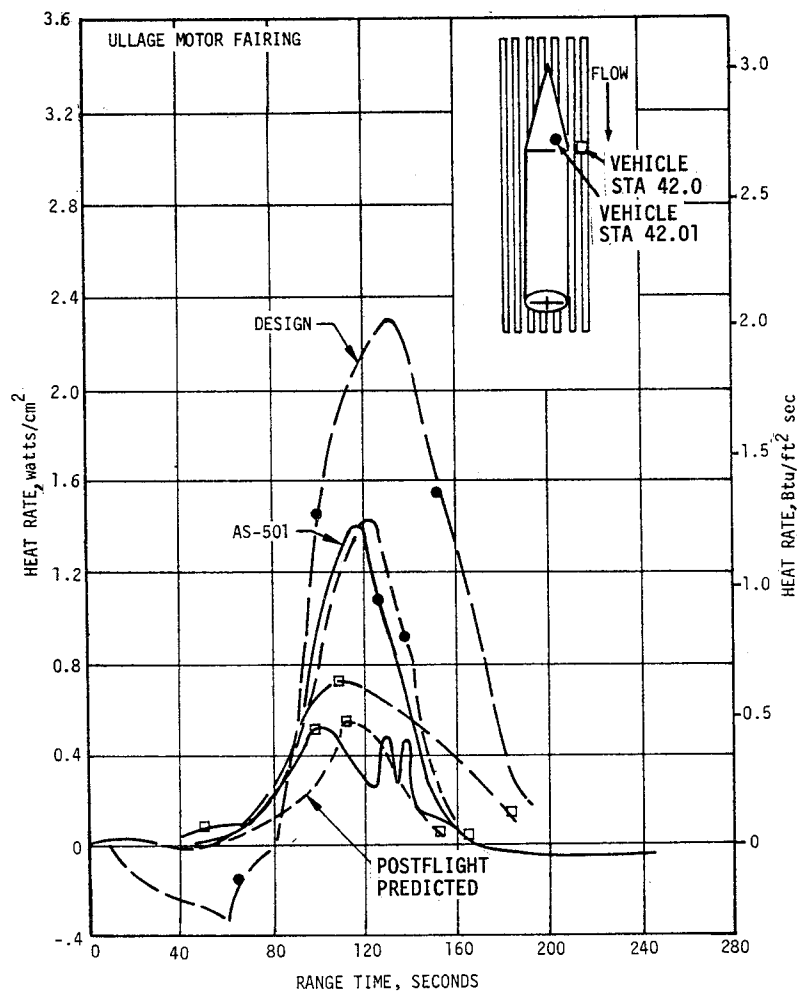


Figure 17-11. Fairing Heat Rate

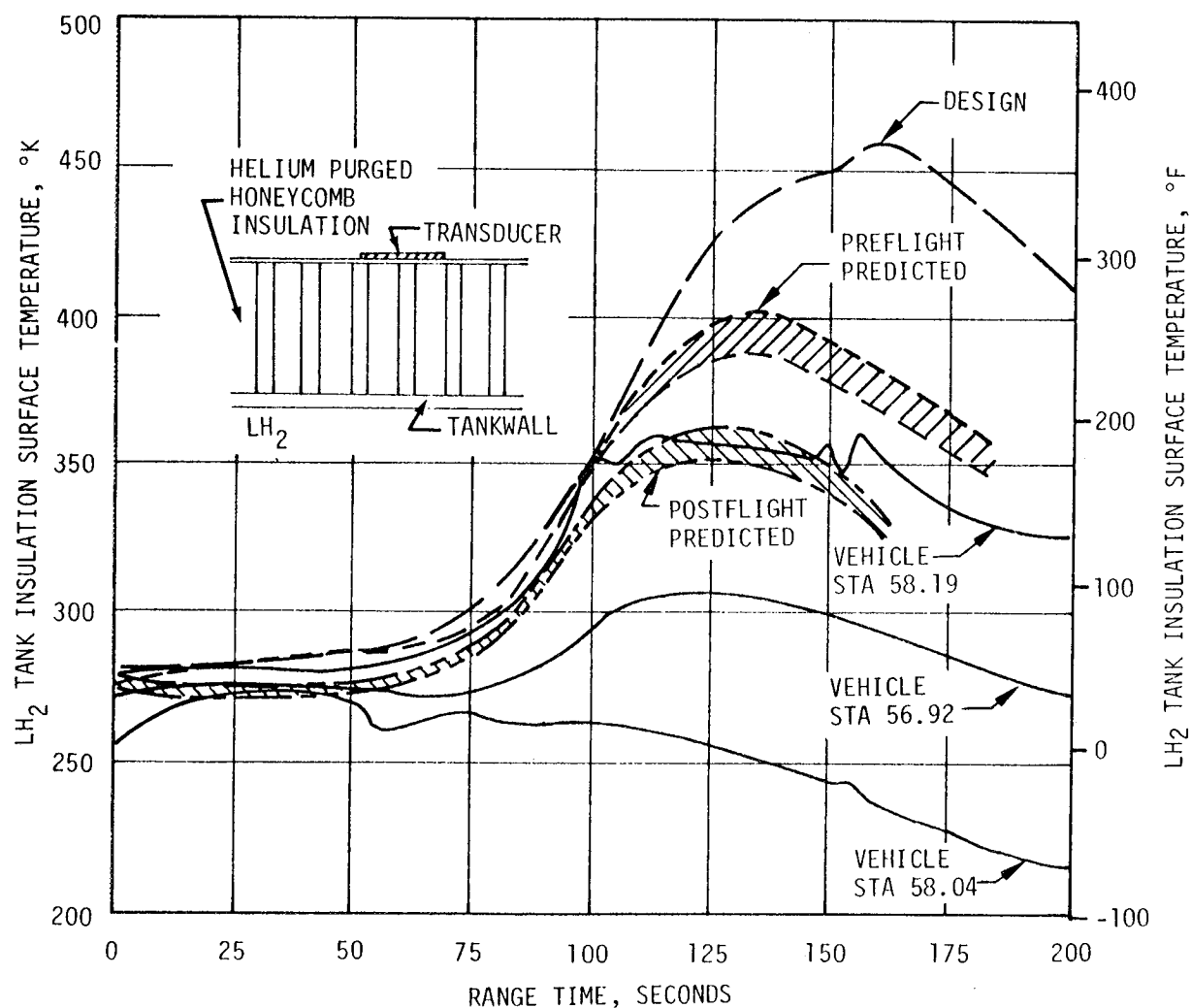
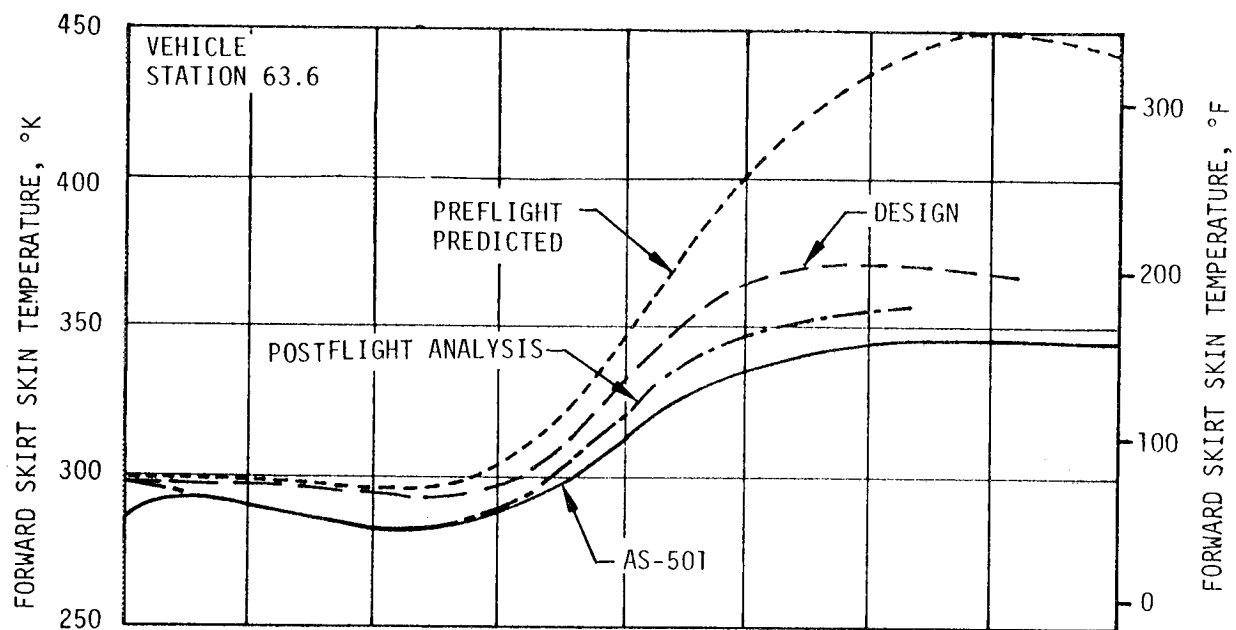


Figure 17-12. Forward Skirt Skin and Insulation Temperatures

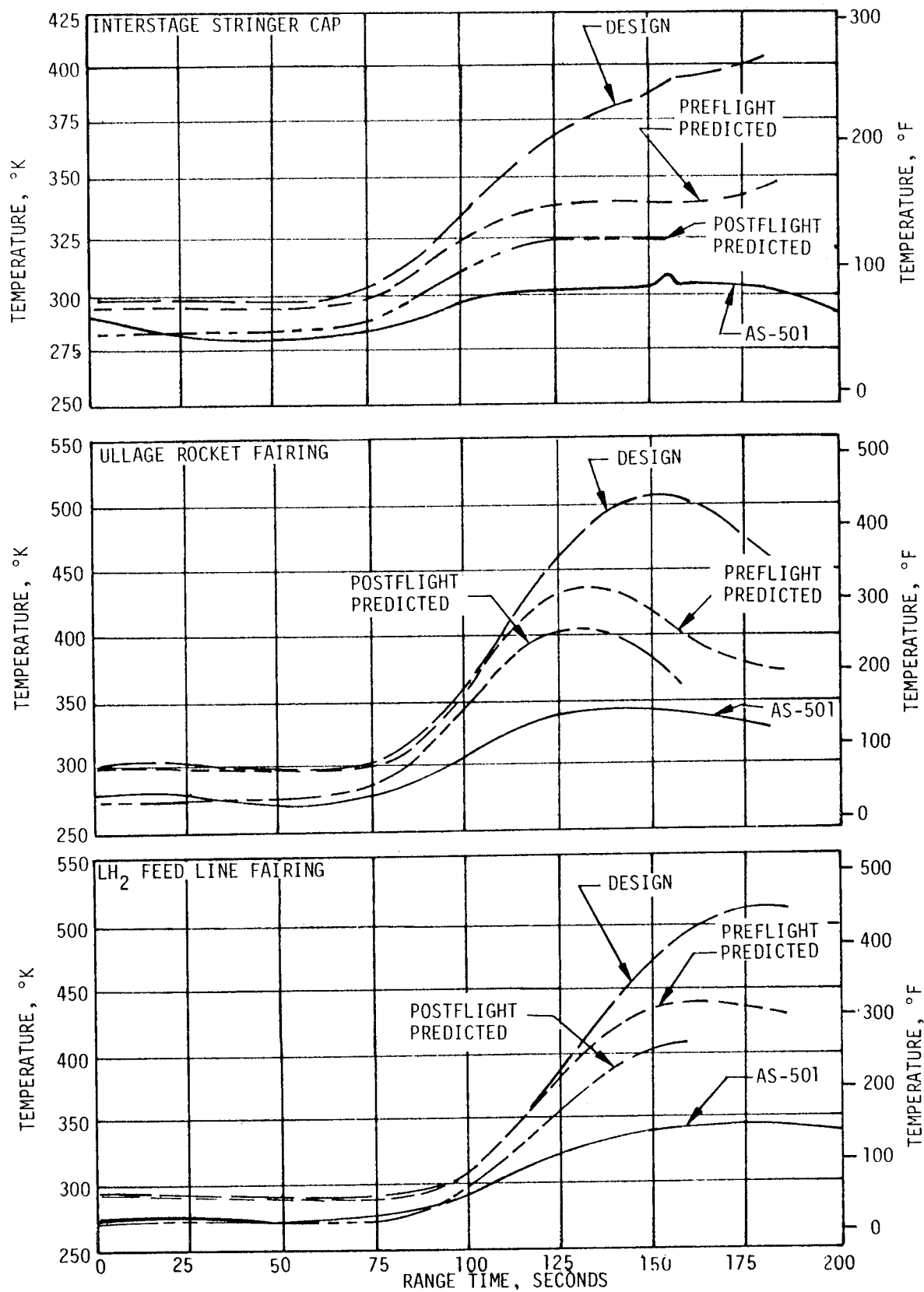


Figure 17-13. S-II Structural Temperatures



### 17.5.3 S-IVB Stage Aeroheating Environment

The forward skirt temperature simulation using the AS-501 trajectory and a transition Reynolds number ( $Re_t$ ) of 500,000 is compared with flight data in Figure 17-14 (upper plot). The simulation is of the sensor temperature.

The  $LH_2$  tank temperatures were either at or below the freezing point of water at liftoff. In Figure 17-14 (center plot), the simulation is compared with the temperature sensor that reached the maximum temperature during boost, 305°K (89°F). The  $LH_2$  tank experienced a temperature rise during retro fire of 2°K (4°F), which was comparable to that experienced on the Saturn IB flights.

The temperature sensors on the aft skirt were located such that some are on uninsulated structure and some are on insulated structure which was subject to protuberance induced heating rates. The simulation of the sensors located on uninsulated structure, shown in Figure 17-14 (lower plot), indicated that a wall to recovery temperature ratio ( $T_w/T_r$ ) of 0.5 should be used as the transition criterion rather than a transition Reynolds number of 500,000. The flight data indicated that the boundary layer flow became laminar at approximately 100 seconds into the flight followed by the maximum temperature at 130 seconds.

Figure 17-15 (upper plot) presents the flight data and sensor simulation for the sensors adjacent to the APS modules. These sensors are covered by 0.0254 centimeter (0.010 in.) of Korotherm and are considered to be in a protuberance induced heating rate area. The aft skirt sensors experienced a temperature rise due to S-II retro motor plume impingement. This temperature was comparable to that experienced on Saturn IB.

Figure 17-15 (center plot) shows the temperatures of the sensors on the aft interstage, which are covered with 0.0254 centimeter (0.010 in.) of Korotherm. The maximum temperature experienced on the aft interstage was 347°K (164.9°F) on the stringer cap. It should be noted that the stringer cap was hotter than the interstage skin; whereas, the simulation indicated the opposite relationship between the skin and stringer temperatures. It is possible that the installation of the stringer sensor employed less mass than the skin installation, or insulation repairs prior to flight introduced insulation thickness variation.

The S-IVB feedline fairing forebody temperatures indicated a maximum temperature of 380°K (224°F) at 150 seconds. The postflight simulation using a transition Reynolds number of 500,000 indicated a maximum temperature of 436°K (325°F). The use of  $T_w/T_r = 0.5$  rather than a transition Reynolds number correlated the flight data to within 3°K (5.4°F) of the maximum temperature. This correlation trend was also noted on the Saturn IB flights.

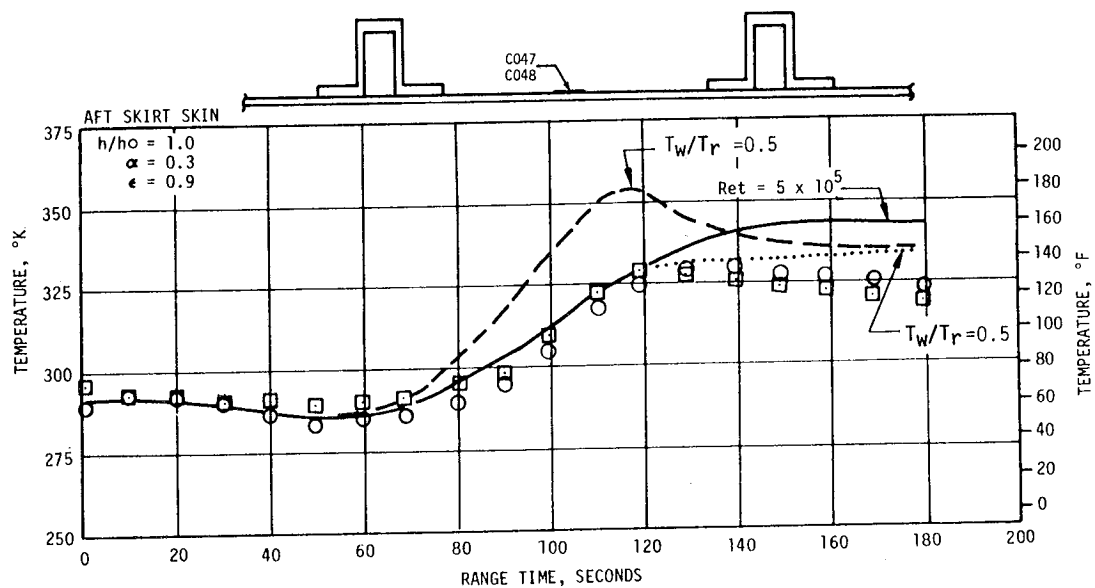
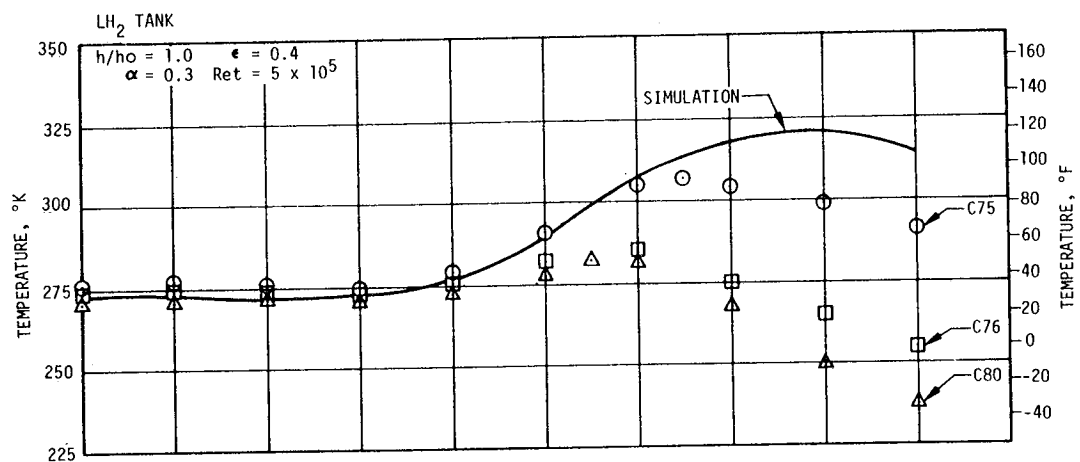
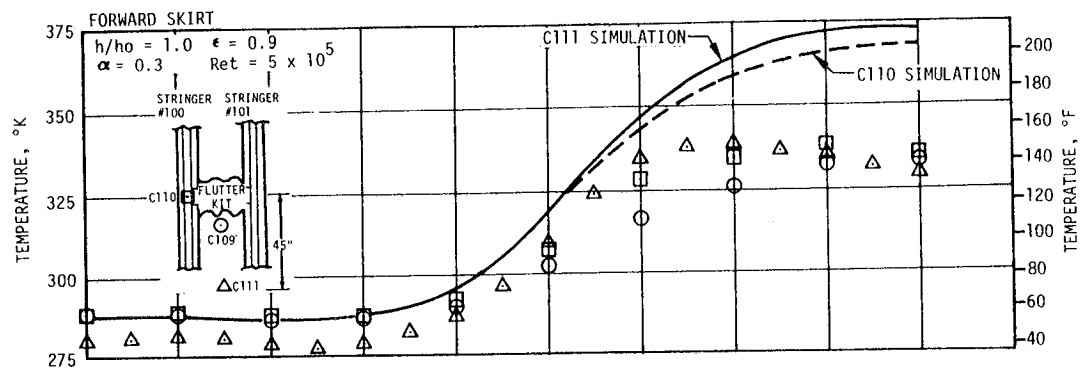


Figure 17-14. S-IVB Aeroheating Environment

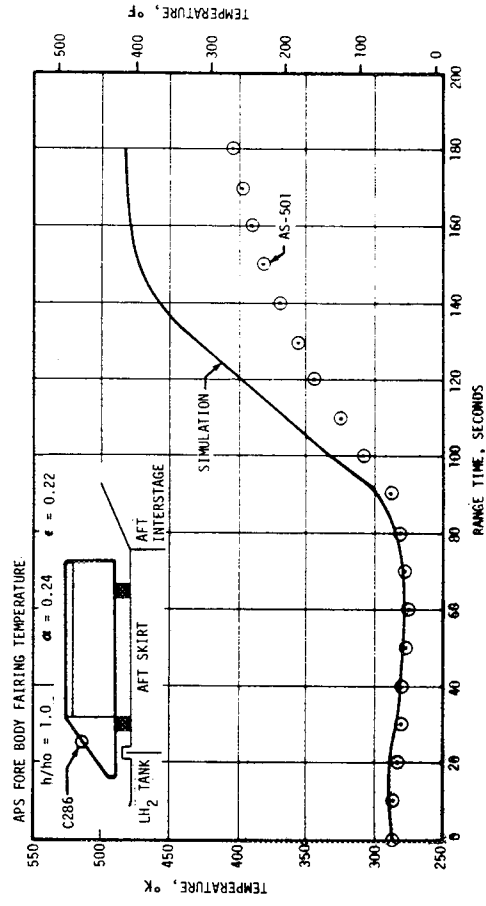
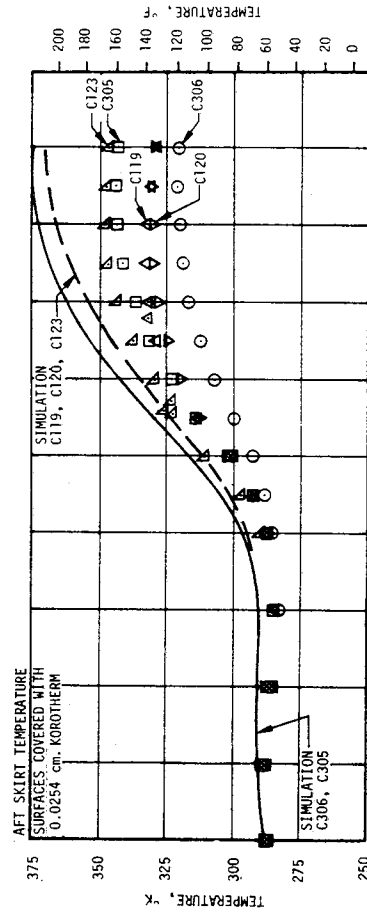
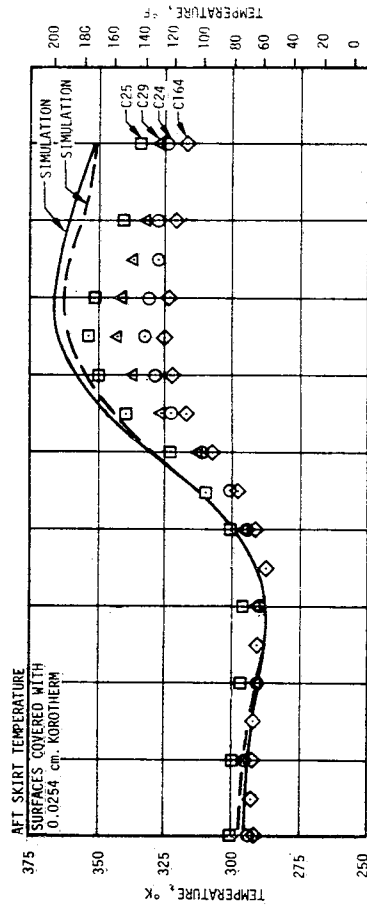


Figure 17-15. S-IVB Protuberance Aeroheating Environment

The sensors located near the APS No. 2 forebody indicated frost formation on the LH<sub>2</sub> tank and aft skirt near the APS. The APS fairing forebody temperature is shown in Figure 17-15 (lower plot) along with the sensor simulation. Better agreement was obtained for the sensor simulation using  $T_w/T_r = 0.5$  rather than  $Re_t = 500,000$  as the criteria for transition to laminar flow. However, the Reynolds number criteria was used for design predictions and thus apparently gives conservative results.

The heat flux measured by two calorimeters on the J-2 engine was approximately one order of magnitude less than expected. The calorimeter located on the J-2 engine in line with the retro motor experienced a maximum heat flux of 0.42 watt/cm<sup>2</sup> (0.37 Btu/ft<sup>2</sup>-sec).

#### 17.5.4 Instrument Unit Aeroheating Environment

The Instrument Unit (IU) aeroheating environment was monitored by eight thermocouples mounted on the inner surface of the honeycomb structure on the low density (49.7 kg/m<sup>3</sup> or 3.1 lbm/ft<sup>3</sup>) core. Seven of the eight measurements indicated temperature rises due probably to internal radiation or local convective heating during the first 30 seconds of flight. This is shown in Figure 17-16. The two sensors located near position IV at station 82.47 meters (3247 in.) and station 82.14 meters (3234 in.) indicated increases of 7°K (13°F) and 11°K (20°F), respectively.

After 30 seconds, these measurements indicated a cooling trend. The IU compartment ambient gas temperature dropped to 273°K (32°F) at 70 seconds. After that time the sensor output was somewhat meaningless since the compartment pressure was approaching 2.7 N/cm<sup>2</sup> (3.9 psia). The inner skin temperature indicated a maximum 348°K (165°F) at approximately 185 seconds at the sensor located near position I at station 82.14 meters and a minimum of 329°K (132°F) near position II at station 82.47 meters. The simulation in Figure 17-16 indicated a maximum external temperature approximately 11°K (20°F) higher than the inner sensor temperature for the no solar heating case. From 185 to 770 seconds, the effects of solar radiation may be noted in the measured data. The simulation of the data was for maximum solar heating and no solar heating; however, it should be noted that the vehicle received considerably less than a maximum solar load. The sensors located at positions I and IV would have experienced the greatest solar heat flux; this was indicated in the measured data. These trends due to solar heating were not noted in the AS-201 and AS-202 data, but were noted in the AS-203 data. The IU for AS-201 and AS-202 was painted white; however, on AS-203 and AS-501, the IU was painted black, and this would account for the difference noted in the data.

#### 17.6 VEHICLE ORBITAL HEATING ENVIRONMENT

The orbital temperatures for the APS were determined by 10 sensors mounted internally on various components and propellant transfer lines and four sensors mounted on the fairing.

One internal component measurement and one fairing measurement were selected for direct correlation with the flight data.

The maximum temperature recorded on the fairing was 361°K (190°F). This exceeded the maximum predicted value by 13.9°K (25°F). The components, however, remained within their allowable temperature limits during low earth orbit.

Figure 17-17 compares the APS fairing orbital temperatures with the design prediction band and the postflight prediction band. Since the flight data exceeded the design prediction, it was suspected that a change in the optical properties of the fairing had occurred. A simulation of the measured data, using revised values of absorptivity ( $\alpha = 0.22$ ) and emissivity ( $\epsilon = 0.14$ ), gave excellent correlation and was used to provide the post-flight prediction bands. The design prediction used values of  $\alpha = 0.24$  and  $\epsilon = 0.22$ .

The propellant control module appeared to exceed its upper allowable temperature limit during the waiting orbit. This could be due to the indicated shift in optical properties on the APS fairings which produce a higher than expected fairing temperatures. The APS fairings, in turn, had a strong influence on component temperatures.

Figure 17-18, upper plot, is a simulation of LH<sub>2</sub> heating using design methods and the initial structural temperatures obtained from the powered flight simulation. Maximum values of internal insulation thermal conductivity ( $k$ ) were used. Tank wall optical properties, solar absorptivity ( $\alpha$ ) of 0.42, and infrared emissivity ( $\epsilon$ ) of 0.87 were used as determined by measurement a few days before the flight. The propellant heating was well within the design range.

Figure 17-18 presents measured tank wall temperature data at two locations together with simulated values which were used in determining LH<sub>2</sub> heating during orbit.

IU inner skin orbital temperatures are shown in Figure 17-19. The effects of the roll maneuvers, before and after spacecraft separation, on the IU heating rates can be seen in the data from 3.2 to 3.6 hours from launch. Data were also available out to 6.9 hours from launch. These data indicated that the minimum inner skin temperatures fell below the lower range of the transducer, 223°K (-58°F), at positions II and III at 5.0 hours from launch. At 6.9 hours from launch one sensor located near position I indicated a maximum temperature of 365°K (198°F), indicating that a temperature differential greater than 142°K (256°F) existed between positions I and III.

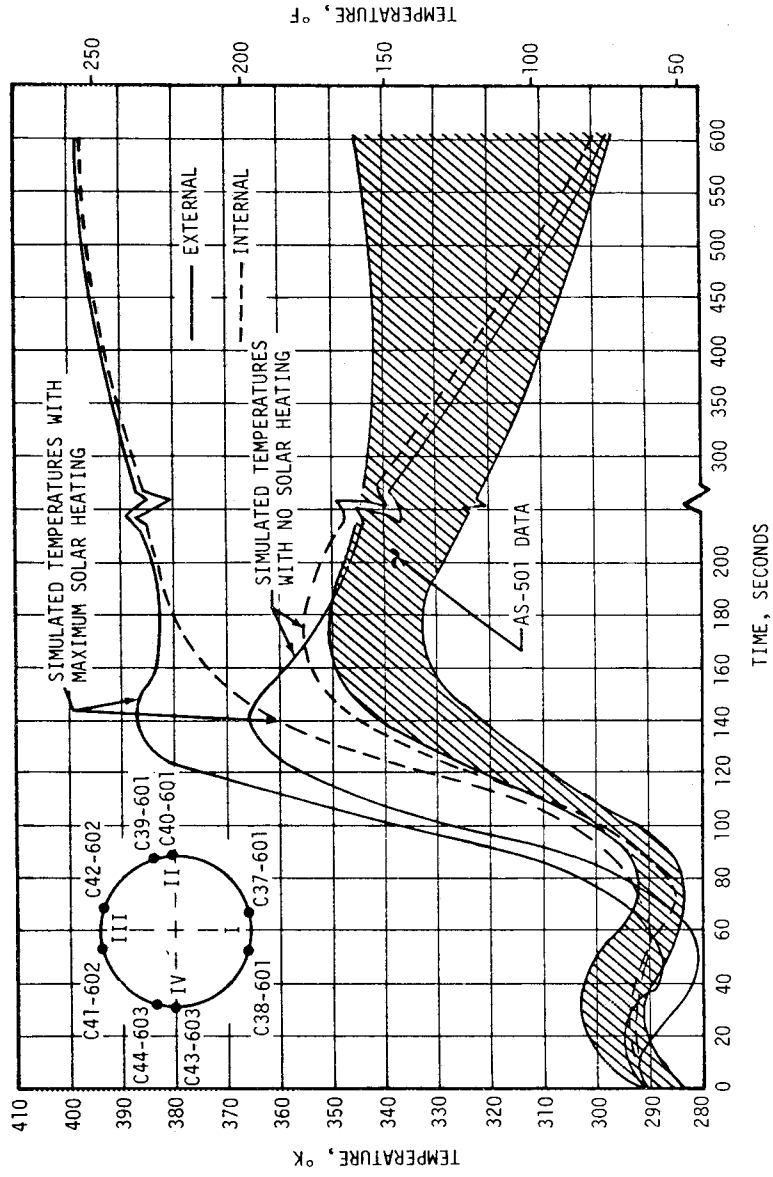


Figure 17-16. Instrument Unit Skin Temperature

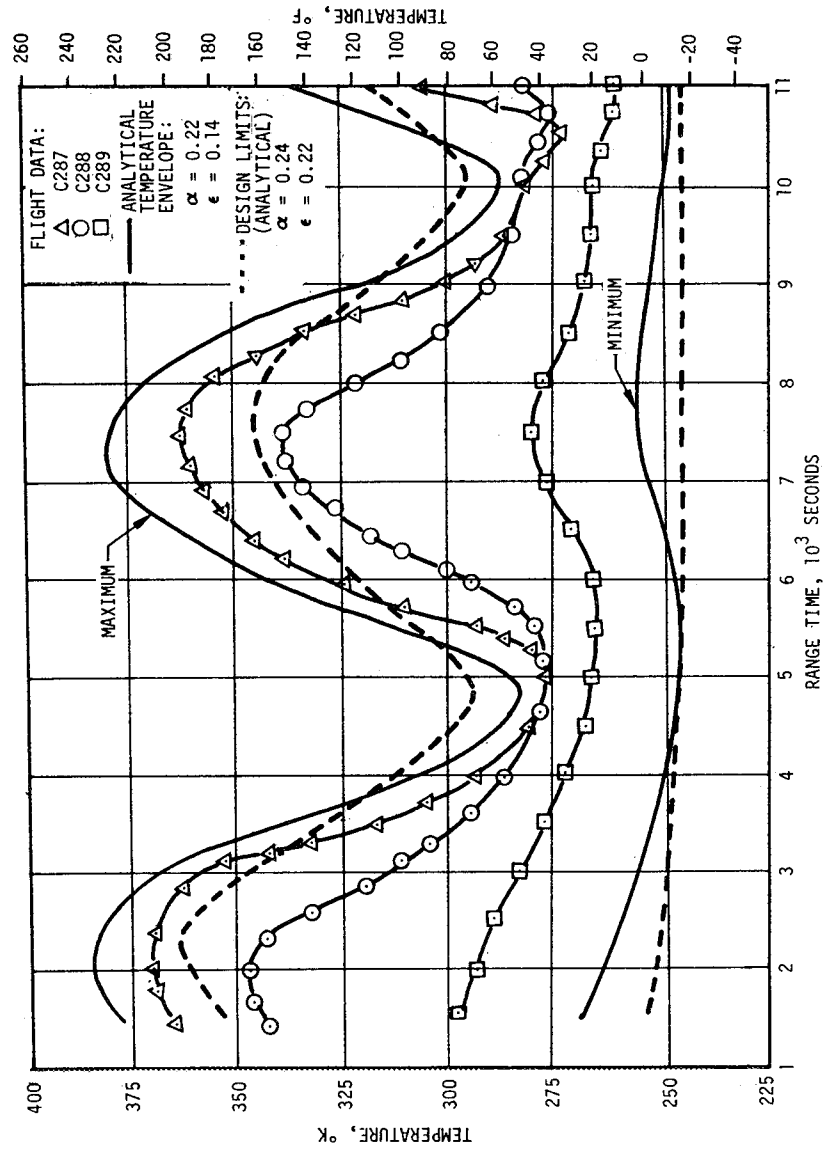


Figure 17-17. APS Firing Orbital Temperature

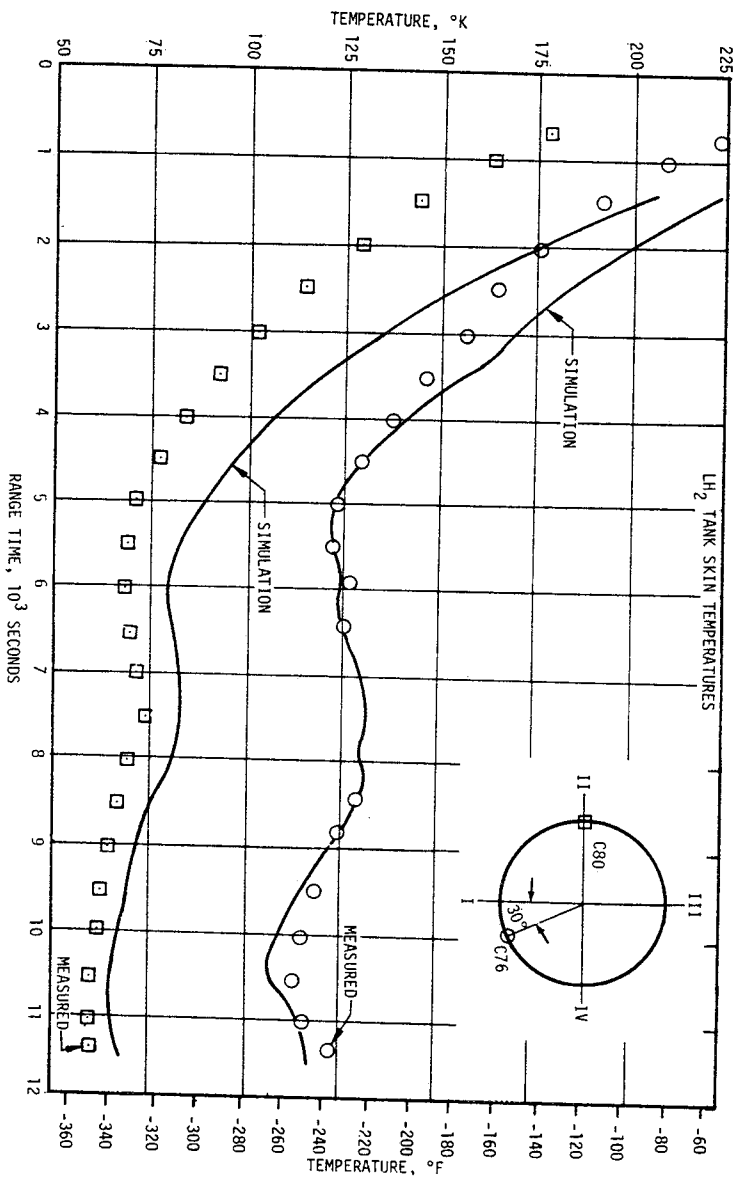
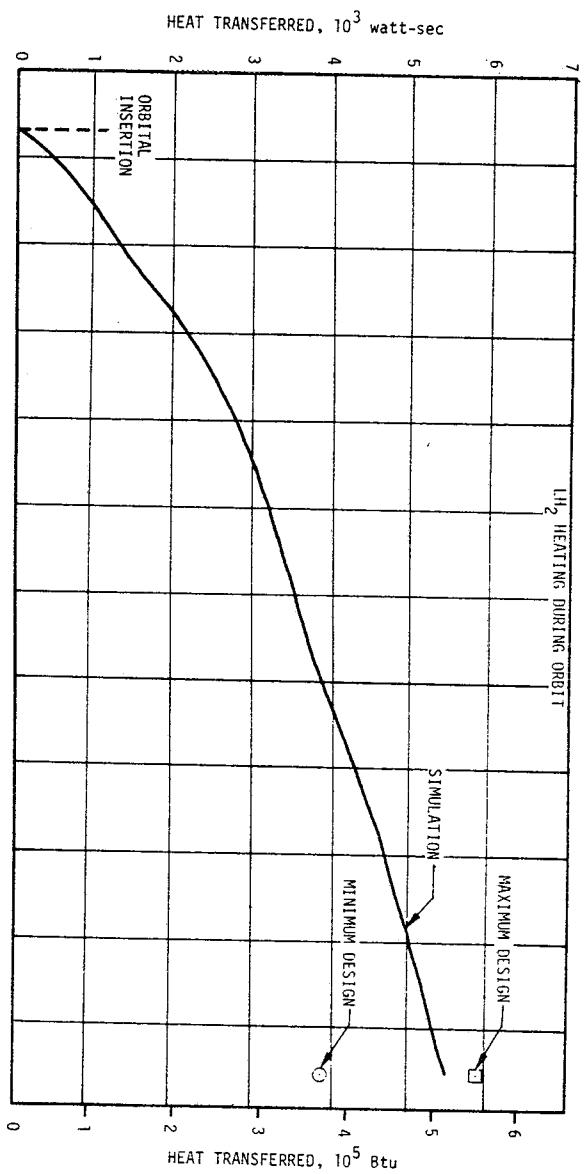


Figure 17-18. LH<sub>2</sub> Heating During Orbit and Tank Skin Temperatures

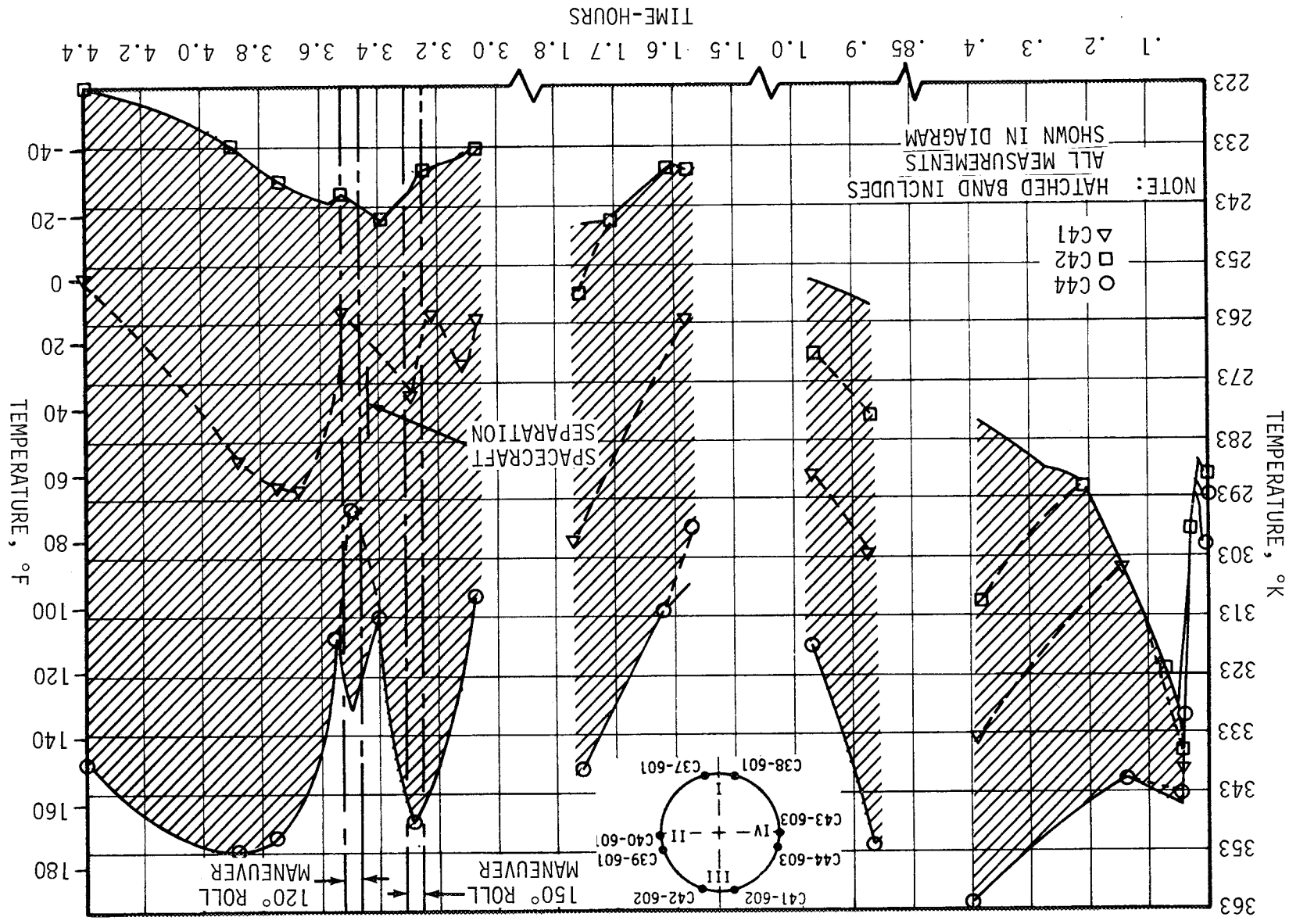


Figure 17-19. Instrument Unit Inner Skin Orbital Temperature



## SECTION 18 ENVIRONMENTAL CONTROL SYSTEM

### 18.1 SUMMARY

The S-IC forward canister conditioning system and the aft environmental conditioning system performed satisfactorily during the AS-501 launch countdown. The compartment ambient and canister temperatures were within the design limits.

The S-II forward and aft thermal control systems maintained container temperatures within mid-range of design limits throughout prelaunch and boost. Both hydrogen and oxygen concentrations were well below the allowable 3 percent maximum.

The S-IVB aft interstage environmental control system maintained an APS temperature within the  $304 \pm 3^\circ\text{K}$  ( $87 \pm 5^\circ\text{F}$ ) design limits.

The IU environmental control subsystem performed well. With only two exceptions; pressures, temperatures, and flow rates were held within the required ranges. The ST-124M internal ambient pressure did not decay to the specified lower limit. However, this did not cause any problem with the platform system operation and was not considered a failure. Also the IU internal ambient temperature dropped below the redline limit prior to liftoff, but a waiver was obtained and no adverse effects were noted. A redline change is being considered.

The water coolant valve opened at 178.318 seconds and sublimator cooling was evident by 300 seconds. By 750 seconds, the modulating flow control valve began diverting the methanol/water through the sublimator bypass, and the methanol/water bulk temperature began to stabilize at approximately  $288.7 \pm 0.2^\circ\text{K}$  ( $60 \pm 0.36^\circ\text{F}$ ). Data at 11,600 seconds showed that the bulk temperature was still holding at  $288.3 \pm 0.2^\circ\text{K}$  ( $59.3 \pm 0.36^\circ\text{F}$ ), indicating a good stable operation of the thermal conditioning system. Environmental control system real-time data indicated good control was maintained through Command Module separation.

### 18.2 S-IC ENVIRONMENTAL CONTROL

The forward canister conditioning system controlled the temperature of the ten equipment canisters in the forward skirt area. Air was used as the conditioning gas until -7 hours 41 minutes. At that time the system was switched to  $\text{GN}_2$ , which was used until umbilical disconnect at -16.7 seconds. The

canister conditioning system performed satisfactorily and held ambient temperature of the canisters within the required  $300 \pm 11.1^{\circ}\text{K}$  ( $80 \pm 20^{\circ}\text{F}$ ) during countdown.

The aft environmental conditioning system controlled the temperature in the aft compartment. The critical components in this compartment were the flight batteries. All recorded temperatures were within the requirements of  $300 \pm 5.5^{\circ}\text{K}$  ( $80 \pm 10^{\circ}\text{F}$ ) except one instrument that had a recorded temperature  $2^{\circ}\text{K}$  ( $3.6^{\circ}\text{F}$ ) below the minimum at liftoff. This instrument was located on the opposite side of the stage from the battery location; therefore, the temperature at that location was not critical.

### 18.3 S-II ENVIRONMENTAL CONTROL

The S-II forward and aft thermal control systems performed satisfactorily during all phases of the countdown and boost of the AS-501 vehicle. Container temperatures were maintained mid-range of design limits throughout prelaunch and boost. Temperature drops in the forward containers were less than the expected  $6^{\circ}\text{K}$  ( $11^{\circ}\text{F}$ ) during S-IC and S-II boost. The container which had the highest internal heat load experienced a temperature rise of  $1^{\circ}\text{K}$  ( $2^{\circ}\text{F}$ ). Aft container temperatures were expected to rise from  $6^{\circ}\text{K}$  to  $17^{\circ}\text{K}$  ( $11$  to  $30^{\circ}\text{F}$ ) during S-II boost due to the effects of base heating; however, base heating was much lower than anticipated, and the aft containers showed a cooling trend similar to the forward containers. All container temperatures were well within limits at the end of S-II boost.

During the first 80 seconds of S-IC boost, the ambient temperature in the S-II engine compartment was expected to drop considerably as the gases expanded due to the drop in pressure with increasing altitude. The data indicated that the ambient temperatures did drop, but not to the extent predicted. One explanation for the difference is that ideal expansion of gases did not occur. A more probable explanation is because of the decrease in thermal capacity of the gas, the transducer indicated the temperature of its sensing element rather than the temperature of the rarefied gas.

Both hydrogen and oxygen concentrations from initiation of tanking until liftoff were maintained well below the allowable maximum (3 percent). During the time interval from 20 percent to 60 percent LOX loading, sporadic indications of oxygen were observed. The highest concentration noted was between 1 and 1.5 percent.

### 18.4 S-IVB ENVIRONMENTAL CONTROL

#### 18.4.1 Ascent Powered Flight Phase

The aft interstage environmental control system functioned properly during the countdown, maintaining an APS temperature within the design limits of  $303.72 \pm 2.78^{\circ}\text{K}$  ( $87 \pm 5^{\circ}\text{F}$ ). At liftoff, the APS temperature was within design limits.

## 18.5 IU ENVIRONMENTAL CONTROL

### 18.5.1 Thermal Conditioning System

The Environmental Control Subsystem (ECS) controlled liquids and gaseous elements of the Instrument Unit (IU) to maintain acceptable operating conditions for all components mounted within the IU and the S-IVB stage forward skirt during preflight and flight operations. The ECS was composed of the Thermal Conditioning System and the Gas Bearing Supply System (GBS). A preflight purge system provided environmental control prior to launch. See paragraph B.5.3, for a description of the IU Environmental Control System.

During portions of the final 90 minutes of the countdown (period following S-IVB stage LH<sub>2</sub> loading) the IU ambient temperature was not maintained above the lower redline value. At liftoff, the ambient temperature was 287.4°K (58°F). This was 1.2°K (2°F) below the initial lower redline limit of  $294.1 \pm 5.5^\circ\text{K}$  ( $70 \pm 10^\circ\text{F}$ ) and 6.6°K (12.0°F) below the design requirement of  $296.8 \pm 2.7^\circ\text{K}$  ( $75 \pm 5^\circ\text{F}$ ). As the ambient temperature approached the lower redline value, a waiver was obtained to allow the redline limit to be lowered to 285.7°K (55°F). The waiver was obtained approximately 11 minutes prior to launch. The reason for the cold ambient temperature is being investigated further.

The methanol/water bulk temperature, shown in Figure 18-1, indicated a 0.4°K (0.7°F) temperature increase from liftoff until 20 seconds. This increase was due to the end of preflight cooling. A 0.8°K (1.4°F) temperature decrease then occurred from 20 until 110 seconds. This 0.8°K (1.4°F) drop resulted from cooling affects of the expanding compartment gases venting during vehicle ascent.

Following the cooling affect of the venting, the bulk temperature increased from 288.13°K (59°F) at 110 seconds to 289.82°K (62°F) at approximately 450 seconds. After 450 seconds, the bulk temperature declined and approached 288.3°K (59°F).

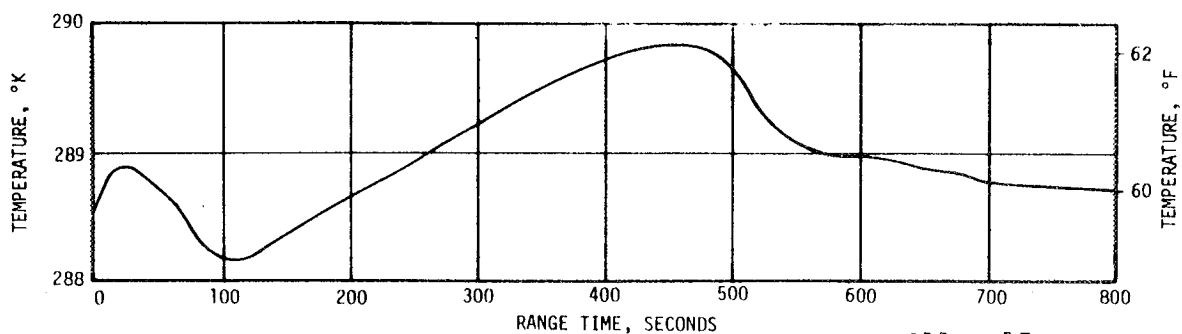


Figure 18-1. Methanol/Water Bulk Temperature  $\frac{C11 + 15}{2}$

The sublimator began operation at 180 seconds when the water control valve was opened. Figures 18-2 and 18-3 show the sublimator performance. A maximum of 7.5 kilowatts of sublimator cooling was observed during sublimator start-up. The sublimator had removed sufficient heat from the system by 530 seconds to allow the modulating flow control valve to begin bypassing fluid around the sublimator. The valve operation is shown in Figure 18-4. The valve had reached 80 percent bypass by approximately 650 seconds. The sublimator cooling rate decreased concurrent with the valve operation.

The TCS  $\text{GN}_2$  supply pressure decay and temperature variation appeared nominal. The pressure decayed at a rate of  $148.09 \text{ N/cm}^2$  (214.8 psia) per hour over an 11,900 second period.

The overall operation of the TCS was nominal for the time period discussed (0 to 750 seconds). Component temperatures were maintained within operational values. Components with integral methanol/water passages maintained very stable temperatures with one exception. The ST-124M inertial gimbal temperature showed a constant increase from  $314.9^\circ\text{K}$  ( $107.13^\circ\text{F}$ ) at 800 seconds to  $319.5^\circ\text{K}$  ( $115.41^\circ\text{F}$ ) at 25,000 seconds. The specification for AS-501 platform inertial gimbal temperature was  $316 \pm 3^\circ\text{K}$  ( $110 \pm 5.4^\circ\text{F}$ ).

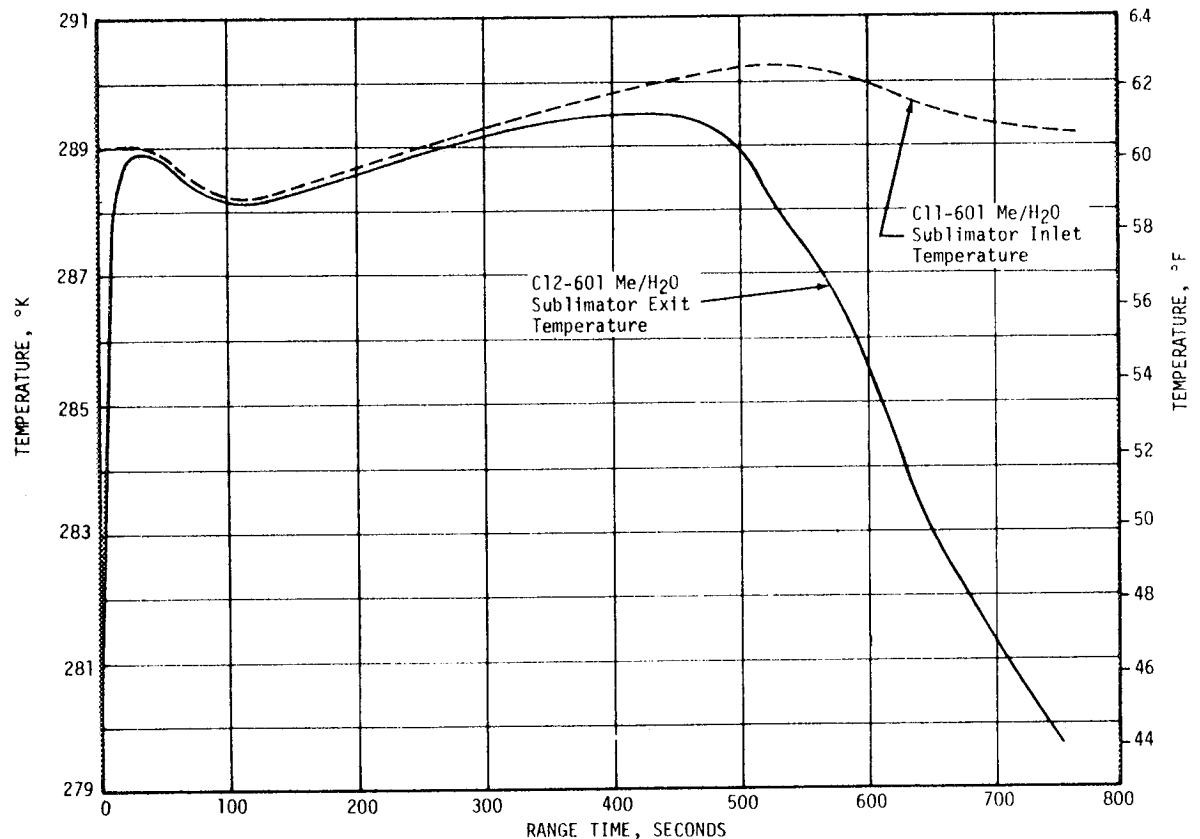


Figure 18-2. Sublimator Inlet and Exit Temperatures

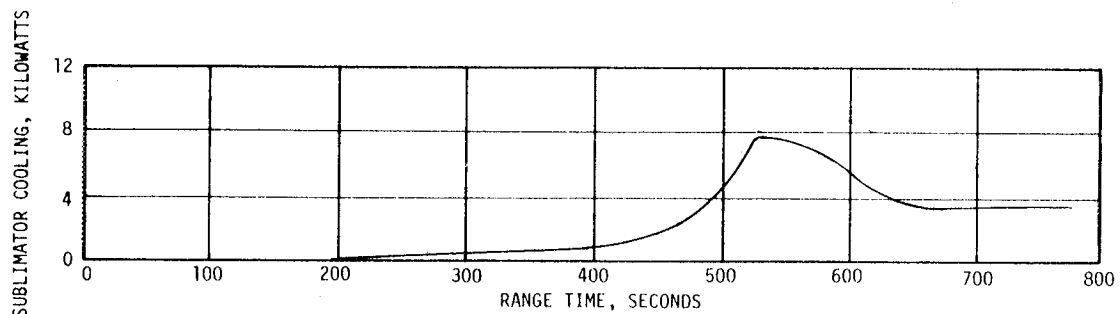


Figure 18-3. Sublimator Cooling Rate

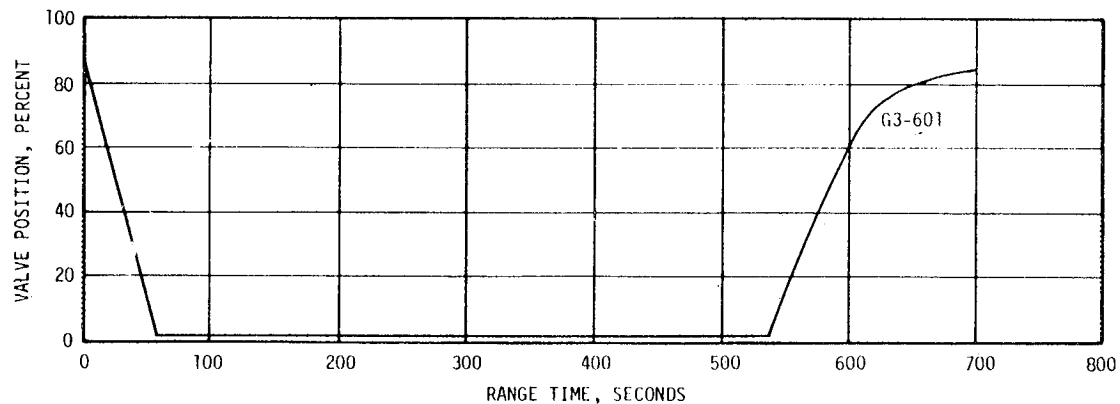


Figure 18-4. Modulating Flow Control Valve Performance

Although the maximum temperature was exceeded by only  $0.5^{\circ}\text{K}$  ( $0.9^{\circ}\text{F}$ ), longer operation would increase the temperature further which could lead to gyro drifts and degraded platform performance. The blower system in the platform has been changed to obtain a better heat distribution. Selected component temperatures are shown on Figure 18-5.

#### 18.5.2 ST-124M Gas Bearing System

Figure 18-6 shows the  $\text{GN}_2$  supply pressure and temperature. The GBS  $\text{GN}_2$  pressure decayed at a rate of  $158.7 \text{ N/cm}^2$  ( $230.2 \text{ psia}$ ) per hour. This decay rate would yield a  $\text{GN}_2$  pressure of  $1408.6 \text{ N/cm}^2$  ( $2043 \text{ psia}$ ) after 4.5 hours or  $236.5 \text{ N/cm}^2$  ( $343 \text{ psia}$ ) above the minimum called for in the system specification.

The platform air bearing  $\text{GN}_2$  inlet pressure was referenced to the platform internal ambient pressure to maintain a constant pressure differential of  $10.34 \pm 0.34 \text{ N/cm}^2$  ( $15 \pm 0.5 \text{ psid}$ ). This pressure differential was maintained between  $10.48 \pm 0.06 \text{ N/cm}^2$  ( $15.2 \pm 0.1 \text{ psid}$ ) which was within the specified limits.

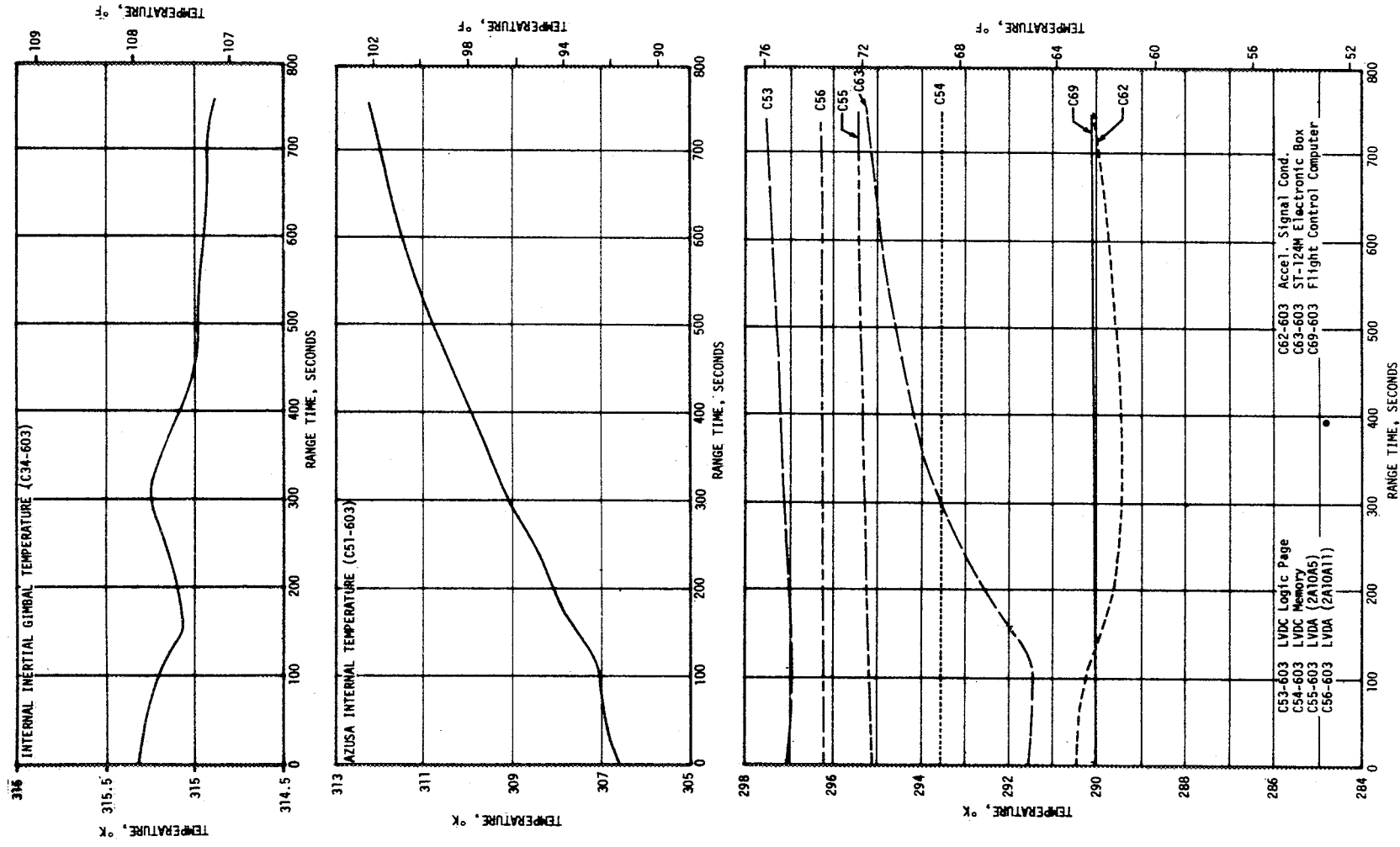


Figure 18-5. Selected Component Temperatures

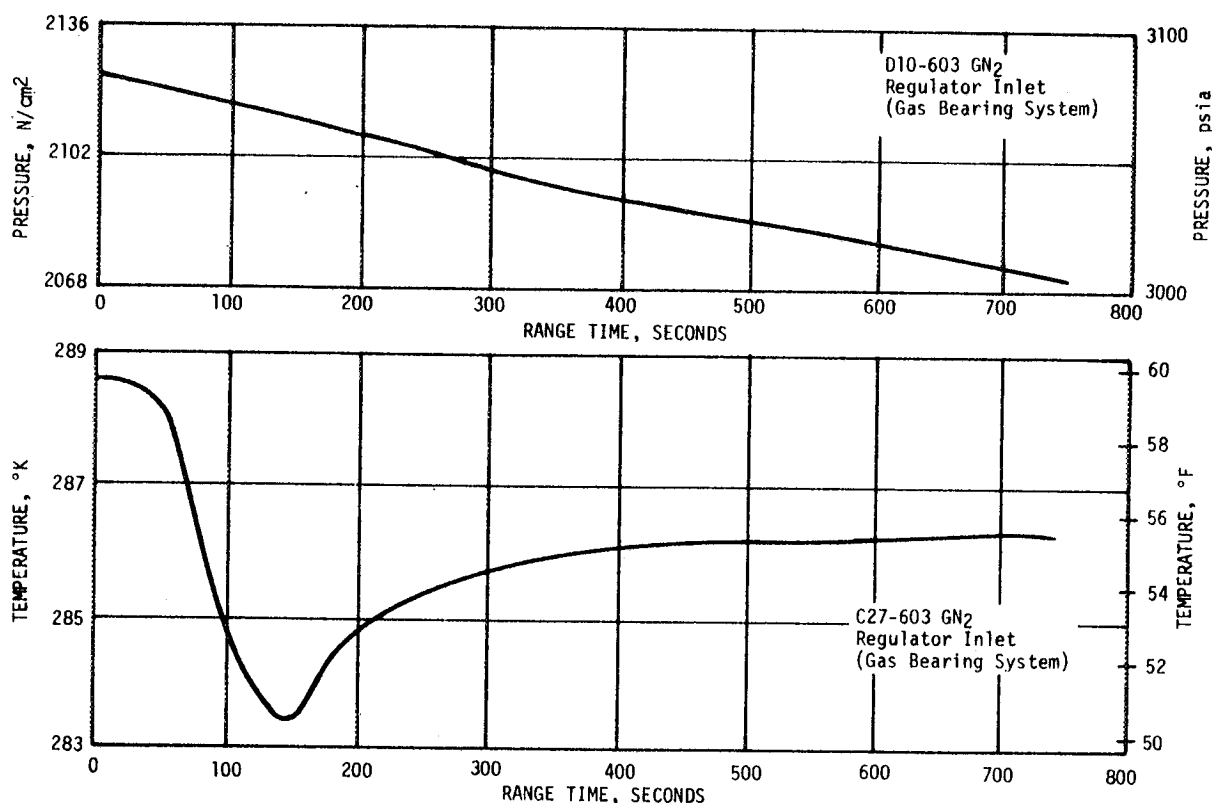


Figure 18-6. GN<sub>2</sub> Supply Pressure and Temperature

The ST-124M platform internal ambient pressure requirement was  $12.76 \pm 1.38 \text{ N/cm}^2$  ( $18.5 \pm 2 \text{ psia}$ ) for preflight and  $8.27 \pm 1.03 \text{ N/cm}^2$  ( $12.0 \pm 1.5 \text{ psia}$ ) for flight. The flight pressure was to be reached within the first hour of operation. The platform internal ambient was  $13.51 \text{ N/cm}^2$  (19.6 psia) at liftoff and decayed to within the specification tolerance at 23,500 seconds. This over-pressure during flight was not considered a serious problem; however, investigation is continuing. Resizing the orifice could help the pressure decay at a faster rate. The platform internal pressure through 750 seconds is shown on Figure 18-7.

Figure 18-8 shows the gas bearing heat exchanger GN<sub>2</sub> and methanol/water temperature. The GN<sub>2</sub> heat exchanger exit temperature was maintained to within 1.1°K (2°F) of the methanol/water temperature.

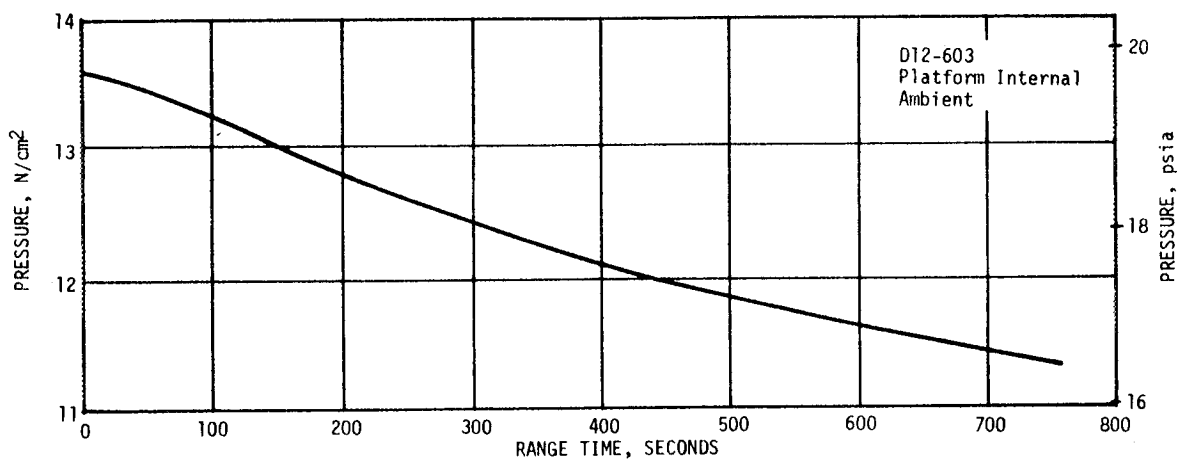


Figure 18-7. Platform Internal Pressure

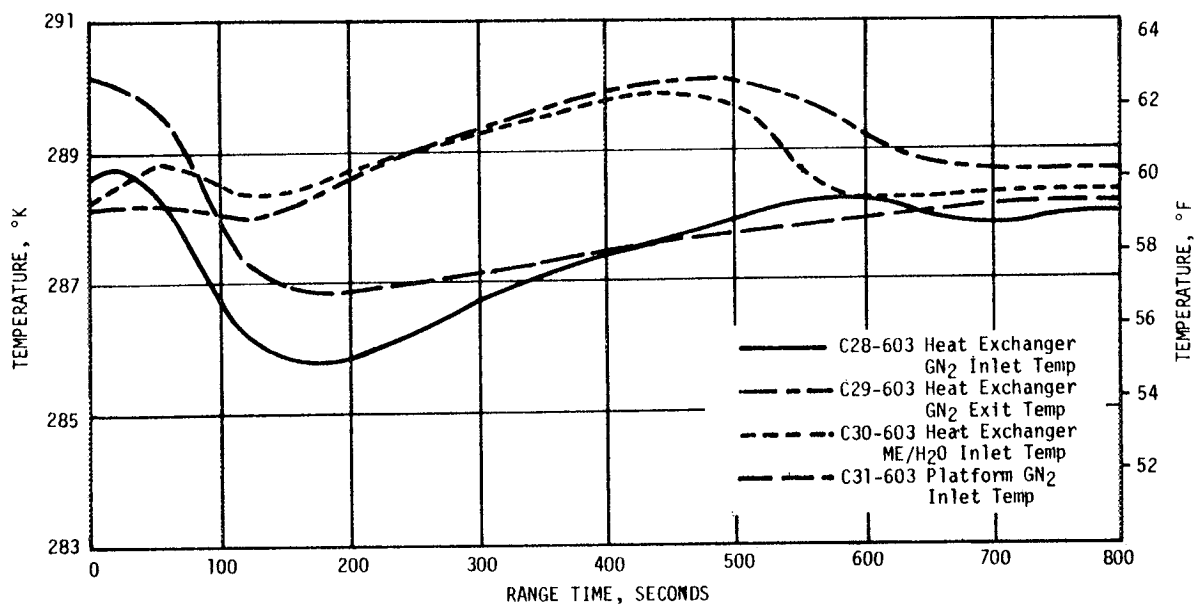


Figure 18-8. Heat Exchanger  $GN_2$  and Methanol/Water Temperatures



## SECTION 19 DATA SYSTEMS

### 19.1 SUMMARY

There were 2687 telemetered measurements active at the start of the AS-501 automatic countdown sequence. Of the 2687 measurements, 45 failed in flight, resulting in an overall measuring system reliability of 98.3 percent.

The Airborne Telemetry System operated satisfactorily, including preflight calibrations, inflight calibrations, and tape recorder operation.

Performance of the RF systems including telemetry, tracking, and command systems was good. Approximately 2 seconds of data on all S-IC stage telemetry links was lost due to an unexpected data dropout at 136.5 seconds. Data on the AF-1 and AF-2 links were recovered from the onboard tape recorder playback.

Ground camera coverage was not entirely satisfactory. Of a total of 85 cameras (68 engineering sequential, 15 tracking, and 2 onboard), 85 percent did not produce all of the required data for evaluation purposes. Thirty-two percent had partial loss and 53 percent had total loss of data for evaluation purposes.

Both onboard cameras viewing the S-IC/S-II stage separation sequence were ejected and recovered successfully, producing excellent quality film.

### 19.2 VEHICLE MEASUREMENTS EVALUATION

The AS-501 measurement systems operated satisfactorily. Lost measurements did not adversely affect vehicle postflight evaluation since sufficient data were acquired to complete the evaluations. There were 2687 telemetered measurements on the vehicle active at the start of the AS-501 automatic countdown sequence. Of these, 854 were on the S-IC stage, 948 on the S-II stage, 548 on the S-IVB stage, and 337 on the Instrument Unit. Of these 2687 measurements, 45 failed in flight, resulting in an overall measuring system reliability of 98.3 percent. Fifty-six measurements were waived prior to the automatic countdown sequence, 37 were partially successful, and 11 had insufficient range. Seventeen of the waived measurements provided good data during flight. A summary of vehicle measurements is presented in Table 19-1.

Table 19-1. Vehicle Measurements Summary

	S-IC STAGE	S-II STAGE	S-IVB STAGE		INSTRUMENT UNIT	TOTAL VEHICLE
			PHASE I	PHASE II		
No. Schedule	872	957	577	577	337	2743
No. Waived	18	9	29*	29*	0	56
No. Failures	22	10	5	13	0	45
No. Partial Successes	27	6	-	-	4	37
No. Insufficient Range	9	2	0	0	0	11
Measurement Reliability	97.4%	98.9%	99.1%	97.6%	100%	98.3%

\* See Table 19-2

#### 19.2.1 S-IC Stage Measurement Analysis

There were 872 flight measurements scheduled for the S-IC stage. Of these, 18 measurements were waived prior to the automatic countdown, 22 failed in flight, 27 were partially successful, and 9 had insufficient range. Eleven of the waived measurements provided useful data during flight. Based upon 854 measurements active at the start of automatic countdown and 22 failures during flight, the reliability is 97.4 percent. Measurements waived prior to launch, measurement failures (including partial failures), and measurements of insufficient range are summarized in Tables 19-2, 19-3, and 19-4, respectively.

#### 19.2.2 S-II Stage Measurement Analysis

There were 957 flight measurements scheduled for the S-II stage. Of these, nine measurements were waived prior to the automatic countdown. Ten failed in flight, four were partially successful and one had insufficient range. Six of the waived measurements provided useful data during flight. Based on 948 measurements active at the start of automatic countdown and 10 failures during flight, the resultant reliability is 98.9 percent. Measurements waived prior to launch, measurement failures (including partial failures), and measurements with insufficient range are summarized in Tables 19-2, 19-3, and 19-4, respectively.

Table 19-2. Measurements Waived Prior to Launch

MEASUREMENT NUMBER	MEASUREMENT TITLE	NATURE OF FAILURE	REMARKS
S-IC STAGE			
A001-118	Acceleration, longitudinal	Measurement installation not according to drawing.	NER 802737, waiver L1A-10 partly valid data good at separation
C102-112	Temperature, skin internal Fin B	Spot weld on thermocouple inside fin broken.	NCR 010729, waiver L1A-7 invalid data.
C103-112	Temperature, skin internal Fin B	Spot weld on thermocouple inside fin broken.	NCR 010731, waiver L1A-7 invalid data.
C120-119	Temperature, LOX tank ullage	Defective transducer in LOX tank. Could not be replaced.	NCR 3648, waiver L1A-6 invalid data
C132-101	Temperature, heat exchanger bellows	Located under engine insulation. Failure mode could not be determined.	NCR 011064, waiver L1A-11 valid data up to liftoff.
D027-101	Pressure, surface outboard engine	Located under engine insulation. Dead band in transducer potentiometer.	NCR 0110076, waiver L1A-12 valid data after liftoff.
D119-101	Pressure, differential, engine gimbal system filter manifold	Transducer bias shifted below telemetry zero level	NCR 011047, waiver L1A-9 valid data.
D119-102	Pressure, differential, engine gimbal system filter manifold	Transducer bias shifted below telemetry zero level.	NCR 011040, waiver L1A-9 valid data.
D119-103	Pressure, differential, engine gimbal system filter manifold	Transducer bias shifted below telemetry zero level.	NCR 4781, waiver L1A-13 valid data.
D119-104	Pressure, differential, engine gimbal system filter manifold	Transducer bias shift and erratic data during CDDT.	NCR 011163, waiver L1A-16 invalid data.
E033-102	Vibration, yaw actuator, pitch	Located under engine insulation. Failure mode could not be determined.	NCR 020118, waiver L1A-20 invalid data.
E036-103	Vibration, combustion chamber dome, longitudinal	Broken mounting stud.	NCR 020117, waiver L1A-21 invalid data.
E084-117	Vibration, LOX inboard tunnel, pitch	Transducer not qualified for flight use.	NER 6430, waiver L1A-1 valid data.
E085-117	Vibration, LOX inboard tunnel, yaw	Transducer not qualified for flight use.	NER 6430, waiver L1A-1 valid data.
E086-117	Vibration, LOX inboard tunnel, pitch	Transducer not qualified for flight use.	NER 6430, waiver L1A-1 valid data.
E087-117	Vibration, LOX inboard tunnel, yaw	Transducer not qualified for flight use.	NER 6430, waiver L1A-1 valid data.
E088-117	Vibration, LOX inboard tunnel, pitch	Transducer not qualified for flight use.	NER 6430, waiver L1A-1 valid data.
E089-117	Vibration, LOX inboard tunnel, yaw	Transducer not qualified for flight use.	NER 6430, waiver L1A-1 valid data.

Table 19-2. Measurements Waived Prior to Launch (Continued)

MEASUREMENT NUMBER	MEASUREMENT TITLE	NATURE OF FAILURE	REMARKS
S-II STAGE			
A003-206	Body modal rad. aft skirt accel. steady state	Intermittent	Gave valid data during flight. Probable ground equipment problems.
A004-206	Body modal lat. aft skirt accel. steady state	Intermittent	Gave valid data during flight. Probable ground equipment problems.
A007-206	Body modal lat. fwd skirt accel. steady state	No RACS	Gave valid data during flight. Probable ground equipment problem.
C032-204	E4 main oxidizer valve temp		Waived by PBC No. M0010 transducer was shorted to the structure and a dummy bridge inserted in the signal conditioner chassis. Measurement not a red line and comparison data could be obtained from same measurement on engine 5. No valid data.
D008-202	E2 LOX turbine inlet press	Not operational	Waived by NAR 4, the transducer was not operational during CDDT and a change could not be made because of schedule constraints. Measurement not a red line and not considered essential in evaluating primary engine performance. No valid data.
D016-203	E2 start tank press	RACS low out	Gave valid data during flight. Probable ground equipment problem.
D021-203	E3 helium tank press	RACS high out	Gave valid data during flight. Probable ground equipment problem.
D021-204	E4 helium tank press	Consistently 140 psi low	Waived by NAR 5. Did not meet specs and criteria document. Is a backup for D015-204 which is a red line and provided usable data. No valid data.
D092-203	E3 engine inlet LH <sub>2</sub> press	RACS high out	Gave valid data during flight. Probable ground equipment problem.
S-IVB STAGE *			
K139-424	Event - oxid SOV chill system - C1	No indication	Micro switch out of adjustment.
<p>* In addition, one measurement was inactive, and 27 measurements were deleted from incentive considerations by installation of the anti-flutter kit on the forward skirt.</p>			

Table 19-3. Measurement Malfunctions During Flight

MEASUREMENT NUMBER	MEASUREMENT TITLE	NATURE OF FAILURE	TIME OF FAILURE (RANGE TIME)	DURATION Satisf. Oper.	REMARKS
TOTAL MEASUREMENT FAILURES, S-IC STAGE					
C010-104	Temperature, engine gimbal system return, yaw actuator	Damaged cable	Prior to Flight	0	Damaged cable noted prior to flight. Did not have time to replace.
C018-101	Temperature, engine total calorimeter	Reading low and trend not as expected	Liftoff	0	Probable failure was wire to foil broken and wire shorted to heat sink.
C039-115	Temperature, heat shield forward surface	Data erratic throughout flight	Liftoff	0	Appears to be open transducer.
C048-101	Temperature, ambient engine compartment	Reading low and trend not as expected	Liftoff	0	Apparent short of thermocouple cable between transducer and zone box.
D048-106	Pressure, air scoop	Data trend higher than expected	Liftoff	0	Excessive transducer zero shift.
E033-101	Vibration, yaw actuator, pitch	Data trend low, PSD not as expected	Liftoff	0	No static firing failure history.
E036-101	Vibration, combustion chamber dome	High amplitude, low frequency noise	Liftoff	0	ECP0333 changes out transducer.
E036-103	Vibration, combustion chamber dome	High amplitude, low frequency noise	Liftoff	0	ECP0333 changes out transducer.
E036-104	Vibration, combustion chamber dome, longitudinal	High amplitude, low frequency noise	Liftoff	0	ECP0333 changes out transducer.
E036-105	Vibration, combustion chamber dome, longitudinal	High amplitude, low frequency noise	Liftoff	0	ECP0333 changes out transducer.
E037-101	Vibration, LOX pump inlet flange, longitudinal	High amplitude data below 500 cps	Liftoff	0	No similar static firing failure history.
E038-101	Vibration, LOX pump inlet flange, radial	High amplitude data below 500 cps	Liftoff	0	No similar static firing failure history.
E040-101	Vibration, fuel pump inlet flange, radial	High amplitude, low frequency noise	Liftoff	0	ECP0333 changes out transducer.
E041-101	Vibration, fuel pump flange, longitudinal	High amplitude, low frequency noise	Liftoff	0	ECP0333 changes out transducer.
E041-102	Vibration, fuel pump flange, longitudinal	High amplitude, low frequency noise	Liftoff	0	ECP0333 changes out transducer.
E041-104	Vibration, fuel pump flange, longitudinal	High amplitude, low frequency noise	Liftoff	0	ECP0333 changes out transducer.
E041-105	Vibration, fuel pump flange, longitudinal	High amplitude, low frequency noise	Liftoff	0	ECP0333 changes out transducer.
E042-102	Vibration, fuel pump flange, radial	High amplitude, low frequency noise	Liftoff	0	ECP0333 changes out transducer.
E042-104	Vibration, fuel pump flange, radial	High amplitude, low frequency noise	Liftoff	0	ECP0333 changes out transducer.
E042-105	Vibration, fuel pump flange, radial	High amplitude, low frequency noise	Liftoff	0	ECP0333 changes out transducer.

Table 19-3. Measurement Malfunctions During Flight (Continued)

MEASUREMENT NUMBER	MEASUREMENT TITLE	NATURE OF FAILURE	TIME OF FAILURE (RANGE TIME)	DURATION SATIS. OPER.	REMARKS
TOTAL MEASUREMENT FAILURES, S-IC STAGE (Cont.)					
E046-120	Vibration, destruct system mounting panel, radial	Loss of data	Prior to flight	0	Measurement failed during ME-01 RACS checked at -20 min.
S049-112	Strain, main spar	Data shifted below expected level	Prior to flight	0	Failure noted on MT-01 at -12 hrs.
TOTAL MEASUREMENT FAILURES, S-II STAGE					
C853-218	E1 LH <sub>2</sub> feedline Q mid	No output	Liftoff	0	No data for entire flight
C893-218	LH <sub>2</sub> tank insulation surface temp	Shorted transducer	Liftoff	0	
D012-205	E5 engine regulator outlet press.	Erratic	Liftoff	0	Data missing for long periods.
D060-200	Ullage rocket # 8 chamber press.	Reads high	Liftoff	0	Reads 250 psi high prior to separation
D131-218	LH <sub>2</sub> tank insulation external press.	Insensitive transducer	Liftoff	0	Press. remains essentially constant with altitude. Insulation allows sensing line to become plugged. Installation to be changed.
D134-218	LH <sub>2</sub> tank insulation external press	Insensitive transducer	Liftoff	0	Press remains constant with altitude. Insulation allows sensing line to become plugged. Installation to be changed.
E012-206	Long. vibration E1 beam at pin	Low readings	Liftoff	0	Appears cables are bad.
E081-214	Radial vibration fwd skirt stringer	No output	Liftoff	0	
E084-219	Radial vibration fwd skirt stringer	No output	Liftoff	0	
E117-228	Radial vibration control upper bracket	Spikes	During S-IC Firing		
TOTAL MEASUREMENT FAILURES, S-IVB STAGE PHASE I					
C121-419	Temp-aft interstage 4	Signal off scale high	Liftoff	0	Temp patch appears to have opened.
C151-401	Temp engine LOX pump surface	Signal off scale high	Liftoff	0	Not properly ranged.
D195-419	Press ext aft interstage 17	Remained at 8.96 N/cm <sup>2</sup> (13 psia)	Liftoff	0	Plugged inlet.
D196-419	Press ext aft interstage 18	Incorrect press ind.	Liftoff	0	Appears that sense line is open or damaged; apparently measuring internal interstage pressures.
D210-402	Press interstage internal 6	Data goes to zero	Liftoff	0	Open circuit in transducer electronics.

Table 19-3. Measurement Malfunctions During Flight (Continued)

MEASUREMENT NUMBER	MEASUREMENT TITLE	NATURE OF FAILURE	TIME OF FAILURE (RANGE TIME)	DURATION SATIS. OPER.	REMARKS
TOTAL MEASUREMENT FAILURES, S-IVB STAGE PHASE II					
C075-409	Temp fuel tank external -1	Off scale high	During orbit	Until 800 sec	OK during boost and S-IVB first burn off scale high at start of second burn
C077-409	Temp fuel tank external -3	Off scale high	During orbit	Until 800 sec	"
C078-409	Temp fuel tank external -4	Off scale high	During orbit	Until 800 sec	"
C079-409	Temp fuel tank external -5	Off scale high	During orbit	Until 800 sec	"
C106-409	Temp fuel tank external -6	Off scale high	During orbit	Until 800 sec	"
C217-401	Temp main hyd. pump flange	Off scale low	During orbit	Until 800 sec	OK during boost and S-IVB first burn off scale low at start of second burn.
D181-409	Press fuel tank continuous vent 1	Erroneous indications	During orbit	Until 800 sec	The parameters displayed acceptable performance during S-IVB first burn and engine cutoff. During orbital periods they displayed unrealistic bias. These bias are apparently due to the transducers being subjected to temperatures lower than they were qualified for. Specification for these units is 78°K (-320°F). They experienced 29°K (-406°F) temperatures during orbital periods.
D182-409	Press fuel tank continuous vent 2	Erroneous indications	During orbit	Until 800 sec	
TOTAL MEASUREMENT FAILURES, S-IVB STAGE NON-INCIDENT					
S056-426	Strain-axial fwd skirt location 11A	No response off scale high	Orbit	800 sec	These measurements operated satisfactorily during first burn and drifted off scale high during orbit. This was apparently due to the temperature comp. limits being exceeded. (Note these are two active arm strain gauge bridges.)
S059-426	Strain-axial fwd skirt location 12B	No response off scale high	Orbit	— —	
S066-426	Strain-axial fwd skirt location 16A	No response off scale high	Orbit	— —	
PARTIAL MEASUREMENT FAILURES, S-IC STAGE					
B002-115	Acoustic, skin flush mounted	Data decreased to zero at 104 sec	104 sec	104 sec	Probable transducer or cable failure.
B003-118	Acoustic, skin flush mounted	High amplitude, low frequency noise after 10 sec	10 sec	10 sec	Appears to be random failure after 15 sec. No static firing failure histories.
C003-103	Temperature, turbine manifold	Data becomes erratic at 20 sec, goes off at 41 sec	20 sec	20 sec	Appears to be random transducer failure.
C004-119	Temperature, LOX bulk	Data noisy & erratic from 0-12 sec	0	140 sec	Valid data after 12 sec.
C042-115	Temperature, heat shield forward surface	Sudden decrease in indicated temperature at 5 sec. Data trend low for the remainder of flight	5 sec	5 sec	Spot weld holding transducer to structure appears to have failed causing transducer to read ambient compartment temperature.

Table 19-3. Measurement Malfunctions During Flight (Continued)

MEASUREMENT NUMBER	MEASUREMENT TITLE	NATURE OF FAILURE	TIME OF FAILURE (RANGE TIME)	DURATION SATIS. OPER.	REMARKS
PARTIAL MEASUREMENT FAILURES, S-IC STAGE (Cont.)					
C044-101	Temperature, ambient engine compartment	Data trend erratic after 80 sec. Off scale high and low	80 sec	80 sec	Apparent random zone box failure.
C081-117	Temperature, fuel tank skin	Data goes off scale high at 115 sec	115 sec	115 sec	Possible zone box failure.
C121-119	Temperature, LOX tank ullage	Data erratic from -3 to 12 sec and 62 to 78 sec	-3 sec and 62 sec	126 sec	Appears to be connector problem. ECP 0241 establishes FIX.
C122-119	Temperature, LOX tank ullage	Data erratic from -3 to 15 sec and 56 to 85 sec	-3 sec and 56 sec	124 sec	Appears to be connector.
C162-115	Temperature, heat shield forward surface	Data shifts and becomes erratic after 112 sec	112 sec	112 sec	Spot weld holding transducer to structure apparently failed.
C173-119	Temperature, LOX tank skin	Sudden increase in indicated temperature at 28 sec	28 sec	28 sec	Indicates possible tab-to-structure bond failure. Problem under investigation.
C176-119	Temperature, LOX tank skin	Data goes abruptly off scale high then low at 33 sec	33 sec	33 sec	Probable tab-to-structure bond failure. Problem under investigation.
C178-119	Temperature, LOX tank skin	Data erratic after 67 sec	67 sec	67 sec	Probable tab-to-structure bond failure. Problem under investigation.
C240-106	Temperature, calorimeter body	Data erratic after 55 sec	55 sec	55 sec	Appears to be connector problem.
D088-115	Pressure, GN <sub>2</sub> sphere, control pressure system	Data decreases abruptly to zero at 75 sec	75 sec	75 sec	Random failure. No static firing failure history.
D150-115	Pressure, LOX pump inlet, high frequency	Data goes off scale high at 7 sec	7 sec	7 sec	Apparent transducer failure. Redundant data on D127-115
D151-115	Pressure, LOX pump inlet, high frequency	Data goes off scale high at 66 sec	66 sec	66 sec	Apparent transducer failure. Redundant data on D131-115.
D159-115	Pressure, thermal conditioning purge	Data decreases in steps after liftoff	Liftoff	— —	Apparent sticky potentiometer wiper arm on transducer.
E036-102	Vibration, combustion chamber dome, longitudinal	High amplitude, low frequency noise on some power spectral densities	Liftoff	60 sec	ECP0333 changes out transducer.
E042-101	Vibration, fuel pump flange, radial	First power spectral density at -2 to -1 seconds shows high amplitude, low freq.	-2 sec	135 sec	Power spectral densities after 19 sec valid, ECP0333 changes out transducer.
E042-103	Vibration, fuel pump flange, radial	Power spectral densities at liftoff and 24 seconds show high amplitude, low freq.	Liftoff	128 sec	Power spectral densities after 24 sec valid; ECP0333 changes out transducer.
F044-101	Flowrate, LOX heat exchanger inlet, D.C.	Data reading low	Liftoff	0	RACS check showed signal conditioner gain decrease. Data can be corrected.
F049-115	Flowrate, joint leakage, PVC aft flange	Data off scale high from 62 sec to 105 sec	62 sec	110 sec	



Table 19-3. Measurement Malfunctions During Flight (Continued)

MEASUREMENT NUMBER	MEASUREMENT TITLE	NATURE OF FAILURE	TIME OF FAILURE (RANGE TIME)	DURATION SATIS. OPER.	REMARKS
PARTIAL MEASUREMENT FAILURES, S-IC STAGE (Cont.)					
L010-119	Segment identification, position II and IV	Erratic switching on Position II discrete sensors after segment number 7	68 sec	68 sec	Appears to be random failure.
S023-118	Strain, intertank skirt, longitudinal	Data trend not as expected after 80	80 sec	80 sec	Appears to be random failure
T001-101	Turbopump RPM	Erratic data between liftoff and 80 sec	Liftoff	72 sec	Threshold on signal conditioner set low. Noise triggers signal conditioner causing erratic data. Threshold level to be increased.
T-001-102	Turbopump RPM	Erratic data between liftoff and 73 sec	Liftoff	79 sec	Same as T001-010. ECP will be submitted.
PARTIAL MEASUREMENT FAILURES, S-II STAGE					
B004-200	Aft internal acoustic	Unknown spikes	After S-IC liftoff	- -	Appears transducer opened. Data step to 589°K (600°F) and erratic.  Transducer intermittent open.
C683-206	Heat shield aft surface temp	Data drops to zero	240 sec	240 sec	
C649-206	O <sub>2</sub> press regulator out temp	Erratic, step change	280 sec	280 sec	
C864-200	Ullage rocket #7 fair surface temp	Data loss	85 sec	85 sec	
C139-217	LOX common bulk-head surface temp	Intermittent		- -	
C820-219	Forward skirt heat rate	Large dropouts	Prior to S-II Ignition	- -	
PARTIAL MEASUREMENT FAILURES, INSTRUMENT UNIT					
C021-603	ST-124M methanol/water exit temperature 273° to 303°K (32° to 86°F)	Instantly dropped from normal 291° to 272°K (64° to 30°F) for 3 sec then went to 273°K (32°F) for remainder of flight until 12,390 sec when normal readings resumed.	80 to 12,390	More than 80 sec	No data is yet available between 700 and 11,100 sec.
C023-603	Cold plate exit coolant temperature 273° to 303°K (32° to 86°F)	Operated thru launch. Off scale high at 11,100 sec, but erratic until it failed at 11,495 sec, at start of S-IVB second burn. Data scattered toward high temp. limit for 105 sec. It then operated normally for 115 sec when indication went off scale high until 12,390 sec when normal readings resumed.	Between 700 and 11,100 to 12,390	More than 700 sec	
C024-603	LVDA/LVDC methanol/water exit temperature 273° to 303°K (32° to 86°F)	Temperature indication suddenly went to 305°K (90°F) and remained there until 12,390 sec when normal readings resumed.	80	More than 80 sec	
C066-601	Battery No. 3 internal temperature 273° to 333°K (32° to 140°F)	OK to 90 sec. Data scattered for about 20 sec before it dropped to 273°K (32°F) at about 105 sec. Normal readings resumed at 12,390 sec	84	More than 84 sec	

Table 19-4. Measurements with Insufficient Range

MEASUREMENT NUMBER	MEASUREMENT TITLE	NATURE OF OFFSCALE OUTPUT	TIME	REMARKS
S-IC STAGE				
C206-120	Temp amb. interstage area	Off scale low	87 sec to 137 sec	ECP changes range to 173° to 298°K (-148° to 77°F)
C207-120	Temp amb. interstage area	Off scale low	Throughout flight	Same as for C206-120. On scale on MTO at -11 hrs. and at -20 min. Goes off during J-2 engine chilldown.
C208-120	Temp amb. interstage area	Off scale low	83 sec to 136 sec	Same as for C206-120.
C209-120	Temp amb. interstage area	Off scale low	After 74 sec	Same as for C206-120.
D096-115	Press diff GOX control valve	Off scale high	At liftoff	Effect noted previously on static firing tests. Not unexpected.
D097-115	Press GOX control valve. LOX tank	Off scale high	At liftoff	Same as for D096-115.
E005-114	Vibration Fin D trailing edge	Insufficient range	Liftoff and 75 sec	Range insufficient for vibration excursion (high and low end of scale).
E009-112	Vibration Fin B leading edge	Insufficient range	Liftoff and 75 sec	Same as for E005-112.
E010-112	Vibration, Fin B trailing edge	Insufficient range	Liftoff and 75 sec	Same as for E005-114.
S-II STAGE				
C701-206	Thrust cone heat rate	Very low signal or no data	Liftoff	
C710-206	Heat shield aft surface temp	Off scale high		Data reads high and tops out. Data is usable.

Interaction was noted on temperature measurements in 11 of the 15 bridge chassis. Temperature measurement interaction occurs whenever a transducer fails or there is a rapid change of state on a measurement, and the effect of the failure or change is observable on all other temperature measurements common to the same power supply. The cause of the interaction has been isolated to a capacitor grounding scheme in the filter module section between the individual bridge modules and the common power supply of the temperature bridge chassis. Although the problem has not seriously affected the usefulness of the data, it is an undesirable condition. Corrective action will be made on S-II-2 and subsequent stages to change the capacitor grounding scheme in the filter modules on each bridge chassis.

The measurement interaction also affected the temperature bridge power supply voltage measurements but did not affect the usefulness of the data. Eleven of the 15 voltage measurements were affected.

A number of temperature measurements did not experience the predicted temperature environment during the flight. As a result, these measurements provided only a minimum of usable data. These measurements are being investigated for range changes on subsequent stages.

The fuel pump inlet temperature measurement on engine No. 2 failed to come into the starting box prior to launch. This problem will be resolved on subsequent vehicles by the deletion of the recirculation delta temperature measurements which contributed to the problem.

The acoustic environment during liftoff and through the MACH 1 and maximum Q portions of the flight was lower than predicted. The feasibility of measurement range and location changes is presently under investigation. One acoustic measurement (B004-200) was listed as a partial measurement failure because of unexplained spikes in the data after S-IC liftoff. Complete analysis of this measurement is dependent on the completion of power spectral density plots.

A group of pressure measurements went to or near the full scale limit during flight. This condition had been noted previously on static firing tests. Range changes are being investigated to correct this problem.

### 19.2.3 S-IVB Stage Measurement Analysis

There were 577 flight measurements scheduled for the S-IVB stage. Of these, one measurement was waived prior to the automatic countdown, 27 measurements were deleted from incentive considerations by installation of the anti-flutter kit on the forward skirt and one measurement was inactive. During Phase I (liftoff to parking orbit insertion) there were five measurement failures. During Phase II (liftoff to S-IVB/Spacecraft separation) there were eight additional failures. Of the 27 measurements that were removed from incentive consideration, three failed in the orbital period. Based

upon 548 measurements active at the start of automatic countdown and five failures during Phase I, the measurement reliability for this period was 99.1 percent. Based upon 548 measurements active at the start of automatic countdown and 13 failures during Phase II, the measurement reliability for this period was 97.6 percent. Measurements waived prior to launch and measurement failures are summarized in Tables 19-2 and 19-3.

Six of the temperature measurement failures appeared to be caused by temperature patch debonding. The original temperature patch installations on S-IVB were fiberglass supported platinum wire units bonded to the structure and potted for mechanical protection. Early static firing acceptance testing proved this method to be unreliable at cryogenic temperatures and a new installation method was devised utilizing ceramic supported platinum wire units bonded to the structure with a swath of fiberglass cemented over each patch for mechanical protection. This method proved successful and all new temperature patch installations were made using this method. All installations on the interior of the LH<sub>2</sub> and LOX tank were reworked to the new installation. External installations were reworked on an as-they-failed basis. As a result, most of the external temperature measurements on AS-501 were still of the old installation at liftoff, and debonding is believed to be the cause of the failures.

The failure of pressure measurements D181-409 and D182-409 (press-fuel tank continuous vent, one and two respectively) is of particular significance. These measurements, prior to S-IVB engine restart, were interpreted as indicating a gas flow in the continuous vent system after the continuous vent control valve had been commanded to close. This resulted in several ground commands, presented in Table 2-4, being issued to close the valve, as discussed in paragraphs 7.5 and 7.10.1. The transducers used for these measurements had a range of 0 to 17.24 N/cm<sup>2</sup> (25 psia). Similar transducers with a range of 0 to 34.47 N/cm<sup>2</sup> (50 psia) were qualified to a low temperature of 77.6°K (-320°F) with an accuracy of  $\pm 2.8$  percent full scale. Except for their range, both units are of identical construction. They were designed to operate to a low temperature of 22°K (-420°F); however, all attempts to qualify these units for reliable data at temperatures below the specification limit of 77.6°K (-320°F) were unsuccessful. Qualification test data indicated that temperature compensation diverged sharply from unit to unit at temperatures below 77.6°K (-320°F) due to erratic characteristics, at these lower temperatures, of the Balco wire used in the temperature compensation circuits. Temperature data from locations near the transducers used for measurements D181-409 and D182-409 indicated that the transducers were subjected to temperatures approaching 29°K (-406°F). Examination of flight data indicated that the transducers were subjected to temperatures approaching 29°K (-406°F). Examination of flight data indicated that transducer outputs began diverging and drifting out of tolerance as soon as they were cooled below 77.6°K (-320°F). This correlates closely with previous experiences in qualification testing and is believed to be the cause of the anomaly. This problem will be eliminated on future stages by relocating the transducers, which are mounted directly on the vent lines.

---

1. Douglas Aircraft Test Report Number TM-DSV-4B-EE-R-5537, paragraphs 5.2.2.2 and 5.2.2.3, pages 46 and 47, and addenda C-106 through C-110.

#### 19.2.4 Instrument Unit Measurement Analysis

There were 337 flight measurements scheduled for the Instrument Unit. No measurements were waived prior to the automatic countdown, none failed in flight, and four were partially successful. Based upon 337 measurements active at the start of automatic countdown with zero failures during flight, the resultant reliability is 100 percent. Partial measurement failures are summarized in Table 19-3.

Three measurements failed during the high vibration period from 80 to 90 seconds. Measurement C023-603 experienced a data dropout from 81 to 83 seconds, failed prior to S-IVB stage second burn, recovered, became erratic, and failed again at S-IVB stage reignition. All four measurements became valid again at approximately 12,390 seconds coincident with a 1.2°K spike in IU internal ambient temperature (C036-601) and LV/SC separation.

Vibration appeared to be the probable cause of failure of three of the measurements. Poor connections somewhere in the measuring system appeared to be the underlying cause for all four measurement failures. The exact nature of the failure has not been determined.

#### 19.3 AIRBORNE TELEMETRY SYSTEMS

There were 23 telemetry links used to transmit flight data on the AS-501 launch vehicle: six on the S-IC stage, six on the S-II stage, five on the S-IVB stage, and six on the Instrument Unit. Performance of the telemetry system was generally satisfactory.

There were approximately 5.3 to 7.8 seconds of real time data lost on all S-IC stage telemetry links. Critical data were recovered, however, by airborne tape recorder playback covering these periods. S-IC stage link AF-1 experienced a considerable reduction in RF power at 158.4 seconds which lasted until loss of received radio signals (410 seconds). Data were lost at CIF and GBI; however, the data were recovered by the airborne recorder playback received at Cape TEL 4. Numerous noisy time periods occurred in the recorder playback of S-II stage telemetry link BF-1. This anomaly was caused by low signal level at Bermuda. All VHF telemetry links were lost in the vehicle for approximately 0.6 to 1.0 second due to S-IC/S-II staging effects. These dropouts were anticipated and data recovery was made via tape recorder playback except for data lost on the S-II stage BF-1 link. With the exceptions noted above, all the telemetry links performed as expected. A summary of the telemetry system performance is shown in Table 19-5.

##### 19.3.1 S-IC Stage Telemetry System

There were six telemetry links used to transmit flight data on the S-IC stage: three PAM/FM/FM links, two SS/FM links, and one PCM/FM link.

Table 19-5. AS-501 Launch Vehicle Telemetry Links

LINK	FREQUENCY (MHz)	MODULATION	STAGE	FLIGHT PERIOD (RANGE TIME, SEC)	PERFORMANCE SUMMARY										
AF-1	240.2	PAM/FM/FM	S-IC	0-410	Satisfactory. AF-1 had a sharp decrease in signal strength 158.4 to 410 sec. (Ref. 19.3.1)  <u>Data Dropouts</u> <table><tr><th>Range Time (sec)</th><th>Duration (sec)</th></tr><tr><td>136.5</td><td>2.0</td></tr><tr><td>151.2</td><td>1.5</td></tr><tr><td>154.5</td><td>1.5</td></tr><tr><td>Approx. 157.5</td><td>0.15 to 2.75 dependent on link</td></tr></table>	Range Time (sec)	Duration (sec)	136.5	2.0	151.2	1.5	154.5	1.5	Approx. 157.5	0.15 to 2.75 dependent on link
Range Time (sec)	Duration (sec)														
136.5	2.0														
151.2	1.5														
154.5	1.5														
Approx. 157.5	0.15 to 2.75 dependent on link														
AF-2	252.4	PAM/FM/FM	S-IC	0-410											
AF-3	231.9	PAM/FM/FM	S-IC	0-410											
AP-1	244.3	PCM/FM	S-IC	0-410											
AS-1	235.0	SS/FM	S-IC	0-410											
AS-2	256.2	SS/FM	S-IC	0-410											
BF-1	241.5	PAM/FM/FM	S-II	0-756*	Satisfactory except for noisy playback of BF-1 as received at Bermuda. (Ref. 19.3.2)  <u>Data Dropouts</u> <table><tr><th>Range Time (sec)</th><th>Duration (sec)</th></tr><tr><td>151.5</td><td>0.6 to 1.0</td></tr></table>	Range Time (sec)	Duration (sec)	151.5	0.6 to 1.0						
Range Time (sec)	Duration (sec)														
151.5	0.6 to 1.0														
BF-2	234.0	PAM/FM/FM	S-II	0-756*											
BF-3	229.9	PAM/FM/FM	S-II	0-756*											
BP-1	248.6	PCM/FM	S-II	0-756*											
BS-1	227.2	SS/FM	S-II	0-756*											
BS-2	236.2	SS/FM	S-II	0-756*											
CF-1	258.5	PAM/FM/FM	S-IVB	Full Duration	Satisfactory. Link CP-1 did not experience this data dropout at the TEL 4 station. (Ref. 19.3.3)  <u>Data Dropouts</u> <table><tr><th>Range Time (sec)</th><th>Duration (sec)</th></tr><tr><td>151.5</td><td>0.6 to 1.0</td></tr></table>	Range Time (sec)	Duration (sec)	151.5	0.6 to 1.0						
Range Time (sec)	Duration (sec)														
151.5	0.6 to 1.0														
CF-2	246.3	PAM/FM/FM	S-IVB	Full Duration											
CF-3	253.8	PAM/FM/FM	S-IVB	Full Duration											
CP-1	232.9	PCM/FM	S-IVB	Full Duration											
CS-1	226.2	SS/FM	S-IVB	Full Duration											
DF-1	250.7	FM/FM	IU	Full Duration	Satisfactory.  <u>Data Dropouts</u> <table><tr><th>Range Time (sec)</th><th>Duration (sec)</th></tr><tr><td>151.5</td><td>1.0</td></tr><tr><td>S-II Retro Firing</td><td>1.0</td></tr></table>	Range Time (sec)	Duration (sec)	151.5	1.0	S-II Retro Firing	1.0				
Range Time (sec)	Duration (sec)														
151.5	1.0														
S-II Retro Firing	1.0														
DF-2	245.3	PAM/FM/FM	IU	Full Duration											
DS-1	259.7	SS/FM	IU	Full Duration											
DP-1	255.1	PCM/FM	IU	Full Duration											
DP-1A	2277.5	PCM/FM	IU	Full Duration											
DP-1B	2282.5	CCS	IU	Full Duration											

\* Only 756 seconds of data were assessed.  
Powered flight ship data not included.

Transmission of data from all six S-IC links was generally satisfactory during flight with the exception of four significant data dropout periods. The first data dropout occurred at approximately 136.5 seconds and lasted for approximately 2 seconds. This dropout is yet to be explained. Three other periods of data loss occurred at 151.2 seconds (1.5 seconds), 154.5 seconds (1.5 seconds), and approximately 157.5 seconds (0.15 to 2.75 seconds); the first two periods were associated with S-IC/S-II staging and S-II stage ignition, respectively, and the third period is as yet unexplained. Data from the AF-1 and AF-2 links were recovered from the airborne tape recorder playback.

Link AF-1 experienced a considerable reduction in RF output power at 158.4 seconds which lasted until loss of received radio signal at 410 seconds. The cause for the reduction of signal strength was believed to be a partial failure of the RF assembly or the cable from the power amplifier to the VSWR monitor. The incident power measured by the VSWR monitor decreased to less than 1 watt at this time with a simultaneous decrease in reflected power, indicating that no anomaly occurred with respect to the antenna subsystem. This reduction in RF power caused loss of data at the CIF ground station but did not cause loss of data at TEL 4 ground station. This was because of the higher gain antenna at TEL 4. The airborne tape recorded data received at TEL 4 during this period were satisfactory. The RF incident power, as indicated by the VSWR monitor for link AP-1, was 11.6 watts during flight. However, watt meter RF power measurements made on this link prior to flight indicated an output power of 16.1 watts, whereas a simultaneous VSWR monitor measurement indicated 11.1 watts. This indication is within VSWR monitor specifications.

Noise analyses were performed on telemetry data recorded on magnetic tapes at the CIF and TEL 4 ground stations. With the exception of the periods of RF dropouts, the 3 sigma noise was less than 3.2 percent of full scale for all six telemetry links, based on TEL 4 data.

Calibration of the subcarrier oscillators, low frequency sampled data channels, and high frequency single sideband channels was conducted satisfactorily twice during flight. These calibrations took place as scheduled beginning at 25.21 seconds and 115.21 seconds. Each of the five step levels initiated by the inflight calibrator was applied to the proper data channel for a period of approximately 140 milliseconds. The duration of each 270 channel multiplexer calibration equaled the prescribed 83.3 milliseconds. Each calibrate level from both the inflight calibrator and multiplexer calibrators was well within 0.5 percent of full scale at the specified level. The frequency of the single sideband inflight calibration was approximately 1700 hertz and calibration magnitudes were approximately 40 percent of full scale. Each single sideband link was calibrated for a period of approximately 1.5 seconds. No data channels were out of calibration.

A summary of telemetry system performance is shown in Table 19-5.

### 19.3.2 S-II Stage Telemetry System

There were six telemetry links used to transmit flight data on the S-II stage: three PAM/FM/FM links, two SS/FM links, and one PCM/FM link. Transmission of data from all six S-II links was satisfactory during flight except for a 0.6 to 1.0 second period at S-IC/S-II separation (approximately 151.5 seconds) during which data were lost from all links due to staging effects. The data from the BF-1, BF-2, and BF-3 links and selected discrete data involved in the separation sequence were recorded during these periods and played back after S-II/S-IVB separation. GBI received data signals through approximately the first 25 seconds of playback while Bermuda, although receiving the entire tape recorder playback, had numerous noisy time periods on link BF-1. Data from the powered flight ship was of such poor quality because of ground receiver problems that it could not be used. All transmitters, multiplexers, and oscillators were operational until S-II flight termination.

Selected measurements were evaluated to determine the proper functional operation of the telemetry equipment to the black box level. All measurements were operable and indicated proper telemetry equipment operation.

The encoding accuracy of the PCM was determined by an evaluation of Frames 9 and 10 of Channel 28 of each time division multiplex (TDM). Frame 9 had a 0 volt level and Frame 10 had a 5 volt level. These evaluations were made just prior to each inflight calibration period (four periods during S-II flight). The encoding accuracy throughout the S-II flight was within 0.5 percent (less than 5 PCM counts).

Four inflight calibrations were performed on the S-II telemetry system. The calibration of the IRIG continuous channels and the TDM's was a five-step calibration at levels of 0, 1.25, 2.5, 3.75, and 5.0 volts. An evaluation of the PCM decimal counts showed that all levels of calibration on the TDM's were within  $\pm 1$  percent. PAM calibration levels were within  $\pm 2$  percent with noise spikes up to 3 percent on BF-2 and BF-3 and up to  $\pm 5$  percent on BF-1. These values were obtained from tapes received from KSC. GBI tapes were much quieter and are being further analyzed for accuracy and noise.

The SS/FM calibration is a single discrete frequency of 1700 hertz. Total evaluation of the SS/FM calibrations could not be made due to the lack of SS/FM data from GBI and the Powered Flight Ship. Correlation of the first two calibrations received at TEL 4 and the three received at Bermuda indicated that the SS/FM was operating properly, and a review of measurements indicated that good data were received. A summary of telemetry system performance is shown in Table 19-5.

### 19.3.3 S-IVB Stage Telemetry System

There were five telemetry links used to transmit flight data on the S-IVB stage: three PAM/FM/FM links, one PCM/FM link, and one SS/FM link.



Transmission from all five links was satisfactory during flight except for a 0.6 to 1.0 second period at S-IC/S-II separation (approximately 151.5 seconds) during which data were lost from all links at all sites, except CP-1 link at TEL 4. Even though link CP-1 was attenuated at the TEL 4 ground receiving station, data were successfully processed from this site. Data from this link were lost at the other sites. The data from the CF-1, CF-2, and CF-3 links were recorded during these periods and played back after S-IVB first cutoff. All transmitters, multiplexers, and oscillators were operational until S-IVB flight termination.

Inflight calibrations of the FM/FM systems were successfully accomplished. The calibration command necessary to calibrate the single sideband system prior to second burn was not in the flight sequence of events. As a result, there were no single sideband calibrations for second burn data. A summary of the telemetry system performance is shown in Table 19-5.

#### 19.3.4 Instrument Unit Telemetry Systems

There were six telemetry links used to transmit flight data in the Instrument Unit: one FM/FM link, one PAM/FM/FM link, one SS/FM link, one PCM/FM link (VHF), one PCM/FM link (S-Band), and one CCS link. Transmission of data from all Instrument Unit VHF links was satisfactory during flight except for a 1.0 second period at S-IC/S-II separation (approximately 151.5 seconds) and a 1.0 second period at S-II interstage jettison during which transmission was lost from some links. The data from the DF-1 and DF-2 links were recorded during retro motor firing periods and played back after S-IVB cutoff. The CCS link lost data during these periods and also lost data at 189.5 seconds and at handover. The length of the data loss on the CCS was greater than the loss on other links because of ground station operational problems. The S-Band PCM/FM link lost data for 0.6 second at S-IC/S-II staging.

All transmitters, multiplexers, and oscillators were operational throughout the entire Instrument Unit flight period. Evaluation of selected measurements indicated proper telemetry equipment operation. Inflight calibrations were successfully accomplished.

A summary of telemetry system performance is shown in Table 19-5.

#### 19.4 AIRBORNE TAPE RECORDERS

The airborne tape recorders record and store for subsequent transmission portions of data that would otherwise be lost due to flame effects or visibility constraints at receiving stations. Performance of all onboard recorders was satisfactory throughout the flight. A summary of vehicle tape recorders is presented in Table 19-6.

Table 19-6. Tape Recorders Summary

RECORDER	LINK RECORDED	RECORD TIME (RANGE TIME)		PLAYBACK TIME (RANGE TIME)	
		START	STOP	START	STOP
LAUNCH PHASE					
S-IC Recorder	AF-1 AF-2	49.72	175.0	175.0	300.3
S-II Recorder #1	BF-1 BF-2	74.32 482.33	162.04 542.2	542.2	640.6
S-II Recorder #2	BF-3 BT-1	74.32 482.33	162.04 542.2	542.2	640.6
S-IVB Recorder	CF-1 CF-2 CF-3	134.12 482.12	162.22 541.02	764.15	854.14
IU Recorder	DF-1 DF-2	134.21 481.94	161.82 538.63	767.33	853.34*
ORBITAL PHASE					
S-IVB Recorder	CP-1				
Playback at:					
Tananarive		954.14	2264.15	2264.35	2429.35
Guaymas		2511.14	5311.78	5311.78	5661.95
Tananarive		5662.15	7765**	7765**	8009.15
Hawaii		8009.35	10257.18	10257.38	10541.37
		10541.57		***	

\* Computed value - not confirmed.

\*\* Programed time. Onsite acquisition did not occur until approximately 7825 seconds.

\*\*\* Not programed for replay.

#### 19.4.1 S-IC Stage Recorder

The S-IC stage recorder successfully recorded telemetry links AF-1 and AF-2. The tape recorder record command and the playback command occurred as scheduled as shown in Table 19-6. The duration of the airborne timer which initiates recorder playback was 23.5 seconds and is within specifications.

Data were recorded by the airborne recorder for a period of 125 seconds. Examination of the playback information from the TEL 4 magnetic tapes indicated excellent reproduction of the recorded signals.

#### 19.4.2 S-II Stage Recorders

The two S-II stage tape recorders successfully recorded and played back the BF-1, BF-2, and BF-3 telemetry links and selected discrete data pertinent to the separation sequence. The discrete data were time division multiplexed via the BTR multiplexer and the playback transmitted on the BS-1 single sideband telemetry link.

The S-II airborne tape recorders and associated hardware performed as required and within specification limits except for BF-1 telemetry link playback. Grand Bahama Island received signals through approximately the first 25 seconds of tape recorder playback, while Bermuda acquired data throughout the total tape recorder playback. The analysis of the tape recorder system was conducted primarily on the data obtained from Bermuda. Numerous noisy time periods occurred in the Bermuda data playback of BF-1.

An analysis was performed on the tape recorder data to determine changes in data levels due to recording and playback of telemetered data. This was accomplished by evaluating oscillograph recordings of continuous channels of BF-1, BF-2, and BF-3 and by comparing the PAM decimal counts data during final inflight calibration between real time transmission and tape recorder playback. The present requirement is that the tape playback data shall be within  $\pm 3$  percent of the real time recorded test data.

The data on the continuous BF-2 and BF-3 channels appears to vary from real time data only to the extent that additional noise was present on the signal. This noise content resulted in a maximum delta in data levels of  $\pm 1.25$  percent, which is within the required  $\pm 3$  percent limit. The PAM calibration data for BF-2 and BF-3 multiplexers also showed agreement between real time and recorder playback. Nominal data level differences were four to five decimal counts out of 227 or approximately 2 percent. The BTR multiplexer calibration levels were all within the required calibration limits of  $\pm 200$  millivolts. The four calibration steps of 1.25, 2.5, 3.75 and 5.0 volts showed very close agreement and fell within 50 millivolts. The 0 volt calibration level, however, was noisier and indicated a level difference of 100 millivolts.

The BF-1 continuous channel data and multiplexer data during tape recorder playback were very noisy. Approximately 5 to 10 percent of the PAM channels were out of the  $\pm 3$  percent tolerance. Since this noise continued on the BF-1 data link after the tape recorder playback was switched off and real time data transmission was resumed, it appears at this time that the problem was not associated with the operation of the tape recorder equipment. This problem is presently under investigation. Table 19-6 summarizes the inflight S-II tape recorder operation.

#### 19.4.3 S-IVB Stage Recorder

The S-IVB stage tape recorder successfully recorded and played back the CF-1, CF-2 and CF-3 telemetry links during the launch phase and the CP-1 telemetry link during the orbital phase. Onsite acquisition at Tananarive occurred at approximately 7825 seconds. Approximately 60 seconds of recorder playback was lost because the station did not acquire signal until 60 seconds after the vehicle appeared over the horizon. Data recorded between Hawaii and Guaymas on the second pass were not played back. The playback of these data was withheld at Guaymas because of flight control constraints.

All airborne tape recorded data were successfully merged with real time data. The airborne tape recorder and playback times available in time for this report are presented in Table 19-6.

#### 19.4.4 Instrument Unit Recorder

The Instrument Unit tape recorder successfully recorded and played back the DF-1 and DF-2 telemetry links.

Two record periods were programed: the first started at 134.21 seconds and ended at 161.82 seconds; the second period started at 481.94 seconds and ended at 538.63 seconds. Data were recorded for approximately 81.4 seconds. Playback reverse command was issued at 767.3 seconds. Playback should have terminated at 852.3 seconds. This has not been confirmed for this report because of the lack of data.

### 19.5 RF SYSTEMS EVALUATION

The overall performance of launch vehicle RF systems was excellent. Based on the analysis performed to date the measured flight data, with few exceptions, agreed favorably with predictions. Telemetry propagation was excellent and data lost due to engine flame and staging effects were recovered by the airborne tape recorder playbacks. Tracking performance throughout the flight was satisfactory. The Command and Communications System performed extremely well.

#### 19.5.1 Telemetry Systems RF Propagation Evaluation

The usual propagation difficulties due to engine flame and staging effects were encountered. S-IC main engine flame effects, resulting in signal strength fluctuation and attenuation, were as predicted. The attenuation at Cape TEL 4 varied between 15 and 25 db, which was less than the signal strength fluctuations experienced with Saturn I and Saturn IB vehicles.

An unexplained dropout of S-IC stage VHF telemetry was experienced between 136.5 and 138.5 seconds. This effect was noted at Cape TEL 4, CIF and GBI.

Tape recorder playback data on the S-IC telemetry links during this time period indicated variations in antenna reflected power and incident power. Abnormal attenuation on the higher frequency systems such as ODOP, UHF telemetry, CCS, AZUSA/GLOTRAC and C-band radar was experienced at this time. Effects on S-II VHF telemetry signals were less severe and no effects were noted on the S-IVB and IU telemetry records. This anomaly occurred within 1 second after the time of S-IC inboard engine cutoff at 135.47 seconds and may be related to this event. The cause of this anomaly has not been conclusively determined and further investigation will be conducted to determine performance impact and recurrence possibilities for future flights.

Staging effects were as expected. All VHF telemetry links went to threshold at 151.5 seconds during S-IC/S-II staging except for the CP-1 telemetry link at TEL 4 receiving station. This resulted in VHF telemetry data loss at all sites for approximately 0.6 to 1.0 second except for the data successfully recovered from the CP-1 link received at TEL 4. No data losses were observed during S-II/S-IVB staging.

Effects of the second stage ignition on the RF systems transmission were more severe than on Saturn IB flights. Cape TEL 4 and CIF data show attenuation up to 20 db for all S-II, S-IVB, and IU VHF links, with no effect on the GBI recorded transmission. S-IC VHF telemetry experienced severe attenuation and approximately 0.15 to 2.75 seconds data loss to both uprange and GBI sites.

The S-IC stage AF-1 telemetry link experienced a sharp decrease in RF output power at 158.4 seconds. The incident power decreased to less than 1 watt at this time with a simultaneous decrease in reflected power, indicating no anomaly in the antenna subsystem. The output power remained low for the remainder of S-IC flight. The cause of this anomaly was believed to be a partial failure of the RF assembly or cable from the power amplifier to the VSWR monitor. This reduction in RF power caused loss of data at the CIF ground station; however, data from this link were recovered from the airborne tape recorder playback at Cape TEL 4.

Effects resulting from the S-II second plane separation were not anticipated, but did result in 20 to 25 db attenuation of the S-II, S-IVB, and IU VHF telemetry systems transmission to the Cape sites. Transmission to GBI was not affected. UHF telemetry experienced 25 db peak attenuation. The CCS data recorded at CIF and MILA/USB show a phase unlock condition at this time (182.2 seconds) lasting until 185.8 seconds at CIF and until 205 seconds at MILA/USB.

Ionospheric effects were as observed on previous flights, posing no threat to telemetry data acquisition. These are phenomena resulting in signal fluctuations to those ground sites looking through the S-II exhaust plume and are believed to be caused by the interaction of the plume and ionospheric layers. Several sharp drops, unlike the usual ionospheric effects, were

observed on the Cape TEL 4 VHF signal strength data but were not present on the GBI data.

Orbital telemetry signal strength levels were as predicted and no major anomalies were observed.

A summary of the telemetry systems general performance is shown in Figures 19-1 and 19-2.

#### 19.5.2 Tracking Systems RF Propagation Evaluation

Tracking performance throughout the flight was satisfactory. No major anomalies occurred, although some minor effects were observed which are being evaluated to determine the potential impact on systems performance and possible improvement for subsequent flights.

The tracking systems for the different stages are tabulated in Table 19-7.

Table 19-7. AS-501 Onboard Tracking Systems

VEHICLE LOCATION	SYSTEM	ONBOARD TRANSMITTER FREQUENCY (MEGAHERTZ)	ONBOARD RECEIVER FREQUENCY (MEGAHERTZ)
S-IC	ODOP	960	890
IU	Azusa/Glotrac	5000	5060.194
IU	C-Band Radar	5765	5690
IU	CCS	2282.5	2101.8

19.5.2.1 ODOP - A performance and coverage summary of the ODOP system on the S-IC stage is shown in Figure 19-3. The ODOP flight data indicate that tracking performance was satisfactory until approximately 105 seconds, when flame effects began to degrade both the interrogation transmission and the ground received signals to a level of marginal performance. Intermittent phase unlock periods at the respective receiving sites continued from this time until S-IC/S-II separation (151.4 seconds), at which time all sites lost phase lock until approximately 180 seconds. The onboard ODOP receiver phase lock measurement indicates loss of lock from 152 to 194 seconds.

An unexplained but short duration (2 to 3 seconds) of low signal level and phase modulation occurred at approximately 44 seconds at all receiving sites. The onboard receiver AGC measurement indicates a gradual decrease of signal strength beginning at 33 seconds and reaching a maximum drop of 35 db in signal level at 42.3 seconds coincident with the effects observed on the received data. No phase unlock conditions were observed nor were postflight tracking data affected at this time.

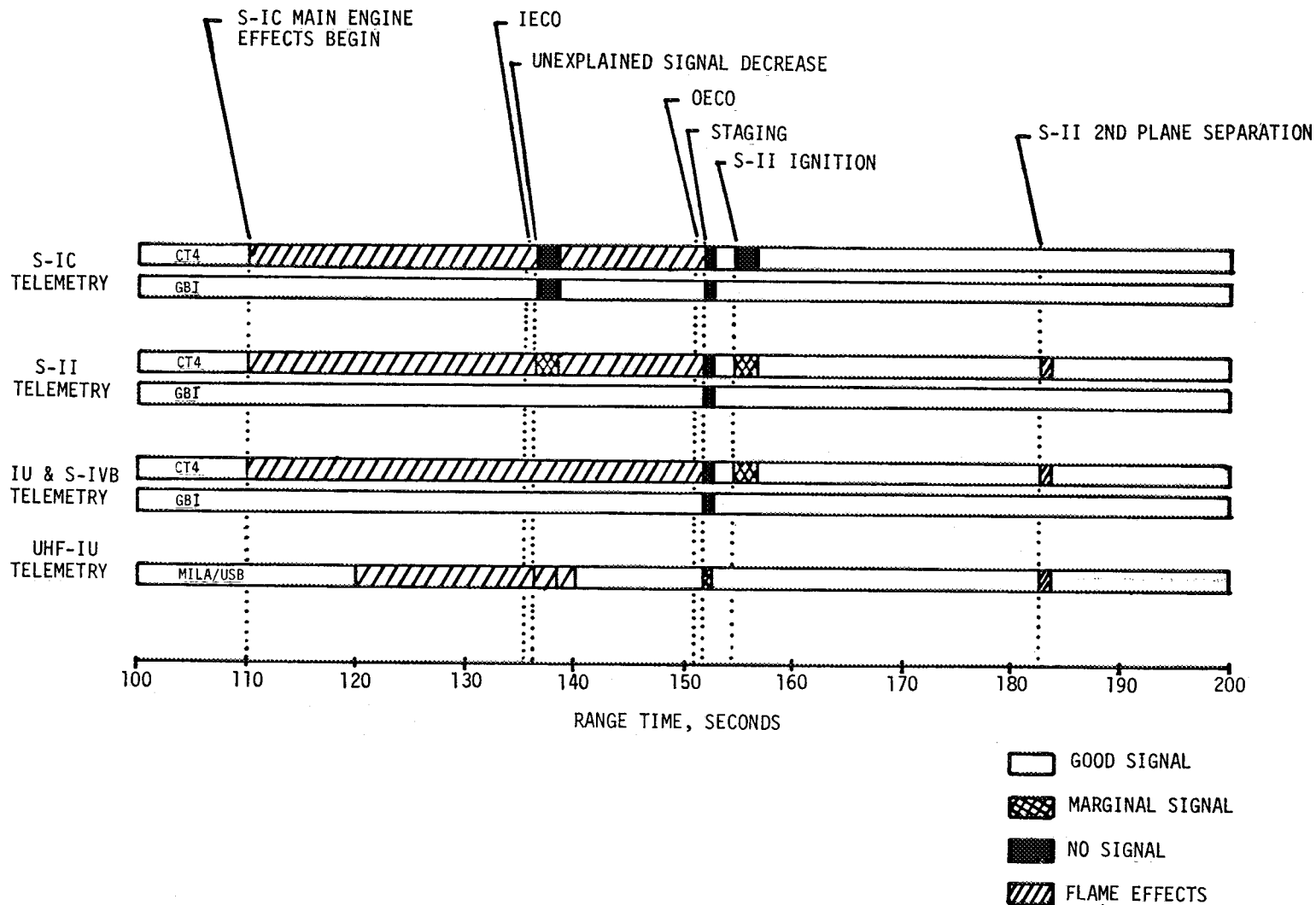


Figure 19-1. VHF Telemetry Coverage, Launch Phase 100 to 200 Seconds

19-24

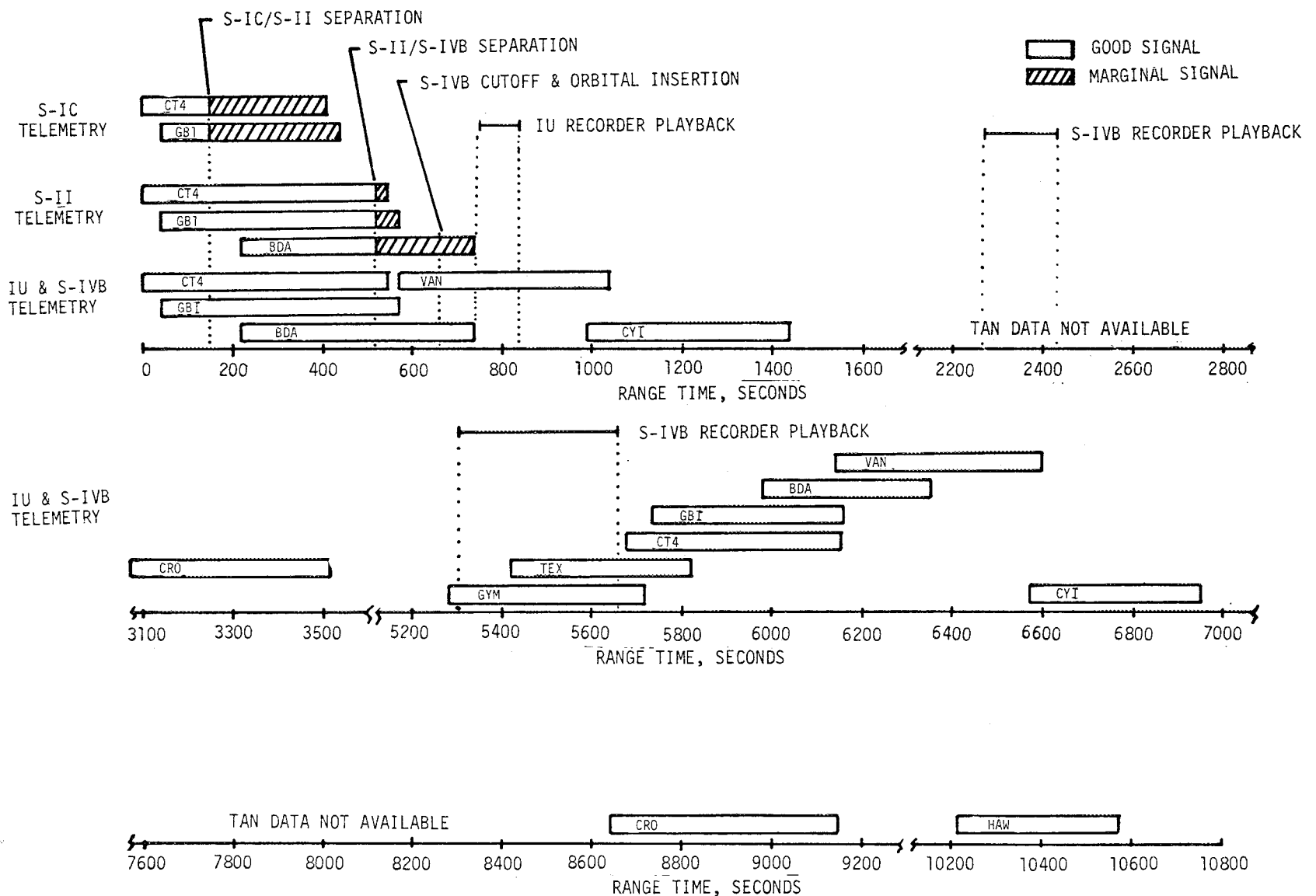
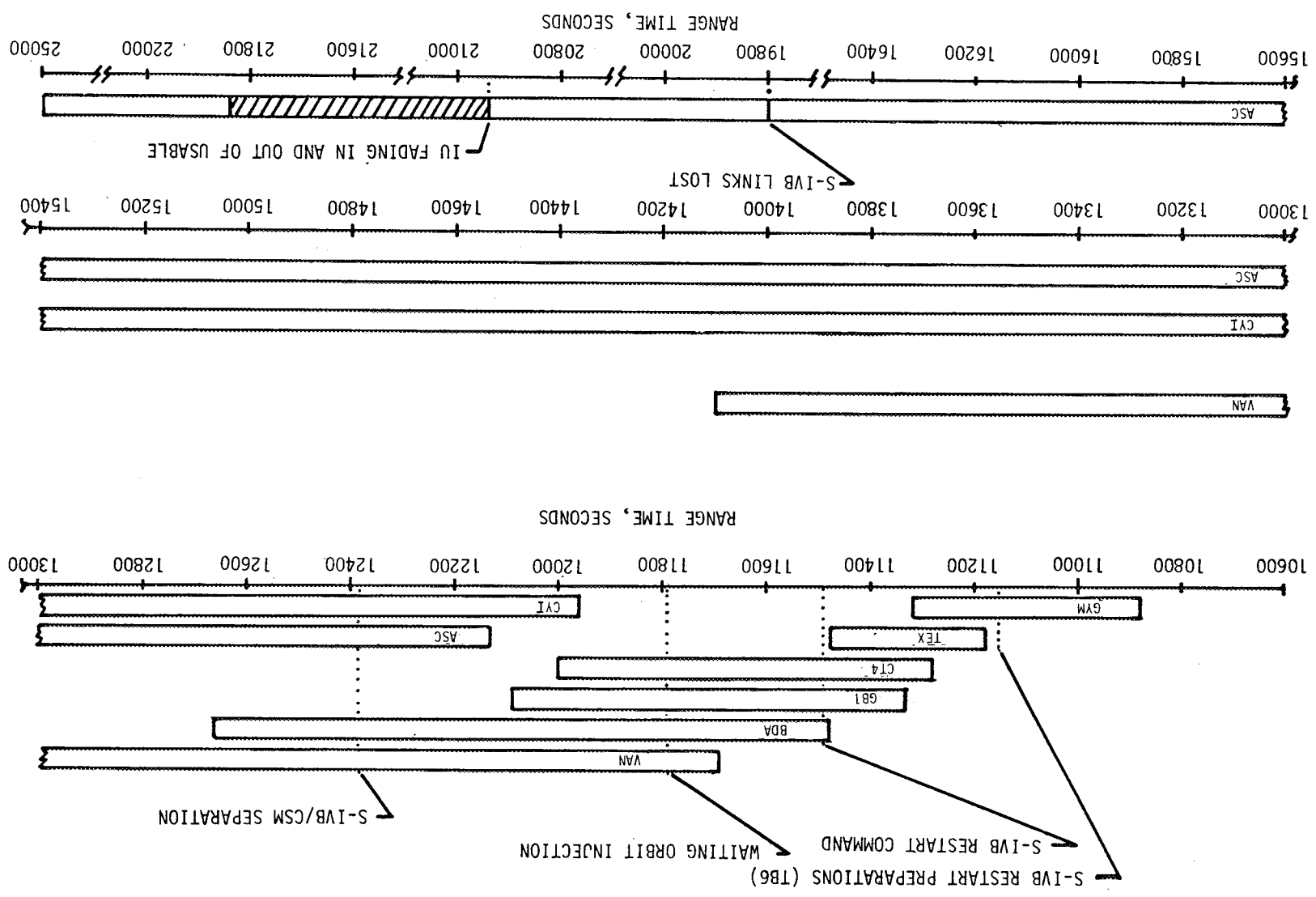


Figure 19-2. VHF Telemetry Coverage Summary, Sheet 1 of 2



Figure 19-2. VHF Telemetry Coverage Summary, Sheet 2 of 2



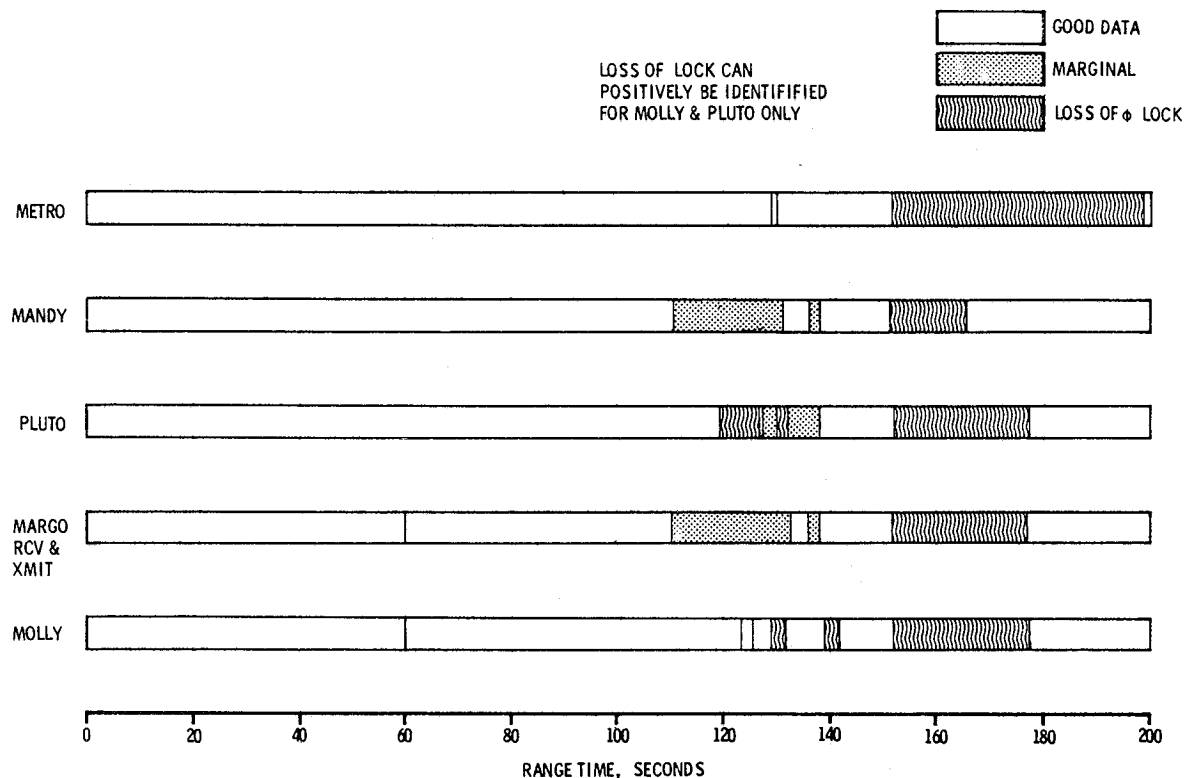


Figure 19-3. ODOP Coverage Summary

Another effect of particular interest was observed between 136.5 and 138.5 seconds when all ODOP receiving sites experienced a drop in signal level. This effect was coincident with S-IC VHF telemetry dropout period and signal attenuation on the IU S-Band and C-Band systems. The cause for this anomaly has not yet been determined.

19.5.2.2 Azusa/Glotrac - The performance of the Azusa/Glotrac system appeared to be satisfactory and in accordance with nominal expectations. Glotrac Station I tracked successfully from liftoff to 260 seconds. Grand Turk accepted active interrogation of the transponder at 283 seconds and maintained track until handover to Bermuda at 564 seconds. Tracking data were simultaneously obtained at all Glotrac stations within view of the vehicle throughout most of the flight.

Flight data indicated that Station I lost phase lock prior to scheduled handover to Grand Turk. This had been a recurring problem on previous flights and was attributed to extremely low aspect angles to this sight. Proper operation of the Azusa transponder was indicated by the steady level of the transponder power output measurement J001-603.

General Azusa/Glotrac coverage summary is shown in Figure 19-4.

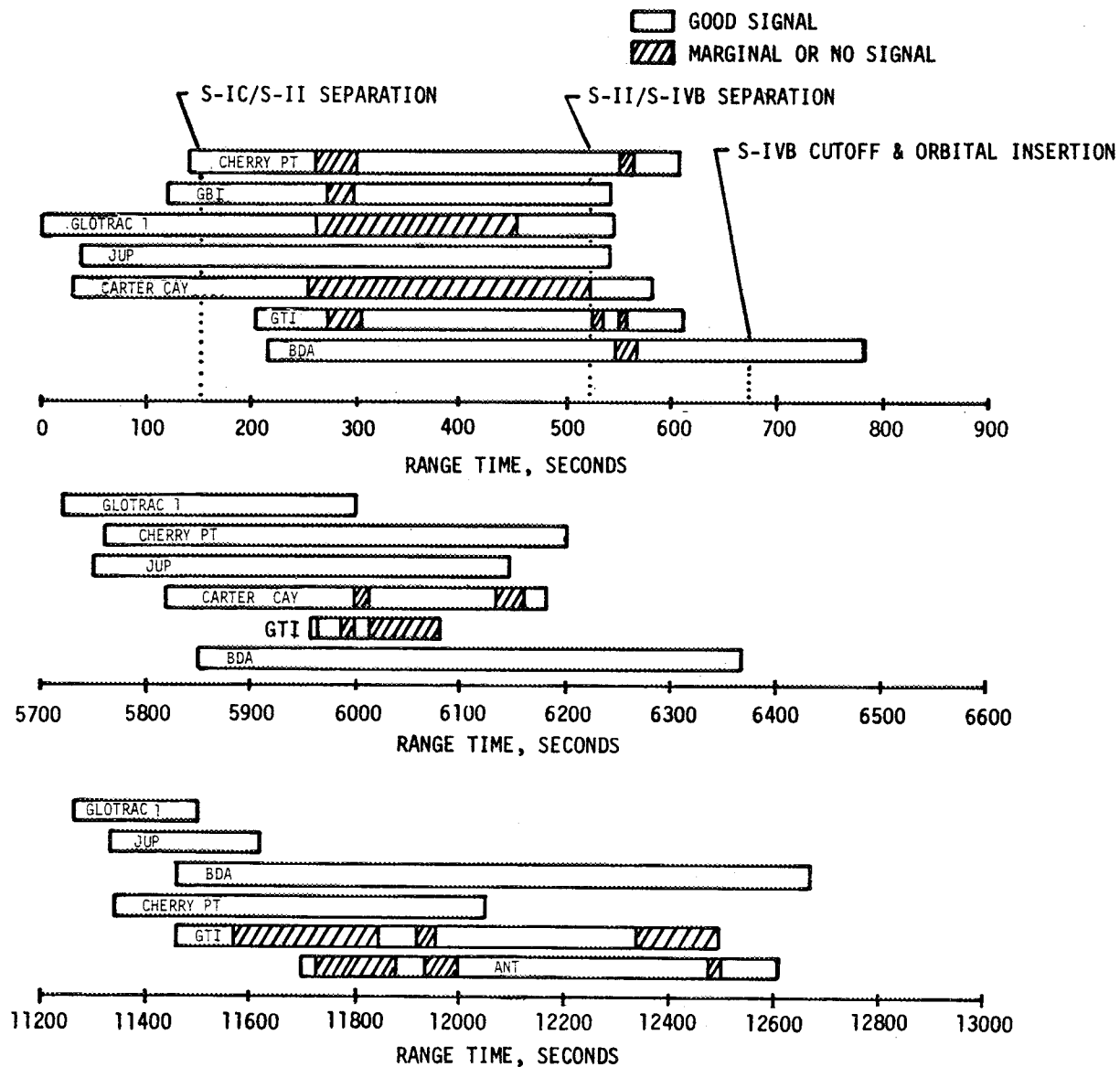


Figure 19-4. Azusa/Glotrac Coverage Summary

19.5.2.3 C-Band Radar - The performance of the launch vehicle C-Band radar systems appeared to be satisfactory throughout the flight. The simultaneous operation of two beacons during the launch phase without data loss was shown to be feasible. The PAFB site was able to satisfactorily track the IU beacons to approximately 410 seconds, losing track slightly earlier than usual because of a low elevation angle and low signal levels resulting from the antenna patterns.

A C-Band flight coverage summary is shown in Figure 19-5.

### 19.5.3 Command Systems RF Evaluation

19.5.3.1 Secure Range Safety Command System - Data indicated that the Secure Range Safety Command System (SRSCS) antennas and receivers operated satisfactorily in the S-IC, S-II, and S-IVB stages. S-IC predicted signal levels were above measured signal levels; however, this has occurred in past flights and is attributed in part to calibration inaccuracies of the onboard system. Signal levels compared favorably with the levels in Saturn IB vehicles.

19.5.3.2 Command and Communications System - The Command and Communications System (CCS) appeared to have performed extremely well. All supporting sites obtained good data, and only minor discrepancies, as indicated in Figures 19-6 through 19-9, were noted. These occurred primarily at the MILA/USB site during the launch phase. This site maintained two-way lock with the IU CCS transponder from liftoff to S-IC/S-II staging. At this time, the adverse effects of the staging exhaust caused the MILA site to lose lock and signal until 165 seconds—approximately 13 seconds of data loss. Lock was lost again due to interstage jettison at 182.4 seconds and downlink lock was not re-established until 205 seconds.

Handover to Bermuda at 420 seconds appeared to have been normal. A two-way lock was established within 4 seconds.

The Ascension Island (ASC) and Carnarvon (CRO) antenna switching tests were performed satisfactorily. Signal levels were near predicted throughout this part of the mission.

Performance of the CCS system is discussed in detail in paragraph 14.3. A coverage summary of the CCS is shown in Figure 19-10.

## 19.6 OPTICAL INSTRUMENTATION

### 19.6.1 Onboard Cameras

The two onboard cameras located on the S-II stage were programmed to record the S-IC/S-II separation sequence. Both cameras were successfully ejected and retrieved. There was no damage to the capsule or film, and the camera coverage and quality of film were excellent. All tracking lights operated and timing and event marks were obtained on the films.

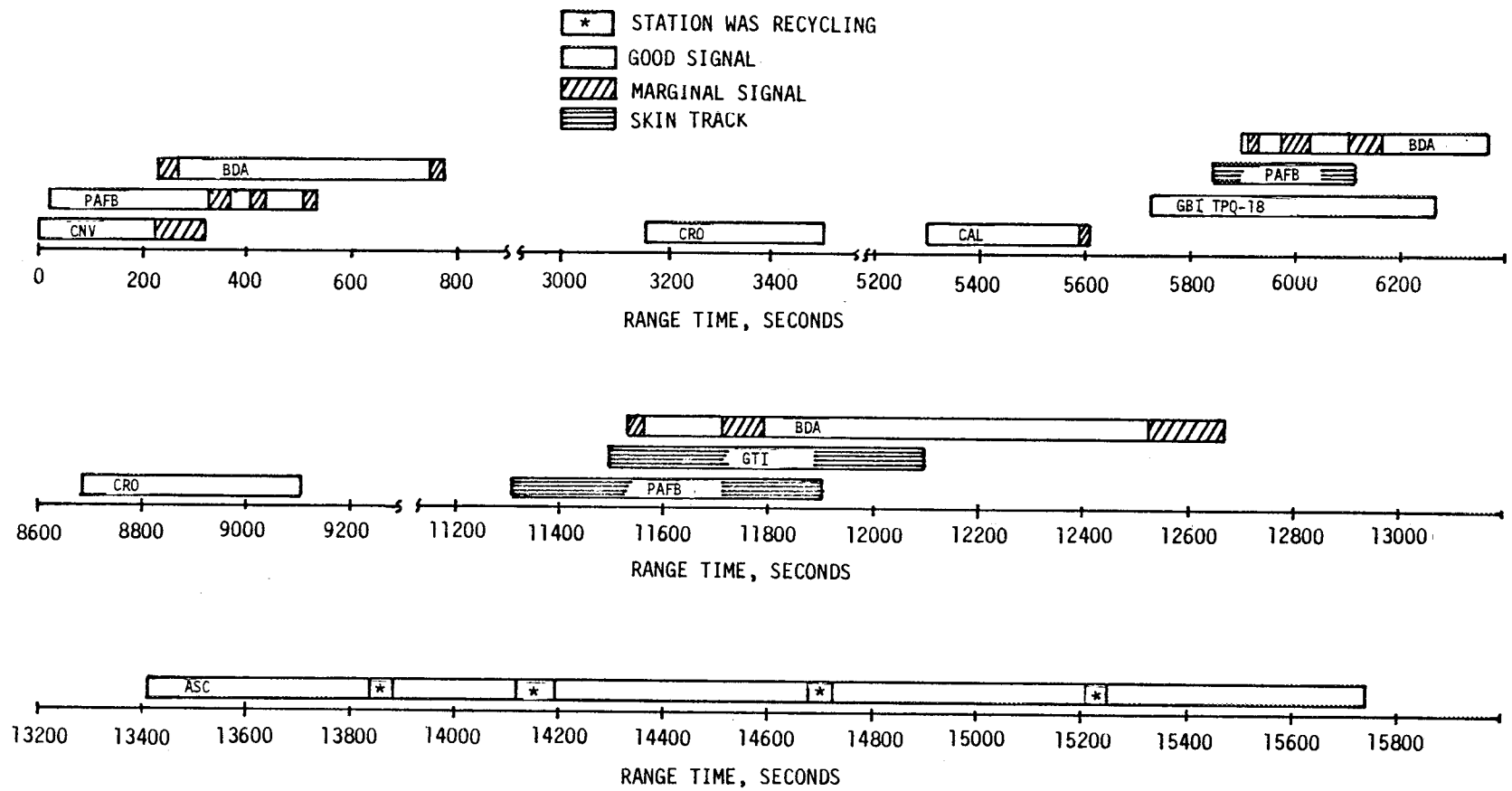


Figure 19-5. C-Band Radar Coverage Summary

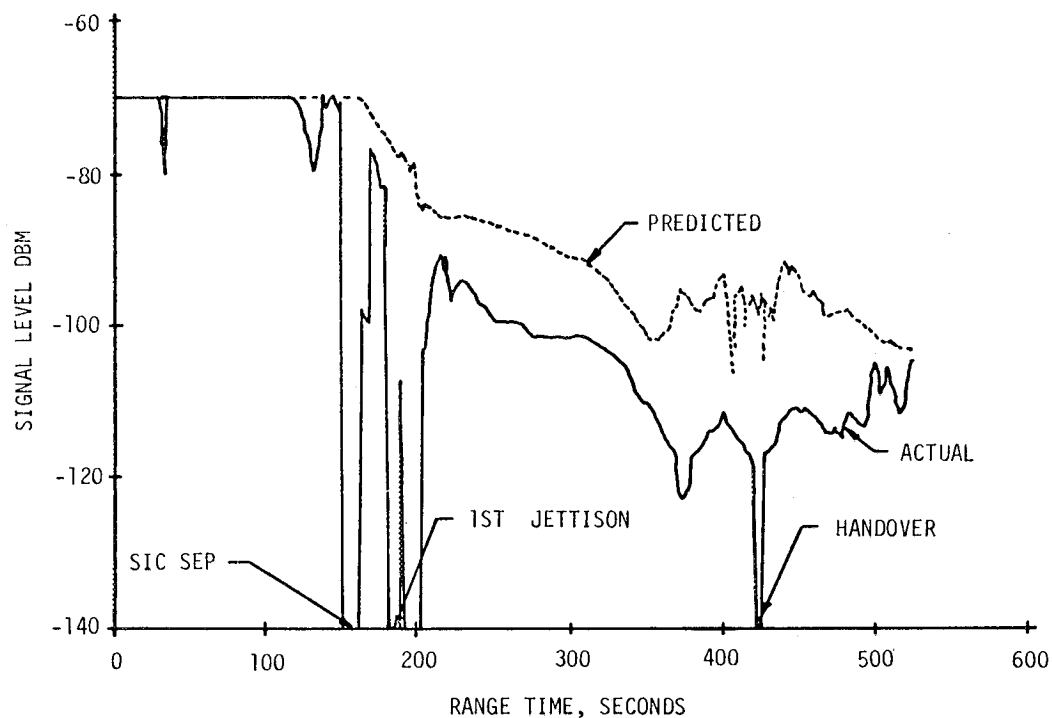


Figure 19-6. Merritt Island CCS Down Link Carrier Signal Strength, AS-501

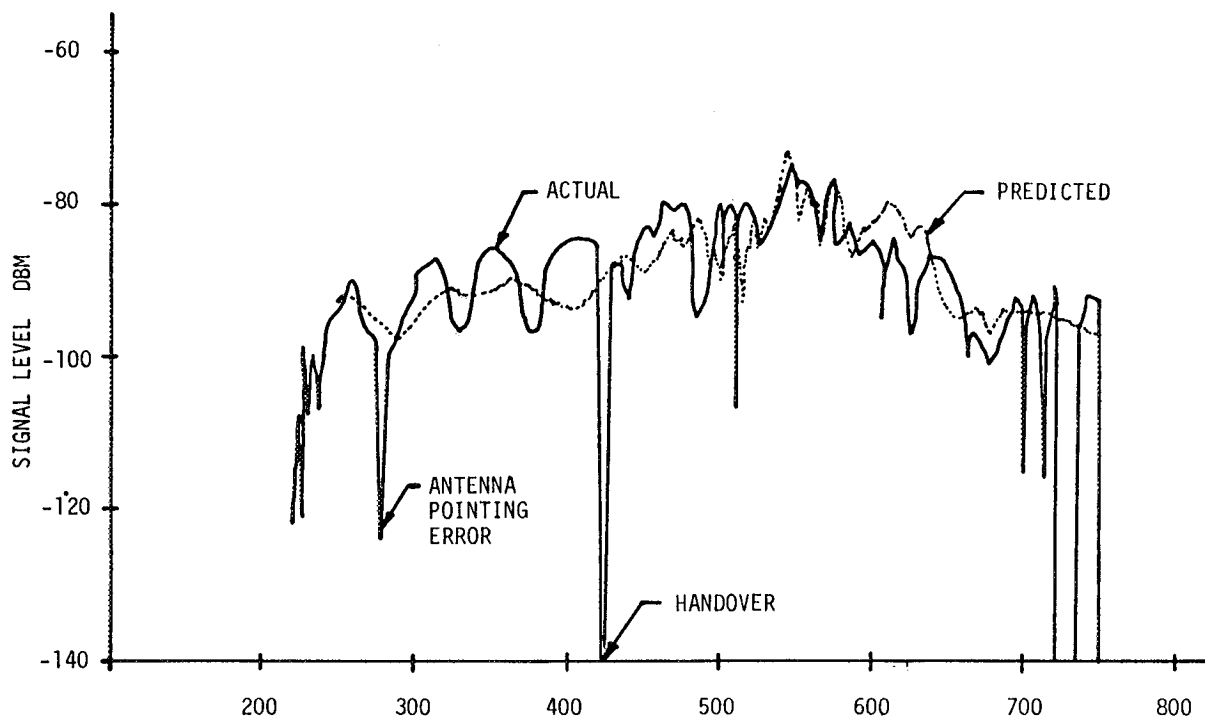


Figure 19-7. Bermuda CCS Down Link Carrier Signal Strength, AS-501

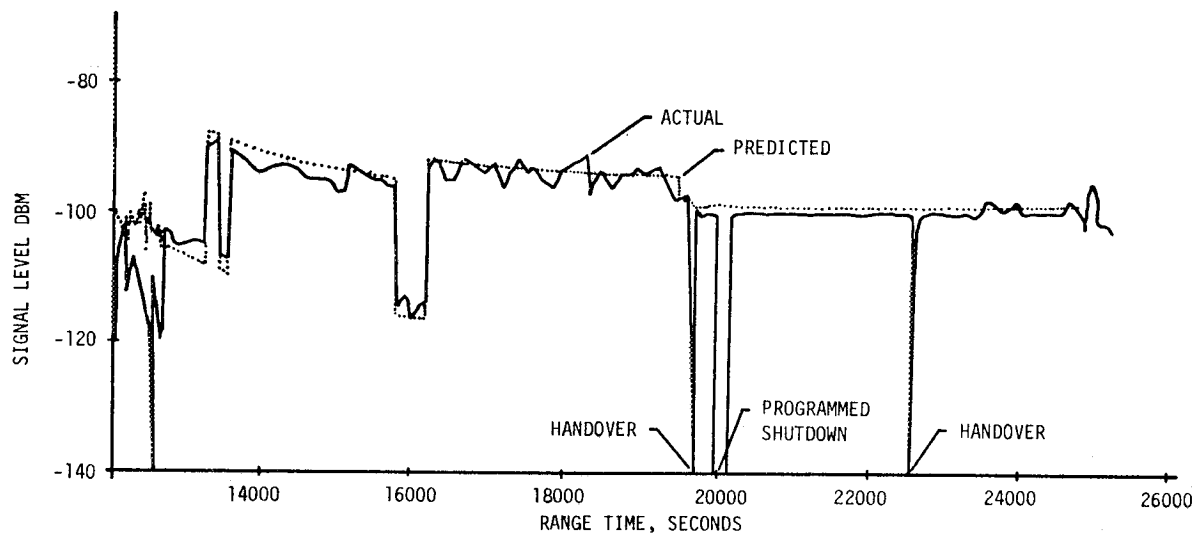


Figure 19-8. Ascension CCS Down Link Carrier Signal Strength, AS-501

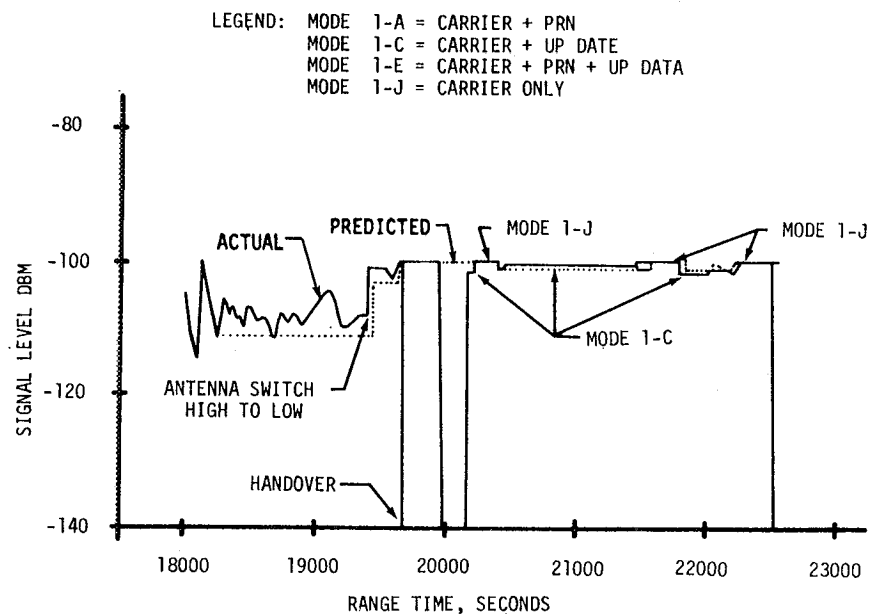


Figure 19-9. Carnarvon CCS Down Link Carrier Signal Strength, AS-501

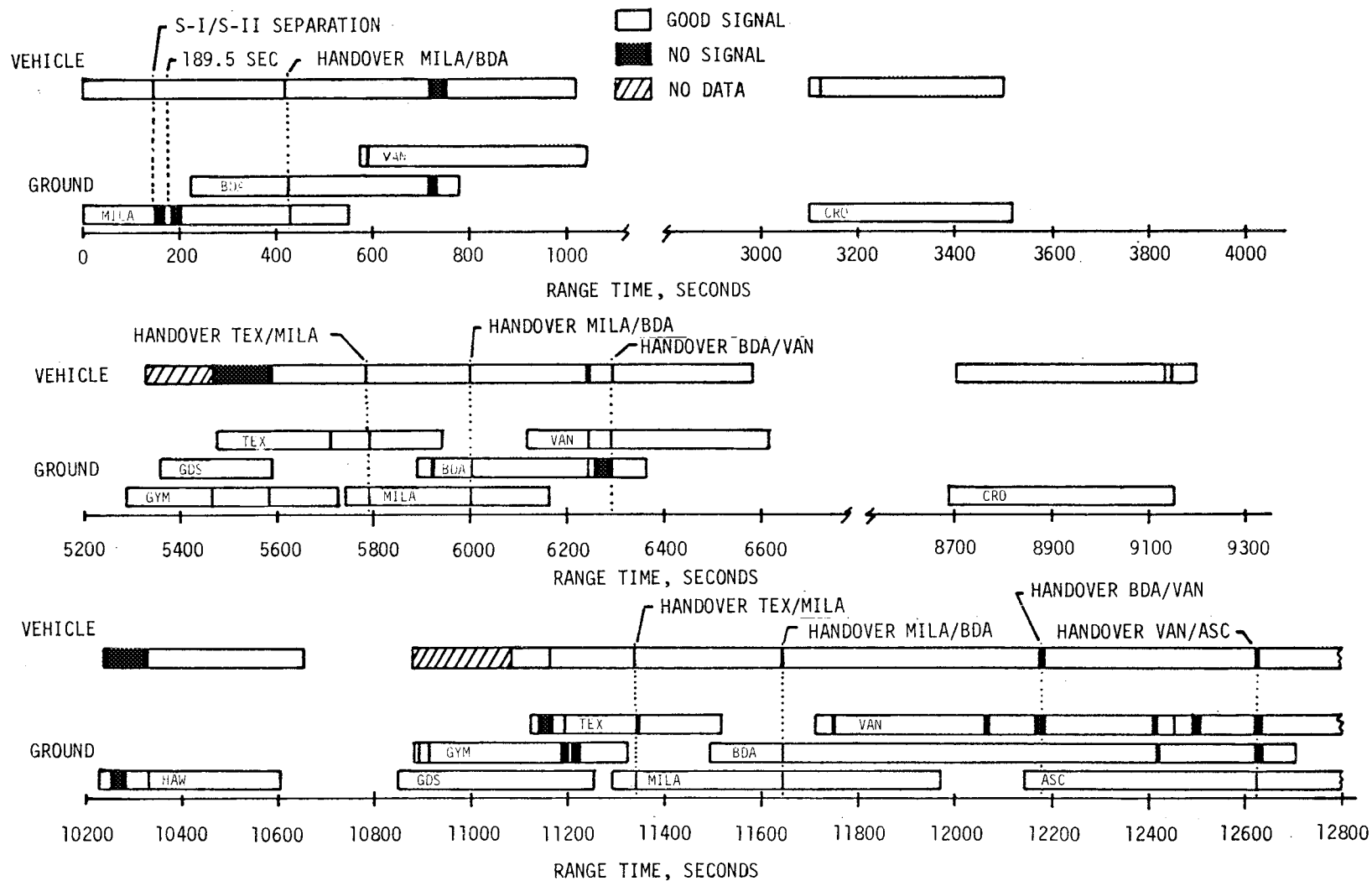


Figure 19-10. Command and Communications (CCS) Coverage Summary, Sheet 1 of 2



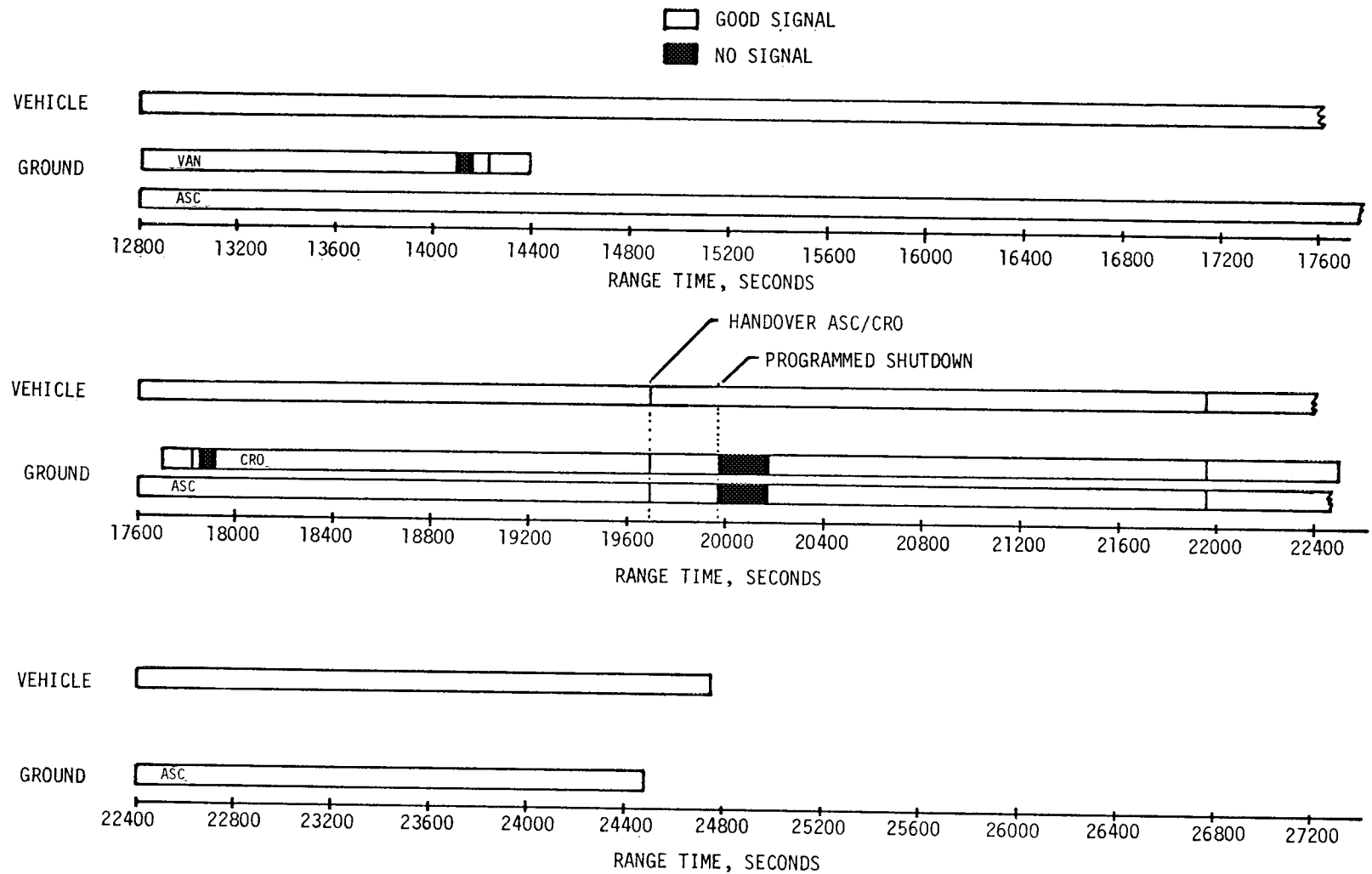


Figure 19-10. Command and Communications (CCS) Coverage Summary, Sheet 2 of 2

During recovery the drag flaps, paraballoons, flashing light beacons, dye markers, and shark repellent operated satisfactorily. One Sarah 242 MC recovery beacon signal was weak and intermittent. It was determined that the antenna did not extend from the capsule. Investigation also disclosed that all control circuitry providing operating current to the squib performed satisfactorily. Therefore, it was concluded that failure of the antenna deployment was most probably due to a malfunctioning squib. ECP 5246 has been approved to replace ordnance with a mechanical system.

#### 19.6.2 Ground Engineering Cameras

The overall ground camera coverage was not entirely satisfactory. There was a total of 83 cameras scheduled for AS-501 coverage: 68 KSC cameras to observe prelaunch and launch sequences and 15 AFETR tracking cameras. Eighty-five percent of the cameras did not produce all of the required data for evaluation purposes. Thirty-two percent contained partial data, and 53 percent had total loss of data for evaluation purposes.

The Launch Complex 39A camera system experienced a control power and timing loss of approximately 1.0 second duration from 12:00:00.381 to 12:00:01.371 Universal Time. The loss of camera control power resulted in a decrease in the programmed speed of the cameras as well as loss of timing signal. Investigation revealed that only four KSC cameras of the total assessed (excluding jammed cameras) did not experience the power outage. KSC has been informed of all aspects in this problem and is taking steps to rectify the problem before the AS-502 launch.

Film jams occurred in all rotary prism type cameras because of the power loss due to the nature of the camera.

Thirteen items of optical data were completely lost and 15 items had partial loss of data as a result of the power loss.

The KSC perimeter trackers (1300 feet from vehicle) malfunctioned when, as power was applied to the trackers (approximately -45 minutes), they dumped backward and could not be returned. As a result, eight cameras observing vehicle and stage structural integrity from liftoff to 1300 feet altitude were lost. Several AFETR tracking cameras acquired the vehicle on the pad and were acceptable for structural integrity; however, due to long focal length and ground haze, the resolution at liftoff was not adequate for detailed analysis.

The ETR tracking system gave satisfactory performance with minor exceptions. The ALOTS camera (aircraft at approximately 20,000 ft altitude) broke film before staging occurred and did not acquire the vehicle on the pad as in past flights.

## SECTION 20 VEHICLE AERODYNAMIC CHARACTERISTICS

### 20.1 SUMMARY

S-IC stage fin loads were measured by 16 static (total) pressure measurements positioned on opposite sides of Fin B and Fin D. Fin loadings were generally low as a result of the low vehicle angle-of-attack.

The axial force coefficient determined from the measured base drag and predicted forebody drag fell below the predicted value from Mach 0.2 to Mach 4.0 due to the lower than predicted base drag. During most of the subsonic flight, the axial force coefficient determined from the trajectory match was considerably higher than the prediction. However, from Mach 0.7 to the end of flight the trajectory match indicated the axial force was in close agreement with the reconstructed and predicted values.

### 20.2 VEHICLE AXIAL FORCE CHARACTERISTICS

The total and base axial force coefficients are shown in Figure 20-1. The base axial force coefficient was calculated from telemetered base pressure measurements. The reconstructed total axial force coefficient was the sum of a predicted forebody coefficient and the calculated base axial force coefficient. The predicted forebody coefficient was based on wind tunnel data. Zero angle-of-attack was assumed for all axial force analyses. The performance simulation (trajectory match) also used the predicted forebody coefficient.

The reconstructed axial force coefficient shown in the upper portion of Figure 20-1 fell below the predicted band from Mach 0.2 to Mach 4.0 due to the lower than predicted base drag. However, the performance simulations indicated a higher than predicted vehicle drag from liftoff until Mach 0.7. Above Mach 0.7 the simulation value was in reasonable agreement with the reconstructed value and near the predicted value. The base axial force coefficient, which was computed from PCM telemetered data from eight static (total) pressure measurements located on the S-IC base heat shield, fell below the prediction from Mach 0.3 to Mach 4.0. The prediction was based on wind tunnel data and Saturn IB flight data. In general, better agreement was obtained for the two derivations of the axial force coefficient for the Saturn IB flight data. The reason for the apparent discrepancy on AS-501 has not been determined, but more refined analyses may improve the comparison.

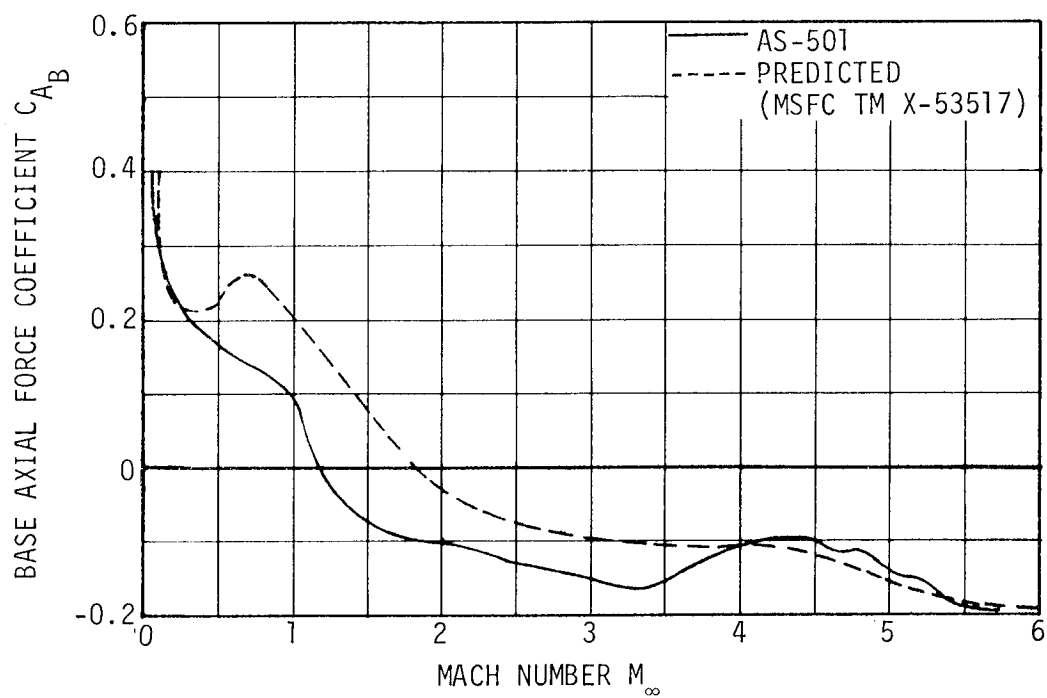
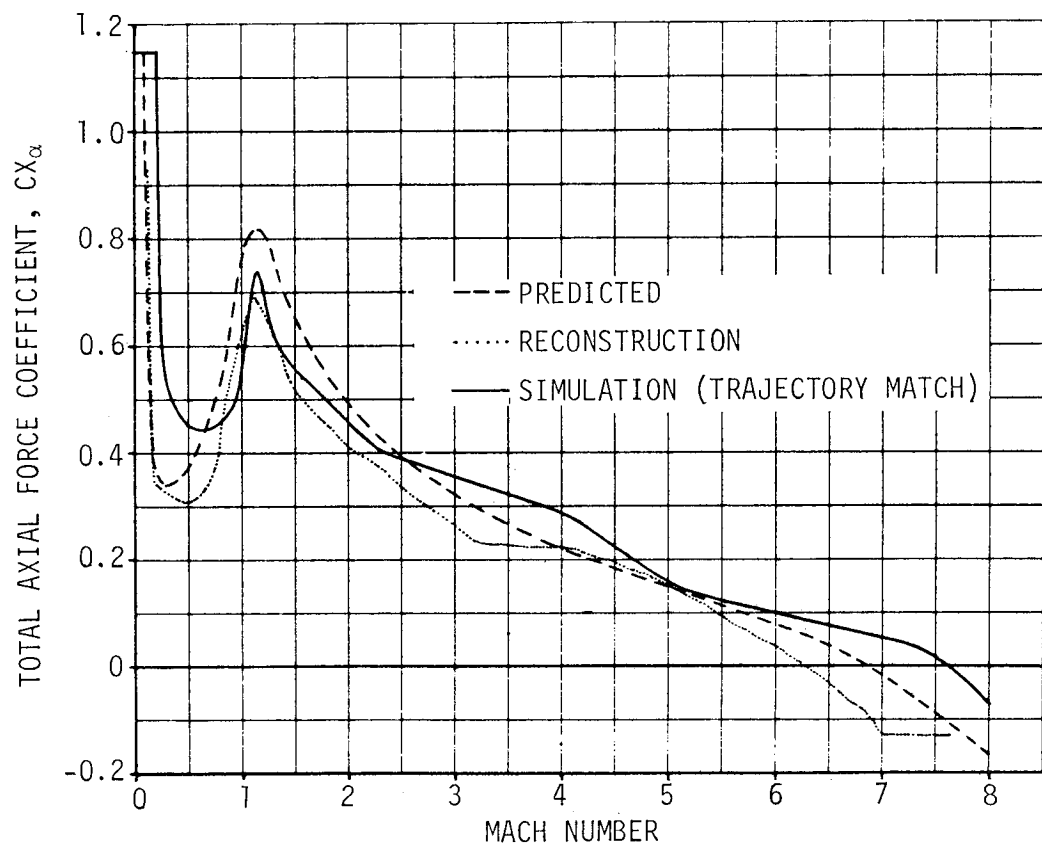


Figure 20-1. Vehicle Axial Force Characteristics

The mutual impingement of J-2 engine exhaust plumes caused reverse flow of the exhaust gases which impinged on the S-II base heat shield and thrust cone surface producing an incremental base thrust force. Figure 20-2 presents this incremental base force history through S-II stage boost. These results were obtained from base region pressure measurements. The major contribution to this thrust force consisted of the pressure acting on the base heat shield while the remainder was due to the pressure acting on the thrust cone. The thrust force dropped approximately 25 percent after second plane separation and an additional 15 percent after PMR step down.

The base region effective surface areas considered in this analysis totalled  $79.4 \text{ m}^2$  (855.3 ft) and consisted of the following:

- a. Base Heat Shield -  $23.2 \text{ m}^2$  (249.9 ft<sup>2</sup>)
- b. J-2 Engine Nozzle Exit Area -  $17.9 \text{ m}^2$  (192.8 ft<sup>2</sup>)
- c. Thrust Cone -  $38.3 \text{ m}^2$  (412.6 ft<sup>2</sup>)

### 20.3 VEHICLE STATIC STABILITY

A reliable evaluation of the static aerodynamic stability characteristics of the AS-501 flight was not possible due to the small vehicle angle-of-attack and the resulting small engine deflections.

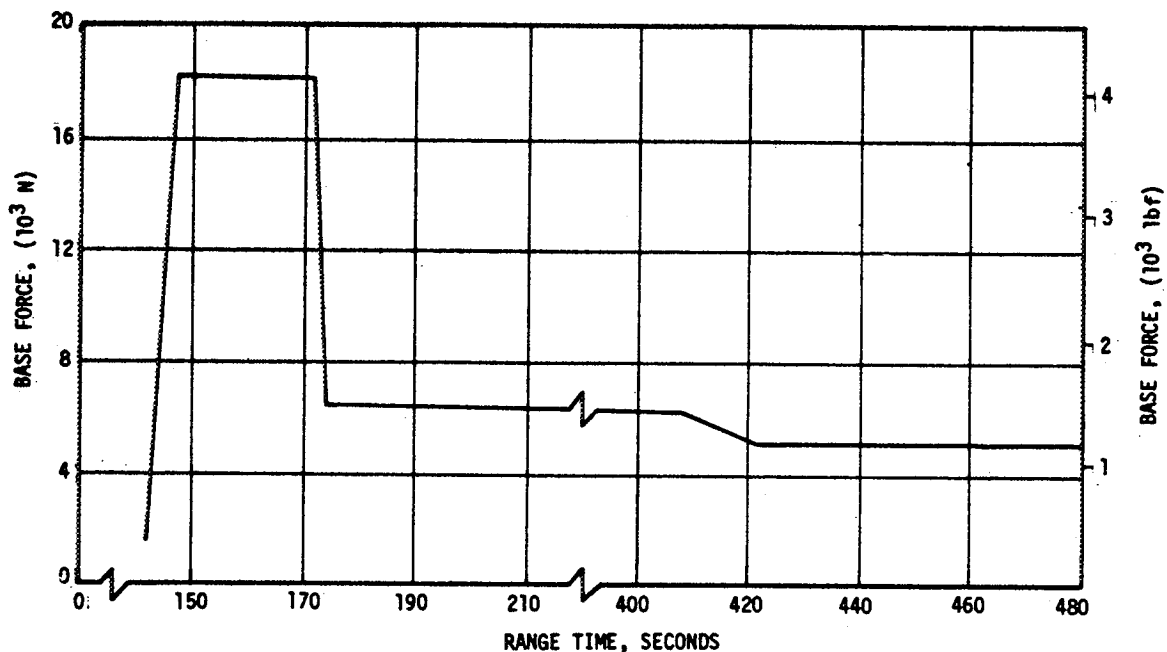


Figure 20-2. Base Pressure Thrust Increment During S-II Boost

#### 20.4 FIN PRESSURE LOADING

External static pressures on the S-IC fins were recorded by sixteen measurements. Each side of two fins had four measurements located in the same relative position.

The pressure differentials across the S-IC fins are shown in Figure 20-3. These differentials were well within the predicted bands as a result of the small angle-of-attack encountered during flight. The bands were predicted using available wind tunnel data and were based on the AS-501 Q-Ball total angle-of-attack.

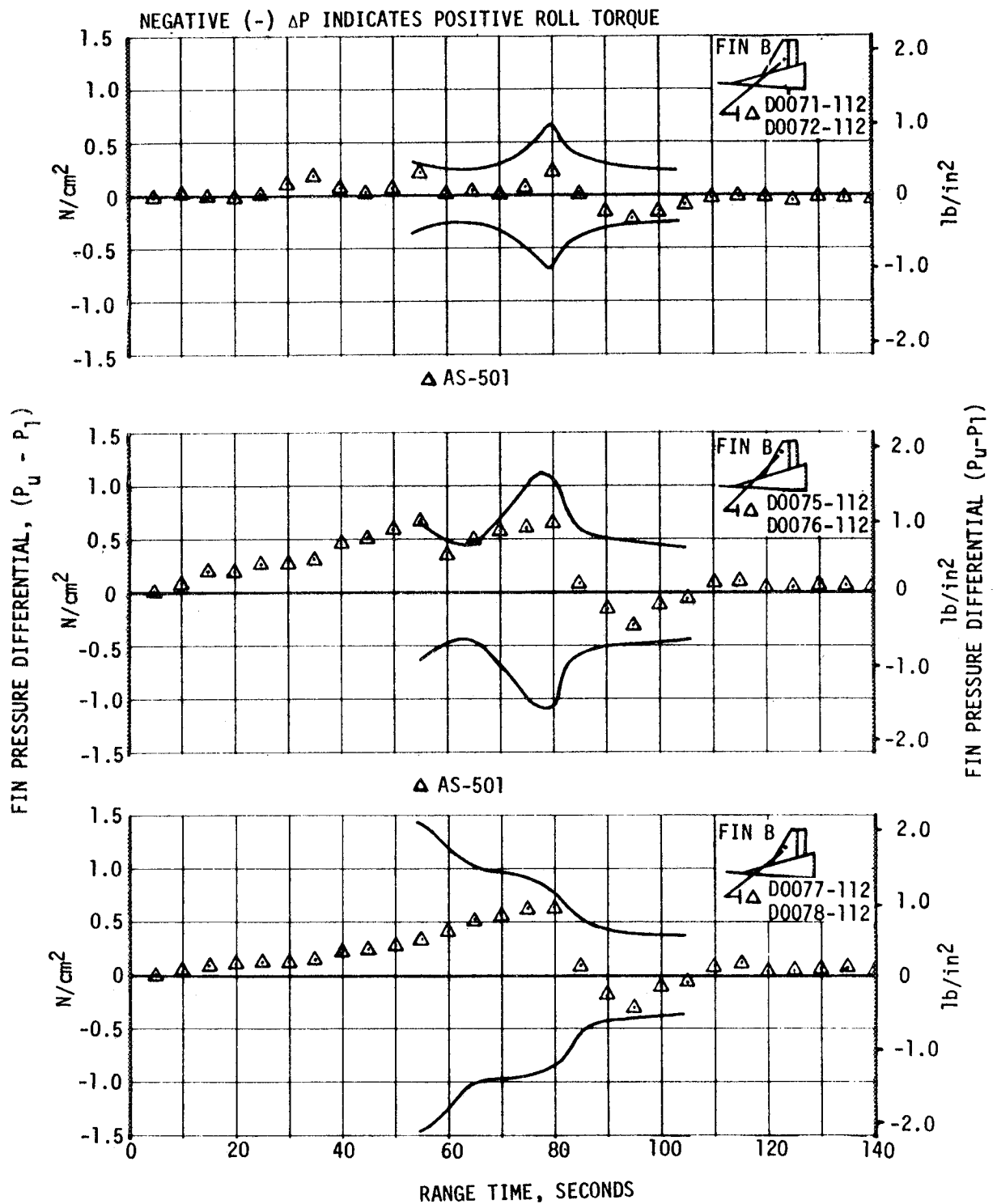


Figure 20-3. S-IC Fin Pressure Differential, Sheet 1 of 2

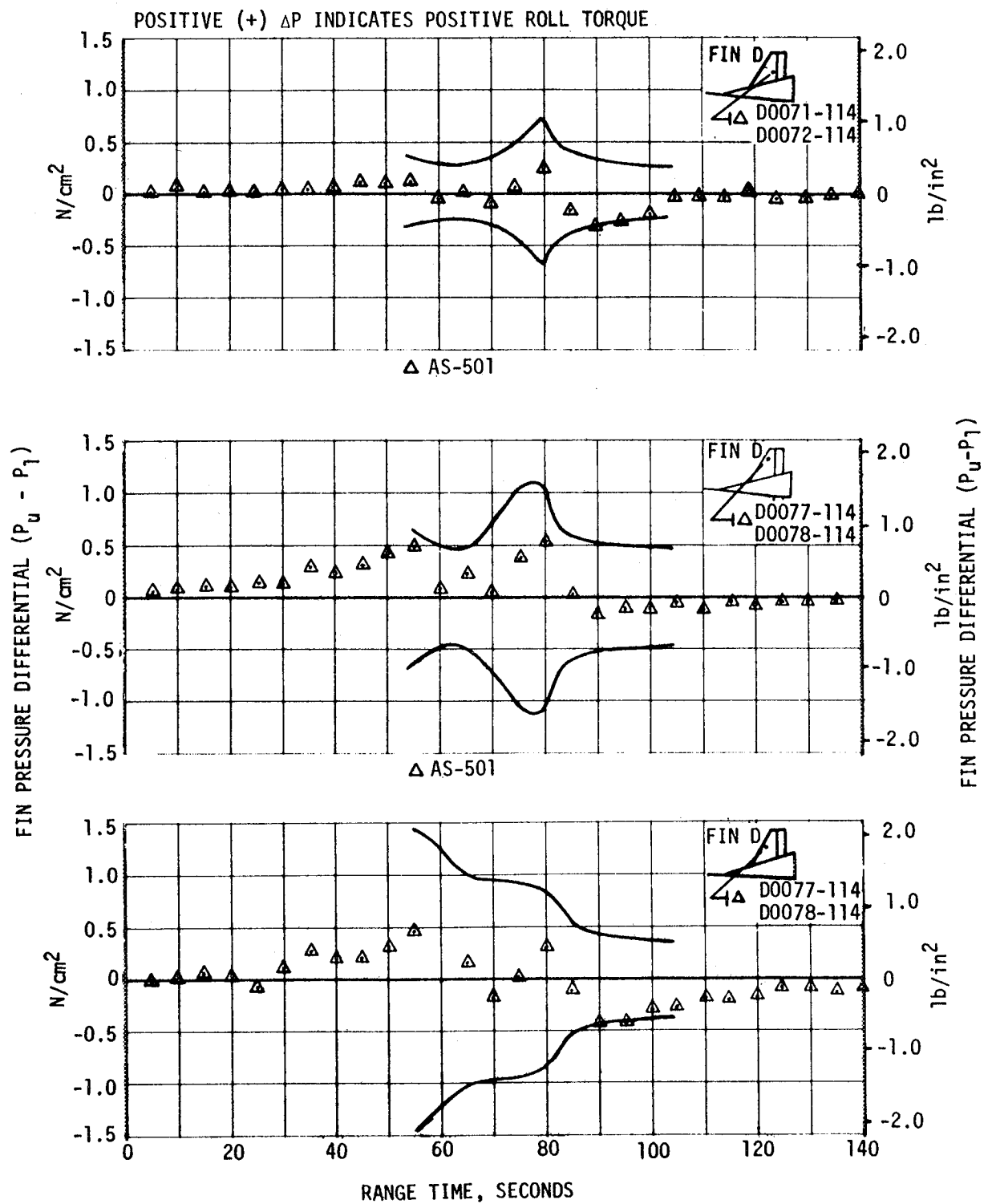


Figure 20-3. S-IC Fin Pressure Differential, Sheet 2 of 2



## SECTION 21 MASS CHARACTERISTICS

### 21.1 SUMMARY

Postflight analysis indicated that the vehicle mass during the boost phase oscillated slightly between higher than predicted and lower than predicted. These deviations can be attributed to:

- a. Higher than predicted stage (except the S-IVB stage which was lower) and interstage, instrument unit and spacecraft weights.
- b. Higher than predicted residual propellants at staging.
- c. Higher than predicted S-IVB stage LOX loading.
- d. Lower than predicted S-IC stage and S-II stage propellant loadings.

### 21.2 MASS EVALUATION

Postflight mass characteristics are compared to the final predicted mass characteristics (R-P&VE-VAW-67-154, November 15, 1967) which were used in determination of the final operational trajectory (R-AERO-FMT-237-67, October 19, 1967).

The postflight mass characteristics were determined from an analysis of all available actual and reconstructed data; from S-IC ignition through S-IVB stage J-2 engine second thrust decay. Dry weights of the launch vehicle were based on an evaluation of the weight and Balance Log Books (MSFC Form 998). Propellant loading and utilization was evaluated from propulsion system performance reconstructions. Spacecraft data was obtained from the Manned Spacecraft Center (MSC).

Deviations in the dry weights of the inert stages and the loaded spacecraft were all within the predicted three sigma deviation limits, except the S-II/S-IVB interstage and the Launch Escape Tower. The S-II/S-IVB interstage was 6.04 percent over predicted or 5.42 percent over tolerance. This overweight was due to a large amount of insulation installed at KSC to protect against possible excessive aerodynamic heating. The Launch Escape

System (LES) was 1.26 percent over predicted or 0.68 percent over tolerance. Since the remainder of the vehicle was under tolerance, the net effect of the excessive weight of these two items was nil.

During S-IC stage powered flight, the weight of the vehicle was determined to be 0.07 percent higher than predicted at liftoff and 0.26 percent higher than predicted at S-IC/S-II separation. These deviations may be attributed to the following:

- a. The inert launch vehicle was 0.25 percent heavier than predicted.
- b. The spacecraft was 0.16 percent heavier than predicted.
- c. S-IVB stage propellant loading was 0.40 percent heavier than predicted.
- d. S-IC stage residuals at separation were 6.36 percent heavier than predicted due to a shorter than anticipated burn time.

S-IC burn phase total vehicle mass is shown in Tables 21-1 and 21-2.

During S-II stage powered flight, the weight of the vehicle was 0.16 percent under predicted at ignition due primarily to the 0.19 percent lower than predicted propellant loading. At S-II/S-IVB separation, the vehicle was 0.24 percent over predicted due to the heavy S-II/S-IVB interstage, heavy spacecraft and heavy S-IVB propellant loading. The total vehicle mass for S-II burn phase is shown in Tables 21-3 and 21-4.

The first burn of the S-IVB stage began at 0.28 percent over predicted mass and ended at 0.49 percent under predicted mass. These deviations are due to the heavy S-IVB propellant loading and a longer than predicted burn time. During earth orbit, vehicle mass loss was 6.58 percent greater than expected. This was due to a larger than predicted fuel tank vent. The total vehicle mass for S-IVB first burn phase is shown in Tables 21-5 and 21-6.

At S-IVB stage reignition the vehicle mass was 0.57 percent under predicted due to the longer first burn and greater than predicted orbit mass loss. At spacecraft separation, the vehicle mass was 3.27 percent greater than predicted due to a 14.20 percent larger than predicted propellant residual. Total vehicle mass for S-IVB second burn phase is shown in Tables 21-7 and 21-8.

A summary of mass utilization and loss, actual and predicted, from first stage ignition to spacecraft payload separation is presented in Table 21-9. A comparison of actual and predicted mass, center of gravity and moment of inertia is presented in Table 21-10. Figure 21-1 through 21-3 present graphically the mass, center of gravity and moment of inertia for each stage burn.

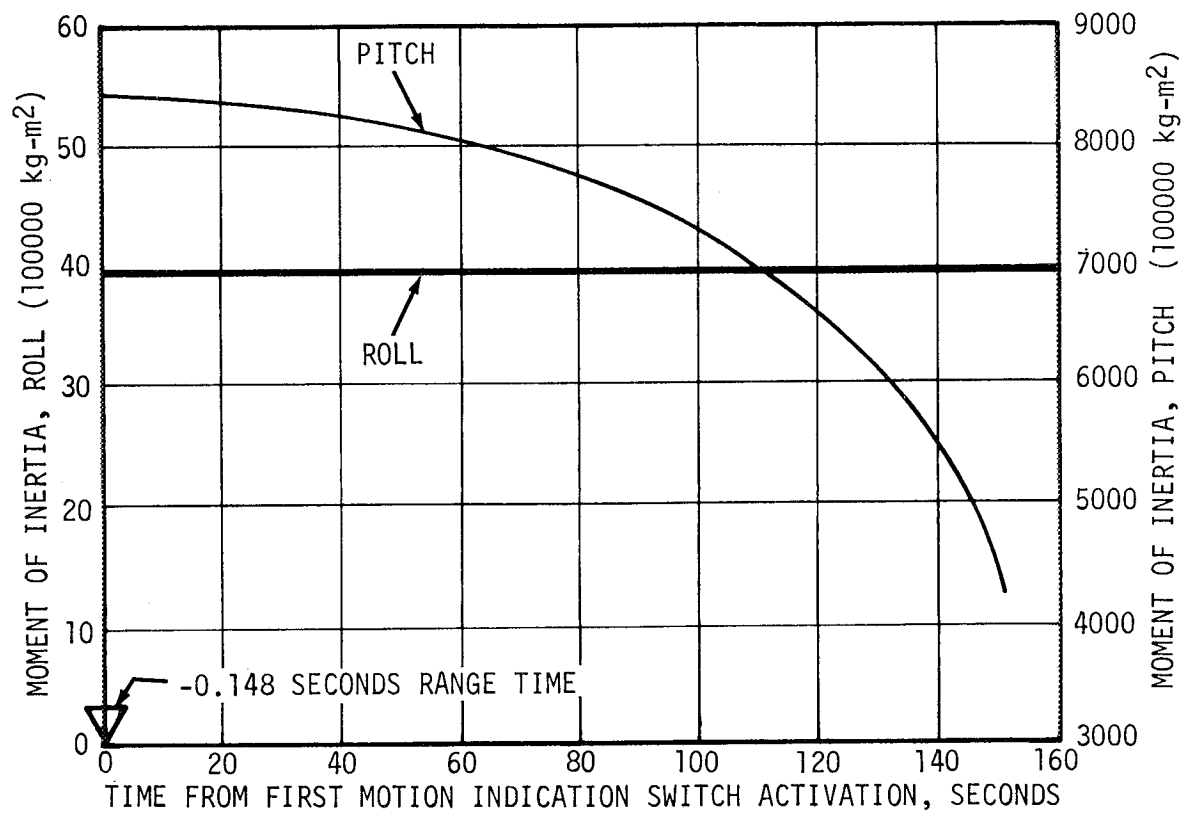
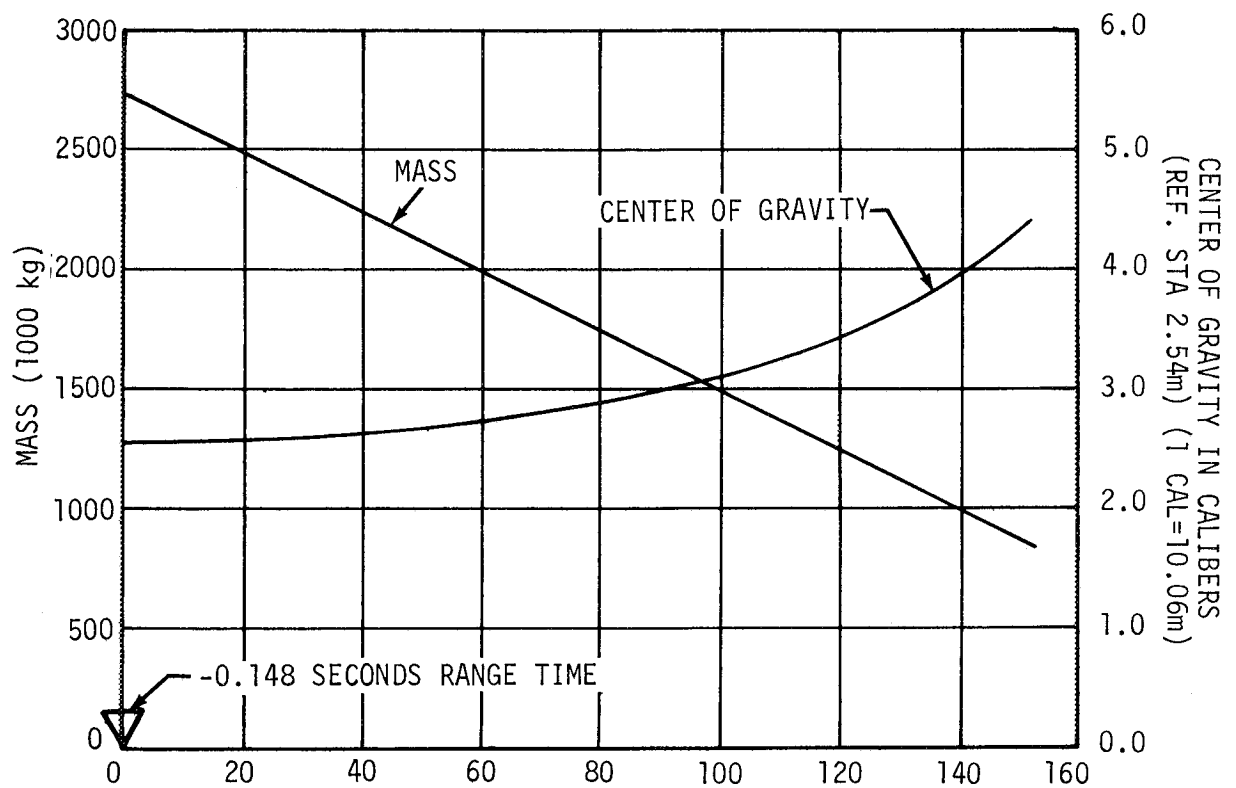


Figure 21-1. Vehicle Mass, Center of Gravity, and Mass Moment of Inertia During S-IC Stage Powered Flight

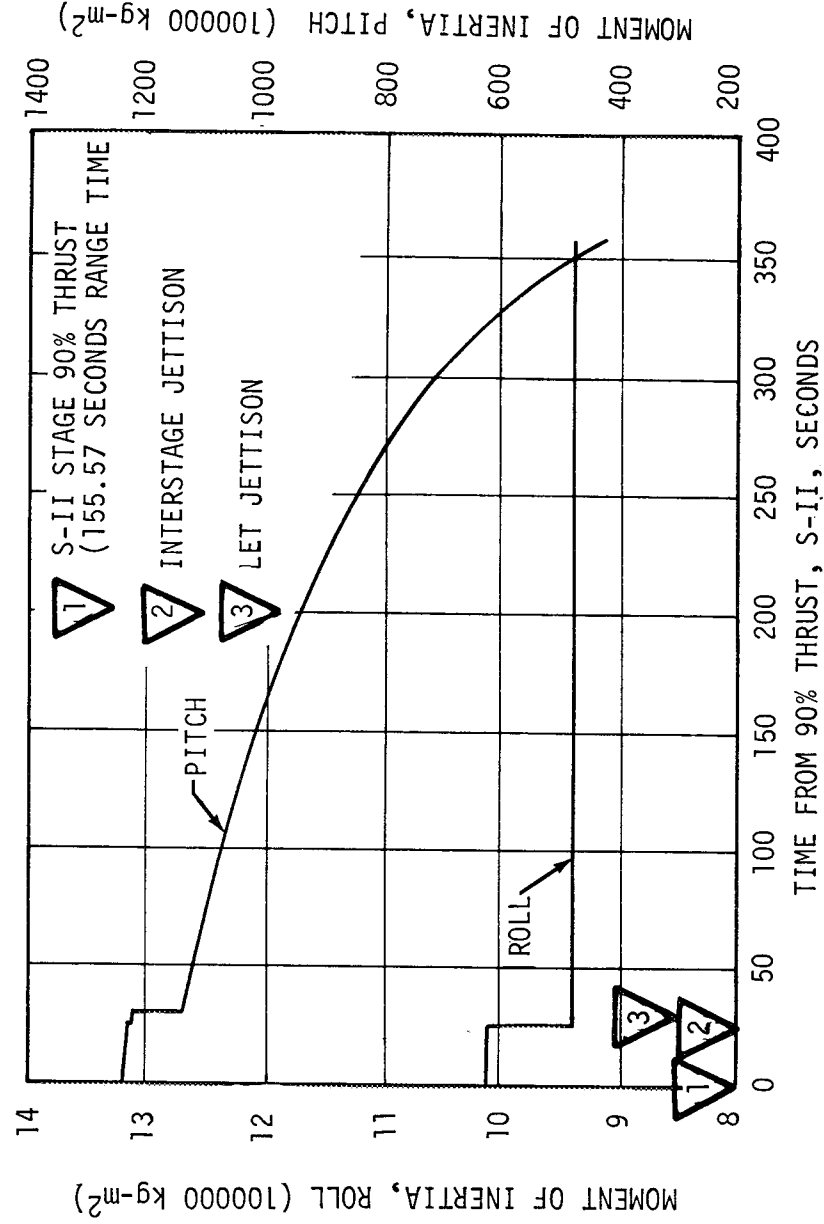
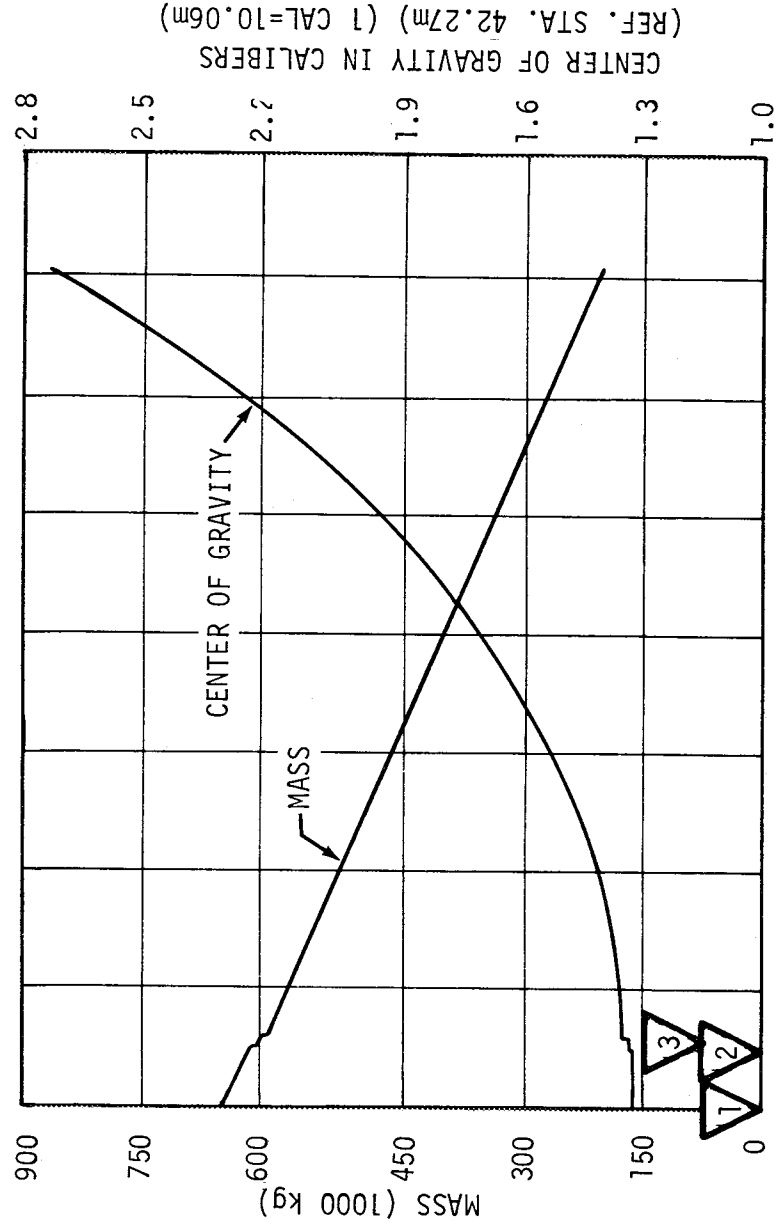


Figure 21-2. Total Vehicle Mass, Center of Gravity, and Mass Moment of Inertia During S-II Stage Powered Flight

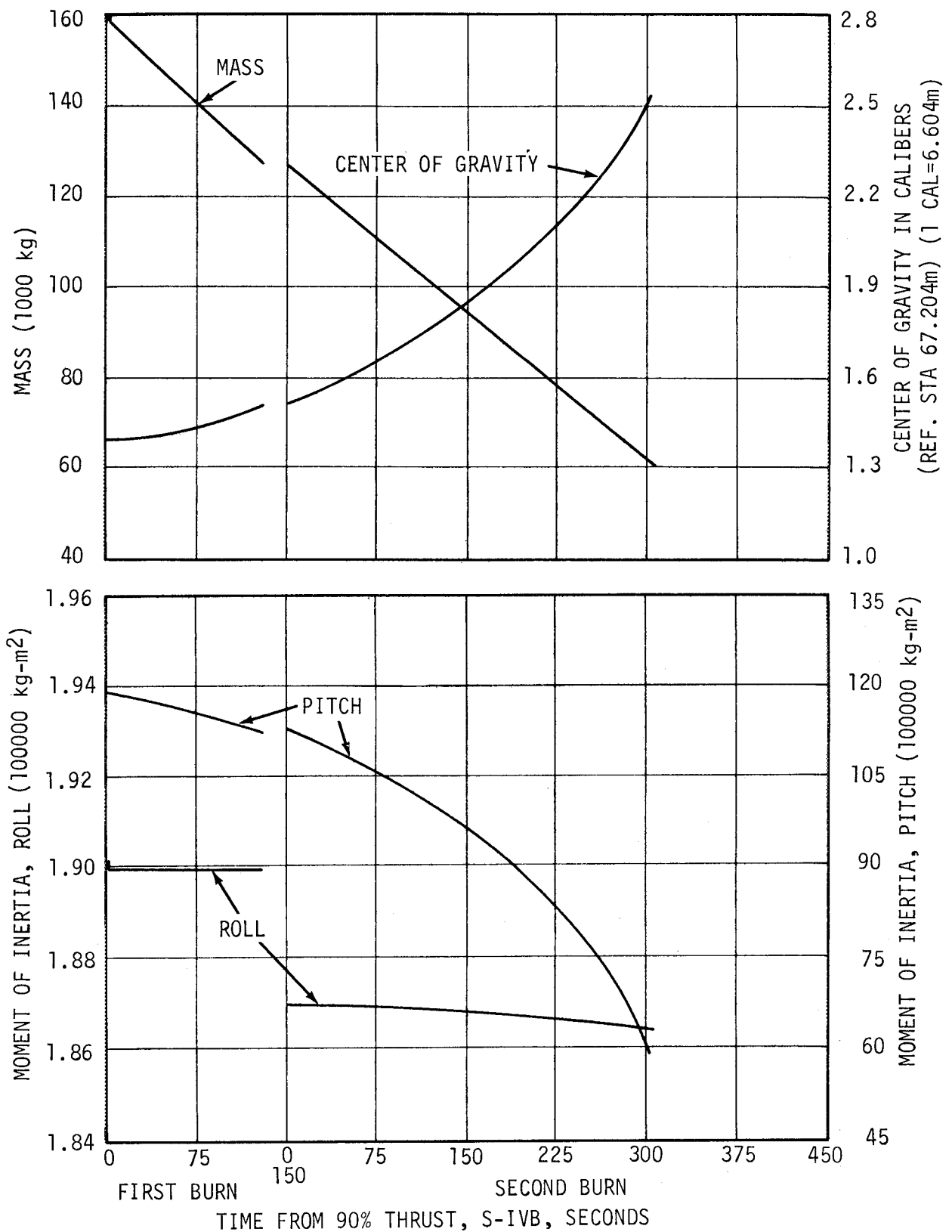


Figure 21-3. Vehicle Mass, Center of Gravity, and Mass Moment of Inertia During S-IVB Stage Powered Flight

Table 21-1. Total Vehicle Mass -- S-IC Burn Phase (Kilograms)

EVENTS	S-IC IGNITION		LIFTOFF		INBOARD ENGINE CUTOFF COMMAND		OUTBOARD ENGINE CUTOFF COMMAND		S-IC/S-II SEPARATION	
	PREDICTED	ACTUAL	PREDICTED	ACTUAL	PREDICTED	ACTUAL	PREDICTED	ACTUAL	PREDICTED	ACTUAL
Time from First Motion Indication Switch Activation (sec)*			0	0.152	135.5	135.694	152.386	150.898	153.087	151.598
S-IC Stage, Dry	139,201.1572	139,502.79	139,201.1	139,502.79	139,201.1	139,502.79	139,201.1	139,502.79	139,201.1	139,502.79
LOX in Tank	1,399,460.92	1,400,522.32	1,362,983.01	1,365,581.19	119,177.32	110,438.86	2,960.21	1,142.14	2,060.21	1,142.14
LOX Below Tank	21,136.95	20,988.62	21,876.8	21,727.98	21,876.8	21,711.20	13,024.0	16,489.89	10,819.5	14,378.87
LOX Ullage Gas	520.724	508.47	555.2	521.63	2,644.4	2,984.18	2,871.2	3,252.25	2,875.3	3,257.24
RP-1 in Tank	612,056.719	610,590.255	592,042.4	598,844.02	62,437.7	57,088.23	8,702.2	7,785.00	7,625.8	6,787.55
RP-1 Below Tank	4,419.804	4,419.80	6,102.6	6,102.63	6,102.6	6,102.63	6,065.0	6,064.98	6,065.0	6,064.98
RP-1 Ullage Gas	83.00	84.82	87.1	88.90	255.8	266.25	277.1	287.12	278.1	287.57
N <sub>2</sub> Purge Gas	34.01	28.57	34.0	28.57	17.2	11.79	17.2	11.79	17.2	11.79
Helium in Bottle	288.48	288.48	284.4	284.40	115.2	106.59	94.3	86.18	93.4	85.72
Frost	635.03	322.05	635.0	322.05	340.2	52.16	340.2	52.16	340.2	52.16
Retro Motor Propellant	1,026.93	1,026.93	1,026.9	1,026.93	1,026.9	1,026.93	1,026.9	1,026.93	1,026.9	1,026.93
Other	135.17	135.17	135.2	135.17	135.2	135.2	135.2	131.08	135.2	135.17
Total S-IC Stage	2,178,998.9	2,178,418.32	2,133,935.42	2,134,166.3	353,830.4	339,426.82	173,814.79	175,836.45	170,538.49	172,732.97
S-IC/S-II Interstage (small)	669.5	671.77	669.5	671.77	669.5	671.77	669.5	671.77	669.5	671.77
S-IC/S-II Interstage (large)	4,830.8	4,818.51	4,830.8	4,818.51	4,830.8	4,818.51	4,830.8	4,818.51	4,830.8	4,818.51
S-IC/S-II Interstage Propellant	1,233.8	1,233.8	1,233.8	1,233.77	1,233.8	1,233.77	1,233.8	1,233.77	1,152.1	1,152.10
Total S-IC/S-II Interstage	6,734.0	6,724.05	6,734.0	6,724.05	6,734.0	6,724.05	6,734.0	6,724.05	6,652.4	6,642.40
Total S-II Stage	469,854.6	469,050.37	469,854.6	469,050.37	469,596.0	468,791.82	469,596.0	468,791.82	469,596.0	468,791.82
Total S-II/S-IVB Interstage	3,459.5	3,681.80	3,459.5	3,681.80	3,459.5	3,681.80	3,459.5	3,681.80	3,459.5	3,681.80
Total S-IVB Stage	119,140.1	119,513.43	119,140.1	119,513.43	119,004.0	119,422.71	119,004.0	118,969.12	119,004.0	118,969.12
Total Instrument Unit	2,154.6	2,157.28	2,154.6	2,157.28	2,154.6	2,157.28	2,154.6	2,157.28	2,154.6	2,157.28
Total Spacecraft	42,456.2	42,525.64	42,456.2	42,525.64	42,456.2	42,525.64	42,456.2	42,525.64	42,456.2	42,525.64
Total Upper Stage	637,065.0	636,928.55	637,065.0	636,928.55	636,670.4	636,579.28	636,670.4	636,579.28	636,670.4	636,579.28
Total Launch Vehicle	2,822,798.94	2,822,070.92	2,777,734.99	2,777,819.36	997,236.04	982,730.16	817,219.28	819,140.70	813,861.338	815,955.57

\* First Motion Indication Switch Activation occurred at -0.148 seconds range time.

Table 21-2. Total Vehicle Mass -- S-IC Burn Phase (Pounds Mass)

EVENTS	S-IC IGNITION		LIFTOFF		INBOARD ENGINE CUTOFF COMMAND		OUTBOARD ENGINE CUTOFF COMMAND		S-IC/S-II SEPARATION	
	PREDICTED	ACTUAL	PREDICTED	ACTUAL	PREDICTED	ACTUAL	PREDICTED	ACTUAL	PREDICTED	ACTUAL
Time from First Motion Indication Switch Activation (sec)*			0	0.152	135.5	135.694	152.386	150.898	153.087	151.598
S-IC Stage, Dry	306,886	307,551	306,886	307,551	306,886	307,551	306,886	307,551	306,886	307,551
Lox in Tank	3,085,283	3,087,623	3,004,863	3,010,591	262,741	243,476	4,542	2,518	4,542	2,518
Lox Below Tank	46,599	46,272	48,230	47,902	48,230	47,865	28,713	36,354	23,853	31,700
Lox Ullage Gas	1,148	1,121	1,224	1,150	5,830	6,579	6,330	7,170	6,339	7,181
RP-1 in Tank	1,349,354	1,346,121	1,305,230	1,320,225	138,754	125,858	19,185	17,163	16,812	14,964
RP-1 Below Tank	9,744	9,744	13,454	13,454	13,454	13,454	13,371	13,371	13,371	13,371
RP-1 Ullage Gas	183	187	192	196	564	587	611	633	613	634
N <sub>2</sub> Purge Gas	75	63	75	63	38	26	38	26	38	26
Helium in Bottle	636	636	627	627	254	235	208	190	206	189
Frost	1,400	710	1,400	710	750	115	750	115	750	115
Retro Motor Propellant	2,264	2,264	2,264	2,264	2,264	2,264	2,264	2,264	2,264	2,264
Other	298	298	298	298	298	298	298	298	298	298
Total S-IC Stage	4,803,870	4,802,590	4,704,522	4,705,031	780,064	748,308	383,196	387,653	375,973	380,811
S-IC/S-II Interstage (small)	1,476	1,481	1,476	1,481	1,476	1,481	1,476	1,481	1,476	1,481
S-IC/S-II Interstage (large)	10,650	10,623	10,650	10,623	10,650	10,623	10,650	10,623	10,650	10,623
S-IC/S-II Interstage Propellant	2,720	2,720	2,720	2,720	2,720	2,720	2,720	2,720	2,540	2,540
Total S-IC/S-II Interstage	14,846	14,824	14,846	14,824	14,846	14,824	14,846	14,824	14,666	14,644
Total S-II Stage	1,035,852	1,034,079	1,035,852	1,034,079	1,035,282	1,033,509	1,035,282	1,033,509	1,035,282	1,033,509
Total S-II/S-IVB Interstage	7,627	8,117	7,627	8,117	7,627	8,117	7,627	8,117	7,627	8,117
Total S-IVB Stage	262,659	263,482	262,659	263,482	262,359	263,282	262,359	262,282	262,359	262,282
Total Instrument Unit	4,750	4,756	4,750	4,756	4,750	4,756	4,750	4,756	4,750	4,756
Total Spacecraft	93,600	93,753	93,600	93,753	93,600	93,753	93,600	93,753	93,600	93,753
Total Upper Stage	1,404,488	1,404,187	1,404,488	1,404,187	1,403,618	1,403,417	1,403,618	1,403,417	1,403,618	1,403,417
Total Launch Vehicle	6,223,206	6,221,601	6,123,857	6,124,043	2,198,529	2,166,549	1,801,660	1,805,896	1,794,257	1,798,874

\* First Motion Indication Switch Activation occurred at -0.148 seconds range time

Table 21-3. Total Vehicle Mass -- S-II Burn Phase (Kilograms)

EVENTS	S-IC IGNITION		S-II IGNITION COMMAND		90% THRUST		ENGINE CUTOFF COMMAND		S-II/S-IVB SEPARATION	
	PREDICTED	ACTUAL	PREDICTED	ACTUAL	PREDICTED	ACTUAL	PREDICTED	ACTUAL	PREDICTED	ACTUAL
Time From 90% Thrust (sec)			-3.00	-3.00	0.0	0.0	359.624	363.752	360.014	363.949
S-IC/S-II Interstage (small)	669.5	671.8								
S-IC/S-II Interstage (large)	4,830.8	4,818.5	4,830.8	4,818.5	4,830.8	4,818.5				
S-IC/S-II Interstage Propellant	1,233.8	1,233.8	662.2	662.2						
Total S-IC/S-II Interstage	6,734.0	6,724.1	5,493.0	5,480.7	4,830.8	4,818.5				
S-II Stage, Dry	40,006.8	40,016.8	40,006.8	40,016.8	40,006.8	40,016.8	40,006.8	40,016.8	40,006.8	40,016.8
LOX in Tank	358,970.7	358,643.2	358,790.2	358,461.8	358,163.3	357,850.8	1,456.0	199.7	1,309.1	1,668.8
LOX Below Tank	737.1	737.1	737.1	737.1	800.1	800.1	800.1	800.1	800.1	800.1
LOX Ullage Gas	23.6	23.6	204.1	205.0	204.6	205.9	1,435.6	1,525.9	1,437.4	1,526.3
LH <sub>2</sub> in Tanks	69,616.9	69,129.7	69,542.5	69,045.8	69,273.1	68,782.7	2,379.5	1,764.0	2,332.4	1,716.8
LH <sub>2</sub> Below Tank	104.8	104.8	104.8	104.8	127.9	127.9	127.9	127.9	127.9	127.9
LH <sub>2</sub> Ullage Gas	30.4	30.4	104.8	114.3	109.8	119.7	674.5	665.0	675.4	665.4
Insulation Purge Gas	54.4	54.4								
Frost	204.1	204.1								
Start Tank Gas	13.6	13.6	13.6	13.6	2.3	2.3	13.6	13.6	13.6	13.6
Cameras	54.4	54.4	54.4	54.4	54.4	54.4				
Others	37.6	37.6	37.6	37.6	37.6	37.6	37.6	37.6	37.6	37.6
Total S-II Stage	469,854.5	469,050.3	469,596.0	468,791.8	468,780.5	467,998.9	46,932.7	46,767.2	46,740.4	46,573.5
Total S-II/S-IVB Interstage	3,459.5	3,681.8	3,459.5	3,681.8	3,459.5	3,681.8	3,459.2	3,681.8	3,459.2	3,681.8
Total S-IVB Stage	119,140.1	119,513.4	119,004.0	119,422.7	119,003.6	119,422.7	119,003.6	119,422.7	119,002.2	119,420.9
Total Instrument Unit	2,154.6	2,157.3	2,154.6	2,157.3	2,154.6	2,157.3	2,154.6	2,157.3	2,154.6	2,157.3
Total Spacecraft	42,456.2	42,525.6	42,456.2	42,525.6	42,456.2	42,525.6	38,555.4	38,574.8	38,555.4	38,574.8
Total Upper Stage	167,210.5	167,878.2	167,074.4	167,787.4	167,073.9	167,787.4	163,173.1	163,836.7	163,173.1	163,834.8
Total Launch Vehicle	643,799.1	636,928.1	642,163.4	642,060.5	640,685.2	640,605.3	210,105.8	210,604.3	209,912.1	210,408.3



Table 21-4. Total Vehicle Mass -- S-II Burn Phase (Pounds Mass)

EVENTS	S-IC IGNITION		S-II IGNITION COMMAND		90% THRUST		ENGINE CUTOFF COMMAND		S-II/S-IVB SEPARATION	
	PREDICTED	ACTUAL	PREDICTED	ACTUAL	PREDICTED	ACTUAL	PREDICTED	ACTUAL	PREDICTED	ACTUAL
Time From 90% Thrust (sec)			-3.00	-3.00	0.0	0.0	359.624	363.752	360.014	363.949
S-IC/S-II Interstage (small)	1,476	1,481								
S-IC/S-II Interstage (large)	10,650	10,623	10,650	10,623	10,650	10,623				
S-IC/S-II Interstage Propellant	2,720	2,720	1,460	1,460						
Total S-IC/S-II Interstage	14,846	14,824	12,110	12,083	10,650	10,623				
S-II Stage, Dry	88,200	88,222	88,200	88,222	88,200	88,222	88,200	88,222	88,200	88,222
Lox in Tank	791,395	790,673	790,997	790,273	789,615	788,926	3,210	4,003	2,886	3,679
Lox Below Tank	1,625	1,625	1,625	1,625	1,764	1,764	1,764	1,764	1,764	1,764
Lox Ullage Gas	52	52	450	452	451	454	3,165	3,364	3,169	3,365
LH <sub>2</sub> in Tanks	153,479	152,405	153,315	152,220	152,721	151,640	5,246	3,889	5,142	3,785
LH <sub>2</sub> Below Tank	231	231	231	231	282	282	282	282	282	282
LH <sub>2</sub> Ullage Gas	67	67	231	252	242	264	1,487	1,466	1,489	1,467
Insulation Purge Gas	120	120								
Frost	450	450								
Start Tank Gas	30	30	30	30	5	5	30	30	30	30
Cameras	120	120	120	120	120	120				
Other	83	83	83	83	83	83	83	83	83	83
Total S-II Stage	1,035,852	1,034,079	1,035,282	1,033,509	1,033,484	1,031,761	103,469	103,104	103,045	102,677
Total S-II/S-IVB Interstage	7,627	8,117	7,627	8,117	7,627	8,117	7,627	8,117	7,627	8,117
Total S-IVB Stage	262,659	263,482	262,359	263,282	262,358	263,282	262,358	263,282	262,355	263,278
Total Instrument Unit	4,750	4,756	4,750	4,756	4,750	4,756	4,750	4,756	4,750	4,756
Total Spacecraft	93,600	93,753	93,600	93,753	93,600	93,753	85,000	85,043	85,000	85,043
Total Upper Stages	368,636	370,108	368,336	369,908	368,335	369,908	359,735	361,198	359,732	361,194
Total Launch Vehicle	1,419,334	1,404,186	1,415,728	1,415,501	1,412,469	1,412,293	463,204	464,303	462,777	463,871

Table 21-5. Total Vehicle Mass -- S-IVB First Burn Phase (Kilograms)

EVENTS	S-IC IGNITION		S-IVB IGNITION COMMAND FIRST BURN		90% THRUST FIRST BURN		ENGINE CUTOFF COMMAND FIRST BURN		INSERTION (END OF THRUST DECAY, START COAST)	
	PREDICTED	ACTUAL	PREDICTED	ACTUAL	PREDICTED	ACTUAL	PREDICTED	ACTUAL	PREDICTED	ACTUAL
Time From 90% Thrust (sec)			-2.533	-2.500	0.067	0.0	132.968	139.200	133.168	141.203
S-IVB Stage, Dry	12,036.5	12,024.7	12,012.9	12,000.7	12,012.9	12,000.7	11,955.3	11,941.7	11,955.3	11,941.7
LOX in Tank	87,516.6	87,936.1	87,500.2	87,927.1	87,317.4	87,780.6	60,065.6	59,613.4	59,993.9	59,580.7
LOX Below Tank	167.4	166.5	167.3	166.5	180.1	180.1	180.1	180.1	180.1	180.1
LOX Ullage Gas	2.3	2.3	18.1	11.3	18.6	11.3	58.9	34.5	58.9	34.5
LH <sub>2</sub> in Tank	18,698.9	18,705.7	18,671.7	18,669.4	18,611.8	18,616.8	13,693.5	13,491.2	13,680.8	13,477.1
LH <sub>2</sub> Below Tank	20.4	21.8	24.9	26.3	24.9	26.3	24.9	26.3	24.9	26.3
LH <sub>2</sub> Ullage Gas	7.7	7.7	30.4	38.6	30.8	38.6	62.1	68.5	62.1	68.5
Ullage Motor Propellant	55.3	55.3	10.0	10.0						
APS Propellant	284.9	280.8	284.9	280.8	284.9	280.8	283.9	280.3	283.9	280.3
Helium in Bottle	181.9	186.4	181.9	186.4	181.9	186.0	162.4	166.0	162.4	166.0
Start Tank Gas	2.3	2.3	2.3	2.3	.5	.5	3.2	3.2	3.2	3.2
Frost	136.1	90.7								
Other	33.1	33.1	33.1	33.1	33.1	33.1	33.1	33.1	33.1	33.1
Total S-IVB Stage	119,144.1	119,513.4	118,939.2	119,352.4	118,698.3	119,155.5	86,523.7	85,839.2	86,439.3	85,792.9
Total Instrument Unit	2,154.6	2,157.3	2,154.6	2,157.3	2,154.6	2,157.3	2,154.6	2,157.3	2,154.6	2,157.3
Total Spacecraft	42,456.2	42,525.6	38,555.4	38,574.9	38,555.4	38,574.9	38,555.4	38,574.9	38,555.4	38,574.9
Total Upper Stage	44,610.8	44,682.9	40,709.9	40,732.1	40,709.9	40,732.1	40,709.9	40,732.1	40,709.9	40,732.1
Total Vehicle	163,754.1	164,196.4	159,649.8	160,085.0	159,409.0	159,888.1	127,233.1	126,571.3	127,148.7	126,525.1

Table 21-6. Total Vehicle Mass -- S-IVB First Burn Phase (Pounds Mass)

EVENTS	S-IC IGNITION		S-IVB IGNITION COMMAND FIRST BURN		90% THRUST FIRST BURN		ENGINE CUTOFF COMMAND FIRST BURN		INSERTION (END OF THRUST DECAY START COAST)	
	PREDICTED	ACTUAL	PREDICTED	ACTUAL	PREDICTED	ACTUAL	PREDICTED	ACTUAL	PREDICTED	ACTUAL
Time From 90% Thrust (sec)			-2.533	-2.500	0.067	0.0	132.968	139.200	133.168	141.203
S-IVB Stage, Dry	26,536	26,510	26,484	26,457	26,484	26,457	26,357	26,327	26,357	26,327
LOX in Tank	192,941	193,866	192,905	193,846	192,502	193,523	132,422	131,425	132,264	131,353
LOX Below Tank	369	367	369	367	397	397	397	397	397	397
LOX Ullage Gas	5	5	40	25	41	25	130	76	130	76
LH <sub>2</sub> in Tank	41,224	41,239	41,164	41,159	41,032	41,043	30,139	29,743	30,161	29,712
LH <sub>2</sub> Below Tank	45	48	55	58	55	58	55	58	55	58
LH <sub>2</sub> Ullage Gas	17	17	67	85	68	85	137	151	137	151
Ullage Motor Propellant	122	122	22	22						
APS Propellant	628	619	628	619	628	619	626	618	626	618
Helium in Bottles	401	411	401	411	401	410	358	366	358	366
Start Tank Gas	5	5	5	5	1	1	7	7	7	7
Frost	300	200								
Other	73	73	73	73	73	73	73	73	73	73
Total S-IVB Stage	262,668	263,482	262,216	263,127	261,685	262,693	190,752	189,243	190,566	189,141
Total Instrument Unit	4,750	4,756	4,750	4,756	4,750	4,756	4,750	4,756	4,750	4,756
Total Spacecraft	93,600	93,753	85,000	85,043	85,000	85,043	85,000	85,043	85,000	85,043
Total Upper Stage	98,350	98,509	89,750	89,799	89,750	89,799	89,750	89,799	89,750	89,799
Total Vehicle	361,018	361,991	351,966	352,927	351,435	352,493	280,501	279,042	280,315	278,940

Table 21-7. Total Vehicle Mass -- S-IVB Second Burn Phase (Kilograms)

EVENTS	S-IVB IGNITION COMMAND SECOND BURN		90% THRUST SECOND BURN		ENGINE CUTOFF COMMAND SECOND BURN		END THRUST DECAY SECOND BURN		SPACECRAFT SEPARATION	
	PREDICTED	ACTUAL	PREDICTED	ACTUAL	PREDICTED	ACTUAL	PREDICTED	ACTUAL	PREDICTED	ACTUAL
Time From 90% Thrust (sec)	-2.567	-2.500	0.033	0.000	304.177	289.700	304.377	291.703		
S-IVB Stage, Dry	11,955.3	11,941.7	11,955.3	11,941.7	11,955.3	11,941.7	11,955.3	11,941.7	11,955.3	11,941.7
LOX in Tank	59,885.1	59,502.2	59,739.0	59,389.8	5,816.4	6,775.3	5,755.2	6,747.2	5,755.2	6,747.2
LOX Below Tank	167.4	166.5	180.1	180.1	180.1	180.1	175.5	180.1	175.5	166.5
LOX Ullage Gas	167.8	123.8	168.3	122.9	210.9	148.7	210.9	148.7	210.9	148.7
LH <sub>2</sub> in Tank	12,478.3	12,071.9	12,422.1	12,023.4	1,526.3	1,743.2	1,514.5	1,730.0	1,514.5	1,730.0
LH <sub>2</sub> Below Tank	24.9	26.3	24.9	26.3	24.9	26.3	24.9	26.3	20.4	21.8
LH <sub>2</sub> Ullage Gas	146.5	220.9	148.0	220.9	224.1	313.4	224.1	311.2	224.1	311.2
Ullage Motor Propellant										
APS Propellant	108.4	147.9	108.4	147.9	106.6	147.0	106.6	147.0	92.1	132.4
Helium in Bottle	136.1	132.9	136.1	132.4	94.8	94.3	94.8	94.3	94.8	94.3
Start Tank Gas	2.3	2.3	.5	.5	2.7	2.7	2.7	2.7	2.7	2.7
Frost										
Other	33.1	33.1	33.1	33.1	34.0	33.1	34.5	33.1	34.5	33.1
Total S-IVB Stage	85,105.3	84,370.0	84,914.8	84,220.3	20,176.2	21,407.3	20,103.7	21,363.3	20,071.9	21,330.6
Total Instrument Unit	2,154.6	2,157.3	2,154.6	2,157.3	2,154.6	2,157.3	2,154.6	2,157.3	2,154.6	2,157.3
Total Spacecraft	38,555.4	38,574.9	38,555.4	38,574.9	38,555.4	38,574.9	38,555.4	38,574.3	15,100.1	15,119.6
Total Upper Stage	40,709.9	40,732.2	40,709.9	40,732.2	40,709.9	40,732.2	40,709.9	40,732.2	17,254.7	17,276.9
Total Vehicle	125,815.2	125,102.2	125,624.7	124,952.5	60,886.1	62,139.5	60,813.6	62,095.5	37,326.6	38,587.5

Table 21-8. Total Vehicle Mass -- S-IVB Second Burn Phase (Pounds Mass)

EVENTS	S-IVB IGNITION COMMAND SECOND BURN		90% THRUST SECOND BURN		ENGINE CUTOFF COMMAND SECOND BURN		END THRUST DECAY SECOND BURN		SPACECRAFT SEPARATION	
	PREDICTED	ACTUAL	PREDICTED	ACTUAL	PREDICTED	ACTUAL	PREDICTED	ACTUAL	PREDICTED	ACTUAL
Time From 90% Thrust (sec)	-2.567	-2.500	0.033	0.000	304.177	289.700	304.377	291.703		
S-IVB Stage, Dry	26,357	26,327	26,357	26,327	26,357	26,327	26,357	26,327	26,357	26,327
LOX in Tank	132,024	131,180	131,702	130,932	12,823	14,937	12,688	14,875	12,688	14,875
LOX Below Tank	369	367	397	397	397	397	397	397	369	367
LOX Ullage Gas	370	273	371	271	465	328	465	328	465	328
LH <sub>2</sub> in Tank	27,510	26,614	27,386	26,507	3,365	3,843	3,339	3,814	3,339	3,814
LH <sub>2</sub> Below Tank	55	58	55	58	55	58	55	58	45	48
LH <sub>2</sub> Ullage Gas	323	487	324	487	494	691	494	686	494	686
APS Propellant	239	326	239	326	235	324	235	324	203	292
Helium in Bottle	300	293	300	292	209	208	209	208	209	208
Start Tank Gas	5	5	1	1	6	6	6	6	6	6
Frost										
Other	73	73	73	73	75	73	76	73	76	73
Total S-IVB Stage	187,625	186,004	187,205	185,674	44,481	47,195	44,321	47,098	44,251	47,026
Total Instrument Unit	4,750	4,756	4,750	4,756	4,750	4,756	4,750	4,756	4,750	4,756
Total Spacecraft	85,000	85,043	85,000	85,043	85,000	85,043	85,000	85,043	33,290	33,333
Total Upper Stage	89,750	89,799	89,750	89,799	89,750	89,799	89,750	89,799	38,040	38,089
Total Vehicle	277,375	275,803	276,955	275,473	134,231	136,993	134,071	136,897	82,291	85,072

Table 21-9. Flight Sequence Mass Summary

MASS HISTORY	ACTUAL		PREDICTED	
	kg	lbm	kg	lbm
S-IC Stage at S-IC Ignition	2,178,418.3	4,802,590	2,178,999.37	4,803,871
S-IC/S-II Interstage (small) at S-IC Ignition	671.77	1,481	669.5	1,476
S-IC/S-II Interstage (large) at S-IC Ignition	6,052.28	13,343	6,064.53	13,370
S-II Stage at S-IC Ignition	469,050.375	1,034,079	469,854.6	1,035,852
S-II/S-IVB Interstage at S-IC Ignition	3,681.80	8,117	3,459.5	7,627
S-IVB Stage at S-IC Ignition	119,513.43	263,482	119,140.1	262,659
Vehicle Instrument Unit at S-IC Ignition	2,157.28	4,756	2,154.6	4,750
Nominal Payload (Including LES)	42,525.65	93,753	42,456.2	93,600
First Flight Stage at S-IC Ignition	2,822,070.93	6,221,601	2,822,798.9	6,223,206
S-IC Thrust Buildup	-44,251.57	-97,558	-45,063.5	-99,348
First Flight Stage at Liftoff	2,777,819.36	6,124,043	2,777,734.99	6,123,857
S-IC Mainstage	-1,957,081.56	-4,314,626	-1,958,786.9	-4,318,386
S-IC Frost	-269.88	-595	-294.8	-650
S-II Frost	-204.11	-450	-204.1	-450
S-IVB Frost	-90.7	-200	-136.1	-300
S-IC N <sub>2</sub> Purge	-16.0	-37	-16.8	-37
S-II Insulation Purge Gas	-54.4	-120	-54.4	-120
S-IC Inboard Engine Thrust Decay Propellant	-775.6	-1,710	-836.4	-1,844
S-IC Inboard Engine Expended Propellant	-185.5	-409	-185.5	-409
First Flight Stage at Outboard Engine Cutoff Signal	819,140.7	1,805,896	817,219.28	1,801,660
S-IC Outboard Engine Thrust Decay Propellant	-3,103.47	-6,842	-3,276.3	-7,223
S-IC/S-II Ullage Motor Propellant	-81.64	-180	-81.6	-180
First Flight Stage at S-IC/S-II Separation	815,955.57	1,798,874	813,861.33	1,794,257
S-IC Stage at Separation	-172,733.42	-380,812	-170,538.49	-375,973
S-IC/S-II Interstage (small)	-67.77	-1,481	-669.5	-1,476
S-IC/S-II Ullage Motor Propellant	-489.87	-1,080	-489.9	-1,080
Second Flight Stage at S-II Ignition	642,060.4	1,415,501	642,163.4	1,415,728
S-II Thrust Buildup Propellant	-781.539	-1,723	-804.2	-1,773
S-II Start Tank	-11.339	-25	-11.3	-25
S-IC/S-II Ullage Motor Propellant	-662.2	-1,460	-662.2	-1,460
Second Flight Stage at 90% Thrust	640,605.37	1,412,293	640,685.2	1,412,469

Table 21-9. Flight Sequence Mass Summary (Continued)

MASS HISTORY	ACTUAL		PREDICTED	
	kg	lbm	kg	lbm
Launch Escape System	-3,950.78	-8,710	-3,900.9	-8,600
S-IC/S-II Interstage (large)	-4,818.51	-10,623	-4,830.7	-10,650
S-II Mainstage Propellant	-421,177.32	-928,537	-421,793.3	-929,895
S-II Cameras	-54.4	-120	-54.4	-120
Second Flight Stage at S-II Cutoff Signal	210,604.3	464,303	210,105.8	463,204
S-II Thrust Decay Propellant	-193.7	-427	-191.9	-423
S-IVB Ullage Propellant	-2.3	-5	-2.3	-5
Second Flight Stage at S-II/S-IVB Separation	210,408.36	463,871	209,911.7	462,776
S-II Stage at Separation	-46,573.96	-102,678	-46,740.4	-103,045
S-II/S-IVB Interstage-Dry	-3,194.19	-7,042	-2,971.9	-6,552
S-II/S-IVB Interstage Propellant	-487.61	-1,075	-487.6	-1,075
S-IVB Aft Frame	-21.77	-48	-21.8	-48
S-IVB Ullage Motor Propellant	-24.94	-55	-24.9	-55
S-IVB Detonation Package	-2.267	-5	-1.8	-4
Third Flight Stage at First Start Sequence Command	160,103.60	352,968	159,662.7	351,996
S-IVB Ullage Motor Propellant	-18.1	-40	-18.1	-40
S-IVB Fuel Lead Loss	-0.5	-1	0.0	0
Third Flight Stage at First S-IVB Ignition	160,085.0	352,927	159,645.0	351,957
S-IVB Ullage Motor Propellant	-10.0	-22	-10.0	-22
S-IVB H <sub>2</sub> in Start Tank	-1.8	-4	-1.8	-4
S-IVB Thrust Buildup Propellant	-185.1	-408	-229.1	-505
Third Flight Stage at 90% Thrust	159,888.1	352,493	159,404.2	351,426
S-IVB Ullage Motor Cases	-59.0	-130	-57.6	-127
S-IVB Mainstage Propellant	-33,257.3	-73,320	-32,115.7	-70,803
S-IVB APS Propellant Power Roll	-0.5	-1	-.9	-2
Third Flight Stage at First S-IVB Cutoff Signal	126,571.3	279,042	127,229.5	280,493
S-IVB Thrust Decay Propellant	-46.2	-102	-84.4	-186
Third Flight Stage at Start of Coast	126,525.1	278,940	127,145.1	280,307

Table 21-9. Flight Sequence Mass Summary (Continued)

MASS HISTORY	ACTUAL		PREDICTED	
	kg	lbm	kg	lbm
S-IVB Engine Propellant Expended	-18.1	-40	-17.2	-38
S-IVB Fuel Tank Vented in Orbit	-1,261.9	-2,782	-1,126.7	-2,484
S-IVB LOX Tank Vented in Orbit	0	0	0.0	0
S-IVB APS Propellant Loss in Orbit	-132.5	-292	-175.5	-387
S-IVB Start Tank	-.9	-2	-.9	-2
S-IVB O <sub>2</sub> /H <sub>2</sub> Burner	0	0	0.0	0
Third Flight Stage at Second Start Sequence Command	125,111.7	275,824	125,824.7	277,396
S-IVB Fuel Lead Loss	-9.1	-20	-9.5	-21
Third Flight Stage at Second S-IVB Ignition	125,102.6	275,804	125,815.2	277,375
S-IVB Start Tank	-1.8	-4	-1.8	-4
S-IVB Thrust Buildup Propellant	-148.3	-327	-188.7	-416
Third Flight Stage at 90% Thrust	124,952.4	275,473	125,624.7	276,955
S-IVB Mainstage Propellant Second Burn	-62,787.2	-138,422	-64,736.2	-142,719
S-IVB APS Propellant Power Roll	-.9	-2	-1.8	-4
S-IVB Venting	-25.4	-56	0.0	0
Third Flight Stage at Second S-IVB Cutoff Command	62,139.0	136,993	60,886.6	134,231
S-IVB Thrust Decay Propellant	-43.6	-96	-72.6	-160
Third Flight Stage at End Second Thrust Decay	62,095.4	136,897	60,813.6	134,071
S-IVB Engine Propellant Expended	-18.1	-40	-17.2	-38
S-IVB APS Propellant	-14.5	-32	-14.5	-32
Spacecraft Less LEM and SLA	-23,474.8	-51,753	-23,455.3	-51,710
Third Flight Stage at Spacecraft Separation	38,588.0	85,072	37,326.6	82,291
LEM	-13,381.0	-29,500	-13,381.0	-29,500
SLA	-1,719.1	-3,790	-1,719.1	-3,790
Vehicle Instrument Unit	-2,157.3	-4,756	-2,154.6	-4,750
S-IVB Stage at Separation	-21,330.6	-47,026	-20,071.9	-44,251



Table 21-10. Mass Characteristics Comparison

MASS ITEM		MASS		LONGITUDINAL C.G. (X STA)		RADIAL C.G.		ROLL MOMENT OF INERTIA		PITCH MOMENT OF INERTIA		YAW MOMENT OF INERTIA	
		KILOGRAMS POUNDS	% DEV.	METERS INCHES	ACT- PRED	METERS INCHES	ACT- PRED	KG-M <sup>2</sup> X10 <sup>6</sup>	% DEV	KG-M <sup>2</sup> X10 <sup>6</sup>	% DEV	KG-M <sup>2</sup> X10 <sup>6</sup>	% DEV
S-IC STAGE, DRY	PREDICTED	139,201		9.5500		0.0774		2.778		17.984		17.904	
		306,886		376.100		2.9428							
	ACTUAL	139,503		9.6600	.11	0.0775	.0001	2.788		18.282		18.201	
		307,551	.22	380.500	4.4	3.4793	.5365		.36		1.63		1.63
S-IC/S-II INTERSTAGE (INCLUDES ULLAGE PROPELLANT)	PREDICTED	6,734		41.5200		0.1643		0.172		0.100		0.100	
		14,846		1,634.900		6.4219							
	ACTUAL	6,724		41.5000	-.02	0.1643	.0	0.172	.00	0.100	.00	0.100	.00
		14,824	-.15	1,633.700	-1.2	6.4759	.0540						
S-II STAGE, DRY	PREDICTED	40,007		48.2000		0.1095		0.675		2.243		2.252	
		88,200		1,897.600		4.3185							
	ACTUAL	40,017		48.2700	.07	0.1095	0.0	0.675	.00	2.186	-2.61	2.197	-2.50
		88,222	.02	1,900.400	2.8	4.3863	0.0678						
S-II/S-IVB INTERSTAGE (INCLUDES RETRO MOTOR PROPELLANT)	PREDICTED	3,460		66.4400		0.0707		0.061		0.040		0.040	
		7,627		2,615.900		2.9154							
	ACTUAL	3,682		66.4400	.0	0.0707	0.0	0.065	6.15	0.042	4.76	0.043	6.98
		8,117	6.04	2,615.900	.0	2.9154	0.0						
S-IVB STAGE, DRY	PREDICTED	12,037		72.8900		0.1788		0.089		0.342		0.341	
		26,536		2,869.900		7.0263							
	ACTUAL	12,025		72.8900	.0	0.1788	0.0	0.089	.00	0.341	-.29	0.340	-.29
		26,510	-.10	2,869.900	.0	7.0263	0.0						
VEHICLE INSTRUMENT UNIT	PREDICTED	2,155		82.4200		0.2345		0.021		0.011		0.010	
		4,750		3,244.700		9.2003							
	ACTUAL	2,157		82.4200	.0	0.2345	0.0	0.021	.00	0.011	.00	0.010	.00
		4,756	.13	3,244.700	.0	9.2003	0.0						
SPACECRAFT AT S-IC IGNITION	PREDICTED	42,456		91.5400		0.1224		0.078		1.433		1.449	
		93,500		3,603.800		4.7539							
	ACTUAL	42,526		91.5600	.02	0.1264	0.0040	0.078	.00	1.455	.83	1.460	.76
		93,753	.16	3,604.700	.9	5.0447	0.2908						

Table 21-10. Mass Characteristics Comparison (Continued)

MASS ITEM		MASS		LONGITUDINAL C.G. (X STA)		RADIAL C.G.		ROLL MOMENT OF INERTIA		PITCH MOMENT OF INERTIA		YAW MOMENT OF INERTIA	
		KILOGRAMS POUNDS	% DEV	METERS INCHES	ACT- PRED	METERS INCHES	ACT- PRED	KG-M <sup>2</sup> X10 <sup>6</sup>	% DEV	KG-M <sup>2</sup> X10 <sup>6</sup>	% DEV	KG-M <sup>2</sup> X10 <sup>6</sup>	% DEV
FIRST FLIGHT STAGE S-IC IGNITION	PREDICTED	2,822,798		29.9812		.0067606		3.99990		844.8426		844.7562	
		6,223,206		1,180.364		.26616							
	ACTUAL	2,822,070		30.0014	.020	.0070710	.0003	4.00449	.11	845.1271	.03	845.0859	.03
		6,221,601	.03	1,181.158	.794	.27753	.0113						
FIRST FLIGHT STAGE AT LIFTOFF	PREDICTED	2,777,734		29.9262		.006846		4.00248		845.6789		845.5930	
		6,123,857		1,178.197	.075	.269508	.0002						
	ACTUAL	2,779,800	.07	30.001	2.96	.007049	.008	4.0045	.05	845.1271	.07	845.0859	.06
		6,128,411		1,181.158		.27754							
FIRST FLIGHT STAGE AT OUTBOARD ENGINE CUTOFF SIGNAL	PREDICTED	817,219		45.7233		.022485		3.98470		433.8201		433.7374	
		1,801,660		1,800.133	-.046	.88525	.0007						
	ACTUAL	819,141	.23	45.6769	-1.829	.02335	.034	3.992163	.19	435.885	.47	435.847	.48
		1,805,896		1,798.304		.9195							
FIRST FLIGHT STAGE AT S-IC/S-II SEPARATION	PREDICTED	813,861		45.8684		.022574		3.98121		429.5400		429.4573	
		1,794,257		1,805.844	-.055	.88877	.0007						
	ACTUAL	815,956	.26	45.813	-2.153	.02344	.034	3.9886	.19	431.847	.53	431.809	.54
		1,798,874		1,803.691		.923							
SECOND FLIGHT STAGE AT S-II IGNITION	PREDICTED	642,163.3		55.5001		.020827		1.0799		126.0152		126.0264	
		1,415,728		2,185.042	.024	.819960	.0007						
	ACTUAL	642,060.6	-.016	55.5238	.933	.0215	.027	1.0825	.24	126.2342	.17	126.247	.17
		1,415,501		2,185.975		.847							
SECOND FLIGHT STAGE AT S-II 90% THRUST	PREDICTED	640,685		55.5172		.020868		1.06371		125.8562		125.8674	
		1,412,469		2,185.715	.024	.821574	.0007						
	ACTUAL	640,605	-.012	55.5407	.928	.02156	.027	1.066	.21	126.0764	.17	126.0891	.18
		1,412,293		2,186.643		.849							
SECOND FLIGHT STAGE AT S-II ENGINE CUT- OFF SIGNAL	PREDICTED	210,105.9		69.9601		.058562		.940598		43.51140		43.52157	
		463,204		2,754.34	.024	2.305578	.0020						
	ACTUAL	210,604.1	.24	69.984	.950	.06053	.0749	.943518	.31	43.4013	.25	43.413	.25
		464,302.7		2,755.29		2.38044							

Table 21-10. Mass Characteristics Comparison (Continued)

MASS ITEM		MASS		LONGITUDINAL C.G. (X STA)		RADIAL C.G.		ROLL MOMENT OF INERTIA		PITCH MOMENT OF INERTIA		YAW MOMENT OF INERTIA	
		KILOGRAMS POUNDS	% DEV	METERS INCHES	ACT- PRED	METERS INCHES	ACT- PRED	KG-M <sup>2</sup> X10 <sup>6</sup>	% DEV	KG-M <sup>2</sup> X10 <sup>6</sup>	% DEV	KG-M <sup>2</sup> X10 <sup>6</sup>	% DEV
SECOND FLIGHT STAGE AT S-II/S-IVB SEPARATION	PREDICTED	209,911.9		69.9828		.0518616		.940595		43.39244		43.40263	
		462,777		2,755.23	.024	2.307709	.0087						
	ACTUAL	210,408	.24	70.0072	.960	.06059	.0770	.943514	.31	43.2808	.26	43.2925	.25
		463,870.8		2,756.19		2.3847							
THIRD FLIGHT STAGE AT FIRST ENGINE START SEQUENCE COMMAND	PREDICTED	159,663.7		76.4708		.049599		.192552		11.80417		11.80541	
		351,996		3,010.660		1.952712							
	ACTUAL	160,103		76.4654	-.0054	.0508331	.0012	.192271	.14	11.81923	.12	11.82075	.12
		352,968	.28	3,010.450	-.210	2.001375	.0486						
THIRD FLIGHT STAGE AT FIRST S-IVB IGNITION	PREDICTED	159,645		76.4687		.049606		.190237		11.80282		11.80421	
		351,957		3,010.578		1.952936							
	ACTUAL	160,086		76.4656	-.0031	.050842	.0012	.192252	1.05	11.81879	.14	11.82031	.14
		352,927	.28	3,010.460	-.118	2.001589	.0486						
THIRD FLIGHT STAGE AT FIRST S-IVB 90% THRUST	PREDICTED	159,404.2		76.47138		.0496857		.190222		11.80122		11.80261	
		351,426		3,010.685		1.956129							
	ACTUAL	159,888		76.46774	-.0036	.050911	.0012	.192234	1.05	11.81711	.13	11.81863	.14
		352,493	.30	3,010.541	-.144	2.004274	.0481						
THIRD FLIGHT STAGE AT FIRST S-IVB ENGINE CUTOFF COMMAND	PREDICTED	127,229		77.3640		.0618142		.1894239		11.13511		11.13627	
		280,493		3,045.828		2.433753							
	ACTUAL	126,571		77.3924	.0280	.063859	.0020	.191415	1.04	11.12913	.05	11.13042	.05
		279,042	-.52	3,046.946	1.118	2.514306	.0805						
THIRD FLIGHT STAGE AT FIRST END THRUST DECAY (START OF COAST)	PREDICTED	127,145		77.3673		.0618546		.1894235		11.13273		11.13389	
		280,307		3,045.959		2.435368							
	ACTUAL	126,525		77.3942	.0269	.063882	.0020	.191415	1.04	11.12753	.05	11.12881	.05
		278,940	-.49	3,047.017	1.058	2.515181	.0798						
THIRD FLIGHT STAGE AT SECOND S-IVB START SEQUENCE COMMAND	PREDICTED	125,825		77.3781		.0620080		.1870200		11.12378		11.12709	
		277,396		3,046.385		2.441247							
	ACTUAL	125,111		77.4026	.025	.0638	.0018	.189489	1.30	11.12435	.01	11.1272	.01
		275,824	-.57	3,047.349	.964	2.5153	.0741						

Table 21-10. Mass Characteristics Comparison (Continued)

MASS ITEM		MASS		LONGITUDINAL C.G. (X STA)		RADIAL C.G.		ROLL MOMENT OF INERTIA		PITCH MOMENT OF INERTIA		YAW MOMENT OF INERTIA	
		KILOGRAMS POUNDS	% DEV	METERS INCHES	ACT- PRED	METERS INCHES	ACT- PRED	KG-M <sup>2</sup> X10 <sup>6</sup>	% DEV	KG-M <sup>2</sup> X10 <sup>6</sup>	% DEV	KG-M <sup>2</sup> X10 <sup>6</sup>	% DEV
THIRD FLIGHT STAGE AT SECOND S-IVB IGNITION	PREDICTED	125,815		77.3778		.0620046		.1870215		11.12438		11.12754	
		277,375		3,046.370		2.441425							
	ACTUAL	125,102		77.4023	.0245	.0639	.0018	.189491	1.30	11.12503	.01	11.1279	.01
		275,804	-.57	3,047.333	.963	2.5155	.0741						
THIRD FLIGHT STAGE AT SECOND S-IVB 90% THRUST	PREDICTED	125,624		77.3838		.0621128		.1870184		11.12095		11.12426	
		276,955		3,046.607		2.44539							
	ACTUAL	124,953		77.407	.0232	.0640	.0019	.189488	1.30	11.12246	.01	11.12529	.01
		275,474	-.53	3,047.512	.905	2.5188	.0734						
THIRD FLIGHT STAGE AT SECOND S-IVB ENGINE CUTOFF COMMAND	PREDICTED	60,886		83.9168		.1262101		.1861915		5.869533		5.872174	
		134,231		3,303.814		4.96819							
	ACTUAL	62,139		83.6572	-.2596	.1270	.0008	.188702	1.33	6.093668	3.68	6.095885	3.67
		136,994	2.02	3,293.591	-10.223	4.9982	.0300						
THIRD FLIGHT STAGE AT SECOND END THRUST DECAY	PREDICTED	60,813		83.93360		.1263605		.1861903		5.855197		5.857836	
		134,071		3,304.473		4.97491							
	ACTUAL	62,096		83.666	-.268	.1270	.0006	.188702	1.33	6.093333	3.91	6.095549	3.90
		136,898	2.07	3,293.944	-10.529	5.0016	.0267						
THIRD FLIGHT STAGE AT SPACECRAFT SEPARATION	PREDICTED	37,326		77.74686		.076720		.169812		2.057092		2.054140	
		82,291		3,060.900		3.02062							
	ACTUAL	38,588		77.5081	-.238	.073770	.0029	.172646	1.64	2.129249	3.39	2.125836	3.37
		85,072	3.27	3,051.500	-9.400	2.90420	.1164						
SPACECRAFT AT SEPARATION	PREDICTED	23,455		93.76918		.217701		.037520		.096664		.101135	
		51,710		3,691.700		8.57098							
	ACTUAL	23,474		93.7768	.007	.226720	.0090	.037118	1.08	.096938	.28	.101420	.28
		51,753	.08	3,692.000	.300	8.92594	.3549						

## SECTION 22 MALFUNCTIONS AND DEVIATIONS

### 22.1 SUMMARY

Evaluation of the launch vehicle performance during the AS-501 flight test did not reveal any malfunctions or deviations which could be considered a serious system failure. Minor modifications, however, are planned for future flights to improve system operations.

### 22.2 SYSTEM MALFUNCTIONS AND DEVIATIONS

The system malfunctions (abnormal operations) and significant deviations (actual operation deviated from expected operation), and the recommended corrective actions are summarized in Table 22-1. A discussion of each problem area is included in the referenced paragraphs. Items having the statement "(closed out)" included in the Recommended Corrective action column are considered resolved with respect to the AS-502 flight.

Table 22-1. Summary of Malfunctions and Deviations

VEHICLE SYSTEMS	MALFUNCTION	PROBABLE CAUSE	CORRECTIVE ACTION BEING CONSIDERED	PARAGRAPH REFERENCE
INSTRUMENTATION MALFUNCTIONS				
S-II Camera Capsule	Very weak RF beacon signal on one of two recoverable camera capsules.	Antenna erection squib did not fire.	ECP 5246 approved to replace ordnance with mechanical system. (Closed out)	19.6.1
INSTRUMENTATION DEVIATIONS				
DEVIATION				
S-IC RF System	Weak signal on AF-1 data link after separation.	Power drop between power amplifier and stage antenna. Exact cause undetermined.	None, since deviation occurred after separa- tion and no data was lost. (Closed out)	19.3.1 19.5.1
S-IC RF System	Unexpected RF blackout from 137 to 139 seconds range time.	May be associated with center engine cutoff.	None anticipated at this time. Condition to be considered as expected environment on future flights. (Closed out)	19.5.1
S-IVB Instrumentation	Erroneous transducer output on CVS telemetered pressure during orbital coast and second burn.	Probably thermal shock on transducers.	Remote relocation of transducers on AS-502 and subs.	7.5 7.10.1 19.2.5

Table 22-1. Summary of Malfunctions and Deviations (Continued)

VEHICLE SYSTEMS	DEVIATION	PROBABLE CAUSE	CORRECTIVE ACTION BEING CONSIDERED	PARAGRAPH REFERENCE
PROPULSION DEVIATIONS				
S-II Propulsion	LOX ullage pressure approached redline during countdown and decayed at a higher than predicted rate during S-IC boost.	LOX tank vent valve reseal pressure was lower than predicted and heat loss from ullage to LH <sub>2</sub> was higher than predicted.	ECP 5238 approved for S-II-502 and subs to evacuate common bulk-head, lower ullage pressure redline, and eliminate LOX "Hi-Press." (Closed out)	6.1 6.6.2
S-II Propulsion	LOX ullage pressure dropped below control band, approximately 300 seconds after S-II start and continued to decay until cutoff.	Possible restriction in engine 4 heat exchanger system.	None No recurrence on subsequent flights expected.	6.1 6.6.2
S-II Propulsion	Greater than desired LH <sub>2</sub> ullage pressure decay during S-IC boost.	Higher than expected heat loss from ullage gas to LH <sub>2</sub> .	ECP 5182 approved for S-II-502 to change LH <sub>2</sub> "Hi-Press" sequence to assure colder ullage and/or higher pressure at liftoff on AS-502 only. (Closed out)	6.1 6.6.1
S-II Propulsion	Start tank temperatures were on cold side and pressures were to the high side of prelaunch and start boxes.	Different environment in S-IC/S-II inter-stage than expected.	Revise start tank and prechill limits and pressurization sequence.	6.1 6.2

Table 22-1. Summary of Malfunctions and Deviations (Continued)

VEHICLE SYSTEM	DEVIATION	PROBABLE CAUSE	CORRECTIVE ACTION BEING CONSIDERED	PARAGRAPH REFERENCE
S-II Propulsion	High LH <sub>2</sub> bulk temperature	High prelaunch vent stack back pressure	Modify facility vehicle vent system	6.1 6.2
S-II Propulsion	Thrust chamber heatup rates during S-IC boost greater than expected.	Engine environment warmer than expected.	Prechill thrust chamber to lower temperature and revise redline.	6.1 6.2
S-II Propulsion (J-2 engine)	Excessive usage of helium after ESC.	Engine No. 2 helium purge valve operated so slowly as to complete closure 4 seconds after ESC.	ECP 470 R1 approved for all J-2 engine beginning with AS-502 to use modified valve incorporating a filter. (Closed out)	6.1 6.2
22-4 S-IVB Propulsion	During the second revolution the stage pneumatic control sphere pressure began a slow decay and eventually dropped below regulator setting after end of S-IVB mission.	Leak probably associated with one or more of the seven actuation control modules or the regulator back-up calips switches.	(1) Cap calips port on pressure switch to eliminate possible leak path. (2) Use redesigned actuation control module.	7.1 7.11
S-IVB Propulsion	Apparent cold helium gas leakage into LOX tank prior to restart.	Supporting analyses indicate the leakage did not occur and pressure reading is in error.	None (Closed out)	7.1 7.10.2
S-IVB Propulsion	Unexpected decay of LH <sub>2</sub> ullage pressure after termination of repressurization.	Malfunction of diffuser or bubble formation.	(1) Implement diffuser ground test program. (2) Change flight sequence to optimize repressurization cycle. (3) Reorifice repress control module.	7.1 7.10.1



Table 22-1. Summary of Malfunctions and Deviations (Continued)

VEHICLE SYSTEM	DEVIATION	PROBABLE CAUSE	CORRECTIVE ACTION BEING CONSIDERED	PARAGRAPH REFERENCE
S-IVB Propulsion	High LH <sub>2</sub> bulk temperature	High prelaunch vent stack back pressure	Modify vent stack	7.1
S-IVB Propulsion	Apparent deterioration in thrust of the roll and yaw engines of APS Module No. 1 (at Position I) after S/C separation.	Under investigation	None	7.1 7.12
STRUCTURES DEVIATIONS				
IU Structures	Vibration input to the stabilized platform at liftoff exceeded the ran- dom specification limit at the lower frequencies.	Flight environment different than ex- pected.	Revision of specifi- cation to reflect measured flight en- vironment.	9.3.4.2
THERMAL ENVIRONMENT DEVIATIONS				
S-IC Base Heat	Two Temperature measure- ments on the base heat shield showed unexpected trend.	Loss of M-31 and delamination	Special attention to this area on future flights. (Closed out)	17.2
IU Environmental Control	IU ambient temperature dropped below redline limit (70 ± 10°F) prior to liftoff.	Heat loss to S-IVB forward dome.	Change lower redline limit to 55 °F.	18.5.1

22-5/22-6



## SECTION 23 SPACECRAFT SUMMARY

### 23.1 SUMMARY

The AS-501, Apollo 4, mission was successfully accomplished as planned using the Apollo Spacecraft 017, the lunar module LTA-10R and the Saturn Launch Vehicle SA-501.

The spacecraft was an unmanned Block I type incorporating selected Block II hardware for certification. Among these were a Block II heat shield, umbilical from the command module to the service module, VHF and S-band antennas, and a modified crew compartment hatch. As a result of being unmanned, a mission control programmer was installed while the crew couches, certain waste management items, certain displays and controls, and the postlanding ventilation valve were omitted.

### 23.2 SPACECRAFT PERFORMANCE EVALUATION

The spacecraft performed its mission perfectly. After separation from the S-IVB stage of the launch vehicle, the service propulsion engine was initiated to augment the thrust of the S-IVB which had placed the spacecraft into a simulated translunar trajectory. After a 16-second burn, the spacecraft was oriented to place the thickest side of the command module heat shield away from the solar vector. During the approximately 4-1/2 hour cold-soak period, the spacecraft coasted to an apogee of 9769 nautical miles. A total of 715 high resolution photographs were taken of the earth's surface during this time.

At an elapsed time of 8:10:55, the service propulsion system was reignited to simulate the lunar entry velocity. The velocity obtained was 299 feet-per-second greater than planned due to ground control of the maneuver. The heat protection system functioned to provide a temperature rise at the aft heat shield bond line of approximately 310°K (100°F) in spite of a nearly 3003°K (5000°F) temperature at the shield surface. Only a ten degree rise in the crew compartment occurred as a result of the entry heating.

As a result of the loss of the 5-volt reference for the instrumentation system at the separation of the command module from the service module, the discrete events that occur during entry were lost. The reference voltage dropped to unacceptable levels due to the improper fusing of the earth landing system controller circuit.

A lift-drag ratio of  $0.365 \pm 0.015$  was obtained placing the spacecraft within 6 miles of the recovery carrier at landing which was approximately 5 miles from the planned landing point. Recovery of the command module, apex heat shield, and one main parachute was effected in 8-foot swells within 2-1/2 hours after landing.

After recovery, the spacecraft was taken to Hawaii where it was deactivated. It was then flown to the North American Rockwell facility at Downey, California, for postflight testing.

The spacecraft and ground anomalies which occurred during the flight had no adverse effect upon completion of the mission. All spacecraft mission objectives were fully satisfied.

For further details on the spacecraft performance, refer to the Apollo 4 Mission Evaluation Report published by the NASA, Manned Spacecraft Center at Houston, Texas.

## APPENDIX A ATMOSPHERIC SUMMARY

### A.1 SUMMARY

The data presented in this section is a summary of the surface and upper atmospheric environment at the time of AS-501 launch. A general description and specific data for winds and thermodynamic conditions is included.

### A.2 GENERAL ATMOSPHERIC CONDITIONS AT LAUNCH TIME

The southeastern United States was dominated by a high pressure system with the center of the system over northern Alabama and Georgia. The surface wind flow at Cape Kennedy, Florida was from the northeast. The wind flow above 7 kilometer (23,000 ft) was generally from the west.

### A.3 SURFACE OBSERVATIONS AT LAUNCH TIME

At launch time, there were 4/10 stratocumulus clouds with bases at 1370 meters (4500 ft). Visibility was 19 kilometer (12 stat mi). Satisfactory chart records were available for only one anemometer on the launch pad. Five of the eight chart records were not received. Of the three received, one provide speed only while the other chart data was not considered representative of the area. Table A-1 summarizes the surface observations at launch time.

Solar radiation data was measured on the launch pad with total horizontal and normal incident sensors. This data is presented in Table A-2.

### A.4 UPPER AIR MEASUREMENTS

Upper air wind data were obtained from four of the five systems requested, with three being used in the final meteorological tape. Table A-3 summarizes the data used. The data from the Cajun-dart arrived too late to be used in the meteorological tape, but has been added to Figures A-1 and A-2.

#### A.4.1 Wind Speed

The wind speed at the lower altitudes did not exceed 26 m/s (50.5 knots) below 30 kilometers (98,000 ft). The maximum wind in the high dynamic pressure region was 26 m/s (50.5 knots) at 11.5 kilometer (37,700 ft). Between 25 and 50 kilometers (82,000 ft and 164,000 ft), the wind increased, reaching a maximum of 91 m/s (177 knots) at 50 kilometers (164,000 ft) as shown in Figure A-1.

Table A-1. Surface Observations at AS-501 Launch Time

LOCATION	TIME AFTER T-0 (MIN)	PRESS-URE N/CM <sup>2</sup> (PSIA)	TEM-PERATURE °K (°F)	REL. HUM. (%)	VISI-BILITY KM (STA MI)	AMOUNT (TENTHS)	SKY COVER TYPE	HEIGHT OF BASE	WIND	
									SPEED M/S (KNOTS)	DIR. (DEG)
MILA (MSOB)	T-0	--	292.03 (66.0)	--	19 (12)	4 <sup>1</sup>	SC	1370	6.2 <sup>2</sup> (12.0)	040
Cape Kennedy Rawinsonde Measurements	T+10	10.261 (14.9)	285.55 (54.0)	55	N/A	N/A	N/A	N/A	3 (6.0)	060
Pad 34 Light Pole S (19.5 m) <sup>3</sup>	T-0	N/A	N/A	N/A	N/A	N/A	N/A	N/A	8.0 (16.0)	070
LUT Top (135.6 m) <sup>3</sup>	T-0								9.5 (19.0)	--
<sup>1</sup> Vehicle entered cloud base at 7:01:45 EST and exited through cloud top at 7:01:52 EST <sup>2</sup> 10 meter height <sup>3</sup> Above natural grade										

Table A-2. Solar Radiation Data (0.35 to 4.0 microns) at AS-501 Launch

DATE NOV. 1967	HOUR ENDING EST	TOTAL HORIZONTAL SURFACE	NORMAL INCIDENT	DIFFUSE (SKY)
8	0700	0.18	0.00	0.00
8	0800	0.21	0.10	0.19
8	0900	0.75	1.10	0.33
8	1000	1.13	1.44	0.35
8	1100	1.42	1.43	0.50
8	1200	1.61	1.06	0.85
8	1300	1.47	1.15	0.65
8	1400	1.02	0.79	0.51
8	1500	0.88	0.84	0.42
8	1600	0.62	0.48	0.44
8	1700	0.31	0.29	0.26
8	1800	0.03	0.04	0.03
9	0700	0.01	0.00	0.00
9	0800	0.20	0.62	0.09

Units of Data--gm cal cm<sup>-2</sup> min<sup>-1</sup>

Cape Kennedy, Florida, Pad 39 Values are average for each hour

To obtain watt m<sup>-2</sup>, multiply by 697.33To obtain Btu ft<sup>-2</sup> hr<sup>-1</sup>, multiply by 221.20

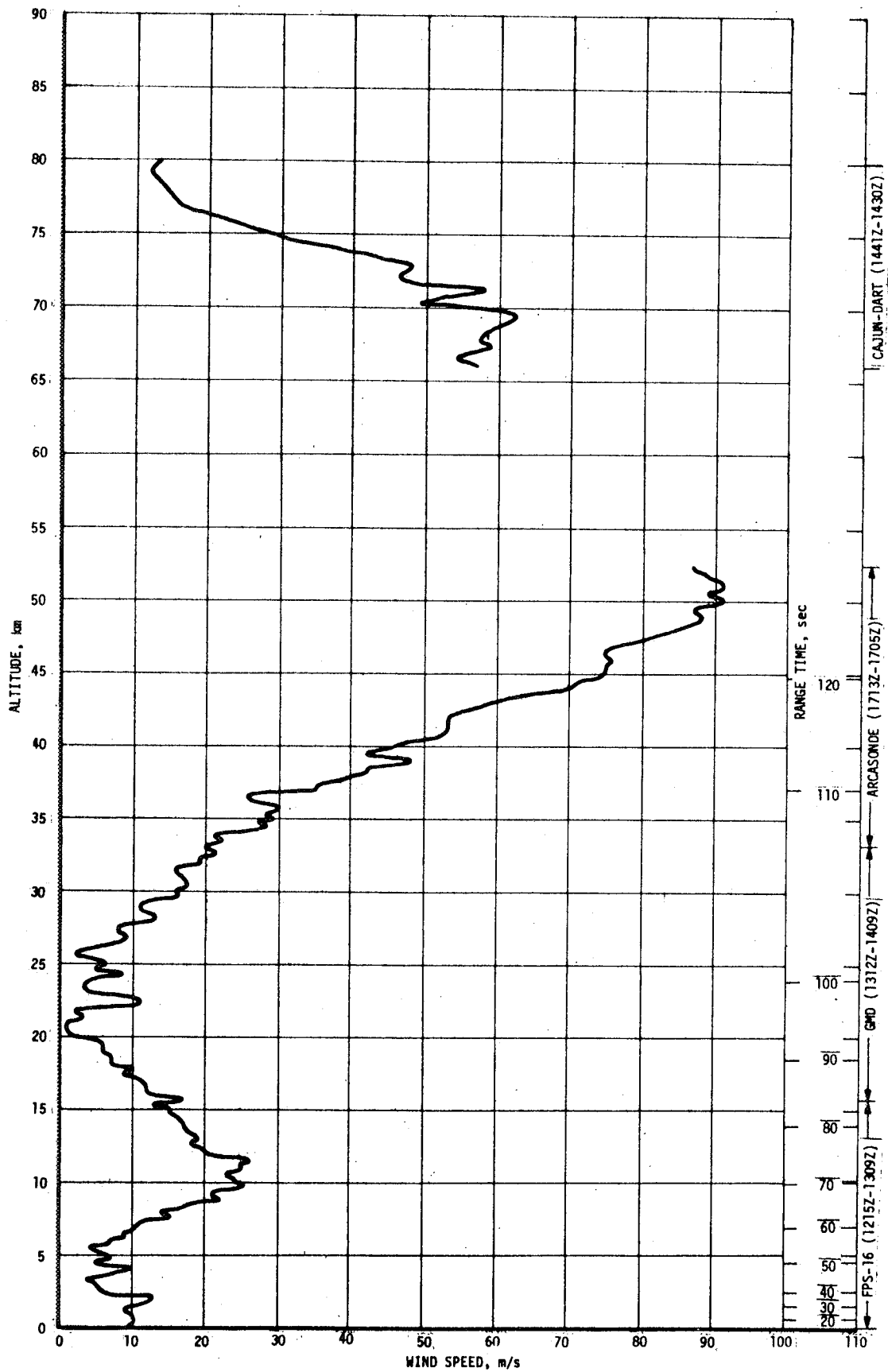


Figure A-1. AS-501 Scalar Launch Wind

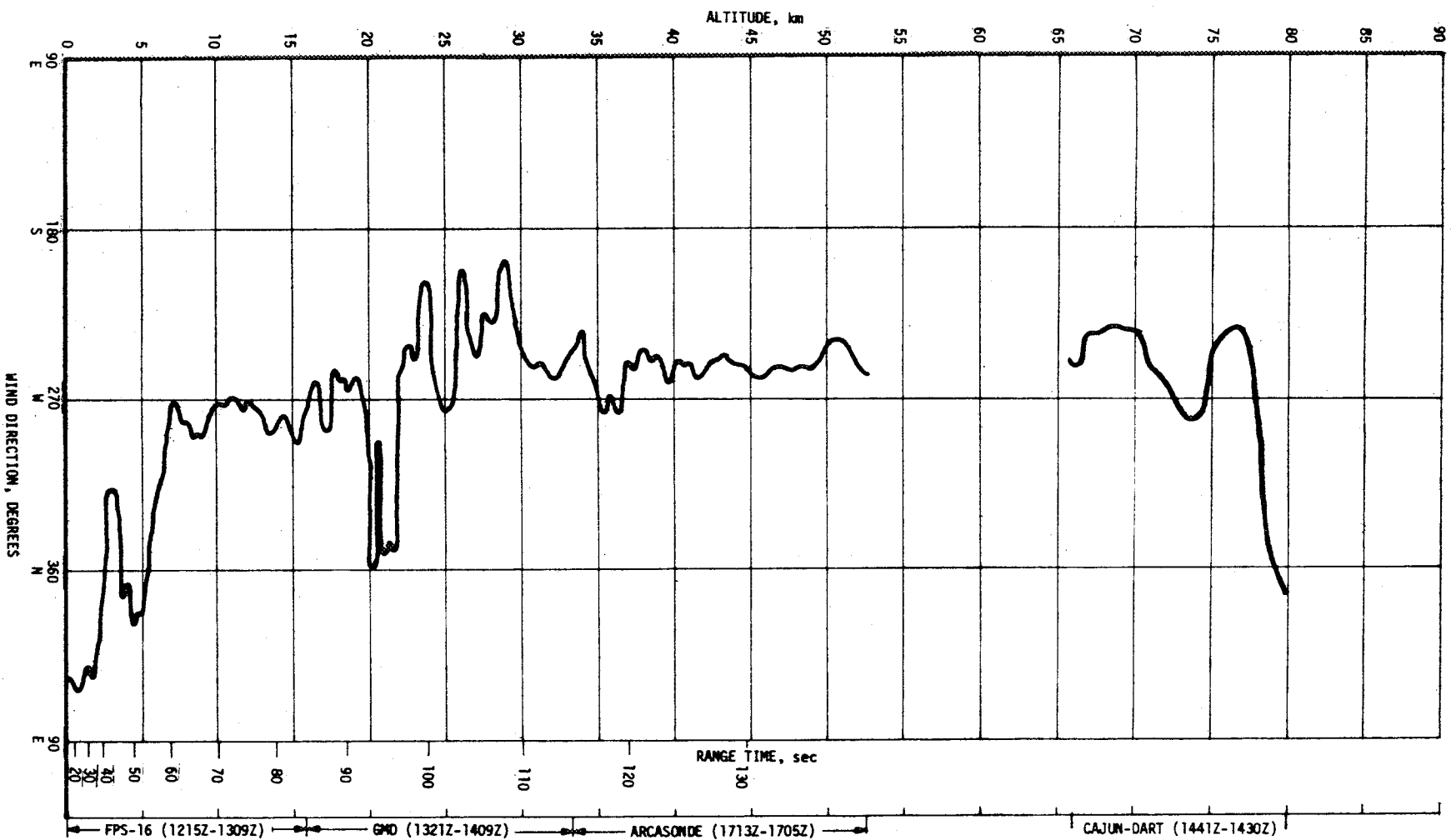




Table A-3. Systems Used To Measure Upper Air Wind Data, AS-501

TYPE OF DATA	RELEASE TIME NOV. 9, 1967		PORTION OF DATA USED			
	TIME (UT)	TIME AFTER T-0 (MIN)	START		END	
			ALTITUDE M (FT)	TIME AFTER T-0 (MIN)	ALTITUDE M (FT)	TIME AFTER T-0 (MIN)
FPS-16 Jimsphere	1215	15	Surface	15	15,750 (51,700)	69
Rawinsonde	1220	20	16,000 (52,500)	72	33,250 (109,000)	129
Arcasonde	1700	300	52,500 (172,000)	305	33,500 (110,000)	313

Table A-4 shows the maximum wind speed and wind speed components in the high dynamic pressure region for AS-501, AS-201, AS-203, AS-202, and Saturn I vehicles.

#### A.4.2 Wind Direction

At the surface the wind was from the northwest. Between the surface and 7 kilometer (23,000 ft) it had shifted (backed) to west. Above 7 kilometer (23,000 ft) the wind direction was generally from the west and southwest as shown in Figure A-2.

#### A.4.3 Pitch Wind Component

Pitch wind components followed the median (or were slightly lower) up to 30 kilometers (98,000 ft). Above 6 kilometers (19,700 ft) the pitch wind components were tail winds. The maximum value was 24.3 m/s (47.2 knots) at 11.5 kilometers (37,700 ft) in the high dynamic pressure region. Above 30 kilometers (98,000 ft) the pitch wind components (tail winds) increased and exceeded the median, reaching a maximum of 91 m/s (177 knots) at 50 kilometer (164,000 ft) as shown in Figure A-3.

#### A.4.4 Yaw Wind Component

The yaw wind component never exceeded 15 m/s (29.2 knots) below 50 kilometers (164,000 ft). Winds were from the left up to 20 kilometers (66,000 ft) reaching a value of 12.9 m/s (25.1 knots) at 9 kilometers (30,000 ft) as shown in Figure A-4.

Table A-4. Maximum Wind Speed in High Dynamic Pressure Region

VEHICLE NUMBER	MAXIMUM WIND			MAXIMUM WIND COMPONENTS			
	SPEED M/S (KNOTS)	DIR (DEG)	ALT KM (FT)	PITCH ( $W_x$ ) M/S (KNOTS)	ALT KM (FT)	YAW ( $W_z$ ) M/S (KNOTS)	ALT KM (FT)
SA-1	47.0 (91.4)	242	12.25 (40,200)	36.8 (71.5)	13.00 (42,600)	-29.2 (-56.8)	12.25 (40,200)
SA-2	33.6 (65.3)	216	13.50 (44,300)	31.8 (61.8)	13.50 (44,300)	013.3 (-25.9)	12.25 (40,200)
SA-3	31.3 (60.8)	269	13.75 (45,100)	30.7 (59.7)	13.75 (45,100)	11.2 (21.8)	12.00 (39,400)
SA-4	51.8 (100.7)	253	13.00 (42,600)	46.2 (89.8)	13.00 (42,600)	-23.4 (-45.5)	13.00 (42,600)
SA-5	42.1 (81.8)	268	10.75 (35,300)	41.1 (79.9)	10.75 (35,300)	-11.5 (-22.4)	11.25 (36,900)
SA-6	15.0 (29.2)	96	12.50 (41,000)	-14.8 (-28.8)	12.50 (41,000)	12.2 (23.7)	17.00 (55,800)
SA-7	17.3 (33.6)	47	11.75 (38,500)	-11.1 (-21.6)	12.75 (41,800)	14.8 (28.8)	12.00 (39,400)
SA-9	34.3 (66.7)	243	13.00 (42,600)	27.5 (53.5)	10.75 (35,300)	23.6 (45.9)	13.25 (43,500)
SA-8	16.0 (31.1)	351	15.25 (50,000)	12.0 (23.3)	11.00 (36,100)	14.6 (28.4)	15.25 (50,000)
SA-10	15.0 (29.2)	306	14.75 (48,400)	12.9 (25.1)	14.75 (48,400)	10.8 (21.0)	15.45 (50,700)
AS-201	70.0 (136.1)	250	13.75 (45,100)	57.3 (111.4)	13.75 (45,100)	-43.3 (-84.2)	13.25 (43,500)
AS-203	18.0 (35.0)	312	13.00 (42,600)	11.1 (21.6)	12.50 (41,000)	16.6 (32.3)	13.25 (43,500)
AS-202	16.0 (31.1)	231	12.00 (39,400)	10.7 (20.8)	12.50 (41,000)	-15.4 (-29.9)	10.25 (33,600)
AS-501	26.0 (50.5)	273	11.50 (37,700)	24.3 (47.2)	11.50 (37,700)	12.9 (25.1)	9.00 (29,500)

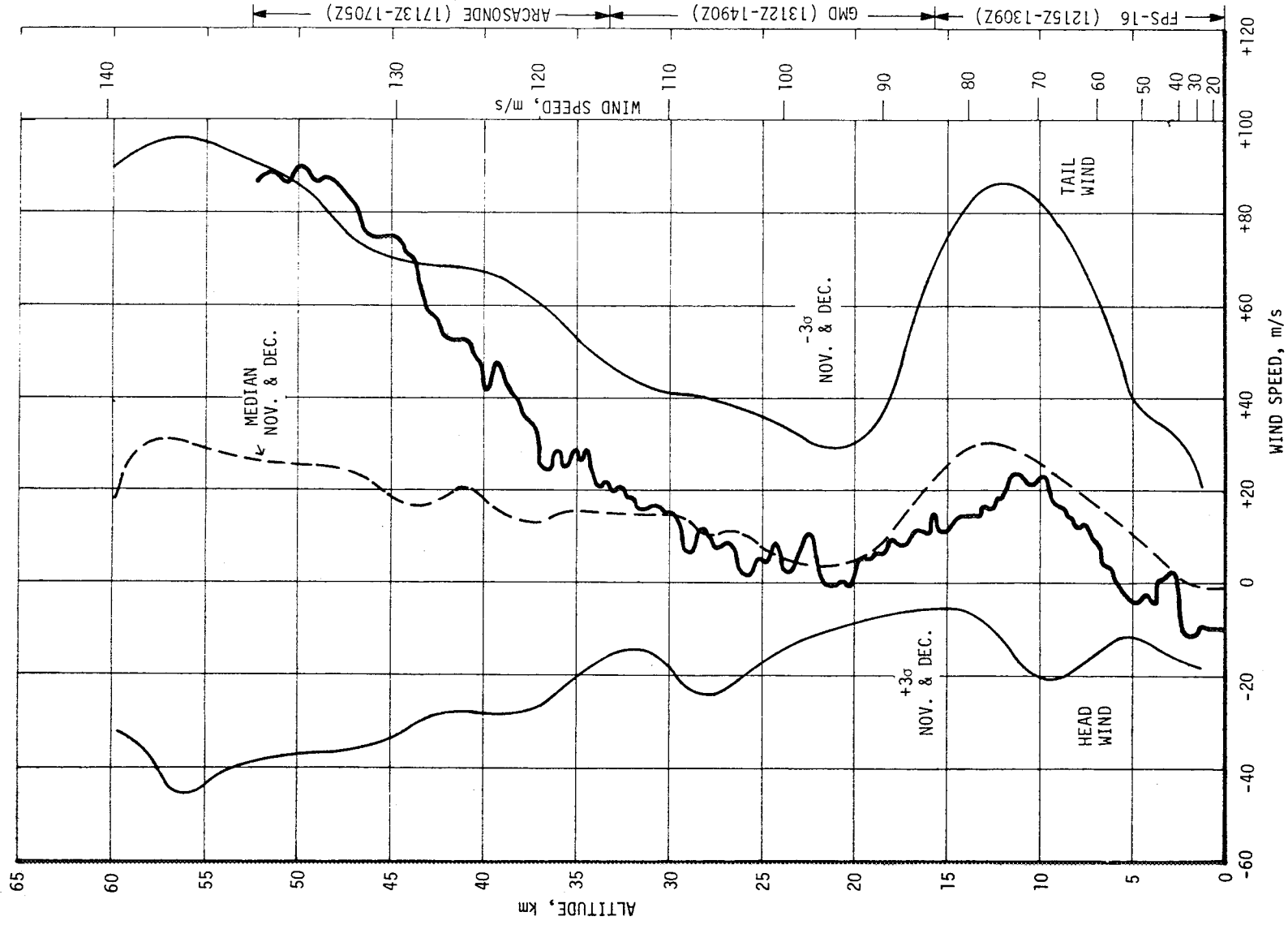


Figure A-3. AS-501 Launch Time Pitch Wind Component ( $W_x$ )

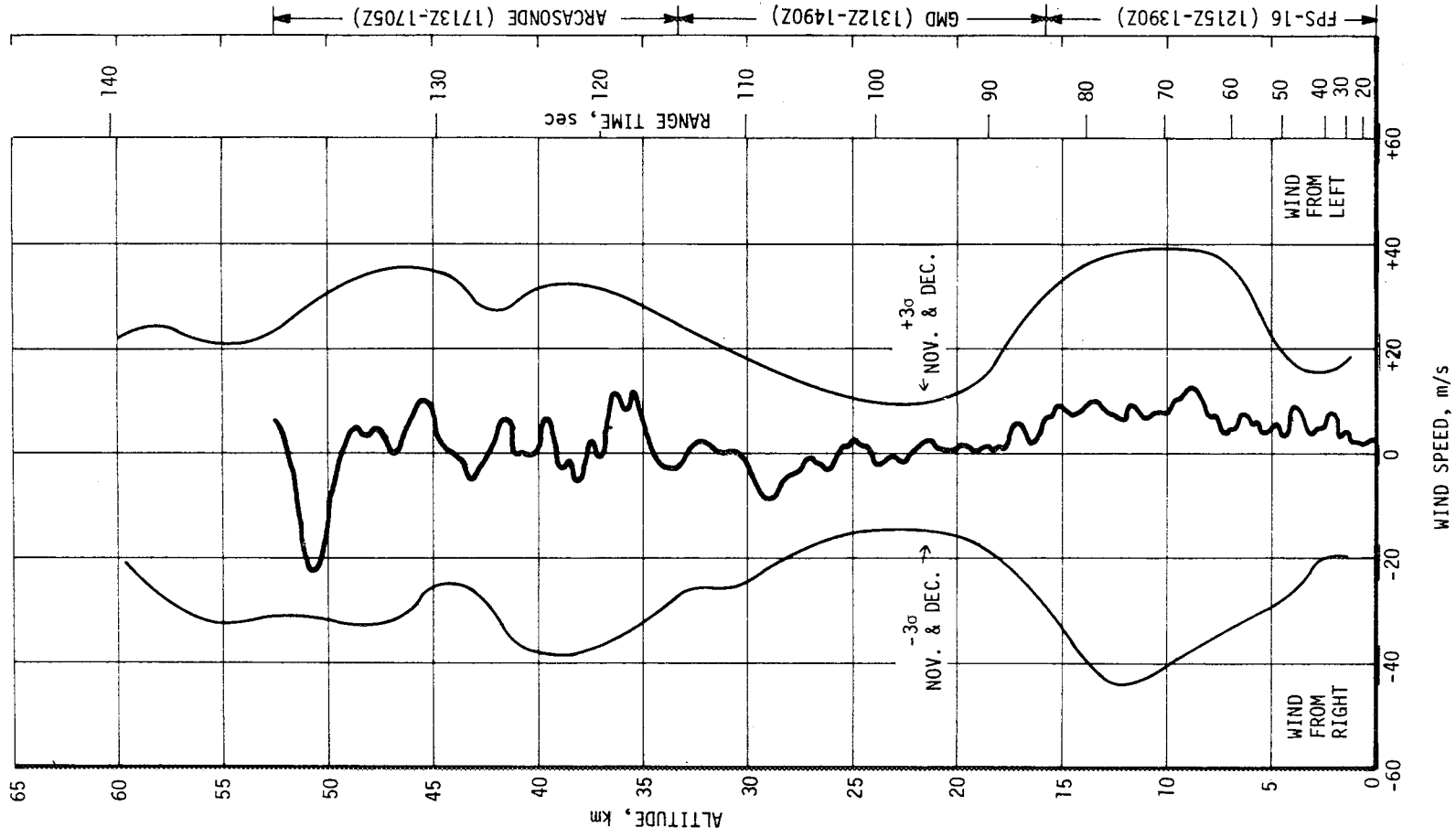


Figure A-4. AS-501 Launch Time Yaw Wind Component ( $W_z$ )

#### A.4.5 Component Wind Shears

Component wind shears ( $\Delta h = 1000$  m) were of low magnitude as shown in Figure A-5. The wind shears are given for AS-501, AS-201, AS-203, AS-202, and Saturn I vehicles in Table A-5.

#### A.5 THERMODYNAMIC DATA

Comparisons of the thermodynamic data taken at launch time with the Patrick Reference Atmosphere (PRA) (1963) for temperature, density, pressure, and optical index of refraction are shown in Figures A-6 and A-7.

##### A.5.1 Temperature

Atmospheric temperatures at launch time were generally lower than that of the PRA temperature. The temperature reached a value of 5.7 percent below the PRA at 2.25 kilometers (7400 ft). Above 42 kilometers (138,000 ft) the relative deviations are greater than the PRA with a maximum of +3.7 percent greater than the PRA at 47.75 kilometers (157,000 ft) as shown in Figure A-6.

##### A.5.2 Density

The surface air density at launch time was +5.5 percent greater than the PRA density. The density remained greater up to 7.0 kilometers (23,000 ft). The maximum value being +5.8 percent at 1.5 kilometers (5000 ft). Above 7 kilometers (23,000 ft) the density is generally lower, with a minimum of -8.9 percent of the Patrick value of density at 47.0 kilometers (154,000 ft) as shown in Figure A-6.

##### A.5.3 Pressure

Launch time atmospheric pressure at the surface was 0.9 percent higher than the pressure of the PRA. Above the surface, the pressure decreased to less than that of the Patrick value, with the greatest difference being -7.9 percent at 31.5 kilometers (103,000 ft). Around 34 kilometers (112,000 ft), the discontinuity shown results from the tie-in of the Radiosonde and the Rocketsonde profiles as shown in Figure A-7.

##### A.5.4 Optical Index of Refraction

At the surface during launch, the optical index of refraction was  $-51.1 (n-1) \times 10^{-6}$  units lower than the corresponding value of the PRA. Above the surface, the value decreased rapidly reaching near zero at 25 kilometers (82,000 ft) as shown in Figure A-7.

Table A-5. Extreme Wind Shear in High  
Dynamic Pressure Region

(Δh = 1000 M)				
VEHICLE NUMBER	PITCH PLANE		YAW PLANE	
	SHEAR (SEC <sup>-1</sup> )	ALTITUDE KM (FT)	SHEAR (SEC <sup>-1</sup> )	ALTITUDE KM (FT)
SA-1	0.0145	14.75 (48,400)	0.0168	16.00 (52,500)
SA-2	0.0144	15.00 (49,200)	0.0083	16.00 (52,500)
SA-3	0.0105	13.75 (45,100)	0.0157	13.25 (43,500)
SA-4	0.0155	13.00 (42,600)	0.0144	11.00 (36,100)
SA-5	0.0162	17.00 (55,800)	0.0086	10.00 (32,800)
SA-6	0.0121	12.25 (40,200)	0.0113	12.50 (41,000)
SA-7	0.0078	14.25 (46,800)	0.0068	11.25 (36,900)
SA-9	0.0096	10.50 (34,500)	0.0184	10.75 (35,300)
SA-8	0.0065	10.00 (32,800)	0.0073	17.00 (55,800)
SA-10	0.0130	14.75 (48,400)	0.0090	15.00 (49,200)
AS-201	0.0206	16.00 (52,500)	0.0205	12.00 (39,400)
AS-203	0.0104	14.75 (48,400)	0.0079	14.25 (46,800)
AS-202	0.0083	13.50 (44,300)	0.0054	13.25 (43,500)
AS-501	0.0066	10.00 (32,800)	0.0067	10.00 (32,800)

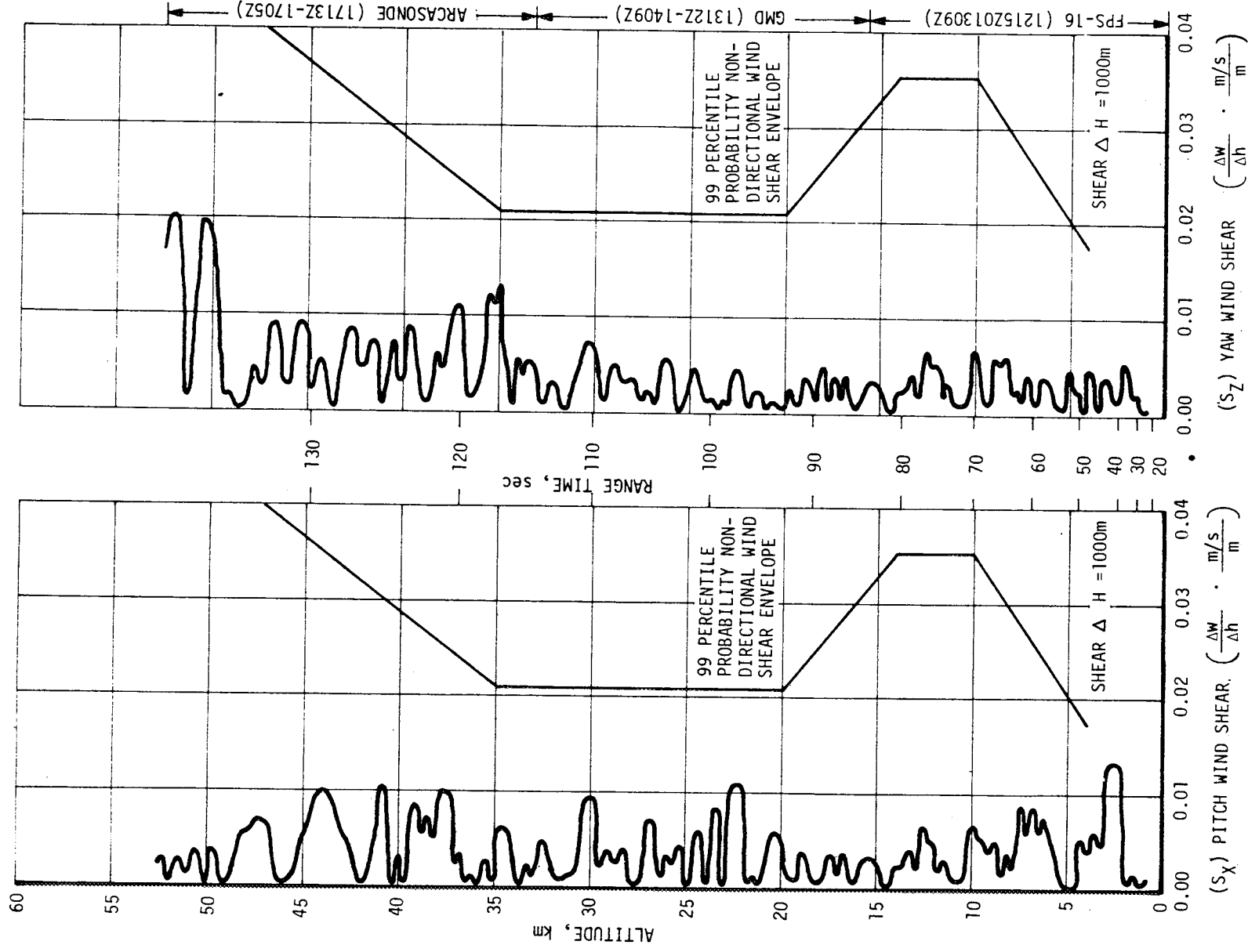


Figure A-5. AS-501 Launch Time Pitch ( $S_X$ ) and Yaw ( $S_Y$ ) Component Wind Shears

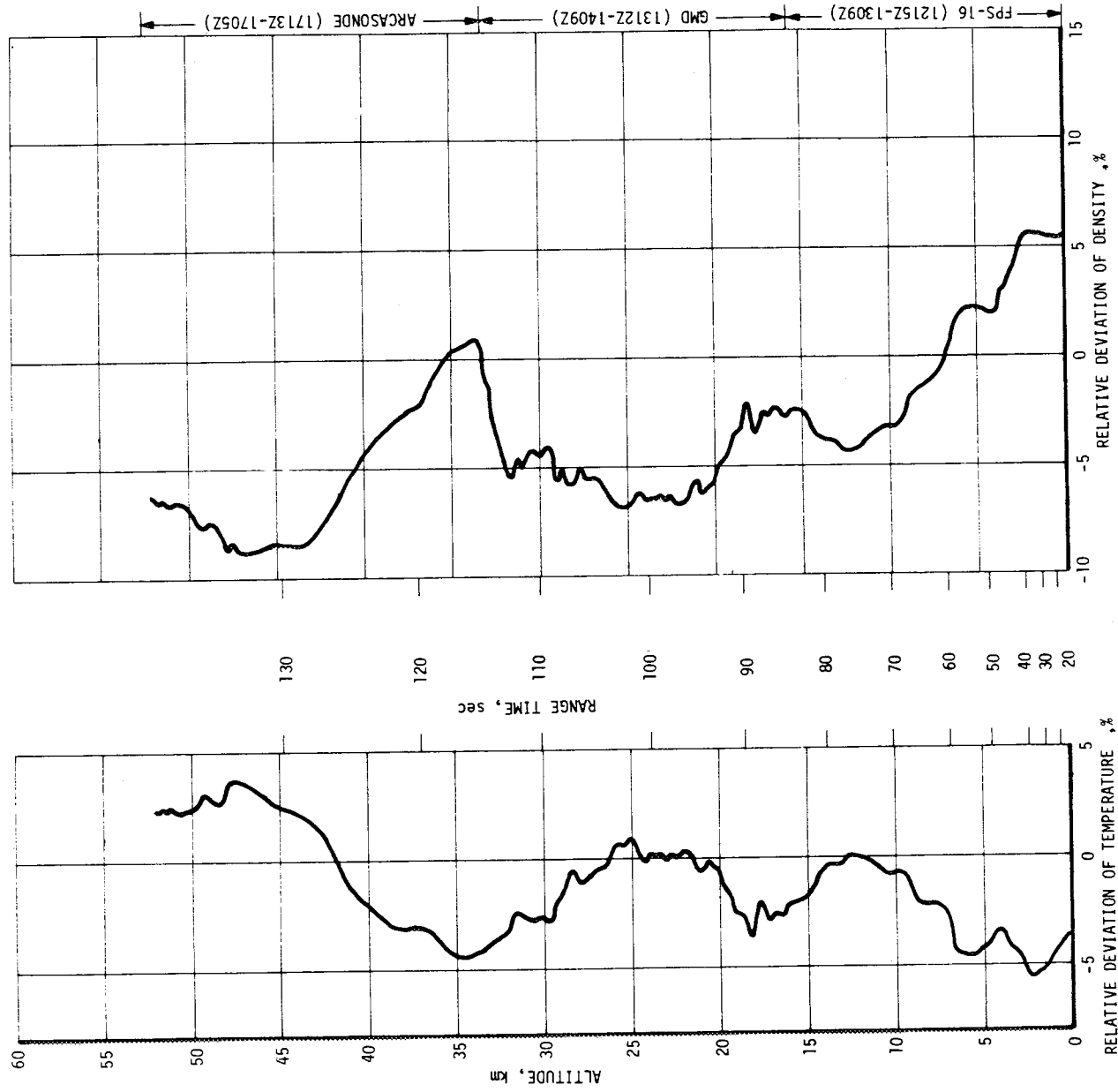


Figure A-6. Relative Deviation of AS-501 Temperature and Density  
From PAFB (63) Reference Atmosphere



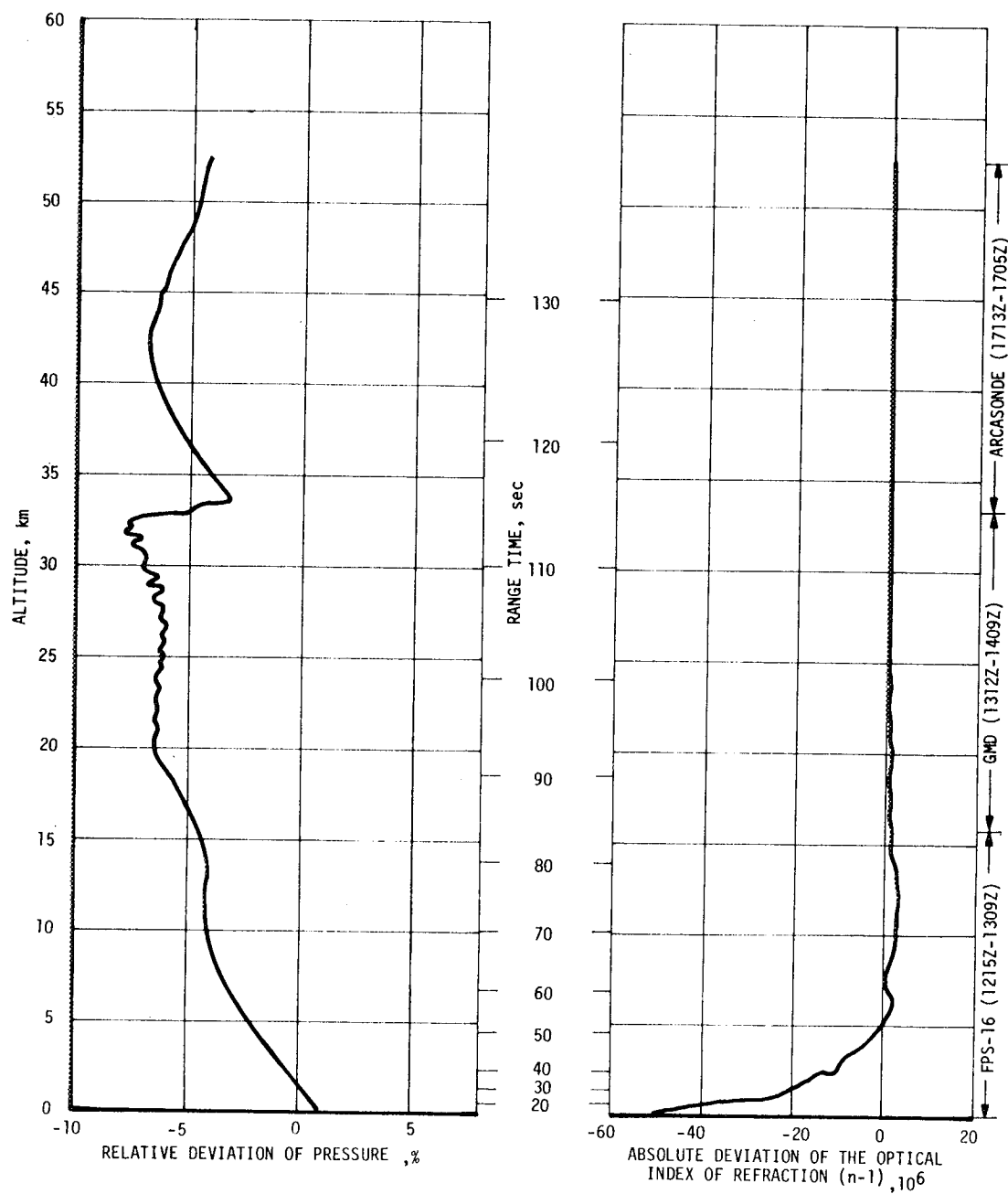


Figure A-7. Relative Deviation of Pressure and Absolute Deviation of the Index Of Refraction from the PAFB (63) Reference Atmosphere AS-501



## APPENDIX B

### AS-501 LAUNCH VEHICLE DESCRIPTION

#### B.1 VEHICLE

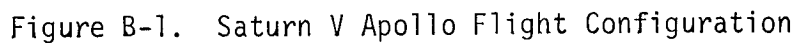
The Saturn V launch vehicle, configured as illustrated in Figure B-1, consists of a booster with three propulsive stages and an instrument unit; and a payload consisting of a refurbished lunar module test article (LTA), generally a Block I command module (CM), a service module (SM), and a launch escape system (LES). The nominal weight of the vehicle is 2,820,000 kilograms (6,220,000 lbm).

##### B.1.1 Vehicle Structure

The vehicle nominal length is 110.7 meters (363.0 ft.). The booster length is 85.7 meters (281.2 ft.) with the S-IC first stage nominal diameter of 10.1 meters (33.1 ft.) and a nominal diameter of 6.6 meters (21.7 ft.) at the uppermost section, the instrument unit (IU). Four fixed fins of equal size are fitted to the first stage for aerodynamic stability.

##### B.1.2 Vehicle Propulsion

The S-IC stage is powered by five bi-propellant F-1 engines developing a combined nominal thrust of 33,400,000 Newtons (7,500,000 lbf), using liquid oxygen (LOX) as the oxidizer and RP-1 as the fuel. The center engine is fixed on the vehicle centerline and the four outboard engines are gimballed by hydraulically operated servoactuators for thrust vector control. The second stage, S-II, is powered by five bi-propellant J-2 engines developing a combined nominal thrust of 4,450,000 Newtons (1,000,000 lbf) using LOX as the oxidizer but liquid hydrogen (LH<sub>2</sub>) as the fuel. The center engine is fixed on the vehicle centerline and the four outboard engines, aligned with the S-IC four outboard engines, are gimballed by hydraulically operated servoactuators for thrust vector control. The third propulsive booster stage, S-IVB, is powered by one J-2 engine with a nominal thrust of 890,000 Newtons (200,000 lbf), LOX and LH<sub>2</sub> as propellants. The engine is gimballed for partial thrust vector control and is aligned at the null position with the vehicle centerline. To settle propellants and to complete thrust vector control the auxiliary propulsion system (APS) is used which consists of two self-contained rocket motor packages attached externally to the stage and located 180 degrees apart. The SM contains the service propulsion system (SPS) which provides the thrust required for large changes in spacecraft (SC) velocity after booster separation. The SPS consists of a gimbal-mounted single-rocket engine, pressurization and propellant tanks, and associated components, all of which are located in the service module. Also located in the SM the reaction control system (RCS) consists of four independent, equally capable, and functionally identical packages. Each package contains four reaction control engines, fuel and oxidizer tanks, a helium tank, and associated components such as regulators valves, filters,



lines, and a nucleonic quantity gauging system.

### B.1.3 Vehicle Systems

The vehicle systems, those systems which are interrelated throughout the vehicle though having in part system and subsystems in certain sections of the vehicle, consist of the guidance, navigation and control system, data system, separation system, range safety system, command and communication system and emergency detection system.

B.1.3.1 The Data System - The data system consists of the measurement system, telemetry system, and tracking system.

The measurement system components are transducers, measuring racks, measuring distributors, measuring rack selectors, and measuring voltage supplies. These components perform the following functions.

- a. The transducers transform the physical quantities being measured into electrical signals.
- b. The signal conditioners convert the transducer output into a signal that is acceptable to telemetry.
- c. The measuring distributors accept the 5-volt outputs from the signal conditioning modules and route them to the proper telemetry channels.
- d. The measuring rack selector is used by the remote automatic calibration system (RACS) to select the proper measurement for calibration prior to launch.
- e. The measuring voltage supplies provide regulated 5-volt power to the measurement system.

The telemetry system on the S-IC is composed of six VHF-RF links. These links are a combination of three PAM/FM/FM links (AF1, AF2, and AF3), two SS/FM links (AS1 and AS2), and one PCM/FM link (AP1) incorporated to handle data and full-fill measurement requirements. These different modulation techniques provide efficient transmission of a large quantity and variety of measuring data that requires different bandwidth and accuracy.

The S-II telemetry system has seven VHF-RF links which are a combination of three PAM/FM/FM links (BF1, BF2, and BF3), one PCM/FM link (BP1), two SS/FM links (BS1 and BS2), and one PAM/FM/FM link (BT1). The PAM/FM/FM and PCM/FM systems are used for airborne telemetry measurements of relatively low-frequency data and SS/FM systems are used for airborne telemetry of high-frequency data. That of the S-IVB requires five VHF-RF links. These links combine three PAM/FM/FM links (CF1, CF2, and CF3), one SS/FM link (CS1), and one PCM/FM link (CP1). However the Instrument Unit (IU) System is composed of four telemetry links. There is one FM/FM (DF1) link, one PAM/FM/FM (DF2) link, one SS/FM link (DS1), and one PCM/FM link (DP1). The PCM/FM information is transmitted by a VHF-RF assembly, a UHF-RF assembly, and the Command

and Communication System (CCS) transponder. The SS/FM and the two FM/FM links are transmitted by separate VHF-RF assemblies.

The tracking system on the S-IC stage is offset Doppler (ODOP) which consists of a transponder and two antennas. The IU contains C-band radar providing radar tracking independent of vehicle attitude, AZUSA/GLOTRAC which consists of a type C-AZUSA transponder and antenna, and the S-band tracking transponder and antenna which supply range and range rate data for precise tracking during orbit.

B.1.3.2 Navigation, Guidance and Control System - The Navigation, Guidance and Control (NGC) system is an all-inertial system utilizing a full-freedom platform for acceleration and attitude measurements. A digital computer is used for guidance computation and an analog computer for the control functions. The navigation, guidance, and control function is achieved by:

- a. A series of attitude, acceleration, velocity, and present-position determinations.
- b. The prediction and compilation of velocity corrections required to attain a desired space position and attitude.
- c. Generation of proper thrust and vehicle attitude control commands.

The NGC system issues commands to the attitude control devices of each stage during powered flight to guide the Apollo vehicle in accordance with a pre-programmed mission.

Before launch, the ST-124M Inertial Platform is erected with the  $X_S$  axis vertical and  $Z_S$  axis pointing in the direction of the launch azimuth. Since the launch azimuth is varying with time, the platform is torqued to maintain this orientation. Just prior to liftoff, the platform is released and becomes space-fixed oriented. The  $Z_S$  axis now determines the flight azimuth.

The vehicle lifts off vertically from the launch pad and maintains its liftoff orientation long enough to clear the ground equipment. It then performs a roll maneuver to align the vehicle with the flight azimuth direction (on the launch pad, the vehicle always has a roll orientation fixed to the launching site) and a yaw maneuver to clear the tower. The roll maneuver gives the vehicle control axes the correct alignment to the flight plane thus simplifying the computations in the attitude control loop.

During first stage propulsion, a time-tilt (pitch) program, stored in the LVDC, is applied simultaneously with the described roll maneuver. The pitch angle of the vehicle is commanded according to the tilt program which is a function of time only and is independent of navigation measurements. However, navigation measurements and computations are performed through the flight, beginning at the time the platform is released (i.e., approximately 8 to 10 seconds before liftoff). Cutoff of the first stage engines occurs when the propellant

level in the tanks reaches a predetermined level. Thereafter, the first stage is separated from the launch vehicle.

After ignition of the S-II stage, adaptive guidance (i.e., the iterative guidance mode) is used during all propelled flight phases of the mission. The iterative guidance mode computes the pitch and yaw angle of the required thrust direction to guide the vehicle on a minimum propellant trajectory into the predetermined parking orbit.

S-II stage engine cutoff is initiated when the propellant in the S-II tank is consumed to a predetermined level. Following separation of the S-II stage, the S-IVB stage engine is ignited. By this time the vehicle has reached the approximate orbital altitude and the S-IVB propulsion provides the necessary velocity for the circular parking orbit. When the predetermined velocity has been obtained, the guidance computations command engine cutoff.

During orbital coast flight, the navigation program continually computes the vehicle position and velocity from the equations of motion based on insertion conditions. Attitude of the vehicle roll axis in orbit is normally maintained at 90 degrees with respect to the local vertical. The local vertical is determined from navigational computations. The time of reignition of the S-IVB engine and the required thrust orientation for powered flight-out-of-orbit are computed during each orbit.

In orbit, navigation and guidance information in the LVDC can be updated by data transmission from ground stations through the IU radio command system.

When the computed time of reignition occurs, the S-IVB engine is ignited. The same guidance equations are used again for the waiting orbit injection. The S-IVB propulsion is cut off when the proper energy (velocity) for injection is achieved. In the following flight phase, up to and through the transposition maneuver, navigation and guidance computations continue.

**B.1.3.3 Separation System** - After the S-IC and S-II stages are severed by a linear-shaped charge, retro motors located in the engine fairings apply a net deceleration force to the S-IC stage, sufficient to effect separation and prevent the S-IC stage from interfering with the upper stages during S-IC/S-II stage separation. The retro motor system is comprised of eight solid propellant motors mounted symmetrically in pairs within each of the four S-IC stage outboard F-1 engine fairings. Each motor burns for approximately 0.6 second and produces a thrust of over 409,000 Newtons (92,000 lbf).

A dual plane method is used for S-IC/S-II separation, and a single plane separation is used between the S-II/S-IVB stages. The separation sequence is controlled by the digital computer located in the Instrument Unit. The separation methods may be divided into five functional areas for S-IC/S-II and two functional areas for S-II/S-IVB.

- a. Acceleration of the vehicle during separation. Propellant settling is required to start the engines in the S-II stage during the weightless period after first plane separation. This is accomplished by the firing of eight ullage motors positioned around the S-II aft interstage. The eight ullage motors will burn for approximately 3 seconds and produce a thrust of 101,400 Newtons (22,800 lbf) per motor.
- b. Severing S-IC/S-II stages. A linear-shaped charge is used to physically sever the stages at the first separation plane. This function is electrically controlled by the S-IC stage.
- c. Retarding the S-IC stage. Retro motors, controlled by and located on the S-IC stage, are ignited to decelerate the stage.
- d. Severing of the S-II interstage at the second separation plane. A linear-shaped charge is also used for separation at this plane. This operation is controlled by electrical signals from the S-II stage-
- e. Retarding the interstage. After J-2 engine stabilization, the combined effect of the S-II stage thrust and the reaction of the J-2 engine exhaust plume impingement forces moves the interstage away from the S-II stage.
- f. Severing of the S-II/S-IVB. A mild detonating fuse is used to physically sever the S-IVB interstage at the S-IVB interstage mating plane. This action is controlled by the S-II stage.
- g. Retarding the S-II stage. Four retro motors embedded around the S-IVB interstage ignite to decelerate the S-II stage for complete separation. Ignition is controlled by the S-II stage.

B.1.3.4 Range Safety System - The range safety command system provides a means to terminate the flight of the vehicle by radio command from the ground in case of emergency situations in accordance with range safety requirements. Each powered stage of the vehicle is equipped with two command receivers/decoders and the necessary antennas to provide omnidirectional receiving characteristics (range safety requirements). The command destruct system in each stage is completely separate and independent of those in other stages. In case of vehicle malfunctions which cause trajectory deviations larger than specified limits, the vehicle will be destroyed by the range safety officer by means of the range safety command system. The range safety system is active until the vehicle has achieved earth orbit, after which the destruct system is deactivated (safed) by command from the ground.

A destruct command results in shutting down the engines and rupturing the propellant tanks of all stages by explosive means. Linear shaped charges will rupture the LOX tanks on one side of stage and the fuel tanks on the other to minimize propellant mixing and resultant explosions.



B.1.3.5 Emergency Detection System - The purpose of the EDS is to sense onboard emergency situations which arise during the boost phase of the flight. On AS-501 the EDS is flown in an open loop configuration which precludes automatic abort.

The EDS is comprised of sensors which detect malfunctions, and logic circuitry which initiate spacecraft displays and, in two cases, automatic abort of the CM. With the exception of the Q-ball, mounted on top of the LET, the EDS sensors are located in the launch vehicle. The system's relay logic is located primarily in the IU EDS distributor and the CM mission events sequence controller.

The EDS has two modes of operation. "Manual", which generates abort cues and "automatic" which initiates firing of the LES, and CM separation in the case of the two S-IC engines out or angular overrates during S-IC powered flight. The automatic abort initiating portion of the system consists of the launch vehicle's rate sensing subsystem, the stage thrust sensing subsystem, and the signal distribution and processing hardware which services these devices.

The angular overrate sensors, three per axis in pitch, yaw, and roll will initiate automatic abort of the CM during the period they are enabled (liftoff to about 136 seconds) whenever two sensors in any one axis simultaneously indicate excessive rates. Detection of the overrates is made by the sensor switch circuitry of the control signal processor in the IU. The settings of these angular rate detectors are 5 degrees per second in pitch and yaw and 20 degrees per second in roll. The majority voting of the three switch outputs in each axis is done by relay logic in the EDS distributor. A valid excess rate decision is forwarded by the EDS distributor to the CM mission events sequence controller for abort initiation.

The S-IC stage engine thrust OK sensors, three per engine on all five engines, will also initiate abort during the period they are enabled (liftoff to about 135 seconds) when the voted output of the sensors from any two engines indicates that the thrust of those engines is below the 89 percent level. These sensors monitor the F-1 engine fuel inlet manifold pressure. Majority voting of the three sensors for each engine is done in the EDS distributor. A valid two engines out decision is sent to the mission events sequence controller for CM abort initiation.

B.1.3.6 Command and Communication System - The Command and Communication System (CCS) is a phase-coherent receiver-transmitter capable of establishing a communication link between the Unified S-Band (USB) ground stations and the IU of the launch vehicle. Specifically, the CCS will:

- a. Receive and demodulate command up-data for the LVDA/LVDC in the IU.
- b. Transmit pulse code modulated (PCM) mission control measurements originating in the S-IVB and IU to the USB ground stations for processing.
- c. Retransmit the pseudo-random noise (PRN) range code that is received from the USB ground stations.

The CCS consists of a transponder, power amplifier, and antenna system.

## B.2 S-IC STAGE

The first stage is approximately 42.1 meters (138 ft.) long, 10.1 meters (33 ft.) in diameter and has five liquid-fueled F-1 engines each of which generates a nominal thrust of 6,700,000 Newtons (1,500,000 lbf). A bi-propellant system of liquid oxygen (LOX) as the oxidizer and RP-1 as the fuel supplies the engines' burn. The four outboard engines are gimballed for directional control and the center engine is stationary.

### B.2.1 S-IC Stage Structure

The S-IC structure is an assembly of a thrust structure, an RP-1 tank, an intertank section, a LOX tank, and a forward skirt which provides an interface surface for the S-II stage. Attached to the thrust structure are a base heat shield, four aerodynamic fins, and four engine fairings. Since both propellants are relatively dense, a separate rather than integral tank configuration is used.

The two primary functions of the thrust structure are to redistribute locally applied loads uniformly about the periphery of the fuel tank at the Y-ring attachment and to support the engines and their accessories, propellant lines and retro motors. The base heat shield thermally protects critical engine components and base region structural components during flight. Each of the four aerodynamically stabilizing fins has a surface area of  $7 \text{ m}^2$  ( $75 \text{ ft}^2$ ). Circumferentially attached, the conically shaped engine fairings protect each outboard engine from aerodynamic loads and also house the retro motors and engine actuator support structure. The fuel tank is a semi-monocoque cylindrical structure closed at each end by an ellipsoidal bulkhead. It has a total volume of 680 cubic meters (24,000 cubic feet), including ullage. Antislosh ring baffles are located on the inside wall of the tank, and an antivortex cruciform baffle in the lower bulkhead area. Five LOX tunnel assemblies extend through the tank from upper to lower bulkhead. The intertank section, composed of skin, longitudinal stringers, and circumferential ring frames, is a structural link between the fuel tank structure and the LOX tank structure. The LOX tank is structured similar to the fuel tank, but four helium bottles are attached to the ring baffles, and its total volume is  $1331 \text{ m}^3$  ( $47,000 \text{ ft}^3$ ) including ullage. The forward skirt is structured similar to the intertank section but is a structural link between the S-IC stage LOX tank top and the S-II stage. External longitudinal wiring and pressurization tunnels, semielliptical in cross-section and hyperbolically faired at the ends, complete the stage structure.

### B.2.2 S-IC Stage Propulsion System

The S-IC propulsion system consists of the F-1 engines, oxidizer system, fuel system, pneumatic control pressure system, and the camera ejection and purge system. Four outboard gimballed engines and one inboard, fixed-mounted engine thrust the launch vehicle during first stage boost.

The F-1 engine is a single-start, 6,670,000 Newton (1,500,000 lbf) fixed-thrust, bipropellant rocket which by the addition of a double-walled extension nozzle increases the expansion area ratio of the bellshaped thrust chamber from 10:1 to 16:1. At a mixture ratio of 2.27:1, the propellants, LOX and RP-1, are supplied to the thrust chamber by each engine's turbopump which is driven by the gas generator (GG) exhaust gases. A ground start signal causes LOX to enter the thrust chamber through the opening LOX valve by pyrotechnics igniting the gas generator thus turning the turbopump. As the LOX and RP-1 flow into the gas generator the turbopump speeds up increasing the propellants pressure. At about 259 N/cm<sup>2</sup> (375 psig), following other start events, fuel enters the hypergol cartridge bursting its diaphragm at about 345 N/cm<sup>2</sup> (500 psig). Hypergol and RP-1 enter the oxygen rich thrust chamber and cause spontaneous primary ignition. The RP-1 valves open as thrust builds up and the engine achieves mainstage operation. The inboard engine is cutoff, IECO, by an instrument unit (IU) signal. Outboard engines are cut off, OECO, by four optical type LOX-level depletion sensors, with fuel depletion sensors as backup, which through their circuitry and a timer cause the prevalves to close stopping propellant flow. From liftoff to about 135 seconds if any two of the three engine thrust OK sensors on each engine's fuel inlet manifold indicate thrust below 89 percent and this indication occurs on two of the five S-IC stage engines' manifolds, the Emergency Detection System (EDS) distributor and its circuitry signal in the command module (CM) that an abort initiation condition exists. Each of the four outboard engines is gimbal mounted on the stage thrust structure to provide engine thrust vectoring for vehicle attitude control and steering. Two hydraulic actuators are utilized to gimbal each engine in response to signals from the flight control computer located in the Instrument Unit. The center engine is fixed on the stage centerline. During preflight operations, an engine purge system supplies gaseous nitrogen (GN<sub>2</sub>) at certain pressures and flowrates, to those stage and engines' components requiring purge.

The hydraulic system supplies high-pressure fluid (RP-1) from a ground source to each engine controlling engine start sequence; also, to the four outboard engines for checkout of the thrust vector control (TVC) system. During engine operation, the fluid is supplied from the No. 1 fuel discharge of the turbopump assembly through the filter manifold to the servo valve and actuators for TVC; and returns through the checkout valve to the No. 2 fuel inlet of the turbopump assembly. The engine control valves are hydraulically closed for engine shutdown.

The stage propellant system is composed of one LOX tank, one RP-1 tank, propellant lines, control valves, vents, and subsystems. Liquid oxygen is stored allowing for a usable oxidizer supply of 1,390,000 kilograms (3,060,000 lbm). The LOX major subsystems are the fill-and-drain, pressurization, and feed systems. The systems' principal functions deliver the proper amount of LOX at the correct rate to meet the minimum net position suction pressure (NPSP) requirements at the engine turbopump inlet.

The fuel system tank stores a usable supply of 608,400 kilograms (1,340,000 lbm) of RP-1. The systems' principal functions provide the proper amount of fuel at the correct rate to meet the minimum NPSP requirements at the engine turbopump's fuel inlet during startup and flight. Its major subsystems are the fill-and-drain, pressurization and feed systems. The loading of LOX and RP-1 tanks is controlled by ground computers. RP-1 loading using the fill-and-drain system takes place prior to the start of LOX loading. LOX bubbling begins and continues through LOX loading to prevent possible geysering. Approximately 90 seconds before ignition command the RP-1 tank is pressurized from a ground source by the fuel pressurization systems, and about 30 seconds later the LOX tank is pressurized by the LOX pressurization system. Up to 72 seconds before liftoff but prior to start of automatic sequence ground-source helium is bubbled through the LOX lines and tank, preventing stratification in the suction lines. After liftoff LOX tank ullage pressure is maintained with gaseous oxygen (GOX) converted from LOX in the engines' heat exchangers. Similarly the RP-1 tank ullage pressure is maintained but by helium (He) heated by passage through the heat exchangers from the four He storage bottles in the LOX tank.

The camera ejection and purge system was inactive on this mission.

The S-IC stage electrical system is comprised of the power supply systems and the power distribution system. Silver-zinc oxide batteries No. 1, power for operating electrical systems, and No. 2, power for instrumentation and telemetry, supply stage 28 volt dc power. A static inverter converts part of this to ac where required. The power distribution system consists of six distributors and the stage switch selector: (1) Main power switches external power to internal (stage) for flight, distributes power by buses and performs time-sensitive switching; (2) measuring power distributes to instrumentation; (3) propulsion system distributes ECO functions from switch selector LOX level and range safety cutoff; (4) thrust OK performs logic and cutoff distribution on engine thrust, distributing the status to the IU; (5) timer distributes time delays for preclude closure and engine cutoff back-up; (6) sequence and control distributes control for exploding bridge wire (EBW) firing units, He flow control valves, tape recorder, separation control logic and retro motor initiation; and the switch selector decodes LVDA/LVDC digital flight sequence commands, and activates the proper stage circuits, via the sequence and control distributor, distributing command execution.

The environmental control system is used to control temperature in the instrumentation canisters, forward skirt compartment, and thrust structure compartment during preflight operations. The conditioning and purge agent (air until 3 minutes before LH<sub>2</sub> loading, gaseous nitrogen thereafter) is provided to the stage from central ground supply.

### B.3 S-II STAGE

The stage is the second of the vehicle and is approximately 24.8 meters (81.4 ft) long, 10.1 meters (33 ft) in diameter and has five J-2 engines

each of which generates a nominal thrust of 890,000 Newtons (200,000 lbf). The engines' burn is supplied by a bi-propellant system of liquid hydrogen (LH<sub>2</sub>) as the fuel and LOX as the oxidizer. The four outboard engines are gimballed for directional control and the center engine is stationary.

### B.3.1 S-II Stage Structure

The stage airframe is comprised of a forward skirt, an aft skirt with thrust structure and heat shield, liquid oxygen (LOX) and hydrogen (LH<sub>2</sub>) tanks, an aft interstage structure, and a system tunnel.

The aft interstage is a semimonocoque structure housing the five J-2 engines. It is approximately 5.56 meters (18.3 ft.) in length and is made of two parts. One 0.58 meters (2 ft.) part from vehicle station 1541 to 1564 remains with the S-IC stage at S-IC/S-II first plane separation. The other part, 4.89 meters (16.3 feet) long from vehicle station 1564 to 1760, is separated from the S-II stage at second plane separation. The aft skirt and thrust structure includes an engine mounting frame, a center engine support assembly, a cone-frustum thrust structure, cylindrical aft skirt, and a heat shield. It is 2.24 meters (7.3 ft.) long. The liquid oxygen tank is 10 meters (33 ft.) in diameter and 7 meters (22 ft.) in height formed by joining ellipsoidal shaped fore and aft halves. The forward half is a common bulkhead exposed to liquid oxygen on one side and liquid hydrogen on the other and is a sandwich structure with an insulation core (phenolic impregnated fiberglass) to minimize heat transfer. Inside the tank are antivortex and slosh suppression baffles. The LOX tank has a capacity of approximately 309 cubic meters (10,900 cubic feet). The liquid hydrogen tank measures 17 meters (56 ft.) in height, 10 meters (33 ft.) in diameter and has a capacity of 1005 m<sup>3</sup> (35,500 ft<sup>3</sup>). Antivortexing baffles are provided at the outlet ducts. An ellipsoidal forward bulkhead, together with the common bulkhead, complete the tank enclosure. The tank sidewalls are insulated with a sealed, plastic honeycomb core partially filled with polyurethane foam. The upper bulkhead is also insulated externally in the same manner as the tank sidewalls. The forward skirt structure includes provisions for installation of flush mounted range safety and telemetry antenna. The systems tunnel is attached vertically to the outside wall of the stage. It protects and supports instrumentation, wiring, and tubing connecting system components located at both ends of the stage. Cabling which connects the S-IC stage to the Instrument Unit also runs through the tunnel.

### B.3.2 S-II Stage Propulsion System

The S-II propulsion system consists of the engine, fuel, oxidizer, leak detection and insulation purge, engine compartment conditioning, propellant management, pneumatic control pressure and the camera ejection systems.

The engine system consists of five J-2 rocket engines using LOX and LH<sub>2</sub> for propellants. Four are located outboard, the fifth on the stage center-line and each vertically lined with the corresponding S-IC stage F-1 engine. The center engine is stationary, the outboard engines are gimballed allowing thrust vector control. The J-2 rocket engine is a high performance 890,000 Newtons (200,000 lbf) thrust engine using LOX and LH<sub>2</sub> at a mixture ratio of 5.0:1, but can vary to as low as 4.5 for the desired propellant utilization at stage cutoff. It features a tubular-wall, bell-shaped thrust chamber (27.5:1 expansion ratio), and two independently driven, direct-drive turbopumps powered in series by a single gas generator.

The LH<sub>2</sub> fuel system consists of a fuel feed system, pressurization system, recirculation system, and a fill-and-drain system. The fuel feed system furnishes LH<sub>2</sub> to the five J-2 engines and includes five 8-inch vacuum-jacketed feed ducts and five normally-open precheck valves. Also, five engine cutoff sensors are located in the LH<sub>2</sub> tank to provide depletion signals for engine cutoff. The LOX fill and drain system provides for filling and draining through a quick-disconnect coupling, fill and drain duct, and fill and drain valve. Loading sensors monitor the LOX level to assure loading to the desired mass. The leak detection and insulation purge system detects hydrogen or air leaking into the LH<sub>2</sub> tank external insulation (accomplished by passing helium purge gas from GSE through honeycomb insulation and back to a gas chromatograph for analysis). The engine compartment conditioning system maintains proper temperature control in the S-II aft compartment and purges it prior to tanking and whenever propellants are on board. The propellant management system maintains closed-loop control of the LOX flow-rate to each engine thus controlling the engine mixture ratio (EMR). The system also controls propellant loading, maintains propellant level during countdown, provides telemetry system propellant mass indication signals, and signals depletion of either propellant thus initiating engine cutoff. The pneumatic control pressure system provides onboard pressurized He for propellant system valve actuation and engine purges in flight but for preflight the system He source is ground supply. Two other onboard He spheres provide gaseous helium (GHe) to the camera ejection system which ejects the two cameras. At an altitude of 4300 meters (14,100 ft) a paraballoon is inflated, stabilizer flaps fall away, a recovery radio transmitter and flashing light beacon turn on, the antenna deploy, and upon impact dye marker and shark repellent are released. Operation of the J-2 engine consists of prestart, start, steady-state operation and cutoff sequences. During prestart, LOX and LH<sub>2</sub> flow through the engine to temperature-condition engine components, and assure the presence of propellant in the turbopumps for starting. After timed cooldown, the start signal is received by a controller which causes the propellant valves to open in the proper sequence. The controller also energizes spark plugs in the gas generator and thrust chamber igniting the propellant and it releases GHe from the start tank providing the initial drive for the turbopumps which deliver propellant to the gas generator and the engine. The propellant ignites, gas generator output accelerates the turbopumps, and engine thrust increases to main stage operation at which time the spark plugs de-energize and the engine is in

steady-state operation. This condition is maintained until a cutoff signal is received by the sequence controller which then causes the engine propellant valves to close in the proper sequence resulting in engine thrust decay and the cutoff sequence is complete. Each outboard engine has an identical hydraulic system for gimbaling. Major system components include an engine-driven main pump, an auxiliary electric motor-driven pump, two electrically controlled, hydraulically powered servoactuators, and an accumulator reservoir manifold assembly. During S-IC powered flight, hydraulic lockup valves are closed, holding the engines in a "toed in" position. After S-IC/S-II stage separation, a signal unlocks the accumulator lockup valves releasing high-pressure fluid to each of the two servoactuators. This fluid provides gimbaling power prior to main hydraulic pump activation, which is driven directly from the accessory drive of the engine LOX pump. Activation provides actuator power during S-II powered flight.

The S-II stage propellant system is composed of integral LOX/LH<sub>2</sub> tanks, propellant lines, control valves, vent, and prepressurization subsystems. Loading of propellant tanks and flow of propellants is controlled by the propellant utilization (PU) system. The LOX/LH<sub>2</sub> tanks are prepressurized by ground source gaseous helium. During powered flight of the S-II Stage, the LOX tank is pressurized by GOX bleed from the LOX heat exchanger. The LH<sub>2</sub> tank is pressurized by GH<sub>2</sub> bleed from the thrust chamber hydrogen injector manifold and pressurization is maintained by the LH<sub>2</sub> pressure regulator. The propellant management system controls loading and engine mixture ratios (LOX to LH<sub>2</sub>) to ensure balanced consumption of LOX and LH<sub>2</sub>. Capacitance probes mounted in the LOX and LH<sub>2</sub> containers monitor the mass of propellants during powered flight. At PU activation (5.5 seconds after J-2 ignition) the capacitance probes sense the LOX to LH<sub>2</sub> imbalance and command the engine to burn at the high rate engine mixture of 5.5:1. When the high mixture ratio is removed, the PU system then commands the engine to burn the reference mixture ratio of 4.7:1, striving for simultaneous depletion of LOX and LH<sub>2</sub> for maximum stage performance. Engine cutoff is initiated when any two of the five capacitance probes in either tank indicate dry.

The S-II stage electrical system is comprised of the power supply system and the power distribution system. Four silver-zinc oxide batteries supply 28 volt dc and 56 volt dc internal power to the stage. The J-2 engines, separation, propellant, flight control, pressurization and one EDS and range safety systems use 28 volt dc from the main battery. Telemetry, instrumentation, tracking and the other EDS and range safety systems use 28 volt dc from the instrumentation battery. Five inverters convert 56 volt dc from two batteries to 42 volt ac, 3 phase, 400 cps supplying the LH<sub>2</sub> recirculation pumps' induction motors. J-2 engine 28 volt dc ignition power comes from one of these batteries. The power distribution system consists of the power transfer switches, distributor buses, sequence controller, separation controller, and the stage switch selector all of which

distribute the power from the batteries. The switch selector decodes LVDA/LVDC digital flight sequence commands and, via the electrical sequence controller for the stage systems and the separation sequence controller for the separation systems, activates the proper circuits.

During propellant loading and later pre-launch operations the stage environmental control system (ECS) purges the engine and aft interstage area using warm ground GN<sub>2</sub> and the engine compartment conditioning system, and it supplies temperature control and inert gas to the engine compartment electronic equipment containers up to liftoff.

#### B.4 S-IVB Stage

The third stage is approximately 18 meters (59 ft.) long, 6.6 meters (22 ft.) in diameter and has one liquid-fueled multiple-start J-2 engine, having a nominal thrust of 890,000 Newtons (200,000 lbf) and gimballed for stage directional control. The stage has an auxiliary propulsion system (APS) providing attitude control and restart propellant settling during engine-off periods. A bi-propellant system of liquid hydrogen (LH<sub>2</sub>) as the fuel and liquid oxygen (LOX) as the oxidizer supplies the J-2 engine burn.

##### B.4.1 S-IVB Stage Structure

The S-IVB structure is the assembly of an aft interstage, an aft skirt, a thrust structure, an integral propellant container, and a forward skirt.

The aft interstage assembly provides structural interface between the S-IVB stage and the S-II stage. It is a truncated cone in shape. The aft skirt assembly, is a cylinder 2.17 meters (7.1 ft.) long and provides the structural interface between the propellant tank and the aft interstage. The thrust structure assembly consists of an inverted, truncated cone, 1.57 meters (5 ft.) high with a base diameter of 4.27 meters (14 ft.) and a top diameter of 0.86 meters (3 ft.). Access to the inside of the thrust structure is provided by two doors. To conserve stage length the propellants are contained in an integral container. The propellant tank assembly consists of a cylindrical tank 6.6 meters (22 ft.) long and 6.4 meters (21 ft.) in diameter, with a hemispherical-shaped dome at each end, and an intermediate spherical radius common bulkhead. The LH<sub>2</sub> tank is internally insulated with type 3-D polyurethane foam on the forward dome and the cylindrical section. The common bulkhead separating the tanks consists of a fiberglass honeycomb core adhesively bonded between two aluminum domes. Antislosh baffles are installed in the LOX and LH<sub>2</sub> tanks. Each tank contains a hinged screen at the tank outlet which acts as a propellant antivortexing device and filter. Under low "G" conditions, the screen opens preventing the accumulation of gas bubbles below the screening. The LOX and LH<sub>2</sub> tanks have capacities of 79 and 294 m<sup>3</sup> (2800 and 10,400 ft<sup>3</sup>), respectively. Cylindrical in shape, the forward skirt extends 3.1 meters (10 ft.) forward from the intersection of the LH<sub>2</sub> tank sidewall and the forward dome, providing a hard attach point for the instrument unit (IU).



#### B.4.2 S-IVB Stage Propulsion System

The stage propulsion system has two propulsion subsystems. The main propulsion system consists of a single, bi-propellant J-2 engine, fuel system, oxidizer system, and a propellant management system. The auxiliary propulsion system (APS) is provided to control the vehicle attitude during S-IVB operation, and position the propellants in the stage after S-II/S-IVB separation. Of two APS, each is a packaged system.

This J-2 engine is a gimbaled high performance, multiple-start engine utilizing two pump-fed propellants and therefore two independently driven direct-drive turbopumps. In a series sequence the gas generator (GG) hot exhaust gases are directed first to the fuel and then to the oxidizer turbopump turbine inlet which provides optimum speed. The engine has a tubular-walled, bell-shaped thrust chamber. At altitude the engine produces a nominal thrust of 890,000 Newtons (200,000 lbf) at a LOX to LH<sub>2</sub> mixture ratio (EMR) of 5:1 but can operate as low as 4.5:1 when the reduction of propellant residuals at engine cutoff (ECO) is desired.

The LH<sub>2</sub> fuel system consists of feed, pressurization, recirculation, fill-and-drain and vent control systems. Through a single suction duct in which the pre valve is located, the feed system supplies turbopumped LH<sub>2</sub> to the engine. The pre valve backs up the main fuel valve and controls recirculation during chilldown. Starting at pre-launch automatic sequence the recirculation system pumps LH<sub>2</sub> from the tank through feed system bleed valves, suction duct, turbopump and the tank return line up to just before first burn and again at repressurization up to just prior to second burn. This keeps the fuel feed system chilled down for engine start. During both engine burns, the fuel pressurization system supplies LH<sub>2</sub> tank pressurization gas from LH<sub>2</sub> converted to GH<sub>2</sub> by the engine heat exchanger; but during engine-off periods GHe is used, first during pre-launch from a ground supply and second during orbital coast by seven storage spheres used to support second burn start requirements. The seven attach to the thrust structure.

Because the venting of the LH<sub>2</sub> tank gases is used to settle propellants during the coast period, the vent control system directs the LH<sub>2</sub> ullage gas in three modes: (1) during pre-launch through the quick-disconnect to the burn pond, (2) inflight through the nonpropulsive vents and (3) during coast starting at approximately 78 seconds after first burn ECO, through the propulsive vents.

The oxidizer system consists of LOX feed, pressurization, recirculation, fill and drain, and vent control systems. Through a single suction duct in which the pre valve is located the feed system supplies turbopumped LOX to the engine. The pre valve backs up the main oxidizer valve and controls recirculation during chilldown. Starting at LOX tank prepressurization the recirculation system pumps LOX from the tank through the feed system bleed valves, suction duct, turbopump, flowmeter and tank return line up to just before first burn ignition and again at repressurization up to just before

second burn ignition. This keeps the LOX feed system chilled down for engine start. During both engine burns, the LOX pressurization system supplies LOX tank pressurization gas, from eight cold GHe storage spheres in the LH<sub>2</sub> tank, and warmed by the engine heat exchanger, but during pre-launch ground GHe is used; and during coast ambient GHe, from two high pressure LOX tank repressurization spheres for second burn engine restart requirements, is used. The LOX fill and drain system provides for LOX filling and draining through a quick-disconnect coupling, fill and drain duct, and fill and drain valve. The system also serves as an exit for the GN<sub>2</sub> and GHe used for LOX tank purging prior to LOX loading. A continuous capacitance probe monitors the LOX level to enable loading to the desired mass. The LOX tank vent control system provides for LOX tank venting during LOX loading and flight. At initiation of LOX loading, the LOX tank vent and relief valve is actuated to the vent position. Vent gas flows from the LOX tank through the vent and relief valve, the overboard vent line, and then to the atmosphere. The propellant management system includes ground and onboard electronics, continuous capacitance probes, a propellant utilization (PU) valve, and discrete liquid level sensors. The system assures simultaneous depletion of propellant accomplished by controlling the flowrate to the engine. Thus propellant loading errors and/or deviations in propellants due to vehicle flight behavior can be corrected and the proper proportion of LOX and LH<sub>2</sub> can be maintained onboard. The system also controls propellant loading, maintains propellant level during countdown, initiates propellant mass indication telemetry signals and initiates the propellant depletion signal thereby initiating ECO. At PU activation (6.3 seconds after first time J-2 ignition and 5.0 seconds after second time J-2 ignition) the capacitance probes sense the LOX to LH<sub>2</sub> imbalance and command the engine to burn at the high rate engine mixture ratio of 5.5 to 1. When the high mixture ratio is removed, the PU system will then command the engine to burn the reference mixture ratio of 4.7:1. J-2 engine operation is included in Section B.3.2. The auxiliary propulsion system (APS) controls the vehicle attitude during S-IVB operation, and positions the propellants in the stage after S-II/S-IVB separation. Nitrogen tetroxide (N<sub>2</sub>O<sub>4</sub>) and monomethyl hydrazine (MMH) are the APS propellants. These propellants are hypergolic and require no ignition system. The APS system is composed of two modules located 180 degrees apart on the aft skirt assembly. All requirements are supplied from within the modules except the electrical signals which are required from the stage. Each module contains three ablative cooled, 667 Newton (150 lbf) thrust, attitude control engines; and one ablative cooled, 311 Newton (70 lbf) thrust, ullage positioning engine. The attitude control engines control S-IVB roll during engine burn; and pitch, yaw, and roll during orbital coast. The ullage positioning engine fires to assure the presence of liquid propellants at the J-2 engine pump inlets during engine chilldown and restart, and to settle the propellants prior to propulsive venting to prevent the loss of liquid propellants through the vent systems.

Engine gimbaling is accomplished by an independent, closed-loop, hydraulic control system consisting of an engine-driven main pump, an auxiliary electric motor-driven pump, two electrically controlled, hydraulically powered

servoactuators, and an accumulator reservoir. During S-IC and S-II powered flight and coast, the auxiliary pump is operating to position the J-2 engine in the null position and to thermally condition the hydraulic fluid. The main hydraulic pump, driven directly from the accessory drive pad of the engine LOX pump, provides actuator power to control pitch and yaw during S-IVB powered flight.

The S-IVB stage electrical system is comprised of the power supply system and the power distribution system. Three 28 volt dc and one 56 volt dc silver-zinc oxide batteries supply internal power of 28 volt dc to instrumentation, switch selector, two range safety command systems, a static PU inverter converter, engines, APS, sequencer, pressurization, ullage motor ignition and jettison; and supply 56 volt dc to the auxiliary hydraulic pump motor and two chilldown inverters which supply ac power to the two recirculation pump motors. The power distribution system consists of the forward power distributor, aft power distributors, forward control distributor, aft control distributor, sequencer, and switch selector. The power distributors distribute the four batteries' power. The control distributors provide distribution paths during tests and countdown. The switch selector consists of electronic and electromechanical components which decode digital flight sequence commands from the LVDA/LVDC and activate the proper stage circuits (through the stage sequencer) to execute the commands. The stage sequencer operates upon receipt of discrete inputs from the switch selector, and other S-IVB stage subsystems, and initiates S-IVB flight functions by supplying or removing power from the appropriate equipment.

The aft skirt and interstage environmental control system provides thermal conditioning of the atmosphere, during ground operations, around electrical equipment in the aft skirt; thermal conditioning of the APS, hydraulic accumulator reservoir, and ambient helium bottle; purging of the aft skirt, aft interstage and thrust structure, and the forward skirt of the S-II stage of oxygen and combustible gases. Temperature controlled air or GN<sub>2</sub> is supplied at the rate of 3500 scfm to accomplish the thermal conditioning. The air purge is initiated at LOX loading. GN<sub>2</sub> flow is initiated at LH<sub>2</sub> loading and terminated at umbilical disconnect.

## B.5 Instrument Unit

The instrument unit (IU) is an assembly approximately 6.6 meters (21.7 ft.) in diameter and 1.1 meters (3 ft.) high. The unit houses most of the critical electronic components of the data system, guidance, navigation and control system, separation systems, safety systems and emergency systems as well as many subsystems. Section B.1 describes these systems.

### B.5.1 Instrument Unit Structure

The IU structure consists of three arc segments (numbered 601, 602, and 603) of sandwiched honeycomb. The three arc segments are joined with splice plates bolted to the skin and the channel ring segments, thus forming a single unit

of honeycomb construction. Brackets are bonded to the inner skin to provide mounting surfaces for 16 cold plates, which are 30 inches square. A coolant fluid is circulated through the cold plates to dissipate heat generated by the electrical components mounted on them. This arrangement provides clearance for the landing gear of the lunar module to be included in later missions, and for the forward bulkhead of the S-IVB hydrogen tank which extends into the IU. A honeycomb-constructed access door provides access to components within the IU after the IU is assembled as part of the vehicle and has been designed to act as a load-carrying part of the structure in flight. In addition, the structure contains an umbilical door which is spring loaded and will close after retraction of the umbilical arm at liftoff. The IU structure provides a path for static and dynamic loads resulting from the payload above the IU.

#### B.5.2 Instrument Unit Electrical System

The IU electrical system is comprised of the power supply system and the power distribution system. The power supply system consists of four 28 volt dc silver-zinc oxide batteries supplying power to the IU power distributors for distribution to the various IU systems; a 56 volt dc power supply which receives power from the IU power distributor and provides operating voltage to the ST-124M gyro, accelerometer servoloops and the accelerometer signal conditioner; and an ac power supply. The power distribution system consists of the power distributor, two auxiliary power distributors, control distributor, EDS distributor, timer measuring distributors, and switch selector. The power distributor receives power from the four 28-volt batteries and distributes power to the various IU systems through the power supplies and other distributors. It contains the power transfer switch which accomplishes the switch from external to internal power. Two auxiliary power distributors take power from the power distributor and distribute it to the astrionics equipment. One auxiliary distributor connects directly to the astrionics equipment, while the other connects directly to the astrionics equipment and also feeds the measuring distributors and the EDS distributor. The control distributor provides a means of routing signals between the flight control computer and other elements of the flight control system. The EDS distributor contains the relay logic needed to monitor and interpret emergency indications and to issue the appropriate commands. The timer is a 40-second EDS cutoff enable timer. The measuring distributors route 5-volt dc power to the various transducers in the IU. The IU switch selector decodes digital flight sequence commands from the LVDA/LVDC, and activates the proper circuits to execute the commands.

#### B.5.3 Instrument Unit Environmental Control System

The environmental control system provides the thermal control of critical components by circulating or dissipating heat energy; it also has the capability of providing thermal-conditioned, pressure regulated nitrogen to the inertial platform of the guidance and control system.

The compartment purge system provides an inert, temperature controlled atmosphere within the Instrument Unit and S-IVB forward skirt prior to launch. Cooling air is forced into the instrument unit to maintain a compartment temperature of 60 to 80° F. The air supply is changed to gaseous nitrogen 30 minutes prior to liquid hydrogen loading. The gaseous nitrogen (GN<sub>2</sub>) system is used by the gas bearing of the ST-124M Stabilized Platform and as a pressure supply for both the methanol/water reservoir and the water accumulator of the thermal conditioning system. The GN<sub>2</sub> is stored in three high-pressure containers located in the instrument unit spheres. The thermal conditioning system absorbs heat generated by electronic components. The various electronic components are mounted on thermal-conditioned panels (cold plates) which are maintained at a maximum of 80° F. The environmental coolant is pumped from a methanol/water reservoir to the cold plates, heat exchanger, stable platform, data adapter, and digital computer in the instrument unit and the S-IVB stage. The coolant absorbs heat from this equipment, dissipates the heat through a heat exchanger (prior to launch) or sublimator (after the initial launch phase), and returns to the methanol/water reservoir.

## B.6 SPACECRAFT

Spacecraft 017, for mission AS-501 is composed of a Launch Escape Tower, Command Module, Service Module, Lunar Module Adapter and a Lunar Module test article.

### B.6.1 Spacecraft Structure

The command module (CM) consists of an inner structure, or pressure vessel, and an outer structure. A layer of insulation separates the inner and outer structures. The heat shield (outer structure) consists of a forward heat shield, a crew compartment heat shield, and an aft heat shield. Ablative material is bonded to the heat shield stainless steel honeycomb structure. The service module (SM) is a cylindrical shell made up of aluminum honeycomb-sandwich panels and forward and aft bulkheads. The SM propulsion engine gimbal is attached to the aft bulkhead. Below the SM gimbal, the engine nozzle extends into the adapter area. The lunar module adapter joins the SM to the S-IVB/IU and encloses the lunar module test article.

### B.6.2 Spacecraft Subsystems

Spacecraft Subsystems include the following:

- |  |                                  |
|--|----------------------------------|
| a. Launch Escape Subsystem             | i. Service Propulsion Subsystem  |
| b. Emergency Detection Subsystem       | j. Reaction Control Subsystem    |
| c. Electrical Power Subsystem          | k. Earth Landing Subsystem       |
| d. Master Event Sequence Controller    | l. Mission Control Programmer    |
| e. Environmental Control Subsystem     | m. Impact and Recovery Subsystem |
| f. Communication Subsystem             | n. Structure Subsystem           |
| g. Instrumentation Subsystem           | o. Heat Shield                   |
| h. Stabilization and Control Subsystem |                                  |



# APPENDIX C MISSION OBJECTIVES

The mission objectives for flight AS-501 are defined in the SA-501 Launch Vehicle Mission Directive document. These objectives are listed in Table C-1 and are identified as either Primary or Secondary by the letters (P) or (S) respectively. Primary objectives are those which are mandatory, and any condition which would result in failure to achieve these objectives would be cause to hold or cancel the mission until the condition has been corrected. Secondary objectives are those which may be cause to hold or cancel the mission as directed in the Mission Rules.

Table C-1. SA-501 Launch Vehicle Flight Objectives

NO.	MISSION OBJECTIVES	CATAGORY
1.	Demonstrate structural and thermal integrity of launch vehicle throughout powered and coasting flight, and determine in-flight structural loads and dynamic characteristics.	P
2.	Determine in-flight launch vehicle internal environment.	P
3.	Verify pre-launch and launch support equipment compatibility with launch vehicle and spacecraft systems.	P
4.	Demonstrate the S-IC Stage propulsion system and determine in-flight system performance parameters.	P
5.	Demonstrate the S-II Stage propulsion system including programmed mixture ratio shift, propellant management systems, and determine in-flight system performance parameters.	P
6.	Demonstrate the S-IVB Stage propulsion system including the propellant management systems, and determine in-flight system performance parameters.	P

Table C-1. SA-501 Launch Vehicle Flight Objectives (Continued)

NO.	MISSION OBJECTIVES	CATAGORY
7.	Demonstrate the launch vehicle guidance and control system during S-IC, S-II, and S-IVB powered flight. Achieve guidance cutoff and evaluate system accuracy.	P
8.	Demonstrate S-IC/S-II dual plane separation.	P
9.	Demonstrate S-II/S-IVB separation.	P
10.	Demonstrate launch vehicle sequencing system.	P
11.	Demonstrate compatibility of the launch vehicle and spacecraft.	P
12.	Evaluate performance of the Emergency Detection System (EDS) in an open loop configuration.	P
13.	Demonstrate the capability of the S-IVB auxiliary propulsion system during S-IVB powered flight and orbital coast periods to maintain attitude control and perform required maneuvers.	P
14.	Demonstrate the adequacy of the S-IVB continuous vent system while in Earth orbit.	P
15.	Demonstrate the S-IVB Stage restart capability.	P
16.	Demonstrate the mission support capability required for launch and mission operations to high post-injection altitudes.	P
17.	Determine launch vehicle powered flight external environment.	S
18.	Determine attenuation effects of exhaust flames on R.F. radiating and receiving systems during main engine, retro, and ullage motor firings.	S



APPENDIX D  
PREFLIGHT VERSUS POSTFLIGHT COMPARISONS  
OF INSERTION AND INJECTION CONDITIONS

Preflight predicted parking orbit insertion and waiting orbit injection conditions are compared with postflight results in Tables D-1 and D-2. Predicted nominal parameter values are shown as well as predicted 3-sigma envelopes based upon predicted launch vehicle, subsystem, and environmental 3-sigma tolerances and dispersions. Preflight predicted trajectory evaluation uncertainties are shown. These values reflect a preflight estimation of the overall uncertainties expected in the postflight trajectory determination. Total parameter dispersions shown are the algebraic sums of the predicted positive and negative system dispersion envelopes and evaluation uncertainties. Comparison of the last two columns in each table shows that the actual insertion and injection conditions lie within the preflight predicted envelopes for all parameters shown.

Table D-1. Parking Orbit Insertion Parameters Comparison

PARAMETER	PREDICTED NOMINAL	$3\sigma$ DISPERSION	EVALUATION UNCERTAINTY	TOTAL DISPERSION	NOMINAL $\pm$ TOTAL DISPERSION	ACTUAL FLIGHT RESULTS
Radius (R, meters)	6,563,431.3	+528.4 -683.0	+800. -800.	+1328.4 -1483.0	6,564,759.7 6,561,948.3	6,564,503.9
Inertial Velocity (m/s)	7793.767	+1.498 -1.403	+3.0 -3.0	+4.498 -4.403	7798.265 7789.364	7791.81
Inertial Flight Path Angle ( $\gamma$ , degrees)	0.0007	+0.0135 -0.0158	+0.05 -0.05	+0.0635 -0.0658	+0.0642 -0.0651	+0.0136
Range (D, meters)*	2,475,759.	+89,282. -94,067.	+800. -800.	+90,082. -94,867.	2,565,841. 2,380,892.	2,520,006.
Orbit Inclination (i, degrees)	32.5612	+0.0070 -0.0078	+0.0160 -0.0160	+0.0230 -0.0238	32.5842 32.5374	32.5730
Orbit Descending Node** ( $\lambda_N$ , degrees)	123.1743	+0.0236 -0.0335	+0.0280 -0.0280	+0.0516 -0.0615	123.2259 123.1128	123.2059

\* Arc length measured along the earth's surface from the launch site to the instantaneous vehicle position vector at orbit insertion.

\*\* Angle in the equatorial plane from the space-fixed launch meridian to the descending nodal line of the terminal orbital plane, measured positive in the direction of earth's spin.

Table D-2. Waiting Orbit Injection Parameters Comparison

PARAMETER	PREDICTED NOMINAL	3 $\sigma$ DISPERSION	EVALUATION UNCERTAINTY	TOTAL DISPERSION	NOMINAL ± TOTAL DISPERSION	ACTUAL FLIGHT RESULTS
C3 (m <sup>2</sup> /s <sup>2</sup> )	-26,484,660.	+328,894. -542,394.	+73,700. -73,700.	+402,594. -616,094.	-26,082,066. -27,100,754.	-26,672,329.
Eccentricity (e)	0.5817	+0.0046 -0.0073	+0.0010 -0.0010	+0.0056 -0.0083	0.5873 0.5734	0.5789
Argument of Perigee* ( $\alpha_D$ , degrees)	108.8915	+0.3723 -0.3874	+0.0960 -0.0960	+0.4683 -0.4834	109.3598 108.4081	108.7893
Orbit Inclination (i, degrees)	30.3132	+0.0425 -0.0988	+0.0160 -0.0160	+0.0585 -0.1148	30.3717 30.1984	30.3022
Orbit Descending Node** ( $\alpha_N$ , degrees)	135.4307	+0.1894 -0.1935	+0.0280 -0.0280	+0.2174 -0.2215	135.6481 135.2092	135.4354
<p>* Angle from the radius of perigee to the descending node, measured positively as a right-hand rotation about the orbital angular momentum vector.</p> <p>** Angle in the equatorial plane from the space-fixed launch meridian to the descending nodal line of the terminal orbital plane, measured positive in the direction of earth's spin.</p>						

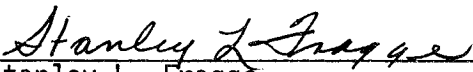


APPROVAL

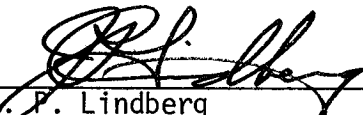
RESULTS OF THE FIRST SATURN V LAUNCH VEHICLE TEST FLIGHT  
AS-501, APOLLO 4 MISSION

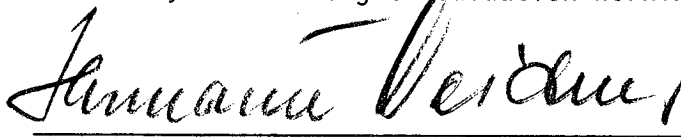
By Saturn Flight Evaluation Working Group

The information in this report has been reviewed for security classification. Review of any information concerning Department of Defense or Atomic Energy Commission programs has been made by the MSFC Security Classification Officer. The highest classification has been determined to be Unclassified.

  
Stanley L. Fragge  
Security Classification Officer

This report has been reviewed and approved for technical accuracy.

  
J. P. Lindberg  
Chairman, Saturn Flight Evaluation Working Group

  
Hermann K. Weidner  
Director, Research and Development Operations

  
A. Rudolph  
Saturn V Program Manager

## DISTRIBUTION:

## MSFC:

Dr. von Braun, DIR  
Mr. Shepherd, DIR  
Dr. Rees, DEP-T  
Mr. Gorman, DEP-A

## E-S

Mr. Maus, E-DIR  
Mr. Abbott, E-P  
Mr. Smith, E-S

## I

Gen. O'Connor, I-DIR  
Dr. Mrazek, I-DIR  
Mr. Andressen, I-RM-CH  
Col. Teir, I-I/IB-MGR  
Dr. Speer, I-MO-MGR (4)  
Mr. Belue, I-S/AA-MGR  
Mr. Brown, I-E-MGR  
Mr. Morea, I-E-J  
Mr. Stewart, I-E-F  
Dr. Rudolph, I-V-MGR  
Mr. Bramlet, I-V-MGR-O  
Mr. Murphy, I-V-MGR-M  
Mr. Burns, I-V-T  
Mr. Bell, I-V-E  
Mr. Rowan, I-V-F  
Mr. Moody, I-V-Q  
Mr. Sneed, I-V-P  
Mr. Urlaub, I-V-SIC  
Mr. Godfrey, I-V-SII  
Mr. McCulloch, I-V-SIVB  
Mr. Duerr, I-V-IU  
Mr. Smith, I-V-G  
Col. Montgomery, I-K  
Col. Murphy, I-K-V (15)  
Mr. Slattery, PA  
Mr. Peters, I-V-SIVB  
Mr. Galey, I-V-IU  
Mr. Ferrell, I-E-J (3)  
Mr. Wood, I-SC-C  
Dr. Constan, I-MICH-MGR  
Mr. Riemer, I-MICH-QP  
Mr. Balch, I-MT-MGR  
Mr. Auter, I-MT-H  
Mr. Wofford, CC-P  
Mr. Sanders, I-V-G  
Mr. Ginn, I-V-E  
Mr. Haley, I-V-SIC  
Mr. Higgins, I-V-SIVB  
Mr. Odom, I-V-SII  
Mr. Stover, I-V-SII  
Mr. Bender, I-V-Q  
Mr. Wheeler, I-E-F  
Mr. Frye, I-V-T  
Mr. Robertson, I-V-T  
Mr. Cushman, I-V-T (40)

Mr. Phillips, TBC-JA-52 (12)

## R&amp;D

Mr. Weidner, R-DIR  
Dr. Johnson, R-EO-DIR  
Mr. Williams, R-AS-DIR (2)  
Mr. Messer, R-OM-V  
Mr. Hamilton, MSC-RL  
Mr. Richard, R-SE-DIR

## R-AERO

Dr. Geissler, R-AERO-DIR  
Mr. Jean, R-AERO-DIR  
Mr. Dahm, R-AERO-A (2)  
Mr. Holderer, R-AERO-A  
Mr. Wilson, R-AERO-AT  
Mr. Jones, R-AERO-AT  
Mr. Reed, R-AERO-AU  
Mr. Horn, R-AERO-D  
Mr. Deaton, R-AERO-DA  
Mr. Ryan, R-AERO-DD  
Dr. McDonough, R-AERO-D  
Mr. Lindberg, R-AERO-F (33)  
Mr. Baker, R-AERO-G  
Mr. McNair, R-AERO-P (3)  
Mr. Jackson, R-AERO-P  
Mr. Cummings, R-AERO-T  
Mr. Vaughan, R-AERO-Y  
Mr. O. E. Smith, R-AERO-Y

## R-ASTR

Dr. Haeserermann, R-ASTR-DIR  
Mr. Hoberg, R-ASTR-DIR  
Mr. Digesu, R-ASTR-A  
Mr. Fichtner, R-ASTR-E  
Mr. Vann, R-ASTR-EA  
Mr. Stroud, R-ASTR-EA  
Mr. Robinson, R-ASTR-ESA  
Mr. Erickson, R-ASTR-ESA  
Mr. Darden, R-ASTR-F  
Mr. Justice, R-ASTR-FA  
Mr. Vallely, R-ASTR-FO  
Mr. Mink, R-ASTR-FO  
Mr. Mandel, R-ASTR-G  
Mr. Ferrell, R-ASTR-GSA  
Mr. Powell, R-ASTR-I  
Mr. Avery, R-ASTR-IM  
Mr. Ely, R-ASTR-IR  
Mr. Threlkeld, R-ASTR-IT  
Mr. Boehm, R-ASTR-M  
Mr. Moore, R-ASTR-N  
Mr. Lominick, R-ASTR-NFS  
Mr. Nicaise, R-ASTR-NGI  
Mr. Taylor, R-ASTR-R  
Mr. Mack, R-ASTR-S  
Mr. Hammers, R-ASTR-S  
Mr. Wolfe, R-ASTR-S

## R-COMP

Dr. Hoelzer, R-COMP-DIR  
Mr. Prince, R-COMP-DIR  
Mr. Fortenberry, R-COMP-A  
Mr. Cochran, R-COMP-RR  
Mr. Houston, R-COMP-RRM

## R-ME

Mr. Kuers, R-ME-DIR  
Mr. Wuencher, R-ME-DIR  
Mr. Orr, R-ME-M  
Mr. Franklin, R-ME-T

## R-P&amp;VE

Dr. Lucas, R-P&VE-DIR  
Mr. Hellebrand, R-P&VE-DIR  
Mr. Palaoro, R-P&VE-DIR  
Mr. Goerner, R-P&VE-A  
Mr. Stein, R-P&VE-A  
Mr. Kingsbury, R-P&VE-M  
Mr. Thompson, R-P&VE-PA  
Mr. Fuhrmann, R-P&VE-PM (2)  
Mr. McKay, R-P&VE-PP  
Mr. Cobb, R-P&VE-PPE  
Mr. Wood, R-P&VE-PT  
Mr. Hunt, R-P&VE-S  
Mr. Beam, R-P&VE-SLA  
Mr. Blumrich, R-P&VE-SA  
Mr. Katz, R-P&VE-SER  
Mr. Showers, R-P&VE-SL  
Mr. Frederick, R-P&VE-SS  
Mr. Furman, R-P&VE-SJ  
Mr. Green, R-P&VE-SVM  
Mr. Aberg, R-P&VE-V  
Mr. Marmann, R-P&VE-VAW  
Mr. Lutonsky, R-P&VE-VAW (2)  
Mr. Devenish, R-P&VE-VNP  
Mr. Sells, R-P&VE-VOO (2)  
Mr. Schulze, R-P&VE-V  
Mr. Rothe, R-P&VE-XA  
Mr. Griner, R-P&VE-XSJ  
Mr. Boone, R-P&VE-XEK

## R-QUAL

Mr. Grau, R-QUAL-DIR  
Mr. Chandler, R-QUAL-DIR  
Mr. Henritze, R-QUAL-A  
Mr. Corder, R-QUAL-A  
Mr. Klauss, R-QUAL-J  
Mr. Brooks, R-QUAL-P  
Mr. Peck, R-QUAL-QVS  
Mr. Brien, R-QUAL-R  
Mr. Smith, R-QUAL-R  
Mr. Wittmann, R-QUAL-T

## R-RP

Dr. Stuhlinger, R-RP-DIR  
Mr. Heller, R-RP-T

## R-TEST

Mr. Heimbarg, R-TEST-DIR  
Mr. Grafton, R-TEST-C  
Dr. Sieber, R-TEST-I  
Mr. Edwards, R-TEST-M  
Mr. Driscoll, R-TEST-S  
Mr. Reilmann, R-TEST-SB

## MS

## MS-H

## MS-I

## MS-IP

## MS-IL

## MS-D

## CC-P

Mr. Wofford, CC-P

## KSC

Dr. Debus, CD  
Adm. Middleton, AP (5)  
Mr. Petrone, LO  
Dr. Gruene, LV  
Mr. Rigell, LV-ENG  
Mr. Sendler, IN  
Mr. Mathews, AP-SAT  
Dr. Knothe, EX-SCI  
Mr. Edwards, LV-INS  
Mr. Fannin, LV-MEC  
Mr. Pickett, LV-TOM  
Mr. Rainwater, LV-TOM  
Mr. Bell, LV-TOM-3  
Mr. Lealman, LV-GDC  
Mr. Preston, DE

EXTERNAL

Headquarters, National Aeronautics & Space Administration  
Washington, D. C. 20546

Dr. Mueller, M  
Gen. Phillips, MA  
Gen. Stevenson, MO (3 copies)  
Mr. Schneider, MO-2  
Capt. Freitag, MC  
Capt. Holcomb, MAO  
Mr. White, MAR (2 copies)  
Mr. Day, MAT (10 copies)  
Mr. Wilkinson, MAB  
Mr. Kubat, MAP  
Mr. Wagner, MAS (2 copies)  
Mr. Armstrong, MB  
Mr. Mathews, ML (3 copies)  
Mr. Lord, MT  
Mr. Lederer, MY

Director, Ames Research Center: Dr. H. Julian Allen  
National Aeronautics & Space Administration  
Moffett Field, California 94035

Director, Flight Research Center: Paul F. Bikle  
National Aeronautics & Space Administration  
P. O. Box 273  
Edwards, California 93523

Goddard Space Flight Center  
National Aeronautics & Space Administration  
Greenbelt, Maryland 20771  
Attn: Herman LaGow, Code 300

John F. Kennedy Space Center  
National Aeronautics & Space Administration  
Kennedy Space Center, Florida 32899  
Attn: Technical Library, Code RC-42  
Mrs. L. B. Russell

Director, Langley Research Center: Floyd L. Thompson  
National Aeronautics & Space Administration  
Langley Station  
Hampton, Virginia 23365

Director, Lewis Research Center: Dr. Abe Silverstein  
National Aeronautics & Space Administration  
21000 Brookpark Road  
Cleveland, Ohio 44135

Lewis Research Center  
National Aeronautics & Space Administration  
21000 Brookpark Road  
Cleveland, Ohio 44135  
Attn: Robert Washko, Mail Stop 86-1  
E. R. Jonash, Centaur Project Mgr.  
Manned Spacecraft Center  
National Aeronautics & Space Administration  
Houston, Texas 77058  
Attn: Director: Dr. Robert R. Gilruth, AA  
Mr. Low, PA  
Mr. Mardel, PT  
Mr. McKann, PT-121 (15 copies)

Director, Wallops Station: R. L. Krieger  
National Aeronautics & Space Administration  
Wallops Island, Virginia 23337

Director, Western Operations Office: Robert W. Kamm  
National Aeronautics & Space Administration  
150 Pico Blvd.  
Santa Monica, California 90406

Scientific and Technical Information Facility  
P. O. Box 5700  
Bethesda, Maryland 20014  
Attn: NASA Representative (S-AK/RKT) (25 copies)

Jet Propulsion Laboratory  
4800 Oak Grove Drive  
Pasadena, California 91103  
Attn: Irl Newlan, Reports Group (Mail 111-122)  
H. Levy, CCMTA (Mail 179-203) (4 copies)

Office of the Asst. Sec. of Defense for Research  
and Engineering  
Room 3E1065  
The Pentagon  
Washington, D. C. 20301  
Attn: Tech Library

Director of Guided Missiles  
Office of the Secretary of Defense  
Room 3E131  
The Pentagon  
Washington, D. C. 20301

Central Intelligence Agency  
Washington, D. C. 20505  
Attn: OCR/DD/Publications (5 copies)

Director, National Security Agency  
Ft. George Mead, Maryland 20755  
Attn: C3/TDL

U. S. Atomic Energy Commission, Sandia Corp.  
University of California Radiation Lab.  
Technical Information Division  
P. O. Box 808  
Livermore, California 94551  
Attn: Clovis Craig

U. S. Atomic Energy Commission, Sandia Corp.  
Livermore Br., P. O. Box 969  
Livermore, California 94551  
Attn: Tech Library

Commander, Armed Services Technical Inf. Agency  
Arlington Hall Station  
Arlington, Virginia 22212  
Attn: TIPCR (Transmittal per Cognizant Act  
Security Instruction) (5 copies)

Commanding General  
White Sands Proving Ground  
New Mexico 88002  
Attn: ORD BS-OMTIO-TL (3 copies)

Chief of Staff, U. S. Air Force  
The Pentagon  
Washington, D. C. 20330  
1 Cpy marked for DCS/D AFDRD  
1 Cpy marked for DCS/D AFDRD-EX

Commander-in-Chief  
Strategic Air Command  
Offutt AFB, Nebraska 68113  
Attn: Director of Operations, Missile Division

Commander  
Arnold Engineering Development Center  
Arnold Air Force Station, Tennessee 37389  
Attn: Tech Library (2 copies)

Commander  
Air Force Flight Test Center  
Edwards AFB, California 93523  
Attn: FTOTL

Commander  
Air Force Missile Development Center  
Holloman Air Force Base  
New Mexico 88330  
Attn: Tech Library (SRLT)

Headquarters  
6570th Aerospace Medical Division (AFSC)  
U. S. Air Force  
Wright-Patterson Air Force Base, Ohio 45433  
Attn: H. E. Vongierke

Systems Engineering Group (RTD)  
Attn: SEPIR  
Wright-Patterson, AFB, Ohio 45433

AFETR (ETLLG-1)  
Patrick AFB, Florida 32925

EXTERNAL (CONC)

Director  
U. S. Naval Research Laboratory  
Washington, D. C. 20390  
Attn: Code 2027

Chief of Naval Research  
Department of Navy  
Washington, D. C. 20390  
Attn: Code 463

Chief, Bureau of Weapons  
Department of Navy  
Washington, D. C. 20390  
1 Cpy to RESI, 1 Cpy to SP,  
1 Cpy to AD3, 1 Cpy to REW3

Commander  
U. S. Naval Air Missile Test Center  
Point Mugu, California 93041

AMSMI-RBLD; RSIC (3 copies)  
Bldg. 4484  
Redstone Arsenal, Alabama 35809

Aerospace Corporation  
2400 East El Segundo  
El Segundo, California 90245  
Attn: D. C. Bakeman

Aerospace Corporation  
Reliability Dept.  
P. O. Box 95085  
Los Angeles, California 90045  
Attn: Don Herzstein

Bellcomm, Inc.  
1100 Seventeenth St. N. W.  
Washington, D. C. 20036  
Attn: Miss Scott, Librarian

The Boeing Company  
P. O. Box 1680  
Huntsville, Alabama 35807  
Attn: S. C. Krausse, Mail Stop AD-60  
(10 copies)

The Boeing Company  
P. O. Box 29100  
New Orleans, Louisiana 70129  
Attn: R. H. Nelson, Mail Stop LA-42  
(3 copies)  
T. J. Kornell, Mail Stop LS-63  
(10 copies)

Chrysler Corporation Space Division  
Michoud Operations  
Dept. 2712, Bldg. 350  
P. O. Box 29200  
New Orleans, Louisiana 70129  
Attn: Mr. Leroy Smith (5 copies)

Chrysler Corporation Space Division  
Huntsville Operation  
1312 N. Meridian Street  
Huntsville, Alabama 35807  
Attn: H. D. Bader, Dept. 4800 (3 copies)  
M. L. Bell, Dept. 4830 (2 copies)  
G. Martin, Dept. 4820 (2 copies)

Douglas Aircraft Company  
Missile & Space Systems Division/SSC  
5301 Bolsa Avenue  
Huntington Beach, California 92647  
Attn: R. J. Calkins (40 copies)

Grumman Aircraft Engineering Corp.  
Bethpage, Long Island, N. Y. 11714  
Attn: NASA Resident Office  
John Johansen

International Business Machine  
Flight Evaluation Dept., K-11  
150 Sparkman Dr. NW  
Huntsville, Alabama 35808  
Attn: H. H. Weaver (10 copies)

Martin Company  
Space Systems Division  
Baltimore, Maryland 21203  
Attn: W. P. Sommers

North American Aviation  
Space & Information Division Systems  
12214 S. Lakewood Blvd.  
Downey, California 90241  
Attn: W. J. Strittmatter (35 copies)

Radio Corporation of America  
Defense Electronic Products  
Data Systems Division  
8500 Balboa Blvd.  
Van Nuys, California 91406

Rocketdyne  
6633 Canoga Avenue  
Canoga Park, California 91303  
Attn: T. L. Johnson (10 copies)

Foreign Technology Division  
FTD (TDBDP)  
Wright-Patterson Air Force Base, Ohio 45433